VOLUME 108 PART C NUMBER 14 SEPTEMBER 1961

The Proceedings

OF

THE INSTITUTION OF ELECTRICAL ENGINEERS

FOUNDED 1871: INCORPORATED BY ROYAL CHARTER 1921

PART C

MONOGRAPHS Nos. 422–454

Price Fifteen Shillings

The Institution of Electrical Engineers

FOUNDED 1871

INCORPORATED BY ROYAL CHARTER 1921

PATRON: HER MAJESTY THE QUEEN

COUNCIL 1960–1961

President

SIR HAMISH D. MACLAREN, K.B.E., C.B., D.F.C.*, LL.D., B.Sc.

Past-Presidents

W. H. ECCLES, D.Sc., F.R.S.
THE RT. HON. THE EARL OF MOUNT EDGCUMBE, T.D.
J. M. DONALDSON, M.C.
PROF. E. W. MARCHANT, D.Sc.
H. T. YOUNG.
SIR GEORGE LEE, O.B.E., M.C.
J. R. BEARD, C.B.E., M.Sc.
SIR NOEL ASHBRIDGE, B.Sc.(Eng.).
SIR HARRY RAILING, D.Eng.
P. DUNSHEATH, C.B.E., M.A., D.Sc.(Eng.), LL.D.
SIR VINCENT Z. DE FERRANTI, M.C.
T. G. N. HALDANE, M.A.
PROF. E. B. MOULLIN, M.A., Sc.D., LL.D.
SIR ARCHIBALD J. GILL, B.Sc.(Eng.).
SIR JOHN HACKING.
COL. B. H. LEESON, C.B.E., T.D.
SIR HAROLD BISHOP, C.B.E., B.Sc.(Eng.), F.C.G.I.
SIR JOSIAH ECCLES, C.B.E., D.Sc.
THE RT. HON. THE LORD NELSON OF STAFFORD.
SIR W. GORDON RADLEY, K.C.B., C.B.E., Ph.D.(Eng.).
S. E. GOODALL, M.Sc.(Eng.), F.Q.M.C.
SIR WILLIS JACKSON, D.Sc., D.Eng., LL.D., F.R.S.

Vice-Presidents

B. DONKIN, B.A.
O. W. HUMPHREYS, C.B.E., B.Sc.
G. S. C. LUCAS, O.B.E., F.C.G.I.
C. T. MELLING, C.B.E., M.Sc.Tech.
A. H. MUMFORD, O.B.E., B.Sc.(Eng.).

Honorary Treasurer

C. E. STRONG, O.B.E., B.A., B.A.I.

Ordinary Members of Council

J. C. ARKLESS, B.Sc.
PROF. H. E. M. BARLOW, Ph.D., B.Sc.(Eng.)., F.R.S.
D. A. BARRON, M.Sc.
C. O. BOYSE, B.Sc.(Eng.).
F. H. S. BROWN, C.B.E., B.Sc.
PROF. M. W. HUMPHREY DAVIES, M.Sc.
SIR JOHN DEAN, B.Sc.
L. DRUCQUER.
J. M. FERGUSON, B.Sc.(Eng.).
D. C. FLACK, B.Sc.(Eng.), Ph.D.
R. J. HALSEY, C.M.G., B.Sc.(Eng.), F.C.G.I.
R. A. HORE, M.A., B.Sc., Ph.D.
J. S. MCCULLOCH.
PROF. J. M. MEEK, D.ENG.
THE HON. H. G. NELSON, M.A.
H. V. PUGH.
J. R. RYLANDS, M.Sc., J.P.
R. L. SMITH-ROSE, C.B.E., D.Sc., Ph.D., F.C.G.I.
G. A. V. SOWTER, Ph.D., B.Sc.(Eng.).
H. G. TAYLOR, D.Sc.(Eng.).
D. H. TOMPSETT, B.Sc.(Eng.).

Chairmen and Past-Chairmen of Sections

Electronics and Communications:
T. B. D. TERRONI, B.Sc.
†M. J. L. PULLING, C.B.E., M.A.

Measurement and Control:
C. G. GARTON.
†PROF. A. TUSTIN, M.Sc.

Supply:
E. L. ROBINSON, M.Sc.
†J. R. MORTLOCK, Ph.D., B.Sc.(Eng.).

Utilization:
J. M. FERGUSON, B.Sc.(Eng.).
†T. E. HOUGHTON, M.Eng.

Chairmen and Past-Chairmen of Local Centres

East Midland Centre:
LT.-COL. W. E. GILL, T.D.
†D. H. PARRY, B.Sc.

North-Western Centre:
F. LINLEY.
†F. J. HUTCHINSON, M.Eng.

Mersey and North Wales Centre:
D. A. PICKEN.
†T. A. P. COLLEDGE, B.Sc.(Eng.).

Northern Ireland Centre:
J. MCA. IRONS.
†T. S. WYLIE.

Southern Centre:
R. GOFORD.
†W. D. MALLINSON, B.Sc.(Eng.).

North-Eastern Centre:
D. H. THOMAS, M.Sc.Tech., B.Sc.(Eng.).
†H. WATSON-JONES, M.Eng.

Scottish Centre:
R. B. ANDERSON.
†J. A. AKED, M.B.E.

Western Centre:
A. C. THIRTLE.
†H. JACKSON, B.Sc.(Eng.).

North Midland Centre:
F. W. FLETCHER.
†PROF. G. W. CARTER, M.A.

South Midland Centre:
BRIGADIER F. JONES, C.B.E., M.Sc.
†G. F. PEIRSON.

† Past Chairman.

Secretary

W. K. BRASHER, C.B.E., M.A., M.I.E.E.

Deputy Secretary

F. JERVIS SMITH, M.I.E.E.

Principal Assistant Secretary

F. C. HARRIS.

Editor-in-Chief

G. E. WILLIAMS, B.Sc.(Eng.), M.I.E.E.

THE PROCEEDINGS OF
THE INSTITUTION OF ELECTRICAL ENGINEERS

EDITED UNDER THE SUPERINTENDENCE OF W. K. BRASHER, C.B.E., M.A., M.I.E.E., SECRETARY

VOL. 108. PART C. NO. 14. SEPTEMBER 1961

621.313.333.2: 621.316.718.5

The Institution of Electrical Engineers
Monograph No. 422 U
Dec. 1960

INTERCONNECTED ROTOR INDUCTION MOTORS

By N. C. ENSLIN, Ph.D., Associate Member.

(*The paper was first received* 30*th May*, 1959, *in revised form* 14*th June, and in final form* 12*th September*, 1960. *It was published as an* INSTITUTION MONOGRAPH *in December*, 1960.)

SUMMARY

The stators of two identical wound-rotor induction motors are connected to a common supply to produce fields revolving in the same direction. The shafts are coupled mechanically and the rotor circuits are electrically connected together with the voltages initially phased so that no rotor current flows. By rotating one stator relative to the other through an angle β the rotor voltages are no longer in anti-phase, rotor currents flow and the unit produces torque.

Boucherot adopted a similar scheme in the construction of a composite machine with two stators and a common squirrel-cage rotor. The mid-points of the rotor bars were connected together through a resistive element so that currents always flowed in the rotor circuits and zero torque could not be obtained.

Expressions for torque are derived for the shunt-interconnected rotor developed by Boucherot and for the purely series-interconnected motor investigated by the author. It is shown that, for the former, torque cannot be controlled from zero without voltage variation, whereas in the latter arrangement zero torque is always obtained when the phases of the induced rotor voltages are in opposition.

The properties and applications of the series interconnected motor circuit are discussed. By the insertion of impedance the torque/speed characteristics of the motors can be modified retaining the zero torque position. Possible applications include small hoists, cranes or lifts, and positioning, manipulating or tensioning drives for which precise control is required.

LIST OF SYMBOLS

V_1 = Stator terminal voltage.
V_2 = Rotor terminal voltage.
I = Current, amp.
R_1 = Stator resistance per phase.
R_2 = Rotor resistance per phase.
X_1 = Stator leakage reactance per phase.
X_2 = Rotor leakage reactance per phase.
R_e = Rotor inserted series resistance per phase.
X_e = Rotor inserted series reactance per phase.
R_h = Rotor inserted shunt resistance per phase.
β = Phase angle introduced by the rotation of the stators or rotors relative to one another.
N = Speed, r.p.m.
s = Fractional slip.
T = Torque, synchronous watts.

Voltages, currents and impedances are all referred to either the stator or rotor, and for simplicity magnetizing and iron-loss components of current are neglected.

(1) INTRODUCTION

For constant-speed drives the polyphase induction motor has the advantages of simplicity of construction and robustness. System supplies are usually alternating current and the elimination of converting equipment is desirable.

Many attempts have been made to vary the speed of this machine while retaining these advantages. The developments have followed two lines: first, those in which the speed is varied by changing the speed, or effective speed, of the revolving field. Examples are pole-changing,[1, 2] pole-amplitude modulation[3] or the spherical motor[4] and subsequent work.[5] In the second group the constant speed of the revolving field produced by the stator is accepted and the rotor speed is varied by inserting impedance or injecting a voltage in the rotor circuit. Wound-rotor motors with resistance control in the rotor, the Schrage motor, the Kraemer and Scherbius systems[6] and cascading of more than one machine, employ this principle.

The interconnected rotor arrangement, falling into the second category, differs from cascading in that the stators of two motors are connected in parallel to a common supply, the shafts are mechanically coupled and the rotor circuits have their common terminals connected together. By introducing a phase shift between the supply and the voltages applied to one of the stators, or simply by swinging one of the stators mechanically relative to the other, the rotor currents can be controlled. The introduction of impedances between the rotor interconnections, the 'series connection', or between the three phases of the rotor interconnections, the 'shunt connection', results in modified

Correspondence on Monographs is invited for consideration with a view to publication.
Dr. Enslin is in the Department of Electrical Engineering, University of Cape Town, South Africa.

torque/speed characteristics controlled by the phase shift and amount and nature of impedance introduced.

Earlier work based on a patent by Boucherot[8] and described by Luraschi[9] and Brunswick[10, 11, 12] employs the 'shunt connection' in the construction and control of mine-haulage and pump motors.

(2) BOUCHEROT'S SHUNT INTERCONNECTION

The development of the circuit followed Boucherot's work on the double-squirrel-cage rotor.[13] Whereas, in the double-squirrel-cage rotor, frequency was used to discriminate in the circulation of current through the high-resistance circuit at start and the low-resistance circuit at speed, with the modification

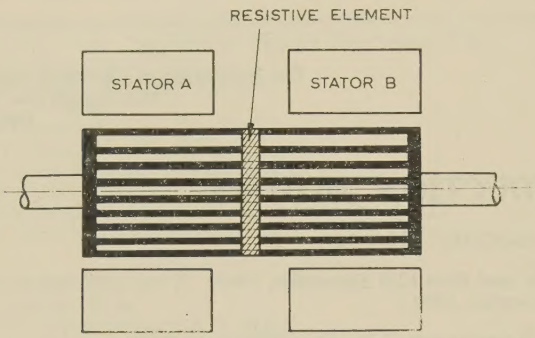

Fig. 1.—Boucherot's motor.

the stator now was split in two, retaining a single squirrel-cage rotor. The rotor bars were connected at their mid-points by a resistive ring, as in Fig. 1. At start the voltages in the two halves of a bar were arranged to be in opposition, thus forcing the rotor currents to circulate through the shunting resistive elements. Once the motor had gained speed the stator B was either rotated until the voltages in the two halves of the bar were in the same direction or the phase of the voltages applied to the stator B was phase-shifted until this was the case. No current would then circulate through the resistive element. The efficiency of the single-cage low-resistance rotor motor is retained while the torque at start can be controlled.

(2.1) Characteristics of the Boucherot Motor

Fig. 2 is the circuit for the motor in Fig. 1 or for two wound-rotor machines with resistors connected externally. In Sec-

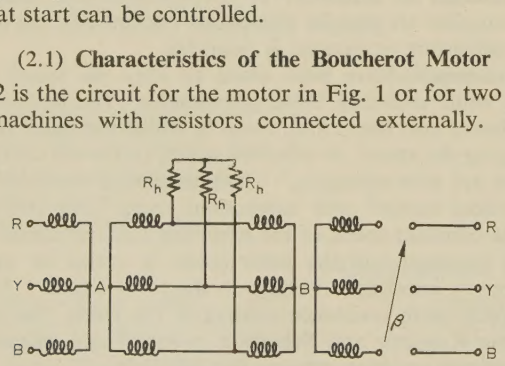

Fig. 2.—Circuit diagram of Boucherot's motor.

tion 10.1 the expression for the total torque of the motors in terms of the short-circuit constants, the applied voltage, the slip and phase angle β is evaluated. Magnetizing and iron-loss components of current have been neglected.

$$T_{A+B} = \frac{2V_1^2 \sin^2 \beta/2 s R_2}{(sR_1 + R_2)^2 + s^2(X_1 + X_2)^2} + \frac{2V_1^2 \cos^2 \beta/2 s(2R_h + R_2)}{(sR_1 + R_2 + 2R_h)^2 + s^2 (X_1 + X_2)^2}$$

synchronous watts per phase (1)

This expression is of the form

$$T_{A+B} = 2T_1 \sin^2 \beta/2 + 2T_2 \cos^2 \beta/2$$

where T_1 is the torque as a function of s of one of the motor with its rotor short-circuited, and T_2 is the torque with resistance $2R_h$ inserted in the rotor circuit.

Fig. 3 shows torque/speed characteristics recorded with tw

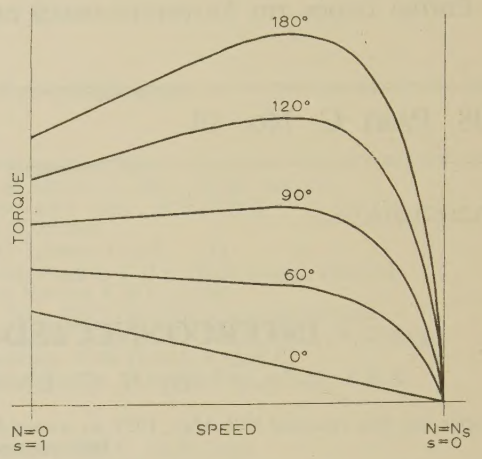

Fig. 3.—Torque/speed characteristics of Boucherot's motor for different values of β.

4 h.p. wound-rotor motors interconnected as in Fig. 2. Th curves are dependent on the chosen value of R_h.

It is clear that zero torque at standstill with rated voltag applied to the stators is not attainable for any value of β.

(2.2) Application of Boucherot's Method

Boucherot's patent[8] covers both squirrel-cage and wound rotor motors, although the applications were confined t squirrel-cage motors. In addition, owing to the difficulty o swinging one of the stators, the specification deals with tw types of external phase-shifting apparatus. The first is th standard 2-winding arrangement in which the shift is produce by revolving a rotor relative to a stator, which, in conjunctio with the motor combination, did not give a position for zer torque. Boucherot realized the advantage of controlling th motors from zero output torque to the full value, and th second type of phase-shifter therefore incorporates voltag control. A drum winding is fed at three symmetrically tappe points, and a large number of tappings from the winding ar connected to a commutator. The output is taken from thre brushes which are moved on the commutator to produce phas and voltage variation.

Boucherot's motors of the squirrel-cage construction wer installed at the Blanzy and Valdonne mines as hoist drives. Rated at 80 and 32 metric horse-power in the two cases, respec tively, the phase shift was produced in three steps by switchin the six ends of the windings of one of the stators, each transitio producing a 60° phase change. No voltage control was applie

The principle was also extended to pump motors of 130 metri horse-power running at 2730 r.p.m. and fan motors of 86 metri horse-power.[12] Squirrel-cage construction and the eliminatio of slip-rings were an advantage on account of the high speed Phase shift was produced by three connections:

(*a*) Stator phases in opposition.
(*b*) Second stator disconnected and short-circuited.
(*c*) Second stator excited in phase with the first.

The motors were no doubt successful in giving improved starting control, and they retained the advantages of low-resistance squirrel-cage machines.

Boucherot states in his specification that the proposed control does what a wound-rotor motor with rotor resistance variation achieves. For large motors when swinging the stator becomes impractical, the control must be by a separate phase-shifter with a rating equal to that of one of the motors. The costly additional control gear makes this impractical. Alternatively the motors can be controlled by switching in the stator circuit, as in the applications referred to.

A wound-rotor motor with resistance variation by means of a liquid controller or switched resistors in the rotor circuit would provide a better control than Boucherot's more difficult switching in the stator. In addition, it is an advantage to have the rotor circuit loss external to the machine, particularly when accelerating loads with appreciable inertia. In large motors which have to deliver a controlled torque during the starting period, the wound-rotor motor has therefore been retained in preference to Boucherot's system.

For smaller motors one stator can be revolved to control torque and speed. Unfortunately the torque cannot be controlled from zero with the shunt interconnection. To achieve this it is necessary to use a separate phase-shifter as described by Boucherot,[8] permitting voltage control as well.

(3) A MODIFIED INTERCONNECTED ROTOR CIRCUIT

In an attempt to obtain better control and simplify the equipment, the series-connected circuit characteristics have been investigated and applied.

(3.1) Characteristics of Series Interconnected Circuit

The expressions for the torque developed by two motors connected according to Fig. 4 are derived in Section 10.2:

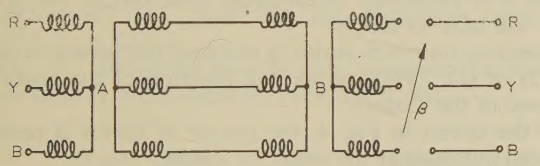

Fig. 4.—Simple series-interconnected circuit.

$$T_A = \frac{V_1^2 \sin^2 \beta/2 s R_2}{(sR_1 + R_2)^2 + s^2(X_1 + X_2)^2} + \frac{V_1^2 s^2 (X_1 + X_2) \sin \beta}{2(sR_1 + R_2)^2 + s^2(X_1 + X_2)^2}$$

synchronous watts per phase (2)

$$T_B = \frac{V_1^2 \sin^2 \beta/2 s R_2}{(sR_1 + R_2)^2 + s^2(X_1 + X_2)^2} - \frac{V_1^2 s^2 (X_1 + X_2) \sin \beta}{2(sR_1 + R_2)^2 + s^2(X_1 + X_2)^2}$$

synchronous watts per phase (3)

$$T_{A+B} = \frac{2V_1^2 \sin^2 \beta/2 s R_2}{(sR_1 + R_2)^2 + s^2(X_1 + X_2)^2}$$

synchronous watts per phase (4)

Eqn. (4) is of the form

$$T_{A+B} = 2T_1 \sin^2 \beta/2$$

where T_1 is the torque as a function of s of one of the motors with rotor short-circuited. The combination of the two motors reduces to the following equivalent: a variable-voltage transformer with a range from zero to the rated value, feeding the stator of a short-circuited rotor induction motor having a rating equal to the sum of that of the two motors, and a torque/speed characteristic the two motors would have if their rotor circuits were short-circuited. This equivalent and the torque characteristics are given in Fig. 5. The voltage reduction factor is $\sin \beta/2$ and at $\beta = 0$ the torque is zero and the machines draw their magnetizing current.

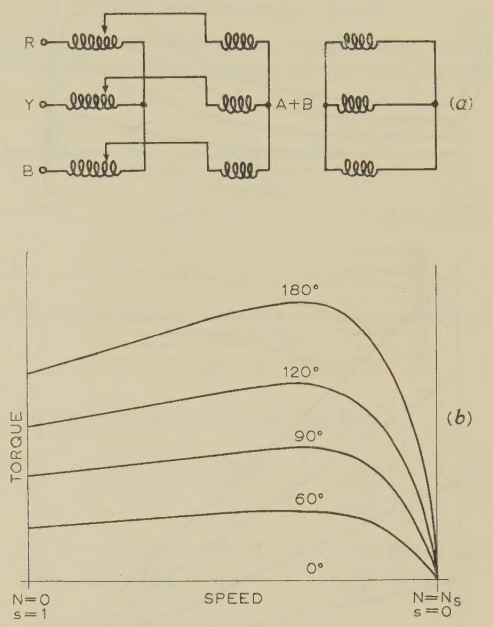

Fig. 5.—Simple series-interconnected motors.
(*a*) Single-motor equivalent arrangement.
(*b*) Torque/speed characteristics for different values of β.

(3.2) Addition of Series Impedance

It has been shown how the torque at a given slip can be varied smoothly from zero to its full value by swinging one of the stators. Adapting the principles established by Boucherot for double-cage induction motors, the torque/speed characteristic of a wound-rotor motor can be varied by inserting impedance as in Fig. 6.

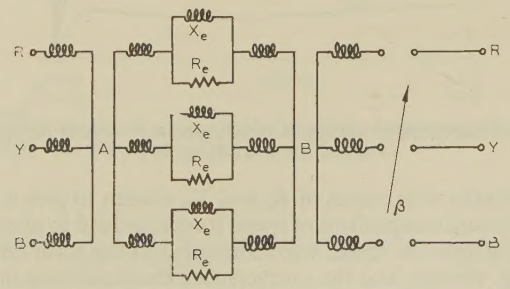

Fig. 6.—Addition of impedance in series.

The average slope of the characteristics can be adjusted to fall anywhere between the typical limits shown in Fig. 7. The modified characteristics of the 2-motor combination are given by the expression

$$T_{A+B} = \frac{2V_1^2 \sin^2 \beta/2s \left[R_2 + \frac{R_e(sX_e)^2}{2(R_e^2 + s^2X_e^2)} \right]}{\left[sR_1 + R_2 + \frac{R_e(sX_e)^2}{2(R_e^2 + s^2X_e^2)} \right]^2 + s^2 \left[X_1 + X_2 + \frac{R_e^2 X_e}{2(R_e^2 + s^2 X_e^2)} \right]^2} \text{ synchronous watts per phase} \quad . \quad . \quad (3$$

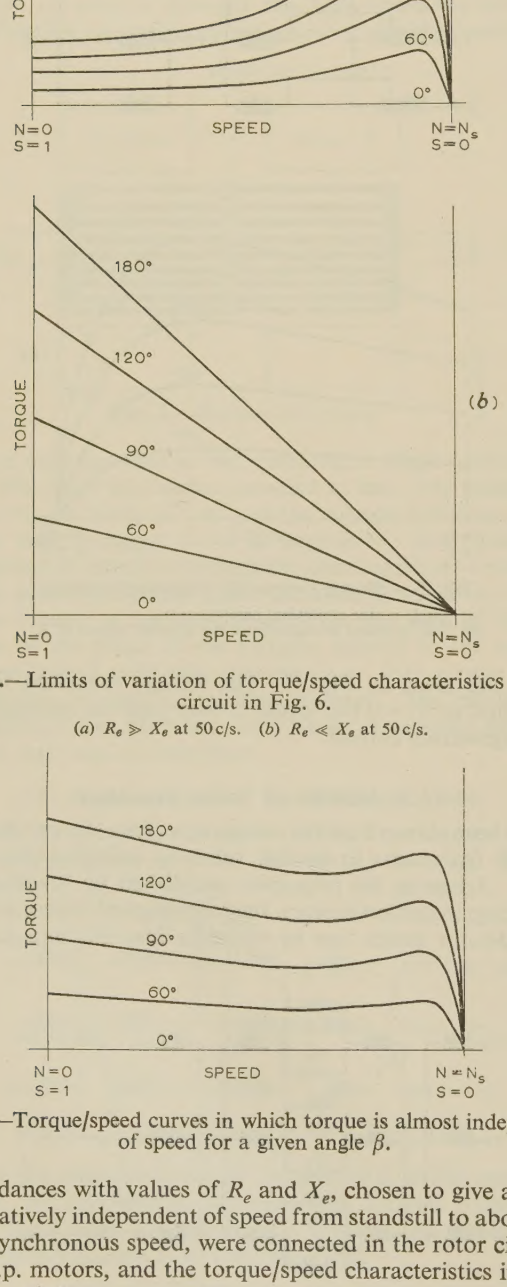

Fig. 7.—Limits of variation of torque/speed characteristics of the circuit in Fig. 6.
(*a*) $R_e \gg X_e$ at 50 c/s. (*b*) $R_e \ll X_e$ at 50 c/s.

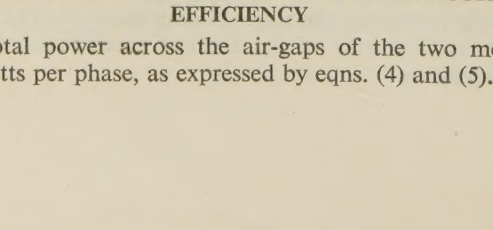

Fig. 8.—Torque/speed curves in which torque is almost independent of speed for a given angle β.

Impedances with values of R_e and X_e, chosen to give a torque comparatively independent of speed from standstill to about 90% of the synchronous speed, were connected in the rotor circuit of two 4 h.p. motors, and the torque/speed characteristics in Fig. 8 were recorded.

(4) POWER DISSIPATED IN THE ROTOR CIRCUIT AND EFFICIENCY

The total power across the air-gaps of the two motors is T_{A+B} watts per phase, as expressed by eqns. (4) and (5). As in the case of a single motor $(1 - s)T_{A+B}$ is delivered mechanical to the shaft and sT_{A+B} is dissipated in the rotor circuit. For fixed torque the power delivered from the stator is constant, th output varies with the speed and the balance is lost in the rotc circuit. At standstill all the power is lost in the rotor circu and adequate provision must be made for this dissipation i the resistors. Neglecting the influence of the constant loss and the stator copper loss, the efficiency is almost proportion to the speed, over its range, for a fixed output torque.

With the interconnection of Fig. 4 and $\beta = 180°$ two moto retain their original efficiency at full load and rated speed. Th efficiency will be reduced when series impedance is added, in Fig. 6, since the reactors have some resistance and they c not completely shunt the resistors R_e because of the finite rot frequency.

(5) REVERSING AND BRAKING

To reverse the motors, the directions of the revolving fiel of both motors have to be reversed by reconnecting the stato

The motors will only brake by regeneration above the synch nous speed. Between synchronous speed and standstill, brak is achieved by reversing the stator revolving fields. Energ then dissipated in the rotor circuit and no regeneration occu

The braking or regenerating torques are controlled as bef by varying β. Eqns. (4) and (5) apply with the appropria value of s substituted.

(6) TORQUE REQUIRED TO REVOLVE ONE OF THE STATORS

When the motors are controlled by revolving one of t stators, it is important to establish what torque the actuati device will have to supply.

Depending on which stator is revolved the torque is given eqn. (2) or (3). This torque is a function of the angle β a the speed of the motors.

For the circuit in Fig. 4, the torque of motor B reverses the speed increases at the point for which

$$\tan \beta/2 = \frac{s(X_1 + X_2)}{R_2}$$

When impedance is inserted in series as in Fig. 6, eqns. (2) a (3) are modified by substituting equivalent values of reactan and resistance as has been done for eqn. (5).

(7) APPLICATIONS OF THE SERIES-INTERCONNECTE CIRCUIT

The connection permits the smooth control of torque a speed with two standard wound-rotor motors and no additio control equipment other than the provision for rotating one the stators. Applications are limited to motors with stators a size that can be rotated conveniently.

The motors operate efficiently at one speed only, their contr being obtained at the expense of dissipation in the rotor circu The use of this method is confined to drives which have starti and stopping periods during which the torque has to be carefu controlled. This must be short compared with the compl load cycle to improve the overall efficiency. Such applicatio exist in small lifts, hoists and cranes, where the drive oft consists of a constant-speed motor and a clutch or a d.c. mot with armature-circuit resistance control. Where the dissipati

of energy occurred in the clutch or the armature-circuit resistors, it is now dissipated in the resistors in the rotor circuit. These can be mounted on the shaft to improve their ventilation and eliminate the slip-rings.

If efficiency can be sacrificed the series-interconnected rotor circuit can be used over its complete speed range to control torque and speed continuously. The ability to control the motors smoothly makes the circuit applicable to positioning or manipulating drives. A torque/speed characteristic as shown in Fig. 8 may be suitable for a tensioning drive. The torque is almost constant over the speed range and can be set to the desired value by varying β.

(8) ACKNOWLEDGMENTS

The author wishes to thank Prof. R. W. Guelke and Col. G. H. Webster for their assistance and useful discussions. The mounting of the experimental motors was effectively carried out by Mr. J. N. Wright.

(9) REFERENCES

(1) RAWCLIFFE, G. H., and JAYAWANT, B. V.: 'The Development of a New 3 : 1 Pole-Changing Motor', *Proceedings I.E.E.*, Paper No. 1958 U, December, 1955 (**103** A, p. 306).

(2) RAWCLIFFE, G. H., and JAYAWANT, B. V.: 'An Asymmetrical Induction-Motor Winding for 6 : 3 : 2 : 1 Speed Ratios', *ibid.*, Paper No. 2180 U, December, 1956 (**103** A, p. 599).

(3) RAWCLIFFE, G. H., BURBRIDGE, R. F., and FONG, W.: 'Induction-Motor Speed-Changing by Pole-Amplitude Modulation', *ibid.*, Paper No. 2597 U, August, 1958 (**105** A, p. 411).

(4) WILLIAMS, F. C., LAITHWAITE, E. R., and PIGGOT, L. S.: 'Brushless Variable-Speed Induction Motors', *ibid.*, Paper No. 2097 U, June, 1956 (**104** A, p. 102).

(5) MIDGLEY, D.: 'A Sliding-Rotor Induction Motor', *ibid.*, Paper No. 3016 U, October, 1959 (**106** A, p. 337).

(6) ADKINS, B., and GIBBS, W. J.: 'Polyphase Commutator Machines', *ibid.*, Paper No. 782, November, 1948 (**103**, Part II, p. 233).

(7) DÉRI, M.: 'Induction Motors with Large Starting Torque', *Zeitschrift Electrotechnik*, 1898, **16**, p. 285.

(8) BOUCHEROT, P. J. J.: 'Improved Method of Starting and Regulating Multiphase-Current Motors', British Patent No. 9534, 1900.

(9) LURASCHI, A.: 'Boucherot's 3 Phase Induction Motor', *Elettricita Milan*, 1901, **20**, pp. 598 and 611.

(10) BRUNSWICK, E. J.: 'Asynchronous Motors', *Électricien*, 1898, **15**, pp. 305, 321 and 340.

(11) BRUNSWICK, E. J.: 'Various Applications of Boucherot Induction Motors in Mines', *ibid.*, 1904, **27**, p. 385, and **28**, p. 3.

(12) BRUNSWICK, E. J.: 'Boucherot's Polyphase Induction Motors', *Industrie Électrique*, 1905, **14**, p. 536.

(13) HOBART, M. H.: 'Electric Motors' (Whittaker, 1910), pp. 325–337.

(10) APPENDICES

(10.1) Derivation of Torque/Speed Relations for Shunt-Interconnected Rotors

To simplify the derivation the magnetizing and iron-loss components of the usual equivalent circuit have been neglected.

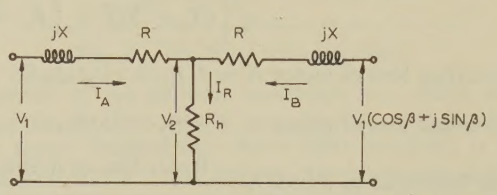

Fig. 9.—Equivalent circuit of motors with shunt-connected rotor resistance R_h.

$X = (X_1 + X_2)$ $R = (R_1 + R_2)$

Solving for the currents and V_2 in Fig. 9,

$$I_A = \frac{V_1}{2}\left[\frac{1 + \cos\beta - j\sin\beta}{(R + 2R_h) + jX} + \frac{1 - \cos\beta + j\sin\beta}{R + jX}\right]$$

$$I_B = \frac{V_1}{2}\left[\frac{1 + \cos\beta - j\sin\beta}{(R + 2R_h) + jX} - \frac{1 - \cos\beta + j\sin\beta}{R + jX}\right]$$

$$V_2 = V_1\frac{(1 + \cos\beta - j\sin\beta)R_h}{(R + 2R_h + jX)}$$

Rotor loss of motor A $= |I_A|^2R_2 + |I_A| \times |sV_2| \times \cos$ of the included angle.

Torque developed by motor A $= \dfrac{\text{Rotor loss of motor A}}{s}$

which can be shown to be

$$T_A = \frac{V_1^2 \sin^2\beta/2sR_2}{(sR_1 + R_2)^2 + s^2(X_1 + X_2)^2} + \frac{V_1^2\cos^2\beta/2s(2R_h + R_2)}{(sR_1 + R_2 + 2R_h)^2 + s^2(X_1 + X_2)^2} + \frac{V_1^2 s(R_h + R_2)\sin(\theta - \alpha)\sin\beta}{\sqrt{\{[(sR_1 + R_2)^2 + s^2(X_1 + X_2)^2][(sR_1 + R_2 + 2R_h)^2 + s^2(X_1 + X_2)^2]\}}} \text{ synchronous watts per phase} \quad (6)$$

Similarly the torque developed by motor B is

$$T_B = \frac{V_1^2 \sin^2\beta/2sR_2}{(sR_1 + R_2)^2 + s^2(X_1 + X_2)^2} + \frac{V_1^2\cos^2\beta/2s(2R_h + R_2)}{(sR_1 + R_2 + 2R_h)^2 + s^2(X_1 + X_2)} - \frac{V_1^2 s(R_h + R_2)\sin(\theta - \alpha)\sin\beta}{\sqrt{\{[(sR_1 + R_2)^2 + s^2(X_1 + X_2)^2][(sR_1 + R_2 + 2R_h)^2 + s^2(X_1 + X_2)^2]\}}} \text{ synchronous watts per phase} \quad (7)$$

$$\theta = \arctan\frac{X_1 + X_2}{(R_1 + R_2/s)}, \text{ and } \alpha = \arctan\frac{X_1 + X_2}{R_1 + \dfrac{R_2 + 2R_h}{s}}$$

(10.2) Derivation of Torque/Speed Relations for Simple Series-Interconnected Motors

The magnetizing and iron-loss components of the motor equivalent circuits have been neglected, as in Fig. 10.

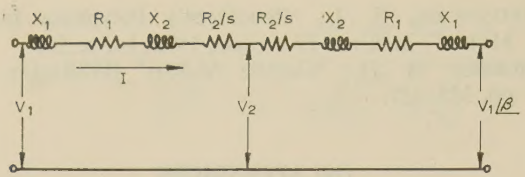

Fig. 10.—Equivalent circuit of simple series-interconnected rotors.

From the vector diagram of Fig. 11,

$$V_2 = V_1 \cos \beta/2 \text{ and } \sin \theta = \frac{X_1 + X_2}{\sqrt{\left[(X_1 + X_2)^2 + \left(R_1 + \frac{R_2}{s}\right)^2\right]}}$$

Rotor-circuit loss of motor A $= I^2R_2 + sV_2I \sin \theta$

Rotor-circuit loss of motor B $= I^2R_2 - sV_2I \sin \theta$

$$\text{Torque developed by motor A} = \frac{\text{Rotor loss of motor A}}{s}$$

$$T_A = \frac{V_1^2 \sin^2 \beta/2 sR_2}{(sR_1 + R_2)^2 + s^2(X_1 + X_2)^2} + \frac{V_1^2 \sin \beta s^2(X_1 + X_2)}{2[(sR_1 + R_2)^2 + s^2(X_1 + X_2)^2]}$$

synchronous watts per phase (8)

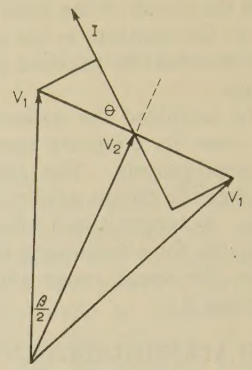

Fig. 11.—Vector diagram for two motors with series-interconnec rotors.

Similarly the torque developed by motor B is

$$T_B = \frac{V_1^2 \sin^2 \beta/2 sR_2}{(sR_1 + R_2)^2 + s^2(X_1 + X_2)^2} - \frac{V_1^2 \sin \beta s^2(X_1 + X_2)}{2[(sR_1 + R_2)^2 + s^2(X_1 + X_2)^2]}$$

synchronous watts per phase

$T_B = 0$ when $\tan \beta/2 = \dfrac{s(X_1 + X_2)}{R_2}$

621.375.13:621.318.5:621.526

The Institution of Electrical Engineers
Monograph No. 423 M
Dec. 1960

FREQUENCY RESPONSE OF FEEDBACK RELAY AMPLIFIERS

By ZE'EV BONENN, B.Sc.

(*The paper was first received* 10*th May, and in revised form* 19*th September*, 1960. *It was published as an* INSTITUTION MONOGRAPH *in December*, 1960.)

SUMMARY

The frequency response of feedback relay amplifiers is analysed by the dual-input describing-function method. At low signal frequencies, the amplifier behaves like a saturating linear amplifier. This picture is modified at higher frequencies, owing to synchronous effects, and it is difficult to achieve satisfactory operation when the ratio of the input-signal frequency to the periodic excitation frequency is appreciable. To eliminate synchronous effects within the signal band, restrictions must be imposed on the forward linear-transfer function. The theory is compared with an experimental example.

LIST OF SYMBOLS

A_{mn} = Fourier coefficient of relay output.
a = Carrier amplitude.
b = Signal amplitude.
$G(j\omega)$ = Forward linear-transfer function.
$G_c = |G(j\omega_c)|$.
$k = b/a$.
N_c = Describing function for carrier.
N_s = Describing function for signal.
$U(\omega) = \mathscr{R}G(j\omega)$.
$u(t)$ = Amplifier input.
u_s = Signal input amplitude.
$V(\omega) = \mathscr{I}G(j\omega)$.
$v(t)$ = Amplifier output.
v_s = Signal output amplitude.
$y(t)$ = Relay output.
y_c = Relay carrier output amplitude.
y_s = Relay signal output amplitude.
ϕ = Phase angle between carrier and signal at relay input.
ω = Angular frequency.
ω_c = Carrier frequency.
ω_s = Signal frequency.

(1) INTRODUCTION

A *relay amplifier* is a device in which the on/off output characteristic of a relay is modified by means of a periodic excitation added to the input signal. The aim is, usually, to obtain a linear relationship between the average output and the input, although other characteristics are also possible.

In the relay amplifier with external excitation the additional

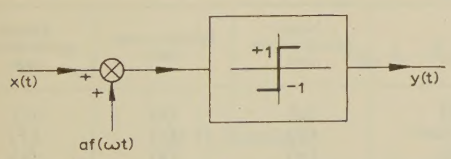

Fig. 1.—Relay amplifier.

periodic excitation is obtained from an external source (Fig. 1), whereas in the feedback relay amplifier the periodic excitation is furnished by a feedback circuit (Fig. 2).

The relay amplifier operates as a square-wave generator at

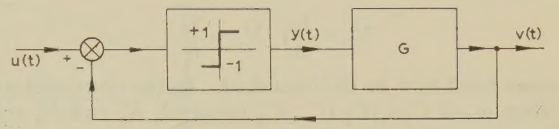

Fig. 2.—Feedback relay amplifier.

the frequency of the periodic excitation, ω_c, which is width modulated by the input signal. ω_c is chosen high compared with the signal frequencies. As a relay amplifier is usually connected to a system which behaves like a low-pass filter, relay output components at ω_c and its harmonics are attenuated. If the attenuation is sufficient, these components have negligible influence on the system output, which essentially contains only signal components.

The main use of a relay amplifier is as a power amplifier in a control system, where it combines very high power gain with a linear characteristic. In some cases the gain obtained is sufficiently high, so that no other amplifying elements are necessary. A relay amplifier is particularly useful in a dual-mode control system,[1] where a small linear range is combined with on/off operation for large errors. A dual-mode system can thus combine the optimal properties of on/off control for large errors with the more convenient and easier linear design for small errors. An example of such a system using a relay amplifier was given recently by Buland and Furomoto.[2]

The concept of 'linearizing' a relay by means of an additional periodic excitation was apparently introduced by MacColl[3] in his analysis of the so-called 'oscillating servomechanisms'. There have been many publications on this subject,[4–9] dealing primarily with the analysis of d.c. response. The main result is that for a d.c. input signal the relay amplifier behaves like a saturating linear amplifier. The departure from linearity within the unsaturated range is usually quite small.

The present paper is devoted to the analysis of the frequency response of relay amplifiers. In general, the device behaves like a saturating linear amplifier. However, several problems arise: first, the nature of the error between input and output; secondly, the practical linear range of the amplifier for a.c. inputs; and thirdly, the permissible bandwidth of the signal frequencies. (Though in theory[10] the input frequency may approach $\frac{1}{2}\omega_c$, in practice it must stay lower.) It is difficult to give exact solutions to the above problems because of the extreme non-linearity of the device. The paper attempts to give approximate answers which may be useful in engineering design.

The analysis will be carried out using the dual-input describing functions[11] of the relay, assuming that its input contains only two frequencies, the input frequency, ω_s, and the internal oscillation frequency, ω_c, called the 'carrier frequency'. This method is also applicable to other on/off control systems whenever the same assumption is justified.

(2) DUAL-INPUT DESCRIBING FUNCTIONS FOR THE IDEAL RELAY

(2.1) General

When the input of the ideal relay is given by

$$a \sin \omega_c t + b \sin (\omega_s t + \phi) \quad . \quad . \quad . \quad . \quad (1)$$

Correspondence on Monographs is invited for consideration with a view to publication.

Mr. Bonenn is in the Department of Engineering, University of Cambridge (on leave of absence from the Israel Ministry of Defence).

the output may be expressed by the double Fourier series

$$y(t) = \sum_{m=0}^{\infty} \sum_{n=-\infty}^{\infty} A_{mn} \sin [m\omega_c t + n(\omega_s t + \phi)] \quad (\text{for } m = 0, n > 0) \quad (2)$$

The coefficients A_{mn} have been calculated by Bennett and Kalb,[12] and are expressed by combinations of various complete elliptic integrals with argument $k = b/a$.

We may now define

$$N_c = \frac{y_c}{a}; \quad N_s = \frac{y_s}{b} \quad . \quad . \quad . \quad . \quad . \quad (3)$$

Two cases must now be distinguished. In the non-synchronous case when $\omega_c \neq C_1\omega_s/C_2$ (C_1, C_2 integers), N_c and N_s are real and functions of the amplitudes a and b only. In the synchronous case they become complex and dependent also on the phase angle ϕ.

(2.2) Non-Synchronous Case

The components of interest in the non-synchronous case are

$$\left.\begin{aligned} y_s(t) &= A_{01} \sin (\omega_s t + \phi) \\ \text{and} \quad y_c(t) &= A_{10} \sin \omega_c t \end{aligned}\right\} \quad . \quad . \quad . \quad . \quad (4)$$

where

$$A_{01} = \begin{cases} \frac{8}{\pi^2} k\mathrm{B}(k) & k < 1 \\ \frac{8}{\pi^2}\mathrm{E}\left(\frac{1}{k}\right) & k > 1 \end{cases}$$

$$A_{10} = \begin{cases} \frac{8}{\pi^2}\mathrm{E}(k) & k < 1 \\ \frac{8}{\pi^2 k}\mathrm{B}\left(\frac{1}{k}\right) & k > 1 \end{cases}$$

and E and B are complete elliptic integrals.[13]

Instead of using the describing functions directly, it is more convenient to use the following functions which depend on k only:

$$aN_s = \frac{y_s}{k} = \frac{A_{01}}{k}; \quad bN_c = ky_c = kA_{10} \quad . \quad . \quad (5)$$

These are plotted together with y_c and y_s in Fig. 3. Note that signal gain is almost constant (for constant a) for $k < \frac{4}{3}$, and

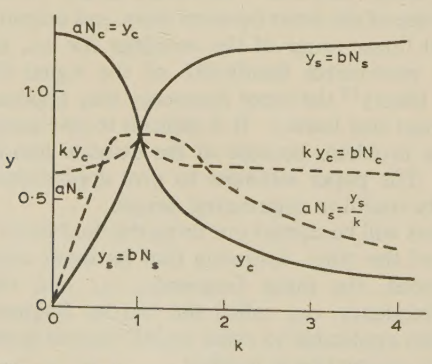

Fig. 3.—Relay output: non-synchronous case.

indeed its general character is quite similar to that of a saturating amplifier. It should be realized that for large k, i.e. greater than unity, the distortion terms, A_{mn} ($m, n \neq 0, 1$), increase rapidly and become comparable to y_c. This should be borne in mind in further analysis.

(2.3) Synchronous Case

There are many possible synchronous cases. The one most practical importance for the relay, owing to its chara teristic (Fig. 1), is $\omega_c = 3\omega_s$. Signal and carrier outputs a in this case given by

$$\left.\begin{aligned} y_s(t) &= A_{01} \sin (\omega_s t + \phi) + A_{1,-2} \sin (\omega_s t - 2\phi) \\ &\quad - A_{1,-4} \sin (\omega_s t + 4\phi) - \ldots \\ y_c(t) &= A_{10} \sin \omega_c t + A_{2,-3} \sin (\omega_c t - 3\phi) \\ &\quad + A_{03} \sin (\omega_c t + 3\phi) + \ldots \\ & \qquad k < 1 \end{aligned}\right\}$$

The convergence of these series deteriorates as k tends to uni The first terms for y_s and y_c are the same as before. The oth come from various combinations of m and n yielding differe frequencies equal to ω_s or ω_c. For $k > 1$ a similar series m be written but its convergence is very slow. Thus the use these series for practical computation is not convenient. Inste y_s and y_c were computed on Edsac II. They are drawn in Fig $-1/bN_c$ and $-1/aN_s$ are given in Fig. 5.

Up to $k = 0{\cdot}75$ the difference from the non-synchron case is small. For larger k there is a marked dependence amplitude and phase on ϕ. In Fig. 6, y_s and y_c are drawn the case $\omega_c = 5\omega_s$ for comparison. Synchronous effects much less pronounced here, and diminish rapidly for the e case $\omega_c = 4\omega_s$ and higher-order cases.

The coefficients A_{mn}, while not very useful in the series mentioned above, are valuable for assessing the effect of vari neglected distortion terms separately. Thus, for third-or synchronization ($\omega_c = 3\omega_s$), the first one is at $\omega = 5\omega_s$ and of some importance for $k > 1$ (see Section 3.3.3). On the ot hand, for fifth-order synchronization ($\omega_c = 5\omega_s$), the first tortion term is at $\omega = 3\omega_s$ and when k increases it eclip components at $5\omega_s$. Therefore, for large k, the fifth-or synchronous describing function (Fig. 6) is not representative the output.

(2.4) Almost Synchronous Case

If $\omega_c \simeq C_1\omega_s/C_2$ and $\Delta\omega = \omega_s - C_2\omega_c/C_1$ is small, difference frequencies do not become exactly ω_s or ω_c. Th is now a complete spectrum of output frequencies around and ω_c. In Fig. 7, examples are given for $\omega_s = 1$, $\omega_c =$ (third-order synchronization) and $k = 1$ and 2. It is conven to regard this case as a synchronous case with varying ϕ, wh $\dot{\phi} = \Delta\omega$. Thus y_s and y_c will be slowly varying vectors (Fig over all values of ϕ. In other words, relay gain for both and ω_c will vary continually in magnitude and phase.

Table 1

k	Non-synchronous case	Synchronous case	Almost synchronous case
Small ..	(*a*)	(*b*)	(*c*)
Medium ..	(*d*)	(*e*)	(*f*)
Large ..	(*g*)	(*h*)	(*i*)

(*a*)–(*c*) Small-signal region, practically a constant gain. Disto negligible.

(*g*)–(*i*) Saturation region, output practically a square wave a carrier influence diminishes and becomes negligible (large k).

(*a*), (*d*), (*g*) Non-synchronous case, behaves like a saturating l amplifier (Fig. 3).

(*e*) Synchronous case (Figs. 4 and 5). Output depends on ϕ.

(*f*) Almost synchronous case (Figs. 4 and 5). ϕ varies and ou varies with it continually.

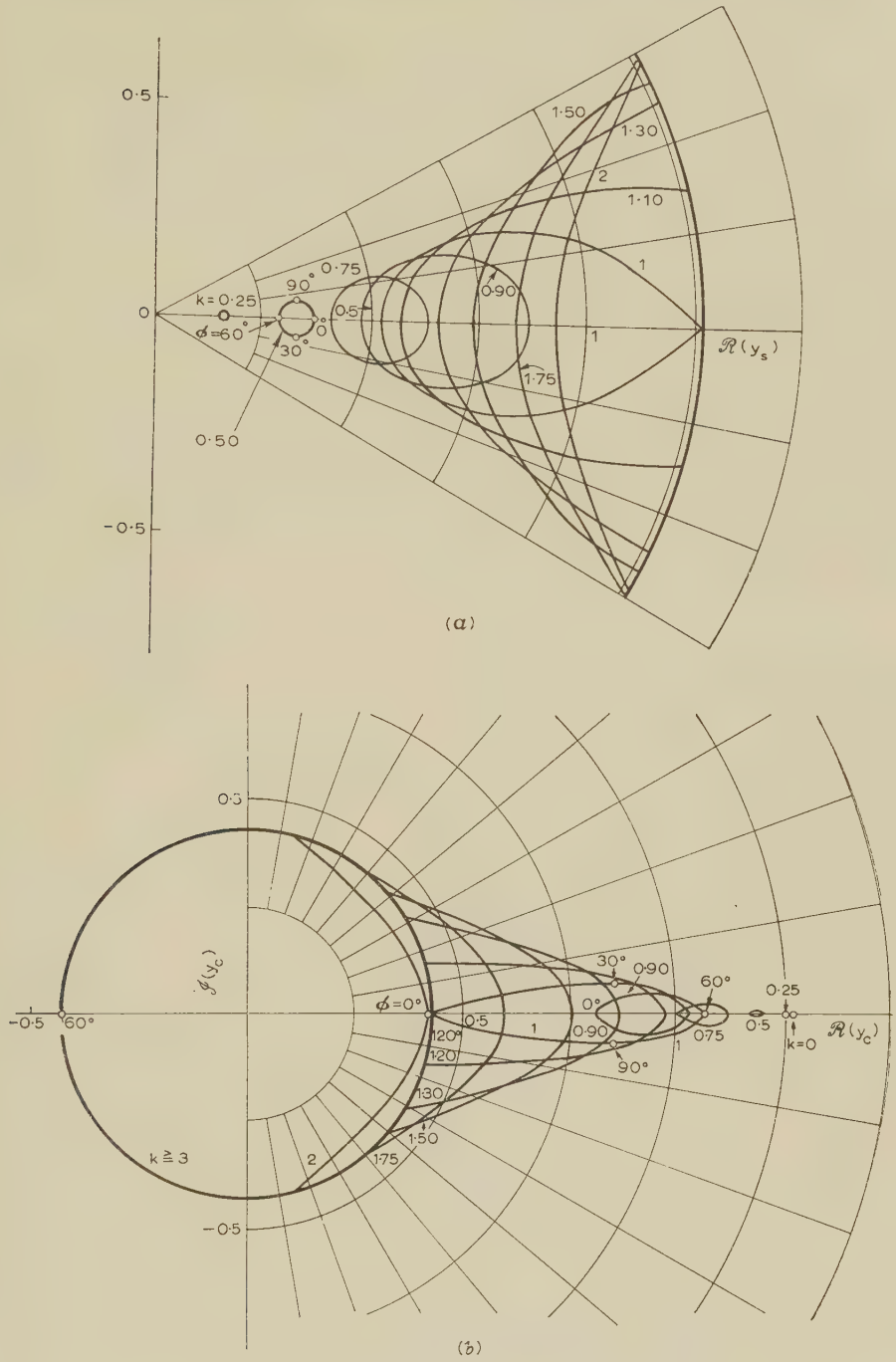

Fig. 4.—Relay output: third-order synchronous case.
(*a*) Signal.
(*b*) Carrier.

(2.5) Summary

The results of this Section may be summarized with the help of Table 1. The non-synchronous case applies when $\omega_s \ll \omega_c$. The synchronous case applies when $\omega_s = C_2\omega_c/C_1$ and in particular when $\omega_s = \frac{1}{3}\omega_c$. The almost synchronous case applies in the neighbourhood of the synchronous case.

(3) FREQUENCY RESPONSE ANALYSIS

(3.1) General

When an input, u_s, at frequency ω_s is applied to the feedback relay amplifier (Fig. 2), the response is given by two complex equations:

Signal equation

$$b + v_s = u_s$$

where

$$v_s = y_s G(j\omega_s) \quad . \quad . \quad . \quad . \quad . \quad (7a)$$

Carrier equation

$$a + y_c G(j\omega_c) = 0 \quad (7b)$$

together with the relationship

$$b = ka \quad (7c)$$

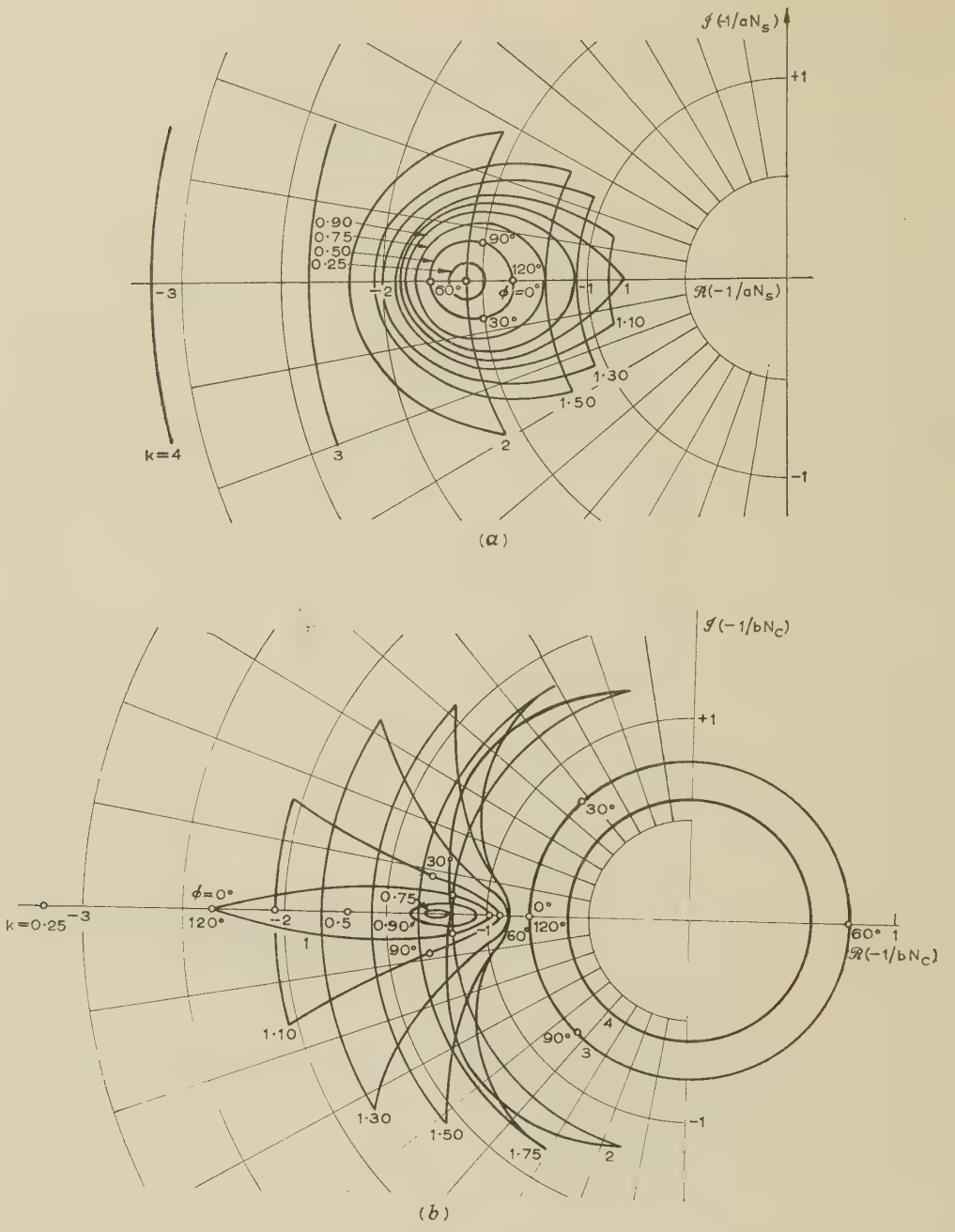

Fig. 5.—Inverse describing function: synchronous case.
(*a*) $-1/aN_s$
(*b*) $-1/bN_c$

y_s and y_c are given by the results of the last Section. These equations are based on the assumption that components at all other frequencies appearing in the relay output, which are relatively small, are sufficiently attenuated around the loop and may be ignored. The validity of this assumption will be discussed separately in every case.

The analysis is divided into two parts. The first part deals with low frequencies ($\omega_s \ll \omega_c$) where the interaction between signal and carrier frequencies is negligible and where the non-synchronous describing functions will be used. The second part deals with higher frequencies where synchronous and almost synchronous phenomena predominate.

(3.2) Low Frequencies

(3.2.1) Analysis.

This is the simplest case. y_s and y_c are real and function k only (Fig. 3). Therefore, the carrier frequency is constant given by the phase condition $\angle G(j\omega_c) = -180°$. Here using eqns. (7), we obtain the following results:

$$a = y_c(k)G_c \quad . \quad . \quad . \quad . \quad . \quad . \quad . \quad . \quad (\ )$$

$$b = ka = ky_c(k)G_c \quad . \quad . \quad . \quad . \quad . \quad . \quad (\ )$$

where $G_c = |G(j\omega_c)|$, and the signal equation becomes

$$ky_c(k)G_c + y_s(k)G(j\omega_s) = u_s \quad . \quad . \quad .$$

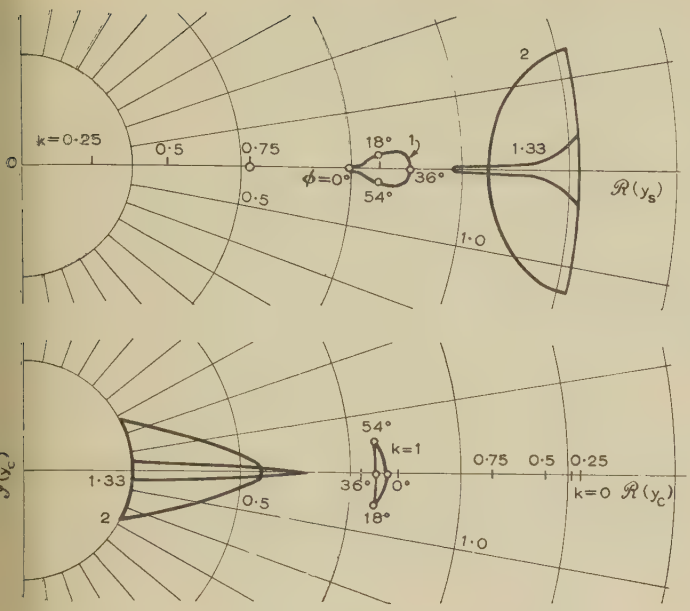

Fig. 6.—Relay output: fifth-order synchronous case.

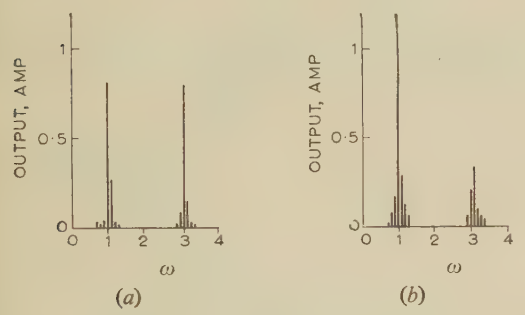

Fig. 7.—Output spectrum.
$\omega_s = 1$, $\omega_c = 3{\cdot}1$.
(*a*) $k = 1$. (*b*) $k = 2$.

This equation may be solved graphically for a given frequency, ω_s, and all k to yield $v_s = f(u_s)$. Note that the actual solution proceeds from output to input.

In the saturation region ($k > 1{\cdot}2$), however, the accuracy of this procedure decreases considerably because it ignores the distortion terms which, as mentioned in Section 2.2, become large in this region. For this reason, it is also very difficult to calculate the behaviour more accurately here.

The signal error for a given output (or given k) is directly proportional to G_c [eqn. (8*b*)], the magnitude of the transfer function at the carrier frequency. Thus, to reduce signal error, G_c must be reduced. This demonstrates the most salient feature of relay amplifiers. Error at signal frequencies depends directly on circuit behaviour at the carrier frequency. Proper design must therefore exercise control over the transfer function in both ranges, at the low signal frequencies and at the high frequencies near ω_c. If the signal error is very small compared with the output, $b \ll v_s$, the signal equation becomes $y_s(k)G(j\omega_s) \simeq u_s$. The practical linear input range is then $4|G(j\omega_s)|/\pi$.

Calculation of the input required for complete saturation (relay output a square wave at ω_s) will be dealt with in Section 3.4. It is usually of limited interest.

(3.2.2) **Experimental Circuit and Results.**

The experimental arrangement used to verify the above theory is shown in Fig. 8. One side only of the 3-positions relay was used as an ideal relay. One coil is in the main circuit with input and output feeding at opposite ends. The second coil is used for zeroing. One time-constant in G is provided by the relay coils, the two others by the operational amplifiers. The low carrier frequency of 12·5 c/s was selected to make mechanical dynamic effects of the relay of negligible importance. This circuit was used for all the experimental measurements given in the paper.

Comparison of the calculated and experimental results for this circuit and three frequencies in the low-frequency region is given in Fig. 9. It shows clearly the good agreement in the linear region and the discrepancy in the saturation region. Despite this discrepancy, the analysis gives a good approximation of the practical linear range of the amplifier. This is

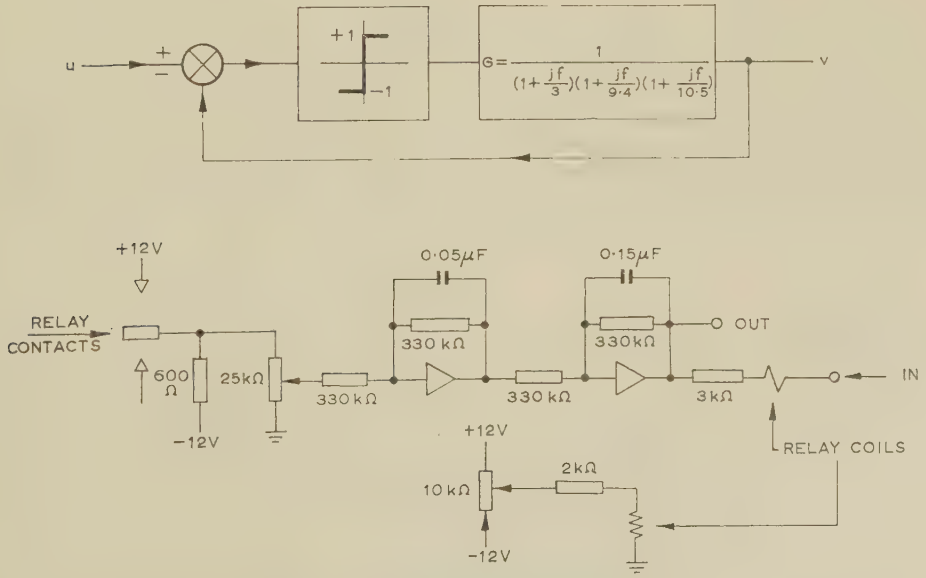

Fig. 8.—Experimental circuit.

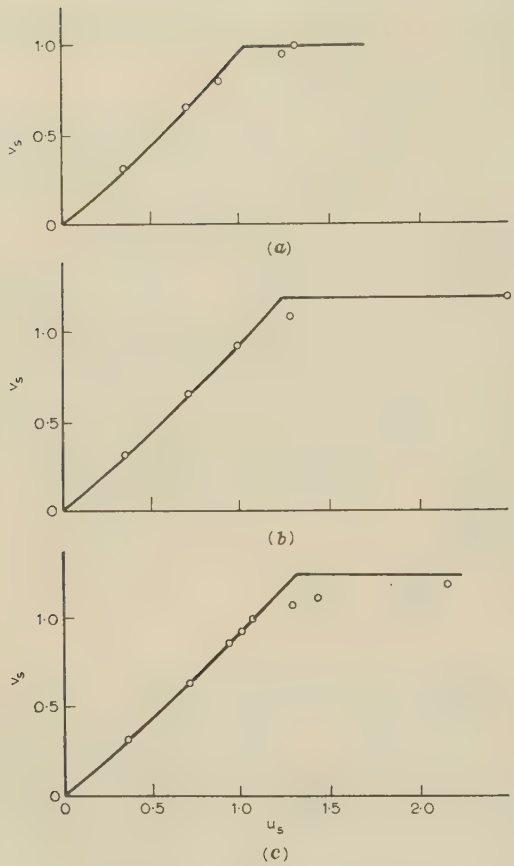

Fig. 9.—Frequency response.
(*a*) $f = 2$ c/s.
(*b*) $f = 1$ c/s.
(*c*) $f = 0{\cdot}5$ c/s.
—— Calculated.
○ Measured.

the range which is of interest in design, rather than the complete saturation range, which may be much bigger.

(3.3) Higher Frequencies

(3.3.1) General.

When we discuss the response of the relay amplifier at higher signal frequencies, two distinct problems arise. The first is the behaviour of the amplifier itself. The second is concerned with the problem of carrier filtering in the system to which the relay amplifier is connected. This, naturally, becomes more difficult as the ratio ω_s/ω_c increases, and implies that the ratio must be kept rather small. However, as it is desired to keep this discussion general and not tied to any particular system used with the relay amplifier, the frequency response of the amplifier its will be investigated at higher frequencies without regard to la filtering difficulties. These, of course, must be dealt with each system separately.

(3.3.2) Qualitative Response Picture.

Before embarking on detailed analysis it is advantageous have a qualitative picture of the phenomena. Suppose we ha a signal at frequency, ω_s, a little smaller than $\frac{1}{3}\omega_{c0}$. As t input signal, u_s, increases, the relay output will contain increasing component at the fifth-harmonic signal, $5\omega_s$, whi will interfere with the carrier. At a certain u_s synchronizati will take place and ω_c will become equal to $5\omega_s$. If ω_s is n reduced, a larger input will be required to effect synchronizatio This phenomenon is somewhat similar to ordinary synchroni tion of oscillators where $\omega_s \simeq \omega_c$. Here, however, there are ma possible fractional-order synchronous bands ($3\omega_s$, $5\omega_s$, . . . Even-order synchronization ($2\omega_s$, $4\omega_s$, . . .) may occur if t characteristic of the relay is not symmetrical.

A qualitative picture of the various synchronization bands given in Fig. 10. In the small-signal region, they become li

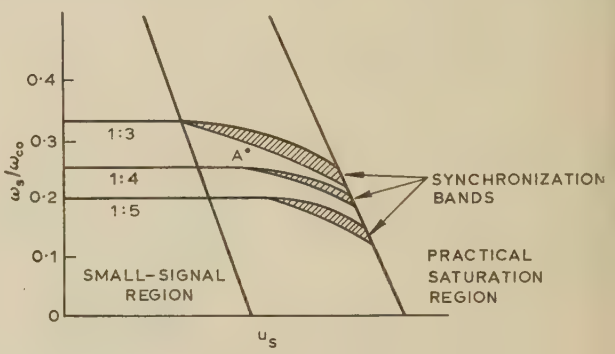

Fig. 10.—Qualitative overall-response diagram.

at ω_{c0}/n. There is little real synchronization here: there merely a coincidence of frequencies. At larger inputs app ciable synchronization occurs and the carrier frequency reduced. This synchronized carrier frequency may be mu lower than ω_c when the input is large. The experimental ti graphs of Fig. 11 show the transition between the various sy chronization modes for $f_s = 3$ c/s and a gradually increasi sinusoidal input signal.

The significance of these phenomena lies in the effect of sy chronization on relay gain, which may change abruptly, bo in magnitude and in phase. This may be seen by co paring the non-synchronous with the synchronous relay outp (Figs. 3, 4, 5 and 6). Therefore, $v_s = f(u_s)$ may also chan However, the situation is more disturbing in the almost s

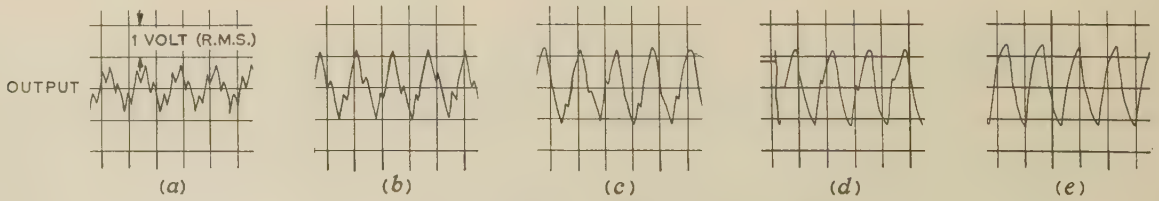

Fig. 11.—Transition between synchronization modes.
$f = 3$ c/s.
(*a*) Input, 0·5 volt (r.m.s.); IV → III
(*b*) Input, 0·95 volt (r.m.s.); III
(*c*) Input, 1·1 volts (r.m.s.); III → II
(*d*) Input, 1·2 volts (r.m.s.); II
(*e*) Input, 1·3 volts (r.m.s.); Complete saturation.

chronous case (Section 2.4). Suppose u_s now corresponds to point A (Fig. 10). It is just a little smaller than that required to synchronize. Consequently, $\omega_c = 3(\omega_s + \Delta\omega)$. Carrier and signal will not stay in step and the phase between them will vary continually. Hence relay gain will vary periodically at $3\Delta\omega$—a very low frequency—and at a constant u_s, v_s will not be constant but will vary with relay gain. It is these low-frequency almost-synchronous variations which impose the ultimate limit on high-frequency operation rather than synchronization itself.

It is quite difficult to calculate higher-order synchronous bands (Fig. 10) and variations around them. Fortunately, it is often sufficient to plot the line of onset of third-order synchronization and calculate output variations just below it, as variations connected with higher-order cases are much smaller. We shall deal only with the third-order case.

(3.3.3) Synchronization.

Eqns. (7) are used again, but now signal and carrier outputs, $y_s = y_s(k, \phi)$ and $y_c = y_c(k, \phi)$, are complex (Section 2.3). Graphical solution of the carrier equation now gives $\omega_c < \omega_{c0}$ and $\angle G(j\omega_c) > -180°$. The extra phase shift to sustain oscillations is supplied by y_c. With these values of k, ω_c and ϕ, we can proceed to solve the other equations as in Section 3.2, finally arriving at the signal input, u_s, required for synchronization. ω_s is, of course, equal to $\frac{1}{3}\omega_c$. Note that, as now $\omega_c < \omega_{c0}$, the signal error $b = ky_cG_c$ is usually larger.

The calculated and experimental curves where third-order synchronization starts for the same circuit as in Section 3.2.2 are compared in Fig. 12. The discrepancy between calculation and experiment increases as ω_s decreases. This is owing to the increasing importance of the term at $5\omega_s$. Indeed, as ω_s decreases, we pass gradually into the saturation region at low frequencies where an increasing number of distortion terms is involved.

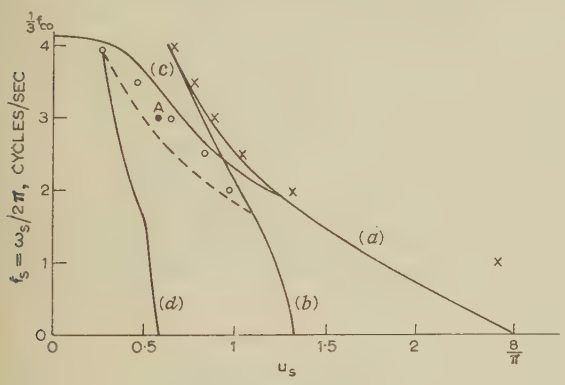

Fig. 12.—Overall-response diagram.

× Experimental results
(*a*) Synchronous case } Saturation.
(*b*) Non-synchronous case
(*c*) Synchronous case
○ Experimental results } Synchronization.
(*d*) Non-synchronous case, $k = 0{\cdot}75$.

(3.3.4) Almost Synchronous Variations.

If $\omega_s \neq \frac{1}{3}\omega_c$ but $\Delta\omega = \omega_s - \frac{1}{3}\omega_c$ is very small, we may still follow the same approach as in the synchronous case. As ϕ is not constant now, we must add to eqns. (7*a*) and (7*b*)—the signal and carrier equations—a third one, the synchronization equation:

$$\dot{\phi} = \Delta\omega = \omega_s - \tfrac{1}{3}\omega_c \quad . \quad . \quad . \quad . \quad (9)$$

A similar approach has been employed successfully for simple synchronization[14] ($\omega_s \simeq \omega_c$). The synchronization equation can be integrated step by step in conjunction with the other two equations to yield $y(t)$ explicitly. From $y(t)$, the time variation of all other variables may be found. Usually this is not necessary, as only the maximum amplitude variation of v_s for constant u_s is required. For this purpose only the signal and carrier equations have to be solved.

Before detailing the procedure it is necessary to examine the approximation involved in this approach. It is essentially in writing $v_s = y_s(k, \phi)G(j\omega_s)$ and $a = -y_c(k, \phi)G(j\omega_c)$ when ϕ is not constant. Referring to Section 2.4 and Fig. 7, it is seen that, when $\Delta\omega \neq 0$, $y(t)$ contains a spectrum of frequencies around ω_s and ω_c. The approximation is in assuming that this spectrum is sufficiently narrow so that G remains almost constant within it. This is justified when $\Delta\omega$ is very small.

The method of solution is essentially, as before, but as ϕ is not constant all variables are functions of both k and ϕ. Solving the signal equation we obtain $u_s(k, \phi)$, which can be plotted as function of ϕ with k as parameter. By superimposing a straight line corresponding to a constant input signal, u_s, on this graph, the relation $k(\phi)$ for this u_s is obtained. When this $k(\phi)$ locus is plotted on the $v_s(k, \phi)$ graphs, we arrive at the variation of v_s for the given constant u_s. If $v_s(t)$ is desired, the synchronization equation must be integrated.

As an example, the almost synchronous variations are calculated for point A of Fig. 12. This calculation is presented in Fig. 13. Fig. 13(*a*) shows $u_s(\phi)$ with k as parameter. The locus

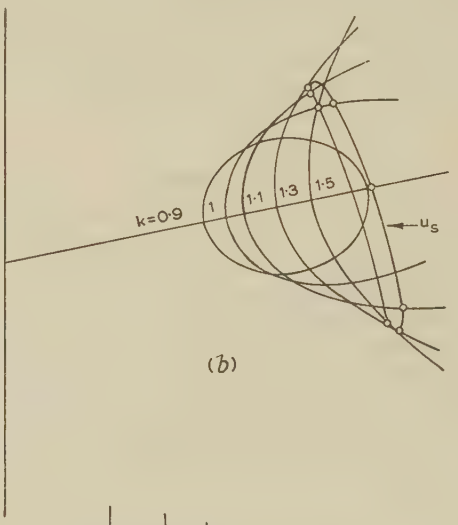

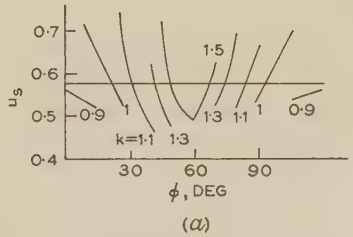

Fig. 13.—Almost synchronous variations.
$u_s = 0{\cdot}58$, $f_s = 3$ c/s.

of v_s for $u_s = 0{\cdot}58$ is given in Fig. 13(*b*). From this locus the maximum variation of the output is found to be 13% of the input. Experiment yields 15%.

(3.4) Complete Saturation and the 'Jump' Phenomenon

The synchronous case can also be used for calculating approximately the line of complete saturation. (Relay output a square wave at ω_s). The relevant loci for this calculation in Figs. 4

and 5 are those formed by circular arcs. This procedure improves the result given by the non-synchronous case (Section 3.2) because it takes into account the term at $3\omega_s$. A comparison of these results with experiment for our circuit (Fig. 8) is also shown in Fig. 12: (*b*) pertains to the non-synchronous case and (*a*) to the synchronous case. At very low frequencies, where higher terms, $5\omega_s$, . . ., are important, the experimental results (marked X) show that complete saturation occurs at a much larger input than that given by the synchronous case. It may be calculated exactly by a formula given by Zypkin,[6] which takes into account all harmonics:

$$u_s = \frac{4}{\pi}\left|\sum_{m=1}^{\infty} \mathrm{U}[(2m-1)\omega_s] + j\frac{\mathrm{V}[(2m-1)\omega_s]}{2m-1}\right| \quad . \quad (10)$$

It is necessary to stress again that this complete saturation is of limited interest and that, for assessing the practical range, curve (*b*) of Fig. 12, which is calculated by the non-synchronous case, is preferable.

There is a case where complete saturation is important. This is when the amplifier saturates at input signals well within the linear range, thus curtailing the effective range. It is known as the 'jump' phenomenon. Lozier,[15] taking into account the fundamental component only (at ω_s), has shown that a 'jump' may occur whenever $\angle \mathrm{G}(j\omega_s) < -90°$, i.e. $\mathrm{G}(j\omega_s)$ lies in the third quadrant. When we apply the synchronous describing functions, it is seen that some excursion into the third quadrant is possible, owing to the signal phase advance upon synchronization (Figs. 4 and 5). This problem, which will be discussed elsewhere, will not be dealt with here any more, as usually the signal frequencies in the relay amplifier lie well within the fourth quadrant for other reasons (Section 4).

(3.5) Summary

A picture of overall behaviour is obtained from the diagram of ω_s versus u_s (Fig. 12). To the left of curve (*d*), calculated for $k = 0{\cdot}75$ (non-synchronous case), the response is quite linear and distortion is negligible. Curve (*b*), calculated for $k = \infty$ (non-synchronous case), gives the practical range of the amplifier, and at higher frequencies it merges with the synchronous-case saturation curve (*a*). Curve (*c*) gives approximately the onset of third-order synchronization. The almost synchronous variations below it may be calculated as in Section 3.3.4. The magnitude of allowed variation will fix the limit of operation in this region. Such a limit may be like the broken line in the diagram.

(4) DESIGN CONSIDERATIONS

It is appropriate to conclude with a discussion of the influence of the shape of the linear transfer function, *G*, on amplifier performance in the various regions. For small inputs the forward gain of the amplifier is, from eqns. (4) and (8),

$$\frac{v_s}{b} = \frac{\mathrm{G}(j\omega_s)y_s(k)}{G_c k y_c(k)} \xrightarrow[k\to 0]{} \frac{\mathrm{G}(j\omega_s)}{2G_c} \quad . \quad . \quad . \quad (11)$$

Error is minimized by reducing G_c as far as possible.

As $\angle \mathrm{G}(j\omega) > -180°$ for $\omega < \omega_c$, the maximum slope which may be used for reducing *G* from $|\mathrm{G}(j\omega_s)| \simeq 1$ to $G_c \angle -180°$ is limited. (The limit is slightly over -40 dB/deg and its exact value depends on ω_c). Thus a requirement for a higher open-loop gain, i.e. small G_c, calls for a higher ω_c. This is similar to the linear feedback amplifier where a higher open-loop gain leads to higher crossover frequency.[16]

However, the design of *G* in the transition band from ω_{smax} to ω_c is also affected by the consideration of the influence of synchronous effects within the signal band ($\omega_s < \omega_{smax}$) wh the input is large. From Fig. 5(*b*) it is seen that these effects a negligible when $\angle \mathrm{G}(j3\omega_s) \geqslant -105°$ (the angle of the tip of t locus for $k = 2$). Hence, by fixing $\angle \mathrm{G}(j\omega) \geqslant -105°$ f $\omega \leqslant 3\omega_{smax}$, synchronous effects can be eliminated inside t signal band. The design requirements are summarized in Fig. 1

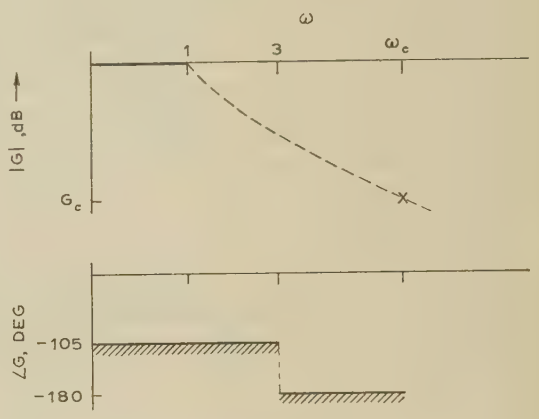

Fig. 14.—Restrictions on *G*.
$\omega_{s\,max} = 1$

The attenuation characteristic for $\omega_s > \omega_{smax}$ should be desig to minimize G_c without violating the phase barriers.

On the other hand, we may attempt to operate at hig frequencies, despite the almost synchronous variations whi disturb the operation, by minimizing their influence with hi forward gain. However, the gain in the synchronous case is

$$\frac{v_s}{b} = \frac{\mathrm{G}(j\omega_s)y_s(k,\phi)}{|\mathrm{G}(3j\omega_s)|ky_c(k,\phi)} < \frac{3\mathrm{G}(j\omega_s)}{k|\mathrm{G}(3j\omega_s)|} \quad . \quad . \quad (1$$

where, usually, $1 < k < 2$. It is rather difficult to design so that the gain will be sufficiently high to reduce the almo synchronous variations to a tolerable value. It therefore appea that operation at higher frequencies, if at all feasible, is limit to the small-signal region.

(5) CONCLUSIONS

The analysis and experiments described in the paper sh that the feedback relay amplifier is similar to a saturating lin amplifier when the input signal frequency is low. As this f quency is increased, operation is disturbed by interaction betwe signal and carrier frequencies, mainly in the form of alm synchronous variations, which put an upper limit on sig frequencies. Restrictions must be placed on *G* to elimin synchronous effects within the signal band.

(6) ACKNOWLEDGMENTS

The author is indebted to Dr. A. T. Fuller for many help discussions during the preparation of the paper; to the Dep ment of Engineering, University of Cambridge, for the use its facilities; and to the Israel Ministry of Defence for provid a grant supporting this work.

(7) REFERENCES

(1) McDonald, D.: 'Nonlinear Techniques for Improv Servo Performance', *Proceedings of the National E tronic Conference*, 1950, **6**, p. 400.

(2) BULAND, R. N., and FURUMOTO, N.: 'Dual Mode Relay Servos', *Transactions of the American I.E.E.*, 1959, **78**, Part II, p. 405.

(3) MACCOLL, L. A.: 'Fundamental Theory of Servomechanisms' (Van Nostrand, 1945, p. 78).

(4) LOZIER, J. C.: 'Carrier-Controlled Relay Servos', *Electrical Engineering*, 1950, **69**, p. 1052.

(5) GIBSON, J. E., and TUTEUR, F. B.: 'The Response of Relay Amplifiers with Feedback', *Transactions of the American I.E.E.*, 1957, **76**, Part II, p. 303.

(6) ZYPKIN, J. S.: 'Theorie des Relaissysteme der Automatischen Regelung' (Oldenburger, Munich, 1958), Chapters 7–11.

(7) SMITH, O. J. M.: 'Feedback Control Systems' (McGraw-Hill, 1958), Chapter 11.

(8) KRUTOVA, I. N.: 'The Behaviour of a Vibration Servo in an Electrical Autopilot', *Automation and Remote Control*, 1959, **20**, p. 113.

(9) KRUTOVA, I. N.: 'The Dynamics of a Vibration Servo in an Electrical Servo During Free Oscillations', *ibid.*, 1959, **20**, p. 409.

(10) SHANNON, C. E.: 'Communication in the Presence of Noise', *Proceedings of the Institute of Radio Engineers*, 1949, **37**, p. 10.

(11) WEST, J. C., DOUCE, J. L., and LIVESLEY, R. K.: 'The Dual-Input Describing Function and its use in the Analysis of Non-Linear Feedback Systems', *Proceedings I.E.E.*, Paper No. 1877 M, July, 1955 (**103** B, p. 463).

(12) BENNETT, W. R., and KALB, R. M.: 'Ferromagnetic Distortion of a Two-Frequency Wave', *Bell System Technical Journal*, 1935, **14**, p. 335.

(13) JAHNKE, R., and EMDE, F.: 'Tables of Functions' (Dover Publications, 1945).

(14) HUNTOON, R. D., and WEISS, A.: 'Synchronization of Oscillators', *Proceedings of the Institute of Radio Engineers*, 1947, **35**, p. 1415.

(15) LOZIER, J. C.: 'Steady State Approach to Saturable Servomechanisms', *Transactions of the Institute of Radio Engineers*, May, 1956, **PGAC-1**, p. 19.

(16) BODE, H. W.: 'Network Analysis and Feedback Amplifiers Design' (Van Nostrand, 1945), Chapter 18.

621.372.6

The Institution of Electrical Engineers
Monograph No. 424 E
Dec. 1960

SIGN MATRICES AND REALIZABILITY OF CONDUCTANCE MATRICES

By Professor G. BIORCI.

(*The paper was first received 5th July, and in revised form 17th September*, 1960. *It was published as an* INSTITUTION MONOGRAPH *in December*, 1960.)

SUMMARY

Given a conductance matrix G of order n, the problem of realizing it by a network with $n + 1$ nodes can be split in two parts: to find the tree of the ports corresponding to the given matrix G; and to determine the actual resistances of the branches of the network.

A procedure to solve the first (topological) problem is proposed, which is simply concerned with the signs of the elements of the given matrix G. The successful development of the procedure can be considered as a necessary and sufficient condition for the existence of a tree corresponding to G.

(1) INTRODUCTION

In order to describe the behaviour of a given resistive network with $n + 1$ nodes one has to choose n independent voltages across pairs of nodes of the network. Such pairs of nodes are called 'ports' of the network. The set of branches of the network connected to the ports is an open graph (since it cannot include loops) called the 'tree' of the ports.

Obviously, for a given network one can draw many trees of the ports (one for each choice of n pairs of nodes making no loops), but, once a tree has been selected, the relationship between the currents and voltages of the ports is determined uniquely, namely

$$I = GV \quad . \quad . \quad . \quad . \quad . \quad . \quad . \quad (1)$$

where I and V are column matrices of the port currents and voltages, and G is a square matrix of order n.

It follows that the matrix G is determined by the choice of the ports and by the resistances of the branches of the network.

If G is given, the problem is to find the network of $n + 1$ nodes which is consistent with G, i.e. to draw a tree of the ports on $n + 1$ nodes; to determine which branches comprise the network; and to find the values of the branch resistances, in such a way that eqn. (1) holds.

This realizability problem is being widely discussed,[1] since it is recognized as an important step in the problem of the synthesis of multi-terminal systems.

Cederbaum[2] was the first to give a realizability criterion, leading from the conductance matrix to the corresponding cut-set matrix. The procedure suggested by him, however, leaves open the problem of realizing a cut-set matrix—a problem which has been solved in various ways by Guillemin,[3] Gould,[4] Löfgren[5] and others.

A direct approach to the realizability problem has recently been proposed by Guillemin[6] and, independently, by Biorci and Civalleri.[7] These authors have proved that the tree of the ports depends solely on the distribution of signs in the conductance matrix and not upon the numerical values of its elements.

In this paper we wish to show that the method proposed by Biorci and Civalleri[7] can be greatly modified and simplified, by making use of some simple development of the theory of the signs in a conductance matrix.

Correspondence on Monographs is invited for consideration with a view to publication.

Professor Biorci is at the Istituto Elettrotecnico Nazionale Galileo Ferraris, Torino, Italy.

(2) DEFINITIONS AND FUNDAMENTAL THEOREMS

First, we resume some definitions and properties previously given in a somewhat different form.[7]

(*a*) Given a tree of the ports, the 'tree path' $[i, j]$ is that path of the tree which joins i and j. The orientation of $[i, j]$ is the same as that of port i.

(*b*) The following property can be considered intuitively; if and only if, G_{ij} is positive (negative) the orientation of the port j is the same as (opposite to) that of the tree path $[i, j]$.

(*c*) From (*b*) it follows that, if the orientation of port i is changed, so also are those of the tree paths $[i, j]$ $(j = 1, 2 \ldots n)$, and hence all the off-diagonal elements of the ith row and column of G change sign.

Conversely, if the signs of all the off-diagonal elements of the ith row and column of G are changed, the orientation of the port i will change.

Guillemin[6] has stressed the importance of reducing the given conductance matrix G to its standard form, G', in which all the elements of the first row and column are positive. For any G, the corresponding G' can be obtained very rapidly. In fact, if the first row of G has some negative elements G_{1r}, G_{1s}, . . . G_{1t}, one simply has to change the signs of all elements of the rth, sth, . . . tth rows and columns in sequence. From (*c*) this operation changes the orientation of ports r, s, . . . t. Once this is done, each port k is oriented as the corresponding tree path $[l, k]$ [point (*b*)], as shown in Fig. 1.

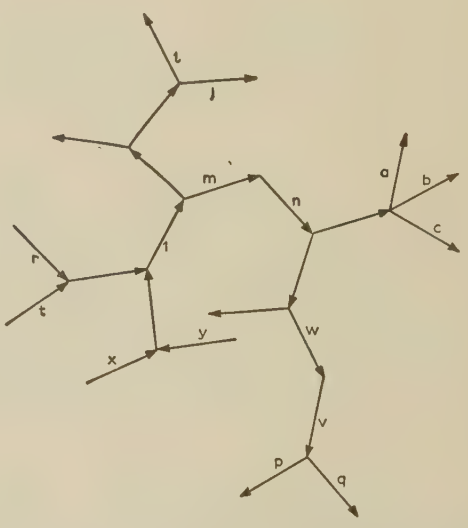

Fig. 1.—Tree with orientation chosen so that G_{1k} is positive for all k.

L sets of tree; (m, n) and (w, v).
V sets of tree; (a, b, c), (i, j), (r, t), (p, q), (x, y).

In the following, we shall neglect all degenerate cases, i.e. we shall assume that no G_{ij} is zero, and that port 1 is not a tip of the tree, i.e. both nodes of port 1 are connected to some other ports. The latter assumption will be removed in a following Section.

In the tree, or sub-trees, of the ports, we call L a set of two (or more) ports which form a linear graph, and V a set of two (or more) ports which form a star of tips (Fig. 1).

If the conductance matrix is reduced to its standard form, G', since each port i, as explained above, has the same orientation as the tree path $[1, i]$ and 1 is not a tip of the tree, the ports of each L set of the tree have like orientation, and the orientations of the ports of each V set are all divergent or all convergent (Fig. 1).

Therefore, taking into account property (b), we can state the following theorem, valid for conductance matrices in standard form G':

Theorem 1.—The ports of each L set of the tree have positive mutual conductances, whereas those of the ports of each V set of the tree are negative (we have excluded the case of the port 1 being a tip of the tree).

(3) THE SIGN MATRIX

Since we are interested in the properties which depend only upon the signs of the elements of G', we introduce[6] the 'sign matrix' corresponding to the given conductance matrix (in standard form) as a matrix S in which the site (i, j) is occupied by a plus if G'_{ij} is positive, a minus otherwise.

Denoting the plus or minus at the site (i, j) by s_{ij}, we say that $s_{ij} = s_{pq}$ if both sites (i, j) and (p, q) are occupied by the same sign, and that $s_{ij} = -s_{pq}$ if those sites are occupied by opposite signs.

We can now prove the following theorem:

Theorem 2.—If, and only if, two ports i and j belong to an L set, $s_{ik} = s_{jk}$ for all k.

In fact, since the conductance matrix is in standard form, it follows from Theorem 1 and property (b) that ports i and j have like orientations, and since they belong to an L set, the orientation of the tree path $[i, k]$ is the same as that of the tree path $[j, k]$ for all k [Fig. 2(a)]. Instead, if the two ports i and

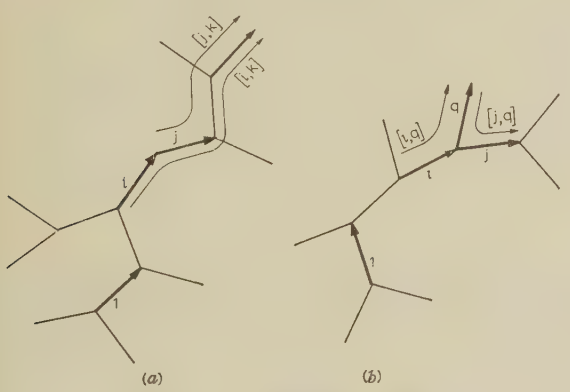

Fig. 2.—Conditions for L sets.

(a) Ports i and j belong to an L set, and thus orientations of the tree paths $[i, k]$ and $[j, k]$ are the same.
(b) Ports i and j do not belong to an L set, and thus there is at least one port q for which $s_{iq} = -s_{jq}$.

j do not belong to an L set, there is at least one port q such that the tree paths $[i, q]$ and $[j, q]$ have opposite orientation, and hence $s_{iq} = -s_{jq}$ [Fig. 2(b)].

Now we define a new sign matrix S' as that whose terms s' are given by

$$\left.\begin{aligned} s'_{ij} &= s_{ij} \quad \text{for } i \neq j \\ s'_{ii} &= -s_{ii} \end{aligned}\right\} \quad . \quad . \quad . \quad . \quad . \quad (2)$$

Then the following theorem can be proved.

Theorem 3.—If, and only if, two ports i and j belong to a V set, $s'_{ik} = s'_{jk}$ for all k.

In fact, since the conductance matrix is in standard form and port 1 is not a tip of the tree, if ports i and j belong to a V set, their orientations are both convergent or divergent (Fig. 3).

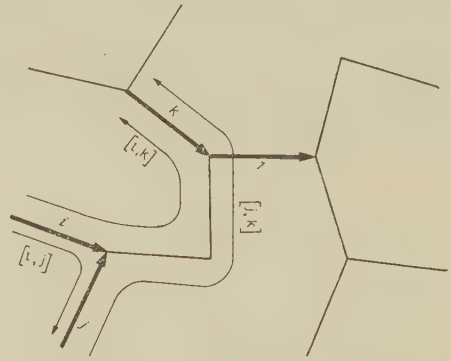

Fig. 3.—If two ports i and j belong to a V set $s'_{ik} = s'_{jk}$ but s'_{ij} is a minus.

Therefore, tree paths $[i, k]$ and $[j, k]$ have like orientations for all values of k except i and j, whereas port j has orientation opposite to tree path $[i, j]$. So $s'_{ik} = s'_{jk}$ for all values of k except i and j, whereas s'_{ij} is a minus, as well as s'_{ii} and s'_{jj}.

Conversely, if the ports i and j do not belong to a V set—this can happen because at least one of them is not a tip of the tree [Fig. 4(a)] or because, being both tips of the tree, there is

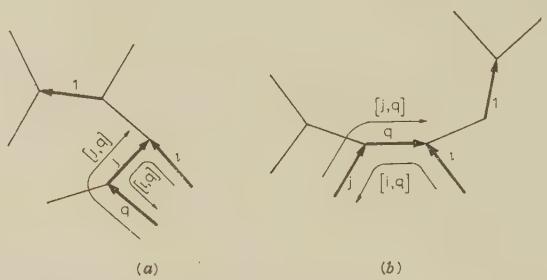

Fig. 4.—If two ports i and j do not belong to a V set (or to an L set) there is at least one port q for which $s'_{iq} = -s'_{jq}$.

at least one port between them [Fig. 4(b)]—there is at least one port q for which $s'_{iq} = -s'_{jq}$. The port q is indicated in Figs. 4(a) and (b), and its orientation has no importance in this respect.

(4) TREE OF THE PORTS

By making use of the preceding theorems, the procedure to find the tree of the ports becomes very simple.

(a) Given a conductance matrix G, the first step in the synthesis is to reduce it to standard form G', and to write down the sign matrices S and S'. Actually, only one sign matrix need be written, putting in the main diagonal double signs, the plus holding for S and the minus for S'. However, in the following, for the ease of the reader, we shall refer to S and S' as two distinct matrices.

(b) The second step is to examine S for equal rows. Each group of equal rows makes an L set of the tree. The order of the ports of each L set cannot be deduced from the sign matrix, but from G. We do not discuss this point here,[6, 7] since it is not immediately relevant.

Once the L sets are found, we can cancel, for each L, the

rows (and columns) of S and S' corresponding to all the ports of that L set but one (arbitrarily chosen). Physically, this means that we short-circuit, for each L set, all ports but one. Provided that note is taken of which ports are short-circuited, the building of the tree can proceed.

(*c*) At this point we examine S' for groups of equal rows. Each group (Theorem 3) is a V set of the tree. We take note of the V sets, and again cancel the rows (and columns) of S and S' corresponding, in each V, to all ports but one. This operation makes new L sets. In fact, for each V, the uncancelled port remains 'in series' with one (and only one) port of the tree (Fig. 5).

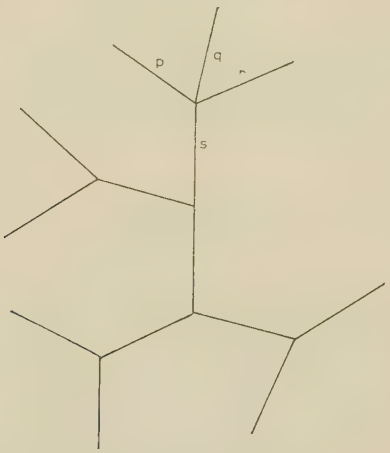

Fig. 5.—If ports p and q are short-circuited, ports r and s make an L set.

(*d*) Let us suppose that the uncancelled ports of the V sets are $m, n, \ldots s$. We examine S and find the rows equal to rows m, n, etc. Let $a, b, \ldots f$ be such rows. We know that a makes an L set with m (once the other ports of the V sets are cancelled) and so on. Therefore we can attach the ports $a, b, \ldots f$ to the V sets in their proper position.

Once this is done, we can cancel the rows (and columns) $m, n, \ldots s$ of S and S'.

(*e*) We now go back to the matrix S' and look for rows equal to rows $a, b, \ldots f$. In this case we may find none [Fig. 6(*a*)],

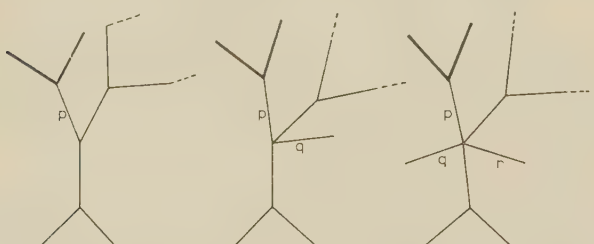

Fig. 6.—Tree with heavily drawn ports short-circuited.
(*a*) Port p makes a V set with no other port.
(*b*) Port p makes a V set with port q.
(*c*) Port p makes a V set with ports q and r.

one [Fig. 6(*b*)] or several [Fig. 6(*c*)] rows equal to a given row. These rows make V sets with $a, b, \ldots f$.

(*f*) The procedure ends when all ports have found their place in the tree.

(5) EXAMPLE

In this Section we shall develop the same example treated previously,[7] in order to show the speed with which the present procedure can be used.

Table 1

SIGNS OF THE OFF-DIAGONAL ELEMENTS OF A GIVEN CONDUCTANCE MATRIX G

	1	2	3	4	5	6	7	8	9	10	11	12	13	14	15
1		−	−	−	−	+	−	+	+	−	−	−	+	+	−
2			+	+	+	+	+	−	−	−	+	+	−	−	+
3				−	−	−	+	−	−	+	+	+	+	−	−
4					+	−	+	−	−	+	−	+	+	−	−
5						−	+	−	−	+	−	+	−	−	−
6							+	−	+	+	−	+	+	−	−
7								+	−	−	+	−	−	−	+
8									+	+	−	+	+	+	−
9										+	−	−	+	+	−
10											+	−	−	+	+
11												+	+	−	+
12													−	+	+
13														+	+
14															−
15															

Table 1 shows the signs of the off-diagonal elements of given conductance matrix G. If we make positive the signs the first row and column by the procedure suggested in Section we obtain the sign matrices S and S' shown in Table 2. T diagonal elements are all plus in S, and all minus in S', where the off-diagonal elements are the same in both matrices.

Now we look for equal rows in S (upper signs in the diagon elements) in order to find the L sets of the tree [Section 4(*b*

Table 2

MATRICES S AND S'

		1	*e* 2	*b* 3	*b* 4	*d* 5	*f* 6	*b* 7	*a* 8	*f* 9	10	*c* 11	*d* 12	*a* 13	*c* 14	*a* 15
	1	±	+	+	+	+	+	+	+	+	+	+	+	+	+	+
e	2	+	±	+	+	+	−	+	+	+	−	+	+	+	+	+
b	3	+	+	±	−	−	+	+	+	+	+	+	+	−	+	−
b	4	+	+	−	±	+	+	+	+	+	+	−	+	−	+	−
d	5	+	+	−	+	±	+	+	+	+	+	−	+	+	+	−
f	6	+	−	+	+	+	±	−	−	+	−	+	−	+	−	+
b	7	+	+	+	+	+	−	±	−	+	−	+	−	+	+	+
a	8	+	+	+	+	+	−	−	±	+	−	+	−	+	+	+
f	9	+	+	+	+	+	+	+	+	±	−	+	+	+	+	+
	10	+	−	+	+	+	−	−	−	−	±	+	−	+	−	+
c	11	+	+	+	−	−	+	+	+	+	+	±	+	−	+	+
d	12	+	+	+	+	+	−	−	−	+	−	+	±	+	−	+
a	13	+	+	−	−	+	+	+	+	+	+	−	+	±	+	−
c	14	+	+	+	+	+	−	+	+	+	−	+	−	+	±	+
a	15	+	+	−	−	−	+	+	+	+	+	+	+	−	+	±

In the diagonal elements, the upper signs refer to S and the lower to S'.

No such rows are found, and hence the tree has no L set Then we look for equal rows of S' (lower signs in the diagon elements) in order to find the V sets of the tree [Section 4(*c*) We find that

$$s'_{3k} = s'_{15k} \quad s'_{4k} = s'_{13k} \quad s'_{7k} = s'_{8k}$$

for all k. Hence the V sets are those indicated in Fig. 7(*a* Now we cancel the rows and columns 15, 13, 8 and examine to find the rows equal to the 3rd, 4th and 7th [Section 4(*d*)].

These are rows 11, 5 and 14, respectively. The correspondi ports make L sets with the not-short-circuited ports, i.e. wit ports 3, 4 and 7, respectively [Fig. 7(*b*)].

We now cancel the rows and columns 3, 4 and 7 and look S' in order to find the rows equal to the 11th, 5th and 14t We find that rows 5 and 11 are equal, and that row 12 is equa to the 14th. Thus the situation is that shown in Fig. 7(*c*).

The procedure is now clear. The order in which the row and columns are cancelled is indicated in Table 2 by the letter $a, b, c, \ldots$ and those ports which have been successively short circuited are shown in Fig. 7.

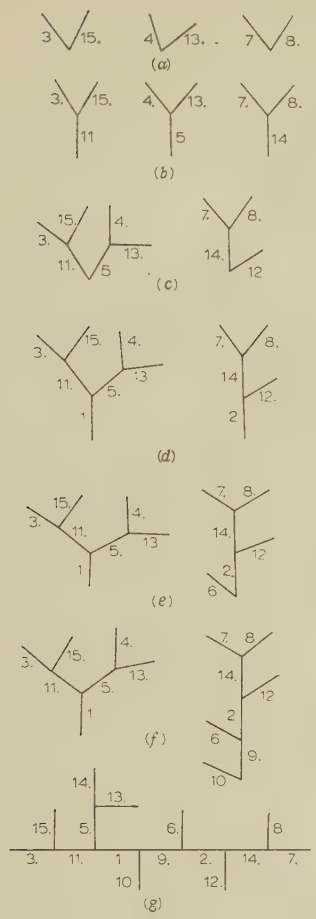

Fig. 7.—Successive steps in growing the tree.
● Short-circuited ports.

Once the tree has been found the orientation of port 1 can be chosen arbitrarily, and the orientations of the other ports can be determined easily by making use of property (*b*), Section 2, applied to the first row of the conductance matrix G (if one wants to have the original orientations) or to the first row of G' (if one prefers to have the orientations corresponding to the standard form of the conductance matrix).

(6) FINAL REMARKS

First, the procedure indicated is straightforward, and therefore any inconsistency found at any step of the development means that the given conductance matrix G is not realizable, at least with a network with only $n + 1$ nodes.

Secondly, to proceed with the synthesis once the tree of the ports is found, one can, for instance, introduce very simply a new set of independent voltages (e.g. a set of node-to-datum voltages) for which the synthesis is well known. The problem is widely treated by Guillemin[6] and mentioned also by Biorci and Civalleri.[7]

Finally, we have to remove the assumption, made in the preceding Sections, that port 1 is not a tip of the tree. This case (Fig. 8) is very simple: the procedure is fully valid and the various steps of the synthesis can be performed without special care. The only difference is that the V set to which port 1 belongs does not show up at step (*c*), Section 4, as the other V sets do, but only at the end of the procedure. In fact, if the port 1, in its V set, is divergent, the other ports of the same V set are convergent, and vice versa (Fig. 8).

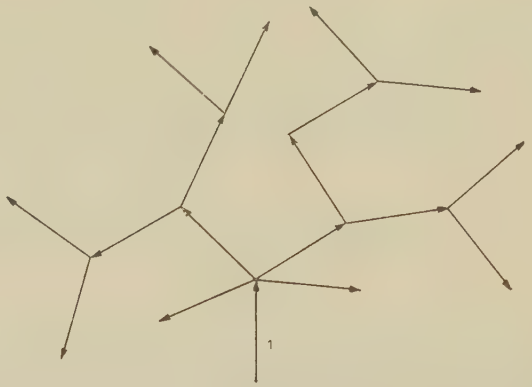

Fig. 8.—A tree in which the port 1 is a tip.

(7) CONCLUSION

A rapid procedure has been given for determining the tree of the ports from the signs of the elements of a given conductance matrix G. The procedure is valid for the realization of a conductance matrix G of order n with a fully resistive network having only $n + 1$ nodes.

The first step of the procedure is to reduce the matrix G to its standard form, G', in which all the elements of the first row are positive. The physical meaning of the transformation from G to G' is a proper reorientation of the ports of the tree.

The tree is built, step by step, by examining the signs of the elements of G' to find simple relationships between them, e.g. equal signs in two rows.

Since the proposed procedure is straightforward, the possibility of applying it successfully to a given conductance matrix G can be considered as the necessary and sufficient condition for G to have a corresponding tree of the ports.

(8) ACKNOWLEDGMENT

The author wishes to thank Dr. P. P. Civalleri for helpful discussions, and Prof. R. Sartori, Director of the Institute, for his kind suggestions and encouragement.

(9) REFERENCES

(1) WEINBERG, L.: 'Report on Circuit Theory', submitted to the XIIIth Triennial General Assembly of U.R.S.I., London, September, 1960.

(2) CEDERBAUM, I.: 'Application of Matrix Algebra to Network Theory', *Transactions of the Institute of Radio Engineers*, 1959, **CT–6**, Special Supplement, p. 127.

(3) GUILLEMIN, E. A.: 'How to Grow Your Own Trees from Given Cut-Set or Tie-Set Matrices', *ibid.*, 1959, **CT–6**, Special Supplement, p. 110.

(4) GOULD, R.: 'Graphs and Vector Spaces', *Journal of Mathematics and Physics*, 1958, **37**, p. 193.

(5) LÖFGREN, L.: 'On the Realizability Problem for Irredundant Boolean Networks', *Nuovo Cimento*, 1959, **13**, Supplement, p. 1400.

(6) GUILLEMIN, E. A.: 'On the Analysis and Synthesis of Single Element Kind Networks', M.I.T. Quarterly Progress Report, Research Laboratory of Electronics, 1960, No. 56, p. 213.

(7) BIORCI, G., and CIVALLERI, P. P.: 'On the Synthesis of Resistive N-Port Networks', *Transactions of the Institute of Radio Engineers* (to be published).

621.372.6

The Institution of Electrical Engine
Monograph No. 425
Jan. 19

TRAVELLING-WAVE ANALYSIS OF GENERALIZED NETWORKS

By J. ZAWELS, Ph.D., Associate Member.

(*The paper was first received 22nd March, and in revised form 8th August*, 1960. *It was published as an* INSTITUTION MONOGRAPH *in January*, 1961.)

SUMMARY

The behaviour of networks, whether lumped, distributed, active or passive, is analysed from a fundamental travelling-wave point of view. Generalized wave parameters are derived for a 2-port network from which image, conjugate and iterative parameters follow as special cases. The relationship of these to short- and open-circuit parameters are also given.

A matrix organization of waves in a multi-port network is next presented, which distinguishes between waves internal and external to the network. Through special transformations, voltage- and power-gain matrices are derived and their relationship to the conventional scattering matrix is shown.

Finally, a visual representation of the wave trains set up in cascaded stages is given in the form of wave flow diagrams, reminiscent of Mason's feedback graphs.

(1) INTRODUCTION

Before the present development of modern lumped network theory, workers were strongly influenced by the travelling-wave treatment of the propagation of electromagnetic energy in continuous media and distributed networks, and have endeavoured to carry over various travelling-wave concepts into lumped network studies. However, these analyses invariably apply only to special cases and the writers warn against carrying the analogy any further. For example, Shea,[1] Guillemin[2, 3], and Terman,[4] treat a series of 2-port networks in cascade, using wave terminology such as reflection coefficient, propagation coefficient, image and iterative matching, etc. Also, the treatment is restricted to passive networks. This paper makes no such reservations and throughout employs a travelling-wave point of view.

Present-day writers on network synthesis, in dealing with multi-port lumped networks, prefer the short-circuit and open-circuit parameter specification, z, y, h, g, a and b, which are formally devoid of any travelling-wave notions. The only major modern development in the travelling-wave approach appears to be the scattering matrix,[5] which has its origin in nuclear physics[6] and in its circuit application is specifically concerned with resistive terminations. Also, the wave amplitudes have dimensions of (volt-ampere)$^{1/2}$ instead of the more familiar volts or amperes.

It is worth while noting some of the merits and demerits of the use of the travelling-wave approach and the specification of a general network by image parameters, as compared with the open- and/or short-circuit description. Amongst the advantages of short- and open-circuit parameters is the fact that, particularly at low frequencies, it is comparatively easy to open- or short-circuit a pair of terminals and conduct a particular set of measurements accordingly. For example, in transistors the measurement of h-parameters has been widely adopted owing to the fact that they often have comparatively low input and high output impedances and so an open-circuit at the input and a short-circuit at the output terminals is easi achieved at low and medium frequencies. In contrast, it is mo difficult to measure the image parameters directly, whatever th frequency. With new transistors, however, operating in th v.h.f. and u.h.f. ranges, a good open- or short-circuit is not easily achieved[7] by virtue of stray capacitance and lead indu tance, and termination on a known finite impedance becom more practical. Indeed, the insertion of some impedance at th output when the current gain is measured is essential at a frequencies. Using these finite impedances and the resulta readings, a set of parameters must then be calculated, and th is as easily done for z, y or h as for image parameters.

Amongst the advantages of image parameters, on the oth hand, is that a circuit designer probably gets more usef information about the amplification capabilities of the devic from an inspection of the image than of, say, the h-parameter since practical loads are closer to the value of an image matche impedance than to a short-circuit when good power gain is requirement. Furthermore, once the image parameters a available, whether measured directly or calculated from th other parameters,* the algebraic expressions used in desig calculations such as input impedance, etc., are believed to b simpler. At ultra-high frequencies, where components such a coaxial cables are specified on an image parameter basis, imag specification of the other components would be an adde advantage.

The paper first deals with a perfectly general linear networ which may contain lumped and/or distributed elements an which, in addition, may be either active or passive, from fundamental travelling-wave point of view, by considering wav trains inside the network. An analogy is drawn from electro magnetic wave travel in anisotropic media, which, in practice occurs with wave propagation in the ionosphere in the presenc of the earth's magnetic field, and in some modern microwav devices such as circulators, gyrators and isolators.[8]

The paper next shows how the short- and open-circuit para meters may be obtained from general wave parameters b inspection, and gives Tables of the relationships between them Indeed, other design quantities such as voltage gain, inpu impedance, etc., may also be obtained by inspection, since eac term in the expressions represents a wave at a particular poin travelling in a particular direction. From these Tables it i clear that computation of image parameters from z, y, h, etc or vice versa, involves no more labour than conversion from say, h to y, which is most desirable if parallel (or y) feedback i applied to a device that has been specified in h-parameters.[9] I is believed that these Tables† will also be found useful in 4-pol synthesis or filter design, where the pole-zero approach an short- and open-circuit parameters have in some instances, bu by no means all, ousted filter design based on image parameter or reflection coefficients,[10] by permitting the design to be see from both points of view.

Correspondence on Monographs is invited for consideration with a view to publication.

Dr. Zawels is with the South African Iron and Steel Industrial Corporation, Ltd., Pretoria.

* The practical determination of image parameters for transistors from both th equivalent circuit and experimental data is given in References 11 and 12.

† A complete Table involving the conversion of z, y, h, g, a, b, image an unnormalized scattering parameters which involve termination with an arbitrar finite impedance is given in Reference 12.

The use of image parameters leads naturally to a circle diagram, of which the well-known Smith chart used in microwave calculations is a special case.[11] The use of this chart for the determination of various design quantities, including stability and power gain of 4-terminal networks, is treated elsewhere.[12] Thus, even if a device is specified in other than image parameters, it is believed worth while to convert it first to image parameters so as to make use of the computational advantage offered by these charts.

Finally, two powerful tools in modern network theory are considered as they apply to travelling waves. The first involves matrix methods, the results of which are related to the scattering matrix. The second is related to flow graphs,[13] where the treatment is empirical and a more systematic approach must still be developed.

(2) TRAVELLING WAVES IN A 4-TERMINAL NETWORK

Let a voltage wave V_{f1} be injected slightly to the right of point 1 in the 4-terminal network shown in Fig. 1(*a*). The network may

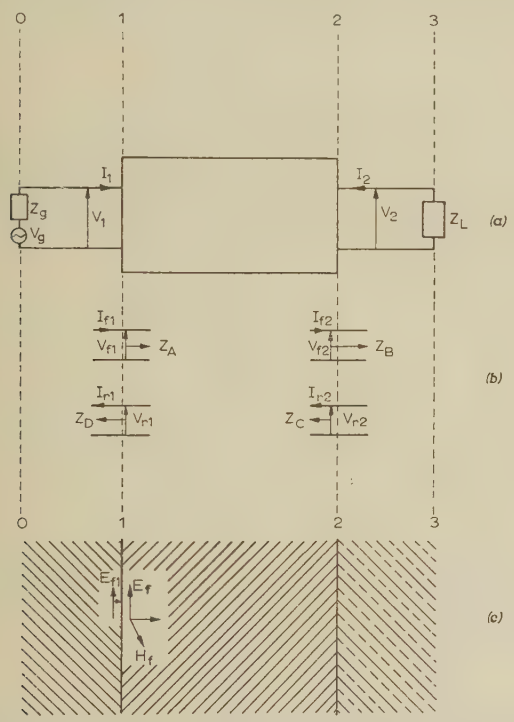

Fig. 1.—Flow of electromagnetic energy in a generalized 4-terminal network and anisotropic medium.

be lumped or distributed, active or passive. Analogously, one may consider a disturbance situated in the centre anisotropic linear medium of Fig. 1(*c*) in the form of the component E_f of a plane-polarized wave. This wave, shown in Fig. 1(*b*), in proceeding from point 1 to point 2 is amplified or attenuated by a factor p_{21} or p_f (f for forward), i.e. its voltage is now $V_{f2} = V_{f1}p_f$. At point 2 it experiences a discontinuity due to impedance Z_L, so that a reflection occurs, the ratio of the reflected to incident wave being r_{23}. The reflected wave is thus $V_{r2} = V_{f1}p_f r_{23}$. The wave proceeds back to point 1, again being amplified or attenuated by a factor p_{12} or p_r (r for reverse) and is now $V_{r1} = V_{f1}p_f r_{23}p_r$. Let it now be specified that the source impedance is of such a magnitude that no reflection occurs there, i.e. matching is present and the signal is completely absorbed by the source impedance, causing no further disturbance to the system. [In the case of Fig. 1(*c*) this implies that no discontinuity exists at point 1, i.e. there are now two semi-infinite media which join at point 2 and the signal proceeds to the left *ad infinitum*, causing no further disturbance. The case of a mismatch at point 1 is treated later.] The voltages at points 1 and 2 will be the sum of the forward and reverse waves. Thus at point 1,

$$V_1 = V_{f1} + V_{r1} = V_{f1}(1 + p_f p_r r_{23}) \quad . \quad . \quad . \quad . \quad (1)$$

and at point 2,

$$V_2 = V_{f2} + V_{r2} = V_{f1}(1 + r_{23})p_f \quad . \quad . \quad . \quad . \quad . \quad (2)$$

To find the associated incident and reflected current waves, it is assumed that, in general, a disturbance experiences an impedance solely determined by the direction in which it travels and by the local conditions, i.e. it is unaffected by impedances at any further point. Thus, let V_{f1} experience at point 1 an impedance Z_A; the incident current wave, I_{f1}, is then V_{f1}/Z_A. Similarly, just prior to emerging at point 2, the forward voltage wave V_{f2} will have an associated current wave $I_{f2} = V_{f2}/Z_B$; the reflected current wave at point 2 is $I_{r2} = V_{r2}/Z_C$, and finally at point 1 it is $I_{r1} = V_{r1}/Z_D$.

At point 1,

$$I_1 = I_{f1} - I_{r1} = V_{f1}\left(\frac{1}{Z_A} - \frac{p_f p_r r_{23}}{Z_D}\right) \quad . \quad . \quad . \quad . \quad (3)$$

and at point 2,

$$-I_2 = I_{f2} - I_{r2} = V_{f1}p_f\left(\frac{1}{Z_B} - \frac{r_{23}}{Z_C}\right) \quad . \quad . \quad . \quad . \quad (4)$$

where the positive and negative signs arise out of the sign convention shown in Figs. 1(*a*) and (*b*).

Eqns. (1)–(4) contain six parameters which are solely functions of the 4-terminal network, namely p_f, p_r, Z_A, Z_B, Z_C and Z_D. Since four quantities are sufficient to specify it uniquely, two of these have to be eliminated by, for example, expressing them in terms of two others. These parameters will then become recognizable in terms of the conventional ones, as shown in Sections 4 and 5. At present some implications of eqns. (1)–(4) will be examined.

The voltage reflection coefficient may be expressed in terms of impedances by dividing eqn. (2) by eqn. (4):

$$-\frac{V_2}{I_2} = Z_L = \frac{1 + r_{23}}{1/Z_B - r_{23}/Z_C}$$

or

$$r_{23} = \frac{Z_L/Z_B - 1}{Z_L/Z_C + 1} \quad . \quad . \quad . \quad . \quad . \quad . \quad . \quad (5)$$

From eqn. (5) it is clear that there will be no reflection, i.e. complete absorption or matching will occur, when

$$Z_L = Z_B \quad . \quad . \quad . \quad . \quad . \quad . \quad . \quad (6)$$

Under this condition, putting $r_{23} = 0$ in eqns. (1) and (3), the input impedance is

$$Z_{in} = V_1/I_1 = Z_A \quad . \quad . \quad . \quad . \quad . \quad (7)$$

Analogously, matching occurs at the input when

$$Z_g = Z_D \quad . \quad . \quad . \quad . \quad . \quad . \quad . \quad (8)$$

resulting in an output impedance

$$Z_{out} = Z_C \quad . \quad . \quad . \quad . \quad . \quad . \quad . \quad (9)$$

From eqn. (5) it is also clear that, for total reflection at a junction, i.e. $Z_L = 0$ or $Z_L = \infty$, the voltage reflection coefficient r_{23} is -1 or Z_C/Z_B, respectively. In general, the magnitude of r_{23} may be either smaller or larger than unity, exceptions being in resistance networks and lossless transmission lines.

Finally, eqns. (1) and (2) define the quantities p_f and p_r more closely than hitherto. Letting r_{23} equal zero in eqns. (1) and (2), it is seen that $V_2/V_1 = p_f$ and therefore p_f and p_r are the forward and reverse voltage transfer ratios, respectively, of a 4-terminal network matched at both terminal pairs.

The above expressions are all in terms of an incident voltage wave, V_{f1}. Obviously, dual expressions in terms of an incident current wave are possible. Of special interest may be the current reflection coefficient, which, from eqn. (4), is $r'_{23} = I_{r2}/I_{f2} = -r_{23}Z_B/Z_C$. Thus, if $Z_L = \infty$, $r'_{23} = -1$.

At a discontinuity between two media or at a terminal pair which connects two networks, the sums of the incident and reflected waves on each side are equal, and in the case of networks this sum equals the net voltage or current measured at the terminal pair. When there is wave flow from one semi-infinite medium containing a generator across the discontinuity to another that is passive (i.e. it does not possess a generator, which is the condition at point 2 in Fig. 1), then the passive side possesses only a wave which travels away from the junction. This is termed the 'transmitted wave'. The transmission coefficient is defined as the ratio of the transmitted wave to the incident wave at such a discontinuity. From eqn. (2) the voltage transmission coefficient is

$$t_{v23} = \frac{V_{f2} + V_{r2}}{V_{f2}} = \frac{V_2}{V_{f2}} = 1 + r_{23} \quad . \quad . \quad (10)$$

and from eqn. (4) the current transmission coefficient is

$$t_{i23} = \frac{I_{f2} + I_2}{I_{f2}} = \frac{-I_2}{I_{f2}} = 1 + r'_{23} \quad . \quad . \quad (11)$$

Consider now power flow. The power delivered to a load, i.e. the transmitted power, is

$$P_T = \tfrac{1}{2}\mathscr{R}(V_2 I_2^*)$$

where $\mathscr{R}$ symbolizes 'the real part of'. From eqns. (10) and (11) this may be written

$$P_T = \tfrac{1}{2}\mathscr{R}(t_{v23} t_{i23}^* V_{f2} I_{f2}^*) \quad . \quad . \quad . \quad . \quad (12)$$

The incident power is

$$P_i = \tfrac{1}{2}\mathscr{R}(V_{f2} I_{f2}^*) \quad . \quad . \quad . \quad . \quad . \quad (13)$$

The reflected power is analogously

$$P_r = \tfrac{1}{2}\mathscr{R}(V_{r2} I_{r2}^*) = \tfrac{1}{2}\mathscr{R}(r_{23} r'^*_{23} V_{f2} I_{f2}^*) \quad . \quad . \quad . \quad . \quad (14)$$

Note that $P_T = P_i + P_r$ only if $Z_B = Z_C$, i.e. if $r_{23} = -r_{23}$ (which, as shown in Section 4, implies 'image' waves) and if $V_{f2} I_{f2}^*$ is real, i.e. if $V_{f2}/I_{f2} = Z_B$ is real. Under these conditions the power transmission coefficient is

$$t_{p23} = \frac{P_T}{P_i} = 1 + \frac{P_r}{P_i} = 1 - |r_{23}|^2 \quad . \quad . \quad . \quad . \quad . \quad (15)$$

This implies that r_{23} may be used as a measure of power mismatch at a junction only when driving from a resistive source or from a medium having a characteristic impedance which is real.

(3) WAVE TRAINS IN 4-TERMINAL NETWORKS WITH MISMATCHED SOURCE

Let a wave V'_{f1} be emitted by the generator which is placed to the left of the network in Fig. 1(*a*). (By analogy, an incident wave E_{f1} is generated at a point close to the boundary 1 in Fig. 1(*c*) and to the left of it.) It first experiences a discontinuity at the input to the network [or at boundary 1 in Fig. 1(*c*)]. The reflected wave will proceed to the left and disappear. The transmitted wave is instantaneously 'unaware' of the type of termination at points 2 and 3 and hence its magnitude will be $V'_{f1}(1 + r_{12})$, analogous to eqn. (10), where [analogous to eqn. (5)]

$$r_{12} = \frac{Z_A/Z_g - 1}{Z_D/Z_g + 1} \quad . \quad . \quad . \quad . \quad . \quad (16)$$

As before, it continues to travel to the right towards point 2 while having its magnitude changed by a factor p_f, and becomes $V'_{f1}(1 + r_{12})p_f$; next it is reflected and becomes $V'_{f1}(1 + r_{12})p_f r_{23}$ at point 2, and when finally arriving at point 1 it is $V'_{f1}(1 + r_{12})p_f r_{23} p_r$. Now, however, it suffers another reflection at the input by a factor r_{21}, given by [analogous to eqn. (5)]

$$r_{21} = \frac{Z_g/Z_D - 1}{Z_g/Z_A + 1} \quad . \quad . \quad . \quad . \quad . \quad (16)$$

resulting in a wave of magnitude $V'_{f1}(1 + r_{12})p_f r_{23} p_r r_{21}$ commencing its journey to the right. All waves proceeding to the left of point 1 again disappear. This process is repeated over and over again, and hence the total voltage of all the waves leaving point 1 and travelling to the right or in the forward direction is

$$\begin{aligned} V_{f1t} &= V'_{f1}(1 + r_{12}) + V'_{f1}(1 + r_{12})p_f p_r r_{23} r_{21} \\ &\quad + V'_{f1}(1 + r_{12})(p_f p_r r_{23} r_{21})^2 + \ldots \\ &= V'_{f1}(1 + r_{12}) \sum_{n=0}^{n=\infty} (p_f p_r r_{23} r_{21})^n \end{aligned}$$

This series can be expressed in closed form if it converges, i.e. if $|p_f p_r r_{23} r_{21}| < 1$:

$$V_{f1t} = \frac{V'_{f1}(1 + r_{12})}{1 - p_f p_r r_{23} r_{21}} \quad . \quad . \quad . \quad . \quad (17)$$

The quantity $p_f p_r r_{23} r_{21}$ will later be referred to as the wave loop gain. Similarly it can be shown that the total voltage for all the waves travelling to the right at point 2 is

$$V_{f2t} = \frac{p_f(1 + r_{12})V'_{f1}}{(1 - p_f p_r r_{21} r_{23})} = p_f V_{f1t} \quad . \quad . \quad . \quad (18)$$

while the total reflected voltages at points 2 and 1 are $V_{r1t} = p_f r_{23} V_{f1t}$ and $V_{r2t} = p_f r_{23} p_r V_{f1t}$ respectively. The actual voltage at point 1 is $V_1 = V_{f1t} + V_{r1t}$ and at point 2 it is $V_2 = V_{f2t} + V_{r2t}$.

Thus it is clear that eqns. (1)–(4), which assume a matched generator, also describe the unmatched case, provided that V_f is substituted for V_{f1}.

The relation of the initial incident voltage V'_{f1} to the generator voltage V_g in Fig. 1(*a*) is clear if one substitutes the expression for V_{f1t} from eqn. (17) for V_{f1} in eqn. (1):

$$V_1 = \frac{V'_{f1}(1 + r_{12})(1 + p_f p_r r_{23})}{1 - p_f p_r r_{21} r_{23}} \quad . \quad . \quad . \quad (19)$$

If both ends of the network are matched, $r_{12} = 0$, $r_{23} = 0$ and from eqn. (19), $V_1 = V'_{f1}$, while from eqns. (7) and (8), $V_1 = Z_{in} V_g/(Z_{in} + Z_g) = Z_A V_g/(Z_A + Z_D)$. Hence

$$V'_{f1} = V_g Z_A/(Z_A + Z_D) \quad . \quad . \quad . \quad . \quad (19)$$

while V_{f1} in eqns. (1)–(4) is

$$V_{f1} = \frac{V_g Z_A (1 + r_{12})}{(Z_A + Z_D)(1 - p_f p_r r_{21} r_{23})} \quad . \quad . \quad . \quad (20)$$

(4) RELATION BETWEEN TRAVELLING WAVE AND SHORT- AND OPEN-CIRCUIT PARAMETERS

The open-circuit (z), short-circuit (y), h, g, a, and b parameters, as well as other properties, are easily derived from eqns. (1)–(4) by substituting the proper value for r_{23} (depending on the terminating impedance) and dividing the appropriate two equations one by the other, which results in V_{f1} being cancelled. Thus, for example, for the open-circuit input impedance, z_{11}, we put $I_2 = 0$. Hence, $r_{23} = Z_C/Z_B$, and dividing eqn. (1) by eqn. (3),

$$z_{11} = \frac{V_1}{I_1} = \frac{1 + p_f p_r Z_C/Z_B}{1 - p_f p_r Z_A Z_C/Z_D Z_B} Z_A$$

For the open-circuit output impedance, z_{22}, we put $I_1 = 0$ in eqn. (3); then $r_{23} = Z_D/Z_A p_f p_r$, and dividing eqn. (2) by eqn. (4),

$$z_{22} = \frac{V_2}{I_2} = \frac{1 + p_f p_r Z_A/Z_D}{1 - p_f p_r Z_A Z_C/Z_D Z_B} Z_C$$

which, as expected, is of the same form as z_{11}, with Z_C and Z_B interchanged with Z_A and Z_D.

Besides open-circuit and short-circuit terminations, there are, out of an infinite number, three special types of terminations to a 4-terminal network which are frequently encountered, as follows.

Case I.—$Z_g = Z_{in}$ and $Z_L = Z_{out}$.

This is the image matched case and hence, from eqns. (6)–(9),

$$Z_D = Z_A \text{ and } Z_B = Z_C$$

Case II.—$Z_g = Z_{in}^*$ and $Z_L = Z_{out}^*$.

This is the conjugate matched case and hence, as above,

$$Z_D = Z_A^* \text{ and } Z_B = Z_C^* \quad . \quad . \quad . \quad . \quad . \quad (22)$$

Case III.—$Z_g = Z_{out}$ and $Z_L = Z_{in}$.

This is the iterative matched case and hence, as above,

$$Z_D = Z_C \text{ and } Z_B = Z_A \quad . \quad . \quad . \quad . \quad (23)$$

Since, in each of these cases, two of the six parameters of the network may be eliminated, the 4-terminal network is completely specified by p_f (or p_{21}), p_r (or p_{12}), an input impedance Z_{01}, and an output impedance Z_{02}. By definition, if a network is specified according to Case I, then p_{21}, p_{12}, Z_{01} and Z_{02} are image parameters and we utilize image waves. Similarly, Cases II and III give rise to conjugate and iterative parameters and waves respectively.

For uniform transmission lines the analysis has conventionally been carried out using image waves. The image impedance is then referred to as the characteristic impedance. Using conjugate waves, on the other hand, the 'characteristic' impedance is quite different, since in measuring it for a given length of line, different terminating impedances, i.e. conjugate matched impedances, must be used. Obviously the iterative matched parameters and image matched parameters are here identical. Only at frequencies where the characteristic impedance is real, or for lossless transmission lines, are the image, conjugate and iterative impedances identical.

It is clear from the above that there is no unique set of waves by which a distributed or lumped network can be analysed. Furthermore, 'matching' or 'no reflection', implying $r_{23} = 0$, does not at the same time uniquely define the magnitude of the terminating impedance in terms of the network, since it may be equal to either the image, conjugate, iterative, or indeed any of an infinite number of terminating impedances.

Finally, we note that for image waves [using eqn. (21)], eqns. (16a) and (16b) may be written

$$r_{12} = \frac{Z_{01}/Z_g - 1}{Z_{01}/Z_g + 1} \text{ and } r_{21} = \frac{Z_g/Z_{01} - 1}{Z_g/Z_{01} + 1}$$

and therefore $r_{12} = -r_{21}$.

Table 1 lists various properties of a 4-terminal network expressed in terms of the above wave parameters. The first and second rows state the basic wave parameters and the manner in which the image, conjugate and iterative columns are obtained from the general wave parameters; the third and fourth rows [based on eqns. (1)–(4)] define the network completely, while the fifth, sixth and seventh rows define the remaining symbols in eqns. (3) and (4). The other formulae in the Table may be derived from the third and fourth rows by inspection, simply by dividing the appropriate two equations one by the other as was done for z_{11} above.

It may also be noted that the voltage transfer expressions have an identical form for the various types of parameters, which is due to an incident voltage wave having been used as the reference disturbance.

Table 2 is an extension of Table 1 but deals with the open- and short-circuit parameters. The conjugate and iterative parameters have been omitted but are easily found by using the first row of Table 1.

It is obvious from these Tables that the expressions corresponding to image parameters are algebraically the simplest, and this is one reason why they will be used more often than the others. Another important property is that they may be written without any difficulty in the form $q = (1 + ar)/(1 + br)$. As an example, in the expression for Z_{in} (eighth row of Table 1), $r = r_{23}$, $a = -b = p_{12}p_{21}$ and $q = Z_{in}/Z_{01}$. The expression for q, which is a bi-linear form in complex variable theory, is known to transform lines and circles in the q-plane into lines and circles in the r-plane. The resulting chart, of which the Smith chart is a special case, considerably facilitates computational labour. Its uses in practical design problems are discussed elsewhere.[11, 12]

(5) WAVE MATRIX TREATMENT OF MULTI-PORT NETWORKS

Fig. 2 is a general multi-port network showing waves both internal and external to it. In Fig. 1(c) internal waves would be those inside the centre medium, while external waves would be those on the sides, assuming generators to be present in the two side media. In a typical port in Fig. 2, such as that connected to generator V_{g2}, having a source impedance Z_{g2}, v'_{i2} and v'_{r2} are the external incident and reflected waves respectively, while v_{i2} and v_{r2} are the internal waves. Equating voltages on each side of every port,

$$v'_{i1} + v'_{r1} = v_{i1} + v_{r1} = V_1$$

$$v'_{i2} + v'_{r2} = v_{i2} + v_{r2} = V_2, \text{ etc.}$$

where V_1, V_2, etc., are the actual voltages measured at the terminals. In matrix notation, using single-column matrices,

$$\boldsymbol{v}'_i + \boldsymbol{v}'_r = \boldsymbol{v}_i + \boldsymbol{v}_r = V \quad . \quad . \quad . \quad . \quad (24)$$

Table 1 PROPERTIES OF A 4-TERMINAL NETWORK EXPRESSED IN TERMS OF GENERAL, IMAGE, CONJUGATE AND ITERATIVE PARAMETERS

	General	Image	Conjugate	Iterative
Matched input impedances, Z_{01} Matched output impedances, Z_{02}	$Z_A\ Z_B\ Z_C\ Z_D$	$Z_{01} = Z_D = Z_A$ $Z_{02} = Z_B = Z_C$	$Z_{01} = Z_D^* = Z_A$ $Z_{02} = Z_B^* = Z_C$	$Z_{01} = Z_B = Z_A$ $Z_{02} = Z_D = Z_C$
Matched forward voltage gain Matched reverse current gain	p_{21} p_{12}	p_{21} p_{12}	p_{21} p_{12}	p_{21} p_{12}
Input voltage, V_1 .. .. Output voltage, V_2	$V_1 = V_{f1}(1 + p_{21}p_{12}r_{23})$ $V_2 = V_{f1}p_{21}(1 + r_{23})$	$V_1 = V_{f1}(1 + p_{21}p_{12}r_{23})$ $V_2 = V_{f1}p_{21}(1 + r_{23})$	$V_{f1}(1 + p_{21}p_{12}r_{23})$ $V_{f1}p_{21}(1 + r_{23})$	$V_{f1}(1 + p_{21}p_{12}r_{23})$ $V_{f1}p_{21}(1 + r_{23})$
Input current, I_1 .. .. Output current, I_2	$I_1 = \frac{V_{f1}}{Z_A}\left(1 - \frac{p_{21}p_{12}Z_Ar_{23}}{Z_D}\right)$ $I_2 = -\frac{V_{f1}p_{21}}{Z_B}\left(1 - \frac{Z_Br_{23}}{Z_C}\right)$	$I_1 = \frac{V_{f1}}{Z_{02}}(1 - p_{21}p_{12}r_{23})$ $I_2 = -\frac{V_{f1}p_{21}}{Z_{02}}(1 - r_{23})$	$\frac{V_{f1}}{Z_{01}}\left(1 - \frac{p_{21}p_{12}Z_{01}}{Z_{01}^*}.r_{23}\right)$ $\frac{-V_{f1}p_{21}}{Z_{02}}\left(1 - \frac{Z_{02}^*r_{23}}{Z_{02}}\right)$	$\frac{V_{f1}}{Z_{02}}\left(1 - \frac{p_{21}p_{12}Z_{01}}{Z_{02}}.r_{23}\right)$ $\frac{V_{f1}p_{21}}{Z_{01}}\left(1 - \frac{Z_{01}r_{23}}{Z_{02}}\right)$
Incident voltage..	$V_{f1} = \frac{V_gZ_A(1 + r_{12})}{(Z_A + Z_D)(1 - p_{21}p_{12}r_{21}r_{23})}$	$\frac{V_g(1 + r_{12})}{2(1 - p_{21}p_{12}r_{23}r_{21})}$	$\frac{V_gZ_{01}(1 + r_{12})}{(Z_{01} + Z_{01}^*)(1 - p_{12}p_{21}r_{21}r_{23})}$	$\frac{V_gZ_{01}(1 + r_{12})}{(Z_{01} + Z_{02})(1 - p_{21}p_{12}r_{21}r_{23})}$
Reflection voltage coefficient, incident wave towards load	$r_{23} = \frac{\frac{Z_L}{Z_B} - 1}{\frac{Z_L}{Z_C} - 1}$	$r_{23} = \frac{\frac{Z_L}{Z_{02}} - 1}{\frac{Z_L}{Z_{02}} + 1}$	$\frac{\frac{Z_L}{Z_{02}^*} - 1}{\frac{Z_L}{Z_{02}} + 1}$	$\frac{\frac{Z_L}{Z_{01}} - 1}{\frac{Z_L}{Z_{02}} + 1}$
Reflection voltage coefficients, generator end	$r_{21} = \frac{\frac{Z_G}{Z_D} - 1}{\frac{Z_G}{Z_A} + 1}, r_{12} = \frac{\frac{Z_A}{Z_G} - 1}{\frac{Z_D}{Z_G} + 1}$	$r_{21} = \frac{\frac{Z_G}{Z_{01}} - 1}{\frac{Z_G}{Z_{01}} + 1} = -r_{12} = -\frac{\frac{Z_{01}}{Z_G} - 1}{\frac{Z_{01}}{Z_G} + 1}$	$r_{21} = \frac{\frac{Z_G}{Z_{01}^*} - 1}{\frac{Z_G}{Z_{01}} + 1}, r_{12} = \frac{\frac{Z_{01}}{Z_G} - 1}{\frac{Z_{01}^*}{Z_G} + 1}$	$r_{21} = \frac{\frac{Z_G}{Z_{02}} - 1}{\frac{Z_G}{Z_{01}} + 1}, r_{12} = \frac{\frac{Z_{01}}{Z_G} - 1}{\frac{Z_{02}}{Z_G} + 1}$
Input impedance, Z_{in}	$\frac{(1 + p_{21}p_{12}r_{23})Z_A}{1 - \frac{p_{21}p_{12}Z_Ar_{23}}{Z_D}}$	$\frac{(1 + p_{21}p_{12}r_{23})Z_{01}}{1 - p_{21}p_{12}r_{23}}$	$\frac{(1 + p_{21}p_{12}r_{23})Z_{01}}{1 - \frac{p_{21}p_{12}Z_{01}r_{23}}{Z_{01}^*}}$	$\frac{(1 + p_{21}p_{12}r_{23})Z_{01}}{1 - \frac{p_{21}p_{12}Z_{02}r_{23}}{Z_{01}}}$
Output impedance, Z_{out} ..	$\frac{(1 + p_{21}p_{12}r_{21})Z_A}{1 - \frac{p_{21}p_{12}Z_Cr_{21}}{Z_B}}$	$\frac{(1 + p_{21}p_{12}r_{21})Z_{02}}{1 - p_{21}p_{12}r_{21}}$	$\frac{(1 + p_{21}p_{12}r_{21})Z_{02}}{1 - \frac{p_{21}p_{12}Z_{02}r_{21}}{Z_{02}^*}}$	$\frac{(1 + p_{21}p_{12}r_{21})Z_{02}}{1 - \frac{p_{21}p_{12}Z_{02}r_{21}}{Z_{01}}}$
Forward voltage gain, $\frac{V_2}{V_1}$ ..	$\frac{(1 + r_{23})p_{21}}{1 + p_{21}p_{12}r_{23}}$	$\frac{(1 + r_{23})p_{21}}{1 + p_{21}p_{12}r_{23}}$	$\frac{(1 + r_{23})p_{21}}{1 + p_{21}p_{12}r_{23}}$	$\frac{(1 + r_{23})p_{21}}{1 + p_{21}p_{12}r_{23}}$
Forward current gain, $\frac{I_2}{I_1} = \frac{-V_2}{V_1} \times \frac{Z_{in}}{Z_L}$ ..	$\frac{-Z_A\left(1 - \frac{Z_Br_{23}}{Z_C}\right)p_{21}}{Z_B\left(1 - \frac{p_{21}p_{12}Z_Ar_{23}}{Z_D}\right)}$	$\frac{-Z_{01}(1 - r_{23})p_{21}}{Z_{02}(1 - p_{21}p_{12}r_{23})}$	$\frac{-\left(1 - \frac{Z_{02}^*r_{23}}{Z_{02}}\right)p_{21}Z_{01}}{\left(1 - \frac{p_{21}p_{12}Z_{01}r_{23}}{Z_{01}^*}\right)Z_{02}^*}$	$\frac{-\left(1 - \frac{Z_{01}r_{23}}{Z_{02}}\right)p_{21}}{1 - \frac{p_{21}p_{12}Z_{01}r_{23}}{Z_{02}}}$
Matched forward current gain Matched reverse current gain ..	$p_{21}.\frac{Z_A}{Z_B}$ $p_{12}.\frac{Z_C}{Z_D}$	$p_{21}.\frac{Z_{01}}{Z_{02}}$ $p_{12}.\frac{Z_{02}}{Z_{01}}$	$p_{21}.\frac{Z_{01}}{Z_{02}^*}$ $p_{12}.\frac{Z_{02}}{Z_{01}^*}$	p_{21} p_{12}
Matched forward power gain, $\frac{\text{Power in load}}{\text{Input power}} G_{PF}$	$\lvert p_{21}\rvert^2\frac{\mathscr{R}\left(\frac{1}{Z_B}\right)}{\mathscr{R}\left(\frac{1}{\quad}\right)}$	$\lvert p_{21}\rvert^2\frac{\mathscr{R}\left(\frac{1}{Z_{02}}\right)}{\mathscr{R}\left(\frac{1}{\quad}\right)}$	$\lvert p_{21}\rvert^2\frac{\mathscr{R}\left(\frac{1}{Z_{02}^*}\right)}{\mathscr{R}\left(\frac{1}{\quad}\right)}$	$\lvert p_{21}\rvert^2$

Table 2

z, *y*, *h*, *g*, *a* AND *b* PARAMETERS EXPRESSED IN TERMS OF GENERAL AND IMAGE PARAMETERS

Parameters		General		Image	
z_{11}	z_{12}	$\frac{\left(1+p_{21}p_{12}\frac{Z_C}{Z_B}\right)Z_A}{\left(1-p_{21}p_{12}\frac{Z_AZ_C}{Z_DZ_B}\right)}$	$\frac{\left(1+\frac{Z_A}{Z_D}\right)Z_Cp_{12}}{1-p_{21}p_{12}\frac{Z_AZ_C}{Z_DZ_B}}$	$\frac{(1+p_{21}p_{12})Z_{01}}{1-p_{21}p_{12}}$	$\frac{2Z_{02}p_{12}}{1-p_{21}p_{12}}$
z_{21}	z_{22}	$\frac{\left(1+\frac{Z_C}{Z_B}\right)Z_Ap_{21}}{1-p_{21}p_{12}\frac{Z_AZ_C}{Z_DZ_B}}$	$\frac{\left(1+p_{21}p_{12}\frac{Z_A}{Z_D}\right)Z_C}{1-p_{21}p_{12}\frac{Z_AZ_C}{Z_BZ_D}}$	$\frac{2Z_{01}p_{21}}{1-p_{21}p_{12}}$	$\frac{(1+p_{21}p_{12})Z_{02}}{1-p_{21}p_{12}}$
y_{11}	y_{12}	$\frac{\left(1+p_{21}p_{12}\frac{Z_A}{Z_D}\right)}{(1-p_{21}p_{12})Z_A}$	$-\frac{\left(1+\frac{Z_D}{Z_A}\right)p_{12}}{(1-p_{21}p_{12})Z_D}$	$\frac{1+p_{21}p_{12}}{(1-p_{21}p_{12})Z_{01}}$	$-\frac{2p_{12}}{Z_{01}(1-p_{21}p_{12})}$
y_{21}	y_{22}	$-\frac{\left(1+\frac{Z_B}{Z_C}\right)p_{21}}{Z_B(1-p_{21}p_{12})}$	$\frac{1+p_{21}p_{12}\frac{Z_C}{Z_B}}{(1-p_{21}p_{12})Z_C}$	$-\frac{2p_{21}}{Z_{02}(1-p_{21}p_{12})}$	$\frac{1+p_{21}p_{12}}{(1-p_{21}p_{12})Z_{02}}$
h_{11}	h_{12}	$\frac{(1-p_{21}p_{12})Z_A}{\left(1+p_{21}p_{12}\frac{Z_A}{Z_D}\right)}$	$\frac{\left(1+\frac{Z_A}{Z_D}\right)p_{12}}{\left(1+p_{21}p_{12}\frac{Z_A}{Z_D}\right)}$	$\frac{(1-p_{21}p_{12})Z_{01}}{1+p_{21}p_{12}}$	$\frac{2p_{12}}{1+p_{21}p_{12}}$
h_{21}	h_{22}	$-\frac{Z_A\left(1+\frac{Z_B}{Z_C}\right)p_{21}}{Z_B\left(1+p_{21}p_{12}\frac{Z_A}{Z_D}\right)}$	$\frac{1-p_{21}p_{12}\frac{Z_AZ_C}{Z_BZ_D}}{\left(1+p_{21}p_{12}\frac{Z_A}{Z_D}\right)Z_C}$	$-\frac{2Z_{01}p_{21}}{Z_{02}(1+p_{21}p_{12})}$	$\frac{1-p_{21}p_{12}}{(1+p_{21}p_{12})Z_{02}}$
g_{11}	g_{12}	$\frac{\left(1-p_{21}p_{12}\frac{Z_AZ_C}{Z_DZ_B}\right)}{\left(1+p_{21}p_{12}\frac{Z_C}{Z_B}\right)Z_A}$	$\frac{\left(1+\frac{Z_D}{Z_A}\right)\frac{Z_C}{Z_D}p_{12}}{\left(1+p_{21}p_{12}\frac{Z_C}{Z_B}\right)}$	$\frac{1-p_{21}p_{12}}{(1+p_{21}p_{12})Z_{01}}$	$-\frac{2p_{12}\frac{Z_{02}}{Z_{01}}}{1+p_{21}p_{12}}$
g_{21}	g_{22}	$\frac{\left(i+\frac{Z_C}{Z_B}\right)p_{21}}{\left(1+p_{21}p_{12}\frac{Z_C}{Z_B}\right)}$	$\frac{(1-p_{21}p_{12})Z_C}{\left(1+p_{21}p_{12}\frac{Z_C}{Z_B}\right)}$	$\frac{2p_{21}}{1+p_{21}p_{12}}$	$\frac{(1-p_{21}p_{12})Z_{02}}{1+p_{21}p_{12}}$
a_{11}	a_{12}	$\frac{\left(1+p_{21}p_{12}\frac{Z_C}{Z_B}\right)}{\left(1+\frac{Z_C}{Z_B}\right)p_{21}}$	$\frac{Z_B(1-p_{21}p_{12})}{\left(1+\frac{Z_B}{Z_C}\right)p_{21}}$	$\frac{1+p_{21}p_{12}}{2p_{21}}$	$\frac{Z_{02}(1-p_{21}p_{12})}{2p_{21}}$
a_{21}	a_{22}	$\frac{\left(1-p_{21}p_{12}\frac{Z_AZ_C}{Z_DZ_B}\right)}{\left(1+\frac{Z_C}{Z_B}\right)Z_Ap_{21}}$	$\frac{Z_B\left(1+p_{21}p_{12}\frac{Z_A}{Z_D}\right)}{Z_A\left(1+\frac{Z_B}{Z_C}\right)p_{21}}$	$\frac{1-p_{21}p_{12}}{2Z_{01}p_{21}}$	$\frac{Z_{02}(1+p_{21}p_{12})}{2Z_{01}p_{21}}$
b_{11}	b_{12}	$\frac{\left(1+p_{21}p_{12}\frac{Z_A}{Z_D}\right)}{\left(1+\frac{Z_A}{Z_B}\right)p_{12}}$	$\frac{Z_D(1-p_{21}p_{12})}{\left(1+\frac{Z_D}{Z_A}\right)p_{12}}$	$\frac{1+p_{21}p_{12}}{2p_{12}}$	$\frac{Z_{01}(1-p_{21}p_{12})}{2p_{12}}$
b_{21}	b_{22}	$\frac{1-p_{21}p_{12}\frac{Z_AZ_C}{Z_DZ_B}}{\left(1+\frac{Z_A}{Z_D}\right)Z_Cp_{12}}$	$\frac{\left(1+p_{21}p_{12}\frac{Z_C}{Z_B}\right)}{\left(1+\frac{Z_D}{Z_A}\right)\frac{Z_C}{Z_D}p_{12}}$	$\frac{1-p_{21}p_{12}}{2Z_{02}p_{12}}$	$\frac{1+p_{21}p_{12}}{2\frac{Z_{02}}{Z_{01}}p_{12}}$

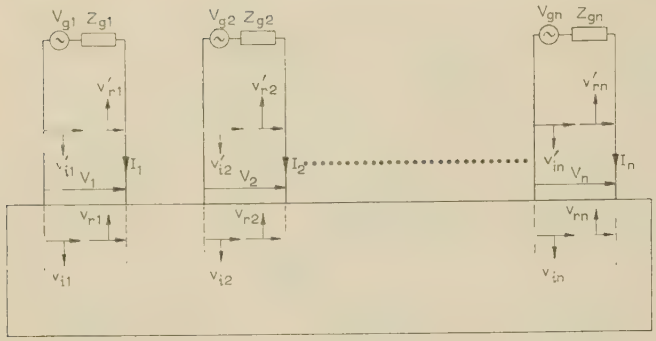

Fig. 2.—Internal and external waves associated with a multi-port network.

Assume image waves and consider the associated current waves. The external and internal waves move in media of characteristic impedance Z_{g1}, Z_{g2}, etc., and Z_{01}, Z_{02}, etc., respectively, where Z_{01}, Z_{02}, etc., are the image impedances at each port. As before, equating conditions on each side of the boundary,

$$Z_g^{-1}(\boldsymbol{v}_i' - \boldsymbol{v}_r') = Z_0^{-1}(\boldsymbol{v}_i - \boldsymbol{v}_r) = \boldsymbol{I} \quad . \quad . \quad (25)$$

where Z_g^{-1} and Z_0^{-1} are diagonal matrices, with elements $1/Z_{g1}$, $1/Z_{g2}$, etc., and $1/Z_{01}$, $1/Z_{02}$, etc., respectively, and $\boldsymbol{I}$ is a column matrix having elements I_1, I_2, etc., which are the actual currents at the terminals.

Each internal reflected wave at a port (e.g. v_{r2}) is now viewed as the result of every internal incident wave at all the other ports having arrived at this port; during their travel each is modified by a factor p_{xy}, i.e.

$$\boldsymbol{v}_r = \boldsymbol{p}\boldsymbol{v}_i \quad . \quad . \quad . \quad . \quad . \quad . \quad . \quad (26)$$

where $\boldsymbol{p}$ is the propagation matrix

$$\boldsymbol{p} = \begin{bmatrix} 0 & p_{12} & p_{13} \cdots & p_{1n} \\ p_{21} & 0 & p_{23} \cdots & p_{2n} \\ p_{31} & p_{32} & 0 \quad \cdots & p_{3n} \\ \cdot & \cdot & \cdot \quad \cdots & \cdot \\ \cdot & \cdot & \cdot \quad \cdots & \cdot \\ \cdot & \cdot & \cdot \quad \cdots & \cdot \\ p_{n1} & p_{n2} & p_{n3} & 0 \end{bmatrix}$$

Finally, by definition the external reflected wave at a port is taken to be a linear combination of all external incident waves, including that at the port under consideration, i.e.

$$\boldsymbol{v}_r' = \boldsymbol{s}'\boldsymbol{v}_i' \quad . \quad . \quad . \quad . \quad . \quad . \quad . \quad (27)$$

where

$$\boldsymbol{s}' = \begin{bmatrix} s'_{11} & s'_{12} & s'_{13} \cdots & s'_{1n} \\ s'_{21} & s'_{22} & s'_{23} \cdots & s'_{2n} \\ s'_{31} & s'_{32} & s'_{33} \cdots & s'_{3n} \\ \cdot & \cdot & \cdot \quad \cdots & \cdot \\ \cdot & \cdot & \cdot \quad \cdots & \cdot \\ & & \cdots & \cdot \\ s'_{n1} & s'_{n2} & s'_{n3} \cdots & s'_{nn} \end{bmatrix}$$

$\boldsymbol{s}'$ will be termed the un-normalized scattering matrix.

Eliminating $\boldsymbol{v}_r'$, $\boldsymbol{v}_r$, $\boldsymbol{v}_i'$ and $\boldsymbol{v}_i$ from eqns. (24)–(27) yields

$$(\boldsymbol{1} + \boldsymbol{s}')(\boldsymbol{1} - \boldsymbol{s}')^{-1}Z_g = (\boldsymbol{1} + \boldsymbol{p})(\boldsymbol{1} - \boldsymbol{p})^{-1}Z_0 = \boldsymbol{V}\boldsymbol{I}^{-1} = \boldsymbol{z} = \boldsymbol{y}^{-1} \quad (28)$$

where $\boldsymbol{1}$ is the unit or identity matrix, and $\boldsymbol{z}$ and $\boldsymbol{y}$ are the open-circuit impedance and short-circuit admittance matrices respectively. From eqn. (28),

$$\boldsymbol{s}' = (\boldsymbol{z}Z_g^{-1} - \boldsymbol{1})(\boldsymbol{z}Z_g^{-1} + \boldsymbol{1})^{-1} \quad . \quad . \quad (29)$$

$$\boldsymbol{p} = (\boldsymbol{z}Z_0^{-1} - \boldsymbol{1})(\boldsymbol{z}Z_0^{-1} + \boldsymbol{1})^{-1} \quad . \quad . \quad (30)$$

and expressing $\boldsymbol{s}'$ in terms of $\boldsymbol{p}$ and vice versa,

$$\left.\begin{aligned} \boldsymbol{s}' &= 2[\boldsymbol{1} - Z_gZ_0^{-1} + 2Z_gZ_0^{-1}(\boldsymbol{1} + \boldsymbol{p})^{-1}]^{-1} - \boldsymbol{1} \\ \text{and} \quad \boldsymbol{p} &= 2[\boldsymbol{1} - Z_0Z_g^{-1} + 2Z_0Z_g^{-1}(\boldsymbol{1} + \boldsymbol{s}')^{-1}]^{-1} - \boldsymbol{1} \end{aligned}\right\} \quad (31)$$

It is clear that, if $Z_g = Z_0$, $\boldsymbol{s}' = \boldsymbol{p}$.

In order to relate the above to the conventional scattering matrix, the following normalized quantities are defined:

$$\boldsymbol{v}_r'' \equiv \sqrt{Z_g^{-1}}\boldsymbol{v}_r'; \boldsymbol{v}_i'' \equiv \sqrt{Z_g^{-1}}\boldsymbol{v}_i' \text{ and } \boldsymbol{s}'' \equiv \sqrt{Z_g^{-1}}\boldsymbol{s}'\sqrt{Z_g} \quad (32)$$

where $\sqrt{Z_g}$ is the diagonal matrix with terms $\sqrt{Z_{g1}}$, $\sqrt{Z_{g2}}$, etc. From eqn. (27) it now follows that $\boldsymbol{v}_r'' = \boldsymbol{s}''\boldsymbol{v}_i''$. Now if $Z_g = R_g$, i.e. if the terms of $\boldsymbol{Z}_g$ are all real, then $\boldsymbol{s}''$ becomes the conventional scattering matrix $\boldsymbol{s}$.

It is clear that, analogous to $\boldsymbol{s}''$, normalized quantities may be defined for the $\boldsymbol{p}$ matrix:

$$\boldsymbol{v}_r' \equiv \sqrt{Z_0^{-1}}\boldsymbol{v}_r; \boldsymbol{v}_i' \equiv \sqrt{Z_0^{-1}}\boldsymbol{v}_i \text{ and } \boldsymbol{p}' \equiv \sqrt{Z_0^{-1}}\boldsymbol{p}\sqrt{Z_0} \quad (33)$$

Eqns. (29)–(31) also hold for $\boldsymbol{s}''$ and $\boldsymbol{p}'$ provided that $\sqrt{Z_g^{-1}}\boldsymbol{z}\sqrt{Z_g^{-1}}$ and $\sqrt{Z_0^{-1}}\boldsymbol{z}\sqrt{Z_0^{-1}}$ are substituted for $\boldsymbol{z}Z_g^{-1}$ and $\boldsymbol{z}Z_0^{-1}$, respectively. $\boldsymbol{s}''$ reduces to $\boldsymbol{p}'$ for $Z_g = Z_0$.

The properties of the matrix $\boldsymbol{s}$ have been well covered in the literature. Concerning the other matrices mentioned here, however, the following is noted.

(*a*) The $\boldsymbol{s}$ as well as the $\boldsymbol{s}'$, $\boldsymbol{s}''$, $\boldsymbol{p}$ and $\boldsymbol{p}'$ matrices exist for many networks, even though they may not possess a $\boldsymbol{z}$ or $\boldsymbol{y}$ matrix, e.g. ideal transformers. The image impedances of such networks do not have a unique value, so that, for example, in the case of a simple transformer, a value for one port may be assumed and then the value for the other port will follow from the impedance transformation ratio.

(*b*) It follows from eqn. (27) that

$$s'_{11} = \frac{v'_{r1}}{v'_{i1}}$$

and

$$s'_{21} = \frac{v'_{r2}}{v'_{i1}}$$

if $v'_{i2} = 0, v'_{i3} = 0$, etc. The condition that $v'_{i2} = 0, v'_{i3} = 0$, etc., implies that all the generator voltages V_{g2}, V_{g3}, etc., are zero except for V_{g1}. Since v'_{r1} and v'_{i1} are external waves, s'_{11} as well as all other diagonal terms are reflection coefficients of an apparent 2-terminal impedance Z_{in}:

$$s'_{11} = \frac{Z_{in}/Z_{g1} - 1}{Z_{in}/Z_{g2} + 1} \quad . \quad . \quad . \quad . \quad (34a)$$

where Z_{in} is the input impedance of the network at port 1. Also, from eqn. (24), since $v'_{i2} = 0$, then $v'_{r2} = V_2$ and from eqn. (19*b*) it follows that, for image waves ($Z_A = Z_D$), $V'_{f1} = V_g/2$ and therefore $V_{i1} = V_{g1}/2$. Hence,

$$s'_{21} = 2V_2/V_{g1} \quad . \quad . \quad . \quad . \quad . \quad (34b)$$

i.e. s'_{21} is twice the voltage gain between the open-circuit voltage of the generator at port 1 and the load, Z_{g2}, at 2, and similarly for the other non-diagonal terms.

Eqns. (34) and (31) have considerable practical significance in the actual determination of the parameters of a device, since the values of Z_{g1} and Z_{g2} are arbitrary and therefore may conveniently be chosen on practical grounds. For a 4-terminal

network the image parameters as a function of the unnormalized scattering parameters are[12]

$$Z_{01} = Z_{g1}\gamma/T\beta \quad . \quad . \quad . \quad . \quad . \quad . \quad . \quad . \quad (35)$$

$$Z_{02} = Z_{g2}\gamma/T\alpha \quad . \quad . \quad . \quad . \quad . \quad . \quad . \quad . \quad (36)$$

$$p_{12} = -\alpha s'_{12}(T-1)/2 \quad . \quad . \quad . \quad . \quad (37)$$

$$p_{21} = -\beta s'_{21}\beta(T-1)/2 \quad . \quad . \quad . \quad . \quad (38)$$

where

$$T = (\alpha\delta/\alpha\beta)^{1/2}$$

$$\alpha = \frac{(s'_{11}+1)(s'_{22}-1)}{s'_{12}s'_{21}} + 1$$

$$\beta = \frac{(s'_{11}-1)(s'_{22}+1)}{s'_{12}s'_{21}} + 1$$

$$\gamma = \frac{(s'_{11}+1)(s'_{22}+1)}{s'_{12}s'_{21}} - 1$$

and

$$\delta = \frac{(s'_{11}-1)(s'_{22}-1)}{s'_{12}s'_{21}} - 1$$

(*c*) It is easily shown that the diagonal terms of the s'' matrix are the same as those of s' and, of course, also of s if Z_g is real. As regards the other terms of s',

$$|s_{21}|^2 = 4\left|\frac{V_2}{V_{g1}}\right|^2 \frac{R_{g1}}{R_{g2}}$$

which is the available power gain between the two real terminations R_{g1} and R_{g2}.

(*d*) In p the diagonal terms are zero and the other terms, such as p_{21}, correspond to the voltage transfer ratio between ports 1 and 2, when all ports are image matched. In the normalized propagation matrix, p', each term is such that, for example, $|p'_{21}|^2$ is the power gain between ports 1 and 2 providing that all ports are image-matched, and $Z_{01} = R_{01}$, $Z_{02} = R_{02}$, etc., i.e. that the relevant image impedances are real. In the case of complex image impedances, the transformation $p'' = \sqrt{G_0}p\sqrt{G_0^{-1}}$ will yield an image-matched power-gain matrix. A typical term is $|p''_{21}|^2 = |p_{21}|^2 \frac{G_{02}}{G_{01}}$, which is the power gain between ports 1 and 2 under image-matched conditions at all ports. Here, G_0 represents a diagonal matrix with terms G_{01}, G_{02}, etc., where G_{01} is the real part of $1/Z_{01}$, G_{02} is the real part of $1/Z_{02}$, etc.

(*e*) The right-hand side of eqn. (28) presents an alternative method for deriving the z and y parameters given in Table 2 in terms of the internal wave parameters Z_{01}, Z_{02}, p_{21} and p_{12}. It differs from the scattering matrix approach by not requiring the specification of external impedances (Z_{g1}, Z_{g2}, etc.).

(6) TRAVELLING-WAVE FLOW DIAGRAMS

The hypothesis that forward and return waves take different paths in space leads to the visualization of wave flow diagrams recalling Mason's flow diagrams.[13] Here the return wave is the feedback wave, since a network having $p_{12} = 0$ is unilateral. Image waves will be used.

Fig. 3(*a*) symbolizes a path wherein a disturbance is only capable of moving in the direction of the arrow. If a unit wave commences on the left-hand side, it changes in magnitude by a factor p by the time it reaches the right-hand side. Hence Fig. 3(*a*) symbolizes multiplication by p. Fig. 3(*b*) symbolizes a discontinuity which is the junction between two media, 1 and 2. Fig. 3(*c*) symbolizes a wave being reflected from a junction. If a unit incident wave impinges on it the magnitude of the reflected

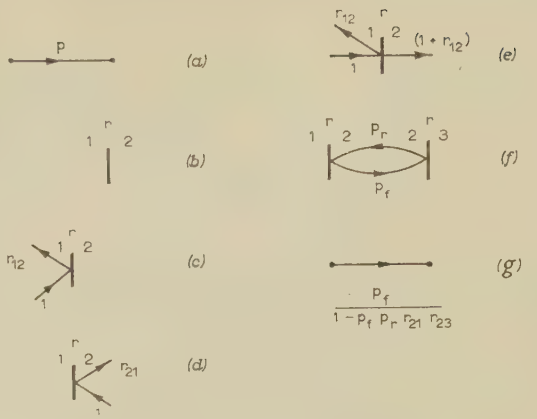

Fig. 3.—Wave flow symbols.

wave is r_{12}. Note that the incident wave is travelling in the direction $1 \rightarrow 2$. Had the incident wave approached the junction from the other side, as in Fig. 3(*d*), the magnitude of the reflected wave would be r_{21}, and $r_{12} = -r_{21}$. Fig. 3(*e*) symbolizes a wave proceeding across the discontinuity from the left. In doing so it is multiplied by $(1 + r_{12})$, i.e. by the sum of the incident and reflected waves.

Fig. 3(*f*) is a closed loop and represents a wave which moves to and fro between two junctions. Thus, a unit wave commencing at any point will, in one complete cycle, be multiplied by $p_f r_{23} p_r r_{21}$. This is defined as the wave loop gain. Over many cycles, the sum of all the waves at a point is found by summing the resulting power series, as in eqn. (17), resulting in $1/(1 - p_f p_r r_{21} r_{23})$, i.e. the denominator consists of unity minus the wave loop gain. A unit wave commencing on the left will have a magnitude $p_f/(1 - p_f p_r r_{21} r_{23})$ by the time it has made all its circulations and finished on the right-hand side, i.e. Fig. 3(*f*) may be replaced by Fig. 3(*g*) as far as its forward transmission properties are concerned.

Let the voltage gain in Fig. 1(*a*) be required, when neither the source nor the load is matched. With reference to Fig. 4(*a*),

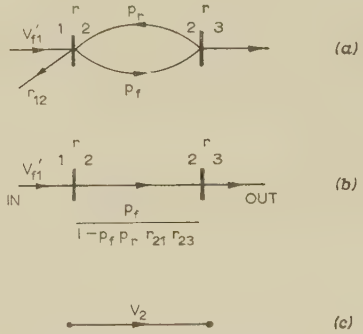

Fig. 4.—Wave flow diagram for single 4-terminal network.

eliminating the loop as before results in Fig. 4(*b*). (The initial reflected wave r_{12} is lost, and is thus ignored.) Using the principles of Figs. 3(*a*), 3(*e*) and 3(*g*), the output voltage is reduced to a line, as shown in Fig. 4(*c*), where

$$V_2 = V'_{f1}(1 + r_{12})\frac{p_f}{1 - p_f p_r r_{21} r_{23}}(1 + r_{23}) \quad . \quad (39)$$

which is identical to eqn. (2) with V_{f1t} from eqn. (17) replacing V_{f1}, as discussed in Section 3. Eqn. (39) yields the voltage gain since $V'_{f1} = V_g/2$.

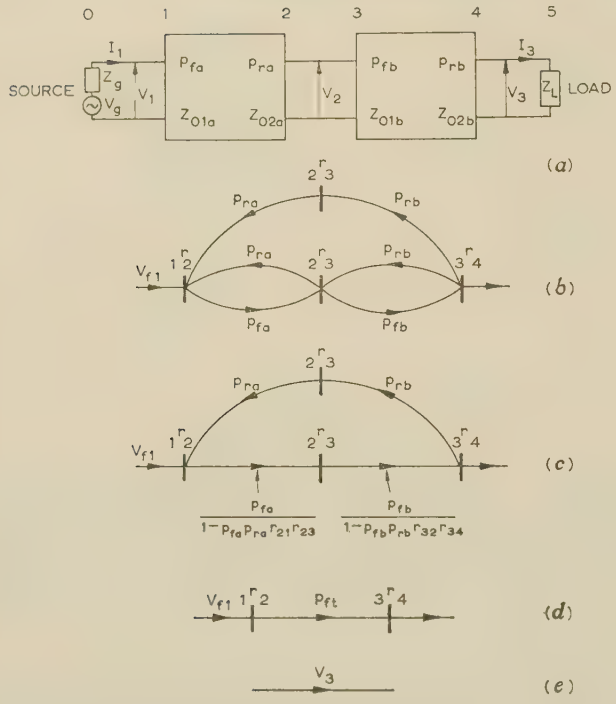

Fig. 5.—Wave flow diagram for a 2-stage cascade network.

Consider now the wave trains in two cascaded stages *a* and *b* as shown in Fig. 5(*a*) and suppose the overall voltage gain is required. It is clear that there will be wave trains set up in network *a*, which will cause wave trains in network *b*, for each wave that arrives at their junction. This is, however, not the complete situation, since the wave trains in network *b* will set up further wave trains in network *a*, for each wave of network *b* that arrives at the junction. With good reason it may be assumed that all the wave trains will be accounted for if one considers that there is one primary wave train in each of the networks and, in addition, there is a secondary wave train whose excursion is the full length of both networks together. Fig. 5(*b*) describes the total situation, where a large loop is introduced to show the secondary wave train. Fig. 5(*c*) now eliminates the two small loops by the method of Fig. 3(*g*). The large loop has now a wave loop gain of

$$G_1 = \frac{p_{fa}(1 + r_{23})}{1 - p_{fa}p_{ra}r_{21}r_{23}} \frac{p_{fb}}{1 - p_{fb}p_{rb}r_{32}r_{34}} r_{34}p_{rb}(1 + r_{32})p_{ra}r_{21}$$

Hence, in Fig. 5(*d*), applying the principles of Fig. 3(*g*).

$$p_{ft} = \frac{\dfrac{p_{fa}}{1 - p_{fa}p_{ra}r_{21}r_{23}}(1 + r_{23})\dfrac{p_{fb}}{1 - p_{fb}p_{rb}r_{32}r_{34}}}{1 - G_1}$$

Using the principle of Fig. 4 results in Fig. 5(*e*). Hence, t voltage gain is, from Fig. 5(*e*),

$$V_3/V_g = V_3/2V'_{f1} = (1 + r_{12})p_{ft}(1 + r_{34})/2 \quad . \quad (4$$

When the interconnection of two ports becomes more co plex, the wave flow diagrams become more involved. Howev it would appear that in any physical situation involving wa flow, provided that the wave trains can be identified, the over effect can systematically be deduced by the use of these wa diagrams.

(7) REFERENCES

(1) SHEA, T. E.: 'Transmission Networks and Wave Filte (Van Nostrand, 1929).
(2) GUILLEMIN, E.: 'Communication Networks' (Wiley, 193 p. 161.
(3) GUILLEMIN, E.: 'Synthesis of Passive Networks' (Chapm and Hall, 1957), p. 190.
(4) TERMAN, F. E.: 'Radio Engineer's Handbook' (McGra Hill, 1943), p. 205.
(5) Scattering Matrix Issue, *Transactions of the Institute Radio Engineers*, June, 1956, **CT–3**.
(6) WHEELER, J. H.: 'On the Mathematical Description of t Light Nuclei by the Method of Resonating Gro Structures', *Physical Review*, 1937, **52**, p. 1107.
(7) BICKLEY, J.: 'Measurement of Transistor Characteris Frequencies in the 20–1000 Mc/s Range', *Proceedin I.E.E.*, Paper No. 3206 M, May, 1960 (**107 B**, p. 301).
(8) GRUBBS, W. J.: 'The Hall Effect Circulator—a Passi Transmission Device', *Proceedings of the Institute Radio Engineers*, 1959, **47**, p. 528.
(9) GUILLEMIN, E.: 'Communication Networks' (Wiley, 193 p. 146.
(10) GUILLEMIN, E.: 'Synthesis of Passive Networks' (Chapm and Hall, 1957), p. 461.
(11) ZAWELS, J.: 'Graphical Methods for Network Desi including Transistor Circuits', *Proceedings I.E.E.*, Pap No. 3116 E, March, 1960 (**106 B**, Suppl. No. 17, p. 110
(12) ZAWELS, J.: 'Determination of Circuit Properties of Fou Poles from the Reflection Plane Diagram' (to be publishe
(13) MASON, S. J.: 'Feedback Theory—Some Properties of Sign Flow Graphs', *Proceedings of the Institute of Rad Engineers*, 1953, **41**, p. 1144.

621—52

The Institution of Electrical Engineers
Monograph No. 426 M
Jan. 1961

OPTIMUM SAMPLED-DATA CONTROL

By R. JACKSON, M.A.

(*The paper was first received* 23rd *July, and in revised form* 6th *October*, 1960. *It was published as an* INSTITUTION MONOGRAPH *in January*, 1961.)

SUMMARY

A method of rendering feedback control systems amenable to treatment by the Wiener theory is applied to the case in which the controller operates on a sampled measurement. An explicit expression is obtained for the minimum attainable mean-square error for certain classes of system transfer functions and disturbance power spectra, and the form of the optimum controller is derived. The results show the inherent limitations in controllability imposed by the structure of the controlled system and by the sampling process.

(1) INTRODUCTION

The Wiener optimum filter theory[2] cannot be applied directly to the problem of the optimum feedback regulator because of difficulties in imposing the condition of physical realizability on the control mechanism to be placed in the feedback loop. However, the closed-loop configuration can always be formally reduced to an equivalent open-loop configuration, and it was recently shown by Price[1] that this can always be done in such a way that the realizability condition takes a simple form in the open-loop case.

Price used this method to investigate the inherent limitations on the attainable control quality imposed by the structure of the controlled system when the controller is allowed to be any linear, continuous device, but a slight modification of the method allows it to be applied to the case in which the controller operates on samples of the measured variable taken at equal intervals of time. In this way it is possible to calculate the best control quality attainable with a linear sampled-data controller of given sampling interval and to derive the form of the optimum controller.

In this paper, the main interest is in the calculation of the best attainable control quality (measured by the mean-square error) and in comparing this with the best control quality obtainable with a continuous controller. This gives a direct measure of the reduction in controllability which must necessarily accompany the loss of information involved in the sampling process. The results have proved useful in estimating the frequency with which automatic batch-analytical instruments on a chemical plant must operate if their signals are to be useful for automatic control.

The type of system to be treated is shown in Fig. 3. A disturbance $d(t)$ causes the controlled quantity $e(t)$ to deviate from its desired value, which is taken as zero for convenience, and the controller operates on samples of $e(t)$ taken at intervals T. Given the fixed element P, the object is to find that physically realizable, linear operation C on the samples $e(rT)$ which will minimize $e^2(t)$, averaged in the manner discussed below over a statistical assembly of disturbances, and to calculate the minimum value of this quantity.

(2) STOCHASTIC SIGNALS IN SAMPLED SYSTEMS

The Wiener theory, as developed by solution of the Wiener–Hopf integral equation, leads to a solution of problems of the above type which minimizes the time average $\langle e^2(t)\rangle$. However, in practice, the ability of the system to reduce this time average for one particular disturbance is of less interest than its ability to keep $e^2(t)$ small, on the average, for all disturbances belonging to some statistically defined assembly. With the usual assumptions that the assembly in question, $\{d(t)\}$, is stationary and ergodic, it follows for continuous systems that the assembly average $\overline{e^2(t)}$ is independent of time t and is equal to the time average $\langle e^2(t)\rangle$ for any member function of the assembly (with the possible exception of a subset of measure zero).

These hypotheses of stationary and ergodic signals throughout the system are not tenable in sampled-data systems, since the result of sampling a stationary, ergodic signal is not stationary and ergodic; in fact, its statistical properties vary periodically with period equal to the sampling interval. There are two different but closely related methods of dealing with this situation. In the first, which is adopted by Ragazzini and Franklin,[3] the assembly considered is enlarged by considering an assembly of systems (as well as disturbances) which are physically identical but have their set of sampling instants displaced in a random manner relative to each other. The complete assembly of outputs, generated by all the signals of the assembly of disturbances applied to all these systems of identical structure, is stationary and ergodic if the assembly of disturbances was stationary and ergodic. Alternatively, it is not difficult to show that, if the assembly of functions $\{y(t)\}$ is generated from the stationary ergodic assembly $\{x(t)\}$ by any linear sampled-data filter, then

$$\langle y^2(t)\rangle = \frac{1}{T}\int_{-T/2}^{+T/2} \overline{y^2(t)}dt \quad . \quad . \quad . \quad . \quad . \quad (1)$$

Thus the Wiener theory, which minimizes $\langle y^2(t)\rangle$, will lead to a system which minimizes the assembly average $\overline{y^2(t)}$, further averaged with respect to time over a sampling interval, and it is in this sense that the control systems discussed here are optimum systems.

(3) REPRESENTATION OF LINEAR SAMPLED-DATA FILTERS

A linear sampled-data filter is a device which linearly relates an output function of time, $y(t)$, to values of an input function, $x(t)$, at the sampling instants $t = rT$. Thus

$$y(t) = \sum_{r=-\infty}^{+\infty} h(t - rT)x(rT) \quad . \quad . \quad . \quad . \quad (2)$$

where $h(u)$ is a function characterizing the particular filter considered. In a physically realizable system, $h(u) = 0$ for $u < 0$.

Filters of this type may be represented by shaded blocks [Fig. 1(*a*)] to distinguish them from continuous filters, which are normally represented by unshaded blocks. An alternative representation may be obtained by considering a continuous filter with weighting function $k(u) \equiv h(u)$ and input consisting of the following sequences of delta functions:

$$x^*(t) = \sum_{r=-\infty}^{+\infty} x(rT)\delta(t - rT) \quad . \quad . \quad . \quad . \quad (3)$$

Correspondence on Monographs is invited for consideration with a view to publication.

Mr. Jackson is with Imperial Chemical Industries, Ltd., Billingham Division.

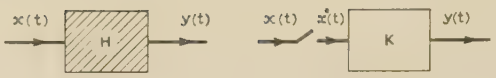

(a) (b)

Fig. 1.—Sampled-data filters.

Then

$$y(t) = \int_0^{\infty} k(u)x^*(t-u)du = \sum_{r=-\infty}^{+\infty} x(rT)\int_0^{\infty} k(u)\delta(t-u-rT)du$$

or

$$y(t) = \sum_{r=-\infty}^{+\infty} k(t-rT)x(rT) \quad . \quad . \quad . \quad . \quad (4)$$

which is identical with eqn. (2) since $k(t-rT) = h(t-rT)$. This arrangement may be represented in a block diagram as shown in Fig. 1(*b*). It is clear from this discussion that every sampled-data filter may be represented in this form and it is often convenient to do so; nevertheless some caution must be used in discussing the behaviour of this representation. In general, the division into a sampler and a continuous linear filter does not correspond to any physical division in the actual filter, and, in particular, no attempt must be made to discuss the response of K to a continuous input at the point x^*. Even if the sampled-data filter may be physically divided into a sampler and a subsequent filter, this filter need not be identical with the continuous filter K.

As an example, consider a system with the structure shown in Fig. 2(*b*). The relation between $x(t)$ and $y(t)$ is clearly linear if

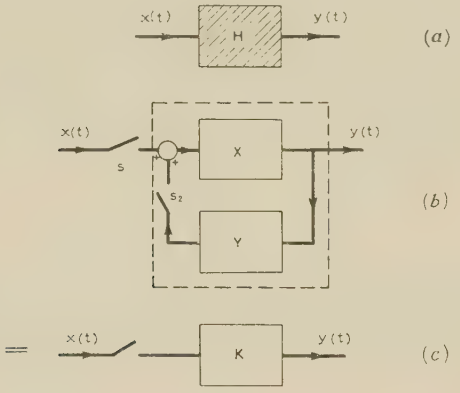

Fig. 2.—Filters with equivalent input-output relations.

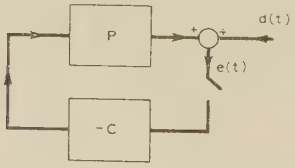

Fig. 3.—Sampled-data controller.

the filters X and Y are linear, and the presence of the sampler S_1 ensures that $y(t)$ can depend only on the values of $x(t)$ at the sampling instants. Thus the system is a linear sampled-data filter according to the definition given at the beginning of this Section and, as shown in eqn. (4), it is certainly possible to find a system of the form shown in Fig. 2(*c*) which will give an equivalent relation between $x(t)$ and $y(t)$, where K is a suitably chosen continuous linear filter. Although the relation between $x(t)$ and $y(t)$ is unaltered by replacing the contents of the dotted boundary in Fig. 2(*b*) by the continuous filter K of Fig. 2(c this does not, of course, mean that K and the contents the dotted boundary have identical dynamical properties. Th are only known to have the same effect on the special class inputs which consist of a sequence of delta-function impuls synchronized with the sampling instants of the samplers and S_2.

(4) CORRELATION FUNCTIONS AND SPECTRA IN SAMPLED-DATA SYSTEMS

Various auto- and cross-correlation functions and the cor sponding spectral densities will be required for the sampled-da filter shown in Fig. 1(*b*). These are given by Ragazzini a Franklin[3] and are listed below, with a complete derivation one case to illustrate the method.

The cross-correlation function, Φ_{ab}, of two functions $a(t)$ a $b(t)$ will be defined by

$$\Phi_{ab}(u) = \lim_{T_0\to\infty} \frac{1}{2T_0}\int_{-T_0}^{+T_0} a(t)b(t+u)dt = \langle a(t)b(t+u)\rangle \quad .$$

and since the functions are assumed to be members of a statio ergodic random process, the time average could be replace an assembly average if desired. When $b(t) \equiv a(t)$, the functi $\Phi_{aa}(u)$ is known as the auto-correlation function of $a(t)$. T cross spectral density, $S_{ab}(s)$, of $a(t)$ and $b(t)$ is defined as Fourier transform of $\Phi_{ab}(u)$, i.e.

$$\left.\begin{aligned} S_{ab}(s) &= \int_{-\infty}^{+\infty} \Phi_{ab}(u)\varepsilon^{-j\omega u}du \qquad \text{for } s = j\omega \\ &= \text{analytic continuation for other values of } s \end{aligned}\right\} .$$

and when $b(t) \equiv a(t)$, the corresponding function $S_{aa}(s)$ is call the power spectrum of $a(t)$. Corresponding to eqn. (6). course, is the inverse transform

$$\Phi_{ab}(u) = \frac{1}{2\pi j}\int_{-j\infty}^{+j\infty} S_{ab}(s)\varepsilon^{su}ds$$

The required relations for the system of Fig. 1(*b*) will now dealt with in turn; the complete derivation given of result typifies the methods used in handling sampled time series.

(i) For the system in Fig. 1(*b*),

$$y(t) = \int_{-\infty}^{+\infty} k(u)x^*(t-u)du \quad [k(u) = 0 \text{ for } u < 0] \quad .$$

$$x^*(t) = \sum_{r=-\infty}^{+\infty} x(rT)\delta(t-rT) \quad . \quad . \quad . \quad .$$

(ii) Since K is a continuous filter, the output spectral dens and the cross spectral density of input and output are given the well-known relations[4]

$$S_{yy}(s) = K(s)K(-s)S_{x^*x^*}(s) \quad . \quad . \quad . \quad .$$

$$S_{x^*y}(s) = K(s)S_{x^*x^*}(s) = S_{yx^*}(-s) \quad . \quad . \quad (1$$

(iii) As shown by Ragazzini and Franklin,[3] the auto-corre tion function and corresponding spectral density of $x^*(t)$ given by

$$\Phi_{x^*x^*}(u) = \frac{1}{T}\sum_{r=-\infty}^{+\infty} \Phi_{xx}(rT)\delta(u-rT) \quad . \quad . \quad (1$$

$$S_{x_*x_*}(j\omega) = \frac{1}{T}\sum_{r=-\infty}^{+\infty} \Phi_{xx}(rT)\varepsilon^{-j\omega rT} \quad . \quad . \quad . \quad (1$$

(iv) Finally, the cross-correlation function and cross spect

density for $x(t)$ and $y(t)$ will be derived as an illustration of the methods used.

From the definition given in eqn. (5), by splitting the range of integration into segments of length T, we obtain

$$\Phi_{xy}(u) = \lim_{N\to\infty} \frac{1}{(2N+1)T} \sum_{n=-N}^{+N} \int_{(n-\frac{1}{2})T}^{(n+\frac{1}{2})T} x(t)\,y(t+u)dt$$

$$= \lim_{N\to\infty} \frac{1}{(2N+1)T} \sum_{n=-N}^{+N} \int_{(n-\frac{1}{2})T}^{(n+\frac{1}{2})T} x(t-u)\,y(t)dt$$

Substituting for $y(t)$ from eqn. (2) gives

$$\Phi_{xy}(u) = \lim_{N\to\infty} \frac{1}{(2N+1)T} \times \sum_{n=-N}^{+N} \int_{(n-\frac{1}{2})T}^{(n+\frac{1}{2})T} x(t-u) \sum_{r=-\infty}^{+\infty} k(t-rT)x(rT)dt$$

or

$$\Phi_{xy}(u) = \lim_{N\to\infty} \frac{1}{(2N+1)T} \times \sum_{n=-N}^{+N} \int_{(n-\frac{1}{2})T}^{(n+\frac{1}{2})T} \sum_{r=-\infty}^{+\infty} x(t-u)x(rT+nT)k(t-rT-nT)dt$$

Now put $v = t - nT$, which reduces the above to

$$\Phi_{xy}(u) = \lim_{N\to\infty} \frac{1}{(2N+1)T} \times \sum_{n=-N}^{+N} \int_{-\frac{1}{2}T}^{+\frac{1}{2}T} \sum_{r=-\infty}^{+\infty} k(v-rT)x(rT+nT)x(v-u+nT)dv$$

$$= \frac{1}{T} \sum_{r=-\infty}^{+\infty} \int_{-\frac{1}{2}T}^{+\frac{1}{2}T} k(v-rT) \times \left[\lim_{N\to\infty} \frac{1}{(2N+1)} \sum_{n=-N}^{+N} x(rT+nT)x(v-u+nT)\right]dv$$

and it may be proved that, when $x(t)$ is stationary and ergodic,

$$\lim_{N\to\infty} \frac{1}{(2N+1)} \sum_{n=-N}^{+N} x(nT)x(nT+t) = \Phi_{xx}(t) \text{ (exactly)}$$

Using this result, the expression for $\Phi_{xy}(u)$ becomes

$$\Phi_{xy}(u) = \frac{1}{T} \sum_{r=-\infty}^{+\infty} \int_{-\frac{1}{2}T}^{+\frac{1}{2}T} k(v-rT)\Phi_{xx}(v-u-rT)dv$$

$$= \frac{1}{T} \int_{-\infty}^{+\infty} k(w)\Phi_{xx}(w-u)dw \text{ (say)}$$

since Φ_{xx} is an even function of its argument, this reduces finally to

$$\Phi_{xy}(u) = \frac{1}{T} \int_{-\infty}^{+\infty} k(w)\Phi_{xx}(u-w)dw \quad . \quad . \quad . \quad (13)$$

and correspondingly,

$$S_{xy}(s) = \frac{1}{T}K(s)S_{xx}(s) = S_{yx}(-s) \quad . \quad . \quad . \quad (14)$$

This completes the set of spectrum relations which will be needed, but before leaving this topic it is worth defining two operations on spectra which will be required in the discussion of the Wiener optimum controller.

A power spectrum, $S_{aa}(s)$, is said to be *Wiener-factorizable* if it is possible to write

$$S_{aa}(s) = S^1_{aa}(s)S^2_{aa}(s) \quad . \quad . \quad . \quad . \quad . \quad (15)$$

where $S^1_{aa}(s)$ has all the zeros and singularities of $S_{aa}(s)$ in the left half-plane and is free from zeros and singularities in the right half-plane, while $S^2_{aa}(s)$ has all the zeros and singularities of $S_{aa}(s)$ in the right half-plane and is free from them in the left half-plane.

The decomposition of a function, $F(s)$, of the complex variable s given by

$$F(s) = [F(s)]_+ + [F(s)]_- \quad . \quad . \quad . \quad . \quad (16)$$

will also be important, where

$$[F(s)]_+ = \frac{1}{2\pi j}\int_0^\infty \varepsilon^{-j\omega t}\left[\int_{-\infty}^{+\infty} F(ju)\varepsilon^{jut}du\right]dt \text{ for } s = j\omega$$
$$= \text{analytic continuation} \quad \text{for } s \neq j\omega \quad . \quad (17)$$

$[F(s)]_+$ is then analytic and bounded in the right half-plane, while $[F(s)]_-$ is analytic and bounded in the left half-plane.

(5) A REARRANGEMENT ANALOGOUS TO PRICE'S METHOD FOR CONTINUOUS SYSTEMS

Returning now to the basic sampled-data regulator of Fig. 3, the block diagrams shown in Fig. 4(*a*) represent systems which give the same relation between $e(t)$ and $d(t)$. C_1 is physically realizable because it is constructed by physical interconnection of the two physically realizable blocks P and C, and so to every system of type A [Fig. 4(*a*)] there corresponds a physically realizable system of type B. The truth of the converse follows in the same way from the second sequence of equivalent systems given in Fig. 4(*b*), so arrangements A and B are completely equivalent so far as the relation between $e(t)$ and $d(t)$ is concerned.

From Fig. 4(*b*) it might appear that even the best C_1 would only correspond to the best C of a particular class of sampled-data filters with a sampler in the feedback loop. However, in view of the remarks in Section 3, this is not the case, and the equivalent C gives the optimum controller for the conventional arrangement represented by A in the class of all linear sampled-data filters.

Having established the equivalence of arrangements A and B, it is now possible to proceed to find the optimum linear C_1 which minimizes $\langle e^2 \rangle$. This can quite easily be done after re-drawing B in the equivalent form shown in Fig. 5. It is permissible to invert the order of the blocks P and C_1, as shown, since each is a continuous linear filter.

(6) OPTIMUM C_1 AND MINIMUM MEAN-SQUARE ERROR

The C_1 which minimizes $\langle e^2 \rangle$ follows immediately from the arrangement shown in Fig. 5 using the conventional Wiener theory:

$$C_1(s) = \frac{1}{S^1_{gg}(s)}\left[\frac{S_{gd}(s)}{S^2_{gg}(s)}\right]_+ \quad . \quad . \quad . \quad . \quad (18)$$

where $S^1_{gg}(s)$ and $S^2_{gg}(s)$ are the Wiener factors of $S_{gg}(s)$ (assuming this is factorizable); the notation $[F(s)]_+$ has been explained in Section 4.

The various terms in eqn. (18) will now be evaluated for the system shown in Fig. 5. The following relations arise from the results given in Section 4:

$$S_{gd}(s) = \frac{1}{T}P(-s)S_{dd}(s) \quad . \quad . \quad . \quad . \quad (19)$$

$$S_{gg}(s) = P(s)P(-s)S_{d^*d^*}(s) \quad . \quad . \quad . \quad (20)$$

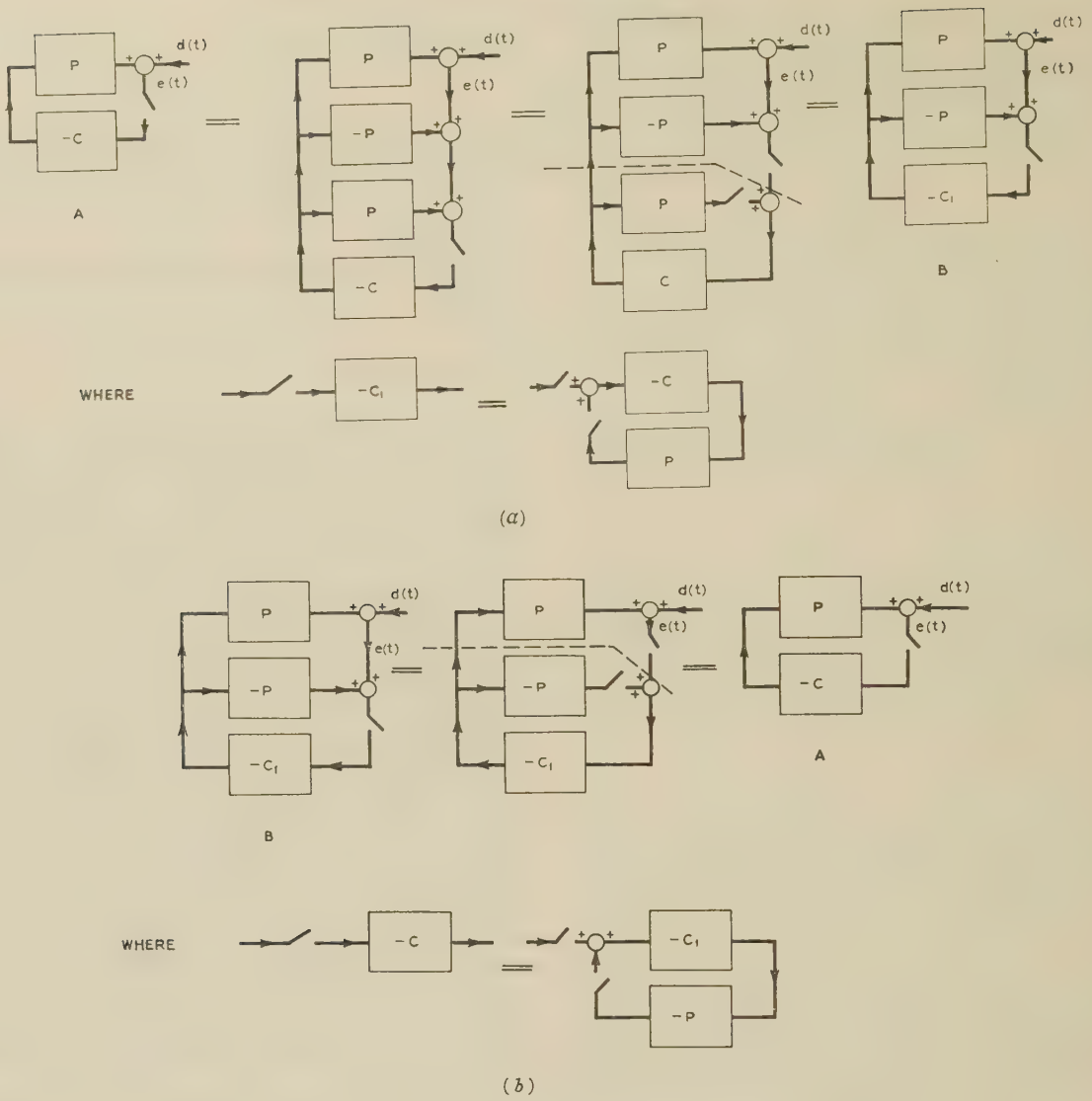

Fig. 4.—Block diagrams of equivalent arrangements.
(*a*) Relation of C_1 to C.
(*b*) Relation of C to C_1.

Attention will be restricted to stable transfer functions $P(s)$ of the form

$$P(s) = P^1(s)P^2(s)\varepsilon^{-s\tau} \quad . \quad . \quad . \quad . \quad . \quad (21)$$

where $P(s)\varepsilon^{s\tau}$ is a rational function, and $P^1(s)$ and $P^2(s)$ have the properties of Wiener factors. Then

$$S_{gd}(s) = \frac{1}{T}P^1(-s)P^2(-s)\varepsilon^{s\tau}S_{dd}(s) \quad . \quad . \quad . \quad (22)$$

$$S^1_{gg}(s) = P^1(s)P^2(-s)S^1_{d^*d^*}(s) \quad . \quad . \quad . \quad . \quad (23)$$

$$S^2_{gg}(s) = P^1(-s)P^2(s)S^2_{d^*d^*}(s) \quad . \quad . \quad . \quad . \quad (24)$$

Substituting these in eqn. (18) gives the optimum $C_1(s)$ in the form

$$C_1(s) = \frac{1}{P^1(s)P^2(-s)S^1_{d^*d^*}(s)}\left[\frac{\varepsilon^{s\tau}}{T}\frac{P^2(-s)}{P^2(s)}\frac{S_{dd}(s)}{S^2_{d^*d^*}(s)}\right]_+ \quad . \quad (25)$$

All the quantities appearing in this are known, so it gives the

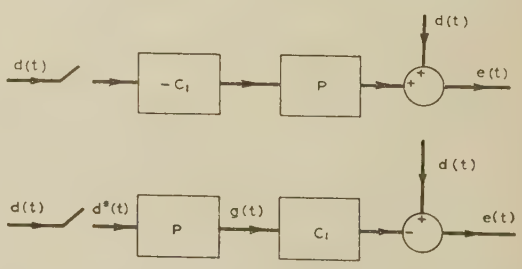

Fig. 5.—Open-loop configuration for control system.

desired solution of the problem. It will be convenient also to have the result in the slightly rearranged form

$$C_1(s) = \frac{1}{P^1(s)P^2(-s)S^1_{dd}(s)} \times \frac{1}{S^1_{d^*d^*}(s)} \times S^1_{dd}(s) \times \left[\frac{\varepsilon^{s\tau}}{S^1_{dd}(s)}\frac{P^2(-s)S^1_{dd}(s)}{P^2(s)}\frac{1}{T}\frac{S_{dd}(s)}{S^2_{d^*d^*}(s)}\right]_+ \quad . \quad (

Notice that, when $P(s) \equiv 1$, $C_1(s)$ becomes simply the optimum filter for reconstructing $d(t)$ from the sampled signal $d^*(t)$. Denoting this by $C_{1r}(s)$, eqn. (25) gives

$$C_{1r}(s) = \frac{1}{S^1_{d^*d^*}(s)}\left[\frac{1}{T}\frac{S_{dd}(s)}{S^2_{d^*d^*}(s)}\right]_+ \quad . \quad . \quad . \quad (27)$$

These results should be compared with Price's optimum $C_1(s)$ for the continuous case, which will be denoted by $C_{1c}(s)$:

$$C_{1c}(s) = \frac{1}{P^1(s)P^2(-s)S^1_{dd}(s)}\left[\frac{P^2(-s)S^1_{dd}(s)\varepsilon^{s\tau}}{P^2(s)}\right]_+ \quad . \quad (28)$$

Comparing eqns. (27) and (28) with eqn. (26) it is seen that the optimum $C_1(s)$ for the sampled-data case is Price's optimum continuous $C_{1c}(s)$ in series with the optimum data reconstruction filter if, and only if,

$$\left[\frac{1}{S^1_{dd}(s)}\frac{P^2(-s)S^1_{dd}(s)\varepsilon^{s\tau}}{P^2(s)}\frac{1}{T}\frac{S_{dd}(s)}{S^2_{d^*d^*}(s)}\right]_+ \equiv \frac{1}{S^1_{dd}(s)} \times \left[\frac{P^2(-s)S^1_{dd}(s)\varepsilon^{s\tau}}{P^2(s)}\right]_+ \times \left[\frac{1}{T}\frac{S_{dd}(s)}{S^2_{d^*d^*}(s)}\right]_+ \quad . \quad (29)$$

One obvious case in which this factorization is valid arises when $P(s)$ is minimum phase, in which case $\tau = 0$, $P^1(s) \equiv P(s)$ and $P^2(s) \equiv 1$; other cases will be discussed later.

Having obtained the optimum $C_1(s)$, it is of direct interest to calculate the corresponding value of the mean-square error. The power spectrum of $e(t)$ is

$$S_{ee}(s) = S_{dd}(s) - \frac{1}{T}P(s)C_1(s)S_{dd}(s) - \frac{1}{T}P(-s)C_1(-s)S_{dd}(s) + C_1(s)C_1(-s)P(s)P(-s)S_{d^*d^*}(s) \quad . \quad (30)$$

from which $\langle e^2 \rangle$ can be obtained using

$$\langle e^2 \rangle = \frac{1}{2\pi j}\int_{-j\infty}^{+j\infty} S_{ee}(s)ds \quad . \quad . \quad . \quad . \quad . \quad (31)$$

Although the method used here gives the form of the optimum filter $C_1(s)$ directly, the form of the optimum $C(s)$ is of greater interest for the purpose of synthesizing an approximate optimum controller. From consideration of the block diagram in Fig. 4(*b*) showing the relation between C and C_1, it follows in a straightforward manner that

$$C(s) = \frac{C_1(s)}{[1 - PC_1(z)]_{z=\varepsilon^{s\tau}}} \quad . \quad . \quad . \quad . \quad (32)$$

where $PC_1(z)$ is the z-transform[3] corresponding to the Laplace transform $P(s)C_1(s)$. The explicit form of $C(s)$ for a particular simple system is given in Section 9.

(7) OPTIMUM CONTROLLER FOR A CLASS OF DISTURBANCE SPECTRA

$C_1(s)$ and $\langle e^2 \rangle$ will be evaluated for a particular but very extensive class of disturbance spectra.

Laning and Battin[4] show that any bounded auto-correlation function, the square of whose magnitude is integrable over the infinite interval, can be approximated in the mean by a sequence of terms of the form $A_k\varepsilon^{-c_k|u|}$ with $c_k > 0$. Thus any auto-correlation function likely to be of interest can be approximated arbitrarily closely, for the purpose of computing mean-square errors, by a sum of the form

$$\Phi_{dd}(u) = \sum_{k=1}^{n} A_k\varepsilon^{-c_k|u|} \quad . \quad . \quad . \quad . \quad (33)$$

If $S_{dd}(s)$ is the power spectrum corresponding to $\Phi_{dd}(u)$, and $S_{d^*d^*}(s)$ the spectral density of the corresponding sampled signal, using eqns. (6), (11) and (12) it is not difficult to show that

$$S_{dd}(s) = \sum_{k=1}^{n} \frac{2A_kc_k}{c_k^2 - s^2} \quad . \quad . \quad . \quad . \quad (34)$$

and that

$$S_{d^*d^*}(s) = \frac{1}{T}\sum_{k=1}^{n} \frac{A_k(1 - \varepsilon^{-2c_kT})}{(1 - \varepsilon^{-c_kT}\varepsilon^{-sT})(1 - \varepsilon^{-c_kT}\varepsilon^{sT})} \quad . \quad (35)$$

Eqn. (25) for $C_1(s)$ will now be evaluated for spectra of this particular form. Paying attention first to the square bracket on the right-hand side of eqn. (25), and denoting its contents by $F(s)$, it follows from eqns. (16) and (17) that it is possible to write

$$[F(s)]_+ = \int_0^\infty f(t)\varepsilon^{-st}dt \text{ with } s = j\omega$$

where

$$f(t) = \frac{1}{2\pi j}\int_{-j\infty}^{+j\infty} F(s)\varepsilon^{st}ds$$

When $S_{dd}(s)$ and $S_{d^*d^*}(s)$ are given by eqns. (34) and (35), inspection of the form taken by $F(s)$ shows that, in evaluating $f(t)$, the integration contour may be closed by a large semicircle in the left half-plane when $t > 0$, so that

$$f(t) = \sum \text{res}\,[F(s)\varepsilon^{st}] \quad (\text{for } t > 0) \quad . \quad . \quad . \quad (36)$$

the sum of the residues being taken over all poles of $F(s)\varepsilon^{st}$ in the left half-plane. The factors $P^2(s)$ and $S^2_{d^*d^*}(s)$ which appear in the denominator of $F(s)$ have, by definition, no zeros in the left half-plane, while the possibility of $P^2(-s)$ having singularities in the left half-plane is excluded by the fact that attention is limited to stable transfer functions $P(s)$. Thus, the only singularities of $F(s)\varepsilon^{st}$ in the left half-plane are the simple poles of $S_{dd}(s)$ at $s = -c_k$, and eqn. (36) may be evaluated immediately:

$$f(t) = \sum_{k=1}^{n} \frac{\varepsilon^{-c_k\tau}}{T}\frac{P^2(c_k)}{P^2(-c_k)}\frac{\varepsilon^{-c_kt}}{S^2_{d^*d^*}(-c_k)} \lim_{s\to -c_k}[(s + c_k)S_{dd}(s)]$$

or

$$f(t) = \frac{1}{T}\sum_{k=1}^{n} \varepsilon^{-c_k\tau}\frac{P^2(c_k)}{P^2(-c_k)}\frac{\varepsilon^{-c_kt}}{S^2_{d^*d^*}(-c_k)}A_k \quad (\text{for } t > 0)$$

whence

$$[F(s)]_+ = \frac{1}{T}\sum_{k=1}^{n} \frac{P^2(c_k)}{P^2(-c_k)}\frac{A_k\varepsilon^{-c_k\tau}}{S^2_{d^*d^*}(-c_k)}\frac{1}{s + c_k}$$

and the optimum $C_1(s)$ then follows from eqn. (25) as

$$C_1(s) = \frac{1}{P^1(s)P^2(-s)S^1_{d^*d^*}(s)}\frac{1}{T}\sum_{k=1}^{n} \frac{P^2(c_k)}{P^2(-c_k)}\frac{A_k\varepsilon^{-c_k\tau}}{S^2_{d^*d^*}(-c_k)}\frac{1}{s + c_k} \quad . \quad . \quad . \quad . \quad (37)$$

Since the following combination of factors will occur frequently from now on, it will be convenient to define

$$Q(A_k, c_k) = Q_k = \frac{1}{T}\frac{P^2(c_k)}{P^2(-c_k)}\frac{A_k\varepsilon^{-c_k\tau}}{S^2_{d^*d^*}(-c_k)} \quad . \quad (38)$$

when eqn. (37) takes the form

$$C_1(s) = \frac{1}{P^1(s)P^2(-s)S^1_{d^*d^*}(s)}\sum_{k=1}^{n} \frac{Q_k}{s + c_k} \quad . \quad . \quad (39)$$

The main difficulty in handling this when $n > 1$ is the cumbersome algebraic form of the factors $S^1_{d^*d^*}(s)$ and $S^2_{d^*d^*}(s)$ when written out explicitly.

Before going on to deal with the mean-square error, however, it is interesting to consider some special results which hold for $n = 1$. In this particular case, eqn. (37) becomes

$$C_1(s) = \frac{1}{P^1(s)P^2(-s)S^1_{d^*d^*}(s)} \frac{1}{T} \frac{P^2(c)}{P^2(-c)} \frac{A\varepsilon^{-c\tau}}{S^2_{d^*d^*}(-c)} \frac{1}{s+c} \quad . \quad (40)$$

(where $c = c_1$) while, from eqn. (27), the optimum data-reconstruction filter is

$$C_{1r} = \frac{1}{S^1_{d^*d^*}(s)} \frac{1}{T} \frac{A}{S^2_{d^*d^*}(-c)} \frac{1}{s+c} \quad . \quad . \quad . \quad (41)$$

Since $S_{dd}(s) = 2Ac/(c^2 - s^2)$ in this case, the right-hand side of eqn. (28) can easily be evaluated, and the optimum continuous controller is

$$C_{1c} = \frac{1}{P^1(s)P^2(-s)} \frac{P^2(c)}{P^2(-c)} \varepsilon^{-c\tau} \quad . \quad . \quad . \quad (42)$$

Comparison of eqns. (41) and (42) with eqn. (40) shows immediately that

$$C_1(s) = C_{1r}(s)C_{1c}(s)$$

so again we have the result that the optimum sampled-data C_1 is equivalent to the optimum continuous C_{1c} in series with the optimum data reconstruction filter C_{1r}. This may also be proved by checking directly that the factorization condition, eqn. (29), is satisfied. It should be noted that, although this attractively simple result is valid for this very popular spectrum, it does not appear to be generally true when $n > 1$.

(8) MINIMUM MEAN-SQUARE ERROR

Returning now to the general case, $n > 1$, the minimum attainable value of $\langle e^2 \rangle$ is calculated by using eqns. (30) and (31) with $C_1(s)$ given by eqn. (39). The terms in eqn. (30) can be integrated separately, the first giving immediately

$$\frac{1}{2\pi j}\int_{-j\infty}^{+j\infty} S_{dd}(s)ds = \sum_{k=1}^{n} A_k \quad . \quad . \quad . \quad . \quad . \quad (43)$$

Considering the second term of eqn. (30), it is necessary to evaluate the contribution to eqn. (31) from

$$\frac{1}{T}P(s)C_1(s)S_{da}(s) = \frac{1}{T} \frac{P^1(s)P^2(s)\varepsilon^{-s\tau}}{P^1(s)P^2(-s)S^1_{d^*d^*}(s)} \times \sum_{k=1}^{n} \frac{Q_k}{s+c_k} \times \sum_{l=1}^{n} A_l\left(\frac{1}{c_l+s} + \frac{1}{c_l-s}\right) \quad . \quad (44)$$

Now $S^1_{d^*d^*}$ has the form

$$\frac{N(s)}{\prod_{k=1}^{n}(1 - \varepsilon^{c_k T}\varepsilon^{-sT})}$$

where $N(s)$ is a polynominal in ε^{-sT} of degree not exceeding $n-1$. Thus $1/S^1_{d^*d^*}(s)$ remains bounded when $|s| \to \infty$ provided that $\mathscr{R}(s) > 0$, and it is seen that every term of eqn. (44) tends to zero faster than $1/|s|$ when $|s| \to \infty$ with $\mathscr{R}(s) > 0$. The contour of integration in eqn. (31) may therefore be closed by a large semicircle in the right half-plane; it is then necessary to remember that the closed contour is described in a negative sense. The only poles of the integrand in eqn. (44) in the right half-plane are at $s = c_l$, and they are simple, so the residues can be obtained by multiplying through by $s - c_l$ and letting $s \to c_l$, with the result

$$\frac{1}{2\pi jT}\int_{-j\infty}^{+j\infty} P(s)C_1(s)S_{dd}(s)ds = \frac{1}{T}\sum_{l=1}^{n} \frac{A_l}{S^1_{d^*d^*}(c_l)} \frac{P^2(c_l)}{P^2(-c_l)}\varepsilon^{-c_l\tau} \sum_{k=1}^{n} \frac{Q_k}{c_k + c_l} \quad . \quad (4$$

In a similar way, by closing the contour with a semicircle the left half-plane, it can be shown that the same contributi is obtained from the third term of eqn. (30).

When written out fully the contribution from the last term eqn. (30) arises from the integrand

$$\frac{1}{S^1_{d^*d^*}(s)S^1_{d^*d^*}(-s)} \sum_{k=1}^{n} \frac{Q_k}{c_k + s} \sum_{l=1}^{n} \frac{Q_l}{c_l - s} S_{d^*d^*}(s) \quad . \quad (4$$

Now $$S_{d^*d^*}(s) = S^1_{d^*d^*}(s)S^2_{d^*d^*}(s)$$

while $$S_{d^*d^*}(-s) = S^1_{d^*d^*}(-s)S^2_{d^*d^*}(-s) = S_{d^*d^*}(s)$$

since $S_{d^*d^*}(s)$ is even. Further, $S^1_{d^*d^*}(-s)$ has all its poles a zeros in the right half-plane, while $S^2_{d^*d^*}(-s)$ has all its pol and zeros in the left half-plane. $S^1_{d^*d^*}(-s)$ and $S^2_{d^*d^*}(-s)$ c therefore differ only by constant factors from $S^2_{d^*d^*}(s)$ a $S^1_{d^*d^*}(s)$ respectively, and the factorization can be carried out such a way that $S^1_{d^*d^*}(-s) = S^2_{d^*d^*}(s)$. Introducing this in integrand (46), the first and last factors cancel. The contrib tion to eqn. (31) may then be evaluated by closing the cont with a semicircle in either half-plane. Choosing a semicirc in the left half-plane, the contour is described in a positive sen and it is only necessary to sum the residues at the poles $s = -c_k$, with the result

$$\sum_{k=1}^{n}\sum_{l=1}^{n} \frac{Q_kQ_l}{c_k + c_l} \quad . \quad . \quad . \quad . \quad . \quad . \quad (4$$

which is seen to be identical with eqn. (45), remembering th $S^2_{d^*d^*}(-c_l) = S^1_{d^*d^*}(c_l)$ with the present choice of factorization

Collecting together the terms contributing to eqn. (31) gives

$$\langle e^2 \rangle = \sum_{k=1}^{n} A_k - \sum_{k=1}^{n}\sum_{l=1}^{n} \frac{Q_kQ_l}{c_k + c_l} \quad . \quad . \quad . \quad (4$$

When the system is without control, $\langle e^2 \rangle = \langle e^2 \rangle_0 = \langle d^2 \rangle$ $\sum_{k=1}^{n} A_k$, so that the mimimum attainable value of $\langle e^2 \rangle / \langle e^2 \rangle_0$ given by

$$\xi = \min \frac{\langle e^2 \rangle}{\langle e^2 \rangle_0} = 1 - \frac{1}{T^2 \sum_{k=1}^{n} A_k} \sum_{k=1}^{n}\sum_{l=1}^{n} \frac{A_kA_l}{S^1_{d^*d^*}(c_k)S^1_{d^*d^*}(c_l)} \times \frac{P^2(c_k)}{P^2(-c_k)} \frac{P^2(c_l)}{P^2(-c_l)} \times \frac{\varepsilon^{-(c_k+c_l)\tau}}{c_k + c_l} \quad . \quad (4$$

where the explicit forms of Q_k and Q_l have been re-introduce and it is assumed that the factorization is carried out in such way that $S^1_{d^*d^*}(s) = S^2_{d^*d^*}(-s)$.

As in the case of $C_1(s)$, the greatest difficulty in handling t is the clumsy algebraic form of the factors $S^1_{d^*d^*}(s)$ when $n >$

(9) EVALUATION OF THE RESULTS FOR SIMPLE EXAMPLES

A programme to evaluate the right-hand side of eqn. (49) h been written for a digital computer. This deals with the c where $n = 2$ [i.e. two terms in expression (35) for $S_{d^*d^*}(s)$] a $P^2(s)$ is a polynomial of degree not greater than two. It v used initially to calculate ξ for the system shown in Fig. 6, which the continuous case has been treated by Price.[1]

The plant consists of a transfer lag with unit time-consta

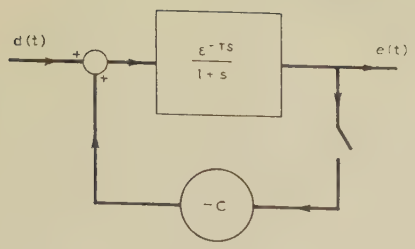

Fig. 6.—System used in illustrative examples.

ogether with a distance-velocity lag, τ, while the disturbance, with spectrum $D(s) = 2c/(c^2 - s^2)$, enters through the plant by he same path as the correction. For the corresponding continuous system, Price obtains the result

$$\left.\begin{aligned} \xi &= 1 - (1 + 2\tau + 2\tau^2)\varepsilon^{-2\tau} && \text{when} \quad c = 1 \\ &= 1 - \frac{2c(1+c)}{(1-c)^2}[\phi(2) - 2\phi(1+c) + \phi(2c)] && \text{when} \quad c \neq 1 \end{aligned}\right\} \quad . \quad (50)$$

where $\phi(x) = \varepsilon^{-\tau x}/x$.

Using the programme described above, corresponding calculations have been carried out for sampled systems with various values of c. The results for $c = 0{\cdot}05$ and for $c = 100$ are recorded in Figs. 7 and 8. Note that:

(i) For fixed values of c and τ, ξ increases with T. This increase is much more rapid for large values of c than for small values.
(ii) For fixed values of c and T, ξ increases with τ and approaches unity as $\tau \to \infty$.

These properties are all as expected intuitively. The curves for $T = 0$ are drawn using Price's formulae above; the convergence of the computed curves to these when T becomes small provides a check on the theory and the programme for the sampled case.

The form of $C(s)$ will also be obtained and compared with the optimum continuous controller for the system shown in Fig. 6, but to avoid unnecessary algebraic complication the disturbance with the spectrum considered above will be replaced by white noise. This affects the measured variable only after passing through the block representing the controlled plant, so

$$S_{dd}(s) = \frac{2}{1 - s^2} \quad \text{and} \quad P(s) = \frac{\varepsilon^{-s\tau}}{1 + s}$$

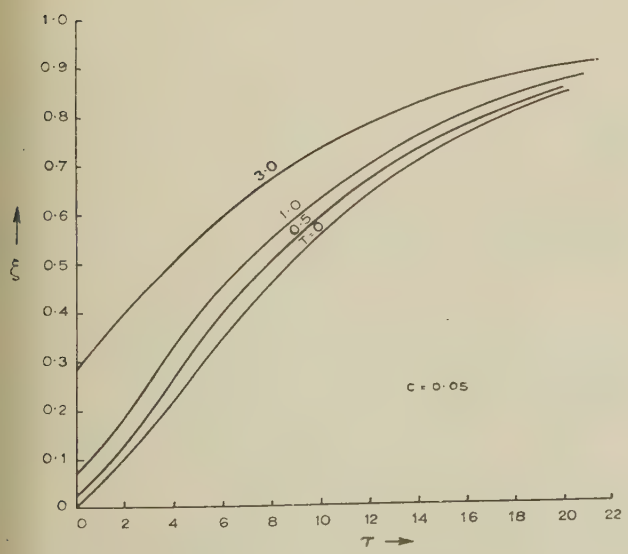

Fig. 7.—ξ as a function of τ for $c = 0{\cdot}05$.

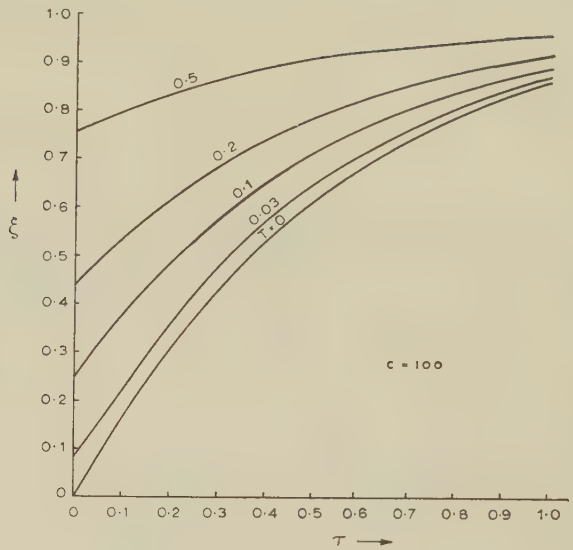

Fig. 8.—ξ as a function of τ for c = 100.

and correspondingly,

$$P^1(s) = \frac{1}{1 + s} \quad \text{and} \quad P^2(s) = 1$$

The sampled spectrum $S_{d^*d^*}(s)$ corresponding to the above form of $S_{dd}(s)$ is given by eqn. (35):

$$S_{d^*d^*}(s) = \frac{1}{T}\,\frac{(1 - \varepsilon^{-2T})}{(1 - \varepsilon^{-T}\varepsilon^{-sT})(1 - \varepsilon^{-T}\varepsilon^{sT})}$$

From eqn. (40) it now follows that

$$C_1(s) = \varepsilon^{-\tau}(1 - \varepsilon^{-T}\varepsilon^{-sT}) \quad . \quad . \quad . \quad . \quad (51)$$

and hence that

$$P(s)C_1(s) = \frac{\varepsilon^{-\tau}(1 - \varepsilon^{-T}\varepsilon^{-sT})\varepsilon^{-s\tau}}{1 + s} \quad . \quad . \quad (52)$$

If τ is written in the form $\tau = (p - \lambda)T$, where p is an integer and $0 \leqslant \lambda < 1$, the z-transform corresponding to eqn. (52) is

$$PC_1(z) = \varepsilon^{-pT}z^{-p} \quad . \quad . \quad . \quad . \quad . \quad (53)$$

$C(s)$ for the optimum controller may now be obtained by substituting from eqns. (51) and (53) into eqn. (32):

$$C(s) = \frac{\varepsilon^{-\tau}[1 - \varepsilon^{-(1+s)T}]}{1 - \varepsilon^{-p(1+s)T}} \quad . \quad . \quad . \quad . \quad (54)$$

The transfer function of the optimum continuous controller can be obtained by substituting the above form of $P(s)$ in eqn. (42) to give $C_{1c}(s)$. Then if $C_c(s)$ is the corresponding filter for use in a simple feedback loop,

$$C_c(s) = \frac{C_{1c}(s)}{1 - P(s)C_{1c}(s)} \quad . \quad . \quad . \quad . \quad (55)$$

which corresponds to eqn. (32) for the sampled case. In the present example,

$$C_c(s) = \frac{(1 + s)\varepsilon^{-\tau}}{1 - \varepsilon^{-\tau(1+s)}} \quad . \quad . \quad . \quad . \quad . \quad (56)$$

Difficulty is experienced in comparing $C_c(s)$ with the limiting behaviour of $C(s)$ when $T \to 0$, because $C(s)$ is assumed to

operate on a sequence of delta functions. This difficulty can be avoided by representing $C(s)$ as a zero-order hold, with transfer function $(1 - \varepsilon^{-sT})/s$, in series with a filter $C'(s)$. We must then have

$$C'(s) = \frac{sC(s)}{1 - \varepsilon^{-sT}} = \frac{s}{1 - \varepsilon^{-sT}} \frac{\varepsilon^{-\tau}[1 - \varepsilon^{-(1+s)T}]}{1 - \varepsilon^{-p(1+s)T}} \quad . \quad (57)$$

The zero-order hold converts the sequence of delta functions leaving the sampler into a 'staircase' function, which approximates to the continuous function at the sampler input more and more closely as $T \rightarrow 0$. Correspondingly, $C'(s)$ would be expected to approximate in the limit to the transfer function $C_c(s)$ of the continuous controller.

In examining the behaviour of eqn. (57) for small values of T, it must be remembered that $p \rightarrow \infty$ as $T \rightarrow 0$ in such a way that $pT \rightarrow \tau$; thus, $\varepsilon^{-p(1+s)T} \simeq \varepsilon^{-\tau(1+s)}$ when $T \rightarrow 0$. The remaining exponentials in eqn. (57) may be expanded in their exponents, neglecting powers beyond the first, when it follows that $C'(s) \rightarrow C_c(s)$ when $T \rightarrow 0$ for each value of s. The convergence of $C'(s)$ to $C_c(s)$ is not uniform in s, but we may say that the behaviour of the optimum sampled-data controller with very short sampling interval approximates to that of the optimum continuous controller, except at very high frequencies. The frequency range over which the approximation is good may be extended as far as we please by taking a sufficiently sh sampling interval.

(10) ACKNOWLEDGMENTS

The author wishes to thank Dr. P. C. Price for making results available prior to publication and for much useful cussion. Valuable suggestions were also made by Mr. Hext. The programme described in Section 9 was written Mr. D. B. Swinson during his tenure of a Vacation Scholars at Billingham in 1959.

The work described forms part of the research programme Imperial Chemical Industries Limited, Billingham Division.

(11) REFERENCES

(1) PRICE, P. C.: 'An Analytical Treatment of Process C trollability' (to be published).

(2) WIENER, N.: 'The Extrapolation, Interpolation and Smoo ing of Stationary Time Series with Engineering Appl tions' (Wiley, 1948).

(3) RAGAZZINI, J. R., and FRANKLIN, G. F.: 'Sampled-D Control Systems' (McGraw-Hill, 1958).

(4) LANING, J. H., and BATTIN, R. H.: 'Random Processes Automatic Control' (McGraw-Hill, 1956).

621.318.25

The Institution of Electrical Engineers
Monograph No. 427 M
Jan. 1961

THE STABILITY OF PERMANENT MAGNETS

By C. E. WEBB, B.Sc.(Eng.), Associate Member.

(*The paper was first received* 23*rd August, and in revised form* 21*st October*, 1960. *It was published as an* INSTITUTION MONOGRAPH *in January*, 1961.)

SUMMARY

The paper describes tests made to compare the magnetic stability of representative martensitic and precipitation-hardening (isotropic and anisotropic) permanent-magnet materials. The weakening of magnets with time after magnetization, when left as free from disturbance as possible, was measured over a period of about three years, both on unstabilized magnets and on magnets artificially stabilized by weakening them 1% or 5% by applying demagnetizing fields. Anisotropic alloys were found to be much more stable than isotropic alloys, the stability of Columax being outstanding. Alnico, in spite of its much higher coercive force, was not more stable than the martensitic steels.

The effect on stability of the working-point of the permanent-magnet material was also examined and found to be small above the $(BH)_{max}$ point on the demagnetization curve. Below the $(BH)_{max}$ point, however, the stability of both isotropic and anisotropic materials was considerably reduced.

Further tests were made on the effects of heating at various temperatures up to 220° C and of mechanical stress and impact. Stability in high-temperature treatment is only roughly related to stability in time tests. The results of the mechanical tests were inconclusive as the magnet assemblies available, designed primarily for long-term tests, were not suitable for subjection to severe mechanical treatment.

LIST OF SYMBOLS

B = Flux density, gauss.
H = Magnetizing force, oersteds.
$(BH)_{max}$ = Maximum value of BH on demagnetization curve.
I = Current, amp.
θ = Scale reading of balance, divisions.
k = Balance constant = $\delta I/I\delta\theta$.
$\tan\psi$ = Slope of permeance line = $-H/B$.
W = Weakening of magnet, parts in 10^4.
t = Time after magnetization, days.

(1) INTRODUCTION

An investigation was undertaken to compare systematically the stability of the chief types of permanent-magnet material.

Early work in this field was summarized in a previous E.R.A. report,[1] when it was concluded that, while adequate information was available on ageing due to metallurgical or structural instability of the material, there was need for further investigation into the magnetic instability of so-called 'permanent' magnets resulting from disturbing factors, such as mechanical vibration or shock, and temperature variation, or occurring with the passage of time when these disturbing factors were reduced to the smallest possible magnitude.

The precipitation-hardening alloys used in most permanent magnets at the present time are known to show no significant structural changes at temperatures below about 500° C, so that consideration of metallurgical ageing is of even less importance than when the previous report was drawn up. Attention has therefore been confined to magnetic instability.

As representative of the range of permanent-magnet materials in present-day use the following were tested:*

Cobalt-chrome steel (2% Co, 4% Cr).	Alcomax II.
35% Cobalt steel.	Alcomax III.
Alnico.	Alcomax IV.
	Columax.

Since magnets are usually designed to operate near the $(BH)_{max}$ point on the demagnetization curve of the material, each material was to be tested when working in approximately this condition, but in order to determine the effect of the working-point on the stability it was decided that one isotropic and one anisotropic alloy (Alnico and Alcomax III) should also be tested at working-points considerably higher and lower than the $(BH)_{max}$ point. A total of eleven types of magnet were thus to be tested.

Each type of magnet was to be investigated both unstabilized and after artificial stabilization. It was considered desirable, therefore, in order that each kind of test could be carried out on more than one magnet and the risk of misleading results being obtained on an unrepresentative sample could be avoided, that at least six magnets of each type should be available.

(2) METHOD OF TESTING

(2.1) Requirements and Preliminary Trials

It was required to make comparable measurements of the strengths of individual magnets before and after subjection to various treatments, and also after the lapse of periods of time up to, say, three years, to an accuracy, if possible, within 1 part in 10^4. For this purpose it was necessary to compare, to this degree of accuracy, the flux maintained by the magnet in precisely reproducible conditions.

An attempt was first made to achieve this by means of specially constructed moving-coil galvanometers in which the working flux was produced by the magnet under test. A determination by potentiometer of the current in the moving-coil required to produce a standard deflection then gave a measure of the flux set up in a standard gap and pole-piece assembly. By reading the deflections of the galvanometer for opposite directions of the current in the coil by means of the reflection of a fixed scale in two suitably placed telescopes, ample sensitivity was obtained. The reproducibility of the readings, however, was much below the desired level unless the magnet remained permanently mounted in the galvanometer, which would have necessitated a complete instrument for each magnet under investigation. Further, independent tests on the constancy, over a period of some months, of the effective area of coils similar to those used in the galvanometers indicated variations of the order of 2 parts in 10^4, while the possibility of additional variations due to the suspension and assembly suggested that, even with the magnet permanently mounted, the reproducibility attainable would not reach the level aimed at.

(2.2) Balance Method—General Principle

It was therefore decided to try the method based on the use of a sensitive balance which was developed by Knight.[2] For a

Correspondence on Monographs is invited for consideration with a view to publication.

The paper is based on Report Ref. N/T84 of the British Electrical and Allied Industries Research Association.

* The nominal compositions and magnetic characteristics of these, together with the names of similar alloys, are given in Table 4 (page 324).

detailed account of the factors involved in the design of the balance reference may be made to Knight's paper, and as experience of its use largely confirmed his observations, no major modifications of his form of the apparatus were made.

The general principle of the balance is shown in Fig. 1. It consists essentially of a beam, AA′, suspended centrally on

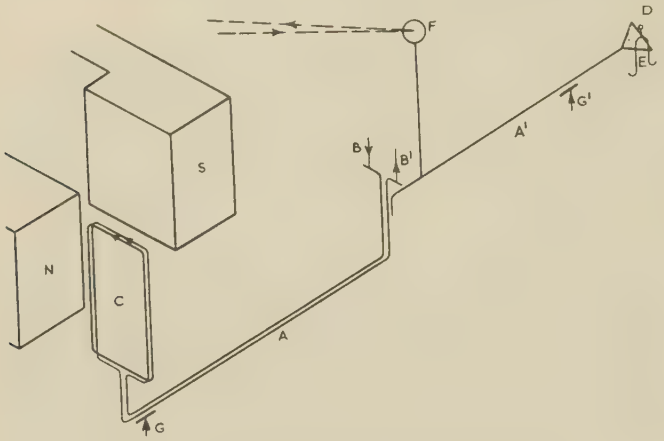

Fig. 1.—Diagram showing principle of balance.

two ligaments, B, B′, and carrying at one end a rectangular coil, C, of two turns of stout copper wire with its plane vertical and perpendicular to the length of the beam, and at the other end a knife-edge, D, on which a rider, E, may be placed. The magnet under test (NS) is placed so that the upper horizontal side of the coil is at the centre of its air-gap, and when a current in the appropriate direction is passed through the coil a downward force is exerted on it which, by varying the current, can be adjusted to balance the weight of the rider on the knife-edge. Balance is detected by means of a mirror, F, carried on a short vertical rod mounted near the point of suspension on the beam and reflecting an image of a horizontal cross-wire on a vertical scale. Adjustable stops, G, G′, are provided to allow only a very small displacement of the beam from the balance position.

With a given rider the current required for balance is inversely proportional to the gap flux density of the magnet, and variations of the gap flux density may be determined to a high degree of accuracy by measuring the balance current with a potentiometer.

(2.3) Construction of Balances

Three balances operating on this principle were made up, the practical details of the construction being as follows.

The two turns of the coil are of 0·05 in-diameter enamelled copper wire and the arm supporting the coil consists of the ends of the same wire, serving also as leads. The wires, both of the arm and of the coil, are bound together with thread and varnished, forming a satisfactorily rigid unit. The rectangular coil is approximately $\frac{3}{4}$ in wide and 2 in deep.

The rider arm is also of stout copper wire and carries, besides the knife edge and mirror, a small adjustable balance weight, allowing the balance position of the beam to be set as desired. The total length of the beam is about 8 in and it is suspended on the two ligaments (which also feed the current into the coil) from two brass rods carried in two blocks of Tufnol, which are mounted on a substantial $\frac{1}{4}$ in-thick brass base.

The magnet under test is precisely located relative to the balance coil, vertically by means of three beryllium-bronze screws in the base-plate and horizontally by means of three similar screws in brackets mounted on the base-plate, one at the end of each pole and one on the side of the magnet. Each locating screw has a specially hardened point and can be locked securely in position after being correctly adjusted.

The knife edge at the end of the rider arm is set accurately perpendicular to the length of the beam and has two notches placed symmetrically in relation to its mid-point, to facilitate locating the rider centrally. The riders used were made of tinned wire or thin sheet metal, weighing 0·1–0·3 g according to the strength of the magnet under test.

The mirror is 1 cm in diameter and has a radius of curvature of 2 m giving a scale distance of approximately 2 m.

Each balance on its massive brass base is placed in a separate brass tank filled with switch oil so that the balance and the magnet are completely immersed except for the mirror and a short length of the rod carrying it. The base is supported on three levelling screws on a hole, slot and plane mounting on the bottom of the tank.

The use of oil immersion has the advantages that

(*a*) It provides nearly critical damping.
(*b*) It facilitates temperature control.
(*c*) It allows much larger currents to be passed through the suspension ligaments so that the forces operating the balances can be greatly increased relative to the mechanical control forces.
(*d*) It minimizes disturbance due to air currents; the remaining disturbance due to currents acting on the mirror is practically eliminated by placing a cover over the mirror having only a small window by which the light beam can enter and leave.

Preliminary tests were made on the operation of the balance using two or three magnets of suitable shape which were available. Considerable trouble was experienced from control exerted on the balance arm by the suspension ligaments, and from zero drifts of the balances, which were apparently mainly due to thermal effects of the coil current. Various materials and sizes were tried for the ligaments, and satisfactory results were obtained using phosphor-bronze strip rolled down to 0·013 in to 0·000 3 in, provided that the coil current did not exceed about 0·8 amp. As the potentiometer could be read to 0·000 05 amp using a standard resistance of 1 ohm, the required discrimination of reading was available.

(2.4) Technique of Operation

To maintain constancy in the performance of the balances it was necessary to avoid any considerable shock to the suspension system. With this object the stops were set to limit the movement of the ends of the balance arms to 0·5 mm, and the following technique was developed for loading, balancing and unloading the beam in carrying out a measurement.

With the magnet in position the zero setting of the balance was read on the scale. A current slightly less than that expected to balance the rider was switched on in the coil circuit with the coil itself short-circuited by a switch, the direction of the current being such as to lift the coil arm. Owing to the comparatively low resistance of the coil this usually deflected the beam sufficiently to bring the rider arm gently on to its stop. The short-circuiting switch was then opened so that the arm was held firmly against the stop, and the rider was placed on the knife edge. The current in the coil was next reversed, but since its value was less than the balance value, the rider arm still remained on its stop. The current was then gradually increased until the force on the coil balanced the weight of the rider as indicated by the return of the balance to its zero position.

After measuring the balance current on the potentiometer, the current was slightly reduced to bring the rider arm back on to stop, the current was again reversed, the rider was removed from the knife edge, the coil short-circuited by the switch, the current in the coil circuit was switched off and the zero position was again read to check that no drift had occurred during the measurement.

(2.5) Reproducibility and Sensitivity

To obtain an indication of the reproducibility of reading likely to be attainable, the effects of displacing the magnet slightly in the vertical and two perpendicular horizontal directions were explored. The variation in the balance current was found to be small enough to be negligible for the displacements likely to occur in practice, except in the vertical direction.

To investigate this variation the stops on the balance arms were withdrawn to allow large deflections, and curves were plotted for two magnets showing the relation between the balance current and the relative vertical position of balance coil and magnet as shown by the scale reading at balance (the change in coil position at balance was produced by placing one or more small riders on one arm of the balance). This relation was found to be accurately linear over the working range of the balance (see Fig. 2), the slopes of the curves for the two magnets being proportional to the balance currents. Thus, for a given balance an equation can be established of the form

$$\delta I/\delta\theta = kI$$

where δI is the correction to be applied to the observed balance current, I, for any relative vertical displacement of coil and magnet expressed as a variation in scale reading, $\delta\theta$, and k is a constant applicable to any magnet.

To check the sensitivity obtainable with the balances, the variation of scale reading produced by a variation of the coil current was determined for the same two magnets. The curves obtained, Fig. 2, show that the minimum readable scale deflection

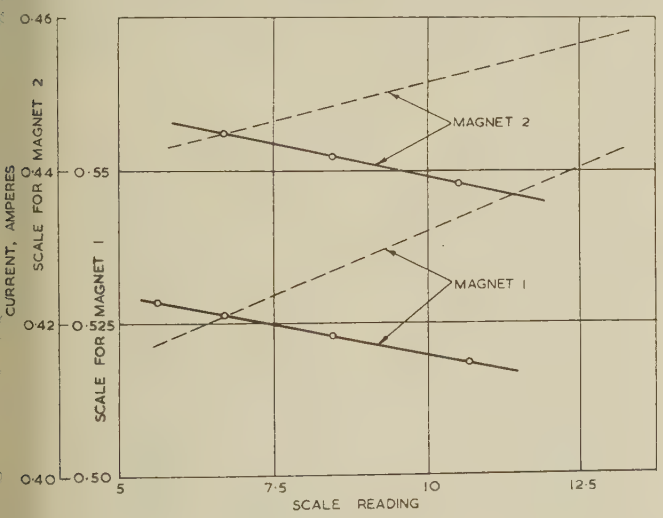

Fig. 2.—Relations between current and scale reading for magnetic balance.

—— Variation of balance current with scale reading.
---- Variation of scale reading with current.

of 0·01 division corresponds, for magnets 1 and 2, to current variations of 0·8 and 0·5 parts in 10^4, respectively. The gap flux densities in these magnets were about 1 000 and 1 600 gauss respectively. It appears, therefore, that the required sensitivity of 1 part in 10^4 can be obtained provided that the gap flux density is not less than about 800 gauss. Since a measurement of change of strength of a magnet involves two readings it is not, in general, possible to make such measurements to a greater accuracy than 2 parts in 10^4.

(3) TEST SAMPLES

To facilitate satisfactory location of the magnets in the balances for testing, it was desirable that they should all operate on a gap of the same geometrical form. For the high-coercivity materials which must be used in block form, a standard pattern of combined limbs and pole-pieces, made of soft iron, was therefore adopted, while for the lower-coercivity materials, requiring a greater length of magnet material to provide a suitable working-point, the same pole-piece assembly was fitted to magnets of horseshoe shape.

The general form of the samples for high-coercivity alloys, 35% cobalt-steel and cobalt-chrome steel are shown in Figs. 3(*a*), (*b*) and (*c*) respectively, and a number of assemblies including samples of each type of magnet to be tested were prepared.

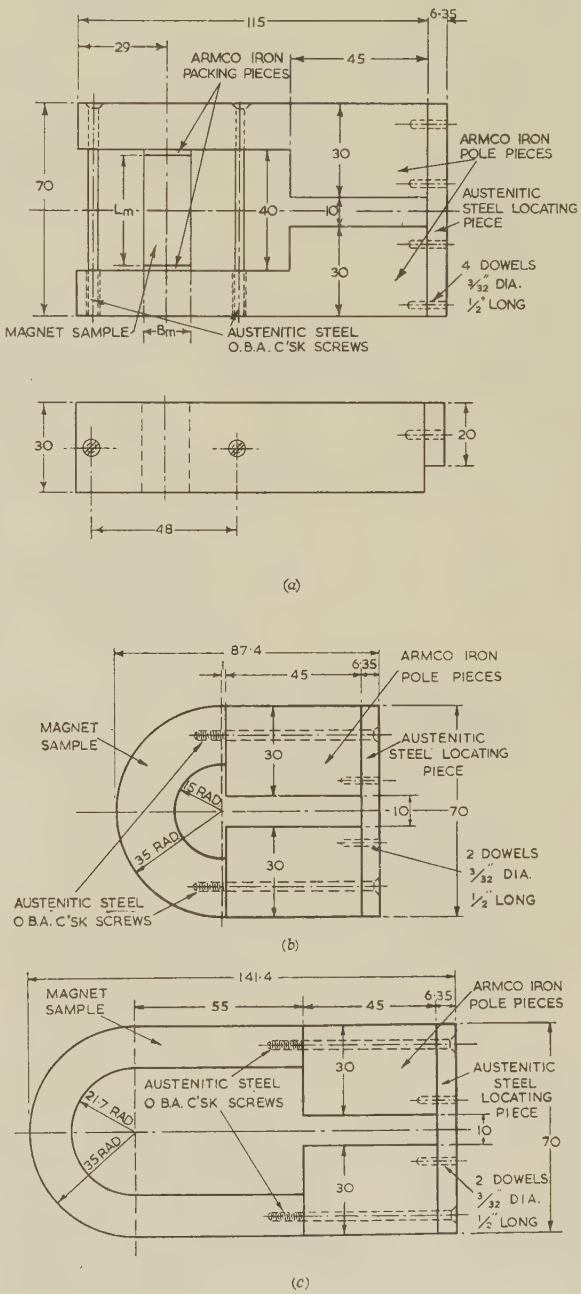

Fig. 3.—Form of magnet assemblies.

(*a*) Block magnets (groups C–G).
(*b*) 35% cobalt-steel magnets (group B).
(*c*) 2% Co 4% Cr steel magnets (group A).

Dimensions are in millimetres unless otherwise indicated.

It will be seen that the standard gap used had a length of 1 cm and a cross-section of $4{\cdot}5 \times 3\,cm^2$. Particular care was taken to make the pole-faces parallel in the direction perpendicular to the plane of the magnetic circuit, and precise location of the pole-pieces was ensured by a non-magnetic locating piece dowelled to the outer ends of the pole-pieces. The dowel pins were kept well away from the gap to minimize distortion of the gap flux.

In the assemblies involving horseshoe magnets the pole-pieces were screwed to the ends of the limbs: in those involving block magnets, two non-magnetic countersunk screws were used to hold the magnet, with soft-iron packing pieces at each end, between the limbs. The assembly in the latter case was permanently maintained by the outer countersunk screw and the dowelled locating piece, the inner screw being provided only for convenience in assembling.

All the soft-iron components in the assemblies were of Armco iron, while the non-magnetic components were of austenitic steel, having approximately the same temperature coefficient of expansion as the magnetic components, so that high-temperature tests could be made without significant disturbance of the assemblies.

The design of the assemblies to provide the desired working-points in the permanent-magnet material was carried out by Hadfield, applying the principles described in his paper.[3] The working-point is most conveniently defined in terms of $\tan\psi\,(=-H/B)$, and the values of $\tan\psi$ for the various types of magnet, together with the dimensions required to provide these conditions, are given in Table 1. The Table also includes a code mark for each group of magnets and the estimated gap flux densities. It will be seen that only in group C′ [Alnico magnets with $\tan\psi$ less than at the $(BH)_{max}$ point] is the flux density significantly below the minimum value of 800 gauss required for a sensitivity of 1 part in 10^4. For magnets in this group the sensitivity will therefore be little more than 2 parts in 10^4.

To determine the actual demagnetization curves of the materials, tests were made on representative magnets and the curves obtained are given in Fig. 4. The working-point of the material at which each group of magnets was designed to operate is also indicated by the points P, P′, P″, denoting respectively the $(BH)_{max}$ point and points with smaller and larger $\tan\psi$ values than that for $(BH)_{max}$.

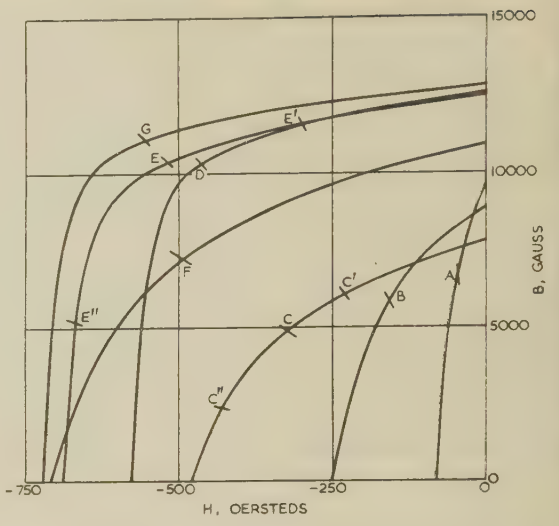

Fig. 4.—Demagnetization curves of magnet materials.
A. 2% Co 4% Cr steel.
B. 35% Co steel.
C, C′, C″. Alnico.
D. Alcomax II.
E, E′, E″. Alcomax III.
F. Alcomax IV.
G. Columax.

In the horseshoe magnets of groups A and B the act working-point of the material varies considerably, owing leakage, between the middle and ends of the magnet. In remaining magnet assemblies, in which most of the magn circuit consists of soft iron, the variation of working-po along the length of the block magnet is very small. No atte was made at precise quantitative determination of the worki point as its effect is comparatively a secondary one, and approximate values derived from design data were conside adequate.

Table 1

PARTICULARS OF MAGNET ASSEMBLIES

Material	Working condition*	Group mark	tan ψ	Length	Section	Estimated gap flux density
				cm	cm²	gauss
Cobalt-chrome steel (2% Co 4% Cr)	(*a*)	A	0·007	20	4·0	830
35% Cobalt steel	(*a*)	B	0·027	8	6·0	1070
Alnico	(*a*)	C	0·066	2·7	5·0	740
	(*b*)	C′	0·038	2·8	3·0	580
	(*c*)	C″	0·18	2·5	12·3	910
Alcomax II	(*a*)	D	0·045	4·0	5·0	1500
Alcomax III	(*a*)	E	0·05	3·6	5·0	1500
	(*b*)	E′	0·026	4·0	3·0	1000
	(*c*)	E″	0·13	3·5	12·3	1830
Alcomax IV	(*a*)	F	0·069	2·6	5·0	1180
Columax	(*a*)	G	0·05	3·6	5·0	1650

* Working condition (*a*) At $(BH)_{max}$ point.
(*b*) Above $(BH)_{max}$ point.
(*c*) Below $(BH)_{max}$ point.

(4) DESCRIPTION OF TESTS

To allow a large number of magnets (about 70) to be tested a stored for long periods free from thermal, mechanical or magn disturbance, use was made of an underground air-raid she remote from other laboratories and running machinery.

(4.1) Temperature Control

The maximum temperature attained naturally in the shelter during the year was just below 18° C and electrical heating, thermostatically controlled to give a temperature of approximately 18° C, was therefore installed. By this means the temperature of the oil baths was maintained constant from day to day within very close limits, but there was an annual temperature cycle of a total range of about 1° C. By careful adjustment of the thermostats this could have been practically eliminated, but instead, temperatures were recorded and a correction applied for temperature variation assuming a temperature coefficient of -2×10^{-4} per deg C. (This was known to be the usual value for permanent magnets of the types tested and was checked by direct tests on two magnets.)

(4.2) Interaction with Magnets or Soft Iron

The three balances were set up on pillars spaced as far apart as the width of the shelter allowed—approximately 2 ft 6 in. Tests were made to check whether a magnet in one balance affected the reading of the neighbouring one, and it was found that the reversal of a magnet produced a just detectable change, equivalent to a current variation of not more than 1 part in 10^4. It was concluded that the direct effect of 1 part in 2×10^4 could be neglected.

Tests were also made to determine the permanent effects on the strength of a magnet produced by interaction between magnets and by contact or near-contact with soft magnetic material. To take the worst case, a cobalt-chrome steel magnet was used, since this material had the smallest coercive force. The magnet was placed in one of the balances and the balance current for a suitable rider was determined. One of the stronger magnets (Alcomax III) was then brought up successively to various distances and withdrawn, and the balance current was determined again after each withdrawal. This was repeated for various angles of approach and it was found that the maximum distance at which a detectable change in the balance current occurred was about 6 in. It was therefore decided to maintain a minimum distance of 12 in between magnets throughout the investigation, and wooden storage racks were constructed providing definite positions 12 in apart, both in the vertical and horizontal directions.

The effects of soft magnetic material naturally depend on the size of the object concerned. A 20 s.w.g. steel wire placed across the gap in contact with the poles produced no detectable permanent change in the balance current, but touching the poles with a small spanner produced a change of about 5 parts in 10^4. Provided that the spanner was not brought within 1 in of the magnet, however, no permanent change was observed, and care was taken during the investigation not to bring any magnetic object within 2 in of the magnet assemblies.

On the very few occasions when magnets or soft iron were inadvertently brought within these limiting distances of a magnet under test, the readings obtained were examined carefully and, unless it was clear that no significant disturbance had occurred, the test in progress was abandoned or the series of observations was restarted.

(4.3) Standardization of Balances

Since, for long-term tests, the constancy of the performance of the balances was of the first importance, provision was made for regular checks using as standards three magnets of types (Alcomax III and IV) expected to have the highest stability, subjected to a large measure of both natural and artificial stabilization. By making comparisons between these three magnets in each of the three balances it was thought that reliable indications would be obtained of changes, either in the standard magnets or in the balances.

In the event, one of the balances proved relatively unstable, and its readings were only of value over short periods, balance 2 was used for most of the routine observations, while balance 3 was used mainly for periodic comparison tests on the standard magnets.

During the four years over which the tests extended, the ratios between the readings obtained on the three standard magnets remained constant within the accuracy of the measurements. The readings on balance 3, although showing irregular variations from time to time of a few parts in 10^4, revealed no secular changes and the final values agreed almost exactly with the initial ones. Readings on the standard magnets on balance 2 showed much less casual variation than on balance 3—in fact, the readings remained almost constant except for abrupt changes on two occasions, the first when the balance mirror became loose and had to be refixed, and the second (a much smaller change about two years later) believed to be due to the arm being slightly jolted when removing a rider. On each occasion a correction factor was derived from readings on the three standard magnets and when this was applied to the readings on other magnets under test, the corrected curves showed no appreciable discontinuity.

It was concluded that the standard magnets had remained satisfactorily constant and that the corrected readings on balance 2 could be taken to give accurately comparable measurements of magnet strength.

(4.4) Time Tests on Unstabilized Magnets

Tests were made on magnets of each group without artificial stabilization, to compare the rates at which they weaken with time when left as free from disturbance of any kind as possible. Each magnet was magnetized by means of a winding of five turns through which a current impulse of approximately 8 kA was passed three times.

Using a rider which gave a balance current in the range 0·5–0·8 amp, comparative measurements of the gap flux density were made, at first at intervals of a few hours, then daily, and finally at increasing intervals over periods up to about 3 years. It was found that readings during the first day after magnetization showed widely differing rates of change for magnets of the same type, but subsequently their rates of change became much more nearly the same. It was concluded that the early readings were influenced by transient effects, probably due to flux redistribution in the magnet. The practice was therefore adopted of measuring the weakening after any given period from the value obtained 24 h after magnetization.

Typical curves are given in Fig. 5 showing the percentage

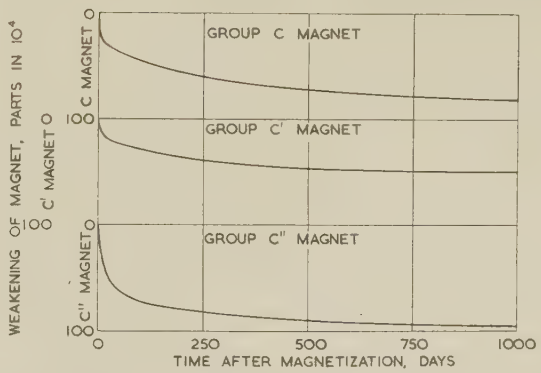

Fig. 5.—Typical curves of weakening with time for Alnico magnets (unstabilized).

weakening, W, as a function of the time, t, for 1 000 days after magnetization, of an Alnico magnet in each of the groups C, C′ and C″. The form of these curves suggests a linear relation between W and log t, and plotting W/log t curves confirms that, for most magnets, a close approximation to a linear relation, though with some scatter of individual points, is obtained.

The W/log t curves for all the Alnico magnets of groups C, C′ and C″, together with the mean curve for each group, are given in Fig. 6, showing the amount of variation between the individual magnets of a particular group.

The mean W/log t curves for all the groups of magnets are collected in Fig. 7, from which it will be seen that a systematic divergence from a linear relation is found only in the martensitic steels of groups A and B and, to a much smaller extent, in one or two Alnico magnets of group C.

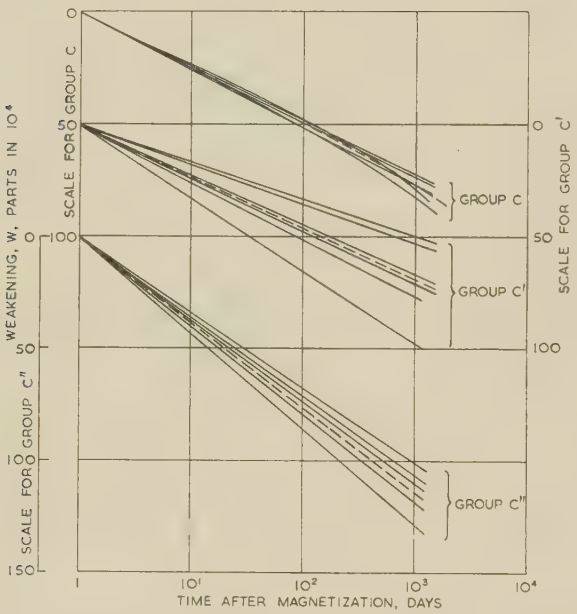

Fig. 6.—Curves connecting weakening with logarithm of time after magnetization for Alnico magnets (unstabilized).
—— Individual magnet.
---- Mean of group.

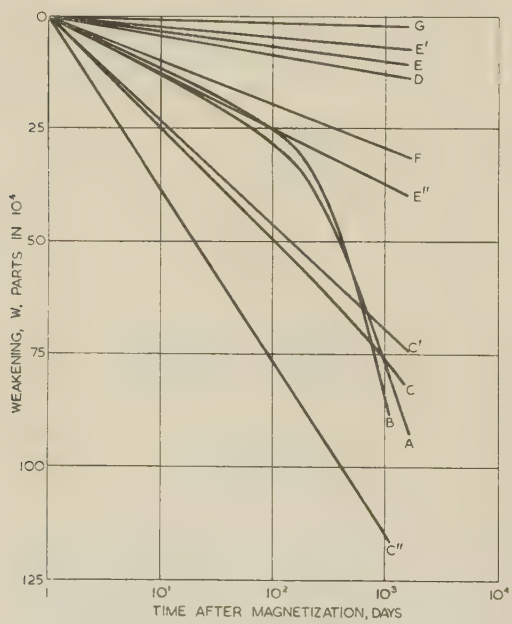

Fig. 7.—Mean W/log t curves for all groups of magnets (unstabilized).

It was thought that the large departure from a linear relat in the martensitic steels might be due, largely at least, to superposition of a metallurgical ageing effect on the effects magnetic instability. Since the magnets had been prepa many months before the magnetization for the time test carried out, weakening due to ageing would be taking place rate more nearly proportional to t and would thus give increasing slope relative to log t. Remagnetization of magnets at the end of the time tests did not, however, indic any considerable weakening due to ageing of the material, it appears that the curvature of W/log t curves for groups and B magnets is mainly, if not entirely, due to the magn weakening following a different law of variation with time.

It should be noted that the curve for Columax represents maximum value of weakening set by the limit of detectio 2 parts in 10^4 which was not exceeded in 1 000 days.

In view of the generally linear relation found between W log t, the slope dW/d (log t) may be taken as a measure of stability—or rather instability—of the various types of mag

Table 2

MEAN VALUES OF dW/d (LOG t) IN TIME TESTS

Magnet group	$\mid dW/d$ (log t)		
	Unstabilized	Artificially stabilized	
		by 1%	by 5%
A	13(26)	6(12)	3
B	11(28)	3(7)	2
C	25(26)	3	2·5
C′	23	2	—
C″	38	7	4
D	4	<1	—
E	3·5	<1	<1
E′	2·5	<1	—
E″	12·5	<1	<1
F	10	<1	<1
G	<1	—	—

The values obtained are given in Table 2. For groups A, B C two values are given, the initial slope and (in brackets) mean value for 1 000 days.

(4.5) Time Tests on Artificially Stabilized Magnets

Artificial stabilization was carried out by the usual metho applying a demagnetizing field to reduce the gap flux density a small percentage, and long-term tests on the strength of magnet were then carried out, as on the unstabilized magn Reduction of the gap flux density by 1% and 5% was u except on the more stable alloys for which there was no detect instability after weakening by 1% and it was, therefore, point to apply the larger amount of stabilization.

The demagnetizing field was applied, either by placing magnet assembly at the centre of a large circular coil, or winding a few turns on the magnet, and passing a suit current through the coil or the winding. Three types of dem netizing treatment were tried:

(*a*) An alternating current was switched on and gradually redu to zero.

(*b*) A direct current was switched on and reduced to zero ei suddenly or gradually.

(*c*) A direct current was switched on and reversed repeat while being gradually reduced to zero.

The long-term weakening which occurred after stabilization appeared to be independent of the type of demagnetizing treatment applied, but with treatments (*a*) and (*b*) there were considerable variations—usually increases—in strength during the first few days, while with treatment (*c*) these initial effects either did not occur or were much smaller. They were presumably due to flux redistribution such as occurred after magnetization and, after treatment (*b*), possibly to a drift in the condition of the material from that represented by a point on the ascending limb of the recoil loop to a more stable condition on or near the axis of the recoil loop.

The long-term behaviour of the magnets after artificial stabilization appeared to approximate to a law of the same form, a linear $W/\log t$ relation, as that found for the unstabilized magnets. The mean values of $dW/d(\log t)$ for stabilized magnets are therefore given in Table 2 for comparison with those for unstabilized magnets.

(4.6) Thermal Tests

To investigate the permanent effects of heating to various temperatures on the strength of the various types of magnet, samples of each type were subjected to successive temperature increases of 50, 100, 150 and 200° C by placing them in a thermostatically-controlled electric oven for a period of three hours. This period was adopted because preliminary tests showed that it was sufficient to bring the magnets to an approximately constant strength at each temperature. Subsequently a repetition of some of the heat treatments indicated that this was not quite true and that a small further weakening occurred in some cases after more than three-hours heating at a given temperature. The three-hour heating period was, however, adopted as the basis of comparison of the stability of the various types of magnet under thermal treatment.

After each heat treatment the magnets were cooled to room temperature and retested in the balance. Magnets were tested in unstabilized and artificially stabilized conditions, and the results obtained are given in Table 3.

Table 3

WEAKENING OF MAGNETS BY HEATING

Magnet group	Weakening after artificial stabilization	Weakening after heating to 70° C	120° C	170° C	220° C	Weakening after remagnetization
	%	parts in 10^4	parts in 10^4	parts in 10^4	parts in 10^4	parts in 10^4
A	0	80	290	1 070	—	250
	1	22	120	—	—	—
	5	11	85	650	—	—
B	0	110	560	1 340	—	680
	1	21	285	—	—	—
	5	15	200	480	—	—
C	0	30	75	130	195	$\gtrsim 2$
	1	10	20	35	—	—
	5	8	16	28	50	—
C′	0	30	65	95	130	—
	5	7	14	20	35	—
C″	0	90	150	240	370	—
	1	55	105	180	290	—
	5	10	25	45	100	—
D	0	5	12	20	25	—
	1	$\gtrsim 2$	$\gtrsim 2$	$\gtrsim 2$	$\gtrsim 2$	—
E	0	6	10	14	18	—
	1	$\gtrsim 2$	$\gtrsim 2$	$\gtrsim 2$	$\gtrsim 2$	—
	5	$\gtrsim 2$	$\gtrsim 2$	$\gtrsim 2$	$\gtrsim 2$	—
E′	0	2	5	8	14	$\gtrsim 2$
	1	$\gtrsim 2$	$\gtrsim 2$	$\gtrsim 2$	$\gtrsim 2$	—
E″	0	25	52	77	100	—
	1	8	15	26	40	—
	5	$\gtrsim 2$	$\gtrsim 2$	$\gtrsim 2$	$\gtrsim 2$	—
F	0	10	20	25	40	—
	1	$\gtrsim 2$	3	5	7	—
G	0	$\gtrsim 2$	$\gtrsim 2$	$\gtrsim 2$	$\gtrsim 2$	—
	1	$\gtrsim 2$	$\gtrsim 2$	$\gtrsim 2$	$\gtrsim 2$	—

For the martensitic steels of groups A and B the effects of metallurgical ageing at increased temperature are superimposed on those of magnetic instability. To indicate the magnitude of the ageing effects some of the magnets in these groups were remagnetized after the final heat treatment and retested in the balance. The weakening recorded after remagnetization shows how much of the weakening after the highest temperature treatment was due to metallurgical ageing, only the remainder being due to magnetic instability.

For the Alnico and Alcomax groups there is no significant weakening after remagnetization, and in many cases the percentage weakening after heating to various temperatures increases almost linearly with the temperature. In a number of cases, however, chiefly magnets operating at a high value of tan ψ, the percentage weakening tends to increase more rapidly at higher temperatures.

Artificial stabilization produces a considerable reduction in the weakening caused by heating but its effect is much less than in the time tests.

(4.7) Mechanical Tests

An attempt was made to examine the effects of stress, static or dynamic, under precisely defined conditions using a large press and an impact tester. By means of the press a static load of 5 or 10 tons was applied and removed a number of times: by means of the impact tester a known weight was repeatedly dropped on the magnet from a measured height, giving a number of impacts of approximately 3 or 6 ft-lb.

In both cases it was, of course, necessary to ensure that the force was applied to the magnet through blocks of non-magnetic material. A more serious difficulty was that, with the heavy loads needed to produce significant weakening, the magnets were liable to be displaced relative to the soft-iron limbs and packing pieces of the assemblies.

In the static tests, repeated loading appeared to add little to the effects of the first application of stress: in the impact tests, the weakening produced was still increasing slowly after 30 or 40 impacts. The weakening produced by the maximum static or dynamic loads applied was of the order of 1% in unstabilized cobalt-chrome steel and Alnico magnets, but in Alcomax was much less. Spurious effects, however, were too large relative to the effects under examination for quantitative results of any value to be obtained, and the results on nominally similar samples were inconsistent.

It was concluded that the form of magnet assembly designed primarily for long-term tests was unsuitable for testing the effects of mechanical treatment. This was of less importance as, since the investigation started, results have been obtained by Hadfield[4] on the effects of shock and vibration on ellipsoidal magnets.

(5) CONCLUSIONS

(*a*) In long-term tests under undisturbed conditions anisotropic alloys are much more stable than isotropic alloys, whether they are compared unstabilized or after artificial stabilization. The high stability of anisotropic alloys is particularly marked in Columax which, even unstabilized, weakens not more than 2 parts in 10^4 in 1 000 days.

(*b*) In long-term stability, Alnico is not better than the much-lower-coercivity martensitic alloys (cobalt-chrome steel and 35% cobalt-steel).

(*c*) The long-term stability depends little on the working-point of the material above the $(BH)_{max}$ point on the demagnetization curve. Below the $(BH)_{max}$ point the stability is substantially reduced, both in isotropic and anisotropic alloys.

(*d*) In Alnico and Alcomax alloys the relation between t percentage weakening and the logarithm of the time elaps after magnetization is approximately linear.

(*e*) The stability of the various types of magnet after hig temperature treatment is roughly related to their stability in tir tests, but Alnico is relatively more stable as compared with t martensitic steels.

(*f*) In Alnico and Alcomax alloys the relation between t percentage weakening and the temperature of heat treatment approximately linear, but in Alnico working at large values tan ψ the weakening increases slightly more rapidly in t neighbourhood of 200° C than at lower temperatures.

(*g*) In anisotropic alloys, 1% artificial stabilization is genera adequate except at large values of tan ψ. In isotropic allo even 5% artificial stabilization does not give immunity fr further weakening with high-temperature treatment or t passage of time.

(*h*) Since the completion of this work, comparable resu obtained under substantially different conditions have be published by Clegg and McCaig[5] and by Gould.[6] It is sat factory that, while their results differ appreciably in detail fr those recorded in this paper, they show similar variations f different materials, and for different working-points in the tw materials (Alnico and Alcomax III) in which the working-poi was varied.

(6) ACKNOWLEDGMENTS

Thanks are due to Messrs. Swift, Levick and Sons, Ltd., f providing the magnet assemblies tested, and for the informa given in Table 4; and to Mr. D. Hadfield, of that firm, f designing the assemblies to provide the desired worki conditions.

The work in connection with the paper was carried out in t Electricity Division of the National Physical Laboratory on b half of the Electrical Research Association, and the paper is pu lished by permission of the Director of the Laboratory and wi the approval of the Director, Electrical Research Association

(7) REFERENCES

(1) Webb, C. E.: 'Summary of Published Information on Stability of Perman Magnets', E.R.A. Report Ref. N/T12: 1938.
(2) Knight, S. F.: 'A Sensitive Balance of Stability Tests on Permanent Magne *Proceedings I.E.E.*, Paper No. 850 M, August, 1949 (96, Part II, p. 635).
(3) Hadfield, D.: 'Permanet Magnet Design', *Electrical Times*, 1947, 111, p. 323.
(4) Hadfield, D.: 'The Magnet Stability of Some Permanent Magnet Materia Ph.D. Thesis, University of London, 1956.
(5) Clegg, A. G., and McCaig, M.: 'The High Temperature Stability of Perman Magnets of the Iron-Nickel-Aluminium System', *British Journal of Appl Physics*, 1958, 9, p. 194.
(6) Gould, J. E.: 'Permanent Magnet Stability', *Instrument Practice*, 1958, 12, p. 10

Table 4.—Nominal Compositions and Properties of Materials Used (with Names of Equivalent Alloys)

Material	C	Cr	Co	W	Fe	B_{rem}	H_c	$(BH)_{max}$
						gauss	oersteds	MGOe
2% Co 4% Cr	1·0	3·8	2·3	0·5	Bal.	9 800	70	0·28
35% Co	0·8	3·5	35·0	6·3	Bal.	9 000	250	0·95
	Ni	Co	Al	Cu	Nb	Fe		
Alnico (British) / Alnico 2 (U.S.A.) ..	17	13·5	9·5	6	—	Bal.	8 000	500	1·7
Alcomax II (British) ..	11·5	25	8	5·5	—	Bal.	12 400	570	4·3
Alcomax III (British) / Ticonal G (Mullard) / Alnico 5 (U.S.A.) ..	13·5	24	8	3	0·7	Bal.	12 200	650	4·8
Alcomax IV (British) / Ticonal H (Mullard) / Alnico 6 (U.S.A.) ..	13·5	24	8	3	2·5	Bal.	11 200	750	4·3
Columax (British) / Ticonal GX (Mullard) / Alnico 5DG (U.S.A.) ..	13·5	24	8	3	0·7	Bal.	13 200	740	7·0

[A discussion on the above monograph will be found on page 535.]

621.372.6

The Institution of Electrical Engineers
Monograph No. 428 E
Feb. 1961

TOPOLOGICAL SYNTHESIS OF NON-RECIPROCAL RESISTANCE NETWORKS

By R. ONODERA

(*The paper was first received* 15*th July*, 1959, *and in revised form* 16*th December*, 1960. *It was published as an* INSTITUTION MONOGRAPH *in February*, 1961.)

SUMMARY

The paper deals with the topological synthesis of non-reciprocal resistance networks specified by the so-called driving-conductance matrix. Synthesis of non-reciprocal networks has already been treated by H. J. Carlin and Y. Oono, and their networks are specified by scattering matrices and consequently n-port impedance matrices. One of the merits of this paper, which differs from their paper, is in the determination of the connection and ideal transformers. Factors which determine the network are the connection and element resistances, and they therefore make possible the determination of the node-branch incidence matrix and resistances so that the driving-conductance matrix may equal the given matrix. When we denote the branch e.m.f. matrix by V and the branch-current matrix by I, $I = GV$, where G is called the driving-conductance matrix, which is assumed to be given, and, in general, $G' \neq G$. If a maximal set of solutions for $Gx = 0$ and $x'G = 0$ is denoted by X as the matrix expression, X is called the zero factor of G. Provided that the zero factor X satisfies the character of a node-branch incidence matrix, the connection can be fixed directly. If not, the connection is determined by the part of X which satisfies the character of a node-branch incidence matrix, and the ideal transformers needed are determined by the other part. After the connection and the ideal transformers are determined, the branch resistances are determined by comparing the given matrix with the matrix calculated from the newly determined connection and the unknown branch resistances.

LIST OF SYMBOLS

D = Node-branch incidence matrix.
$\tilde{D}$ = D without an arbitrary row.
R = Loop-branch incidence matrix.
N = Turns-ratio matrix of ideal transformers.
$B = \begin{bmatrix} \tilde{D} \\ N \end{bmatrix}$.
C = Transposed matrix of zero factor on the right-hand side of B.
V = Branch-e.m.f. matrix (of one column).
I = Branch-current matrix (of one column).
U = Element voltage-drop matrix (of one column), including voltage drops across gyrator ports but omitting voltage drops across ideal transformer coil winding.
J = Generalized loop-current matrix in general (= Loop-current matrix if ideal transformers do not exist).
r = Branch-resistance matrix including gyrator elements.
$\overset{(+)}{r}$ = Symmetrical component of r.
$\overset{(-)}{r}$ = Alternative component of r.
$Z = CrC'$.
$\overset{(+)}{Z} = \overset{(+)}{C}\,r\,\overset{(+)}{C}'$.
$\overset{(-)}{Z} = \overset{(-)}{C}\,r\,\overset{(-)}{C}'$.
G = Driving-conductance matrix.

Correspondence on Monographs is invited for consideration with a view to publication.
Mr. Onodera is in the Department of Electrical Engineering, Yamagata University, Japan.

(1) INTRODUCTION

Needless to say, combinatorial topology is important in electrical networks. It is useful for handling not only various problems in analysis[1–14] but also in synthesis.[15–16] The paper deals with the topological synthesis of non-reciprocal resistance networks specified by the so-called driving-conductance matrix. Factors which determine the network are the connection* and element resistances, and they therefore enable the determination of the node-branch incidence matrix† and resistances, so that the driving-conductance matrix of the network may be equal to the given matrix. The paper deals mainly with the topological method of determining the node-branch incidence matrix.

When we denote the branch-e.m.f. matrix by V and the branch-current matrix by I,

$$I = GV,$$

where, in general,

$$G' \neq G \quad . \quad . \quad . \quad . \quad . \quad . \quad . \quad . \quad (1)$$

and G is the driving-conductance matrix.

If we denote the node-branch incidence matrix (1-incidence matrix) by D, from Kirchhoff's first law we have the relation

$$DI = 0 \quad . \quad . \quad . \quad . \quad . \quad . \quad . \quad . \quad (2)$$

Therefore, from eqns. (1) and (2),

$$DGV = 0$$

In order to satisfy any value of V, the following relation must hold:

$$DG = 0 \quad . \quad . \quad . \quad . \quad . \quad . \quad . \quad (3)$$

A suitable value of D is determined by a linear combination of a maximal set $X[\overset{1}{x}, \overset{2}{x}, \ldots, \overset{m}{x}]$‡ of independent solutions x (unknown matrices of one row), for

$$x'G = 0 \quad . \quad . \quad . \quad . \quad . \quad . \quad . \quad . \quad (4)$$

namely

$$D = KX' \quad . \quad . \quad . \quad . \quad . \quad . \quad . \quad (5)$$

where K is a square matrix with

$$|K| \neq 0, \text{ and } X' = \begin{bmatrix} \overset{1}{x'} \\ \overset{2}{x'} \\ \vdots \\ \overset{m}{x'} \end{bmatrix} = \begin{bmatrix} \overset{1}{x_1} & \overset{1}{x_2} & \overset{1}{x_3} & \ldots & \overset{1}{x_n} \\ \overset{2}{x_1} & \overset{2}{x_2} & \overset{2}{x_3} & \ldots & \overset{2}{x_n} \\ \cdot & \cdot & \cdot & & \cdot \\ \overset{m}{x_1} & \overset{m}{x_2} & \overset{m}{x_3} & \ldots & \overset{m}{x_n} \end{bmatrix}$$

Of course, we have

$$X'G = 0 \quad . \quad . \quad . \quad . \quad . \quad . \quad . \quad . \quad (6)$$

When the driving conductance G is given, we can determine a connection specified by this value of G from eqns. (4) and (5). If D, as determined by eqns. (4) and (5), satisfies the character

* For the foundations of network topology, see References 17–22, etc.
† The 'node-branch incidence matrix' is also called '1-incidence matrix', or 'incidence matrix'.
‡ $m = n - k$, where n = dim (G) and k = rank (G).

of a node-branch incidence matrix, we can determine the connection directly by means of D. Otherwise the connection is determined by the part of D which satisfies the character of a node-branch incidence matrix, and the ideal transformers are determined by the other part. Therefore, the question of whether ideal transformers are necessary depends on whether D, given by a linear combination of x's, satisfies the character of a node-branch incidence matrix.* After the connection and ideal transformers are determined, branch resistances can be determined by comparing the given matrix with the matrix calculated from the newly determined connection and the unknown branch resistances.

(2) GENERAL CONSIDERATION OF RESISTANCE NETWORKS

This Section gives the general outline of a.c. resistance networks and introduces some algebraic treatments preliminary to topological consideration of network synthesis.

(2.1) Node-Branch Incidence matrix

When several sub-networks are isolated, each is called a 'disconnected sub-network'. If a network consists of p_0 disconnected sub-networks, the number p_0 is called the 'zero Betti number'[2]. In the paper we put $p_0 = 1$ for simplicity, because the distribution of branch currents is invariant even if each of the sub-networks has a common point, assuming that the only sources are the branch e.m.f.'s, V. First we denote the node-branch incidence matrix by D. This is an $\alpha_0 \times \alpha_1$ matrix, where α_0 is the number of nodes and α_1 is the number of branches. For example, in Fig. 1 the node-branch incidence matrix[2] is

$$D = \begin{bmatrix} 1 & 0 & -1 & -1 & 0 & 0 \\ -1 & 0 & 0 & 0 & -1 & -1 \\ 0 & 1 & 1 & 0 & 1 & 0 \\ 0 & -1 & 0 & 1 & 0 & 1 \end{bmatrix} \quad . \quad . \quad . \quad (7)$$

The column corresponding to each branch has one $+1$, one -1 and all the other elements 0. Thus one row of D is linearly dependent on the others. In general, p_0 rows are linearly dependent. Therefore if we denote D without an arbitrary row by $\tilde{D}$, it is frequently sufficient to use $\tilde{D}$ instead of D, and we also call $\tilde{D}$ the 'node-branch incidence matrix' as well as D. Hence $\tilde{D}$ is an $(\alpha_0 - p_0) \times \alpha_1$ matrix, and is an $(\alpha_0 - 1) \times \alpha_1$ matrix if the network is connected.

For example, in Fig. 1 $\tilde{D}$ is given by

$$\tilde{D} = \begin{bmatrix} 1 & 0 & -1 & -1 & 0 & 0 \\ -1 & 0 & 0 & 0 & -1 & -1 \\ 0 & 1 & 1 & 0 & 1 & 0 \end{bmatrix} \quad . \quad . \quad . \quad (8)$$

If we determine $\tilde{D}$ algebraically, it satisfies the necessary and sufficient condition that each column corresponding to each branch has either a single '+1' or a single '—1' as elements or it may have both, and all the other elements are zero. This characteristic is very important to the topological synthesis. If current sources do not exist, Kirchhoff's first law is given by

$$DI = 0 \text{ or } \tilde{D}I = 0 \quad . \quad . \quad . \quad . \quad . \quad . \quad (9)$$

* Since, in the paper, transfer resistances may be positive or negative it does not give the direct solution of the important unsolved problem of the necessary and sufficient conditions for the realizability by an n-port network of resistances without ideal transformers. But it gives one of the necessary conditions, and also it seems very useful for consideration of the sufficient conditions.

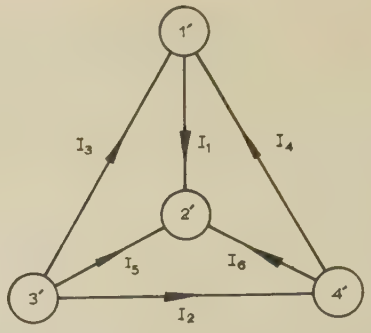

Fig. 1.—The connection without ideal transformers.

For example, in Fig. 1,

$$\begin{bmatrix} 1 & 0 & -1 & -1 & 0 & 0 \\ -1 & 0 & 0 & 0 & -1 & -1 \\ 0 & 1 & 1 & 0 & 1 & 0 \\ 0 & -1 & 0 & 1 & 0 & 1 \end{bmatrix} \begin{bmatrix} I_1 \\ I_2 \\ I_3 \\ I_4 \\ I_5 \\ I_6 \end{bmatrix} = \begin{bmatrix} 0 \\ 0 \\ 0 \\ 0 \end{bmatrix}$$

or

$$\begin{bmatrix} 1 & 0 & -1 & -1 & 0 & 0 \\ -1 & 0 & 0 & 0 & -1 & -1 \\ 0 & 1 & 1 & 0 & 1 & 0 \end{bmatrix} \begin{bmatrix} I_1 \\ I_2 \\ I_3 \\ I_4 \\ I_5 \\ I_6 \end{bmatrix} = \begin{bmatrix} 0 \\ 0 \\ 0 \end{bmatrix}$$

(2.2) Ideal Transformers[23]

With ideal transformers having no magnetic leakage flux a infinite permeance, it is sufficient to consider only those id transformers which each have a magnetic circuit consisting o of a single-loop core, with the coil m.m.f.'s in series and common magnetic flux, and it follows that

$$NI = 0 \quad . \quad . \quad . \quad . \quad . \quad . \quad (1$$

where each element of N is the number of turns of a windi coil in each magnetic core of the ideal transformers, a each sign is positive or negative according to the bran

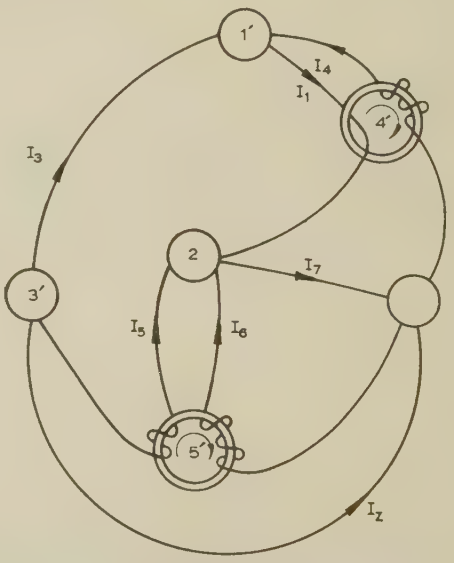

Fig. 2.—The connection with ideal transformers.

orientation for the core. Here N is a $t \times \alpha_1$ matrix, where t is the number of ideal transformers, and is called a 'winding matrix' or 'turns-ratio matrix'. For example, in Fig. 2,

$$N = \begin{bmatrix} -1 & 0 & 0 & 4 & 0 & 0 & 0 \\ 0 & 0 & 0 & 0 & 2 & 3 & 0 \end{bmatrix} \quad . \quad . \quad (11)$$

Each element of a winding matrix is a real integer, positive or negative. With the following definition:

$$B = \begin{bmatrix} \tilde{D} \\ \\ N \end{bmatrix} = \left[\begin{bmatrix} 1 & 0 & -1 & -1 & 0 & 0 & 0 \\ -1 & 0 & 0 & 0 & -1 & -1 & 1 \\ 0 & 1 & 1 & 0 & 1 & 0 & 0 \end{bmatrix} \begin{bmatrix} -1 & 0 & 0 & 4 & 0 & 0 & 0 \\ 0 & 0 & 0 & 0 & 2 & 3 & 0 \end{bmatrix}\right] \quad (12)$$

B is an $(\alpha_0 - 1 + t) \times \alpha_1$ matrix, and we have

$$BI = \mathbf{0} \quad . \quad . \quad . \quad . \quad . \quad . \quad . \quad (13)$$

i.e.

$$\left[\begin{bmatrix} 1 & 0 & -1 & -1 & 0 & 0 & 0 \\ -1 & 0 & 0 & 0 & -1 & -1 & 1 \\ 0 & 1 & 1 & 0 & 1 & 0 & 0 \end{bmatrix} \begin{bmatrix} -1 & 0 & 0 & 4 & 0 & 0 & 0 \\ 0 & 0 & 0 & 0 & 2 & 3 & 0 \end{bmatrix}\right] \begin{bmatrix} I_1 \\ I_2 \\ I_3 \\ I_4 \\ I_5 \\ I_6 \\ I_7 \end{bmatrix} = \begin{bmatrix} \begin{bmatrix} 0 \\ 0 \\ 0 \end{bmatrix} \\ \\ \begin{bmatrix} 0 \\ 0 \end{bmatrix} \end{bmatrix}$$

Provided that the number of magnetic cores of the ideal transformers is given by t, the ranks of $\tilde{D}$, N and B, respectively, are given by

$$\rho_D = \rho(D) = \rho(\tilde{D}) = \alpha_0 - p_0 = \alpha_0 - 1$$
$$\rho_N = \rho(N) = t$$
and $$\rho_B = \rho(B) = \rho_D + \rho_N = \alpha_0 - p_0 + t = \alpha_0 - 1 + t$$

where it is postulated that $\tilde{D}$ and N are mutually linearly-independent, so that $t \leqslant \alpha_1 - \alpha_0 + 1 = p_1$, the number of independent loops. Any winding matrix N which depends linearly on the node-branch incidence matrix $\tilde{D}$ is not admissible, because the result is the same whether it exist or not; B is called the 'generalized node-branch incidence matrix'.

(2.3) Generalized Loop-Branch Incidence Matrices[8, 25]

Let C be an $(\alpha_1 - \rho_B) \times \alpha_1$ matrix formed by a maximal set of linearly independent solutions, x', of the following equation:

$$Bx = \mathbf{0} \quad \text{or} \quad x'B' = \mathbf{0} \quad . \quad . \quad . \quad . \quad (14)$$

i.e.

$$BC' = \mathbf{0} \quad \text{or} \quad CB' = \mathbf{0} \quad . \quad . \quad . \quad . \quad (15)$$

namely C is a $(\alpha_1 - \alpha_0 + 1 - t) \times \alpha_1$ matrix. For example, in Fig. 2, relation (14) is denoted as follows:

$$Bx = \left[\begin{bmatrix} 1 & 0 & -1 & -1 & 0 & 0 & 0 \\ -1 & 0 & 0 & 0 & -1 & -1 & 1 \\ 0 & 1 & 1 & 0 & 1 & 0 & 0 \end{bmatrix} \begin{bmatrix} -1 & 0 & 0 & 4 & 0 & 0 & 0 \\ 0 & 0 & 0 & 0 & 2 & 3 & 0 \end{bmatrix}\right] \begin{bmatrix} x_1 \\ x_2 \\ x_3 \\ x_4 \\ x_5 \\ x_6 \\ x_7 \end{bmatrix} = \begin{bmatrix} \begin{bmatrix} 0 \\ 0 \\ 0 \end{bmatrix} \\ \\ \begin{bmatrix} 0 \\ 0 \end{bmatrix} \end{bmatrix}$$

Thus one example of C is

$$C = \begin{bmatrix} 1 \\ x' \\ \\ 2 \\ x' \end{bmatrix} = \begin{bmatrix} 4 & -3 & 3 & 1 & 0 & 0 & 4 \\ \\ 0 & 3 & 0 & 0 & -3 & 2 & 1 \end{bmatrix}$$

B and C are zero factors of each other. If ideal transformers do not exist, B equals $\tilde{D}$, and C can be equal to a loop-branch incidence matrix* R. Then B is called the 'generalized loop-branch incidence matrix'.

For example, in Fig. 1, since we make

$$B = \tilde{D} = \begin{bmatrix} 1 & 0 & -1 & -1 & 0 & 0 \\ -1 & 0 & 0 & 0 & -1 & -1 \\ 0 & 1 & 1 & 0 & 1 & 0 \end{bmatrix}$$

the maximal set C of the independent solutions, x', of the equation

$$Bx = \tilde{D}x = \begin{bmatrix} 1 & 0 & -1 & -1 & 0 & 0 \\ -1 & 0 & 0 & 0 & -1 & -1 \\ 0 & 1 & 1 & 0 & 1 & 0 \end{bmatrix} \begin{bmatrix} x_1 \\ x_2 \\ x_3 \\ x_4 \\ x_5 \\ x_6 \end{bmatrix} = \begin{bmatrix} 0 \\ 0 \\ 0 \end{bmatrix}$$

is determined as follows:

$$C = \begin{bmatrix} 1 & 0 & 1 & 0 & -1 & 0 \\ -1 & 0 & 0 & -1 & 0 & 1 \\ 0 & -1 & 0 & 0 & 1 & -1 \end{bmatrix} = R$$

Evidently this is a loop-branch incidence matrix[2, 25] when the

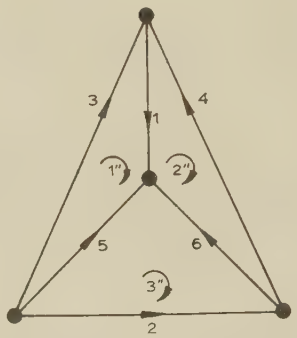

Fig. 3.—Loop-branch incidence relation.

independent loops are chosen as in Fig. 3, and the relation is denoted by

$$DR' = \mathbf{0} \quad \text{or} \quad RD' = \mathbf{0} \quad . \quad . \quad . \quad . \quad (16)$$

i.e. D and R are zero factors of the other. From eqns. (13) and (15), I can be a linear combination of the columns of C'. If J is an adequate matrix of one column for coefficients of the above combination, we have

$$I = C'J \quad . \quad . \quad . \quad . \quad . \quad . \quad . \quad (17)$$

J is called the 'generalized loop-current matrix', and if $B = \tilde{D}$, i.e. $C = R$, J is an ordinary loop-current matrix. The rank of C is equal to

$$\rho_C = \alpha_1 - \rho_B = \alpha_1 - (\alpha_0 - p_0 + t) = p_1 - t_1 = \alpha_1 - (\alpha_0 - 1 + t)$$

where α_1 is the number of branches, and p_1 is the first Betti number, which is the number of independent loops.

(2.4) Principle of the Conservation of Energy and the Generalized Kirchhoff's Second Law

The powers of the active and passive elements are calculated as follows: the power in the ideal transformer is zero, and if there is no current source, we may consider only $\bar{I}'U$ in passive

* D and R, respectively, correspond to div and curl in a vector field, and thus we specifically use D and R to denote the corresponding matrices.

elements other than ideal transformers, and $\bar{I}'V$ in voltage sources, where $\bar{I}'$ is the conjugate matrix of the branch-current matrix of one row. From the general principle of the conservation of energy, therefore, we have

$$\bar{I}'U - I'V = 0$$

Therefore $$I'(U - V) = 0$$

From eqn. (17) we have

$$J'C(U - V) = 0 \quad . \quad . \quad . \quad . \quad . \quad (18)$$

In order to make eqn. (18) hold for any value of J, we must have

$$C(U - V) = 0 \quad . \quad . \quad . \quad . \quad . \quad (19)$$

i.e. $$CU = CV \quad . \quad . \quad . \quad . \quad . \quad . \quad . \quad (20)$$

which is the same as Kirchhoff's second law if ideal transformers do not exist, since $C = R$ in this case.*

(2.5) Fundamental Equations of a Network Problem and the Driving-Conductance Matrix

The fundamental equations of an electrical network can be arranged as follows:

Generalized first law of Kirchhoff: $BI = 0 \quad . \quad . \quad (21)$

Generalized second law of Kirchhoff: $CU = CV \quad . \quad . \quad (22)$

Ohm's law: $U = rI \quad . \quad . \quad (23)$

where r is a branch-impedance matrix. If V is given, U and I are determined by eqns. (21), (22) and (23). When we wish to determine branch currents I caused by branch-voltage sources V, the matrix G in the solution of the form

$$I = GV \quad . \quad . \quad . \quad . \quad . \quad . \quad . \quad (24)$$

is generally called the 'transfer-admittance matrix'. Using matrix calculations this may be determined as follows. From eqns. (22) and (23) we have

$$CrI = CV$$

As in eqn. (17), changing the variable I to J, we have

$$CrC'J = CV$$
$$J = (CrC')^{-1}CV$$

Then from eqn. (17)

$$I = C'(CrC')^{-1}CV \quad . \quad . \quad . \quad . \quad . \quad (25)$$

Therefore the driving-conductance matrix is determined by

$$G = C'(CrC')^{-1}C = C'Z^{-1}C, \text{ where } Z = CrC' \quad . \quad (26)$$

If there is no ideal transformer, we may change C to R, and it is then determined by

$$G = R'(RrR')^{-1}R \quad . \quad . \quad . \quad . \quad . \quad (27)$$

(3) TOPOLOGICAL SYNTHESIS OF THE DRIVING-CONDUCTANCE MATRIX

(3.1) Topological Method

In the previous Section, we determined the distribution of currents I caused by the given voltage sources V about the given network. But frequently we must determine a network which has the given distribution of currents I caused by the give voltage sources V. Here the problem is to determine the ne work which is specified by the given driving-conductance matr G. If the frequency of the voltage sources is constant, we ma treat this problem by the topological synthesis of the netwo which is specified by the driving-conductance matrix given arbitrary real numbers, where, in general,

$$G' \neq G \quad . \quad . \quad . \quad . \quad . \quad . \quad . \quad (2$$

For the practical problem, a few conditions must be attache One of these is that G must not be negative, because the el ments of the considered network are passive and dissipative.

From eqns. (15) and (26), whatever the voltage sources B must be both a left and (as B') a right zero factor of G

i.e. $$BG = O \quad \text{or} \quad GB' = O \quad . \quad . \quad (29'), (29$$

where, in general, $G' \neq G$ and the rank of G is, from eqn. (2

$$\rho_t = \rho(G) = \rho_c = p_1 - t$$

The maximum number of independent solutions of $Gx = O$ is

$$\alpha_1 - \rho_t = \alpha_1 - (p_1 - t) = a_1 - (a_1 - \alpha_0 + p_0 - t)$$
$$= \alpha_0 - p_0 + t = \alpha_0 - 1 +$$

where x is an unknown matrix of one column. If we indicate maximal set of independent solutions $x, x, \ldots, x (m = \alpha_0 - 1$ by

$$X = \begin{bmatrix} x_1 \\ x_2 \\ \cdot \\ \cdot \\ \cdot \\ x_m \end{bmatrix} = \begin{bmatrix} x_1 & x_1 & \cdots & x_1 \\ 1 & 2 & & m \\ x_2 & x_2 & \cdots & x_2 \\ 1 & 2 & & m \\ & & & \\ & \cdots & & \\ & & & \\ x_n & x_n & \cdots & x_n \\ 1 & 2 & & m \end{bmatrix} \quad . \quad (3$$

we have $$GX = 0 \quad . \quad . \quad . \quad . \quad . \quad . \quad (3$$

From eqns. (29) and (31), it follows that X and B are linea transformations of each other, since B' also has m column and these are linearly independent. Hence we may put

$$B = KX' \quad . \quad . \quad . \quad . \quad . \quad . \quad (3$$

where K is an arbitrary transformation matrix, and det (K) $\neq$ [so that, from eqns. (29), (31) and (32), X must also be a le zero factor of G, i.e. $X'G = O$]. Therefore we can determine from X by a suitable linear transformation, so that B ma satisfy the character of a node-branch incidence matrix and winding matrix. If the rows of B do not satisfy the charact of a node-branch incidence matrix, we must use ideal tran formers. In other words, the determinant of B is a set of linea combinations of rows of X', and it is written like eqn. (32) as matrix expression. Generally the character of the 1-incidenc matrix, whose elements are $+1$, -1, or 0, is special, and ca not be algebraically treated. But one solution at least of B ca be X' itself, and we can obtain a solution or sometimes severa algebraically by inspection. If some systematic method wer found, it should give the direct solution of the importan unsolved problem of the necessary and sufficient conditions fo the realizability of an n-port network without ideal transformer (see the end of example 2). After we have determined th connection and ideal transformers, we can determine the branc impedances. We find the general inverse C^{-1} of C satisfying

$$CC^{-1} = 1 \quad . \quad . \quad . \quad . \quad . \quad . \quad (3$$

* This method of deriving Kirchhoff's second law from the energy principle is called 'Planck's logic'.

where **1** is a unit matrix of dimension $(\alpha_1 - \rho_B)$, and C is generally a rectangular matrix, namely, an $(\alpha_1 - \rho_B) \times \alpha_1$ one. C^{-1} is not determined uniquely, but it may be an arbitrary matrix satisfying eqn. (33). Hence it follows that

$$(C^{-1\prime}GC^{-1})^{-1} = \{C^{-1\prime}[C'(CrC')^{-1}C]C^{-1}\}^{-1} = CrC' = Z \quad . \quad . \quad . \quad . \quad . \quad . \quad . \quad . \quad . \quad (34)$$

We can determine the branch-resistance matrix r by comparing $(C^{-1\prime}GC^{-1})^{-1}$ with CrC', since G, C and C^{-1} are already known. If we put

$$\begin{cases} {}^{(+)}_{r} = 1/2(r + r') \\ {}^{(-)}_{r} = 1/2(r - r') \end{cases} \quad \text{and} \quad \begin{cases} {}^{(+)}_{Z} = 1/2(Z + Z') \\ {}^{(-)}_{Z} = 1/2(Z - Z') \end{cases}$$

the comparison is done more easily, since we use such branch elements as resistances and real gyrators.

(3.2) Necessary Conditions for G

Of necessity, r must be positive, and the necessary conditions for G are as follows:

(a) G must not be negative

i.e. $$x'Gx \geqslant 0 \quad . \quad . \quad . \quad . \quad . \quad . \quad . \quad . \quad (35)$$

for any matrix x of one column, the elements of which are real numbers.

(b) G must have the same zero factor of rank n–k on the right and the left sides of G.

Thus each of the dependent rows (or columns) is a linear combination of the other independent rows (or columns) with real coefficients, with the same linear combinations for corresponding rows and columns. Only if the given value of G satisfies conditions (a) and (b) can we produce a network having this value of G. This network is shown algebraically as both B and r. In order to have the smallest number of ideal transformers, it would be better for the driving-conductance matrix G to satisfy the following condition (b') instead of (b):

(b') Each of the dependent rows (or columns) of G is a linear combination of the other independent rows (or columns) only for the coefficients ± 1. It is because each element in the zero factor becomes only ± 1 or 0 if (b') holds.

(4) EXAMPLES

(4.1) Problem 1

Design a network specified by the driving-conductance matrix*

$$G = \begin{bmatrix} 26 & -24 & 2 & 20 & -4 & 6 \\ -14 & 31 & 17 & -18 & 13 & 4 \\ 12 & 7 & 19 & 2 & 9 & 10 \\ 16 & -22 & -6 & 34 & 12 & -18 \\ 2 & 9 & 11 & 16 & 25 & -14 \\ 10 & -2 & 8 & -14 & -16 & 24 \end{bmatrix}$$

The first row in G equals the fourth row plus the sixth row in G, the second equals the fifth minus the fourth, and the third row equals the fifth plus the sixth. The rank k of G is then 3. As these relations similarly hold in the transposed matrix of G, G has the same zero factor of rank 3 on the right and the left sides. Since we have

$$24 > 0, \quad \begin{vmatrix} 25 & -14 \\ -16 & 24 \end{vmatrix} > 0, \quad \begin{vmatrix} 34 & 12 & -18 \\ 16 & 25 & -14 \\ -14 & -16 & 24 \end{vmatrix} > 0,$$

$$\begin{vmatrix} 19 & 2 & 9 & 10 \\ -6 & 34 & 12 & -18 \\ 11 & 16 & 25 & -14 \\ 8 & -14 & -16 & 24 \end{vmatrix} = 0, \ldots = 0$$

G must be negative. Thus conditions (a), (b) and (b') in Section 3.2 hold for this value of G.

In order to determine a set of independent solutions of $Gx = \mathbf{0}$, we must exclude from G the row linearly dependent on the others, as follows:

$$\begin{bmatrix} 16 & -22 & -6 & 34 & 12 & -18 \\ 2 & 9 & 11 & 16 & 25 & -14 \\ 10 & -2 & 8 & -14 & -16 & 24 \end{bmatrix} \begin{bmatrix} x_1 \\ x_2 \\ x_3 \\ x_4 \\ x_5 \\ x_6 \end{bmatrix} = \mathbf{0}$$

Then

$$\begin{bmatrix} 34 & 12 & -18 \\ 16 & 25 & -14 \\ -14 & -16 & 24 \end{bmatrix} \begin{bmatrix} x_4 \\ x_5 \\ x_6 \end{bmatrix} = - \begin{bmatrix} 16 & -22 & -6 \\ 2 & 9 & 11 \\ 10 & -2 & 8 \end{bmatrix} \begin{bmatrix} x_1 \\ x_2 \\ x_3 \end{bmatrix}$$

Therefore

$$\begin{bmatrix} x_4 \\ x_5 \\ x_6 \end{bmatrix} = - \begin{bmatrix} 34 & 12 & -18 \\ 16 & 25 & -14 \\ -14 & -16 & 24 \end{bmatrix}^{-1} \begin{bmatrix} 16 & -22 & -6 \\ 2 & 9 & 11 \\ 10 & -2 & 8 \end{bmatrix} \begin{bmatrix} x_1 \\ x_2 \\ x_3 \end{bmatrix}$$

$$= \frac{1}{4418} \begin{bmatrix} 188 & 0 & 141 \\ -94 & 282 & 94 \\ 47 & 188 & 329 \end{bmatrix} \begin{bmatrix} 16 & -22 & -6 \\ 2 & 9 & 11 \\ 10 & -2 & 8 \end{bmatrix} \begin{bmatrix} x_1 \\ x_2 \\ x_3 \end{bmatrix}$$

Putting $$\begin{bmatrix} x_1 \\ x_2 \\ x_3 \end{bmatrix} = \begin{bmatrix} 1 \\ 0 \\ 0 \end{bmatrix}, \quad \begin{bmatrix} 0 \\ 1 \\ 0 \end{bmatrix} \text{ or } \begin{bmatrix} 0 \\ 0 \\ 1 \end{bmatrix}$$

we have

$$\begin{bmatrix} x_4 \\ x_5 \\ x_6 \end{bmatrix} = \frac{1}{4418} \begin{bmatrix} 188 & 0 & 141 \\ -94 & 282 & 94 \\ 47 & 188 & 329 \end{bmatrix} \begin{bmatrix} 16 & -22 & -6 \\ 2 & 9 & 11 \\ 10 & -2 & 8 \end{bmatrix} \left\{ \begin{bmatrix} 1 \\ 0 \\ 0 \end{bmatrix}, \quad \begin{bmatrix} 0 \\ 1 \\ 0 \end{bmatrix} \text{ or } \begin{bmatrix} 0 \\ 0 \\ 1 \end{bmatrix} \right\}$$

$$= \frac{1}{4418} \begin{bmatrix} 188 & 0 & 141 \\ -94 & 282 & 94 \\ 47 & 188 & 329 \end{bmatrix} \left\{ \begin{bmatrix} 16 \\ 2 \\ 10 \end{bmatrix}, \quad \begin{bmatrix} -22 \\ 9 \\ -2 \end{bmatrix} \text{ or } \begin{bmatrix} -6 \\ 11 \\ 8 \end{bmatrix} \right\} = \left\{ \begin{bmatrix} -1 \\ 0 \\ -1 \end{bmatrix}, \quad \begin{bmatrix} 1 \\ -1 \\ 0 \end{bmatrix} \text{ or } \begin{bmatrix} 0 \\ -1 \\ -1 \end{bmatrix} \right\}$$

Let a maximal set of the independent solutions be denoted by X. We can determine X from the above result as follows:

$$X' = \begin{bmatrix} 1 & 0 & 0 & -1 & 0 & -1 \\ 0 & 1 & 0 & 1 & -1 & 0 \\ 0 & 0 & 1 & 0 & -1 & -1 \end{bmatrix}$$

as we saw at the beginning. In order to have a set of linear

* This example is made up as follows: choosing arbitrarily the square matrix of the fifth to sixth rows and columns, which must be positive-definite, the others are given as the linear combinations of the above rows and columns.

combinations of rows in X' satisfying the character of a connection matrix, we may put

$$B = KX' = \begin{bmatrix} -1 & -1 & 1 \\ 0 & 1 & 0 \\ 1 & 0 & 0 \end{bmatrix} \begin{bmatrix} 1 & 0 & 0 & -1 & 0 & -1 \\ 0 & 1 & 0 & 1 & -1 & 0 \\ 0 & 0 & 1 & 0 & -1 & -1 \end{bmatrix}$$

$$= \begin{bmatrix} -1 & -1 & 1 & 0 & 0 & 0 \\ 0 & 1 & 0 & 1 & -1 & \\ 1 & 0 & 0 & -1 & 0 & -1 \end{bmatrix}$$

Therefore $$D = \begin{bmatrix} \begin{bmatrix} -1 & -1 & 1 & 0 & 0 & 0 \\ 0 & 1 & 0 & 1 & -1 & 0 \\ 1 & 0 & 0 & -1 & 0 & -1 \end{bmatrix} \\ \begin{bmatrix} 0 & 0 & -1 & 0 & 1 & 1 \end{bmatrix} \end{bmatrix}$$

This connection matrix shows the network in Fig. 4. A set of

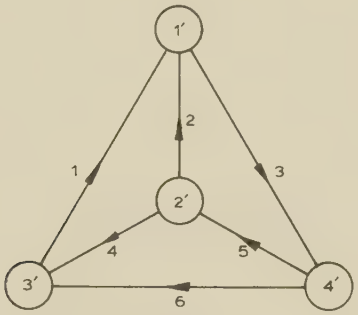

Fig. 4.—The connection determined in problem 1.

independent loops is determined as indicated in Fig. 5, and the loop matrix is then given by

$$R = \begin{bmatrix} 1 & -1 & 0 & 1 & 0 & 0 \\ 0 & 1 & 1 & 0 & 1 & 0 \\ 0 & 0 & 0 & -1 & -1 & 1 \end{bmatrix}$$

R^{-1}, satisfying $RR^{-1} = \mathbf{1}$ where $\mathbf{1}$ is a unit matrix, is determined as follows:

$$R^{-1} = \begin{bmatrix} 1 & 0 & 0 \\ 0 & 0 & 0 \\ 0 & 1 & 0 \\ 0 & 0 & 0 \\ 0 & 0 & 0 \\ 0 & 0 & 1 \end{bmatrix}$$

Therefore we can calculate Y as follows:

$$Y = R^{-1\prime}GR^{-1} = \begin{bmatrix} 1 & 0 & 0 & 0 & 0 & 0 \\ 0 & 0 & 1 & 0 & 0 & 0 \\ 0 & 0 & 0 & 0 & 0 & 1 \end{bmatrix}$$

$$\begin{bmatrix} 26 & -24 & 2 & 20 & -4 & 6 \\ -14 & 31 & 17 & -18 & 13 & 4 \\ 12 & 7 & 19 & 2 & 9 & 10 \\ 16 & -22 & -6 & 34 & 12 & -18 \\ 2 & 9 & 11 & 16 & 25 & -14 \\ 10 & -2 & 8 & -14 & -16 & 24 \end{bmatrix} \begin{bmatrix} 1 & 0 & 0 \\ 0 & 0 & 0 \\ 0 & 1 & 0 \\ 0 & 0 & 0 \\ 0 & 0 & 0 \\ 0 & 0 & 1 \end{bmatrix} = \begin{bmatrix} 26 & 2 & 6 \\ 12 & 19 & 10 \\ 10 & 8 & 24 \end{bmatrix}$$

Then

$$Z = Y^{-1} = \underbrace{\begin{bmatrix} 4 & 0 & -1 \\ -2 & 6 & -2 \\ -1 & -2 & 5 \end{bmatrix}}_{94} = \underbrace{\begin{bmatrix} 4 & -1 & -1 \\ -1 & 6 & -2 \\ -1 & -2 & 5 \end{bmatrix}}_{94} + \underbrace{\begin{bmatrix} 0 & 1 & 0 \\ -1 & 0 & 0 \\ 0 & 0 & 0 \end{bmatrix}}_{94}$$

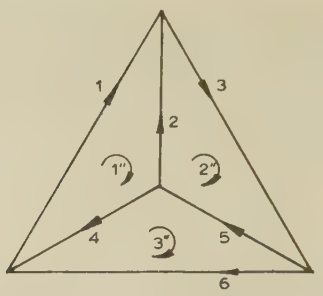

Fig. 5.—A set of the independent loops.

Namely $$\overset{(+)}{Z} = \underbrace{\begin{bmatrix} 4 & -1 & -1 \\ -1 & 6 & -2 \\ -1 & -2 & 5 \end{bmatrix}}_{94} \quad . \quad . \quad . \quad . \quad (+$$

and $$\overset{(-)}{Z} = \underbrace{\begin{bmatrix} 0 & 1 & 0 \\ -1 & 0 & 0 \\ 0 & 0 & 0 \end{bmatrix}}_{94} \quad . \quad . \quad . \quad . \quad . \quad (-$$

On the other hand, we can directly show the symmetric part $\overset{(+)}{r}$ of the loop-resistance matrix r as follows:

$$\overset{(+)}{Z} = R\overset{(+)}{r}R' =$$

$$\begin{bmatrix} 1 & -1 & 0 & 1 & 0 & 0 \\ 0 & 1 & 1 & 0 & 1 & 0 \\ 0 & 0 & 0 & -1 & -1 & 1 \end{bmatrix} \begin{bmatrix} r_1 & 0 & 0 & 0 & 0 & 0 \\ 0 & r_2 & 0 & 0 & 0 & 0 \\ 0 & 0 & r_3 & 0 & 0 & 0 \\ 0 & 0 & 0 & r_4 & 0 & 0 \\ 0 & 0 & 0 & 0 & r_5 & 0 \\ 0 & 0 & 0 & 0 & 0 & r_6 \end{bmatrix}$$

$$\begin{bmatrix} 1 & 0 & 0 \\ -1 & 1 & 0 \\ 0 & 1 & 0 \\ 1 & 0 & -1 \\ 0 & 1 & -1 \\ 0 & 0 & 1 \end{bmatrix} = \begin{bmatrix} r_1 + r_2 + r_4 & -r_2 & -r_4 \\ -r_2 & r_2 + r_3 + r_5 & -r_5 \\ -r_4 & -r_5 & r_4 + r_5 + r_6 \end{bmatrix} . \quad (+$$

Comparing eqns. (+A) and (+B), we determine the eleme impedances as

$$r_1 = 0{\cdot}0212,\ r_2 = 0{\cdot}0106,\ r_3 = 0{\cdot}0318,\ r_4 = 0{\cdot}0106,$$
$$r_5 = 0{\cdot}0212,\ r_6 = 0{\cdot}0212.$$

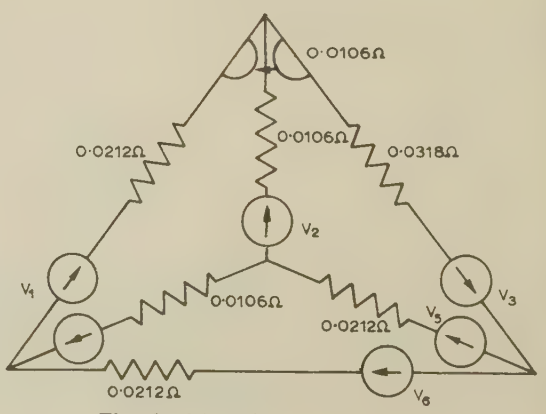

Fig. 6.—The solution of problem 1.

In order to obtain the unsymmetrical part $\overset{(-)}{Z}$, we have

$$r_{13} = 0{\cdot}0106, \quad r_{31} = -0{\cdot}0106$$

by comparing (−A) with Fig. 5. We then have a network as shown in Fig. 6.

(4.2) Problem 2

Let us design a network specified by the driving-conductance matrix*

$$G = \begin{bmatrix} 5 & -2 & 3 & -1 & 8 & -3 & 5 & -3 \\ -4 & 3 & -1 & 2 & 4 & 5 & 9 & -8 \\ 1 & 1 & 2 & 1 & 12 & 2 & 14 & -11 \\ -3 & 1 & -2 & 2 & 0 & 3 & 5 & -3 \\ -8 & 8 & 4 & 12 & 48 & 20 & 84 & -68 \\ -7 & 4 & -3 & 4 & 4 & 8 & 12 & -11 \\ -15 & 12 & -3 & 16 & 52 & 28 & 90 & -67 \\ 13 & -10 & 3 & -13 & -40 & -23 & -71 & 53 \end{bmatrix}$$

A maximal set of independent rows is the second, third and fourth, while, in the transposing matrix of G, similar relations hold. Dependent relations are similar on the right and the left sides, and dependent rows or columns are linear combinations of independent rows or columns with real coefficients. Therefore G has the same zero factor on both sides.

$$Gx = \begin{bmatrix} -4 & 3 & -1 & 2 & 4 & 5 & 9 & -8 \\ 1 & 1 & 2 & 1 & 12 & 2 & 14 & -11 \\ -3 & 1 & -2 & 2 & 0 & 3 & 5 & -3 \end{bmatrix} \begin{bmatrix} x_1 \\ x_2 \\ x_3 \\ x_4 \\ x_5 \\ x_6 \\ x_7 \\ x_8 \end{bmatrix} = \mathbf{0}$$

Therefore
$$X' = \begin{bmatrix} 1 & 1 & -1 & 0 & 0 & 0 & 0 & 0 \\ 0 & 0 & -4 & -4 & 1 & 0 & 0 & 0 \\ 0 & -1 & 0 & -1 & 0 & 1 & 0 & 0 \\ 0 & -1 & -4 & -5 & 0 & 0 & 1 & 0 \\ 0 & 1 & 3 & 4 & 0 & 0 & 0 & 1 \end{bmatrix}$$

If we put
$$K = \begin{bmatrix} 1 & 0 & 0 & 0 & 0 \\ -1 & 1 & 0 & 0 & 1 \\ 0 & 0 & 1 & 0 & 0 \\ 0 & 0 & 0 & -1 & -1 \\ 0 & 3 & 4 & 0 & 4 \end{bmatrix}$$

$$B = KX' = \begin{bmatrix} 1 & 0 & 0 & 0 & 0 \\ -1 & 1 & 0 & 0 & 1 \\ 0 & 0 & 1 & 0 & 0 \\ 0 & 0 & 0 & -1 & -1 \\ 0 & 3 & 4 & 0 & 4 \end{bmatrix} \times$$

$$\begin{bmatrix} 1 & 1 & -1 & 0 & 0 & 0 & 0 & 0 \\ 0 & 0 & -4 & -4 & 1 & 0 & 0 & 0 \\ 0 & -1 & 0 & -1 & 0 & 1 & 0 & 0 \\ 0 & -1 & -4 & -5 & 0 & 0 & 1 & 0 \\ 0 & 1 & 3 & 4 & 0 & 0 & 0 & 1 \end{bmatrix}$$

$$= \begin{bmatrix} 1 & 1 & -1 & 0 & 0 & 0 & 0 & 0 \\ -1 & 0 & 0 & 0 & 1 & 0 & 0 & 1 \\ 0 & -1 & 0 & -1 & 0 & 1 & 0 & 0 \\ 0 & 0 & 1 & 1 & 0 & 0 & -1 & -1 \\ 0 & 0 & 0 & 0 & 3 & 4 & 0 & 4 \end{bmatrix}$$

* This example is made up from $\begin{bmatrix} 3 & -1 & 2 \\ 1 & 2 & 1 \\ 1 & -2 & 2 \end{bmatrix}$.

Then we obtain

$$D = \left[\begin{bmatrix} 1 & 1 & -1 & 0 & 0 & 0 & 0 & 0 \\ -1 & 0 & 0 & 0 & 1 & 0 & 0 & 1 \\ 0 & -1 & 0 & -1 & 0 & 1 & 0 & 0 \\ 0 & 0 & 1 & 1 & 0 & 0 & -1 & -1 \end{bmatrix}\right.$$

$$\left.\begin{bmatrix} 0 & 0 & 0 & 0 & -1 & -1 & 1 & 0 \end{bmatrix}\right]$$

and
$$N = [0 \;\; 0 \;\; 0 \;\; 0 \;\; 3 \;\; 4 \;\; 0 \;\; 4]$$

Therefore we have the connection shown in Fig. 7.

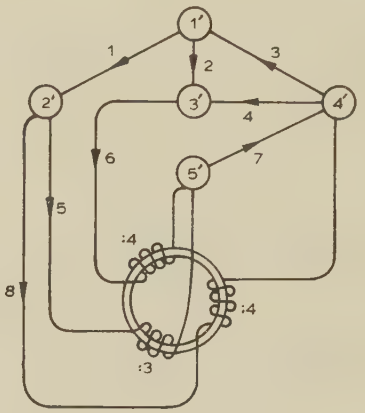

Fig. 7.—The connection and the ideal transformer determined in problem 2.

A maximal set of independent solutions for

$$Bx = \mathbf{0}$$

$$C = \begin{bmatrix} -1 & 1 & 0 & 0 & 0 & 1 & 1 & -1 \\ 1 & 0 & 1 & 0 & 4 & 0 & 4 & -3 \\ 0 & 0 & 0 & 1 & 4 & 1 & 5 & -4 \end{bmatrix}$$

The generalized inverse of C is

$$C^{-1} = \begin{bmatrix} 0 & 1 & 0 & 0 & 0 & 0 & 0 & 0 \\ 0 & 0 & 1 & 0 & 0 & 0 & 0 & 0 \\ 0 & 0 & 0 & 1 & 0 & 0 & 0 & 0 \end{bmatrix}$$

On the one hand,

$$Z = Y^{-1} = (C^{-1}GC^{-1})^{-1} = \begin{bmatrix} 3 & -1 & 2 \\ 1 & 2 & 1 \\ 1 & -2 & 2 \end{bmatrix} = \frac{1}{11}$$

$$\begin{bmatrix} 6 & -2 & -5 \\ -1 & 4 & -5 \\ -4 & 5 & 7 \end{bmatrix} = \underline{\begin{bmatrix} 12 & -3 & 9 \\ -3 & 8 & 0 \\ 9 & 0 & 14 \end{bmatrix}} + \underline{\begin{bmatrix} 0 & -1 & -1 \\ 1 & 0 & -10 \\ 1 & -10 & 0 \end{bmatrix}}$$
$$22 \qquad\qquad 22$$

Therefore
$$\overset{(+)}{Z} = \underline{\begin{bmatrix} 12 & -3 & 9 \\ -3 & 8 & 0 \\ 9 & 0 & 14 \end{bmatrix}}$$
$$22$$

and
$$\overset{(-)}{Z} = \underline{\begin{bmatrix} 0 & -1 & -1 \\ 1 & 0 & -10 \\ 1 & -10 & 0 \end{bmatrix}} \quad . \quad . \quad (+A), (-A)$$
$$22$$

On the other hand,

$$\overset{(+)}{Z} = \begin{bmatrix} r_1 + r_2 + r_6 + r_7 + r_8 & -r_1 + 4r_7 + 3r_8 & r_6 + 5r_7 + 4r_8 \\ -r_1 + 4r_7 + 3r_8 & r_1 + r_3 + 16r_5 + 16r_7 + 9r_7 & 16r_5 + 20r_7 + 12r_8 \\ r_6 + 5r_7 + 4r_8 & 16r_5 + 20r_7 + 12r_8 & r_4 + 16r_5 + r_6 + 25r_7 + 16r_8 \end{bmatrix} \quad . \ . \ . \ . \ (+B$$

Comparing relations (+A) and (+B), we have

$$r_1 = 1{\cdot}6 \times 10^{-1},\ r_2 = r_3 = r_4 = 0,\ r_5 = 7{\cdot}1 \times 10^{-3},$$
$$r_6 = 3{\cdot}8 \times 10^{-1},\ r_7 = 4{\cdot}3 \times 10^{-3},\ r_8 = 2{\cdot}3 \times 10^{-3}$$

From the elements in C, by inspection, it can be stated that only three gyrators exist among the branches 2, 3 and 4. Therefore, in this case, $\overset{(-)}{Z}$ is written as

$$\overset{(-)}{Z} = \begin{bmatrix} 0 & r_{23} & r_{24} \\ r_{32} & 0 & r_{34} \\ r_{42} & r_{43} & 0 \end{bmatrix} \quad . \ . \ . \ . \ (-B)$$

Comparing (−A) with (−B), we have

$$r_{32} = -r_{23} = 4{\cdot}55 \times 10^{-2},\ r_{42} = -r_{24} = 4{\cdot}55 \times 10^{-2},$$
$$r_{43} = -r_{34} = 4{\cdot}55 \times 10^{-1}$$

Finally we have the network of the type of Fig. 8.

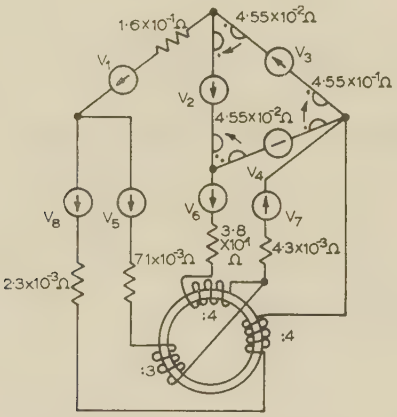

Fig. 8.—The solution of problem 2.

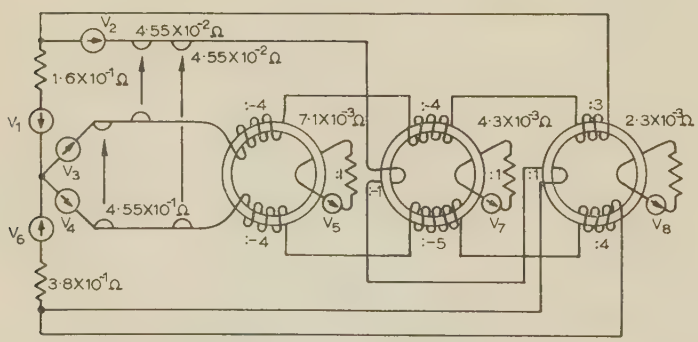

Fig. 9.—The solution with many ideal transformers.

On determination of the connection, the minimum number of ideal transformers are not given, but by inspection the rest are given and several solutions for the problem are provided. For instance, B satisfying this problem is as follows: Arranging the rows of X' only, we have

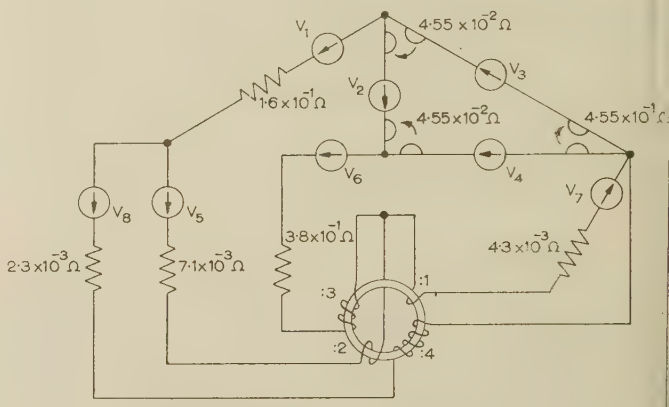

Fig. 10.—The solution given by $\tilde{B}$.

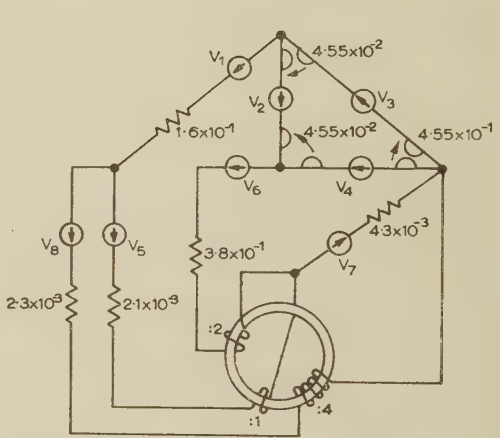

Fig. 11.—One of the solutions given by $\tilde{B}$.

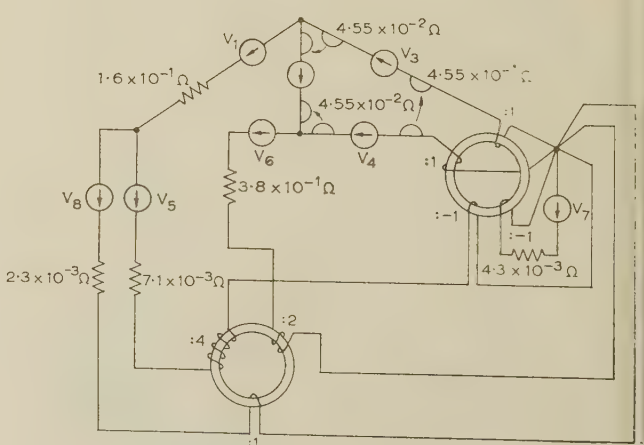

Fig. 12.—One of the solutions given by $\tilde{B}$.

$$B = KX' = \begin{bmatrix} 1 & 0 & 0 & 0 & 0 \\ 0 & 0 & 1 & 0 & 0 \\ 0 & 1 & 0 & 0 & 0 \\ 0 & 0 & 0 & 1 & 0 \\ 0 & 0 & 0 & 0 & 1 \end{bmatrix} \begin{bmatrix} 1 & 1 & -1 & 0 & 0 & 0 & 0 & 0 \\ 0 & 0 & -4 & -4 & 1 & 0 & 0 & 0 \\ 0 & -1 & 0 & -1 & 0 & 1 & 0 & 0 \\ 0 & -1 & -4 & -5 & 0 & 0 & 1 & 0 \\ 0 & 1 & 3 & 4 & 0 & 0 & 0 & 1 \end{bmatrix} = \begin{bmatrix} 1 & 1 & -1 & 0 & 0 & 0 & 0 & 0 \\ 0 & -1 & 0 & -1 & 0 & 1 & 0 & 0 \\ 0 & 0 & -4 & -4 & 1 & 0 & 0 & 0 \\ 0 & -1 & -4 & -5 & 0 & 0 & 1 & 0 \\ 0 & 1 & 3 & 4 & 0 & 0 & 0 & 1 \end{bmatrix}$$

Determining this as an arbitrary set of linear combinations which differs from it in the above example, we have

$$\tilde{B} = \tilde{K}X' = \begin{bmatrix} 1 & 0 & 0 & 0 & 0 \\ -1 & 1 & 0 & 0 & 1 \\ 0 & 0 & 1 & 0 & 0 \\ 0 & 0 & 0 & -1 & -1 \\ 0 & 2 & 3 & 1 & 4 \end{bmatrix} \begin{bmatrix} 1 & 1 & -1 & 0 & 0 & 0 & 0 & 0 \\ 0 & 0 & -4 & -4 & 1 & 0 & 0 & 0 \\ 0 & -1 & 0 & -1 & 0 & 1 & 0 & 0 \\ 0 & -1 & -4 & -5 & 0 & 0 & 1 & 0 \\ 0 & 1 & 3 & 4 & 0 & 0 & 0 & 1 \end{bmatrix} = \begin{bmatrix} 1 & 1 & -1 & 0 & 0 & 0 & 0 & 0 \\ -1 & 0 & 0 & 0 & 1 & 0 & 0 & 1 \\ 0 & -1 & 0 & -1 & 0 & 1 & 0 & 0 \\ 0 & 0 & 1 & 1 & 0 & 0 & -1 & -1 \\ 0 & 0 & 0 & 0 & 2 & 3 & 1 & 4 \end{bmatrix}$$

It is also given as an arbitrary set of linear combinations of the rows in B or $\tilde{B}$,

$$\text{i.e. } B = K\tilde{B} = \begin{bmatrix} 1 & 0 & 0 & 0 & 0 \\ 0 & 1 & 0 & 0 & 0 \\ 0 & 0 & 1 & 0 & 0 \\ 0 & 0 & 0 & 1 & 0 \\ 1 & 1 & 1 & 1 & 1 \end{bmatrix} \begin{bmatrix} 1 & 1 & -1 & 0 & 0 & 0 & 0 & 0 \\ -1 & 0 & 0 & 0 & 1 & 0 & 0 & 1 \\ 0 & -1 & 0 & -1 & 0 & 1 & 0 & 0 \\ 0 & 0 & 1 & 1 & 0 & 0 & -1 & -1 \\ 0 & 0 & 0 & 0 & 2 & 3 & 1 & 4 \end{bmatrix} = \begin{bmatrix} 1 & 1 & -1 & 0 & 0 & 0 & 0 & 0 \\ -1 & 0 & 0 & 0 & 1 & 0 & 0 & 1 \\ 0 & -1 & 0 & -1 & 0 & 1 & 0 & 0 \\ 0 & 0 & 1 & 1 & 0 & 0 & -1 & -1 \\ 0 & 0 & 0 & 0 & 1 & 2 & 0 & 4 \end{bmatrix}$$

Therefore Figs. 9–11 are also the solutions of example 2. And assuming only the first to third rows as the 1-incidence matrix, the network shown in Fig. 12 is also a solution.

(5) CONCLUSION

Synthesis of non-reciprocal networks has already been treated by Carlin[26] and Oono,[27] and their networks are specified by scattering matrices and consequently n-port impedance matrices. But in this paper the author treats topologically the synthesis of the non-reciprocal network employing the transfer-conductance matrix (the driving-conductance matrix) instead. In addition, the determination of its connection is treated algebraically and topologically, namely the connection is algebraically determined as a 1-incidence matrix which is a set of linear combinations of rows in the transposed matrix of a zero factor of the driving-conductance matrix. If the given value of G is symmetrical, the zero factor X need be considered only on one side of G, namely the left or right as $G' = G$. If $\overset{(-)}{G} = G$, i.e. $\overset{(\div)}{G} = 0$, this network is a gyrator circuit and the treatments can be applied to Carlin's method[28] in gyrator circuits. These are investigated. In conclusion the author introduces topological synthesis of a.c. resistance networks. The solution of this problem is not unique, and generally needs ideal transformers.

(6) REFERENCES

(1) FOSTER, R. M.: 'Topological and Algebraic Considerations in Network Synthesis', *Proceedings of the Symposium on Modern Network Synthesis*, 1952, p. 8.

(2) GUILLEMIN, E. A.: 'Introductory Circuit Theory' (Wiley, 1953), p. 1.

(3) MASON, S. J.: 'Topological Analysis of Linear Non-Reciprocal Networks', *Proceedings of the Institute of Radio Engineers*, 1957, **45–6**, p. 829.

(4) DOYLE, T. C.: 'Topological and Dynamical Invariant Theory of an Electrical Network', *Journal of Mathematics and Physics*, 1955, **34–2**, p. 81.

(5) PERCIVAL, W. S.: 'The Solution of Passive Electrical Networks by means of Mathematical Trees', *Proceedings I.E.E.*, Paper No. 1492, May, 1953 (**100**, Part III, p. 143).

(6) TSANG, N. F.: 'On Electrical Network Determinants', *Journal of Mathematics and Physics*, 1954, **33–2**, p. 185.

(7) CEDERBAUM, I.: 'Invariance and Mutual Relations of Electrical Network Determinants', *ibid.*, 1956, **24–4**, p. 236.

(8) OKADA, S., and ONODERA, R.: 'A Unified Treatise on the Topology of Networks and Algebraic Electromagnetism' (Memoirs of the Unifying Study of the Basic Problems in Engineering Sciences by means of Geometry I, Tokyo, 1955), p. 68.

(9) KRON, G.: 'A Set of Principles Interconnecting the Solutions of Physical Systems', *Journal of Applied Physics*, 1953, **24**, p. 965.

(10) WENGERT, R. E.: 'Simple Diakoptics', *Matrix and Tensor Quarterly*, 1955, **5**, p. 129.

(11) HEYDA, P. G.: 'A Simple Numerical Example for the Beginner of Kron's Method of Tearing and Interconnection', *ibid.*, 1956, **6**, p. 142.

(12) CEDERBAUM, I.: 'On Matrices of Residues of the Impedance or Admittance Matrices of n-Ports', *Transactions of the Institute of Radio Engineers*, 1957, **CT–4–1**, p. 20.

(13) PRIHAR, Z.: 'Topological Consideration of Telecommunication Networks', *Proceedings of the Institute of Radio Engineers*, 1956, **44–7**, p. 927.

(14) FOSTER, R. M.: 'Geometrical Circuit of Electrical Networks', *Transactions of the American I.E.E.*, 1932, **51–2**, p. 309.

(15) SESHU, S.: 'Considerations in Design Driving Point Functions', *Transactions of the Institute of Radio Engineers*, 1955, **CT–2–4**, p. 356.

(16) CEDERBAUM, I.: 'Conditions for Impedance and Admittance Matrices of n-Ports without Ideal Transformers', *Proceedings I.E.E.*, Monograph No. 276, January, 1958 (**105** C, p. 245).

(17) VEBLEN, O.: 'Analysis Situs' (Colloquium Publications, New York, 1931).

(18) STANDARDS ON CIRCUITS: 'Definitions of Terms in Network Topology', *Proceedings of the Institute of Radio Engineers*, 1951, **39–1**, p. 27.

(19) KÖNIG, D.: 'Theorie der Endlichen und Unendlichen Graphen' (Leipzig, 1936).

(20) IRI, M., ONODERA, R., and KONDO, K.: 'A Theory of Multi-Trees and Multi-Cotrees and its Application to the Analysis of 2-Trees and 2-Cotrees', *R.A.A.G. Research Notes, Tokyo*, 1957, **2–30**, p. 1.

(21) SYNGE, L.: 'The Fundamental Theorem of Electrical Network', *Quarterly of Applied Mathematics*, 1951, **9–2**, p. 113.

(22) LUNELLI, L.: 'Numerazione delle Maglie in Rete Completa', *Istituto Lombardo di Scienze e Lettere*, 1957, **91**, p. 902.

(23) CAUER, W.: 'Theorie der Linearen Wechselstromschaltungen' (Becker und Euler Kom-Gesellschaft, 1941).

(24) STIGANT, S. A.: 'Modern Electrical Engineering Mathematics', 1946.

(25) LE CORBEILLER, P.: 'Matrix Analysis of Electric Networks' (Harvard University Press, Wiley, 1950).

(26) CARLIN, H. J.: 'Synthesis of Non-reciprocal Networks' *Proceedings of the Symposium on Modern Networ Synthesis, Polytechnic Institute of Brooklyn*, April, 1955.

(27) OONO, Y., and YASUURA, K.: 'Synthesis of Finite Passiv $2n$ Terminal Networks with Prescribed Scatterin Matrices', *Annales des Télécommunications*, March–May 1954, Vol. 2.

(28) CARLIN, H. J.: 'Principles of Gyrator Networks', Sym posium on Modern Advances in Microwave Technique *Monograph of the Research Institute of Applied Electricit Symposia Series*, 1954, **4**.

621.372.6:621.375.1:621.397

The Institution of Electrical Engineers
Monograph No. 429 E
Feb. 1961

THE IMPULSE RESPONSE OF A NUMBER OF IDENTICAL CIRCUITS IN CASCADE

A Refined Method

By K. THARMALINGAM, B.A., B.Sc., Graduate.

(*The paper was first received 22nd June, in revised form 28th September, and in final form 24th October*, 1960. *It was published as an* INSTITUTION MONOGRAPH *in February*, 1961.)

SUMMARY

Approximate analytical expressions are derived for the impulse response of identical circuits in cascade. The results obtained from these approximate expressions, tested for an exactly solvable case, show remarkable accuracy. Cruder approximations to obtain a quick estimate of peak-to-peak ring in response to a step function, and the first zero of impulse response, are also given.

LIST OF PRINCIPAL SYMBOLS

p = Variable of Laplace transform.
p_m, q_m = Coefficients in the asymptotic expansion.
Z = Normalized variable of the form p/ω_0.
t = Time.
τ = Normalized time of the form $\omega_0 t$.
$G(Z)$ = Transfer function of a network.
$\chi(Z)$ = $\log G(Z)$.
n = Number of circuits in cascade.
u = Complex variable.
A_i = Airy function.
Z_1, Z_2 = Value of Z at cols.
Z_0 = Value of Z at critical point.
χ_0^{II}, χ_0^{III}, χ_0^{IV} = Derivatives of $\chi(Z)$ at $Z = Z_0$.
λ_0 = Value of λ at critical point.
$F_0 = \lambda_0 Z_0 + \chi(Z_0)$ = Value of F at critical point.

$'$ denotes differentiation with respect to Z.

(1) INTRODUCTION

The response to unit impulse function of a network with transfer function $G(p)$, whose singularities lie to the left of Bromwich contour, is given by

$$A(t) = \frac{1}{2\pi j}\int_{c-j\infty}^{c+j\infty} G(p)\varepsilon^{pt}dp \quad . \quad . \quad . \quad . \quad . \quad (1)$$

For a number n of identical circuits in cascade the response, in terms of the normalized variables $Z = p/\omega_0$ and $\tau = \omega_0 t$, can be written as

$$A_n(\tau) = \frac{1}{2\pi j}\int_{c-j\infty}^{c+j\infty} [G(Z)]^n \varepsilon^{Z\tau}dZ \quad . \quad . \quad . \quad . \quad (2)$$

Introducing the logarithmic gain $\chi(Z)$ defined by $\chi(Z) = \log G(Z)$ we obtain

$$A_n(\tau) = \frac{1}{2\pi j}\int_{c-j\infty}^{c+j\infty} \varepsilon^{nF(Z)}dZ \quad . \quad . \quad . \quad . \quad (3)$$

where
$$F(Z) = \lambda Z + \chi(Z) \quad . \quad . \quad . \quad . \quad . \quad (4)$$

and
$$\lambda = \tau/n$$

In all except simple cases of $G(Z)$ the above integrals are difficult to evaluate, and numerical methods are liable to be tedious when large phase shifts are involved. Approximate analytical expression for $A_n(\tau)$ can, however, be obtained by the method of steepest descents;[1] the standard method[4] is to deform the contour of integration so as to pass through the cols of $F(Z)$, i.e. those points where $dF/dZ = 0$.

Let Z_1 be a col and u a new local variable defined by

$$F(Z) - F(Z_1) = -\tfrac{1}{2}u^2 \quad . \quad . \quad . \quad . \quad (5)$$

Eqn. (3) then becomes

$$A_n(\tau) = \exp[nF(Z_1)]\frac{1}{2\pi j}\int_{C(U)} \varepsilon^{-\frac{1}{2}nu^2}\left(\frac{dZ}{du}\right)du \quad . \quad . \quad (6)$$

where $C(U)$, the contour of integration in the U-plane, corresponds to the line of steepest descent in the Z-plane passing through col Z_1. If $F^{II}(Z_1) \neq 0$, $\frac{dZ}{du}$ can be expanded in the form

$$\frac{dZ}{du} = \Sigma\, C_m u^m \quad . \quad . \quad . \quad . \quad . \quad . \quad (7)$$

(the radius of convergence for such an expansion being, in general, not greater than the distance from Z_1 to the nearest col) and hence $A_n(\tau)$ can be expressed in terms of factorial functions.

It has been shown by Sander[1] that, for cases of practical interest, the main build-up of $A_n(\tau)$ occurs when two saddle points (nearly) coincide, i.e. $F^{II}(Z_1) \to 0$. For this case the circle of convergence of expansion for eqn. (7) tends to zero, and, in this region, the standard method gives results which are not uniformly accurate. In this paper a further extension of the method of steepest descents due to Chester *et al.*,[2] valid in the region of build-up, is used to derive expressions for $A_n(\tau)$.

(2) DESCRIPTION OF METHOD

Consider the transformation

$$F(Z) = \tfrac{1}{3}u^3 - a^2u + A \quad . \quad . \quad . \quad . \quad (8)$$

It has been shown by Chester *et al.*[2] that the transformation $u \leftrightarrow Z$ is uniformly regular and (1, 1), and that there is an expansion of the form

$$\frac{dZ}{du} = \sum_{m=0}^{\infty}[p_m(u^2 - a^2)^m + q_m u(u^2 - a^2)^m] \quad . \quad . \quad (9)$$

Eqn. (3) then becomes

$$A_n(\tau) = \sum_{m=0}^{\infty}\frac{1}{2\pi j}\int_{\infty\varepsilon^{-j\pi/3}}^{\infty\varepsilon^{j\pi/3}}[p_m(u^2 - a^2)^m + q_m u(u^2 - a^2)^m]\,\varepsilon^{n(\frac{1}{3}u^3 - a^2u + A)}du \quad . \quad (10)$$

Correspondence on Monographs is invited for consideration with a view to publication.
Mr. Tharmalingam is in the Department of Physics, University of Reading.

The evaluation of this integral is dealt with in Reference 2, and retaining the significant terms ($m = 0$), we find

$$A_n(\tau) \simeq \varepsilon^{nA}[p_0 n^{-1/3} A_i(n^{2/3}a^2) - q_0 n^{-2/3} A_i'(n^{2/3}a^2)] \quad . \quad (11)$$

where A_i and A_i' are the Airy functions and their derivatives. A, a^2, p_0 and q_0, which are functions of the cols Z_1 and Z_2 and hence of λ, can be obtained as follows:

$$F(Z) \equiv \lambda Z + \chi(Z) = \tfrac{1}{3}u^3 - a^2 u + A \quad . \quad . \quad (12)$$

$F'(Z) \equiv \lambda + \chi'(Z) = 0$ gives the cols Z_1, Z_2, and corresponding to these points in the U-plane we have $u = \pm a$.

Hence at these saddle points,

$$F(Z_1) \equiv \lambda Z_1 + \chi(Z_1) = -\tfrac{2}{3}a^3 + A \quad . \quad . \quad (13)$$

$$F(Z_2) \equiv \lambda Z_2 + \chi(Z_2) = \tfrac{2}{3}a^3 + A \quad . \quad . \quad . \quad (14)$$

from which

$$A = \tfrac{1}{2}[\lambda(Z_1 + Z_2) + \chi(Z_1) + \chi(Z_2)] \quad . \quad . \quad . \quad (15)$$

and

$$a^3 = \tfrac{3}{4}[\lambda(Z_2 - Z_1) + \chi(Z_2) - \chi(Z_1)] \quad . \quad . \quad . \quad (16)$$

Differentiating eqn. (12) twice with respect to u and putting $Z = Z_1$, $u = a$ and $Z = Z_2$, $u = -a$ successively we obtain

$$\chi^{II}(Z_1)\left(\frac{dZ_1}{du}\right)^2 = 2a \quad . \quad . \quad . \quad . \quad . \quad (17)$$

$$\chi^{II}(Z_2)\left(\frac{dZ_2}{du}\right)^2 = -2a \quad . \quad . \quad . \quad . \quad (18)$$

Eqn. (9) at these saddle points gives

$$\frac{dZ_1}{du} = p_0 + q_0 a \quad . \quad . \quad . \quad . \quad . \quad (19)$$

$$\frac{dZ_2}{du} = p_0 - q_0 a \quad . \quad . \quad . \quad . \quad . \quad (20)$$

Solving for p_0 and q_0 from eqns. (17)–(20) we obtain

$$p_0 = \frac{1}{2}\left\{\left[\frac{2a}{\chi^{II}(Z_1)}\right]^{1/2} + \left[\frac{-2a}{\chi^{II}(Z_2)}\right]^{1/2}\right\} \quad . \quad . \quad (21)$$

and

$$q_0 - \frac{1}{2a}\left\{\left[\frac{2a}{\chi^{II}(Z_1)}\right]^{1/2} - \left[\frac{-2a}{\chi^{II}(Z_2)}\right]^{1/2}\right\} \quad . \quad . \quad (22)$$

p_m, q_m for $m > 0$ can similarly be found by considering the higher derivatives of eqns. (9) and (12).

If Z_1 and Z_2 are both real, then A is real and a is real positive or negative. The sign of a will be related to the signs of $\chi^{II}(Z_1)$ and $\chi^{II}(Z_2)$ which will be different, since Z_1 and Z_2 are on either side of the critical point Z_0, i.e. the point at which Z_1 and Z_2 coincide. Hence $2a/\chi^{II}(Z_1)$ and $-2a/\chi^{II}(Z_2)$ will both be positive and p_0, q_0 real.

If Z_1, Z_2 are complex conjugates, A will be real, and equal to $\mathscr{R}(F_1)$. a^3 and hence a will be pure imaginary; $\chi^{II}(Z_1)$, $\chi^{II}(Z_2)$ will now be complex conjugates. It follows that p_0 and q_0 will again be real.

At the critical point $a = 0$, p_0 and q_0 obtained from eqns. (21) and (22) by a limiting process give

$$\left.\begin{aligned} p_0 &= \left(\frac{2}{\chi_0^{III}}\right)^{1/3} \\ q_0 &= -\frac{\chi_0^{IV}}{6\chi_0^{III}}\left(\frac{2}{\chi_0^{III}}\right)^{2/3} \end{aligned}\right\} \quad . \quad . \quad . \quad . \quad (23)$$

From eqn. (15), since, at the critical point $Z_1 = Z_2 = Z_0$ and $\lambda = \lambda_0$,

$$A = F_0 = \lambda_0 Z_0 + \chi(Z_0) \quad . \quad . \quad . \quad . \quad (24)$$

With these values eqn. (11) becomes, for the critical point,

$$A_n(\tau_0) \simeq \varepsilon^{nF_0}\left[\left(\frac{2}{n\chi_0^{III}}\right)^{1/3} A_i(0) + \frac{\chi_0^{IV}}{6\chi_0^{III}}\left(\frac{2}{n\chi_0^{III}}\right)^{2/3} A_i'(0)\right]$$

The known properties of Airy functions show that this can be expressed in terms of gamma functions, yielding

$$A_n(\tau_0) \simeq \frac{\varepsilon^{nF_0}}{2\pi\sqrt{3}}\left[\left(\frac{6}{n\chi_0^{III}}\right)^{1/3}\Gamma\left(\frac{1}{3}\right) - \frac{1}{6}\frac{\chi_0^{IV}}{\chi_0^{III}}\left(\frac{6}{n\chi_0^{III}}\right)^{2/3}\Gamma\left(\frac{2}{3}\right)\right] \quad . \quad . \quad . \quad . \quad (25)$$

which is identical with the expression, for $A_n(\tau)$ at the critical point, obtained by Sander.[1] Other expressions for $A_n(\tau)$ when $\lambda \neq \lambda_0$ quoted by Sander[1] can be obtained by retaining only the first term of eqn. (11) and with a further approximation for p_0, A and a^2.

(3) APPLICATION

The transfer function in terms of normalized variables, of a coupling circuit characterized by two poles, can be written as

$$G(Z) = \frac{2}{(Z+1)^2 + 1} \quad . \quad . \quad . \quad . \quad . \quad (26)$$

The impulse response of n identical networks of the above function in cascade is given by

$$A_n(\tau) = \frac{1}{2\pi j}\int_{c-j\infty}^{c+j\infty}\left[\frac{2}{(Z+1)^2+1}\right]^n \varepsilon^{Z\tau} dZ$$

$$= \frac{1}{2\pi j} 2^n \varepsilon^{-\tau} \int_{c-j\infty}^{c+j\infty} \frac{\varepsilon^{Z\tau}}{(Z^2+1)^n} dZ \quad . \quad . \quad . \quad . \quad (27)$$

The above integral may be evaluated approximately by using results of Section 2 as follows:

$$\chi(Z) = -\log(Z^2 + 1)$$

The saddle points given by the solutions of the equation

$$\lambda + \chi^{I}(Z) = 0$$

are

$$Z_1 = x + \sqrt{(x^2 - 1)}$$

$$Z_2 = x - \sqrt{(x^2 - 1)}$$

where $x = 1/\lambda = n/\tau$.

With these values for Z_1 and Z_2 using eqns. (15) and (16) we obtain

$$A = 1 - \log 2x$$

$$a^3 = -\frac{3}{2}\left\{\frac{\sqrt{(x^2-1)}}{x} + \log[x - \sqrt{(x^2-1)}]\right\}$$

Since

$$\left[\frac{1}{\chi^{II}(Z_1)}\right]^{1/2} = \frac{x}{(x^2-1)^{1/4}}[x + \sqrt{(x^2-1)}]^{1/2}$$

and

$$\left[\frac{-1}{\chi^{II}(Z_2)}\right]^{1/2} = \frac{x}{(x^2-1)^{1/4}}[x - \sqrt{(x^2-1)}]^{1/2}$$

p_0 and q_0 are easily obtained from eqns. (21) and (22) and the above values of $\left[\frac{1}{\chi^{II}(Z_1)}\right]^{1/2}$, $\left[\frac{-1}{\chi^{II}(Z_2)}\right]^{1/2}$ and a. With these values, $A_n(\tau)$ given by eqn. (11) becomes

$$A_n(\tau) \simeq \left[\frac{\varepsilon^{\left(1-\frac{1}{x}\right)}}{x}\right]^n [p_0 n^{-1/3} A_i(n^{2/3}a^2) - q_0 n^{-2/3} A'(n^{2/3}a^2)] \quad . \quad (28)$$

At the critical point $\lambda = \lambda_0 = 1$ and $A_n(\tau_0)$ given by eqn. (25) becomes

$$A_n(\tau_0) \simeq \frac{0{\cdot}4473}{n^{1/3}} + \frac{0{\cdot}2055}{n^{2/3}} \quad . \quad . \quad . \quad . \quad (29)$$

The integral of eqn. (27) can also be evaluated exactly in terms of Bessel functions, giving

$$A_n(\tau) = \frac{2^n\sqrt{\pi}}{(n-1)!}\left(\frac{\tau}{2}\right)^{n-\frac{1}{2}} \varepsilon^{-\tau} J_{n-\frac{1}{2}}(\tau) \quad . \quad . \quad (30)$$

The results evaluated for $n = 6$, 10 and 15 by the exact and approximate methods are shown in Fig. 1. The accuracy of the present approximate method is remarkably good.

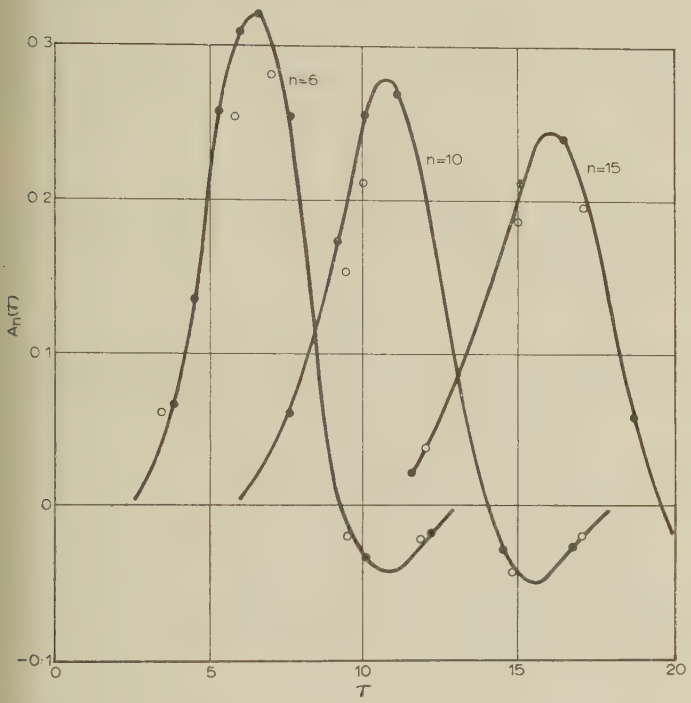

Fig. 1.—Impulse responses for cascaded networks each with transfer function $G(z) = 2[(Z+1)^2 + 1]^{-1}$.

—— Exact, using eqn. (30).
○ From Reference 1.
● Present method, using eqns. (28) and (29).

(4) APPROXIMATION VALID FOR LARGE VALUES OF *n*

$$F(Z\lambda) \equiv \lambda Z + \chi(Z) = \alpha Z + \lambda_0 Z + \chi(Z) \quad . \quad (31)$$

where $\alpha = (\lambda - \lambda_0)$

Expanding $F(z\lambda)$ as a Taylor series about Z_0 we have

$$F(Z\lambda) = (\alpha Z_0 + \lambda_0 Z_0 + \chi_0) + (\alpha + \lambda_0 + \chi_0')(Z - Z_0) + \frac{(Z-Z_0)^2}{2!}\chi_0^{II} + \ldots \quad . \quad (32)$$

Since $\lambda_0 + \chi_0^I = 0$ and $\chi_0^{II} = 0$, $\dfrac{\partial F}{\partial Z} = 0$ gives

$$\alpha + \frac{\chi_0^{III}}{2}(Z-Z_0)^2 + \frac{\chi_0^{IV}}{6}(Z-Z_0)^3 + \ldots = 0 \quad . \quad (33)$$

Putting $$\theta = -\frac{2\alpha}{\chi_0^{III}} \equiv -\frac{2(\lambda-\lambda_0)}{\chi_0^{III}}$$

and by inversion of series given by eqn. (33) we get $(Z - Z_0)$ in terms of θ of the form

$$(Z - Z_0) = \pm\,\theta^{1/2}\left(1 \mp \frac{\chi_0^{IV}}{6\chi_0^{III}}\theta^{1/2} + \ldots\right) \quad . \quad (34)$$

Since $2A = F(Z_1) + F(Z_2)$ and $\frac{4}{3}a^3 = F(Z_2) - F(Z_1)$ from eqns. (32) and (34) we obtain

$$A \simeq F_0 + (\lambda - \lambda_0)Z_0 + \frac{\chi_0^{IV}}{24}\theta^2 \quad . \quad . \quad . \quad (35)$$

and

$$a^2 \simeq \left(\frac{\chi_0^{III}}{2}\right)^{2/3}\theta \quad . \quad . \quad . \quad . \quad . \quad (36)$$

$\chi^{II}(Z)$ can similarly be expanded in terms of θ, and we obtain

$$p_0 \simeq \left(\frac{2}{\chi_0^{III}}\right)^{1/3} \quad . \quad . \quad . \quad . \quad . \quad (37)$$

With these expressions for A, a^2 and p_0, retaining only the first term of eqn. (11), we have

$$A_n(\tau) \simeq \left(\frac{2}{n\chi_0^{III}}\right)^{1/3} A_i\left[\left(\frac{n\chi_0^{III}}{2}\right)^{2/3}\theta\right] \varepsilon^{n[F_0 + (\lambda-\lambda_0)Z_0 + \frac{\chi_0^{IV}}{24}\theta^2]} \quad . \quad (38)$$

This is identical with the expression obtained by Sander,[1] except that the θ^2 term is included in the exponential. Inclusion of the θ^2 term is expected to give better results for peak-to-peak

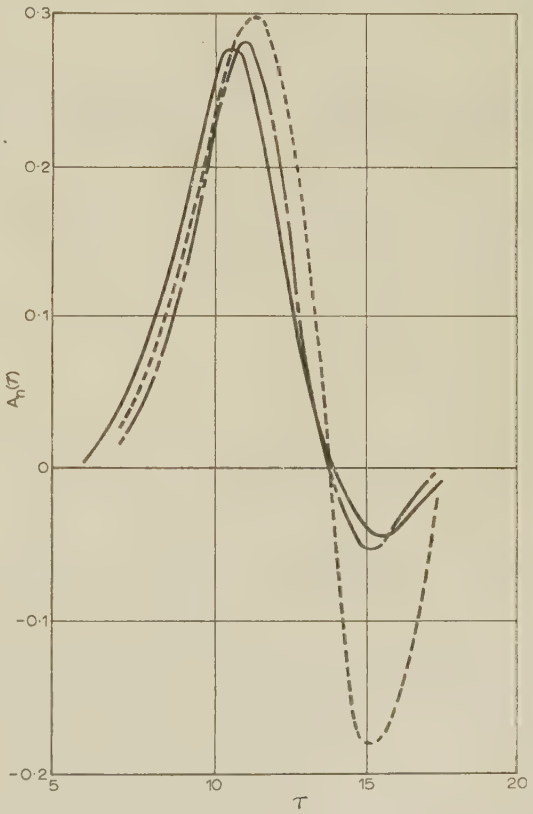

Fig. 2.—Impulse responses for cascaded networks each with transfer function $G(z) = 2[(Z+1)^2 + 1]^{-1}$.
$n = 10$

—— Exact, using eqn. (30).
– – – Approximate, using eqn. (38).
– – – – – Approximate, neglecting θ^2 term in eqn. (38).

ring and shape of response, since, at the second peak of impulse response, the argument of the Airy function is $-3{\cdot}25$, i.e. $\theta \sim -3{\cdot}25\left(\frac{2}{n\chi_0^{III}}\right)^{2/3}$. Therefore the θ^2 term in the exponential is approximately $0(n^{-1/3})$, whereas the next-order term in the coefficient p_0 is $\theta \sim 0(n^{-2/3})$. For the network function $G(Z) = 2[(Z+1)^2+1]^{-1}$, with $n = 10$ we find that the inclusion of the θ^2 term reduces the height of the second peak by a factor of 3, as shown in Fig. 2, giving a good agreement with exact results. It is also evident that the first zero of impulse response, to a good approximation, is given by

$$A_i\left[\left(\frac{n\chi_0^{III}}{2}\right)^{2/3}\theta\right] = 0 \quad . \quad . \quad . \quad . \quad . \quad (39)$$

An estimate of the peak-to-peak ring in the response to a step function may be evaluated by regarding $A_n(\tau)$ as parabolic in the region of the second peak. Since the first and second zeros of $A_i(-x)$ are at 2·34 and 4·09, and its first minimum of magnitude $-0{\cdot}42$ occurs at 3·25, the difference in the first and second ring in the response to the step function is given by

$$\int A_n(\tau)d\tau \simeq -\tfrac{1}{2}\exp\left[nF_0 + 3{\cdot}3Z_0\left(\frac{n\chi_0^{III}}{2}\right)^{1/3} + 5{\cdot}3\left(\frac{\chi_0^{IV}}{6\chi_0^{III}}\right)\left(\frac{n\chi_0^{III}}{2}\right)^{-1/3}\right] \quad . \quad (40)$$

For an inductance-compensated video amplifier where the gain is given by

$$g\left(\frac{Lp+R}{1+Rcp+LCp^2}\right)$$

with normalized variables $\tau = Rt/L$; $Z = Lp/R$; $m = L/CR^2$ and gain normalized to unity at low frequency, we get

$$\chi(Z) = \log[m(1+Z)] - \log(m+Z+Z^2) \quad . \quad (41)$$

Using eqn. (40) the peak-to-peak ring obtained for different values of $K = m^{-1/2}$, and $n = 32$, are given in Table 1.

Table 1

PEAK-TO-PEAK RING IN RESPONSE TO STEP FUNCTION

K	1·66	1·55	1·45
Peak-to-peak ring from Reference 1	0·06	0·5	2·0
Peak-to-peak ring, present method	0·04	0·33	1·18

The results from Reference 3 are

K =	1·61	1·51	1·41
Peak-to-peak ring =	0·07	0·35	1·15

(5) CONCLUSION

The extended method of steepest descents gives uniformly accurate results in regions of interest, i.e. $\lambda \sim \lambda_0$ as indicated in Section 3. The inclusion of the θ^2 term in the exponential factor of expressions in Section 4 gives a much better shape for the response of impulse functions.

(6) ACKNOWLEDGMENTS

The author wishes to acknowledge advice received from Dr K. F. Sander, by whom the developments recorded in this paper were suggested.

(7) REFERENCES

(1) SANDER, K. F.: 'A Method for the Approximate Determination of the Impulse Response of a Number of Identical Circuits in Cascade', *Proceedings I.E.E.*, Monograph No. 189 R, August, 1956 (**104** C, p. 13).

(2) CHESTER, C., FRIEDMAN, B., and URSELL, F.: 'An Extension of the Method of Steepest Descents', *Proceedings of the Cambridge Philosophical Society*, 1957, **53**, p. 599.

(3) BEDFORD, A. V., and FREDENDALL, G. L.: 'Transient Response of Multistage Video Frequency Amplifiers', *Proceedings of the Institute of Radio Engineers*, 1939, **27**, p. 277.

(4) JEFFREYS, H., and JEFFREYS, B. S.: 'Methods of Mathematical Physics' (Cambridge, 1946), p. 472.

621.372.853.2

The Institution of Electrical Engineers
Monograph No. 430 E
Feb. 1961

MICROWAVE PROPAGATION THROUGH ROUND WAVEGUIDE PARTIALLY FILLED WITH FERRITE

By A. J. BADEN FULLER, M.A., Graduate.

(*The paper was first received 22nd August, and in revised form 26th October*, 1960. *It was published as an* INSTITUTION MONOGRAPH *in February*, 1961.)

SUMMARY

The theory of microwave propagation through an unbounded ferrite medium magnetized along the direction of microwave propagation is considered, and expressions are derived for the components of the microwave field. Boundary conditions are applied, and characteristic equations are derived for four circularly symmetric shapes, namely

(*a*) Ferrite-filled round waveguide.
(*b*) Ferrite rod at the centre of round waveguide.
(*c*) Ferrite tube adjacent to the wall of round waveguide.
(*d*) Ferrite tube in the centre of round waveguide.

Some propagation constants have been computed for the last three shapes. The method is such that it may easily be extended to give the characteristic equations for any circularly symmetric shape of ferrite inside round waveguide in addition to the characteristic equations given in the paper. At 9370 Mc/s some computed results of Faraday rotation have shown reasonable agreement with those measured on ferrite rods. The results of a specimen investigation of the variation of the propagation coefficient with change of ferrite dimension are included.

(1) INTRODUCTION

The paper gives a theoretical treatment of the various configurations of ferrite in round waveguide used in Faraday rotation devices. An infinite length of round waveguide is considered with various circularly symmetric shapes of ferrite inside it, the ferrite being longitudinally magnetized up to and just above saturation. If a circularly polarized microwave field is propagated through an infinite ferrite medium which is statically magnetized in the direction of propagation, the effective permeability varies with change of magnetizing field as shown in Fig. 1. The rotation of a linearly polarized wave is given by the difference in propagation coefficient of the two circularly polarized waves of opposite hand.

A Faraday rotation device usually consists of a length of round waveguide with a magnetizing coil wound round it and with a ferrite rod, suitably matched, mounted coaxially in the centre. The rotation varies with applied magnetic field in a manner shown in Fig. 2. The amount of rotation also depends on the ferrite or waveguide dimensions, the microwave frequency and the properties of the particular ferrite used.

Under high-power conditions the ferrite rod is difficult to cool, and a tube whose outside is adjacent to the waveguide wall may be cooler and handle more power. For high-frequency ferrite modulators, where the rotation is varied by the application of an h.f. current to the magnetizing coil, the short-circuited-turn effect of the waveguide sets a frequency limit; but if a ferrite tube is used, the magnetizing coil may be wound on to the outside of the tube so that the coil acts as the waveguide wall.

Owing to the importance of rotators to microwave engineers, many theoretical investigations of microwave propagation through round waveguide filled or partially filled with ferrite have been published. The first theoretical treatment of round waveguide containing gyromagnetic media was given by Gamo,[2] who restricted himself to a completely filled waveguide but considered a material that was gyro-electric as well as gyromagnetic. He gives a study of some cut-off frequencies and shows the variation of propagation coefficient with waveguide radius. Kales[3] gives a similar theoretical treatment of ferrite-filled waveguide and also indicates the solution for a ferrite rod at the centre of the waveguide, but he does not give any results computed from theory. Suhl and Walker[4] have undertaken a more detailed study of the completely filled waveguide; like Gamo, they begin by considering a medium which is both gyro-electric and gyro-

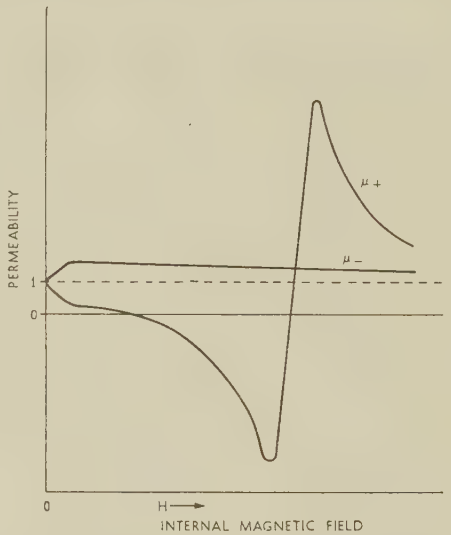

Fig. 1.—Typical ferrite permeability for positive and negative circularly polarized plane waves as a function of internal magnetic field, *H*.

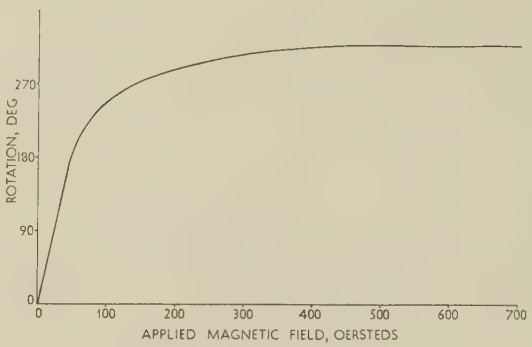

Fig. 2.—Rotation of linearly polarized wave at 9370 Mc/s by a 2 in rod of ferrite 0·25 in in diameter inside a round waveguide 0·9 in in diameter as a function of applied magnetic field.

Correspondence on Monographs is invited for consideration with a view to publication.

Mr. Baden Fuller is with A.E.I. (Rugby), Ltd.

magnetic, but because of the complexity of the solutions, they simplify the problems to the gyromagnetic material only before finding expressions for the propagation coefficient. They give a large number of results of calculations of cut-off frequencies and phase coefficients. They also discuss approximate perturbation methods of calculating the propagation coefficients for the partly filled guide, which confine the problem to very thin ferrite rods or to very dilute ferrite materials. In practice, partially filled ferrite waveguide is used whose dimensions are well outside the realm of validity of these approximate methods. Clarricoates[5] gives a perturbation theory of microwave propagation in round waveguide with a ferrite rod in the centre. He makes the assumption that the ferrite has the same effective permeability to circularly polarized waves inside the waveguide as an infinite ferrite medium has to plane circularly polarized waves; he shows that this method gives ample accuracy for the design of ferrite devices.

Acknowledging the limitation of all previously published results, Waldron[6] gives an exact theoretical analysis of an infinite length of round waveguide with a ferrite rod at the centre. He has computed a large number of curves of cut-off conditions and phase coefficients for various sizes of rod and waveguide and various ferrite parameters. He has also computed[11] values of the microwave field components and density of energy flow for the H_{11} mode as functions of transverse position in the waveguide. Waldron[7] and Mirimanov and Anisimova[8] have also analysed microwave propagation in round waveguide with a tube of ferrite adjacent to the waveguide wall. Waldron gives an expression linking cut-off conditions for ferrite tubes and rods and has computed a few cut-off conditions, but no phase coefficients have been computed. Rizzi[9] also gives theoretical results for a ferrite rod or tube, and also a few results of rotation which were calculated for the design of a particular ferrite device.

In the present paper propagation equations are given for round waveguide with

(*a*) Ferrite filling.
(*b*) Ferrite rod at centre.
(*c*) Ferrite tube adjacent to wall.
(*d*) Ferrite tube in centre.

and propagation coefficients have been computed for the last three. Some specimen results are given.

(2) THEORY

(2.1) Ferrite Properties

For a ferrite material magnetized to saturation in the z-direction the permeability with regard to a time-varying microwave field is given by the tensor

$$\boldsymbol{T} = \mu_0 \begin{vmatrix} \mu_r & -j\kappa_r & 0 \\ j\kappa_r & \mu_r & 0 \\ 0 & 0 & 1 \end{vmatrix} \quad . \quad . \quad . \quad . \quad (1)$$

where

$$\left.\begin{aligned} B_x &= \mu_0\mu_r H_x - j\mu_0\kappa_r H_y \\ B_y &= j\mu_0\kappa_r H_x + \mu_0\mu_r H_y \\ B_z &= \mu_0 H_z \end{aligned}\right\} \quad . \quad . \quad . \quad . \quad (2)$$

and

$$\left.\begin{aligned} \mu_r &= 1 + \frac{\gamma^2 H M_0}{\gamma^2 H^2 - \omega^2} \\ \kappa_r &= \frac{M_0\gamma\omega}{\gamma^2 H^2 - \omega^2} \end{aligned}\right\} \quad . \quad . \quad . \quad . \quad (3)$$

where γ is the gyromagnetic ratio, ω the microwave frequency, H the static applied magnetic field and M_0 the magnetization in the material.

Polder[1] derived eqns. (2) and (3) connecting the periodic part of $\boldsymbol{B}$ and $\boldsymbol{H}$ in a saturated ferrimagnetic medium by assuming that the classical model is applicable. However, eqns. (2) without the additional eqns. (3) have a more general significance than Polder's derivation with the aid of the classical model might suggest. In an isotropic material completely magnetized in the z-direction the most general linear relation between $\boldsymbol{B}$ and $\boldsymbol{H}$, from symmetry considerations, is given exactly by eqns. (2). Strictly, a ferrite is never isotropic, and the permeability tensor will have a more complicated form when the magnetization is arbitrarily directed with respect to the crystallographic axis, but eqns. (2) have been found to be applicable for commercially available ferrites.

For many applications of Faraday rotation the ferrite is magnetized well below saturation, but it is still assumed that eqns. (2) describe the properties of the ferrite. No effect has yet been found to disprove this assumption. μ_r and κ_r are functions of the applied magnetic field, and except for the lossless condition they are complex quantities.

The ferrite has a normal permittivity, so that

$$\boldsymbol{D} = \epsilon_0\epsilon_r \boldsymbol{E} \quad . \quad . \quad . \quad . \quad . \quad . \quad (4)$$

where ϵ_r will be a complex quantity except in the lossless case.

(2.2) Some Special Units

Following Waldron,[6] some special units will be used in order to simplify the computation. For microwaves in round metal waveguide all phenomena may be scaled with dimensions proportional to wavelength. In this paper all dimensions will be measured in units of the free-space wavelength, λ_0, of the microwave energy, so that if the actual dimension is R, the normalized dimension used here will be $r = R/\lambda_0$. Similarly, the propagation coefficient, β, is normalized so that $\beta = \lambda_0/\lambda_g$, where λ_g is the waveguide wavelength. Moreover, the permeability and permittivity of the ferrite are taken relative to the medium filling the rest of the waveguide, whether this be air (vacuum) or any other dielectric material. If the waveguide is filled with a dielectric other than air, the free-space wavelength is taken to be the wavelength in an unbounded dielectric medium. Deducing the mathematics in terms of these normalized units means that the frequency of the microwaves and the permittivity and permeability of free space cancel out in the characteristic equations, so simplifying the computation.

(2.3) Sign Convention

The integer n describes the circular order of the waveguide mode; it is defined to be positive for a right-hand circularly polarized wave in a right-handed cylindrical-co-ordinate system. β is positive for waves travelling in the direction of positive z. The static magnetic field is positive when directed in the positive z-direction. κ_r is negative for a positive static magnetic field if this is below that required for resonance, i.e. $\gamma H = \omega$, as can be seen from eqns. (3).

Circularly polarized modes are the fundamental modes propagating through gyromagnetic material. A negative circularly polarized wave is mathematically described by a negative integer for n. But the propagation coefficient for a negative circularly polarized wave passing through ferrite magnetized positively is the same as that of a positive wave passing through ferrite magnetized negatively, so that changing the sign of κ_r is mathematically equivalent to changing the sign of n and is easier for computation; thus in the computation of the results recorded here a negative polarized wave is considered by a change of sign of κ_r rather than a negative value for n.

(2.4) Differential Equations

In the waveguide Maxwell's equations hold, i.e.

$$\left.\begin{aligned}\operatorname{curl} \boldsymbol{H} &= \frac{\partial \boldsymbol{D}}{\partial t}\\ \operatorname{curl} \boldsymbol{E} &= -\frac{\partial \boldsymbol{B}}{\partial t}\end{aligned}\right\} \quad . \quad . \quad . \quad . \quad . \quad . \quad (5)$$

If the expressions for the properties of the ferrite, eqns. (2) and (4), are substituted into eqns. (5), E_z and H_z are contained in a pair of differential equations and the other field components are expressed in terms of E_z and H_z. Since Waldron and others have derived these expressions already, the intermediate steps will be omitted here. It is assumed that the field components vary by $\varepsilon^{j\omega t}$ and $\varepsilon^{-j\beta z}$. The 2-dimensional differential operator ∇_t is defined to denote $(\partial/\partial x, \partial/\partial y)$ in rectangular co-ordinates. So we have

$$\mu_r \nabla_t^2 H_z + \omega^2 \epsilon_0 \mu_0 (\epsilon_r \mu_r - \beta^2) H_z = j\omega^2 \epsilon_0 \mu_0 \beta \epsilon_r \kappa_r \frac{1}{\eta} E_z \; . \quad (6)$$

$$\mu_r \nabla_t^2 E_z + \omega^2 \epsilon_0 \mu_0 [\epsilon_r (\mu_r^2 - \kappa_r^2) - \mu_r \beta^2] E_z = - j\omega^2 \epsilon_0 \mu_0 \beta \kappa_r \eta H_z \quad (7)$$

where $$\eta = \sqrt{\frac{\mu_0}{\epsilon_0}}$$

Eliminating H_z and E_z in turn from eqns. (6) and (7) gives

$$\left\{(\mu_r \nabla_t^2)^2 + \omega^2 \epsilon_0 \mu_0 [(\epsilon_r \mu_r - \beta^2)(\mu_r + 1) - \kappa_r^2 \epsilon_r] \mu_r \nabla_t^2 + \omega^4 \epsilon_0^2 \mu_0^2 \mu_r [(\epsilon_r \mu_r - \beta^2)^2 - (\epsilon_r \kappa_r)^2]\right\} E_z = 0 \quad (8)$$

and a similar equation for H_z.

Eqn. (8) may be put into the form

$$(\nabla_t^2 + \gamma_1^2)(\nabla_t^2 + \gamma_2^2) E_z = 0 \; . \quad . \quad . \quad . \quad (9)$$

where

$$\gamma^2 = \frac{2\pi^2 \epsilon_r}{\mu_r}\left(\mu_r(\mu_r + 1)(1 - \beta') - \kappa_r^2 \pm \sqrt{\left\{[(1 - \beta')(\mu_r - 1)\mu_r - \kappa_r^2]^2 + 4\kappa_r^2 \mu_r \beta'\right\}}\right) \quad (10)$$

where γ_1 takes the positive sign and γ_2 the negative and

$$\beta' = \frac{\beta^2}{\epsilon_r \mu_r}$$

In cylindrical polar co-ordinates the solution to eqn. (9) is

$$E_z = [K_1 \mathrm{J}_n(\gamma_1 r) + L_1 \mathrm{Y}_n(\gamma_1 r) + K_2 \mathrm{J}_n(\gamma_2 r) + L_2 \mathrm{Y}_n(\gamma_2 r)] \varepsilon^{jn\theta} \quad . \quad . \quad . \quad . \quad (11)$$

where K_1, K_2, L_1 and L_2 are arbitrary constants determined by the boundary conditions. γ may be real or imaginary, and so may the arbitrary constants K and L, so that, in any actual calculation, modified Bessel functions are as likely to occur as not. $\nabla_t^2 E_z$ is given by

$$\nabla_t^2 E_z = [-K_1 \gamma_1^2 \mathrm{J}_n(\gamma_1 r) - L_1 \gamma_1^2 \mathrm{Y}_n(\gamma_1 r) - K_2 \gamma_2^2 \mathrm{J}_n(\gamma_2 r) - L_2 \gamma_2^2 \mathrm{Y}_n(\gamma_2 r)] \varepsilon^{jn\theta} \quad (12)$$

Substituting this value of E_z into eqn. (7) gives an expression for H_z. The other field components are given by the equations

$$\omega \epsilon_r \mu_0 [\kappa_r^2 - \mu_r^2 (1 - \beta')^2] H_r = j\mu_r (1 - \beta')\left(-\epsilon_r \frac{1}{r}\frac{\partial E_z}{\partial \theta} + \beta\eta \frac{\partial H_z}{\partial r}\right) - \kappa_r \left(\epsilon_r \frac{\partial E_z}{\partial r} + \beta\eta \frac{1}{r}\frac{\partial H_z}{\partial \theta}\right) \quad (13)$$

$$\omega \epsilon_r \mu_0 [\kappa_r^2 - \mu_r^2 (1 - \beta')^2] H_\theta = \kappa_r \left(-\epsilon_r \frac{1}{r}\frac{\partial E_z}{\partial \theta} + \beta\eta \frac{\partial H_z}{\partial r}\right) + j\mu_r (1 - \beta')\left(\epsilon_r \frac{\partial E_z}{\partial r} + \beta\eta \frac{1}{r}\frac{\partial H_z}{\partial \theta}\right) \quad (14)$$

$$E_r = \frac{\eta\beta}{\epsilon_r} H_\theta - \frac{j}{\omega \epsilon_r \epsilon_0}\frac{1}{r}\frac{\partial H_z}{\partial \theta} \quad . \quad . \quad . \quad (15)$$

$$E_\theta = -\frac{\eta\beta}{\epsilon_r} H_r + \frac{j}{\omega \epsilon_r \epsilon_0}\frac{1}{r}\frac{\partial H_z}{\partial r} \quad . \quad . \quad . \quad (16)$$

(2.5) Field Components

Appropriate substitution into eqns. (13)–(16) gives the following expressions for the components of the field in the unbounded ferrite medium:

$$E_z = [K_1 \mathrm{J}_n(\gamma_1 r) + L_1 \mathrm{Y}_n(\gamma_1 r) + K_2 \mathrm{J}_n(\gamma_2 r) + L_2 \mathrm{Y}_n(\gamma_2 r)] \exp j(n\theta + \omega t - \beta z) \quad (11)$$

$$H_z = \frac{j}{\eta}\left\{(A_1 - A_2\gamma_1^2)[K_1 \mathrm{J}_n(\gamma_1 r) + L_1 \mathrm{Y}_n(\gamma_1 r)] + (A_1 - A_2\gamma_2^2)[K_2 \mathrm{J}_n(\gamma_2 r) + L_2 \mathrm{Y}_n(\gamma_2 r)]\right\} \exp j(n\theta + \omega t - \beta z) \quad (17)$$

$$H_r = \frac{1}{\eta}\left\{(A_3 - A_4\gamma_1^2)\frac{n}{r}[K_1 \mathrm{J}_n(\gamma_1 r) + L_1 \mathrm{Y}_n(\gamma_1 r)] + (A_3 - A_4\gamma_2^2)\frac{n}{r}[K_2 \mathrm{J}_n(\gamma_2 r) + L_2 \mathrm{Y}_n(\gamma_2 r)] - (A_5 - A_6\gamma_1^2)\gamma_1 [K_1 \mathrm{J}_n'(\gamma_1 r) + L_1 \mathrm{Y}_n'(\gamma_1 r)] - (A_5 - A_6\gamma_2^2)\gamma_2 [K_2 \mathrm{J}_n'(\gamma_2 r) + L_2 \mathrm{Y}_n'(\gamma_2 r)]\right\} \exp j(n\theta + \omega t - \beta z) \quad (18)$$

$$H_\theta = \frac{j}{\eta}\left\{-(A_5 - A_6\gamma_1^2)\frac{n}{r}[K_1 \mathrm{J}_n(\gamma_1 r) + L_1 \mathrm{Y}_n(\gamma_1 r)] - (A_5 - A_6\gamma_2^2)\frac{n}{r}[K_2 \mathrm{J}_n(\gamma_2 r) + L_2 \mathrm{Y}_n(\gamma_2 r)] + (A_3 - A_4\gamma_1^2)\gamma_1 [K_1 \mathrm{J}_n'(\gamma_1 r) + L_1 \mathrm{Y}_n'(\gamma_1 r)] + (A_3 - A_4\gamma_2^2)\gamma_2 [K_2 \mathrm{J}_n'(\gamma_2 r) + L_2 \mathrm{Y}_n'(\gamma_2 r)]\right\} \exp j(n\theta + \omega t - \beta z) \quad (19)$$

$$E_r = j\left\{-(A_9 - A_{10}\gamma_1^2)\frac{n}{r}[K_1 \mathrm{J}_n(\gamma_1 r) + L_1 \mathrm{Y}_n(\gamma_1 r)] - (A_9 - A_{10}\gamma_2^2)\frac{n}{r}[K_2 \mathrm{J}_n(\gamma_2 r) + L_2 \mathrm{Y}_n(\gamma_2 r)] + (A_7 - A_8\gamma_1^2)\gamma_1 [K_1 \mathrm{J}_n'(\gamma_1 r) + L_1 \mathrm{Y}_n'(\gamma_1 r)] + (A_7 - A_8\gamma_2^2)\gamma_2 [K_2 \mathrm{J}_n'(\gamma_2 r) + L_2 \mathrm{Y}_n'(\gamma_2 r)]\right\} \exp j(n\theta + \omega t - \beta z) \quad (20)$$

$$E_\theta = \left\{-(A_7 - A_8\gamma_1^2)\frac{n}{r}[K_1 \mathrm{J}_n(\gamma_1 r) + L_1 \mathrm{Y}_n(\gamma_1 r)] - (A_7 - A_8\gamma_2^2)\frac{n}{r}[K_2 \mathrm{J}_n(\gamma_2 r) + L_2 \mathrm{Y}_n(\gamma_2 r)] + (A_9 - A_{10}\gamma_1^2)\gamma_1 [K_1 \mathrm{J}_n'(\gamma_1 r) + L_1 \mathrm{Y}_n'(\gamma_1 r)] + (A_9 - A_{10}\gamma_2^2)\gamma_2 [K_2 \mathrm{J}_n'(\gamma_2 r) + L_2 \mathrm{Y}_n'(\gamma_2 r)]\right\} \exp j(n\theta + \omega t - \beta z) \quad (21)$$

where

$$\left.\begin{aligned}
A_1 &= \frac{\epsilon_r}{\beta\kappa_r}[\mu_r^2(1-\beta') - \kappa_r^2] \\
A_2 &= \frac{\mu_r}{4\pi^2\beta\kappa_r} \\
A_3 &= \frac{\mu_r(\mu_r+1)(1-\beta') - \kappa_r^2}{2\pi[\kappa_r^2 - \mu_r^2(1-\beta')^2]} \\
A_4 &= \frac{\mu_r}{8\pi^3\epsilon_r[\kappa_r^2 - \mu_r^2(1-\beta')^2]} \\
A_5 &= \frac{\mu_r[\mu_r^2(1-\beta')^2 - \kappa_r^2(1-\beta') + \kappa_r^2/\mu_r]}{2\pi\kappa_r[\kappa_r^2 - \mu_r^2(1-\beta')^2]} \\
A_6 &= \frac{\mu_r^2(1-\beta')}{8\pi^3\epsilon_r\kappa_r[\kappa_r^2 - \mu_r^2(1-\beta')^2]} \\
A_7 &= \frac{\beta}{\epsilon_r}A_3 \\
A_8 &= \frac{\beta}{\epsilon_r}A_4 \\
A_9 &= \frac{\beta}{\epsilon_r}A_5 - \frac{1}{2\pi\epsilon_r}A_1 \\
A_{10} &= \frac{\beta}{\epsilon_r}A_6 - \frac{1}{2\pi\epsilon_r}A_2
\end{aligned}\right\} \quad . \quad (22)$$

and the primed Bessel functions are the differential derivatives with regard to the argument.

Expressions for the components of the microwave field in an unbounded dielectric are obtained similarly to those for the ferrite. They are

$$E_z = [K_3 J_n(\gamma_a r) + L_3 Y_n(\gamma_a r)] \exp j(n\theta + \omega t - \beta z) \quad . \quad . \quad (23)$$

$$H_z = \frac{j}{\eta}[K_4 J_n(\gamma_a r) + L_4 Y_n(\gamma_a r)] \exp j(n\theta + \omega t - \beta z) \quad (24)$$

where

$$\gamma_a^2 = 4\pi^2(1-\beta^2) \quad . \quad . \quad . \quad . \quad . \quad (25)$$

and

$$H_r = \frac{1}{\eta}\left\{A_{11}\frac{n}{r}[K_3 J_n(\gamma_a r) + L_3 Y_n(\gamma_a r)] - A_{12}\gamma_a[K_4 J_n'(\gamma_a r) + L_4 Y_n'(\gamma_a r)]\right\} \exp j(n\theta + \omega t - \beta z) \quad (26)$$

$$H_\theta = \frac{j}{\eta}\left\{-A_{12}\frac{n}{r}[K_4 J_n(\gamma_a r) + L_4(\gamma_a r)] + A_{11}\gamma_a[K_3 J_n'(\gamma_a r) + L_3 Y_n'(\gamma_a r)]\right\} \exp j(n\theta + \omega t - \beta z) \quad (27)$$

$$E_r = j\left\{-A_{11}\frac{n}{r}[K_4 J_n(\gamma_a r) + L_4 Y_n(\gamma_a r)] + A_{12}\gamma_a[K_3 J_n'(\gamma_a r) + L_3 Y_n'(\gamma_a r)]\right\} \exp j(n\theta + \omega t - \beta z) \quad (28)$$

$$E_\theta = \left\{-A_{12}\frac{n}{r}[K_3 J_n(\gamma_a r) + L_3 Y_n(\gamma_a r)] + A_{11}\gamma_a[K_4 J_n'(\gamma_a r) + L_4 Y_n'(\gamma_a r)]\right\} \exp j(n\theta + \omega t - \beta z) \quad (29)$$

where

$$\left.\begin{aligned}
A_{11} &= -\frac{2\pi}{\gamma_a^2} \\
A_{12} &= \beta A_{11}
\end{aligned}\right\} \quad . \quad . \quad . \quad . \quad . \quad (30)$$

(3) CHARACTERISTIC EQUATIONS

The characteristic equation for round waveguide fully o partially filled with ferrite is derived by applying the relevan boundary conditions to the expressions for the microwav field. The method used in this Section may easily be extende to give the characteristic equation for any circularly symmetri shape of ferrite inside round waveguide.

The following constants are used to simplify the expressio for the characteristic equations and are defined here fo convenience.

Define the constants F as follows:

$$\begin{aligned}
F_1 &= J_n(\gamma_1 r_1) \\
F_2 &= Y_n(\gamma_1 r_1) \\
F_3 &= J_n(\gamma_2 r_1) \\
F_4 &= Y_n(\gamma_2 r_1) \\
F_5 &= (A_1 - A_2\gamma_1^2)J_n(\gamma_1 r_1) \\
F_6 &= (A_1 - A_2\gamma_1^2)Y_n(\gamma_1 r_1) \\
F_7 &= (A_1 - A_2\gamma_2^2)J_n(\gamma_2 r_1) \\
F_8 &= (A_1 - A_2\gamma_2^2)Y_n(\gamma_2 r_1) \\
F_9 &= -(A_5 - A_6\gamma_1^2)\frac{n}{r_1}J_n(\gamma_1 r_1) + (A_3 - A_4\gamma_1^2)\gamma_1 J_n'(\gamma_1 r_1) \\
F_{10} &= -(A_5 - A_6\gamma_1^2)\frac{n}{r_1}Y_n(\gamma_1 r_1) + (A_3 - A_4\gamma_1^2)\gamma_1 Y_n'(\gamma_1 r_1) \\
F_{11} &= -(A_5 - A_6\gamma_2^2)\frac{n}{r_1}J_n(\gamma_2 r_1) + (A_3 - A_4\gamma_2^2)\gamma_2 J_n'(\gamma_2 r_1) \\
F_{12} &= -(A_5 - A_6\gamma_2^2)\frac{n}{r_1}Y_n(\gamma_2 r_1) + (A_3 - A_4\gamma_2^2)\gamma_2 Y_n'(\gamma_2 r_1) \\
F_{13} &= -(A_7 - A_8\gamma_1^2)\frac{n}{r_1}J_n(\gamma_1 r_1) + (A_9 - A_{10}\gamma_1^2)\gamma_1 J_n'(\gamma_1 r_1) \\
F_{14} &= -(A_7 - A_8\gamma_1^2)\frac{n}{r_1}Y_n(\gamma_1 r_1) + (A_9 - A_{10}\gamma_1^2)\gamma_1 Y_n'(\gamma_1 r_1) \\
F_{15} &= -(A_7 - A_8\gamma_2^2)\frac{n}{r_1}J_n(\gamma_2 r_1) + (A_9 - A_{10}\gamma_2^2)\gamma_2 J_n'(\gamma_2 r_1) \\
F_{16} &= -(A_7 - A_8\gamma_2^2)\frac{n}{r_1}Y_n(\gamma_2 r_1) + (A_9 - A_{10}\gamma_2^2)\gamma_2 Y_n'(\gamma_2 r_1)
\end{aligned}$$

Define the constants G so that if F_i is a function of r_1 the G_i is the same function of r_2.

Define the constants P as follows:

$$\begin{aligned}
P_1 &= \frac{J_n(\gamma_a r_2)}{Y_n(\gamma_a r_2)} \\
P_2 &= \frac{J_n'(\gamma_a r_2)}{Y_n'(\gamma_a r_2)}
\end{aligned}$$

Define the constants Q so that, if P_i is a function of r_2, Q_i i the same function of r_3.

Define the constants M as follows:

$$\begin{aligned}
M_1 &= J_n(\gamma_a r_1) - P_1 Y_n(\gamma_a r_1) \\
M_2 &= J_n(\gamma_a r_1) - P_2 Y_n(\gamma_a r_1) \\
M_3 &= A_{11}\gamma_a[J_n'(\gamma_a r_1) - P_1 Y_n'(\gamma_a r_1)] \\
M_4 &= -A_{12}\frac{n}{r_1}M_2 \\
M_5 &= -A_{12}\frac{n}{r_1}M_1 \\
M_6 &= A_{11}\gamma_a[J_n'(\gamma_a r_1) - P_2 Y_n'(\gamma_a r_1)]
\end{aligned}$$

Define the constants N so that, if M_i is a function of P and r_1, N_i is the same function of Q and r_2.

Define the constants S as follows:

$$S_1 = \mathrm{J}_n(\gamma_a r_1)$$

$$S_2 = A_{11}\gamma_a \mathrm{J}_n'(\gamma_a r_1)$$

$$S_3 = -A_{12}\frac{n}{r_1}\mathrm{J}_n(\gamma_a r_1)$$

(3.1) Ferrite-Filled Round Waveguide

Although the characteristic equation for round waveguide filled with ferrite has been given before in various forms, it is derived again here for completeness.

Consider a round waveguide of radius r_1 completely filled with ferrite. The boundary condition is that the tangential electric field is zero at the waveguide wall. Since the ferrite medium is continuous through the origin, the constants associated with the Bessel functions of the second kind are zero.

Equating the longitudinal and circumferential electric fields to zero gives

$$\left.\begin{aligned} F_1K_1 + F_3K_2 &= 0 \\ F_{13}K_1 + F_{15}K_2 &= 0 \end{aligned}\right\} \quad . \quad . \quad . \quad . \quad (31)$$

Elimination of K_1 and K_2 gives

$$\begin{vmatrix} F_1 F_3 \\ F_{13} F_{15} \end{vmatrix} = 0 \quad . \quad . \quad . \quad . \quad . \quad . \quad (32)$$

which is the characteristic equation in the ferrite filled round waveguide.

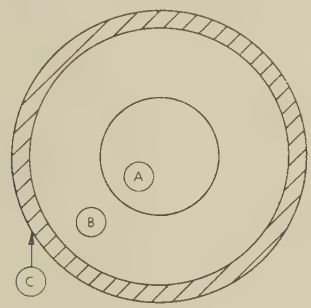

Fig. 3.—Cross-section of waveguide partially filled with ferrite.

(3.2) Ferrite Rod at Centre of Round Waveguide

Consider the waveguide configuration shown in cross-section in Fig. 3.

Area A.—Ferrite medium, $0 \leqslant r < r_1$.

Area B.—Homogeneous dielectric medium, $r_1 \leqslant r < r_2$.

Area C.—Perfectly conducting waveguide wall, $r_2 \leqslant r$.

Because area A is continuous through the origin, the constants associated with the Bessel functions of the second kind will be zero.

For the boundary conditions at the waveguide walls, equating the expression for the longitudinal component of electric field to zero gives

$$K_3\mathrm{J}_n(\gamma_a r_2) + L_3\mathrm{Y}_n(\gamma_a r_2) = 0 \quad . \quad . \quad . \quad (33)$$

Therefore

$$L_3 = -P_1K_3 \quad . \quad . \quad . \quad . \quad . \quad . \quad (34)$$

Similarly, the circumferential component gives

$$L_4 = -P_2K_4 \quad . \quad . \quad . \quad . \quad . \quad . \quad (35)$$

At the ferrite dielectric boundary, where $r = r_1$, the tangential components of the electric and magnetic fields are continuous. Equating the expressions for these field components across the boundary gives

$$\left.\begin{aligned} K_3M_1 &= K_1F_1 + K_2F_3 \\ K_4M_2 &= K_1F_5 + K_2F_7 \\ K_3M_3 + K_4M_4 &= K_1F_9 + K_2F_{11} \\ K_3M_5 + K_4M_6 &= K_1F_{13} + K_2F_{15} \end{aligned}\right\} \quad . \quad . \quad (36)$$

Elimination of K_1, K_2, K_3 and K_4 from eqns. (36) gives

$$\begin{vmatrix} F_1 & F_3 & M_1 & 0 \\ F_5 & F_7 & 0 & M_2 \\ F_9 & F_{11} & M_3 & M_4 \\ F_{13} & F_{15} & M_5 & M_6 \end{vmatrix} = 0 \quad . \quad . \quad . \quad . \quad (37)$$

which is the characteristic equation for the waveguide partially filled with ferrite.

(3.3) Ferrite Tube Adjacent to Wall of Waveguide

Again the configuration in the waveguide is shown in cross-section in Fig. 3, but in this case the ferrite occupies the tubular space inside the waveguide wall.

Area A.—Homogeneous dielectric medium, $0 \leqslant r < r_1$.

Area B.—Ferrite medium, $r_1 \leqslant r < r_2$.

Area C.—Perfectly conducting waveguide wall, $r_2 \leqslant r$.

Because area A is continuous through the origin, the constants associated with the Bessel functions of the second kind will be zero.

For the boundary conditions at the waveguide walls, equating the expression for the longitudinal and circumferential components of the electric field to zero gives

$$\left.\begin{aligned} K_1G_1 + L_1G_2 + K_2G_3 + L_2G_4 &= 0 \\ K_1G_{13} + L_1G_{14} + K_2G_{15} + L_2G_{16} &= 0 \end{aligned}\right\} \quad . \quad . \quad (38)$$

At the ferrite dielectric boundary, where $r = r_1$, the tangential components of the electric and magnetic fields are continuous. Equating the expressions for these field components across the boundary gives

$$\left.\begin{aligned} K_1F_1 + L_1F_2 + K_2F_3 + L_2F_4 &= K_3S_1 \\ K_1F_5 + L_1F_6 + K_2F_7 + L_2F_8 &= K_4S_1 \\ K_1F_9 + L_1F_{10} + K_2F_{11} + L_2F_{12} &= K_3S_2 + K_4S_3 \\ K_1F_{13} + L_1F_{14} + K_2F_{15} + L_2F_{16} &= K_3S_3 + K_4S_2 \end{aligned}\right\} \quad (39)$$

Elimination of K_1, L_1, K_2, L_2, K_3 and K_4 from eqns. (38) and (39) gives

$$\begin{vmatrix} F_1 & F_2 & F_3 & F_4 & S_1 & 0 \\ F_5 & F_6 & F_7 & F_8 & 0 & S_1 \\ F_9 & F_{10} & F_{11} & F_{12} & S_2 & S_3 \\ F_{13} & F_{14} & F_{15} & F_{16} & S_3 & S_2 \\ G_1 & G_2 & G_3 & G_4 & 0 & 0 \\ G_{13} & G_{14} & G_{15} & G_{16} & 0 & 0 \end{vmatrix} = 0 \quad . \quad . \quad . \quad (40)$$

which is the characteristic equation for the waveguide partially filled with ferrite.

(3.4) Ferrite Tube in Centre of Waveguide

Consider the waveguide configuration shown in cross-section in Fig. 4.

Area A.—Homogeneous dielectric medium, $0 \leqslant r < r_1$.

Area B.—Ferrite medium, $r_1 \leqslant r < r_2$.

Area C.—Homogeneous dielectric medium, $r_2 \leqslant r < r_3$.

Area D.—Perfectly conducting waveguide wall, $r_3 \leqslant r$.

Because area A is continuous through the origin, the constants associated with the Bessel functions of the second kind will be zero. In area C the arbitrary constants are K_5, L_5, K_6 and L_6.

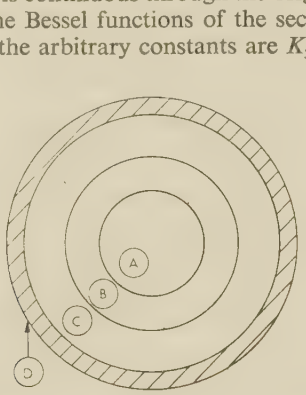

Fig. 4.—Cross-section of waveguide partially filled with ferrite.
Area A.—Dielectric material.
Area B.—Ferrite material.
Area C.—Dielectric material.
Area D.—Perfectly conducting waveguide wall.

At the waveguide wall the boundary conditions are given by [similar to eqns. (34) and (35)].

$$\left.\begin{aligned} L_5 &= -Q_1 K_5 \\ L_6 &= -Q_2 K_6 \end{aligned}\right\} \quad . \quad . \quad . \quad . \quad . \quad (41)$$

At the boundary $r = r_2$ the boundary conditions are given by [similar to eqns. (39)]

$$\left.\begin{aligned} K_5 N_1 &= K_1 G_1 + L_1 G_2 + K_2 G_3 + L_2 G_4 \\ K_6 N_2 &= K_1 G_5 + L_1 G_6 + K_2 G_7 + L_2 G_8 \\ K_5 N_3 + K_6 N_4 &= K_1 G_9 + L_1 G_{10} + K_2 G_{11} + L_2 G_{12} \\ K_5 N_5 + K_6 N_6 &= K_1 G_{13} + L_1 G_{14} + K_2 G_{15} + L_2 G_{16} \end{aligned}\right\} \quad (42)$$

At the boundary $r = r_1$ the boundary conditions are given by eqns. (39).

Elimination of K_1, L_1, K_2, L_2, K_3, K_4, K_5 and K_6 from eqns. (39) and (42) gives

$$\begin{vmatrix} G_1 & G_2 & G_3 & G_4 & 0 & 0 & N_1 & 0 \\ G_5 & G_6 & G_7 & G_8 & 0 & 0 & 0 & N_2 \\ G_9 & G_{10} & G_{11} & G_{12} & 0 & 0 & N_3 & N_4 \\ G_{13} & G_{14} & G_{15} & G_{16} & 0 & 0 & N_5 & N_6 \\ F_1 & F_2 & F_3 & F_4 & S_1 & 0 & 0 & 0 \\ F_5 & F_6 & F_7 & F_8 & 0 & S_1 & 0 & 0 \\ F_9 & F_{10} & F_{11} & F_{12} & S_2 & S_3 & 0 & 0 \\ F_{13} & F_{14} & F_{15} & F_{16} & S_3 & S_2 & 0 & 0 \end{vmatrix} = 0 \quad . \quad . \quad (43)$$

which is the characteristic equation for the waveguide partially filled with ferrite.

(4) SOLUTION OF THE CHARACTERISTIC EQUATIONS

Mathematical expressions have been given in Sections 2 and 3 which define the conditions for microwave propagation in round waveguides partially filled with ferrite. It is now necessary to derive useful results from these expressions. The unknown in any waveguide problem is the propagation coefficient β. As this paper has already shown, the mathematics required to find the condition for propagation in a partially filled waveguide is very involved. Bessel functions enter in all round-waveguide problems, and for those partially filled w ferrite the argument of the Bessel functions is a term wh itself is the solution of a quadratic equation into which t unknown β enters. So it is impossible to solve the equatio for the propagation coefficient except by trial and error, trying values for β to find when the propagation equation zero. The problem is such that it can be solved only by recou to an electronic computer. A programme has been written perform these calculations on a Pegasus computer, and a f details of this programme are given in Section 5.

(4.1) Faraday Rotation

For most applications the microwave engineer is interest in the Faraday rotation effect of waveguide partially filled w ferrite rather than the propagation coefficients of the two han of circular polarization—the difference between which gives t Faraday rotation. Many authors, e.g. Waldron,[6] have deriv the expression connecting rotation with propagation coefficie and the derivation will not be repeated here. The rotation given by

$$\phi = \pi(\beta_+ - \beta_-) \quad . \quad . \quad . \quad . \quad . \quad (4$$

measured in radians per unit length of waveguide, the unit length being λ_0.

(4.2) Identification of Modes

In waveguide partially filled with ferrite there are no mod with either purely transverse-E or transverse-H fields. Th are longitudinal components of both fields, so that the nom clature of E (TM) and H (TE) modes are inapplicable. It possible to use the idea of quasi-E and quasi-H modes by relati them to the modes which propagate in empty waveguide. T propagation coefficient can be followed as the ferrite dimensio change, and at the limit of small ferrite size the mode may identified from that which propagates in empty waveguid The theoretical analysis can distinguish only between modes different circular order, i.e. with H_{nq} and E_{nq} modes it c only distinguish between modes of different n and it cann distinguish between either E or H modes or modes of different To distinguish further between different modes of the same orc it will be necessary to follow the propagation coefficient to t limit of small ferrite dimensions. The author does not belie that this investigation is worth the labour involved, since t computations required are very lengthy and for normal applic tions interest is only in the H_{11} mode and whether any oth mode can propagate.

(5) COMPUTATION OF RESULTS

(5.1) General Principles

The mathematics in Section 3 gives expressions for fo determinants which, when zero, give the propagation coefficie for four different configurations of circularly symmetric ferr loaded round waveguide. Three of these structures are interest to microwave engineers, namely

(*a*) Ferrite rod at centre of waveguide.
(*b*) Ferrite tube adjacent to wall of waveguide.
(*c*) Ferrite tube at centre of waveguide.

The obvious way to solve this ferrite–waveguide problem to write a programme to compute the propagation equation each of the three configurations separately and to incorporate search-for-zero routine in each. But the mathematics leadi to the expressions for the propagation coefficients of the thr configurations are similar and many intermediate results a the same. Moreover, the expressions for the propagati

oefficients of the reverse waves mostly use the same intermediate esults. So it was decided to calculate the value of the deter- ninant for the six different conditions (three forward and three everse) at one time, for a range of propagation coefficients, and hen to determine, by visual inspection of the results, the coeffi- ient for which each determinant was zero. This method of omputation was thought to be more economical in the computer ime than instituting an individual search for zero on each hysical configuration.

(5.2) Inadmissible Cases

If the condition for the unmagnetized ferrite, i.e. $\kappa_r = 0$, is ut into the expression for the propagation coefficient, various erms in the determinants become infinite, so it is necessary to se a different expression to find β when $\kappa_r = 0$. The condition or cut-off, i.e. $\beta = 0$, has the same effect. Separate expressions or the two above special conditions have not been given here, ut Waldron[6, 7] gives very full treatment of the cut-off conditions.

It has also been found that the expressions for the determinants n the propagation equations appear to have infinities as well s zeros as β is varied. At zero, the determinant changes apidly, so that these zeros are observed by a change of sign in his value and there is no indication whether it is zero or infinity. Moreover, if certain terms in the determinant tend to infinity, t is probable that in evaluating the determinant a small difference etween two very large quantities will occur, which the com- uter may register as zero. Such false zeros or infinities occur when $\beta = 1$ as well as for the conditions given above and others which are less easily specified. The propagation equations are equivalent to a physical condition only when the determinant is zero, so that its value has no significance except when it is zero. The infinities are only significant because they may be mistaken for propagating conditions.

(6) EXPERIMENTAL VERIFICATION

A large number of measurements have been made on two equivalent types of ferrite material, R1 and FR3, which are magnesium-manganese ferrites containing approximately 48% iron, 15% magnesium, 3% manganese and 34% oxygen. These measurements have been compared with theory.

(6.1) Test Conditions

For the tests the ferrite rod is 0·25 in in diameter and 2 in long, and the round waveguide has an inside diameter of 0·9 in. The microwave frequency is 9370 Mc/s, i.e. $\lambda_0 = 1{\cdot}26$ in. The saturation magnetization is produced by a current of 115 mA in a coil of 20000 turns wound around the outside of the wave- guide in a length of 3 in.

(6.2) Measured Results

With the ferrite rod matched into the empty round waveguide he saturation magnetized rotation is 320°. The absolute varia- ion on this rotation between different specimens is $\pm 18°$, which s the specification which has been set for this ferrite material.

(6.3) Measured Parameters

The material constants of the two types of ferrite were neasured at microwave frequencies.

The permittivity was measured in an E_{01} resonant cavity on a od of ferrite about $\frac{1}{16}$ in diameter, giving 11·1 for R1 and 1·6 for FR3. These measurements were made at 8930 and 850 Mc/s respectively.

The tensor permeability was measured in a round cavity scillating in the degenerate H_{112} mode excited by positive or egative circularly polarized waves. The method is substantially the same as that used by Spencer, LeCraw and Reggia.[10] The measurements were performed on discs of ferrite, 0·15 in in diameter and 0·05 in thick, magnetized normal to the plane of the disc. The measured effect of the intrinsic tensor per- meability is given in Fig. 5. The components of the tensor permeability, given in Fig. 6, are derived from the results in Fig. 5.

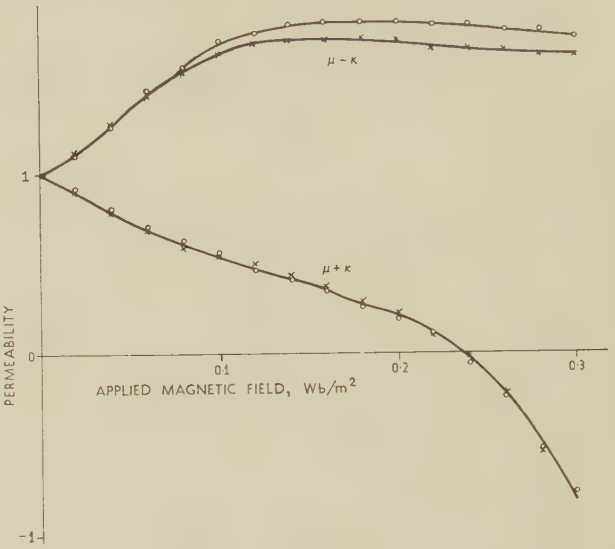

Fig. 5.—Cavity measurement of tensor permeability of ferrite, measured on a disc 0·15 in in diameter and 0·050 in thick magnetized normal to the disc, at 9320 Mc/s, as a function of applied magnetic field.

× × × FR3.
○ ○ ○ R1.

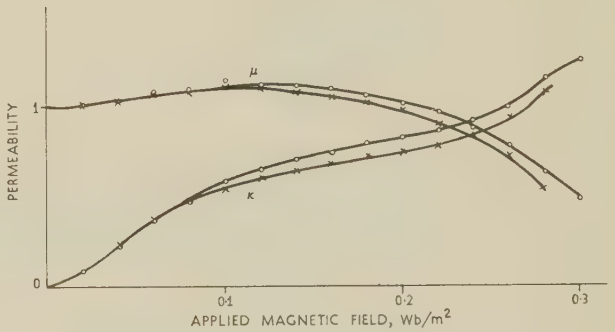

Fig. 6.—Components of the tensor permeability of the ferrite, calculated from the measured results given in Fig. 5, as a function of applied magnetic field.

× × × FR3.
○ ○ ○ R1.

(6.4) Computed Results

For computation the test conditions become

Ferrite rod normalized radius, $r_1 = 0{\cdot}100$.
Waveguide normalized radius, $r_2 = 0{\cdot}357$.

The permittivities are given above and the diagonal and cross-diagonal components of the permeability tensor are given in Fig. 6.

The computed results of the normalized propagation coeffi- cients are given in Fig. 7(*a*), while Fig. 7(*b*) gives the rotation of a linearly polarized wave measured in the units 'twice right angles per free-space wavelength' from eqn. (44). For both types of ferrite the saturation rotation (computed) gives 1·4

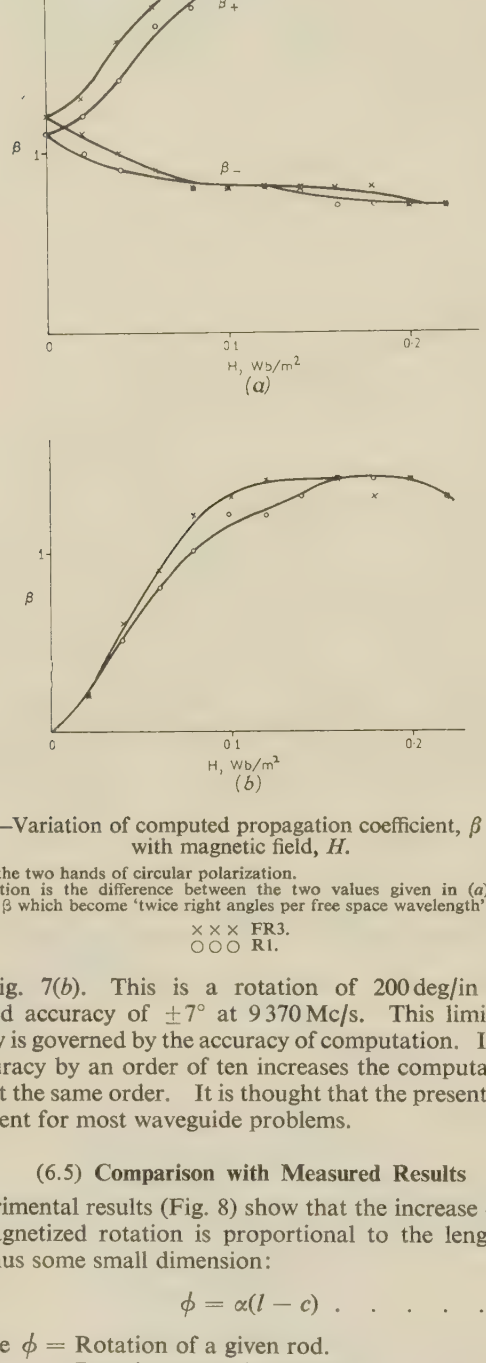

Fig. 7.—Variation of computed propagation coefficient, $\beta = \lambda_0/\lambda_g$, with magnetic field, H.

(*a*) For the two hands of circular polarization.
(*b*) Rotation is the difference between the two values given in (*a*), measured in units of β which become 'twice right angles per free space wavelength'.

× × × FR3.
○ ○ ○ R1.

from Fig. 7(*b*). This is a rotation of 200 deg/in with an estimated accuracy of ±7° at 9370 Mc/s. This limitation on accuracy is governed by the accuracy of computation. Increasing the accuracy by an order of ten increases the computation time by about the same order. It is thought that the present accuracy is sufficient for most waveguide problems.

(6.5) Comparison with Measured Results

Experimental results (Fig. 8) show that the increase of saturation magnetized rotation is proportional to the length of the rod minus some small dimension:

$$\phi = \alpha(l - c) \quad . \quad . \quad . \quad . \quad . \quad . \quad (45)$$

Where ϕ = Rotation of a given rod.
α = Rotation per unit length.
l = Length of the rod.
c = Experimental constant.

Fig. 8 shows that, for our experimental configuration, $c = 0{\cdot}1$ in. This experimental result has a very simple (if not exactly true) physical explanation. The ferrite rod is assumed to be uniformly magnetized, but there will be effects at the end of the rod where this is not true. These effects reduce the effective length of the rod by an amount which appears to be independent of the length, so that, to find the theoretical rotation of a 2 in rod, the rotation per inch must be multiplied by 1·9 in

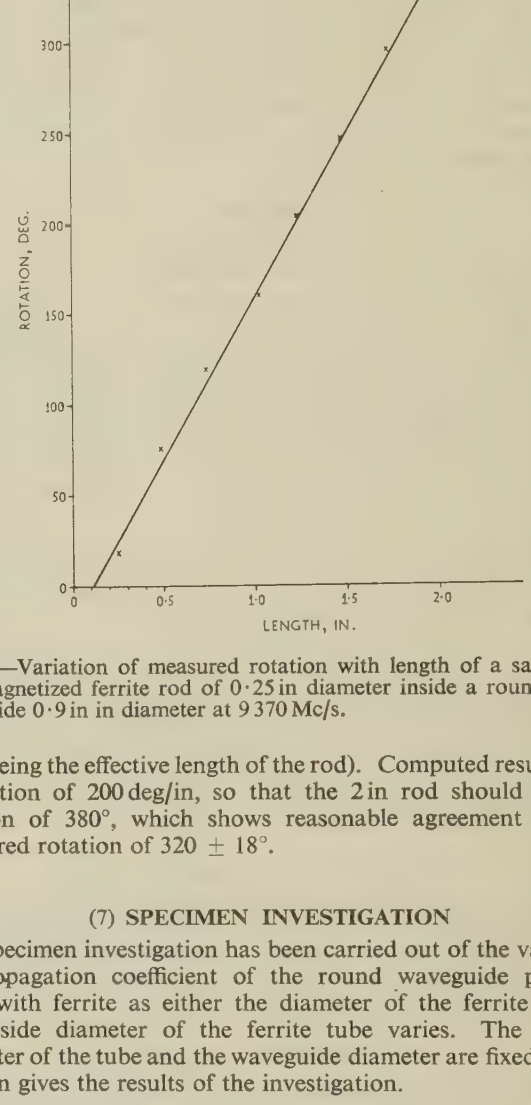

Fig. 8.—Variation of measured rotation with length of a saturated magnetized ferrite rod of 0·25 in diameter inside a round waveguide 0·9 in in diameter at 9370 Mc/s.

(that being the effective length of the rod). Computed results gi a rotation of 200 deg/in, so that the 2 in rod should have rotation of 380°, which shows reasonable agreement with measured rotation of 320 ± 18°.

(7) SPECIMEN INVESTIGATION

A specimen investigation has been carried out of the variatio of propagation coefficient of the round waveguide partial filled with ferrite as either the diameter of the ferrite rod the inside diameter of the ferrite tube varies. The outsi diameter of the tube and the waveguide diameter are fixed. Th Section gives the results of the investigation.

(7.1) Parameters Used

A guess was made for ferrite properties to approximate R1 ferrite when magnetized to saturation. The manufacturer information gave the permittivity as 13, so the ferrite properti chosen were $\mu_r = 1$, $\kappa_r = 0{\cdot}75$ and $\epsilon_r = 13$. It was assum that the rest of the space was filled with air. Subseque measurement, recorded in Section 6, shows that these valu for the ferrite properties are high; the permittivity especially high, but the manufacturer's measurements were possibly carri

Fig. 9.—Variation of normalized propagation coefficient, $\beta = \lambda_0/$ with rod diameter or tube inside diameter, r_1.

Ferrite properties: $\mu_r = 1$, $\kappa_r = 0{\cdot}75$, $\epsilon_r = 13$, $r_2 = 0{\cdot}357$ and $r_3 = 0{\cdot}405$.
(*a*), (*b*), (*c*), (*d*) and (*e*): Ferrite rod of radius r_1 inside waveguide of radius r_2.
(*f*), (*g*), (*h*), (*i*) and (*j*): Ferrite tube of radii r_1 and r_2 inside waveguide of radius r_2.
(*k*), (*l*), (*m*), (*n*) and (*p*): Ferrite tube of radii r_1 and r_2 inside waveguide of radius r_3.
(*a*), (*f*) and (*k*): Positive and negative circularly polarized waves for all circular symmetric modes, i.e. E_{0q} and H_{0q} modes.
(*b*), (*g*) and (*l*): Positive circularly polarized waves } for all modes of circular order
(*c*), (*h*) and (*m*): Negative circularly polarized waves } i.e. E_{1q} and H_{1q} modes.
(*d*), (*i*) and (*n*): Positive circularly polarized waves } for all modes of circular order
(*e*), (*j*) and (*p*): Negative circularly polarized waves } i.e. E_{2q} and H_{2q} modes.

Fig. 9
(see bottom of previous page)

out at low instead of microwave frequencies. The calculation uses three normalized radii, namely

r_1 = Radius of the ferrite rod or inside radius of the ferrite tube.

r_2 = Radius of the waveguide, (*a*) and (*b*), and outside radius of the ferrite tube, (*b*) and (*c*).

r_3 = Radius of the waveguide, (*c*).

(The letters refer to the configurations listed in Section 5.1.)

The investigation uses fixed values of r_2 and r_3 and varies r_1. As already mentioned, many measurements have been made of ferrite rods at 9370 Mc/s, i.e. $\lambda_0 = 1{\cdot}26$ in, inside a waveguide with a diameter of 0·9 in; another size of round waveguide in common use has a diameter of 1·022 in. r_2 and r_3 were taken to be these dimensions respectively, normalized with regard to a free-space wavelength of 1·26 in. They become $r_2 = 0{\cdot}357$ and $r_3 = 0{\cdot}405$.

(7.2) Results

As mentioned in Section 4.2 the theoretical analysis is able to distinguish only between modes of different circular order, i.e. with H_{nq} and E_{nq} modes it can distinguish only between modes of different n. For this reason all the results for a given configuration of ferrite, a given hand of polarization and a given n are recorded on the same graph. Results are given for values of $n = 0$, 1 and 2. In the results, the H_{11} and the E_{01} modes have been labelled by consideration of the mode which can propagate in the limit of small ferrite dimensions; otherwise no attempt has been made to label the other modes which the results show can propagate in the ferrite-loaded waveguide.

Graphs are plotted of normalized propagation coefficient, β, against the normalized radius, r_1, for the different configurations of ferrite and for both hands of circular polarization showing all the modes propagated up to the circular order 2. Points were computed in steps of 0·025 in r_1 and in between if necessary for determining the shape of any curve. β was calculated to the nearest 0·1. The results are given in Fig. 9.

(8) CONCLUSIONS

The method of the theoretical investigation is such that it may easily be extended to give the characteristic equation for any circularly symmetric shape of ferrite inside round waveguide, in addition to the characteristic equations given in the paper. A programme has been written to compute results from this theory and is available to help in the design of reciprocal and non-reciprocal ferrite-waveguide components.

(9) ACKNOWLEDGMENTS

R1 ferrite is manufactured by the Plessey Company, Lt and FR3 by the Research Laboratory of A.E.I. (Rugby), L The microwave cavity measurements of ferrite properties w carried out by Mr. T. H. B. Baker of the Research Laborat of A.E.I. (Rugby), Ltd. The author wishes to acknowle helpful discussions with his colleagues in the Military Ra Engineering Department of the A.E.I. Electronic Appara Division, and also with Mr. P. Hammond and Mr. R. Waldron. Thanks are due to the Executive of the A.E Electronic Apparatus Division and the Board of the A.E Company for permission to publish the paper.

(10) REFERENCES

(1) POLDER, D.: 'The Theory of Ferromagnetic Resonan *Philosophical Magazine*, 1949, **40**, p. 99.

(2) GAMO, H.: 'The Faraday Rotation of Waves in a Circu Waveguide', *Journal of the Physical Society of Jap* 1953, **8**, p. 176.

(3) KALES, M. L.: 'Modes in Wave Guides Containing Ferrite *Journal of Applied Physics*, 1953, **24**, p. 604.

(4) SUHL, H., and WALKER, L. R.: 'Topics in Guided W Propagation through Gyromagnetic Media', *Bell Sy Technical Journal* 1954, **33**, pp. 579, 939 and 1133.

(5) CLARRICOATS, P. J. B.: 'A Perturbation Method for Circu Waveguides containing Ferrites', *Proceedings* I.E Paper No. 2796 E, May, 1959 (**106** B, p. 335).

(6) WALDRON, R. A.: 'Electromagnetic Wave Propagation Cylindrical Waveguides containing Gyromagnetic Me *Journal of the British Institution of Radio Engineers*, 19 **18**, pp. 597, 677 and 733.

(7) WALDRON, R. A.: 'Theory of the Mode Spectra of Cyl drical Waveguides containing Gyromagnetic Media', *ib* 1959, **19**, p. 347.

(8) MIRIMANOV, R. G., and ANISIMOVA, YU. V.: 'Circu Waveguide Partially Filled with Ferrite as a Retardi System', *Radiotekhnika i Elektronika*, 1957, **2**, p. 8 (English Translation in *Radio Engineering and Electroni* 1957, **2**, No. 7, p. 37).

(9) RIZZI, P. A.: 'High-Power Ferrite Circulators', *Transactio of the Institute of Radio Engineers*, 1957, **MTT–5**, p. 2

(10) SPENCER, E. G., LECRAW, R. C., and AULT, L. 'Measurements of Microwave Dielectric Constant a Tensor Permeability of Ferrite Spheres', *Proceedings the Institute of Radio Engineers*, 1956, **44**, p. 790.

(11) WALDRON, R. A.: 'Features of Cylindrical Waveguid containing Gyromagnetic Media', *Journal of the Brit Institution of Radio Engineers*, 1960, **20**, p. 695.

621.372.85

The Institution of Electrical Engineers
Monograph No. 431 E
Feb. 1961

MICROWAVE HALL EFFECT AND THE ACCOMPANYING ROTATION OF THE PLANE OF POLARIZATION

By Professor H. E. M. BARLOW, B.Sc.(Eng.), Ph.D., M.I.Mech.E., Member.

(*The paper was first received 2nd September, and in revised form 25th October*, 1960. *It was published as an* INSTITUTION MONOGRAPH *in February*, 1961.)

SUMMARY

Faraday rotation of the plane of polarization of an electromagnetic wave, propagated through a medium in the direction of an independently applied steady magnetic field, has been interpreted in terms of gyromagnetic action and in certain circumstances as a consequence of Hall effect.

The paper calls particular attention to the Hall-effect mechanism, which is shown to lead to different propagation coefficients for the right-handed and left-handed circularly-polarized components of a plane wave.

The contention is advanced that a Hall effect can be expected to arise from a displacement current in the material medium and that, as a consequence, the Faraday rotation effect in dielectrics and semiconductors may, in some cases, be significantly modified at frequencies above the microwave part of the spectrum. Some elementary calculations are given in support of this argument.

(1) INTRODUCTION

The rotation which occurs in the plane of polarization of an electromagnetic wave propagated through a material in the direction of an independently applied steady magnetic field has been the subject of many investigations since Faraday first discovered it in 1845. This Faraday effect was originally observed with light transmitted through a transparent dielectric medium, but more recently very similar behaviour has been demonstrated at microwave frequencies in both ferrites and semiconductors. According to the particular physical conditions there are several closely allied but nevertheless distinctive mechanisms which have been used to explain Faraday rotation. In most cases the rotation is interpreted in terms of the precession about the direction of the steady applied magnetic field of the axes of spinning or orbital electrons. In a dielectric at optical frequencies or in a ferrite transmitting a microwave, the effect normally arises from bound electrons, their precession under the influence of the applied magnetic field giving rise to different velocities of propagation for the right- and left-hand circularly-polarized components of an incident plane wave. The model on which this kind of analysis is based is in the nature of an atomic gyroscope, but, in general, it forms a unit of a more complex system in accordance with the structure of the substance. As might be expected, the gyromagnetic action leads to resonances at particular Larmor frequencies, and according to their values, they can be ascribed to spinning charges in atomic structures of various kinds. A given resonance is accompanied by an enhanced Faraday rotation and a corresponding increase in the absorption of power.

In a semiconductor mobile charges play a vital part, and at low temperatures, well below ambient, these free electrons or holes can execute orbital motions and so provide for gyromagnetic action associated with cyclotron resonance effects, when under the influence of a microwave and a steady applied magnetic field. At room temperatures, however, the mean free path of the mobile carriers is too small to permit the setting up of orbital motions at microwave frequencies, and consequently the Faraday rotation in semiconductors must then arise from a different source. The essential condition for the gyromagnetic mechanism to operate in these circumstances is clearly that $\omega > \omega_c$, where ω and ω_c are, respectively, the applied and collision angular frequencies. If $\omega < \omega_c$ the Hall effect is known to be practically entirely responsible for the rotation of the plane of polarization of the wave. The present paper is concerned with this high-frequency Hall effect, which is of acknowledged importance at room temperatures in semiconductors, but which may also have an influence on Faraday rotation in other cases.

The discussion, which is in terms of classical theory, treats the medium as a simple one having electrical properties defined by a conductivity σ, a permeability μ and a permittivity ϵ. Analysis on this basis is clearly an oversimplification in many cases, but it does enable a helpful physical picture of the conditions to be obtained. The current produced by the electric field of the wave interacts with the steady applied magnetic field to generate a secondary or Hall electric field in a mutually perpendicular direction and of the same frequency as the wave.* This Hall field, when combined with the incident electric field, will clearly cause a rotation of the plane of polarization of the wave, and since the direction of the current in the medium is always aligned with the resultant electric field at any point, there must be a progressive increase in the angle through which the polarization is rotated as the wave moves forward. The analysis shows that the effect of the Hall electric field is precisely the same as gyromagnetic action causing the right- and left-handed circularly-polarized components of the incident plane wave to propagate with different velocities, giving to the medium an equivalent tensor permittivity. The accompanying rotation of the plane of polarization is always non-reciprocal.

The contention previously advanced by the author[1] that there is a contribution to the Hall electric field from the displacement component of current in the material medium, as well as from the conduction component, has been maintained in the present analysis, and it leads to the expectation that the Hall effect plays a more important part than is usually thought to be the case at frequencies approaching the infra-red part of the spectrum. In this region, even at room temperatures, we should generally have $\omega > \omega_c$, so that gyromagnetic action and cyclotron resonance again become significant, producing pronounced Faraday rotation. The question that arises, therefore, is how far this source of Faraday rotation is supplemented by the Hall effect in such circumstances, or whether the two mechanisms must be regarded as mutually exclusive.

There is a very long list of important papers concerned with

* It will be recalled that a Hall electric field arises without the independently applied steady magnetic field. This is a double-frequency Hall field in the direction of propagation of the wave and is generally of much smaller magnitude, being dependent on the interaction of the current in the medium with the magnetic component of the wave. The double-frequency Hall field is neglected as an insignificant quantity in the present discussion.

Correspondence on Monographs is invited for consideration with a view to publication.

Prof. Barlow is Pender Professor of Electrical Engineering, University College, London.

different aspects of Faraday rotation, but perhaps those most relevant to the present discussion are by Suhl and Walker,[2] Rau and Caspari,[3] Brown and Clarricoats,[4] and Stephen and Lidard.[5]

(2) CASE FOR A CONTRIBUTION TO THE HALL EFFECT FROM DISPLACEMENT CURRENT IN THE MATERIAL MEDIUM

In the first place it is important to recognize that the mechanism of the Hall effect, arising as it does from the interaction of a current and an applied magnetic field, is inherently incapable of distinguishing between conduction and displacement components of that current. At the same time there can clearly be no contribution to the Hall effect from free-space displacement current, because the effect is only manifest in the presence of a material medium. Moreover, mobile charge carriers in the medium must respond to an applied electric field in a way which is different from that of electric dipoles, and consequently in interpreting the result of this mechanism we must use two different Hall coefficients, one for the conduction component and the other for the displacement component of the current concerned. It is well known that an electromagnetic wave incident on a material medium of any kind exerts pressure upon it. This radiation pressure is closely allied to Hall effect, the mechanical force being the direct result of the Hall electric field acting on the mobile charge carriers and on the electric dipoles within the medium.[1]

In the case of a dielectric the radiation pressure must be due to displacement current in the material medium interacting with the magnetic field component of the wave to produce a secondary electric displacement in the direction of propagation of the wave. It seems, therefore, to be an inescapable conclusion that there is a Hall effect and a corresponding Hall coefficient associated with displacement current. We know that any such Hall coefficient associated with displacement current must be a very small quantity compared with the corresponding coefficient for conduction current, so that only at frequencies well above the microwave band is Hall effect from displacement current likely to become of real significance.

(3) ANALYSIS OF ELECTROMAGNETIC WAVE PROPAGATION IN THE PRESENCE OF HALL EFFECT

Consider a TEM wave (Fig. 1) propagated in the $+z$-direction and incident at $z = 0$ normal to the surface of a homogeneous medium of permeability μ, permittivity ϵ and conductivity σ. If E_x and E_y are the electric field components induced by the associated periodically-changing magnetic field components, then, assuming a time factor $\varepsilon^{j\omega t}$, we have

$$\frac{\partial E_x}{\partial z} = -j\omega\mu H_y \quad . \quad . \quad . \quad . \quad . \quad (1)$$

and

$$\frac{\partial E_y}{\partial z} = j\omega\mu H_x \quad . \quad . \quad . \quad . \quad . \quad . \quad (2)$$

With a steady independently applied magnetic field of density B_0 in the direction of propagation of the wave, secondary Hall electric fields E_{xH} and E_{yH} will be set up in the x and y directions, respectively.

Thus we shall have resultant electric fields E_{xR} and E_{yR} along the x and y co-ordinates, and these resultant fields will be responsible for producing the corresponding current densities J_x and J_y, each of which will include both conduction and displacement components.

Thus

$$E_{xR} = E_x + E_{xH} \quad . \quad . \quad . \quad . \quad . \quad . \quad . \quad (3)$$

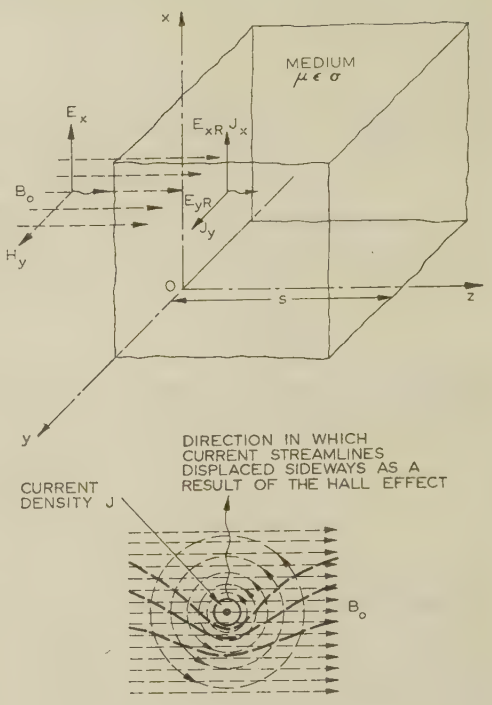

Fig. 1.—Propagation of a TEM wave in the presence of Hall effe

and $$E_{yR} = E_y + E_{yH} \quad . \quad . \quad . \quad . \quad . \quad . \quad . \quad . \quad (4$$

with $$J_x = E_{xR}(\sigma + j\omega\epsilon) = -\frac{\partial H_y}{\partial z} \quad . \quad . \quad . \quad (5$$

and $$J_y = E_{yR}(\sigma + j\omega\epsilon) = \frac{\partial H_x}{\partial z} \quad . \quad . \quad . \quad . \quad (6$$

In accordance with the contention advanced here that the Ha electric fields arise in general both from conduction and displac ment components of current in the material medium interacti with B_0, we have

$$E_{xH} = -[\sigma E_{yR}\mathcal{R}_c B_0 + j\omega(\epsilon - \epsilon_0)E_{yR}\mathcal{R}_d B_0] \quad . \quad (7$$

and $$E_{yH} = +[\sigma E_{xR}\mathcal{R}_c B_0 + j\omega(\epsilon - \epsilon_0)E_{xR}\mathcal{R}_d B_0] \quad . \quad (8$$

where $\mathcal{R}_c$ is the Hall coefficient associated with the conductio component of current in the medium and is normally negati for an n-type semiconductor or positive for a p-type.

$\mathcal{R}_d$ is the Hall coefficient associated with the displaceme component of current in the material medium. This quanti is negative for good high-frequency low-loss materials li polythene, in which the positive charges associated with t atomic nuclei have so large an inertia that they are unable respond to the rapidly alternating applied electric field ar therefore take no significant part in the support of the di placement current.

If m is a factor taking into account the fact that the electr force on the individual mobile charge carriers in the mediu differs from the applied field (for semiconductors, $m = 8/3\pi$ and n is the corresponding factor applicable to the electr dipoles in the medium, we have

$$\mathcal{R}_c = \frac{1}{mq_c N_c} \quad . \quad . \quad . \quad . \quad . \quad (9$$

and $$\mathcal{R}_d = \frac{1}{nq_d N_d} \quad . \quad . \quad . \quad . \quad . \quad (10$$

where q and N are, respectively, the electric charge and the lensity of charges, the subscripts being appropriate to mobile arriers in one case and electric dipoles in the other.

Using eqns. (3), (4), (5), (6), (7) and (8) we have

$$J_x = aE_x - bE_y \quad . \quad . \quad . \quad . \quad . \quad (11)$$

nd

$$J_y = aE_y + bE_x \quad . \quad . \quad . \quad . \quad . \quad (12)$$

here

$$a = \frac{\sigma + j\omega\epsilon}{1 + B_0^2[\sigma\mathscr{R}_c + j\omega(\epsilon - \epsilon_0)\mathscr{R}_d]^2} \quad . \quad . \quad (13)$$

nd

$$b = \frac{B_0(\sigma + j\omega\epsilon)[\sigma R_c + j\omega(\epsilon - \epsilon_0)\mathscr{R}_d]}{1 + B_0^2[\sigma R_c + j\omega(\epsilon - \epsilon_0)\mathscr{R}_d]^2} \quad . \quad . \quad (14)$$

o that eqns. (5) and (6) become

$$-\frac{\partial H_y}{\partial z} = aE_x - bE_y \quad . \quad . \quad . \quad . \quad . \quad (15)$$

nd

$$\frac{\partial H_x}{\partial z} = aE_y + bE_x \quad . \quad . \quad . \quad . \quad . \quad (16)$$

nd combining these with eqns. (1) and (2) we find

$$\frac{\partial^2 E_x}{\partial z^2} = j\omega\mu(aE_x - bE_y) = K^2E_x - j\eta E_y \quad . \quad (17)$$

and

$$\frac{\partial^2 E_y}{\partial z^2} = j\omega\mu(aE_y + bE_x) = K^2E_y + j\eta E_x \quad . \quad (18)$$

where

$$K^2 = j\omega\mu a \quad . \quad . \quad . \quad . \quad . \quad . \quad (19)$$

nd

$$\eta = \omega\mu b \quad . \quad . \quad . \quad . \quad . \quad . \quad (20)$$

Assuming solutions to eqns. (17) and (18) of the form

$$E_x = A\varepsilon^{-\gamma z} \quad . \quad . \quad . \quad . \quad . \quad . \quad (21)$$

nd

$$E_y = pA\varepsilon^{-\gamma z} = pE_x \quad . \quad . \quad . \quad . \quad (22)$$

we have

$$\frac{\partial^2 E_x}{\partial z^2} = \gamma^2 E_x = K^2E_x - j\eta pE_x$$

or

$$\gamma^2 = K^2 - j\eta p \quad . \quad . \quad . \quad . \quad . \quad (23)$$

nd

$$\frac{\partial^2 E_y}{\partial z^2} = \gamma^2 E_y = K^2E_y + \frac{j\eta}{p}E_y$$

or

$$\gamma^2 = K^2 + j\frac{\eta}{p} \quad . \quad . \quad . \quad . \quad . \quad (24)$$

To make eqns. (23) and (24) consistent we must therefore have

$$-j\eta p = j\frac{\eta}{p} \text{ or } p^2 = -1$$

nd

$$p = \pm j$$

iving

$$\gamma^2 = K^2 \pm \eta \quad . \quad . \quad . \quad . \quad . \quad . \quad (25)$$

nd from eqn. (22)

$$E_y = \pm jE_x \quad . \quad . \quad . \quad . \quad . \quad . \quad (26)$$

When $p = -j$ then $E_y = -jE_x$, and E_y lags by 90° behind E_x iving a right-handed circularly-polarized wave with a propaga-ion coefficient γ_r such that

$$\gamma_r^2 = K^2 - \eta \quad . \quad . \quad . \quad . \quad . \quad . \quad (27)$$

lternatively when $p = +j$ then $E_y = +jE_x$ and E_y leads E_x y 90°, giving a left-handed circularly-polarized wave with a ropagation coefficient γ_l such that

$$\gamma_l^2 = K^2 + \eta \quad . \quad . \quad . \quad . \quad . \quad . \quad (28)$$

Starting at $z = 0$ with linear polarization we can therefore write

$$E_x = A\varepsilon^{-\gamma_r z} + A\varepsilon^{-\gamma_l z} \quad . \quad . \quad . \quad (29)$$

and remembering that the corresponding E_y field components are $-jA\varepsilon^{-\gamma_r z}$ for right-handed circular polarization and $+jA\varepsilon^{-\gamma_l z}$ for left-handed circular polarization we find

$$E_y = -jA\varepsilon^{-\gamma_r z} + jA\varepsilon^{-\gamma_l z} \quad . \quad . \quad . \quad . \quad (30)$$

γ_r and γ_l are both complex so that

$$\gamma_r = \alpha_r + j\beta_r \quad . \quad . \quad . \quad . \quad . \quad . \quad (31)$$

and

$$\gamma_l = \alpha_l + j\beta_l \quad . \quad . \quad . \quad . \quad . \quad . \quad (32)$$

The linearly-polarized wave incident on the medium under consideration at $z = 0$ has been resolved into right- and left-handed circularly-polarized waves which proceed to propagate through the medium with attenuation and phase-change coefficients α and β, respectively, the subscripts distinguishing the quantities for the two directions of rotation. On emergence from the medium the two circularly-polarized waves if equally attenuated, would combine to give a linearly-polarized wave* whose direction of polarization is that for which the electric fields of the two circularly-polarized waves are in phase. Since $\beta_r \neq \beta_l$ the two circularly-polarized waves travel with different phase velocities, and the direction of the resulting linearly-polarized wave at emergence from the medium will differ from that of the wave at incidence, giving rotation of the plane of polarization during transmission through the medium. If we suppose that the incident wave is vertically polarized we can resolve it into right-handed and left-handed circularly-polarized waves, so phased that their electric fields are coincident when they are vertical. Thus the two circularly-polarized waves at emergence from the medium of thickness s will have electric fields coinciding in direction at an angle θ from the vertical given by

$$\theta = \tfrac{1}{2}(\beta_r - \beta_l)s \quad . \quad . \quad . \quad . \quad . \quad (33)$$

θ is therefore the angle of rotation of the plane of polarization and this is clockwise when $\beta_r > \beta_l$. To calculate θ some approximations can generally be made without significant error.

Let

$$h = \sigma\mathscr{R}_c B_0 \quad . \quad . \quad . \quad . \quad . \quad . \quad (34)$$

and

$$u = \omega(\epsilon - \epsilon_0)\mathscr{R}_d B_0 \quad . \quad . \quad . \quad . \quad (35)$$

so that from eqns. (13) and (14) we have

$$a = \frac{\sigma + j\omega\epsilon}{1 + (h + ju)^2} \quad . \quad . \quad . \quad . \quad . \quad (36)$$

and

$$b = \frac{(\sigma + j\omega\epsilon)(h + ju)}{1 + (h + ju)^2} \quad . \quad . \quad . \quad . \quad (37)$$

Now h and u are the Hall electric fields arising from conduction and displacement components of current, respectively, per unit applied electric field, so that $h \ll 1$ and $u \ll 1$. We can therefore write with sufficient accuracy

$$a \simeq (\sigma + j\omega\epsilon) \quad . \quad . \quad . \quad . \quad . \quad . \quad (38)$$

and

$$b \simeq (\sigma + j\omega\epsilon)(h + ju) \quad . \quad . \quad . \quad . \quad (39)$$

giving, from eqn. (19),

$$K = \sqrt{[j\omega\mu(\sigma + j\omega\epsilon)]} = \alpha_0 + j\beta_0 \quad . \quad . \quad . \quad (40)$$

and consequently

$$\alpha_0 = \omega\sqrt{(\mu\epsilon)}\left\{\tfrac{1}{2}\sqrt{[1 + (\sigma/\omega\epsilon)^2]} - 1\right\}^{1/2} \quad . \quad (41)$$

* Since $\alpha_r \neq \alpha_l$ the emergent wave is actually slightly elliptically polarized.

with $$\beta_0 = \omega\sqrt{(\mu\epsilon)}\left\{\tfrac{1}{2}\sqrt{[1 + (\sigma/\omega\epsilon)^2]} + 1\right\}^{1/2} \quad . \quad (42)$$

while from eqn. (20) we get

$$\eta = \omega\mu(\sigma + j\omega\epsilon)(h + ju) \quad . \quad . \quad . \quad . \quad (43)$$

and since $|K^2| \gg |\eta|$ we find from eqns. (27), (28), (31) and (32) that

$$(\gamma_r - \gamma_l) = (\alpha_r - \alpha_l) + j(\beta_r - \beta_l) = -\frac{\eta}{K} \quad . \quad (44)$$

or using eqns. (40) and (43) we have

$$(\alpha_r - \alpha_l) = -(u\alpha_0 + h\beta_0) \quad . \quad . \quad . \quad . \quad (45)$$

with $$(\beta_r - \beta_l) = +(h\alpha_0 - u\beta_0) \quad . \quad . \quad . \quad . \quad (46)$$

and from eqn. (33),

$$\theta = \tfrac{1}{2}(\beta_r - \beta_l)s = \frac{B_0 s}{2}[\sigma\mathscr{R}_c\alpha_0 - \omega(\epsilon - \epsilon_0)\mathscr{R}_d\beta_0] \quad (47)$$

or Verdet's constant

$$V = \frac{\theta}{B_0 s} = \tfrac{1}{2}[\sigma\mathscr{R}_c\alpha_0 - \omega(\epsilon - \epsilon_0)\mathscr{R}_d\beta_0] \quad . \quad . \quad (48)$$

(4) CALCULATIONS FOR FARADAY ROTATION ARISING FROM HALL EFFECT IN DIFFERENT MEDIA

(4.1) Semiconductors at Microwave Frequencies

It has already been emphasized that at room temperatures (300° K) and microwave frequencies, semiconductors produce Faraday rotation arising primarily from Hall effect. In spite of the fact that, in the circumstances, the displacement component of current in the material medium is often of the same order of magnitude as the conduction component, we shall still have $u \ll h$ because $R_d \ll R_c$. As a good approximation, therefore, eqn. (47) reduces to

$$\theta = \frac{B_0 s\sigma\mathscr{R}_c\alpha_0}{2} \quad . \quad . \quad . \quad . \quad . \quad (49)$$

α_0 being given by eqn. (41). Two cases of special interest will be considered.

(4.1.1) Germanium.

Rau and Caspari[3] have investigated the behaviour of germanium both analytically and experimentally at a frequency of 8·74 Gc/s. Their work was concerned with *n*-type germanium at room temperature having the following electrical characteristics:

$$\sigma = 6{\cdot}25 \text{ mhos/m}$$
$$\epsilon_r = 16$$
$$s = 4{\cdot}6 \times 10^{-3} \text{ m}$$

Hall mobility = 0·364 m² per volt-sec corresponding to

$$\mathscr{R}_c = -\frac{3\pi \times 0{\cdot}364}{8 \times 6{\cdot}25} = -6{\cdot}87 \times 10^{-2} \text{ m}^3\text{/coulomb}$$

A steady magnetic field $B_0 = 0{\cdot}143$ Wb/m² was applied. Thus $\omega\epsilon = 7{\cdot}77$, and is of the same order of magnitude as σ. From eqns. (41) and (49) we have

$$\theta = \frac{B_0 s\sigma\mathscr{R}_c\omega\sqrt{\epsilon_r}}{2 \times 3 \times 10^8}\left(\tfrac{1}{2}\left\{\sqrt{[1 + (\sigma/\omega\epsilon)^2]} - 1\right\}\right)^{1/2} \quad (50)$$

where $\sqrt{\epsilon_r}$ can be identified as the refractive index. Applying eqn. (50) to this case yields $\theta = -2{\cdot}24°$ instead of the measured value of $-3{\cdot}47°$. The theory given by Rau and Caspari based on the Drude–Zener model of free charges moving under the influence of crossed electric and magnetic fields gives a rather different expression for θ which seems to agree mu more accurately with the experimental result. It is relevant t point out, however, that these authors, in neglecting any standi wave within the germanium on the grounds that the skin dep was rather less than the thickness, seem to overlook the fact th a substantial field (about one-third of the incident value) m arrive at the far side of the crystal, and it so happens that t dimensions are such as to give $s \simeq \lambda/2$ within the cryst From eqn. (45) with $u \ll h$, we find

$$\alpha_r - \alpha_l = -\sigma\mathscr{R}_c B_0\beta_0 \quad . \quad . \quad . \quad . \quad . \quad (5$$

so that for the particular case of

$$z = \frac{1}{\alpha_r - \alpha_l} \quad . \quad . \quad . \quad . \quad . \quad (5$$

$$(\beta_r - \beta_l)z = -\alpha_0/\beta_0 \quad . \quad . \quad . \quad . \quad (5$$

and from eqns. (29), (30), (31) and (32) the ellipticity of t wave at the value of z given by eqn. (52) and represented the ratio of the major to the minor axis is

$$\left|\frac{E_x}{E_y}\right| = \sqrt{\frac{1 + \varepsilon^2 + 2\varepsilon\cos(\alpha_0/\beta_0)}{1 + \varepsilon^2 - 2\varepsilon\cos(\alpha_0/\beta_0)}} \quad . \quad . \quad . \quad (5$$

Thus, for the case of the germanium under discussion, we fi that when $z = \left(\frac{1}{\alpha_r - \alpha_l}\right) \simeq 2$ cm, then $\left|\frac{E_x}{E_y}\right| \simeq 2$ and t attenuation of the wave in passing through this thickness of t crystal is about 50 dB, giving as the operational figure of meri

$$\frac{\theta \text{ (degrees)}}{\text{Attenuation (dB)}} \simeq 0{\cdot}2$$

It is of interest to compare this microwave Faraday rotati in a semiconductor with the corresponding effect in a ferri When the applied magnetic force is well below the resonan value, one finds for a ferrite having a saturation magnetizati of 0·2 Wb/m² and a relative permittivity of 10, a rotation about 100°/cm, and this compares with only some 6°/cm for t semiconductor. The operational figure of merit of the ferrite therefore about 700.

(4.1.2) Indium Antimonide.

In the microwave part of the spectrum indium antimonide h $\sigma \gg \omega\epsilon$ so that eqn. (50) reduces to

$$\theta = 3{\cdot}97 \times 10^{-4} B_0 s\sigma^{3/2}\mathscr{R}_c\omega^{1/2} \quad . \quad . \quad . \quad (5$$

Assuming the same frequency as for the germanium cryst i.e. $f = 8{\cdot}74$ Gc/s, with electrical parameters for *n*-ty indium antimonide of $\sigma = 10^4$ mhos/m and $\mathscr{R}_c = -6$ 10^{-4} m³/coulomb, we have for Verdet's constant in this case

$$V = \frac{\theta}{B_0 s} = -3{\cdot}19 \times 10^6 \text{ degrees per Wb/m}^2 \text{ per metre}$$

which, although nearly 1 000 times greater than for the ge manium sample, can only be demonstrated in practice to t extent of about the skin depth, which is 100 times smaller.

(4.2) Dielectrics at Infra-Red Frequencies

Good low-loss dielectrics (without polar molecules) li polythene carry a current represented almost entirely by t displacement of bound electrons associated with the elect dipoles, when a high-frequency electric field is applied to t material. In these circumstances eqn. (48) for Verdet's consta reduces to

$$V = \frac{\theta}{B_0 s} = -\tfrac{1}{2}\omega(\epsilon - \epsilon_0)\mathscr{R}_d\beta_0 \quad . \quad . \quad . \quad (5$$

where, with $\omega\epsilon \gg \sigma$,

$$\beta_0 = \omega\sqrt{(\mu\epsilon)} \quad . \quad . \quad . \quad . \quad . \quad . \quad (57)$$

Hence we have

$$V = \frac{\theta}{B_0 s} = -\frac{\mathscr{R}_d \omega^2 \epsilon_0 (\epsilon_r - 1)\sqrt{\epsilon_r}}{6 \times 10^8} \quad . \quad . \quad (58)$$

Faraday rotation at optical frequencies has been thoroughly explored in a wide variety of dielectric materials, and the effect is explained in terms of gyromagnetic action. For example, measurements have been made on quartz over a range of frequencies, and it is of interest to consider how far a Hall effect in that medium might be used to interpret the results. Applying eqn. (58) to the following experimental data[6] for quartz at 18° C:

(i) $f = 4{\cdot}66 \times 10^{14}$ c/s. $\epsilon_r = 2{\cdot}37$. $V = 228°$/m per Wb/m^2
(ii) $f = 5{\cdot}09 \times 10^{14}$ c/s. $\epsilon_r = 2{\cdot}385$. $V = 277°$/m per Wb/m^2
(iii) $f = 13{\cdot}7 \times 10^{14}$ c/s. $\epsilon_r = 2{\cdot}59$. $V = 2650°$/m per Wb/m^2

we find corresponding values of $\mathscr{R}_d$ between $-1{\cdot}5 \times 10^{-11}$ and $-1{\cdot}6 \times 10^{-11}$ m^3/C. It therefore appears that, in this case, the Faraday rotation could be very simply explained by the Hall effect, and that the requirements are substantially satisfied with V increasing as the square of the frequency and R_d remaining constant at the very small value of about $-1{\cdot}5 \times 10^{-11}$ m^3/C.

(4.3) Semiconductors at Infra-Red Frequencies

Faraday rotation in semiconductors at infra-red frequencies has been examined by Stephen and Lidard[5] and by Smith, Moss and Taylor.[7] At these frequencies, even at room temperatures, $\omega > \omega_c$ and gyromagnetic effects become predominant, particularly in the vicinity of cyclotron resonance. Work undertaken by these authors shows that a theoretical analysis based on mobile carriers forming an electron gas is capable of giving a good interpretation of the experimental observations over quite a wide range of frequencies. It is of interest, however, to consider what contribution, if any, Hall effect could make to Faraday rotation at these frequencies.

In the first place it is important to remember that, as shown by Kronig,[8] the conductivity σ is a function of frequency and

$$\sigma_f = \frac{\sigma_{d.c.}}{1 + (\omega\tau)^2} \quad . \quad . \quad . \quad . \quad . \quad (59)$$

where τ is the relaxation time of the charge carriers. Kronig also gave an approximate expression for permittivity as a function of frequency, but in the circumstances under consideration where we are only concerned with orders of magnitude, this is not very significant.

From eqn. (59) it will be seen that at infra-red frequencies one can expect σ to be greatly reduced, and bearing in mind that the displacement component of current through the medium is at the same time much enhanced by the high frequency, eqn. (58) applies.

Most of the experimental information available concerns indium antimonide, and we shall therefore discuss this material. It is difficult to estimate the value of $\mathscr{R}_d$, but using the Clausius–Mossotti relation and putting

$$n = \left(\frac{\epsilon_r + 2}{3}\right) \quad . \quad . \quad . \quad . \quad . \quad (60)$$

in eqn. (10) we should expect with $\epsilon_r = 16$ that $\mathscr{R}_d \simeq -10^{-11}$ m^3/C. Inserting this figure in eqn. (58) enables a very rough estimate to be made of a possible Hall contribution to the Faraday rotation. At $f = 3 \times 10^{13}$ c/s we thus find $V = 18°$/m per Wb/m^2. In the experimental work of Smith, Moss and Taylor[7] on a sample of n-type indium antimonide having $1{\cdot}1 \times 10^{22}$ conduction electrons per cubic metre they found a Faraday rotation in a positive direction of about 10^4 deg/m per Wb/m^2 and still larger values at lower frequencies. It seems, therefore, that the usual explanation of the Faraday rotation based on orbital free-electron carriers covers the major part of the phenomenon, and that any Hall effect, whilst not entirely insignificant, is relatively small.

(5) CONCLUSIONS

It is well established that Faraday rotation in a medium arises as a result of the local modification of the motion of the electric or magnetic carriers in the presence jointly of the steady applied magnetic field and the high-frequency wave. The phenomenon includes gyromagnetic action of various origins and Hall effect. The discussion presented here distinguishes the Hall-effect mechanism and identifies it as leading to different propagation coefficients for the right-handed and left-handed circularly-polarized components of the wave. The result is equivalent to giving to the medium a tensor permittivity.

The contention is advanced that a Hall effect can be expected to arise from a displacement current in the material medium, and that, as a consequence, the Faraday-rotation effect in dielectrics and semiconductors may in some cases be significantly modified at frequencies above the microwave part of the spectrum. Some elementary calculations are given in support of this argument.

(6) ACKNOWLEDGMENTS

The author desires to thank the Admiralty (C.V.D.) for their most valuable support of research work in the Electrical Engineering Department at University College, on the behaviour of semiconductors in microwave fields. This work has stimulated the production of the paper. The author is also indebted to his colleague Dr. J. Brown for helpful discussions on the subject.

(7) REFERENCES

(1) Barlow, H. E. M.: 'Hall Effect and its Counterpart, Radiation Pressure, in Microwave Power Measurement', *Proceedings I.E.E.*, Monograph No. 191 R, August, 1956 (**104** C, p. 35).
(2) Suhl, H., and Walker, L. R.: 'Topics in Guided-Wave Propagation through Gyromagnetic Media', *Bell System Technical Journal*, 1954, **33**, pp. 579, 939 and 1133.
(3) Rau, R. R., and Caspari, M.: 'Faraday Effect in Germanium at Room Temperature', *Physical Review*, 1955, **100**, p. 632.
(4) Brown, J., and Clarricoats, P. J. B.: 'Waveguide Components with Non-Reciprocal Properties (Part 1)', *Electronic Engineering*, August, 1956, p. 328.
(5) Stephen, M. J., and Lidard, A. B.: 'The Faraday Effect in Semi-Conductors', *Journal of the Physics and Chemistry of Solids*, 1958, **9**, p. 43.
(6) Kaye, G. W. C., and Laby, T. H.: 'Physical and Chemical Constants' (Longmans, 1911), p. 72 and p. 80.
(7) Smith, S. D., Moss, T. S., and Taylor, K. W.: 'The Infra-red Faraday Effect due to Free Carriers in Indium Antimonide', *Journal of the Physics and Chemistry of Solids*, 1959, **8**, p. 323, and 'The Energy-Dependence of Electron Mass in Indium Antimonide determined from Measurements of the Infra-Red Faraday Effect', *ibid.*, 1959, **11**, p. 131.
(8) Kronig, R. de L.: 'The Quantum Theory of Dispersion in Metallic Conductors', *Proceedings of the Royal Society* (*London*) *A*, 1931, **133**, p. 255.

621.372.542.21

The Institution of Electrical Engine
Monograph No. 432
Feb. 19

A METHOD OF CALCULATING THE TRANSFER FUNCTIONS OF LADDER NETWORKS

By N. REAM, B.A.

(*The paper was first received 20th February, and in revised form 29th October*, 1960. *It was published as an* INSTITUTION MONOGRAPH *in February*, 1961.)

SUMMARY

From the Kirchhoff equations applied to a ladder network, recurrence equations are derived for calculating the voltages and currents in terms of the output voltage and current; from these, another set of equations is obtained for working from the input end of the network. It is shown that either set of equations is particularly suitable for the numerical calculation of transfer functions. A few general formulae are included for the voltage-transfer ratio of an *RC* ladder network.

(1) INTRODUCTION

The analysis and synthesis of ladder networks is important in communication theory and automatic control. In communication theory the problem may be the representation of a transmission line by a lumped-parameter network or the design of a network to have prescribed frequency or transient-response characteristics.[1] In automatic control the ladder network is a convenient form of equalizing circuit for servo mechanisms, and such properties as pole-zero synthesis have been extensively studied.[2] In process control, also, systems of 'interacting transfer lags' occur in the control of temperature and flow,[3] and these can be linearized and represented by an electrical ladder-network analogue; distributed-parameter systems such as heat-exchangers may also be approximately represented in this way.

In spite of the importance of ladder networks in these fields, little attention seems to have been given to the choice of a convenient and comparatively foolproof method of calculating their transfer functions; the need for one was encountered in analysing a demonstration fluid-flow network,[4] though this network can be treated algebraically. The method described here is intended mainly for the numerical calculation of transfer functions of networks with given elements, but a few algebraic expressions are obtained for *RC* networks.

(2) FORMULAE FOR A GENERAL LADDER NETWORK

Fig. 1 shows an n-stage 4-terminal ladder network with input voltage v_n and output voltage v_0. The elements are numbered from the output end and the notation used is as follows:

$z_1 \ldots z_n$ = Impedances of series arms.
$y_1 \ldots y_n$ = Admittances of shunt arms.
$i_1 \ldots i_n$ = Currents through $z_1 \ldots z_n$.
$v_0 \ldots v_{n-1}$ = Voltages across $y_1 \ldots y_n$.

Correspondence on Monographs is invited for consideration with a view to publication.
Mr. Ream is Reader in Control Engineering, Electrical Engineering Department, Battersea College of Technology.

(2.1) Recurrence Equations for Voltages and Currents

The usual network equations give

$$i_m = i_{m-1} + y_m v_{m-1} \quad . \quad . \quad . \quad . \quad . \quad (1)$$

$$v_m = v_{m-1} + z_m i_m \quad . \quad . \quad . \quad . \quad . \quad (1)$$

These are a pair of recurrence equations whereby, starting fr given values of i_0 and v_0, one may derive successive curre and voltages up to v_n. If the load impedance, v_0/i_0, is kno the method gives the transfer functions i_m/v_0 and v_m/v_0 for ea m, and from the final equation the input impedance, v_n/i_n, the network may be obtained. If the network is driven b generator (v_g) via a source impedance z_s, the input current given by

$$i_n = \frac{v_g}{z_s + (v_n/i_n)}$$

and all the other currents and voltages follow from this.

If, on the other hand, v_0/i_0 is initially unknown and is to chosen to give a specified v_n/i_n eqn. (1) may be rewritten as

$$\left.\begin{aligned} v_{m-1} &= v_m - z_m i_m \\ i_{m-1} &= i_m - y_m v_{m-1} \end{aligned}\right\} \quad . \quad . \quad . \quad . \quad .$$

Starting from given values of v_n and i_n, successive applicatio of eqn. (2) yield the voltages and currents up to v_0 and i_0.

Another set of recurrence equations may be derived fr eqns. (1) by introducing quantities a_m and b_m such that

$$1/v_m = a_m + b_m/Z_m \quad . \quad . \quad . \quad . \quad .$$

$$1/i_m = Z_m a_m + b_m \quad . \quad . \quad . \quad . \quad .$$

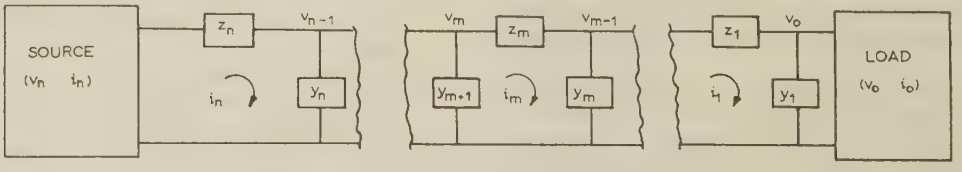

Fig. 1.—n-stage 4-terminal ladder network.

where $Z_m = v_m/i_m$ is the input impedance of the part of network to the right of node v_m. It is shown in the Appen that

$$\left.\begin{aligned} b_{m-1} &= b_m + z_m a_m \\ a_{m-1} &= a_m + y_m b_{m-1} \end{aligned}\right\} \quad . \quad . \quad . \quad .$$

The general solution is a linear combination of the follow particular solutions:

(*a*) $v_n = 1$ giving $a_n = 1$ and $b_n = 0$ from eqn. (3)
(*b*) $i_n = 1$ giving $a_n = 0$ and $b_n = 1$ from eqn. (4).

In case (*a*), repeated applications of eqn. (5) lead to the values $a_0 = A$ and $b_0 = B$ in the equation

$$v_n/v_0 = a_0 + b_0/Z_0$$

or

$$v_n = Av_0 + Bi_0$$

Similarly, in case (*b*) the equations lead to $a_0 = C$ and $b_0 = D$ in

$$i_n = Cv_0 + Di_0$$

These results are clearly equivalent to those obtained from eqn. (1) taking v_0 and i_0 as initial values. Eqns. (5) are useful mainly as a numerical check on the results obtained by the other method; they are not much use by themselves, since they do not yield intermediate voltages and currents directly.

(2.2) Response to Current Injected at an Intermediate Node

Suppose that the network is driven, not from the source (v_n), which is now open-circuited, but from a current source (i) injected at node v_j (this situation may well arise in the fluid-flow

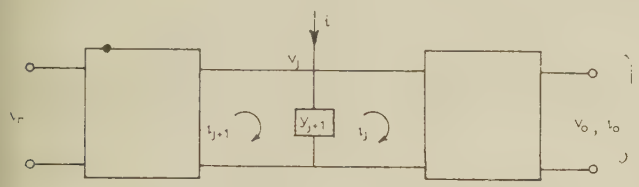

Fig. 2.—Current input at node v_j with v_n open-circuited.

analogy). The network can then be split into two parts, as shown in Fig. 2. We have

$$\left.\begin{aligned} i &= i_j - i_{j+1} + y_{j+1}v_j \\ &= v_j\left(\frac{i_j}{v_j} - \frac{i_{j+1}}{v_j} + y_{j+1}\right) \end{aligned}\right\} \quad . \quad . \quad . \quad . \quad (6)$$

The admittance i_j/v_j is calculated from eqn. (1) using given initial values i_0 and v_0. The admittance i_{j+1}/v_j is calculated from eqn. (2) starting with $v_{n-1} = 1$ and $i_n = 0$ and working with negative i's to avoid introducing minus signs. Each calculation can be checked by using eqns. (5) in their direct or reversed form, as appropriate. Intermediate steps in the calculations using eqns. (1) and (2) give the ratios between i and all voltages and currents.

(3) A SYSTEMATIC PROCEDURE FOR NUMERICAL CALCULATIONS

(3.1) Presentation in Tabular Form

The form of eqns. (1) suggests the method of setting out the calculation of currents and voltages shown in Table 1; here, $i_0 \ldots i_n$ are built up in one column and $v_0 \ldots v_n$ in another, and the left-hand column contains the successive multipliers $y_1 \ldots z_n$ corresponding to each stage of the calculation. Below each multiplication a line is drawn and the new value of current or voltage is found by adding together the entries between this line and the one above. A similar process is followed if eqns. (2) or (5) are used.

(3.2) Transfer-Function Coefficients

The method can be adapted to give the separate coefficients of p^r in a transfer function if this is a sum of powers of p, i.e.

Table 1

TABLE OF CURRENTS AND VOLTAGES

Multiplier	*Current*	*Voltage*
	i_0	
y_1	y_1v_0	v_0
z_1	i_1	z_1i_1
y_2	y_2v_1	v_1
z_2	i_2	z_2i_2
.	.	.
.	.	.
.	.	.
y_n	y_nv_{n-1}	v_{n-1}
z_n	i_n	z_ni_n
		v_n

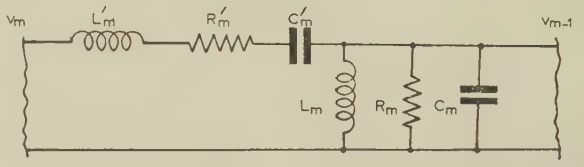

Fig. 3.—*m*th-stage components leading to power-series transfer function.

if each y_m is a parallel combination, and each z_m is a series combination, of LRC elements. As shown in Fig. 3, let

$$\left.\begin{aligned} y_m &= pC_m + 1/R_m + 1/pL_m \\ z_m &= pL'_m + R'_m + 1/pC'_m \end{aligned}\right\} \quad . \quad . \quad . \quad (7)$$

and write

$$\left.\begin{aligned} i_m &= \Sigma i_{mr}p^r \\ v_m &= \Sigma v_{mr}p^r \end{aligned}\right\} \quad . \quad . \quad . \quad . \quad . \quad . \quad (8)$$

The range of summation depends on the value of m, the initial condition and the number of components present in eqn. (7). The recurrence equations (1) become

$$\left.\begin{aligned} i_{mr} &= i_{m-1,r} + C_m v_{m-1,r-1} + \frac{1}{R_m}v_{m-1,r} + \frac{1}{L_m}v_{m-1,r+1} \\ v_{mr} &= v_{m-1,r} + L'_m i_{m,r-1} + R'_m i_{m,r} + \frac{1}{C'_m}i_{m,r+1} \end{aligned}\right\} \quad (9)$$

Table 2 shows the first few stages of Table 1 with the coefficients of different powers of p summed in different columns. In this Table i_0 and v_0 are assumed to be independent of p.

(3.3) Computation

The computation follows the scheme shown in Table 2 in so far as the multipliers are present. To avoid excessive rounding-off errors, one more decimal digit is retained than is required in the answer. When a column builds up to the next higher digit place, the least significant digit is dropped.

The network shown in Fig. 4 is used as a simple illustration of the method. Since the load impedance is known ($i_0 = 0$),

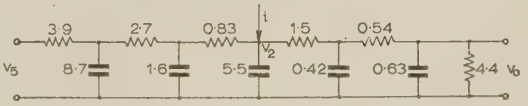

Fig. 4.—Numerical example.

Table 2

TABLE OF TRANSFER-FUNCTION COEFFICIENTS

Multiplier	Current							Voltage				
	Coefficient of							Coefficient of				
	p^{-3}	p^{-2}	p^{-1}	p^0	p^1	p^2	p^3	p^{-2}	p^{-1}	p^0	p^1	p^2
$1/pL_1$				i_{00}								
$1/R_1$			v_{00}/L_1							v_{00}		
pC_1				v_{00}/R_1	$v_{00}C_1$							
$1/pC_1'$			$i_{1,-1}$	i_{10}	i_{11}			$i_{1,-1}/C_1'$	i_{10}/C_1'	i_{11}/C_1'		
R_1'									$i_{1,-1}R_1'$	$i_{10}R_1'$	$i_{11}R_1'$	
pL_1'										$i_{1,-1}L_1'$	$i_{10}L_1'$	$i_{11}L_1'$
$1/pL_2$	$v_{1,-2}/L_2$	$v_{1,-1}/L_2$	v_{10}/L_2	v_{11}/L_2	v_{12}/L_2			$v_{1,-2}$	$v_{1,-1}$	v_{10}	v_{11}	v_{12}
$1/R_2$		$v_{1,-2}/R_2$	$v_{1,-1}/R_2$	v_{10}/R_2	v_{11}/R_2	v_{12}/R_2						
pC_2			$v_{1,-2}C_2$	$v_{1,-1}C_2$	$v_{10}C_2$	$v_{11}C_2$	$v_{12}C_2$					
etc.	$i_{2,-3}$	$i_{2,-2}$	$i_{2,-1}$	i_{20}	i_{21}	i_{22}	i_{13}					

eqns. (1) yield all currents and voltages in terms of v_0. Table 3(*a*) shows the calculations; to three decimal digits the result is

$$i_5/v_0 = 0{\cdot}227 + 31{\cdot}5p + 387p^2 + 720p^3 + 392p^4 + 36{\cdot}8p^5 \quad . \quad . \quad . \quad . \quad (10)$$

$$v_5/v_0 = 3{\cdot}15 + 164p + 1\,590p^2 + 2\,850p^3 + 1\,530p^4 + 143p^5 \quad . \quad . \quad . \quad . \quad (11)$$

A check on v_5/v_0 is provided by eqn. (5), worked out in Table 3(*b*). The rounding-off errors in eqn. (11) are negligible, since the two answers differ by not more than one unit in the fourth digit.

Table 3(*c*) gives the additional calculations needed to find the impedance to current injected at node v_2. Thus

$$-\frac{i_3}{v_2} = \frac{10{\cdot}3p + 37{\cdot}6p^2}{1 + 32{\cdot}0p + 31{\cdot}2p^2} \quad . \quad . \quad . \quad (12)$$

while from Table 3(*a*) we have

$$\frac{i_2}{v_2} = \frac{0{\cdot}227 + 1{\cdot}10p + 0{\cdot}143p^2}{1{\cdot}46 + 1{\cdot}99p + 0{\cdot}214p^2} \quad . \quad . \quad . \quad (13)$$

From eqns. (6), (12) and (13),

$$\frac{i}{v_2} = \frac{0{\cdot}227 + 1{\cdot}10p + 0{\cdot}143p^2}{1{\cdot}46 + 1{\cdot}99p + 0{\cdot}214p^2} + \frac{10{\cdot}3p + 37{\cdot}6p^2}{1 + 32{\cdot}0p + 31{\cdot}2p^2} + 5{\cdot}5p \quad . \quad . \quad . \quad (14)$$

As a check it may be verified that the numerator of i/v_2 is the same as eqn. (10) (this can be shown to follow from an application of the reciprocity theorem).

(4) FORMULAE FOR v_n/v_0 IN A SIMPLE *RC* LADDER

One of the instances where general algebraic formulae may be useful in ladder-network response calculations concerns the simple *RC* circuit shown in Fig. 5. This Section gives a few formulae for v_n/v_0 assuming infinite load impedance ($i_0 = 0$).

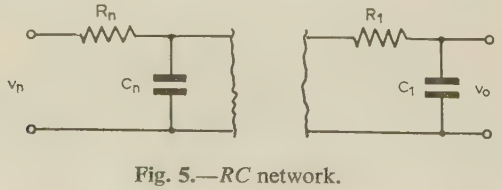

Fig. 5.—*RC* network.

(4.1) General *R* and *C* Values

For Fig. 5 we have $y_m = pC_m$ and $z_m = R_m$ [not R_m' as i eqn. (7)]. In the notation of eqn. (8), eqns. (1) become

$$\left.\begin{aligned} i_{mr} &= i_{m-1,r} + C_m v_{m-1,r-1} \\ v_{mr} &= v_{m-1,\,r} + R_m i_{mr} \end{aligned}\right\} \quad . \quad . \quad . \quad (.$$

The initial conditions are $i_0 = 0$ and $v_0 = 1$, so putting $r =$ in eqn. (15) gives $i_{m0} = 0$ and $v_{m0} = 1$ for all m. Thes $i_{m1} = i_{m-1,1} + C_m$ and $v_{m1} = v_{m-1,1} + R_m i_{m1}$, so that

$$i_{m1} = \sum_1^m C_j \text{ and } v_{m1} = \sum_1^m R_k \sum_1^k C_j$$

The next application of eqn. (15), with $r = 2$, gives, similarly,

$$i_{m2} = \sum_2^m C_p \sum_1^{p-1} R_k \sum_1^k C_j$$

$$v_{m2} = \sum_2^m R_q \sum_2^q C_p \sum_1^{p-1} R_k \sum_1^k C_j$$

where the lower limit of p and q is 2 since $i_{12} = v_{12} =$ (Formulae for higher values of r may be written down by inspec tion. The transfer function v_n/v_0 is now given by

$$\frac{v_n}{v_0} = v_{n0} + pv_{n1} + \ldots + p^n v_{nn}$$

$$= 1 + p\sum_1^n R_k \sum_1^k C_j + p^2 \sum_2^n R_q \sum_2^q C_p \sum_1^{p-1} R_k \sum_1^k C_j + \ldots + p^n \prod_1^n C_{j'}$$

The summations may be rearranged in various ways by algebrai manipulation. In particular, if the order of the R and summations in each (RC) pair is reversed, we arrive at a formul which would have resulted from applying eqns. (5).

(4.2) General *R*'s, Equal *C*'s

In this case the transfer function is expressible in terms of th n time-constants $\tau_m = CR_m$. The following formula for th numerical coefficients of the various τ products in v_n/v_0 wa suggested by inspecting the first few functions v_m/v_0, and may b verified by substitution into eqn. (15):

$$v_{nn} = \Sigma \ldots \Sigma A(a, b, \ldots, k)\tau_a\tau_b \ldots \tau_j\tau_k$$

Table 3

CALCULATIONS FOR NETWORK SHOWN IN FIG. 4

(*a*) Current and Voltage Coefficients with $v_0 = 1$ and $i_0 = 0$.

Multiplier	*Current*						*Voltage*					
	0						1					
$\left\{\begin{matrix}1/4\cdot4\\p0\cdot63\end{matrix}\right.$	0·2273	0·63										
0·54	0·2273	0·63					0·123	0·3402				
*p*0·42		0·4717	0·1429				1·123	0·3402				
1·5	0·2273	1·102	0·1429				0·341	1·653	0·2144			
*p*5·5		8·052	10·96	1·179			1·464	1·993	0·2144			
0·83	0·2273	9·154	11·10	1·179			0·189	7·598	9·213	0·9786		
*p*1·6		2·645	15·35	15·08	1·566		1·653	9·591	9·427	0·9786		
2·7	0·2273	11·80	26·45	16·26	1·566		0·614	31·86	71·41	43·90	4·228	
*p*8·7		19·72	360·6	703·3	390·4	36·78	2·267	41·45	80·84	44·88	4·228	
3·9	0·2273	31·52	387·0	719·6	392·0	36·78	0·886	122·9	1 509	2 806	1 529	143·4
							3·153	164·4	1 590	2 851	1 533	143·4

(*b*) *a* and *b* Coefficients with $1/v_5 = 1$.

Multiplier	*b-Coefficients*					*a-Coefficients*					
	0					1					
3·9	3·9										
*p*8·7	3·9						33·93				
2·7	2·7	91·61				1	33·93				
*p*1·6	6·6	91·61					10·56	146·6			
0·83	0·83	36·93	121·6			1	44·49	146·6			
*p*5·5	7·43	128·5	121·6				40·86	706·8	668·8		
1·5	1·5	128·0	1 280	1 003		1	85·35	853·4	668·8		
*p*0·42	8·93	256·5	1 402	1 003			3·75	107·7	588·8	421·2	
0·54	0·54	48·1	519	679	227·4	1	89·10	961·1	1 258	421·2	
$\left\{\begin{matrix}1/4\cdot4\\p0\cdot63\end{matrix}\right.$	9·47	304·6	1 921	1 682	227·4	2·153	69·24 5·97	436·6 191·9	382 1 210	51·7 1 060	143·3
						3·153	164·3	1 590	2 850	1 523	143·3

(*c*) Current Input at v_2, Calculation of $-i_3$ and v_2 from Eqn. (2).

Multiplier	*Current (reversed)*			*Voltage*		
	0			1		
*p*8·7		8·7				
2·7	0	8·7		0	23·49	
*p*1·6		1·6	37·58	1	23·49	
0·83	0	10·3	37·58	0	8·55	31·19
				1	32·04	31·19

where the summations extend over all values of the suffixes, which are r in number, such that $a > b > \ldots > j > k$, and where the numerical coefficient has the value

$$A = (a - b)(b - c) \ldots (j - k)k$$

For example, with $n = 4$ the formula gives

$$\begin{aligned} v_4/v_0 = 1 &+ p(4\tau_4 + 3\tau_3 + 2\tau_2 + \tau_1) \\ &+ p^2(3\tau_4\tau_3 + 4\tau_4\tau_2 + 3\tau_4\tau_1 + 2\tau_3\tau_2 + 2\tau_3\tau_1 + \tau_2\tau_1) \\ &+ p^3(2\tau_4\tau_3\tau_2 + 2\tau_4\tau_3\tau_1 + 2\tau_4\tau_2\tau_1 + \tau_3\tau_2\tau_1) \\ &+ p^4\tau_4\tau_3\tau_2\tau_1 \end{aligned}$$

(4.3) Equal *R's* and Equal *C's*

Let $\tau = CR$. The coefficients of successive functions v_m/v_0 can be derived very simply by writing eqn. (1) as

$$\frac{i_m}{pC} = \frac{i_{m-1}}{pC} + v_{m-1}$$

$$v_m = v_{m-1} + p\tau\left(\frac{i_m}{pC}\right)$$

and building up the coefficients in a difference Table (Table 4).

Table 4

VOLTAGE-TRANSFER COEFFICIENTS FOR *RC* NETWORK WITH $R = C = 1$, $v_0 = 1$, AND $i_0 = 0$

v_0										1
i_1								1		
v_1							1		1	
i_2						1		2		
v_2					1		3		1	
i_3				1		4		3		
v_3			1		5		6		1	
i_4		1		6		10		4		
v_4	1		7		15		10		1	
i_5		8		21		20		5		
v_5	1		9		28		35		15		1

Thus, for example,

$$v_5/v_0 = 1 + 15p\tau + 35(p\tau)^2 + 28(p\tau)^3 + 9(p\tau)^4 + (p\tau)^5$$

It is clear from the Table that the coefficients are closely related to the binomial coefficients; in fact

$$v_{mr} = \binom{m + r}{2r} = \frac{(m + r)!}{(2m)!\,(m - r)!}$$

(5) CONCLUSIONS

The equations for currents and voltages in a ladder network form a set of linear recurrence equations which are convenient for numerical calculation, and there are computational advantages in calculating transfer functions this way instead of writing down the complete algebraic expression and substituting numerical values. A parallel set of equations provide a numerical check.

Formulae for *RC* networks are comparatively simple, and the general form of the coefficients of certain transfer functions can be calculated in this case.

(6) REFERENCES

(1) GREEN, E.: 'Synthesis of Ladder Networks to give Butterworth or Chebyshev Response in the Pass Band', *Proceedings I.E.E.*, Monograph No. 88 R, January, 1954 (**10**, Part IV, p. 192).

(2) GUILLEMIN, E. A.: 'Communication Networks' (Wiley, New York, 1935), Vol. 2.

(3) YOUNG, A. J.: 'An Introduction to Process-Control System Design' (Longmans, London, 1955), Chapter 15.

(4) D'OMBRAIN, G. L.: 'The Training of the Process-Control Engineer and the Presentation of Control Theory', *Transactions of the Society of Instrument Technology*, 1955, **5**, p. 90.

(7) APPENDIX: PROOF OF EQNS. (5)

Since $Z_m = v_m/i_m$, we have

$$\begin{aligned} v_m/v_{m-1} &= Z_m i_m/v_{m-1} \\ &= Z_m(y_m + 1/Z_{m-1}) \quad . \quad . \quad . \quad (1 \end{aligned}$$

from eqn. (1*a*).

Alternatively, eqn. (1*b*) gives

$$\begin{aligned} v_m/v_{m-1} &= 1 + z_m i_m/v_{m-1} \\ &= 1 + z_m y_m + z_m/Z_{m-1} \quad . \quad . \quad (1 \end{aligned}$$

from eqn. (16).

Suppose it is possible to express any v_m in the form

$$1/v_m = a_m + b_m/Z_m \quad . \quad . \quad . \quad . \quad . \quad (1$$

where a_m and b_m depend only on $y_{m+1} \ldots z_n$. Then

$$\begin{aligned} a_{m-1} + b_{m-1}/Z_{m-1} &= (a_m + b_m/Z_m)(v_m/v_{m-1}) \\ &= [(1 + z_n y_m) + z_m/Z_{m-1}]a_m + (y_m + 1/Z_{m-1})b_m \quad (1 \end{aligned}$$

The coefficient of a_m in eqn. (19) is formed by using eqn. (1 for v_m/v_{m-1}, and the coefficient of b_m by using eqn. (16). Sin Z_{m-1} is independent of $y_m \ldots z_n$, eqn. (19) splits into tw equations, one involving the coefficients of $1/Z_{m-1}$ and one no

$$b_{m-1} = b_m + z_m a_m \quad . \quad . \quad . \quad . \quad . \quad . \quad (5$$

$$\begin{aligned} a_{m-1} &= (1 + z_m y_m)a_m + y_m b_m \\ &= a_m + y_m b_{m-1} \quad . \quad . \quad . \quad . \quad . \quad (5 \end{aligned}$$

from (5*a*).

Since eqn. (18) can be made to hold for $m = n$ by suitable choice of a_n and b_n, it must hold for all m, subject to eqns. (Eqn. (18) is, in fact, equivalent to Thévenin's theorem.

621.372.853.2

The Institution of Electrical Engineers
Monograph No. 433E
Feb. 1961

THE PART PLAYED BY SURFACE WAVES ON THE REFLECTION AT A FERRITE BOUNDARY

By L. LEWIN, Associate Member.

(*The paper was first received* 3*rd August, and in revised form* 18*th November*, 1960. *It was published as an* INSTITUTION MONOGRAPH *in February*, 1961.)

SUMMARY

It is shown that the solution given in a previous paper for the reflection at a ferrite boundary in a rectangular waveguide is invalid in a certain region because it implies a finite power flux into the waveguide walls. This flux can be taken care of by means of Bresler's surface waves, which can propagate in the anomalous region, and which were postulated in order to resolve a thermodynamic paradox. Their reality when the ferrite is lossy, however, requires further elucidation.

(1) INTRODUCTION

In a previous paper[1] (to which reference is made for equations, notation, etc.) the problem was examined of the reflection of a dominant rectangular waveguide mode from a transversely magnetized ferrite region, the guide being empty for $z < 0$ and filled with ferrite for $z > 0$. An expression was given for the discontinuity reactance jX representing the energy stored in higher modes generated at the ferrite boundary, the formula being a function of a parameter

$$p = \frac{1}{2} + \frac{1}{2\pi j} \log \frac{1 + M/K}{1 - M/K}$$

Here, M/K is a measure of the magnetic properties of the ferrite and is zero when the ferrite is unmagnetized, in which case the problem degenerates into the simple one of reflection at the boundary between two uniform media. According to the manner of solution given, the formula should be valid for all values of M/K, but it was apparent that the reactance, which involved $(\frac{1}{2} - p)^2$, would be complex for $M/K > 1$, and it was postulated that the result could be valid only for $|M/K| < 1$, although the reason for such a restriction was not known.

It is the purpose of this further paper to explain why the above restriction is necessary and to examine what alterations are required to give the correct form for X.

(2) FIELD AT THE GUIDE WALL

The axial magnetic field at the guide wall in the ferrite is easily obtained from Sharpe and Heim's paper:[2]

$$H_z = \frac{-j}{\omega\mu_\perp} \frac{\partial E_y}{\partial z} + \frac{\kappa}{\omega(\mu^2 - \kappa^2)} \frac{\partial E_y}{\partial x} \quad . \quad . \quad (1)$$

Here, μ and $j\kappa$ are the components of the permeability tensor and $\mu_\perp = (\mu^2 - \kappa^2)/\mu$.

At the guide wall $E_y = 0$, so that $H_z \propto \partial E_y/\partial x$. Since the flow of power into the wall is given by $H_z \times E_y$, there is a power flow proportional to $E_y\, \partial E_y/\partial x$, and this must be zero since the walls have been assumed to have infinite conductivity. Of course, $E_y = 0$ as $x \to 0$ or a, but $\partial E_y/\partial x$ can become infinite, so that it is also necessary that the product be zero.

According to eqn. (19) of Reference 1 the field as $\cos\phi = \cos(\pi x/a) \to 1$ is

$$\left.\begin{aligned} E_y &\to \phi^{2p} \\ \partial E_y/\partial x &\to \phi^{2p-1} \end{aligned}\right\} \quad . \quad . \quad . \quad . \quad . \quad (2)$$

Hence the power flow at the waveguide wall ($x = 0$) vanishes as ϕ^{4p-1}, and it is necessary that $\mathscr{R}p > \frac{1}{4}$ for a zero power flux. Similarly, as $x \to a$, $\phi = \pi - \psi$ with $\psi \to 0$, giving

$$\left.\begin{aligned} E_y &\to \psi^{2-2p} \\ \partial E_y/\partial x &\to \psi^{1-2p} \end{aligned}\right\} \quad . \quad . \quad . \quad . \quad . \quad (3)$$

The power flow to the wall as $x \to a$ is ψ^{3-4p} so that $\mathscr{R}p < \frac{3}{4}$ for a zero flux. Hence the solution given in Reference 1 has limits of validity

$$\tfrac{1}{4} < \mathscr{R}p < \tfrac{3}{4} \quad . \quad . \quad . \quad . \quad . \quad . \quad . \quad (4)$$

If we put $M/K = \varepsilon^{j\beta}$, then

$$p = \frac{1}{2} + \frac{1}{2\pi j} \log(-j \tan \beta/2) \quad . \quad . \quad . \quad . \quad (5)$$

Hence $\mathscr{R}p = \frac{1}{4}$ or $\frac{3}{4}$ according to the sign of β, and the limits in eqn. (4) correspond to $|M/K| = 1$. This confirms the earlier postulate on the limits of validity of the solution. It is now necessary to see what modifications in the solution are required when $\mathscr{R}p$ is outside the above limits.

(3) A MODIFIED FIELD DISTRIBUTION

Eqn. (19) of Reference 1 has one disposable constant, B, which was chosen to give $E_y = 0$ at the guide wall. If we could dispense with this condition for $\mathscr{R}p < \frac{1}{4}$ or $\mathscr{R}p > \frac{3}{4}$, B could be chosen to give zero power flux to the walls. If $\mathscr{R}p < \frac{1}{4}$ and $B = 0$, eqn. (19) gives

$$E_y = \int_{-1}^{\cos\phi} \left(\frac{1 - x}{1 + x}\right)^p dx$$

As $\phi \to 0$ this gives $E_y \to \text{const.} + \phi^{2p+2}$, $\partial E_y/\partial\phi \to \phi^{2p+1}$ and $E_y\, \partial E_y/\partial\phi \to 0$ as $\phi \to 0$. If $\phi = \pi - \psi$, $E_y \to \psi^{2-2p}$, $\partial E_y/\partial\phi \to \psi^{1-2p}$ and $E_y\, \partial E_y/\partial\phi \to \psi^{3-4p} \to 0$ as $\psi \to 0$.

Similarly, for $\mathscr{R}p > \frac{3}{4}$ take $B = -1$. Then

$$E_y = \int_{1}^{\cos\phi} \left(\frac{1 - x}{1 + x}\right)^{p-1} dx$$

As $\phi \to 0$, $E_y \to \phi^{2p}$, $\partial E_y/\partial\phi \to \phi^{2p-1}$, and $E_y\, \partial E_y/\partial\phi \to \phi^{4p-1} \to 0$. If $\phi = \pi - \psi$, $E_y \to \text{const.} + \psi^{4-2p}$, $\partial E_y/\partial\phi \to \psi^{3-2p}$ and $E_y\, \partial E_y/\partial\phi \to 0$ as $\psi \to 0$.

Hence, in both cases, the necessity for zero power flux to the walls is met at the cost of permitting a non-zero electric field at one of the walls, in the first case at $x = 0$, in the second at $x = a$. What justification could there be for such a procedure? And if justified, why limit it to $\mathscr{R}p < \frac{1}{4}$ or $> \frac{3}{4}$?

Correspondence on Monographs is invited for consideration with a view to publication.
Mr. Lewin is with Standard Telecommunication Laboratories, Ltd.

(4) CONDITIONS AT THE GUIDE WALL

It will help to understand these questions if we note the reasons for choosing $E_y = 0$ at a perfectly conducting wall under more familiar conditions. Since tangential electric fields are continuous, a non-vanishing field would set up an equal field in the metal, and with an infinite conductivity, an infinite current density would be caused. This in itself need not be a reason for dismissing a non-zero field, since such currents can, in fact, be set up—at a sharp edge, for example. But it is essential that such currents be integrable, otherwise they would cause infinite radiation. This is always so with an edge current. In the present case we have a field varying as $C + x^{2p+2}$ across the ferrite face. How does it vary along the wall? (An infinite current density at $z = 0$ would be permissible if it vanished fast enough for $z > 0$.) Close enough to the corner of the ferrite the constant term behaves as a component of a plane wave, giving a finite axial extension along which the field is non-zero. This is impermissible, since a finite region of infinite current density would give infinite radiation. Hence, if we wish to retain the features of the modified field distribution, it is necessary to find some way of reducing the field to zero at the walls—a way which, moreover, is not applicable to the range $\frac{1}{4} < \mathscr{R}p < \frac{3}{4}$, where we have no need for an additional solution.

(5) SURFACE WAVES

Bresler[3] has shown that the commonly accepted set of sinusoidal modes is not complete in a certain range of the material constants and applied magnetostatic field. In brief, he finds that if one examines the problem of a ferrite which does not completely fill the guide cross-section, a surface wave may be formed which hugs the crack between the ferrite and the guide wall, and in the limit in which the crack goes to zero this wave does *not* vanish, but can carry a finite amount of energy. Moreover, its presence is required for the resolution of a thermodynamic paradox, and its reality must therefore be presumed. Although the reason was not given as to why it is essential to start with the analysis involving a finite crack and only at the end proceed to the limit, we will accept here that this process is necessary. We shall examine first the range of parameters over which the surface wave is required.

The equation for the propagation coefficients is given by Bresler's eqn. (37) in which we are interested in the limit $1 - \Delta - D = D \to 0$ (i.e. a crack on each side of the ferrite of width D approaching zero).

The propagation coefficient θ is normalized to the free-space value $k = 2\pi/\lambda$, and in the limit $D \to 0$ we need values of $q = kD\theta$ such that as $D \to 0$, $\theta \to \infty$ in such a way that q is a finite solution of the equation

$$\left(\coth q + \frac{1}{\nu_1} \pm \frac{1}{\nu_2}\right) = 0 \quad . \quad . \quad . \quad . \quad (6)$$

Here ν_1 and ν_2 are related to the material coefficients. Solving eqn. (6) and expressing the constants in terms of the magnetostatic field H and saturation magnetization M_s gives

$$q = \frac{1}{2} \log \frac{\frac{1}{2}\gamma|M_s|}{\omega \pm \gamma(H + \frac{1}{2}M_s)} \quad . \quad . \quad . \quad (7)$$

This obviously gives real values of q, and therefore of $\theta = q/kD$ when $\omega > \gamma|H + \frac{1}{2}M_s|$. In addition, a requirement that θ be positive leads to $\omega < \gamma|H + M_s|$. These are exactly the limits at which, for a lossless ferrite, we have $\mathscr{R}p = \frac{1}{4}$ or $\frac{3}{4}$. Hence we can say that, just at the limits at which the solution in Reference 1 breaks down owing to a non-zero power flux to the waveguide wall, surface waves appear whose physical duty, it now clear, is to convey this flux away.

In the lossy case we rewrite eqn. (7) (for a positive field) as

$$q = \frac{1}{2} \log \frac{\frac{1}{2}\gamma M_s}{\omega - \gamma(H + \frac{1}{2}M_s) - j\alpha} \quad . \quad . \quad . \quad (8$$

The requirement that θ be positive, which is connected with th requirement that $\varepsilon^{-\theta x}$ represent an attenuated wave, mus become $\mathscr{R}\theta > 0$, or

$$\omega < \gamma(H + \tfrac{1}{2}M_s) + \sqrt{[(\tfrac{1}{2}\gamma M_s)^2 - \alpha^2]} \quad . \quad . \quad (9$$

The requirement that q be real is more difficult to deal with since, presumably, we must let q become complex if the ferrit is lossy. This implies a surface wave of infinite attenuation a $D \to 0$, and we must decide the limits at which such a wave i to be no longer considered real. In the lossless case eqn. (gives an imaginary component of 0 or $j\pi$ according to the sig of $\omega - \gamma(H + \frac{1}{2}M_s)$. In general, the imaginary part is

$$j \text{ arc tan } \frac{\alpha}{\omega - \gamma(H + \frac{1}{2}M_s)}$$

and this equals $j\pi/2$ at the cross-over frequency $\omega = \gamma(H + \frac{1}{2}M_s)$ This would seem to be a reasonable limit to choose, and thes considerations therefore indicate surface waves when

$$\gamma(H + \tfrac{1}{2}M_s) < \omega < \gamma(H + \tfrac{1}{2}M_s) + \sqrt{[(\tfrac{1}{2}\gamma M_s)^2 - \alpha^2]} \quad (10$$

Unfortunately, these limits are not the same as $\mathscr{R}p < \frac{1}{4}$ or $> \frac{3}{4}$ in the lossy case. From eqn. (10) of Reference 1 we find th above limits for p when

$$(A^2 - \omega^2 + \alpha^2)(B^2 - \omega^2 + \alpha^2) + 4\omega^2\alpha^2 = 0 \quad (11$$

where $A = \gamma(H + \frac{1}{2}M_s)$ and $B = \gamma(H + M_s)$.
Hence

$$\omega^2 = \tfrac{1}{2}(A^2 + B^2 - 2\alpha^2) \pm \tfrac{1}{2}\sqrt{[(A^2 - B^2)^2 - 8\alpha^2(A^2 + B^2)]} \quad (12$$

and this is the same as eqn. (10) only in the limit $\alpha = 0$.

The lower limit, for α small, is

$$\omega \simeq A + \frac{\alpha^2}{2A} \frac{3A^2 + B^2}{B^2 - A^2} > A \quad . \quad . \quad . \quad (13$$

and hence is contained within eqn. (10).

The upper limit of eqn. (12), for small α, is

$$\omega \simeq B - \frac{\alpha^2}{2B} \frac{3B^2 + A^2}{B^2 - A^2} \quad . \quad . \quad . \quad . \quad (14$$

whilst the upper limit in eqn. (10) is similarly

$$\omega \simeq B - \frac{\alpha^2}{2B} \frac{B(B + A)}{B^2 - A^2} \quad . \quad . \quad . \quad . \quad (15$$

Since $3B^2 + A^2 > B(B + A)$, eqn. (14) is contained within eqn. (15). Hence, surface waves exist in the range $\mathscr{R}p < \frac{1}{4}$ o $\mathscr{R}p > \frac{3}{4}$, but, as defined by eqn. (10), also somewhat outside this range. The significance of these waves existing when they are not wanted is not too clear, since, with their infinite attenuations they could always be considered unreal and ignored; and ye their presence is required within the limits given by eqn. (12) It seems rather arbitrary to keep them when they satisfy eqn. (12 but to write them off over the remainder of the extended range of eqn. (10). Presumably in formulating eqn. (10) we have been too generous; the matter obviously requires further attention.

(6) MODIFIED FIELD DISTRIBUTION

A function such as

$$\sum_{1}^{\infty} \frac{\sin(2n+1)\phi}{2n+1}$$

as the value $\pi/4$ for $0 < \phi < \pi$ but zero at $\phi = 0, \pi$. Hence, in the air-filled part of the waveguide we can contemplate a field which behaves like a constant close to the waveguide wall, but which nevertheless drops to zero just at the wall. In the ferrite-filled region in which a minute crack is supposed to exist between the ferrite and the wall, the field need not drop to zero at the ferrite edge. Field continuity is supplied by the surface wave, which collapses rapidly to zero in the space between the ferrite and the waveguide wall. Hence the surface wave can supply the features postulated at the end of Section 4 to permit a solution of the integral equation which is non-zero at $\phi = (0, a)$.

Unfortunately, the introduction of the surface wave invalidates the whole of the analysis it was introduced to save. For example, eqn. (1) of Reference 1 was obtained by an integration by parts, the integrated part vanishing at the limits. This will now no longer be so, and a further term, corresponding to the magnetic field of the surface wave, is also needed earlier in the formulation. This alteration has not yet been made, and is particularly difficult because of the introduction of the crack. This disappears in the limit, but the earlier part of the analysis is very much complicated thereby.

It is interesting to note that the analysis in Reference 1, if taken at its face value in the invalid range, with the change of permitting the modified field distribution of Section 3, gives, for the discontinuity reactance,

$$X = -\frac{1}{K}\left(1 + \frac{\pi^2}{\log^2 \dfrac{M+K}{M-K}}\right), \quad |M/K| > 1 \quad . \quad (16)$$

This is real, and agrees with Sharpe and Heim's expression for $M \gg K$. It is not believed that it is correct, however, since the accompanying surface waves must obviously be carrying away or absorbing power, so that X should be complex to take this lost power into account. It is just possible, however, that the reactive term might be given correctly by eqn. (16), but the complete analysis is necessary to confirm this.

(7) CONCLUSIONS

A new physical role has been found for the surface waves postulated by Bresler in order to resolve a thermodynamic paradox. Their purpose is to carry away power adjacent to the waveguide wall in an arrangement in which a strong magnetostatic field would otherwise have caused a field distribution to build up with an impermissible power flux into the waveguide wall. The significance of these waves when the ferrite is lossy, however, requires further elucidation, since the accompanying attenuation would be so large that they normally would be taken to be non-existent. So far as the reflection at the ferrite boundary is concerned, the difficult mathematical problem of a guide partially filled with ferrite must first be solved, with the limit of zero crack between ferrite and guide wall taken only at a sufficiently late stage in the analysis.

(8) REFERENCES

(1) LEWIN, L.: 'A Ferrite Boundary-Value Problem in a Rectangular Waveguide', *Proceedings I.E.E.*, Paper No. 3056 E, November, 1959 (**106**B, p. 559).

(2) SHARPE, C. B., and HEIM, D. S.: 'A Ferrite Boundary-Value Problem in a Rectangular Waveguide', *Transactions of the Institute of Radio Engineers*, January, 1958, **MTT-6**, p. 42.

(3) BRESLER, A. D.: 'On the TE_{n0} Modes of a Ferrite-Slab-Loaded Rectangular Waveguide and the Associated Thermodynamic Paradox', *ibid.*, January, 1960, **MTT-7**, p. 81.

621.371.011.21

The Institution of Electrical Engineers
Monograph No. 434
Mar. 19

THE SURFACE IMPEDANCE CONCEPT AND THE STRUCTURE OF RADIO WAVES OVER REAL EARTH

By Z. GODZIŃSKI

(*The paper was first received* 15*th July, and in revised form* 7*th November*, 1960. *It was published as an* INSTITUTION MONOGRAPH *in March*, 1961.)

SUMMARY

The paper is concerned with the concept of surface impedance as applied to the theory of radio-wave propagation over a real, i.e. inhomogeneous and irregular, earth; some of the conclusions may also be of value in the theory of waveguides, cavity resonators and certain types of aerial.

The advantages and limitations of the surface-impedance concept are shown in connection with a very general integral equation for the field strength.

The approximations and physical phenomena underlying the surface-impedance concept are first discussed in the simplest case of a homogeneous and flat earth. The analysis is then extended to a horizontally stratified earth; it is then possible to characterize the earth by certain effective parameters depending on frequency and the geometric structure of the soil. The same is also true in the cases of a spherical or not too excessively irregular earth. The discussion is then generalized to the case of an arbitrarily inhomogeneous earth. The height/gain function and the shape of the ellipse of polarization are discussed. Approximate boundary conditions for the Hertzian vector and Hertzian scalar function are related to the concept of surface impedance.

Practical conclusions are drawn with regard to the existence and measurement of the effective earth constants and to some aspects of geological prospecting by radio methods.

LIST OF PRINCIPAL SYMBOLS

E, H = Electric and magnetic force, respectively.
D = Electric flux density.
ω = Angular frequency.
λ, λ_0 = Actual wavelength and wavelength for free-space propagation.
μ_0, ϵ_0 = Absolute permeability and permittivity of free space.
μ, μ_r = Absolute and relative permeability.
ϵ, ϵ_r = Absolute and relative permittivity.
σ = Conductivity.
ϵ' = Complex absolute permittivity $= \epsilon_r'\epsilon_0 = \epsilon - j\sigma/\omega$.
ϵ_r' = Complex relative permittivity $= \epsilon_r - j\sigma/(\omega\epsilon_0)$.
γ = Propagation coefficient $= \sqrt{(\omega^2\mu\epsilon')}$.
γ_0 = Free-space propagation coefficient $= \omega(\mu_0\epsilon_0)^{1/2} = 2\pi/\lambda_0$.
Z_0 = Intrinsic impedance of free space $= (\mu_0/\epsilon_0)^{1/2} \simeq 376{\cdot}7$ ohms.
Z = Intrinsic impedance $= \gamma/(\omega\epsilon') = \omega\mu/\gamma = (\mu/\epsilon')^{1/2} = Z_0(\mu_r/\epsilon_r')^{1/2}$.
Z_{xy}, Z_{yx} = Impedances for field components E_x/H_y, $E_y/(-H_x)$.
Z_z = Impedance in the direction of the positive z-axis.
Z_s = Surface impedance.
δ = Depth of penetration.

Subscript t denotes the tangential component of a vector.

Subscripts a and e denote that the quantity pertains to atmosphere and earth, respectively.

Rationalized M.K.S. units are used throughout. The time factor $\exp(j\omega t)$ is suppressed.

Correspondence on Monographs is invited for consideration with a view to publication.

Mr. Godziński is at the Instytut Lacznosci, Wroclaw, Poland.

(1) INTRODUCTION

The propagation of radio waves over a real, i.e. inhomogeneo and irregular, earth is an extremely difficult problem in mat mathematical physics. In certain practical applications, such broadcasting, an exact knowledge of the field strength a structure is often not necessary. It is then possible to introdu essential simplifications, for instance to assume that the earth spherical and homogeneous. However, even in this simple case, the rigorous mathematical analysis is very complicated a rigorous analysis by classical methods of the more compl problem of radio-wave propagation over a real earth must considered as almost hopeless. Essential progress has be made possible only by the introduction of approximate bound conditions.

These may be formulated mathematically in a number of wa one of which is the concept of surface impedance. Because its more direct physical significance and its connections with t concept of impedance in circuit theory, the concept of surf impedance has been applied frequently in recent investigation it is used, therefore, as a basis in the present paper.

An attempt is made to give a review of the physical phenome underlying the concept of surface impedance,[1] to show t consequences which follow therefrom with regard to field stru ture and attenuation, and to draw a number of practical co clusions. Special consideration is given to a real (inhom geneous and irregular) earth.

Some of the theoretical remarks may also be of value in t theory of waveguides, cavity resonators and certain types aerial.

(2) INTEGRAL EQUATIONS FOR FIELD STRENGTH

The advantages of surface impedance in the theory of radi wave propagation may be shown most conveniently in connecti with the vector integral equation for the field strength. T derivation of such equation by Monteath[2] was based Ballantine's 'Corollary I' of the electromagnetic reciproci theorem.[3] In the present paper we shall, however, use anoth approach, which is very simple and also shows clearly the orig of certain limitations of the method.

Let V be a closed region of space bounded by a regular surfac S, and let $\boldsymbol{P}$ and $\boldsymbol{Q}$ be two vector functions of position whic together with their first and second derivatives, are continuo throughout V and on the surface S. Then, as shown b Stratton,[4]

$$\int_V (\boldsymbol{Q} \cdot \operatorname{curl}\operatorname{curl} \boldsymbol{P} - \boldsymbol{P} \cdot \operatorname{curl}\operatorname{curl} \boldsymbol{Q})\,dV = \oint_S (\boldsymbol{Q} \times \operatorname{curl} \boldsymbol{P} - \boldsymbol{P} \times \operatorname{curl} \boldsymbol{Q}) \cdot d\boldsymbol{S} \quad . \quad (1)$$

where $d\boldsymbol{S}$ is assumed to be in the direction of the inward norma

Eqn. (1) will be applied to the following problem (Fig. 1).

Real (irregular and inhomogeneous) earth S_1 is surrounde by a not necessarily homogeneous atmosphere. The sho

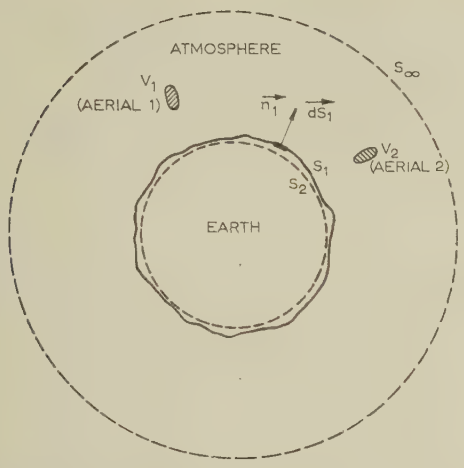

Fig. 1.—Real earth S_1 with transmitting aerial at V_1, and auxiliary fictitious earth S_2 with its transmitting aerial at V_2.

ransmitting aerial (dipole) 1 at V_1 is replaced by an equivalent current distribution of density J_1. The electric and magnetic fields produced by aerial 1 will be denoted by E_1, H_1.

At the same time we consider a second, auxiliary and fictitious problem: the same atmosphere as before, a current distribution, J_2, in a small volume V_2 equivalent to a short aerial (dipole) 2, and an earth S_2 whose surface at no point protrudes above the surface S_1. The electrical properties and shape of the auxiliary earth S_2 may be almost arbitrary; the limitations will be mentioned later. The fields produced by aerial 2 will be denoted by E_2, H_2.

Returning to eqn. (1), we put $Q = E_1$, $P = E_2$. V is assumed to be the volume outside the real earth S_1; it is bounded on the outside by the infinitely distant surface S_∞.

The electromagnetic field in the atmosphere satisfies Maxwell's equations:

$$\text{curl } E = -j\omega\mu_0 H \quad . \quad . \quad . \quad . \quad . \quad (2)$$

$$\text{curl } H = j\omega D + J \quad . \quad . \quad . \quad . \quad . \quad (3)$$

Substituting in eqn. (1) we obtain

$$\int_{V_2} E_1 J_2 dV - \int_{V_1} E_2 J_1 dV + j\omega \int_V (E_1 D_2 - E_2 D_1) dV = \int_{S_1, S_\infty} (E_1 \times H_2 - E_2 \times H_1) dS \quad . \quad (4)$$

Since both aerials have been assumed to be short, the vectors E_1 inside V_2 and E_2 inside V_1 are approximately constant and may be placed outside the integral sign of the first and second volume integrals. The remaining simplified volume integrals over V_1 and V_2 are then proportional to the electric moments p_1 and p_2 of the respective aerials:

$$\left.\begin{aligned} \int_{V_1} J_1 dV &= j\omega p_1 \\ \int_{V_2} J_2 dV &= j\omega p_2 \end{aligned}\right\} \quad . \quad . \quad . \quad . \quad . \quad (5)$$

The surface integral over the infinitely distant surface S_∞ vanishes because of the radiation condition.

The volume integral over V vanishes only if the permittivity of the not necessarily homogeneous atmosphere is a scalar quantity or a symmetrical tensor. The upper atmosphere, however, is a magneto-ionic medium and its permittivity is an antisymmetrical tensor. In the paper—as often in theory—the permittivity of the atmosphere is assumed to be a scalar quantity. Physically, it means neglecting the influence of the ionosphere on the propagation of radio waves, or, more simply, neglecting the ionospheric wave. This is a very serious simplification of the problem and must always be checked very carefully.

It must be emphasized that eqn. (4) has been derived on the assumption that both the vectors E_1 and E_2 are continuous, together with their first and second derivatives. Where there are discontinuities in the electrical properties of the earth or sharp irregularities in its surface, the field will show singularities. The volume and surfaces of integration must then be changed correspondingly in order to avoid discontinuities and thus certain additional terms may be produced at these singularities. Physically, this means that at the respective singularities there appear, for instance, line currents or charges which we must take into account separately (see also Section 5.2). It is not a problem peculiar to radio-wave propagation. It will also be found, for example, in the cases of corrugated waveguides, cavity resonators and aerials. This essential complication seems to have been overlooked.

Returning to eqn. (4), we assume that the electric moments of the aerials are equal ($|p_1| = |p_2| = p$). Eqn. (4) then gives

$$(E_1)_{p2} = (E_2)_{p1} - \frac{j}{\omega p} \int_{S_1} (E_1 \times H_2 - E_2 \times H_1) dS \quad . \quad (6)$$

where $(E_1)_{p2}$, $(E_2)_{p1}$ denote the projections of electric field intensities E_1, E_2 existing inside volumes V_2, V_1 in the directions of electric moments p_2, p_1, i.e. $(E_1)_{p2}$, $(E_2)_{p1}$ are the components of electric force along the directions of aerials 2, 1.

As a consequence of the assumption that the permittivity of the atmosphere is a scalar quantity, the fields satisfy* the reciprocity theorem.[5, 6, 3] Consequently $(E_2)_{p1}$ may be considered as a component in the direction of p_2 of the field existing at V_2 and produced there by aerial 1, if this aerial is placed, not over the real earth S_1, but over the fictitious earth S_2. Consequently, the surface integral in eqn. (6) expresses the change of the field on transition from a fictitious to a real earth.

The case when the transmitting aerial is a magnetic dipole can be dealt with similarly. The current distributions J_1, J_2 within the aerial are replaced by fictitious magnetic polarizations M_1, M_2 ($J = \text{curl } M$), and H_1, H_2 are substituted for Q, P in eqn. (1). In order to avoid volume integrals in connection with the inhomogeneities of the atmosphere we shall assume a homogeneous atmosphere of permittivity ϵ_0. Denoting the magnetic moments of the aerials by m_1, m_2 ($m = \int M dV$), and assuming as before $|m_1| = |m_2| = m$, we obtain an expression similar to eqn. (6):

$$(H_1)_{m2} = (H_2)_{m1} + \frac{j}{\omega\mu_0 m} \int_{S_1} (E_1 \times H_2 - E_2 \times H_1) dS \quad . \quad (7)$$

The integral equation (6) is equivalent to, or represents an alternative formulation or a generalization of, expressions derived previously by a number of authors on the basis of the approximate boundary conditions of Leontovich[7–31] or Ballantine's formulation of the reciprocity theorem.[2, 32–36]

(3) INTRODUCTION OF THE SURFACE IMPEDANCE CONCEPT

To introduce the concept of surface impedance we shall consider eqn. (6) under the following assumptions: an inhomogeneous and spherical earth S_1, a homogeneous and spherical earth S_2, a homogeneous atmosphere and both aerials vertical; consequently we shall consider the vertical component of an electric field, produced by a vertical dipole.

* It is interesting to note that eqn. (4) lends itself readily to a very simple discussion of the problem of reciprocity relations in radio-wave propagation.

The scalar triple products in the integrand of eqn. (6) reduce to products of tangential components. Consequently the integral in eqn. (6) may be written as follows:

$$-\frac{j}{\omega p}\int_{S_1} H_{1t}H_{2t}\left[\frac{E_{1t}}{H_{1t}}\sin(\boldsymbol{E}_{1t}, \boldsymbol{H}_{2t}) - \frac{E_{2t}}{H_{2t}}\sin(\boldsymbol{E}_{2t}, \boldsymbol{H}_{1t})\right]dS \quad . \quad (8)$$

The tangential components $\boldsymbol{E}_{2t}$, $\boldsymbol{H}_{2t}$ of the auxiliary field $\boldsymbol{E}_2$, $\boldsymbol{H}_2$ existing over a homogeneous spherical earth are mutually perpendicular; $\boldsymbol{E}_{2t}$ is directed radially (Fig. 2). The tangential

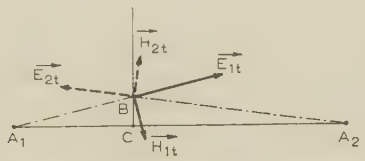

Fig. 2.—Arrangement of the tangential components of the field.

A_1 Real aerial 1 producing the real field $\boldsymbol{E}_1$, $\boldsymbol{H}_1$.
A_2 Auxiliary aerial 2 producing the auxiliary field $\boldsymbol{E}_2$, $\boldsymbol{H}_2$.

components $\boldsymbol{E}_{1t}$, $\boldsymbol{H}_{1t}$ of the field over the inhomogeneous spherical earth are not necessarily mutually perpendicular, nor is $\boldsymbol{E}_{1t}$ always radial; the deviations, however, are generally not very great.

The largest contribution to the integral (8) comes from those parts of the surface S where the phase of the integrand is stationary, i.e. from points such as B lying not too far from the line A_1A_2 (Fig. 2). As a consequence the angles $(\boldsymbol{E}_{1t}, \boldsymbol{H}_{2t})$, $(\boldsymbol{E}_{2t}, \boldsymbol{H}_{1t})$ at such points are nearly right angles, and both sine terms in eqn. (8) may be omitted as an approximation.

The value of E_{2t}/H_{2t} is known from the rigorous theory for a homogeneous spherical earth. Except for points lying very near to the transmitting aerial (A_2 in Fig. 2) E_{2t}/H_{2t} is practically constant and may be calculated readily. We shall show later that the same is true in many cases for E_{1t}/H_{1t}. We thus see that a number of unknown quantities in eqn. (6) may be calculated approximately in advance and the computations are simplified considerably. But at the same time the introduction of a number of approximations may cast doubt upon the results unless the whole procedure is checked very carefully.

The ratio of electric and magnetic forces has the dimension of impedance. Considering a direction $\boldsymbol{n}$, we may introduce orthogonal co-ordinates u, v so that u, v, n form a right-handed triplet. The u- and v-components of the vectors $\boldsymbol{E}$, $\boldsymbol{H}$ may be combined into impedance relations:

$$E_u/H_v = Z_{uv}; \quad E_v/(-H_u) = Z_{vu} \quad . \quad . \quad . \quad . \quad (9)$$

The algebraic signs of the components in the expressions for the *field impedances* Z_{uv}, Z_{vu} are chosen so that in each case the corresponding directions also form with n a right-handed triplet (Z_{uv}: u, v, n; Z_{vu}: v, $-u$, n). If the field impedances Z_{uv}, Z_{vu} are equal, the impedance properties of the field in the direction of $\boldsymbol{n}$ are described in a unique manner by a single quantity $Z_n = Z_{uv} = Z_{vu}$, the (*field*) *impedance in the direction of* $\boldsymbol{n}$.

We are often interested in the impedance properties of the field in a direction $\boldsymbol{n}$ normal to a surface (e.g. a surface of discontinuity); the u- and v-components are then the tangential components of $\boldsymbol{E}$, $\boldsymbol{H}$. If the field impedances Z_{uv}, Z_{vu} are equal, $Z_n = Z_{uv} = Z_{vu}$ is termed the (*field*) *impedance normal to S*.

When the surface S shows a constant normal impedance, Z_n, independent of the field structure, Z_n is called the *surface impedance* of the surface S; we denote it by Z_s.

The field impedances Z_{uv}, Z_{vu} are, in general, not equal; moreover, they change from point to point. The corresponding electromagnetic problems are then almost always very comple In a number of important practical cases the surfaces of di continuity may, however, be assumed to possess approximate a surface impedance; this facilitates the solution of the corr sponding problems considerably. In fact progress has bee achieved in many cases only after the direct or indirect introdu tion of the surface impedance concept.

As shown by eqns. (6) and (7) and the subsequent remark the problem of impedances emerges in a very natural way wh discussing the influence of a body on the field. The simple and very important case is when the body is a good conduct surrounded by a dielectric. The propagation coefficient of t conductor is then very much larger than that of the surroundi medium, and the wavelength, λ, inside the conductor is ve much less than the wavelength outside it. The structure of t field at some point inside the conductor is then determin practically by the field distribution over the adjoining part the surface of the conductor with dimensions of the order magnitude of λ. As λ is very much smaller than the wavelen outside the conductor, the changes of the outside field over distance λ are very small. Thus, when considering the fie inside the conductor we may assume that the 'generating' fie over the adjoining part of the conductor's surface is appro mately constant, i.e. that the surface of the conductor is appro mately an equiphase surface.

As an example, let us consider the case of a good and hom geneous conductor, with permeability μ and complex permittivi ϵ', surrounded by a dielectric. The structure of the field ins the conductor is then approximately the same as that of homogeneous plane wave propagating perpendicularly insi it. But for a homogeneous plane wave inside a homogeneo medium, the impedances Z_{uv}, Z_{vu} in the direction of propagati are equal:

$$Z_{uv} = Z_{vu} = Z \quad . \quad . \quad . \quad . \quad . \quad (1$$

where

$$Z = (\mu/\epsilon')^{1/2} = Z_0(\mu_r/\epsilon_r')^{1/2} \quad . \quad . \quad . \quad (1$$

is the *intrinsic impedance* of the conductor and

$$Z_0 = (\mu_0/\epsilon_0)^{1/2} \simeq 376{\cdot}7 \text{ ohms} \quad . \quad . \quad . \quad (1$$

is the *intrinsic impedance of free space*. Consequently, in t approximation, the surface of the conductor will show a surfa impedance Z_s equal to the intrinsic impedance of the conducto

$$Z_s = Z \quad . \quad . \quad . \quad . \quad . \quad . \quad (1$$

The idea underlying the concept of surface impedance w suggested for the first time by Leontovich in 1940 in unpublished theoretical investigation. The concepts of imp dance and surface impedance were introduced into fie theory by Schelkunoff.[37, 38] Important papers by Leontovich, Rytov,[39] Grünberg,[7] Booker,[40] Monteath,[2] Petrovsky a Feinberg,[24] and Bass[25] must also be mentioned.

The concept of surface impedance and its application analysis involve a number of approximations. The purpose the present paper[1] is to discuss these approximations, especial with regard to real (inhomogeneous and irregular) earth, a to try to show some of the consequences and limitations whi follow therefrom.

(4) SURFACE IMPEDANCE OF A HOMOGENEOUS AN STRATIFIED EARTH

(4.1) Surface Impedance in the Case of a Homogeneous Flat Earth

As the starting-point in the discussion of the surface impedan we choose the case of a flat, homogeneous earth surrounded

homogeneous atmosphere with parameters $\epsilon_a = \epsilon_0$, $\mu_a = \mu_0$, $\gamma_a = 0$. The electromagnetic field over the considered area of earth's surface is assumed for the moment to be without singularities. The xy-plane is the plane of earth's surface with the z-axis directed upwards.

The field inside the earth may be expanded in a finite or infinite sum of suitable orthogonal functions; as such we choose plane waves. We shall consider now the simplest case, when it is sufficient to take into account only the first term of such an expansion, i.e. when it is possible to represent the field by a single, homogeneous or inhomogeneous, plane wave.

A plane wave propagating inside a homogeneous medium is characterized by the components γ_{ex}, γ_{ey}, γ_{ez} of the propagation coefficient γ_e. These components are, in general, complex ($\gamma_{ex} = \alpha_{ex} - j\beta_{ex}$, etc.). Their real and imaginary parts may be considered as components of two vectors $\gamma_{e\mathscr{R}}$, $\gamma_{e\mathscr{I}}$. The vectors $\gamma_{e\mathscr{R}}$ and $\gamma_{e\mathscr{I}}$ fix in space a certain plane which we will denote by S_γ.

To each pair of vectors $\gamma_{e\mathscr{R}}$, $\gamma_{e\mathscr{I}}$ there belong two types of plane waves, a transverse electric and a transverse magnetic one. To simplify the expressions we choose the directions of the x- and y-axes so that the plane S_γ cuts the xy-plane along a line parallel to the x-axis. In such case the field vectors in the atmosphere just above the surface of the earth satisfy the following relations:

(*a*) *Transverse electric wave*:

$$E_{ax} = 0,\ E_{ay} \neq 0,\ E_{az} = \frac{\epsilon'_{re} g_y}{(1 - g_x^2 - g_y^2)^{1/2}} E_{ay} \quad . \quad (14)$$

$$H_{ax} = \frac{1}{Z_e} \frac{1 - g_x^2}{(1 - g_x^2 - g_y^2)^{1/2}} E_{ay} \quad . \quad . \quad . \quad . \quad . \quad . \quad (15)$$

$$H_{ay} = -\frac{1}{Z_e} \frac{g_x g_y}{(1 - g_x^2 - g_y^2)^{1/2}} E_{ay} \quad . \quad . \quad . \quad . \quad . \quad . \quad (16)$$

$$H_{az} = \frac{1}{Z_e} \mu_{re} g_x E_{ay} \quad . \quad . \quad . \quad . \quad . \quad . \quad . \quad . \quad . \quad (17)$$

(*b*) *Transverse magnetic wave*:

$$E_{ax} = -Z_e \frac{1 - g_x^2}{(1 - g_x^2 - g_y^2)^{1/2}} H_{ay} \quad . \quad . \quad . \quad . \quad . \quad . \quad (18)$$

$$E_{ay} = Z_e \frac{g_x g_y}{(1 - g_x^2 - g_y^2)^{1/2}} H_{ay} \quad . \quad . \quad . \quad . \quad . \quad . \quad (19)$$

$$E_{az} = -Z_e \epsilon'_{re} g_x H_{ay} \quad . \quad . \quad . \quad . \quad . \quad . \quad . \quad . \quad . \quad (20)$$

$$H_{ax} = 0;\ H_{ay} \neq 0;\ H_{az} = \frac{\mu_{re} g_y}{(1 - g_x^2 - g_y^2)^{1/2}} H_{ay} \quad . \quad (21)$$

In the above formulae Z_e denotes the intrinsic impedance of the earth, $g_x = \gamma_{ex}/\gamma_e$ and $g_y = \gamma_{ey}/\gamma_e$. The curves of complex relative permittivity ϵ'_r and intrinsic impedance Z for typical soils as functions of frequency are given in Figs. 3 and 4.

It follows from these expressions that the impedances Z_{xy}, Z_{yx} are, in general, different and, consequently, there is—in principle at least—no unique impedance which could be considered as the surface impedance Z_s of the earth/atmosphere interface.

The above results have been obtained on the assumption that the wave inside the earth is plane. As a consequence, the components of field vectors in the atmosphere should change along the surface of the earth all in exactly the same manner as described by the expression $\exp(-j\gamma_{ex}x - j\gamma_{ey}y)$. In the case of radio-wave propagation, the field structure in the atmosphere

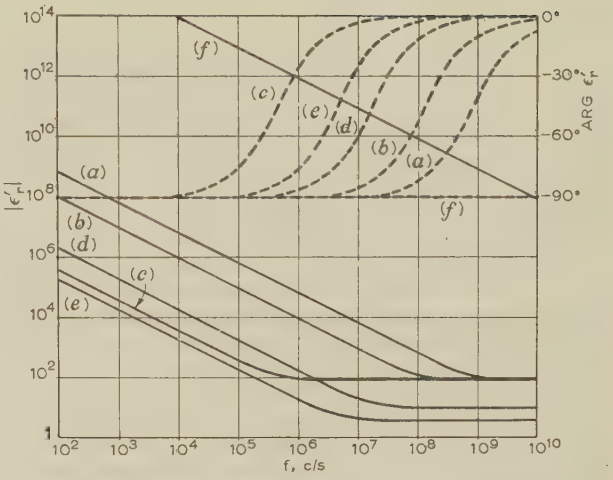

Fig. 3.—Complex relative permittivity, ϵ'_r, for typical soils and copper as a function of frequency, f.

—— $|\epsilon'_r|$
---- arg ϵ'_r

	ϵ_r	σ, mhos/m
(*a*) Sea water	80	4
(*b*) Sea water	80	0·6
(*c*) Fresh water	80	2×10^{-3}
(*d*) Wet ground	10	0·01
(*e*) Dry ground	4	0·001
(*f*) Copper	~1	$5{\cdot}5 \times 10^7$

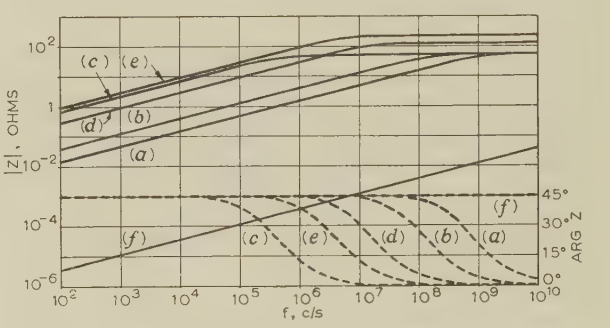

Fig. 4.—Intrinsic impedance, Z, for typical soils and copper as a function of frequency, f.

—— $|Z|$
---- arg Z
(*a*)–(*f*) as in Fig. 3.

is not so simple. The wavelength in the atmosphere, however, is approximately equal to the wavelength in free space, λ_0; consequently γ_{ax}, γ_{ay} and, because of the continuity of tangential components, γ_{ex}, γ_{ey} are of the same order of magnitude as γ_0. We find thus that g_x, g_y are of the order of magnitude of $(\epsilon'_{re}\mu_{re})^{-1/2}$; as follows from Fig. 3, they are generally very small. As a first approximation we may, therefore, assume $g_x = g_y = 0$. This is equivalent to the assumption that the surface of the earth is a plane of constant phase and amplitude and that the waves in the atmosphere and inside the earth are homogeneous plane waves propagating perpendicularly to the earth's surface. As mentioned in Section 3, the surface of the earth shows, in this approximation, a surface impedance equal to the earth's intrinsic impedance. Assuming $\mu_{re} = 1$ we obtain from eqns. (13) and (11)

$$Z_s = Z_e = (\mu_0/\epsilon'_e)^{1/2} = Z_0/(\epsilon'_{re})^{1/2} \quad . \quad . \quad . \quad (22)$$

These are the so-called approximate boundary conditions of Leontovich. We have formulated them in terms of the surface

impedance. Later, in Sections 4.4 and 6.1, we shall give the alternative original expressions.

Under the assumed approximations the field inside the earth may be represented by two homogeneous plane waves propagating perpendicularly to the surface. The electric and magnetic vectors of both waves are mutually perpendicular; their magnitudes and phases depend on the properties of the field above the surface. Consequently, in the general case the field inside the earth is an elliptically polarized plane wave.

The first critical investigation of the approximations underlying the boundary conditions of Leontovich was made by Rytov.[39] He not only discussed the case of a homogeneous conductor with a plane surface but also the cases of inhomogeneous conductors and curved surfaces. He used a perturbation method, taking as the starting-point the field over a perfectly-conducting body of the same shape. The fields outside and inside the conductor he expanded in series according to ascending powers of a small parameter, δ, the depth of penetration of electromagnetic waves into the conductor. For $\delta \to 0$, it is sufficient to consider the zero-order terms only. The outside field is then the same as over a perfect conductor, and the inside field is a wave in agreement with the assumptions of Leontovich. Since it is a perturbation method, its success depends on the difference between the zero-order solution (field over a perfect conductor) and the final solution. In most problems of radio-wave propagation over a real earth this difference is very large and the method is not a convenient one. Some of Rytov's conclusions are, nevertheless, of a fundamental character; they were summarized later by Leontovich[10] as follows:

> The conditions for the application of approximate boundary conditions (of Leontovich) for absorbing bodies are the following: The depth of penetration of the wave into the body (δ) and the wavelength inside it (λ) should be small as compared with the wavelength in the surrounding space (λ_0), the distance to the sources of the field, and the radii of the curvature of the surface of the body. The changes of ϵ' inside the body along the distance of a wavelength λ (or pentration depth δ) should be small.

Fig. 5 gives the curves of λ, δ and λ_0 for typical soils and copper as functions of frequency.

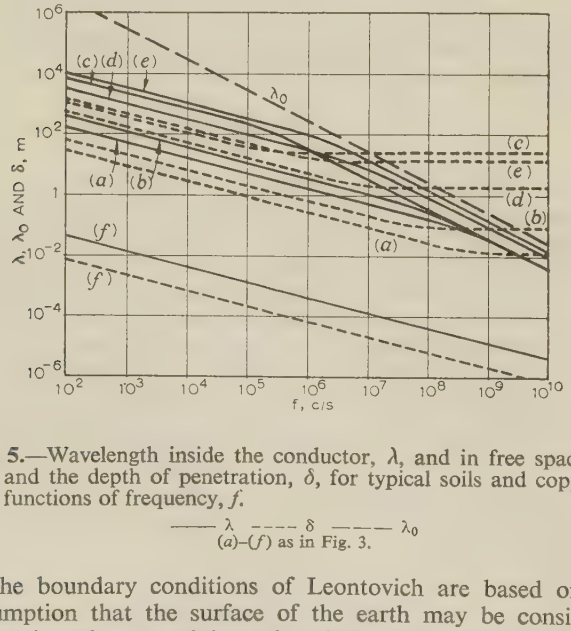

Fig. 5.—Wavelength inside the conductor, λ, and in free space, λ_0, and the depth of penetration, δ, for typical soils and copper as functions of frequency, f.

—— λ ---- δ ——— λ_0
(*a*)–(*f*) as in Fig. 3.

The boundary conditions of Leontovich are based on the assumption that the surface of the earth may be considered approximately as equiphase, i.e. that the changes of the field along it may be approximately disregarded. Any improvement of boundary conditions must, consequently, take into accou the changes of the field along the earth's surface. Accordi to the remarks in Section 3 it is sufficient to consider the chan of the field over comparatively small areas with dimensions the order of λ; these changes are, in general, very sma Expanding the field components in series we may therefo retain the terms of first order only. The comparison of the expressions with an exponential function will then give 'effective' values for γ_x, γ_y.

As an example we shall consider the field produced over homogeneous and flat earth with $\mu_{re} = 1$ by a vertical dipo situated above the surface of the earth. We orient the x-, y- a z-axes as indicated at the beginning of Section 4.1; the axis the dipole coincides with the z-axis. We shall consider t propagation of the wave along the x-axis. If the angle whi the wave normal makes with the surface of the earth (with t x-axis) is ψ, then $\gamma_{ax} \simeq \gamma_0 \cos\psi$, $\gamma_{ay} = 0$; also, because of t continuity of tangential components, $\gamma_{ex} \simeq \gamma_0 \cos\psi$, $\gamma_{ey} =$ The only tangential components of the field are E_x, H_y; cons quently the wave inside the earth is a transverse magnetic wa Eqn. (18) then gives

$$Z_{xy} = \frac{E_{ax}}{H_{ay}} = -Z_e(1-g_x^2)^{1/2} \simeq -Z_e\left(1-\frac{\cos^2\psi}{\epsilon'_{re}}\right)^{1/2}$$

$$= -\frac{Z_0}{\left(\dfrac{\epsilon'^2_{re}}{\epsilon'_{re}-\cos^2\psi}\right)^{1/2}} \simeq -\frac{Z_0}{(\epsilon'_{re}+\cos^2\psi)^{1/2}} \quad . \quad (2$$

The change of sign in eqn. (23) compared with eqn. (22) because the reference directions are different: inside the ea for eqn. (22), and outside for eqn. (23). In this improv approximation, Z_{xy} depends on the properties of the field the atmosphere. Consequently it is not characteristic of t surface alone and we may regard it as the surface impeda in such cases only when we are sure that the structure of t field (i.e. the coefficients γ_x, γ_y) over the considered area sufficiently close to the structure assumed as the basis wh calculating Z_{xy}.

Comparison of eqns. (22) and (23) shows that the improveme consists in the introduction of a factor $(1-g_x^2)^{1/2}$ and, as consequence, in replacing

$$\epsilon'_{re} \text{ by } \left(\frac{\epsilon'^2_{re}}{\epsilon'_{re}-\cos^2\psi}\right) \quad . \quad . \quad . \quad . \quad (2$$

or, approximately, ϵ'_{re} by $(\epsilon'_{re}+\cos^2\psi)$ . . . . . (2

The approximate formula (25) has been obtained previously Soviet scientists by a different method (cf. Feinberg's discu sion,[14] pp. 95 and 96); it also follows from eqn. (5) of Monteath paper.[2] The exact formula (24) has been derived recently different methods by Petrovsky and Feinberg,[24] and Bass. The present derivation shows very clearly the physical sense the approximations underlying formulae (24) and (25). T fundamental approximation consisted in our case in assumi $\gamma_{ax} \simeq \gamma_0 \cos\psi$, $\gamma_{ay} = 0$. This is equivalent, in fact, to t assumption that the wave over the earth's surface is a hom geneous plane wave propagating at the grazing angle ψ.

As can be seen from Fig. 3, the replacement of ϵ'_{re} by t coefficients according to formulae (24) and (25) represents many cases a completely negligible change. In such cases w may use first-order approximation, i.e. the surface impedan according to eqn. (22).

As follows from eqns. (22) and (23), the Z_{xy} impedance ma differ considerably from the intrinsic impedance Z_e in suc cases only when $g_x = \gamma_{ex}/\gamma_e$ is large. If there are no singularit

or rapid changes of the field in the atmosphere, then, as we found previously, g_x is of the order of magnitude of $(\epsilon'_{re})^{-1/2} = [\epsilon_{re} - j\sigma_e/(\omega\epsilon_0)]^{-1/2}$. This expression is large only if the conductivity is small and the frequency high (see Fig. 3). In such cases we must use for the impedance the more complicated expression of the type of eqn. (23), i.e. we must consider the dependence of the impedance on field structure. The failure of the simple equation (22) in such cases may be explained physically by the change of electric properties of the earth. For low frequencies it has the character of a comparatively good conductor $[\epsilon_{re} \ll \sigma_e/(\omega\epsilon_0)]$; for high frequencies it behaves like a dielectric $[\epsilon_{re} > \sigma_e/(\omega\epsilon_0)]$. For high frequencies the propagation coefficient of the earth is not much larger than that of the atmosphere and the wavelength inside the earth is not much smaller than that in the atmosphere; at the same time the ratio of the depth of penetration to wavelength increases with frequency (see Fig. 5). Consequently for high frequencies the great difference between the electrical properties of the earth and the atmosphere which existed at lower frequencies vanishes, but just this difference made it possible to introduce the approximate boundary conditions of eqn. (22).

The coefficient g_x may also be large where the field shows exceptionally rapid changes, e.g. in the immediate neighbourhood of the sources of radiation, or very near a pronounced irregularity or an abrupt change of electrical properties of the earth's surface. In such cases the impedance will certainly change from point to point. When considering it we are faced with two essential difficulties. First, the impedances will depend on the structure of the field, which will be known only after solving the whole problem. Secondly, serious doubts may arise with regard to the simple formulae of the type of eqn. (23). The fundamental basis was there the assumption that the field in the atmosphere may be approximated locally by an exponential expression, i.e. replaced locally by a plane wave; in such a case the wave inside the earth may be also approximated by a plane wave. When the changes of the field in the atmosphere along a distance of the order of a wavelength in the earth become large, the whole previous approximation is doubtful and a more rigorous approach seems necessary [see Monteath[2] eqn. (5), and Bass[25] eqn. (7)].

In the immediate neighbourhood of the sources of radiation an additional difficulty appears in connection with the failure of the conventional method used for the evaluation of the surface integrals of the type found in eqn. (6). In this method the shape of Fresnel zones is described by an approximate formula which fails in the vicinity of the transmitter and receiver. At present there is only an indirect answer to this problem based on a number of investigations[8, 9, 11, 26, 14] of the propagation of radio waves produced by a vertical dipole over a homogeneous earth. The authors used conventional approximations for the shape of Fresnel zones and assumed surface impedance to be constant over the whole surface of the earth. The results which they obtained were equivalent to the results of a rigorous analysis. This seems to indicate that—at least for the vertical dipole—the errors of the conventional surface-impedance method in the immediate neighbourhood of the transmitting and receiving aerials are not very important.

If the field inside the earth be replaced, as previously, by one or by two plane waves (transverse electric and transverse magnetic) with the same propagation coefficients then the changes of all components of field vectors along the surface of the earth are described by the same coefficients γ_x, γ_y. In the majority of practical cases the structure of the field is, however, more complicated. An example of such a field is shown in Fig. 6. The resultant field at the point A is composed of the primary field E_a^0, H_a^0 and the secondary field E_a^s, H_a^s. This latter is produced by some inhomogeneity or irregularity

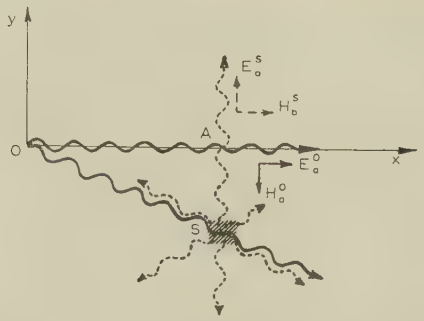

Fig. 6.—Resultant field as a superposition of the primary and the secondary fields.
——→ Primary wave.
- - - - → Secondary wave.

in the earth's surface existing at the point S. The primary field at A is propagating along the x-axis showing the propagation coefficients $\gamma_x \simeq \gamma_0$, $\gamma_y = 0$. The secondary field at A is propagating parallel to the y-axis, its propagation coefficients being $\gamma_x = 0$, $\gamma_y \simeq \gamma_0$. Consequently the components of the resultant field at A show the following propagation coefficients:

$$\begin{array}{llll} E_{ax}(= E_a^0) & \gamma_x \simeq \gamma_0, & \gamma_y = 0 \\ E_{ay}(= E_a^s) & \gamma_x = 0, & \gamma_y \simeq \gamma_0 \\ H_{ax}(= H_a^s) & \gamma_x = 0, & \gamma_y \simeq \gamma_0 \\ H_{ay}(= -H_a^0) & \gamma_x \simeq \gamma_0, & \gamma_y = 0 \end{array}$$

In the general case of a real earth the resultant field is a superposition of the primary field and a number of secondary fields produced by all inhomogeneities and irregularities of the earth's surface. As a consequence, each component of field vectors may show different propagation coefficients γ_x, γ_y. In such cases we may disregard the field changes altogether, assume approximately $\gamma_x = \gamma_y = 0$ and use the approximate boundary conditions of Leontovich. Or we may try to improve the analysis by expanding the field inside the earth in a number of plane waves; the analysis becomes, however, very involved.

The improvements of approximate boundary conditions must always be considered in connection with the properties of the real earth. As we shall show later the inhomogeneity and irregularity of the earth's surface may change the structure of the field inside the earth profoundly. In such cases all previously discussed improvements of boundary conditions may be completely meaningless.

(4.2) Surface Impedance in the Case of an Earth Composed of Parallel Layers

The real earth exhibits very complex and random inhomogeneity, partly because of its complicated geological structure, partly as a result of human activity. This has three consequences. First, it makes the theoretical analysis extremely difficult. Even such a comparatively simple case as plane-wave propagation in a parallel-stratified medium with continuously-changing parameters has not yet found a general and rigorous solution. Consequently a rigorous mathematical analysis of the much more complicated problem of the real earth seems practically hopeless. Secondly, the earth's inhomogeneity is the cause of casual fluctuations of the amplitude and phase of the field vectors in the atmosphere. The knowledge of such field fluctuations is in most practical applications not necessary. Thirdly, the analytical expressions describing the changes of electrical properties of the earth from point to point are in most cases unknown, and there is hardly any hope that they will ever be known. Because of all these reasons it is necessary to

keep a judicious balance between the rigours of analysis, the introduced simplifications and practical needs.

The simplest case of an inhomogeneous earth is a flat earth composed of a number of homogeneous parallel layers; for all of them we assume $\mu_r = 1$. As in Section 4.1, we take the earth's surface as the xy-plane; the z-axis is upwards.

The electromagnetic field inside any of the layers consists of a transmitted and a reflected wave. Such waves may be always represented by an appropriate sum of a number of plane waves. According to our previous remarks it seems admissible to simplify the analysis by approximating the real field by a set of homogeneous plane waves propagating perpendicularly to the boundaries of the layers, i.e. parallel to the z-axis. For such waves the field vectors are parallel to the xy-plane. They are mutually perpendicular and their ratio is equal to the intrinsic impedance of the layer ($E_e/H_e = Z_e$). The resultant field just under the surface of the earth is a superposition of a transmitted (E_e^t, H_e^t) and a reflected (E_e^r, H_e^r) wave. Each of these waves may be resolved into two waves with the components E_x, H_y and E_y, H_x; both behave in exactly the same manner. We assume, therefore, for simplicity that the transmitted wave has components E_{ey}^t, H_{ex}^t only. The components of the reflected wave are then $E_{ey}^r = \zeta E_{ey}^t$, $H_{ex}^r = -\zeta H_{ex}^t$, where the complex factor ζ may be regarded as the reflection coefficient from the interior of the earth; it is, of course, $|\zeta| < 1$.

Adding the transmitted and reflected waves and taking into account the continuity of tangential components of field vectors we obtain the surface impedance Z_s:

$$Z_s = \frac{E_{ay}}{H_{ax}} = \frac{(1+\zeta)E_{ey}^t}{(1-\zeta)H_{ex}^t} = \frac{1+\zeta}{1-\zeta}Z_{e,1} = \frac{1+\zeta}{1-\zeta}\frac{Z_0}{(\epsilon'_{re})_1^{1/2}} \quad . \quad (26)$$

The subscript 1 denotes the intrinsic impedance of the first (top) layer. According to eqn. (26) the surface impedance does not depend on the properties of the field in the atmosphere; consequently eqn. (26) constitutes a generalization of eqn. (22). The errors and limits of application of eqn. (26) may be estimated in the same manner as before in the case of homogeneous soil.

The result obtained shows that, as regards the surface impedance, there is no essential difference between a homogeneous and a parallel-stratified earth. The same is true with respect to the propagation of radio waves; this follows directly from eqns. (6) and (8). In fact, let us take as S_1 a stratified earth and as S_2 a homogeneous earth. The field over the stratified earth is the same as over the homogeneous one if the surface integral (8) vanishes; this takes place when $E_{1t}/H_{1t} = E_{2t}/H_{2t}$, i.e. when the surface impedance of the stratified earth is the same as that of the homogeneous earth.*

We may therefore replace the stratified earth formally by a homogeneous one with the same surface impedance Z_s. The electric parameters of the latter may be then called the effective parameters of the stratified earth; we shall denote them by $(\epsilon'_{re})_{ef}$, $(\epsilon_{re})_{ef}$, $(\sigma_e)_{ef}$. According to eqns. (22) and (26),

$$Z_s^2 = \left(\frac{1+\zeta}{1-\zeta}\right)^2 \frac{Z_0^2}{(\epsilon'_{re})_1} = \frac{Z_0^2}{(\epsilon'_{re})_{ef}} \quad . \quad . \quad . \quad (27)$$

and thus

$$(\epsilon'_{re})_{ef} = (\epsilon_{re})_{ef} - j\frac{(\sigma_e)_{ef}}{\omega\epsilon_0} = \left(\frac{Z_0}{Z_s}\right)^2$$

$$= \left(\frac{1-\zeta}{1+\zeta}\right)^2 (\epsilon'_{re})_1 = \left(\frac{1-\zeta}{1+\zeta}\right)^2 \left[(\epsilon_{re})_1 - j\frac{(\sigma_e)_1}{\omega\epsilon_0}\right] \quad . \quad (28)$$

* The above condition should be fulfilled over the whole surface of the earth, i.e. also in the immediate neighbourhood of the sources of radiation where the field shows very rapid changes. The corresponding changes of impedance for the homogeneous and the stratified earth may be different, but in view of the discussion in Section 4.1 this will probably have no essential influence on the field.

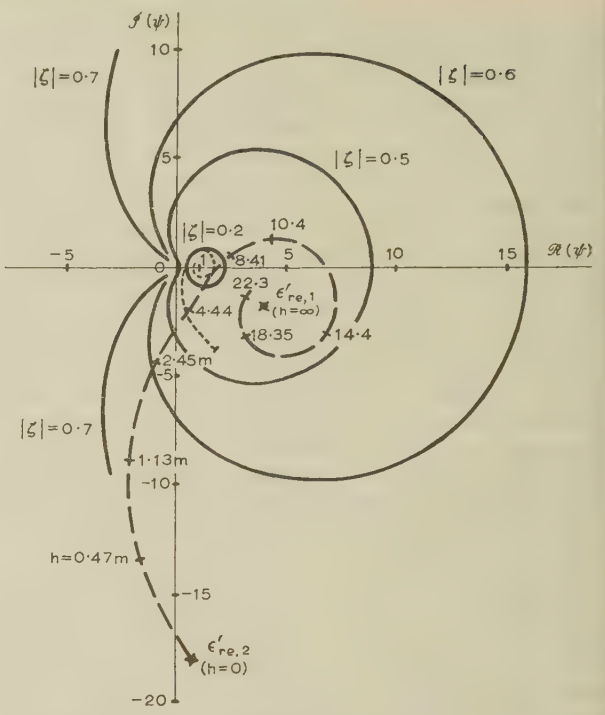

Fig. 7.—Effective electric parameters of a stratified soil as functions of the intensity of the reflected wave.

—— Polar diagrams of the coefficient $\psi = (1-\zeta)^2/(1+\zeta)^2$ for $|\zeta|$ = parameter
The top layer, h metres thick, is fresh water ($\epsilon_{r1} = 80$, $\sigma_1 = 2 \times 10^{-3}$ mhos/m). The bottom layer is wet ground ($\epsilon_{r2} = 15$, $\sigma_2 = 2 \times 10^{-2}$ mhos/m).
---- Polar diagram of $\psi = F(h)$.
– – – Polar diagram of $(\epsilon'_{re})_{ef} = F(h)$ reduced in size 20 times.

In Fig. 7 the solid lines show polar diagrams of $\psi = (1-\zeta)^2/(1+\zeta)^2$ with $|\zeta|$ as the parameter. When the reflected wave is strong ($|\zeta|$ large) the effective complex permittivity $(\epsilon'_{re})_{ef} = \psi \cdot (\epsilon'_{re})_1$ may differ considerably from $(\epsilon'_{re})_1$ as regards both its phase and amplitude. This means that the effective permittivity $(\epsilon_{re})_{ef}$ and the effective conductivity $(\sigma_e)_{ef}$ may both be markedly different from the parameters of the top layer $(\epsilon_{re})_1$, $(\sigma_e)_1$; they may be even negative.

As an example, the dotted lines in Fig. 7 show the polar diagrams of ψ and $(\epsilon'_{re})_{ef}$ for a certain case of a 2-layer earth. The surface impedance may be computed according to the well-known formula for the input impedance of a stratified medium (see, for instance, References 41, 42, 43):

$$Z_s = Z_{e1}\frac{Z_{e2} + Z_{e1}\tanh(j\gamma_{e1}h)}{Z_{e1} + Z_{e2}\tanh(j\gamma_{e1}h)} \quad . \quad . \quad . \quad (29)$$

where h denotes the thickness of the top layer and subscripts 1, 2 refer to the top layer and the underlying ground, respectively.

The diagram of $(\epsilon'_{re})_{ef} = f(h)$ from Fig. 7 is a spiral which starts, for $h = 0$, from the point $(\epsilon'_{re})_{ef} = (\epsilon'_{re})_2$ (the earth is then homogeneous with the parameters of the underlying ground). For $h \to \infty$ this spiral winds around the point $(\epsilon'_{re})_1$ as a consequence of the diminishing intensity of the reflected wave caused by the attenuation inside the top layer. From Fig. 7 and eqn. (28), there are certain thicknesses of the top layer for which $(\epsilon_{re})_{ef}$ or $(\sigma_e)_{ef}$ are negative, or $(\epsilon_{re})_{ef}$ is positive but larger than that for pure water, i.e. larger than is possible for any homogeneous soil constituent. We thus see that the effective electric parameters of a stratified earth are certain formally introduced quantities only, essential for the problem of radio-wave propagation but not representing any conventionally averaged parameters of the stratified medium.

The results obtained are confirmed by experiments of Grosskopf[44–46], who measured the effective electric parameters by the wave-tilt method and in a number of cases found negative values of $(\epsilon_{re})_{ef}$ or $(\sigma_e)_{ef}$.

The amplitude and phase of the reflected wave depend on the reflection coefficients from the boundaries between the layers and on the phase velocity and attenuation factor inside the layers, which change with frequency. Consequently the effective electric parameters of a stratified soil are not constant but also change with frequency.

Conversely there arises a possibility of determining the structure of a stratified earth from the measurements of the frequency characteristics of the effective parameters. We shall discuss it in Section 8.

A parallel-stratified earth with continuously changing properties may be considered as the limiting case of an earth composed of n homogeneous layers when $n \to \infty$. As a result, the physical phenomena and the general conclusions for continuously-changing properties are the same as for the earth composed of only a few homogeneous layers. Mathematical analysis becomes, however, very involved and rigorous solutions have been found only in certain comparatively simple cases. An excellent review of the problem has been given recently by Brekhovskikh.[43]

The whole previous discussion shows that in the case of a stratified earth the effective electric parameters may be used for the calculation of the so-called numerical distance in exactly the same manner as ordinary parameters in the case of a homogeneous earth.

The problem of radio-wave propagation over stratified earth has been investigated by a number of authors; for details we refer to the original papers.[41, 42, 44, 47–57]

(4.3) Surface Impedance in the Case of a Curved Surface

The wave inside the earth may be thought of as being generated by radiation sources distributed over its surface; the properties of this wave depend, consequently, on the shape of earth's surface and on the field distribution over it. As follows from our previous discussion, the wavelength λ_e in the earth serves as a reference distance. Consequently, if the surface of the earth differs from a plane by much less than λ_e over an area with dimensions of the order of λ_e (i.e. if the radii of curvature of the surface are much larger than λ_e) then the structure of the field inside the earth is approximately the same as in the case of a plane earth. This conclusion is in agreement with the remarks of Leontovich quoted in Section 4.1. We thus see that all previous results for a plane earth may be extended to the cases of a spherical or not too irregular surface. Because of this we shall often assume for simplicity in the following Sections the earth's surface to be plane.

As we shall show later the structure of the field just above the surface is determined by the properties of the field inside the earth. Thus a normal to the earth's surface, and not the direction of the vertical, serves as a reference direction for the fields. This conclusion is in agreement with the results of the measurements of the wave tilt in rolling country.[58–60]

Fundamental difficulties arise in the case of sharp irregularities in the earth's surface, such as jagged rocky mountains, etc. Neither of the premisses which are essential for the introduction of approximate boundary conditions are then fulfilled: the radii of curvature of the surface are not much larger than λ_e, and the field in the atmosphere in the neighbourhood of such irregularities shows rapid variations. Consequently, it is not possible to use the concept of surface impedance in such cases, or when using it we must expect considerable errors.

(4.4) Approximate Boundary Conditions for the Hertzian Vector and Hertzian Scalar Function

The boundary conditions for field vectors in the form of surface impedance are useful when using integral equations of the type of eqn. (6). When adopting a different mathematical approach it is necessary to use other formulations of boundary conditions. The approximate boundary conditions for electric force, $\boldsymbol{E}$, Hertzian vector, $\boldsymbol{\Pi}$, and Hertzian scalar function, Π, have been derived previously[7, 8, 10, 13, 14, 24, 25] without any reference to the surface-impedance concept. We shall discuss now the approximate boundary conditions for $\boldsymbol{\Pi}$ and Π in a different manner, using surface impedance as the starting-point. Thus a common basis will be provided and it will not be necessary to repeat the whole discussion. The approximate boundary conditions for $\boldsymbol{E}$ take the form of a partial derivative along the direction of a normal, i.e. the form of a height/gain function; they will be discussed in Section 6.1.

We start with approximate boundary conditions for the electric Hertzian vector $\boldsymbol{\Pi}$. We consider a plane earth, not necessarily homogeneous, surrounded by a homogeneous atmosphere with $\epsilon_a = \epsilon_0$; a vertical dipole is the source of radiation. We introduce cylindrical co-ordinates z, r, ϕ and choose the earth's surface as the r, ϕ plane. The z-axis we direct towards the atmosphere with the dipole situated on it. We assume that the field may be described by means of the vector $\boldsymbol{\Pi}$ parallel to the z-axis, i.e. by the Π_z component only. Outside the sources the field vectors are determined by the relations $\boldsymbol{E} = \operatorname{curl}\operatorname{curl}\boldsymbol{\Pi}$, $\boldsymbol{H} = j\omega\epsilon_0 \operatorname{curl}\boldsymbol{\Pi}$. Substituting it in the expressions for the field impedances at the surface of the earth ($Z_{r\phi} = E_r/H_\phi$, $Z_{\phi r} = -E_\phi/H_r$) we obtain

$$\left.\begin{aligned} \frac{\partial}{\partial r}\left(\frac{\partial \Pi_z}{\partial z}\right) &= -j\omega\epsilon_0 Z_{r\phi}\frac{\partial \Pi_z}{\partial r} \\ \frac{\partial}{\partial \phi}\left(\frac{\partial \Pi_z}{\partial z}\right) &= -j\omega\epsilon_0 Z_{\phi r}\frac{\partial \Pi_z}{\partial \phi} \end{aligned}\right\} \quad . \quad . \quad . \quad (30)$$

The simplest case is that of a homogeneous or parallel-stratified earth. The field is then axially symmetrical, $\partial\Pi_z/\partial\phi = 0$, and only the first of eqns. (30) need be considered. The impedance $Z_{r\phi}$ is approximately constant except in the immediate neighbourhood of the transmitting aerial; we will consider it as constant for all values of r (cf. remarks in Section 4.1). Putting $Z_{r\phi} = -Z_s$ we obtain

$$\partial\Pi_z/\partial z = j\omega\epsilon_0 Z_s \Pi_z \quad . \quad . \quad . \quad . \quad (31)$$

On substituting for Z_s from eqn. (22) this reduces to

$$\frac{\partial \Pi_z}{\partial z} = \frac{j\gamma_0}{(\epsilon'_{re})^{1/2}}\Pi_z \quad . \quad . \quad . \quad . \quad . \quad (32)$$

This is the final form of approximate boundary conditions for Π_z for a homogeneous earth. An improvement might be achieved by using eqn. (23) instead of eqn. (22) for Z_s.

In the general case of an inhomogeneous plane earth the use of a vertical Hertzian vector represents only an approximation. First, the formula $\boldsymbol{H} = j\omega\epsilon_0 \operatorname{curl}\boldsymbol{\Pi}$ always gives $H_z = 0$. Secondly, in a general case the impedances $Z_{r\phi}$ and $Z_{\phi r}$ may be different (cf. Section 5); eqns. (30) then reduce to different expressions for $\partial\Pi_z/\partial z$.

In the case of a homogeneous spherical earth we introduce a radial Hertzian vector $r\Pi$; Π is the so-called scalar Hertzian function. A similar reasoning gives for Π the same boundary condition as before according to eqn. (31)

$$\partial\Pi/\partial r = j\omega\epsilon_0 Z_s \Pi \quad . \quad . \quad . \quad . \quad . \quad (33)$$

In the general case of an inhomogeneous spherical earth the same difficulties appear as in the case of an inhomogeneous plane earth.

(5) SURFACE IMPEDANCE IN THE GENERAL CASE OF AN ARBITRARILY INHOMOGENEOUS EARTH

(5.1) The Case of Oblique Stratification

As the introduction to the general case of an inhomogeneous earth, we shall consider now a plane earth with oblique stratification (Fig. 8); the earth's surface is the xy-plane and a radio wave propagates over it; in Fig. 8 it is indicated by rays 1, 2.

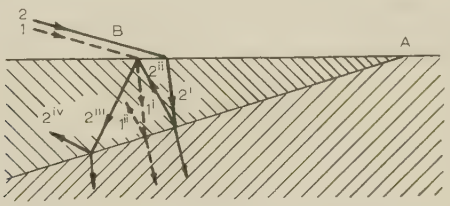

Fig. 8.—Field configuration in the case of oblique stratification.

The problem as outlined above represents a very complicated case of diffraction by a wedge. In the immediate neighbourhood of the edge of the wedge, A, the structure of the field is certainly very complex, but at some distance from A, for instance at B, we may try to represent the field in the earth approximately by a number of plane waves propagating according to geometrical optics. Theoretically multiple reflections appear; because of rapid attenuation of the waves inside the earth we may take into account the strong waves only (waves 2^{ii} and 2^{iii}) and disregard all following reflections (waves 2^{iv}, etc.). The structure of the field inside the earth, and thus the impedances Z_{xy}, Z_{yx}, depend on the superposition of a number of plane waves (transmitted wave 1^{i} and reflected waves 2^{ii}, 2^{iii}). With increasing distance from A the intensity of reflected waves decreases. At the same time the phase difference between the transmitted wave 1^{i} and reflected waves 2^{ii}, 2^{iii} is changing. As a consequence Z_{xy}, Z_{yx} change from point to point. At some distance from A the reflected waves become so weak that they may be disregarded completely. Z_{xy}, Z_{yx} then have values characteristic of a homogeneous earth. We thus see that the changes in impedances are limited to the comparatively small part of the earth's surface in the immediate neighbourhood of the place where the oblique layer meets it.

The impedances depend on the frequency in the same way as for a parallel-stratified earth; they depend also on the direction of wave propagation above the surface. There are three factors which contribute towards it. First, the direction of the propagation of transmitted waves (waves 1^{i} and 2^{i}) is not fixed. However, the transmitted waves propagate in most cases almost exactly perpendicularly and consequently this will not be, in general, of great practical importance. Secondly, the field inside the earth is formed as the superposition of waves travelling along paths of different length. The difference of the path lengths and thus the phase difference between these waves, and consequently also the values of the impedances, depend on the direction of wave propagation above the surface. Thirdly, the reflection coefficient from the oblique boundary and the geometrical configuration of field vectors in the waves 1^{i}, 2^{ii}, 2^{iii} depend on the state of polarization of the waves with respect to the boundary, and consequently on the direction of propagation above the surface.

We thus see that the impedances depend on the properties of the field in the atmosphere. Moreover, as a consequence of the third factor, Z_{xy} may be different from Z_{yx}. As a result there is no unique value of impedance which could be regarded as the surface impedance at the considered point of the earth's surface. These conclusions find confirmation in the results of measurements of the shape of the ellipse of polarization over inhomogeneous earth;[46] we shall return to it in Section 7.

In the case of an oblique stratification with a continuous instead of an abrupt change of electric parameters, the physical phenomena and the conclusions are essentially the same. The only difference is that the changes of the field in the immediate neighbourhood of A in Fig. 8 are more gradual.

(5.2) The General Case of an Arbitrarily Inhomogeneous Earth

In the general case of an arbitrarily inhomogeneous earth the structure of the wave inside the earth is very complex. It is then impossible to approximate to the field by one or a few plane waves and analysis becomes very involved. Consequently it is necessary to introduce serious approximations; however, it is often difficult to estimate the limits of application and the accuracy of final formulae.

Some results for an inhomogeneous earth may be found in Rytov's paper.[39] However, his formulae take into account the influence of horizontal stratification only and disregard changes of electric parameters along the surface of the earth. The problem of an inhomogeneous earth has also been investigated by Feinberg; we shall discuss it shortly in Section 6.1.

Taking as a basis the discussion of oblique stratification we may formulate the following general conclusions for the case of an arbitrarily inhomogeneous earth:

(*a*) The impedances Z_{xy}, Z_{yx} may change over the earth's surface from point to point.

(*b*) The impedances may differ considerably from the value characteristic of a homogeneous soil of the same electric properties as that of the surface layer.

(*c*) The impedances Z_{xy} and Z_{yx} may be different and may depend on the direction of propagation of radio waves above the surface; thus it may be impossible to characterize the earth's surface by a uniquely determined surface impedance.

(*d*) The effective electric properties of the earth may be a function of frequency.

When the changes of electric parameters are very gradual, the earth may be considered locally as homogeneous. According to Leontovich (see Section 4.1) the condition is that the relative changes of electric parameters of the soil along a distance λ be small.

In the case of gradual changes of electric properties there appear in the earth additional distributed currents and charges. A discontinuous change of electric properties may be considered as the limiting case of gradual changes when the thickness of the transition zone decreases towards zero. The distributed charges and currents are then compressed into line or surface charges and currents, i.e. into certain discrete secondary sources of radiation which produce corresponding secondary fields. In the existing theoretical investigations these discrete secondary sources have always been disregarded, but they may be of some importance. The discrete secondary fields show singularities; consequently they change the field considerably in the immediate vicinity of the discontinuity. Moreover, as discussed in Section 4.1, this fact changes the impedances over the whole neighbourhood. The picture is thus quite different from the situation when, for instance, two areas are assumed with different but constant surface impedances and no secondary sources are taken into account at the discontinuity.

Similar phenomena appear in the case of gradual changes of electric properties, only the effect is not so pronounced. The

; the physical background for changes of field and impedances
t the inhomogeneities of the earth's surface.

The above discussion shows qualitatively that inhomogeneities
f the earth's surface may act as secondary sources of radiation;
ıe same conclusion follows formally from eqns. (6) and (7).
Consequently the field at some point of the surface is, in general,
superposition of the primary field produced by the primary
ource of radiation and a number of secondary fields produced
y inhomogeneities of the surface (cf. Fig. 6). The resultant
eld may thus possess field components not present in the
rimary wave.

(6) THE HEIGHT/GAIN FUNCTION

(6.1) The Height/Gain Function for Points immediately above the Earth's Surface

When considering field structure just above the earth's surface
ve may assume for simplicity a homogeneous atmosphere with
$_a = \epsilon_0$. The field in the atmosphere then satisfies the equations

$$\text{div } E_a = 0, \text{ curl } H_a = j\omega\epsilon_0 E_a \quad . \quad . \quad . \quad (34)$$

We assume for simplicity a plane earth and choose a rectangular
ystem of co-ordinates so that the earth's surface is the xy-plane
nd the z-axis is directed towards the atmosphere. Introducing
he impedances $E_{ax}/H_{ay} = Z_{xy}$, $E_{ay}/H_{ax} = -Z_{yx}$ we obtain
rom the first of eqns. (34)

$$\frac{\partial E_{az}}{\partial z} = -Z_{xy}\frac{\partial H_{ay}}{\partial x} + Z_{yx}\frac{\partial H_{ax}}{\partial y} - H_{ay}\frac{\partial Z_{xy}}{\partial x} + H_{ax}\frac{\partial Z_{yx}}{\partial y} \quad . \quad (35)$$

n the case of homogeneous or parallel-stratified earth,
$Z_{xy} \simeq Z_{yx} \simeq -Z_s =$ a constant. Eqn. (35) and the z-com-
ponent of the second of eqns. (34) then give

$$\partial E_{az}/\partial z = j\omega\epsilon_0 Z_s E_{az} \quad . \quad . \quad . \quad . \quad . \quad (36)$$

On substituting for Z_s from eqn. (22), eqn. (36) reduces to

$$\frac{\partial E_{az}}{\partial z} = \frac{j\gamma_0}{(\epsilon'_{re})^{1/2}} E_{az} \quad . \quad . \quad . \quad . \quad . \quad . \quad (37)$$

Eqn. (37) represents approximate boundary conditions for the
ector E as they were frequently applied in theoretical investiga-
ions; they may be improved in suitable cases by using eqn. (23)
or Z_s instead of eqn. (22). Eqn. (37) is at the same time an
xpression for the height/gain function for small heights above
he earth's surface.

In the general case of an inhomogeneous earth, $\partial E_{az}/\partial z$
epends on the local properties of the soil in a complicated
nanner, as shown by eqn. (35). However, if the changes in
lectric parameters of the earth in the horizontal direction are
ery gradual then, according to Section 5.2, the impedances are
pproximately the same as those given by the formulae for a
omogeneous or horizontally stratified earth. Consequently we
ut, as before, $Z_{xy} \simeq Z_{yx} \simeq -Z_s$, but now consider Z_s as a
unction of position; this gives

$$\frac{\partial E_{az}}{\partial z} = j\omega\epsilon_0 Z_s E_{az} - \frac{1}{Z_s} E_a \text{ grad } Z_s \quad . \quad . \quad . \quad (38)$$

Let us consider a special case when the electric properties of
he earth are constant in a vertical direction but are changing
lowly in a horizontal one (i.e. they are functions of x, y only).
On substituting for Z_s from eqn. (22), eqn. (38) reduces to

$$\frac{\partial E_{az}}{\partial z} = \frac{j\gamma_0}{(\epsilon'_{re})^{1/2}} E_{az} + \frac{1}{2\epsilon'_{re}} E_a \text{ grad } \epsilon'_{re} \quad . \quad . \quad . \quad (39)$$

This is eqn. (40.14) in Feinberg's paper;[14] he derived it by
nother method.

(6.2) The Height/Gain Function for Greater Heights

We shall consider the problem of height/gain function for
greater heights from a qualitative point of view only, using the
integral equation (6) as the basis of the discussion. The con-
tributions to the final field from different parts of the earth's
surface are not equally strong. This is mainly the result of
phase relations and may be best visualized by means of the
Fresnel zones[14] (Fig. 9). The parts of the surface which lie

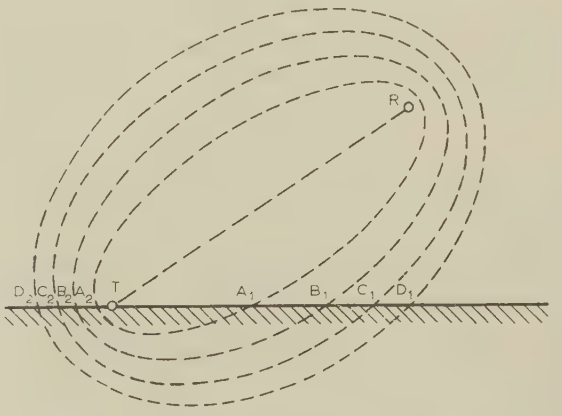

Fig. 9.—Fresnel zones for greater heights of the receiver above the earth's surface.
T Transmitter. R Receiver.

inside the first Fresnel zone, between A_1 and A_2, give contribu-
tions of approximately the same phase; consequently they
interfere constructively and produce a strong field. If we con-
sider, on the other hand, the parts of the surface which lie
outside the first few Fresnel zones we find that they cut the
Fresnel zones at short intervals, at B_1, C_1, D_1, etc. The corre-
sponding field contributions show rapid phase variations, inter-
fere destructively and thus have practically no influence on the
field* at R. Consequently only the points inside the few first
Fresnel zones are of importance for the field at R. With
increasing height of the receiver this area contracts; for great
heights it comprises only the points in the neighbourhood of the
transmitting aerial. Analytically this is clearly a transition
from the diffraction theory for small heights to geometrical-
optical approximation for very large heights.

Whereas for small heights we found that the height/gain
function depends on the local field distribution, for greater
heights it depends on the field distribution over a considerable
part of the earth's surface. It is interesting to note that for
greater heights the height/gain function is influenced not by
the area below the receiver but by a part of the earth's surface
lying closer to the transmitter.[14]

(7) ELLIPSE OF POLARIZATION OF THE FIELD IN THE ATMOSPHERE

As in Section 6.1 we assume a plane earth and a homogeneous
atmosphere with $\epsilon_a = \epsilon_0$. The surface of the earth is the
xy-plane with the z-axis directed towards the atmosphere. The
z-component of the second of eqns. (34) gives

$$j\omega\epsilon_0 E_{az} = \frac{\partial H_{ay}}{\partial x} - \frac{\partial H_{ax}}{\partial y} \quad . \quad . \quad . \quad . \quad (40)$$

For simplicity we assume that the wave propagates along
the x-axis and that $E_{ay} = H_{ax} = 0$. Introducing the surface

* An exception to this general picture is, for instance, a slope of a hill approximately parallel to a corresponding Fresnel zone. Such a slope produces a strong contribution similar to the reflection from a mirror.

impedance $Z_s = -E_{ax}/H_{ay}$ and assuming that $E_{ax} \simeq \exp[-j(\gamma_{ax}x + \xi)]$ we obtain

$$E_{az} = \frac{\gamma_{ax}}{\omega\epsilon_0 Z_s}\left(1 + \frac{1}{\gamma_{ax}}\frac{\partial\xi}{\partial x} - \frac{j}{\gamma_{ax}Z_s}\frac{\partial Z_s}{\partial x}\right)E_{ax} \quad . \quad (41)$$

For a homogeneous or parallel-stratified earth, Z_s = a constant, $\xi \simeq 0$, $\gamma_{ax} \simeq \gamma_0$, and hence

$$E_{ax}/E_{az} = Z_s/Z_0 \quad . \quad . \quad . \quad . \quad . \quad (42)$$

On using for Z_s eqn. (23) ($Z_s = -Z_{xy}$, $\psi = 0$), for a homogeneous earth eqn. (42) reduces to

$$\frac{E_{ax}}{E_{az}} = \frac{(\epsilon'_{re} - 1)^{1/2}}{\epsilon'_{re}} \quad . \quad . \quad . \quad . \quad . \quad (43)$$

This is eqn. (108) in Norton's paper.[61] According to eqn. (43) the electric force is elliptically polarized in a vertical (xz) plane.

In the case of an inhomogeneous earth the shape of the ellipse of polarization as given by eqn. (41) is different from that for a homogeneous earth. Moreover, as the surface impedance Z_s may depend on the direction of wave propagation (cf. Section 5), the shape of the ellipse of polarization also may be different for various directions of propagation. This result is in agreement with experiment. Grosskopf in one of his investigations[46] measured the shape of the ellipse of polarization along a certain inhomogeneous path placing the transmitting aerial first at one end of the path and then at the other. In these two cases he found different shapes of the ellipse of polarization at the same points of the path. The investigated path showed most probably an oblique stratification of the soil.

In the general case of a real earth the inhomogeneities and irregularities of the surface act as secondary sources of radiation; consequently the resultant field may possess field components not present in the primary wave. The tangential components of field vectors may be then elliptically polarized, and not linearly as for a homogeneous earth, and the ellipse of polarization may thus lie in an oblique plane and not in a vertical one. These conclusions are supported by the results of theoretical investigations of coastal refraction by Furutsu[62] and Senior,[63] who found elliptical polarization of tangential components, and by the results of careful measurements of the wave deviation by Pressey, Ashwell and Roberts,[64] who were faced with comparatively strong random secondary fields.

When measuring the shape of the ellipse of polarization we may meet with some difficulties in practice. As discussed in Section 4.3, the normal to the earth's surface and not the vertical serves as a reference direction for the forward tilt; consequently, in rolling country it may sometimes not be easy to determine the angle of the wave tilt experimentally. As suggested by Grosskopf and Vogt,[65, 45] the direct measurement of the axes of the ellipse of polarization may be replaced by an indirect method based on the measurement of angles only. The fundamental assumption with this method is, however, that the tangential component of electric force is linearly polarized; in a general case of an inhomogeneous and irregular earth this condition may be not fulfilled.

(8) PRACTICAL CONCLUSIONS

The problem of effective electric parameters of the earth is of considerable practical importance. In a general case they depend on the structure of the soil, the frequency and the direction of wave propagation. Soil in most cases shows a very random inhomogeneity; the measurements often give markedly different electrical parameters of the earth at comparatively adjacent points.[66, 67, 46] Consequently only suitable averag values are needed for most practical purposes.

In the cases of a homogeneous or parallel-stratified ear the measurement of the shape of the ellipse of polariz tion[44–46, 58–61, 65, 68–73] or the height/gain function for sm heights makes possible the computation of Z_s and thus effective electric parameters [cf. eqns. (36), (37), (42) and (43 In the case of an inhomogeneous earth such simple determinati of local electric parameters is not possible; moreover, it is nece sary to take into account the statistical character of these par meters and to calculate suitable average values.

These effective electric parameters depend on the structure the soil; consequently they show seasonal variations caused the changes in vegetation or in ground-water level, by sno etc.[74–76]

When compiling conductivity maps all these factors, especia the frequency dependence, should be taken into account. seems that a number of problems await solution, both regards theory and methods of measurement.

In the cases of a parallel-stratified earth the shape of t ellipse of polarization and the height/gain function for sm heights depend on the surface impedance, which in turn is function of frequency and soil structure. Conversely, the pos bility arises of determining the local earth structure fro measurements of the frequency dependence of the wa tilt[77, 70, 45, 49] or the height/gain function. It is thus, principle, possible to develop a comparatively simple rad method of geological prospecting.

An obvious limitation of this method is the comparative small depth of penetration of electromagnetic waves into t earth (cf. Fig. 5). Consequently it is possible to investigate this way only the uppermost strata of the earth's crust.

Because of analytical complications and limited accuracy measurements, the practical computations have been made general, on the assumption that the earth is composed of on two homogeneous layers having electric parameters which a independent of frequency. In fact, the changes in electr parameters with depth are generally much more complicate and the parameters show some frequency dependence.[66]

The most fundamental difficulty is, however, caused by t inhomogeneity of the earth's surface in the horizontal directio Consequently, the simple formulae for a homogeneous parallel-stratified earth may be used only if there is reason believe that the structure of the ground is sufficiently hom geneous horizontally, e.g. when at a number of adjacent poin the measurements give approximately the same results. single measurement at an isolated point may be complete meaningless.

As regards the possibility of geological prospecting at great heights above the earth's surface,[49] we refer to Section 6.2.

(9) ACKNOWLEDGMENT

The author wishes to thank the Director of the Institute Telecommunication for his kind permission to publish the pape

(10) REFERENCES

(1) GODZIŃSKI, Z.: 'Surface Impedance Concept in the Theory of Radio Wa Propagation', C.C.I.R. Study Groups, Geneva, 1958, Document IV/17.
(2) MONTEATH, G. D.: 'Application of the Compensation Theorem to Certa Radiation and Propagation Problems', *Proceedings I.E.E.*, Monograph No. 3 June, 1951 (98, Part IV, p. 23).
(3) BALLANTINE, S.: 'Reciprocity in Electromagnetic, Mechanical, Acoustical, a Interconnected Systems', *Proceedings of the Institute of Radio Engineers*, 192 17, p. 929.
(4) STRATTON, J. A.: 'Electromagnetic Theory' (McGraw-Hill, New York, 194 p. 250.
(5) CARSON, J. R.: 'Reciprocal Theorems in Radio Communication', *Proceedings the Institute of Radio Engineers*, 1929, 17, p. 952.
(6) BALLANTINE, S.: 'The Lorentz Reciprocity Theorem for Electric Waves', *ibi* 1928, 16, p. 513.

(7) GRÜNBERG, G. A.: 'Theory of the Coastal Refraction of Electromagnetic Waves', *Journal of Physics* (Moscow), 1942, **6**, p. 185.
(8) LEONTOVICH, M. A.: 'On a Certain Method of the Solution of the Problems of Radio Wave Propagation along Earth's Surface', *Bulletin of the Academy of Sciences of U.S.S.R.* (Physical Series), 1944, **8**, p. 16.
(9) LEONTOVICH, M. A., and FOCK, V. A.: 'Solution of the Problem of Electromagnetic Wave Propagation along the Surface of the Earth by the Parabolic Equation Method', *Journal of Experimental and Theoretical Physics* (Moscow–Leningrad), 1946, **16**, p. 557.
(10) LEONTOVICH, M. A.: 'On the Approximate Boundary Conditions for Electromagnetic Field on the Surface of Well-Conducting Bodies', from 'Investigations of Propagation of Radio Waves', edited by B. A. Vvedensky (Academy of Sciences, U.S.S.R., Moscow, 1948), p. 5.
(11) FOCK, V. A.: 'Ground Wave Propagation around the Earth with Consideration of Diffraction and Refraction', *ibid.*, p. 40.
(12) GRÜNBERG, G. A., and FOCK, V. A.: 'On the Theory of Coastal Refraction o Electromagnetic Waves', *ibid.*, p. 69.
(13) FEINBERG, E. L.: 'Propagation of Radio Waves along a Real Surface', *ibid.*, p. 97.
(14) FEINBERG, E. L.: 'Theory of Ground Wave Propagation along the Earth's Surface' from 'Propagation of Radio Waves', Alpert, J. L., Ginzburg, V. L., and Feinberg, E. L. (GITTL, Moscow, 1953), Chapter IX, p. 184.
(15) 'Ground Wave Propagation over Mixed Paths (A Brief Review of the Present Situation)', C.C.I.R., Warsaw, 1956, Paper No. 501.
(16) FEINBERG, E. L.: 'Theory of Mixed Path Propagation of Radiowaves and Engineering Methods of Calculation', C.C.I.R., Warsaw, 1956, Paper No. 563.
(17) FEINBERG, E. L.: 'Propagation of Radio Waves along an Inhomogeneous Surface', *Nuovo Cimento*, 1959, Suppl. a1 Vol. XI, Ser. X, p. 60.
(18) TRENEV, N. G.: 'Diffraction of Electromagnetic Surface Waves Caused by Impedance Discontinuity', *Radiotechnics and Electronics* (Moscow), 1958, **3**, p. 27.
(19) TRENEV, N. G.: 'Diffraction of Electromagnetic Surface Waves at a Half-infinite Impedance Surface', *ibid.*, p. 163.
(20) KALININ, YU. K.: 'Perturbation of the Field of a Plane Radio Wave by Inhomogeneities of Earth's Surface', *ibid.*, p. 557.
(21) BOTCHAROFF, V. G., and BASS, F. G.: 'On the Diffraction of Electromagnetic Waves by a Statistically Inhomogeneous Surface', *ibid.*, p. 577.
(22) KALININ, YU. K., and FEINBERG, E. L.: 'Ground Wave Propagation over an Inhomogeneous Spherical Earth's Surface', *ibid.*, p. 1122.
(23) KALININ, YU. K.: 'On the Problem of Radio Wave Diffraction over Inhomogeneous Spherical Earth's Surface', *ibid.*, p. 1274.
(24) PETROVSKY, A. D., and FEINBERG, E. L.: 'On the Approximate Boundary Condition in the Theory of Radio Wave Propagation along Earth's Surface', *ibid.*, 1960, **5**, p. 385.
(25) BASS, F. G.: 'Boundary Conditions for the Electromagnetic Field at the Surface with Arbitrary Permittivity', *ibid.*, p. 389.
(26) HUFFORD, G. A.: 'An Integral Equation Approach to the Problem of Wave Propagation over an Irregular Surface', *Quarterly of Applied Mathematics*, 1952, **9**, p. 391.
(27) CLEMMOW, P. C.: 'Radio Propagation over a Flat Earth across a Boundary Separating Two Different Media', *Philosophical Transactions of the Royal Society, A*, 1953, **246**, p. 1.
(28) BREMMER, H.: 'The Extension of Sommerfeld's Formula for the Propagation of Radio Waves over a Flat Earth to Different Conductivities of the Soil', *Physica*, 1954, **20**, p. 441.
(29) BREMMER, H.: 'Application of Operational Calculus to Ground-Wave Propagation, Particularly for Long Waves', *Transactions of the Institute of Radio Engineers*, 1958, AP–6, p. 267.
(30) GODZIŃSKI, Z.: 'The Use of Equivalent Secondary Sources in the Theory of Ground-Wave Propagation over an Inhomogeneous Earth', *Proceedings I.E.E.*, Monograph No. 299 R, April, 1958 (105 C, p. 448).
(31) GODZIŃSKI, Z.: 'A Comparison of Millington's Method and the Equivalent Numerical Distance Method with the Theory of Ground-Wave Propagation over and Inhomogeneous Earth', *ibid.*, Monograph No. 318 R, December, 1958 (106 C, p. 62).
(32) WAIT, J. R.: 'Mixed Path Ground Wave Propagation: 1. Short Distances', *Journal of Research of the National Bureau of Standards*, 1956, **57**, p. 1.
(33) WAIT, J. R., and HOUSEHOLDER, J.: 'Mixed-Path Ground-Wave Propagation: 2. Larger Distances', *ibid.*, 1957, **59**, p. 19.
(34) WAIT, J. R.: 'Amplitude and Phase of the Low-Frequency Ground Wave Near a Coastline', *ibid.*, 1957, **58**, p. 237.
(35) WAIT, J. R.: 'On the Theory of Propagation of Electromagnetic Waves along a Curved Surface', *Canadian Journal of Physics*, 1958, **36**, p. 9.
(36) KAY, A. F.: 'Scattering of a Surface Wave by a Discontinuity in Reactance', *Transactions of the Institute of Radio Engineers*, 1959, AP–7, p. 22.
(37) SCHELKUNOFF, S. A.: 'The Impedance Concept and its Application to Problems of Reflection, Refraction, Shielding and Power Absorption', *Bell System Technical Journal*, 1938, **17**, p. 17.
(38) SCHELKUNOFF, S. A.: 'Electromagnetic Waves' (Van Nostrand, New York, 1943), pp. 80, 296 and 480–484.
(39) RYTOV, S. M.: 'Calcul du skin-effet par la méthode des perturbations', *Journal of Physics* (Moscow), 1940, **2**, p. 233.
(40) BOOKER, H. G.: 'The Elements of Wave Propagation Using the Impedance Concept', *Journal I.E.E.*, 1947, **94**, Part III, p. 171.
(41) WAIT, J. R., and FRASER, W. C. G.: 'Radiation from a Vertical Dipole over a Stratified Ground, Part II', *Transactions of the Institute of Radio Engineers*, 1954, AP–3, p. 144.
(42) WAIT, J. R.: 'Radiation from a Vertical Antenna over a Curved Stratified Ground', *Journal of Research of the National Bureau of Standards*, 1956, **56**, p. 237.
(43) BREKHOVSKIKH, L. M.: 'Waves in Stratified Media' (Academy of Sciences of the U.S.S.R., Moscow, 1957) (in Russian).
(44) GROSSKOPF, J.: 'Das Strahlungsfeld eines vertikalen Dipolsenders über geschichtetem Boden', *Hochfrequenztechnik und Elektroakustik*, 1942, **60**, p. 136.
(45) GROSSKOPF, J.: 'Über Bodenleitfähigkeitsmessungen in Schleswig–Holstein', *Fernmeldetechnische Zeitschrift*, 1949, **2**, p. 211.
(46) GROSSKOPF, J., and VOGT, K.: 'Der Einfluss von Bodeninhomogenitäten auf die Funkbeschickung', *Nachrichtentechnische Zeitschrift*, 1956, **9**, p. 349.
(47) BREKHOVSKIKH, L. M.: 'On the Field of a Point Source of Radiation in a Stratified Medium', *Bulletin of the Academy of Sciences of U.S.S.R.* (Physical Series), 1949, **13**, p. 505.
(48) WAIT, J. R.: 'Radiation from a Vertical Electric Dipole over a Stratified Ground', *Transactions of the Institute of Radio Engineers*, 1953, AP–1, p. 9.
(49) WAIT, J. R.: 'Theory of Electromagnetic Surface Waves over Geological Conductors', *Geofisica Pura e Applicata*, 1954, **28**, p. 47.
(50) WAIT, J. R.: 'Propagation of Radio Waves over a Stratified Ground', *Geophysics*, 1953, **18**, p. 416.
(51) WAIT, J. R.: 'The Fields of a Line Source of Current over a Stratified Conductor', *Applied Scientific Research*, Section B, 1953, **3**, p. 279.
(52) WAIT, J. R.: 'On Anomalous Propagation of Radio Waves in Earth Strata', *Geophysics*, 1954, **19**, p. 342.
(53) LO, Y. T.: 'Electromagnetic Field of a Dipole Source above a Grounded Dielectric Slab', *Journal of Applied Physics*, 1954, **25**, p. 733.
(54) BRICK, D. B.: 'The Radiation of a Hertzian Dipole over a Coated Conductor', *Proceedings I.E.E.*, Monograph No. 113, December, 1954 (102 C, p. 104)
(55) PAVINSKY, P. P., and KOZULIN, YU. N.: 'The Field of a Vertical Magnetic Dipole over a Two-Layer Medium', Scientific Papers of Leningrad State University, Physical Series, No. 9, 'Geophysics' (Leningrad University, 1956), p. 134.
(56) KOZULIN, YU. N.: 'The Field of a Vertical Magnetic Dipole over a Two-Layer Medium. Computation of the Function $T\mu(p, z)$', *ibid.*, p. 158.
(57) LOWNDES, J. S.: 'A Transient Magnetic Dipole Source above a Two-Layer Earth', *Quarterly Journal of Mechanics and Applied Mathematics*, 1957, **10**, p. 79.
(58) SMITH-ROSE, R. L., and BARFIELD, R. H.: 'On the Determination of the Directions of the Forces in Wireless Waves at the Earth's Surface', *Proceedings of the Royal Society, A*, 1925, **107**, p. 587.
(59) GROSSKOPF, J., and VOGT, K.: 'Technische Anwendungen eines Bodenleitfähigkeitsmessers', *Telegraph-, Fernsprech-, Funk- und Fernseh-Technik*, 1941, **30**, p. 352.
(60) GROSSKOPF, J., and VOGT, K.: 'Das Zennecksche Drehfeld im Bereich von Rückstrahlern', *ibid.*, 1943, **32**, p. 102.
(61) NORTON, K. A.: 'The Propagation of Radio Waves over the Surface of the Earth and in the Upper Atmosphere; Part II, The Propagation from Vertical, Horizontal, and Loop Antennas over a Plane Earth of Finite Conductivity', *Proceedings of the Institute of Radio Engineers*, 1937, **25**, p. 1203.
(62) FURUTSU, K.: 'Propagation of Electromagnetic Waves over a Flat Earth across a Boundary Separating Different Media and Coastal Refraction', *Journal of the Radio Research Laboratories, Japan*, 1955, **2**, p. 1.
(63) SENIOR, T. B. A.: 'Radio Propagation over a Discontinuity in the Earth's Electrical Properties—II. Coastal Refraction', *Proceedings I.E.E.*, Monograph No. 201 R, October, 1956 (104 C, p. 139).
(64) PRESSEY, B. G., ASHWELL, G. E., and ROBERTS, R.: 'Further Studies of the Deviation of Low- and Medium-Frequency Ground Waves at a Coast-Line', *ibid.*, Paper No. 3018 E, November, 1959 (106 B, p. 548).
(65) GROSSKOPF, J., and VOGT, K.: 'Zur Messung der Bodenleitfähigkeit', *Telegraphen-, Fernsprech-, Funk- und Fernsehtechnik*, 1942, **31**, p. 22.
(66) SMITH-ROSE, R. L.: 'Electrical Measurements on Soil with Alternating Currents', *Journal I.E.E.*, 1934, **75**, p. 221.
(67) GROSSKOPF, J., and VOGT, K.: 'Ausbreitungsmessungen über inhomogenem Boden', *Hochfrequenztechnik und Elektroakustik*, 1942, **60**, p. 97.
(68) FELDMAN, C. B.: 'The Optical Behaviour of the Ground for Short Radio Waves', *Proceedings of the Institute of Radio Engineers*, 1933, **21**, p. 764.
(69) GROSSKOPF, J., and VOGT, K.: 'Über die Messung der Bodenleitfähigkeit', *Telegraphen-, Fernsprech-, Funk- und Fernsehtechnik*, 1940, **29**, p. 164.
(70) GROSSKOPF, J., and VOGT, K.: 'Die Messung der elektrischen Leitfähigkeit bei geschichtetem Boden', *Hochfrequenztechnik und Elektroakustik*, 1941, **58**, p. 52.
(71) GROSSKOPF, J.: 'Über das Zennecksche Drehfeld im Bodenwellenfeld eines Senders', *ibid.*, 1942, **59**, p. 72.
(72) GROSSKOPF, J., and VOGT, K.: 'Die Messung des elektrischen Drehfeldes im Nahfeld eines Senders', *ibid.*, p. 70.
(73) GILL, E. W. B.: 'A Simple Method of Measuring Electrical Earth-Constants', *Proceedings I.E.E.*, Paper No. 808 R, March, 1949 (96, Part III, p. 141).
(74) GERBER, W., and WERTHMÜLLER, A.: 'Über die vegetabile Absorption der Bodenwelle', *Technische Mitteilungen der Schweizerischen Telegraphen- und Telephonverwaltung*, 1945, **23**, p. 12.
(75) KAPPELHOFF, K. H.: 'Zeitliche Schwankungen der Bodenwellenfeldstärke', Fernmeldetechnisches Zentralamt der Deutschen Bundespost, Technischer Bericht Nr. 5511, June, 1955.
(76) JOSEPHSON, B., and BLOMQUIST, Å.: 'The Influence of Moisture in the Ground, Temperature and Terrain on Ground Wave Propagation in the V.H.F. Band', *Transactions of the Institute of Radio Engineers*, 1958, AP–6, p. 169.
(77) CAIRNS, J. E. I.: 'Experimental Confirmation of the Influence of a Low-Resistivity Layer Subsoil on the Forward Inclination of Radio Waves', *Journal of the Washington Academy of Sciences*, 1927, **17**, p. 264.

621.372.45

The Institution of Electrical Engine
Monograph No. 435
Mar. 19

THE ANALYSIS OF NON-LINEAR RESONANT CIRCUITS

By C. B. NEWPORT, Ph.D., and D. A. BELL, M.A., Ph.D., Member.

(*The paper was first received* 15*th January, in revised form* 4*th August, and in final form* 14*th November*, 1960. *It was published as an* INSTITUTION MONOGRAPH *in March*, 1961.)

SUMMARY

The paper describes two graphical methods of calculating the instantaneous voltages and currents which result from feeding a sinusoidal current to a resonant circuit which employs a non-linear inductor. The voltage-integral method uses a step-by-step approximation to the actual inductor characteristic, including hysteresis. Knowledge of the detailed waveforms facilitates the determination of the optimum magnitude and timing of a pulse to trigger a ferroresonant circuit from the dissonant to the resonant state. Calculated waveforms are satisfactorily confirmed experimentally.

Alternatively, the phase-plane method allows the use of a piecewise linear approximation to the magnetization characteristic of the core of the inductor (e.g. three straight lines), but at the cost of ignoring hysteresis.

(1) INTRODUCTION

A resonant circuit containing a non-linear inductor may exhibit two distinct stable states of voltage and current at one frequency, and is then known as a ferroresonant circuit. The use of such a circuit as a digital computing element has been suggested.[1,2]

Preliminary analysis of the non-linear circuit can be undertaken by various quasi-linear techniques,[3,4] from which it is possible to deduce a figure of merit for a non-linear inductor and the optimum conditions under which it can be used. From their nature these techniques provide no information on the current and voltage waveforms in the circuit, but assume that they are sinusoidal; and even more important, they provide no information on the type of trigger pulse required to switch the circuit from one stable state to the other in the minimum time. In the paper an analytical technique described as the 'voltage-integral method' is developed to take account of the inherent non-linearities in the ferroresonant circuit, and to provide detailed information on transient and steady-state voltage and current waveforms and on the magnitude and duration of the trigger pulse required for optimum triggering. The voltage-integral method is a simple graphical technique by which the required waveforms are built up step by step from small linear segments. Results can be obtained quite rapidly and accurately by hand, but the method is particularly suitable for a digital computer.

Another technique, using a phase-plane method, is useful in certain circumstances and is described briefly in Section 7.1.

(2) VOLTAGE-INTEGRAL METHOD

For a detailed analysis of the non-linear resonant circuit it is necessary to have complete information on the properties of the non-linear reactor. For a non-linear inductor this information is conventionally presented as a B/H loop relating the magnetic flux density in the core to the applied magnetic field, though, for a particular inductor, the same curve drawn to an appropriate scale will relate the total magnetic flux, Φ, to the instantaneous inductor current i_L. A method will be described for analysi the performance of such an inductor when connected in parallel ferroresonant circuit which is fed from a consta current sinusoidal source.

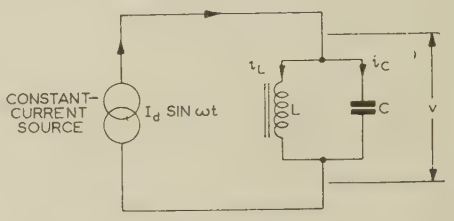

Fig. 1.—Ferroresonant circuit fed from constant-current source.

Referring to Fig. 1, the flux equation for the inductor m be written:

$$n\Delta\Phi = \int_0^t (v - i_L R)dt \quad . \quad . \quad . \quad . \quad . \quad (1)$$

while the circuit voltage, v, across the capacitor is given by

$$v = \frac{1}{C}\int_0^t (I_d \sin \omega t - i_L)dt \quad . \quad . \quad . \quad . \quad (2)$$

Thus, eliminating v between eqns. (1) and (2), flux change given as a function of inductor current, i_L, and the known dri current.

This function is, in fact, already defined by the B/H loop mentioned above. Thus a sequence of values of Φ and i_L, whi satisfy simultaneously eqns. (1) and (2) and the B/H loop, w give the voltage, current and flux waveforms as functions time.

The solution is obtained by a stepwise graphical technique which a value of i_L is chosen and assumed constant for a sho period of time, so that eqn. (2) may be integrated to give v a function of time. This function is then integrated graphica over the same period of time and the resistive loss term su tracted, so that eqn. (1) yields the flux change during that ti interval. This flux change at constant current is then plotted a vertical line on the inductor characteristic (Fig. 2), and it

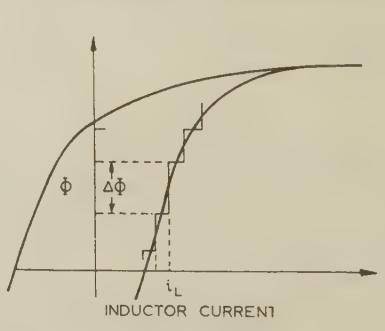

Fig. 2.—Step-by-step approximation to the magnetization process

Correspondence on Monographs is invited for consideration with a view to publication.

Dr. Newport was formerly in the Electrical Engineering Department, University of Birmingham, and is now with the English Electric Company. Dr. Bell is in the Electrical Engineering Department, University of Birmingham.

ssumed that the two match adequately if the characteristic isects the vertical line. In general this will not be the case,) that a step which gives a suitable match must be found by ial. With practice it is possible to choose the correct current nmediately, in at least 90% of the cases, so that complete olutions can be built up quite rapidly.

Direct integration of eqn. (2) with i_L constant gives

$$v = \frac{I_d}{\omega C}(1 - \cos \omega t) - \frac{i_L}{C} t \quad . \quad . \quad . \quad . \quad (3)$$

The first term can be plotted directly (see Fig. 3) and the :cond superimposed step by step as new values of i_L are deter-

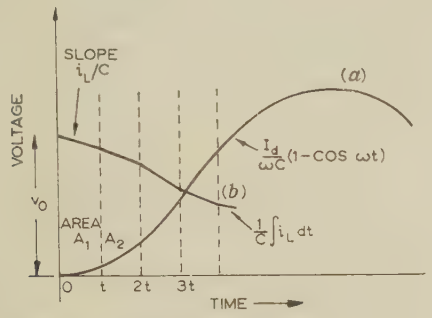

Fig. 3.—Graphical construction for voltage across the circuit of Fig. 1.

ined for each time interval. The difference between the two urves then gives the instantaneous circuit voltage.

Eqn. (1) may be integrated by noting that i_L is constant and riting it in the form

$$n\Delta\Phi = \int_0^t v dt - Ri_L t$$

he voltage integral may be evaluated by measuring the area A_1 etween curves (*a*) and (*b*) of Fig. 3, and thus the flux change ay be found. This flux change at constant current is then lotted on the *B*/*H* loop of Fig. 2 to see if an adequate match as been obtained. If not, the chosen value of i_L must be ltered as described above.

Since this is a second-order system, two initial conditions are equired, and these are conveniently taken as the initial values f voltage and inductor current. These enable the first section f the curve in Fig. 3 to be drawn and the first flux step to be btained. If necessary, initial conditions corresponding to the teady state may be obtained approximately from the resistive-urrent/reactive-current characteristic.[4] The size of step should, f course, be smaller when the flux is near an extreme value and he two curves in Fig. 3 are crossing. It is also helpful to mark he current axis of the hysteresis loop with a scale of volts per illisecond, which corresponds to the slope of curve (*a*) of Fig. 3.

In the dissonant steady state the flux will traverse some minor oop on the *B*/*H* characteristic, and this loop will normally have o be obtained by interpolation from a number of measured alues. The complete hysteresis loop of the inductor usually as very steep sides which are almost straight, and the dissonant oop is essentially contained by these sides. Other minor loops re possible, such as loop (*a*) in Fig. 4, which is not symmetrical bout the current axis but yet has almost the same area as the ue dissonant loop. There is also only a very slight net current o that the damping in traversing loop (*a*) is only very slightly ore than that for the true dissonant loop. Hence, if the rcuit is disturbed so that it traverses loop (*a*), it will take a latively long time to settle back to the true dissonant loop.

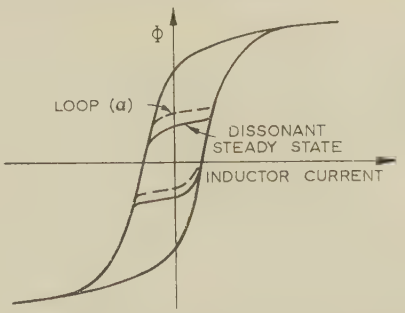

Fig. 4.—Hysteresis loops traced with different voltage swings across the circuit.
—— Symmetrical loop. ---- Loop (*a*).

Thus, slight errors in the initial conditions assumed for the analysis could necessitate iteration round a number of cycles before the steady state was reached. One can, however, note the difference between the end-point of the first cycle and the estimated initial conditions, and use this to modify the initial conditions, rather than continue the first trial. Usually two or three cycles will give sufficiently accurate results.

The hysteresis and resistive losses in the resonant steady state are very voltage dependent, so that this state is very resistant to perturbations and convergence upon it is rapid.

(3) COMPARISON WITH EXPERIMENTAL RESULTS

The experimental check of the method was carried out at 200 c/s, using an iron-cored transformer (the characteristics of which are given in Fig. 5) resonating with a 33 μF capacitor.

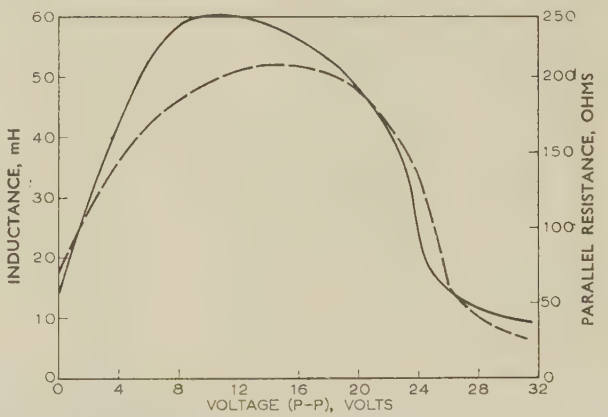

Fig. 5.—Inductance and resistance/voltage characteristics of the experimental inductor at 200 c/s.
—— Inductance. ---- Parallel resistance.

Initial conditions were chosen by trial with the aid of the resistive-current/reactive-current plot as mentioned above, and a steady-state dissonant curve was plotted as shown in Fig. 6(*a*); the corresponding predicted inductor voltage and current waveforms are shown in the left-hand parts of Figs. 7(*a*) and (*b*). These curves show that the voltage is almost a pure sinusoid of amplitude 7 volts, about 83° phase advanced on the drive current. The inductor current waveform contains many harmonics, as would be expected from the nature of the hysteresis loop, and its peak amplitude is about 0·11 amp. Comparison of these calculated waveforms with the measured ones, shown in Fig. 8(*a*), shows that the measured voltage is closely sinusoidal in form and has an amplitude of about 6·7 volts. The calculated

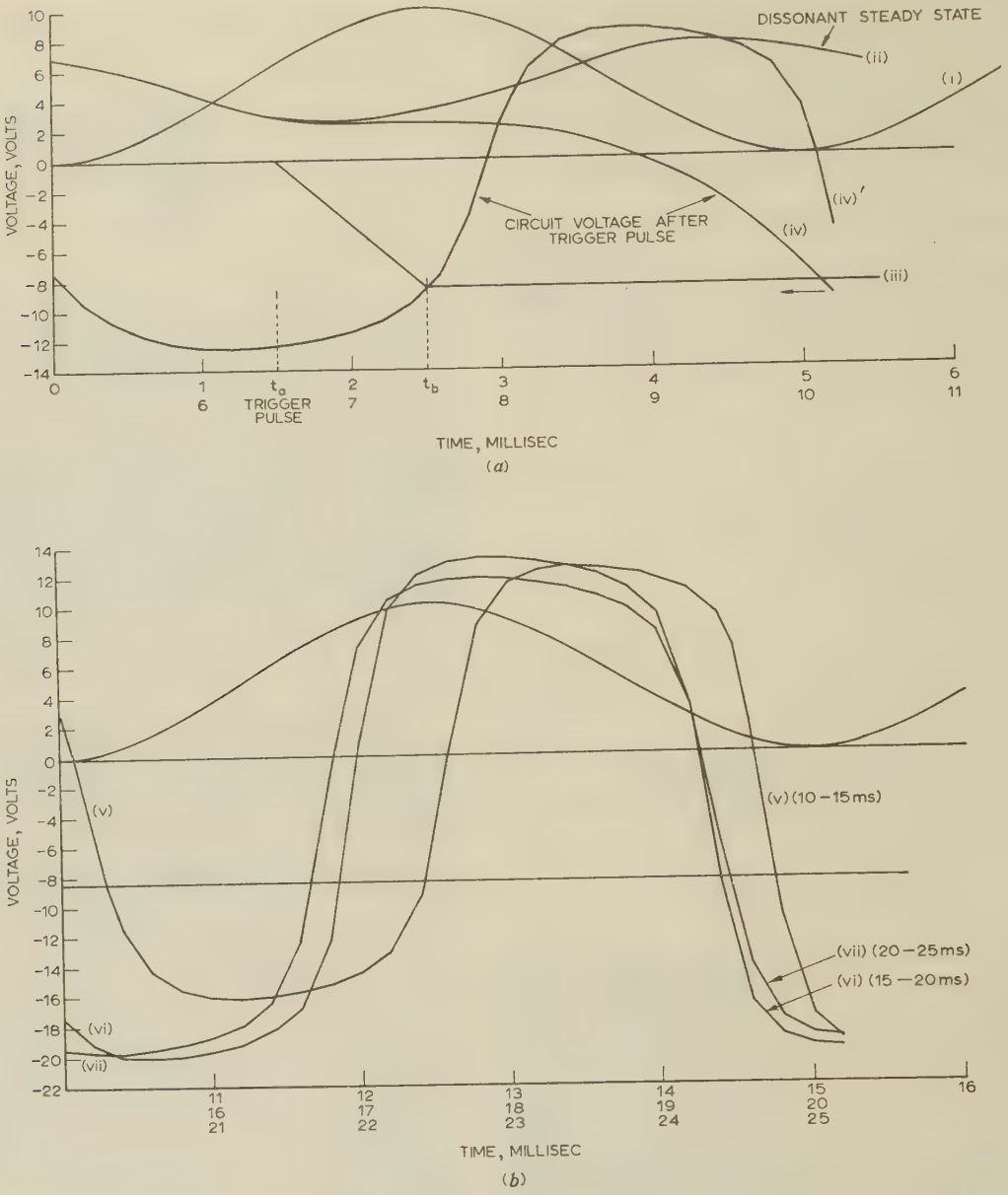

Fig. 6.—Investigation of circuit behaviour by the voltage-integral method.

(*a*) (i) $(I_d/\omega C)(1 - \cos \omega t)$.
(ii) $(1/C) \int i_L dt$ in the dissonant steady state.
(iii) Voltage resulting from the trigger pulse.
(iv) (0–5 millisec) and
(iv)′ (5–10 millisec) $(1/C) \int i_L dt$ after triggering.

(*b*) Continuation of curves (i) and (iv)′ of (*a*). Curve (iv)′ continues to (v) (10–15 millisec), then (vi) (15–20 millisec) and (vii) (20–25 millisec).

and measured current waveforms are also very similar in shape and the measured amplitude is 0·1 amp.

The drive current waveform shown in Fig. 8 contains some higher harmonics which were introduced by non-linearities in the drive oscillator. These harmonics were found to be unimportant since they were strongly attenuated by the resonant circuit. A test was made by introducing considerable additional distortion into the drive current waveform, and it was found that this had negligible effect on the other circuit waveforms.

In the theoretical analysis the voltage waveform is obtained by integrating the drive current [eqn. (2)], and if this contains, say, 10% of the third-harmonic component, the integration reduces this to about 3%. The additional integration of eqn.. to obtain the flux change further reduces the third harmonic about 1%. It was therefore considered adequate in the theoreti analysis to neglect the harmonic content of the actual dr current and assume it to be sinusoidal, for simplicity.

No attempt was made to evaluate the resonant steady st directly, but the state attained some five cycles (25 millisec) af triggering was assumed to be sufficiently close. The calcula waveforms following a trigger pulse are shown in Figs. 7 and (*b*) and their construction is described below. Here bo the inductor current and voltage are definitely non-sinusoid although the current waveform again contains a higher prop

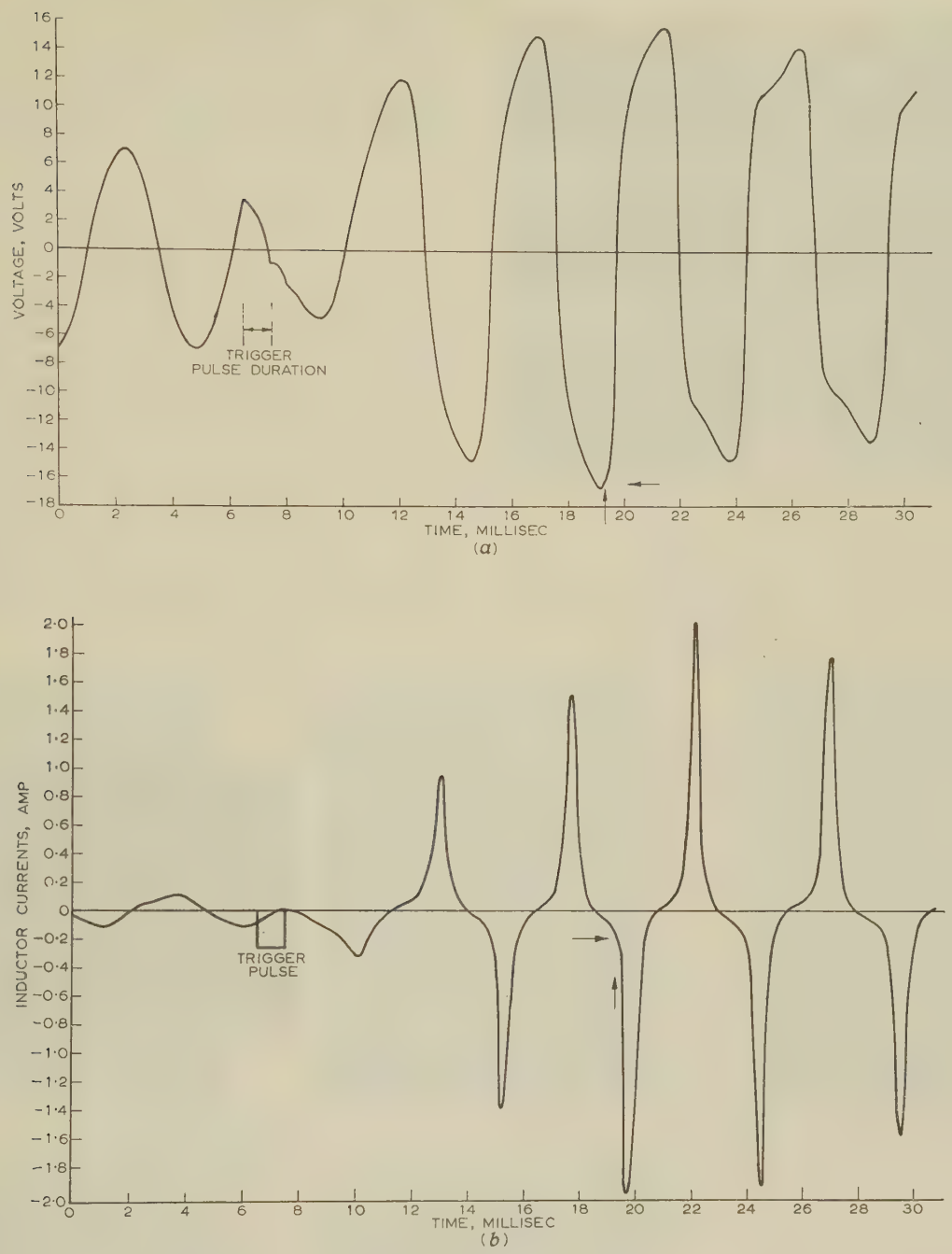

Fig. 7.—Calculated waveforms.

(*a*) Circuit voltage.
(*b*) Inductor current.

on of harmonics than the voltage waveform. The constructions or the fourth and fifth cycles, shown in Fig. 6(*b*) as curves (vi) nd (vii), are almost identical, indicating that they are close to ne steady state. The voltage amplitude for the fifth cycle, ig. 7(*a*), is about 13·5 volts, which compares fairly well with ne measured value of 12·0 volts [Fig. 8(*b*)], and the shapes of ne waveforms are also very similar. Better agreement would e expected if further cycles were calculated.

The calculated peak current on the fifth cycle is 1·6 amp, hich is rather more than the measured current of 1·3 amp. This discrepancy is possibly due to error in the saturation curve of the hysteresis loop for currents above 1 amp, since a very slight error in the slope of this part of the curve would cause considerable error in the current associated with a given flux. Also, the straight-line approximations used in the construction of Fig. 6(*b*) show a considerable change in slope from one line to the next, so introducing further errors. With more elaborate approximations a closer agreement could be expected between the calculated and measured waveforms, but they are already reasonably close in both magnitude and shape.

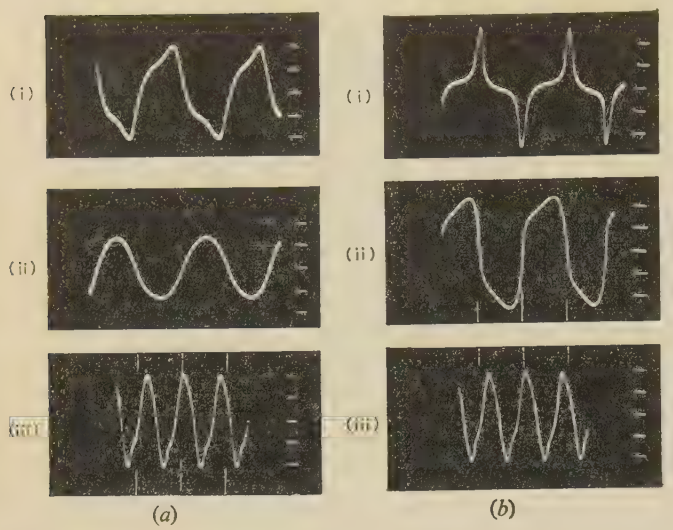

Fig. 8.—Oscillograms of experimental waveforms of drive current, circuit voltage and inductor current.

(*a*) Dissonant.
(i) Inductor current: 0·05 amp/division.
(ii) Voltage: 5 volts/division.
(iii) Drive current: 0·1 amp/division.
(*b*) Resonant.
(i) Inductor current: 0·5 amp/division.
(ii) Voltage: 5 volts/division.
(iii) Drive current 0·1 amp/division.
All waveforms are at 200 c/s.

(4) APPLICATION TO THE TRIGGERING OF A FERRORESONANT CIRCUIT

To enable a ferroresonant circuit to be used as a computing element it is necessary to be able to switch, or trigger, it at will from one stable state to the other. It is desirable that the transition shall take place as rapidly as possible, and also that the output from one ferroresonant circuit can be made to trigger another.

When a ferroresonant circuit is transferred from its dissonant to its resonant state there is an increase in stored energy in the circuit, which can, in principle, be supplied from the trigger mechanism or from the carrier source, or part from each. One method of controlling the circuit is effectively the same as that used in magnetic amplifier; the core is divided into two parallel parts with separate trigger windings on each. These windings are so connected that in the linear regime they have no mutual inductance with the resonant winding. When the core is operated in a non-linear regime, there is interaction between the non-inductive trigger winding and the resonant winding, and most of the energy required to saturate the core is drawn from the drive circuit. (For an analysis of this phenomenon in magnetic amplifiers see Reference 5.)

The alternative method of triggering is to inject the necessary additional energy into the resonant circuit, and if a pulse of correct magnitude and phase is injected the switching is instantaneous. It is, in principle, possible to place an increment of charge on the tuning capacitor at an appropriate time, but, in practice, it is easier to achieve the same effect by injecting a current pulse into the inductor: e.g. by having a separate winding coupled to the resonant winding [Fig. 9(*a*)], a method which is described as the transformer-coupled trigger circuit. The equivalent circuit for the transformer in Fig. 9(*a*) is shown in Fig. 9(*b*). Since the trigger pulse is at constant current the ideal transformer simply alters its amplitude by the turns ratio N, and R_1 and L_1 have no effect on the circuit as seen from A and B. Thus the only impedances of importance are R_2, L_2, R_3 and L_3.

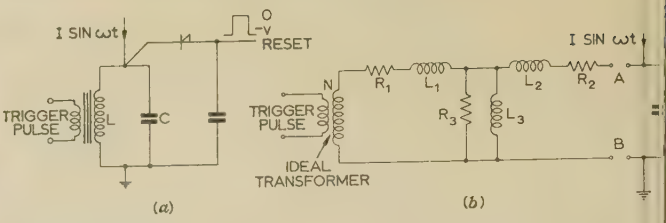

Fig. 9.—Ferroresonant circuit with transformer-coupled triggering.
(*a*) Typical practical circuit.
(*b*) Equivalent circuit.

R_2 is the resistance of the secondary winding, which was measur to be 1·87 ohms in the transformer used for subsequent tes To estimate the significance of the other impedances, t secondary winding was short-circuited and the primary windi fed with a known current pulse. With a rectangular prima input pulse, as in Fig. 10(*a*) curve (i), the secondary curre

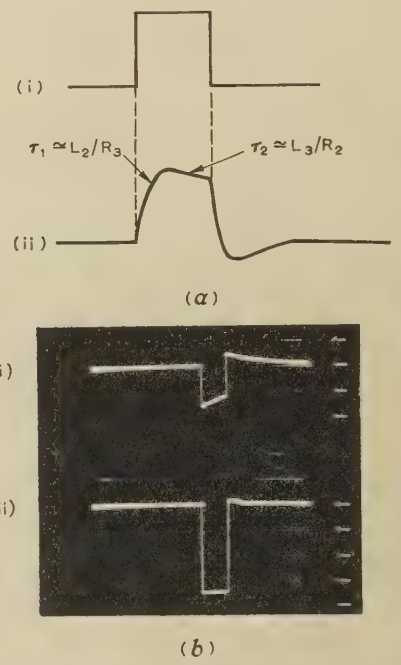

Fig. 10.—Calculation of components of equivalent circuit.
(*a*) Principle of method: transformer response.
(i) Input. (ii) Output.
(*b*) Experimental waveforms.
(i) Secondary current: 0·2 amp/division.
(ii) Primary current: 0·2 amp/division.
Pulse width, 2·5 millisec.

would be of the form shown in curve (ii), and if we assu $L_3 \gg L_2$ and $R_3 \gg R_2$ the rise time-constant, τ_1, is appro mately equal to L_2/R_3 and the decay time-constant, τ_2, approximately L_3/R_2.

The measured waveforms of the primary and seconda currents are shown in Fig. 10(*b*). From the secondary curre waveform it can be seen that the rise time-constant τ_1 is qu negligible, so that the inductance L_2 can be neglected. There a slight decay of secondary current during the pulse because t time-constant $\tau_2 = L_3/R_2$ is not infinite. This time-consta can be estimated from the oscillogram of Fig. 10(*b*); as t initial rate of decay of current is about 38 amp/sec from a curre of 0·31 amp, the time-constant is approximately 0·31/38 sec 8·2 millisec. Taking the measured value of R_2 of 1·87 ohm we have $L_3 = \tau_2 R_2 = 8{\cdot}2 \times 10^{-3} \times 1{\cdot}87 = 15{\cdot}3$ mH.

This agrees well with the low-flux-density inductance of Fig.

ne flux density in the core remained very low during these tests cause the primary and secondary magnetomotive forces were most exactly equal and opposite. In practice, the droop of condary current due to the finite value of τ_2 will be less, because is unlikely that the trigger pulse will be applied at the instant the drive-current cycle when the core flux density is zero.

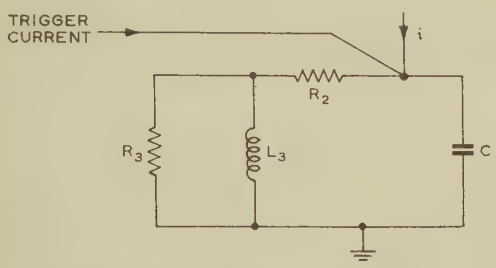

Fig. 11.—Simplified equivalent circuit of triggering system.

hus L_3 will normally be considerably larger than 15 mH (its inimum value) and τ_2 will also be considerably larger. As ost of the actual triggering tests used pulses about 1 millisec ide the effect of the finite value of τ_2 is negligible.

Since τ_2 is very large, the current flowing through R_3 and L_3 negligible, for short trigger pulses, and we may assume that ne trigger current is added to the drive current (Fig. 11). This

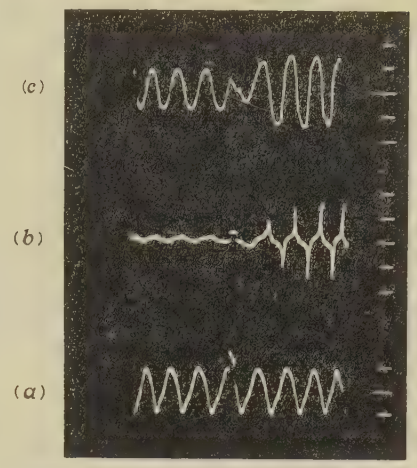

Fig. 12.—Oscillograms resulting from the application of a triggering pulse phased to end at a maximum of the drive current.
(*a*) Drive current and pulse: 0·2 amp/division.
(*b*) Inductor current: 1 amp/division.
(*c*) Voltage: 10 volts/division.

enables the voltage-integral method to be applied during and following a trigger pulse.

The waveforms in Figs. 12 and 13, which show the drive

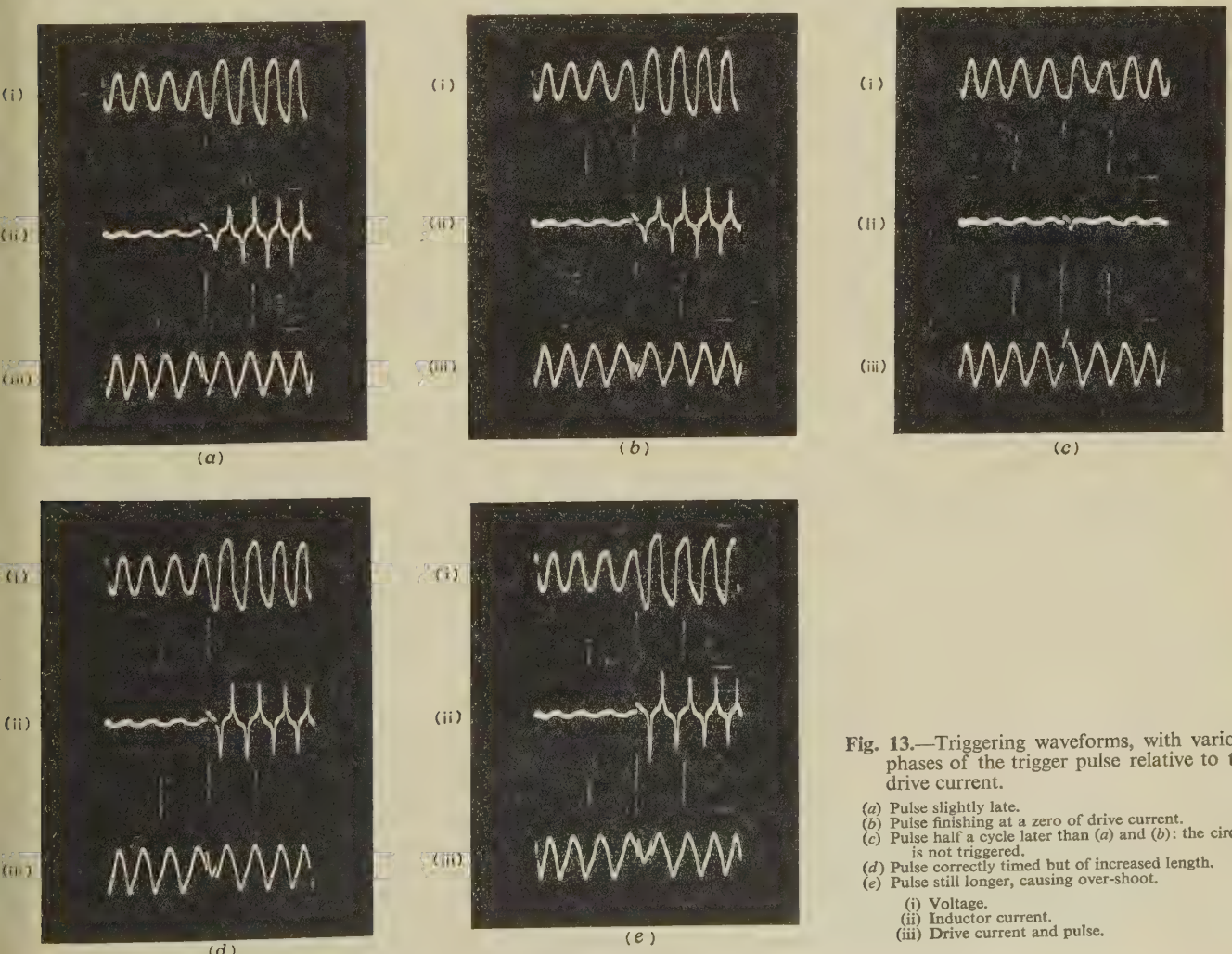

Fig. 13.—Triggering waveforms, with various phases of the trigger pulse relative to the drive current.
(*a*) Pulse slightly late.
(*b*) Pulse finishing at a zero of drive current.
(*c*) Pulse half a cycle later than (*a*) and (*b*): the circuit is not triggered.
(*d*) Pulse correctly timed but of increased length.
(*e*) Pulse still longer, causing over-shoot.
(i) Voltage.
(ii) Inductor current.
(iii) Drive current and pulse.

current and the trigger pulse, were obtained by applying the sum of the two independent waveforms to the oscilloscope, so that they could be compared for phase and pulse durations.

Since negligible trigger current flows through the ferroresonant inductor it must all flow into the capacitor; the interesting result appears that triggering does not affect the inductor but simply adds more charge to the capacitor. In the example analysed, Fig. 6(*a*), the effective trigger current was 0·27 amp lasting for 1 millisec. This is a total charge of 0·27 mC, and so the voltage on the 31·8 μF capacitor should change by about 8·5 volts. Experimentally, Fig. 6(*a*) indicates a voltage change of about 7·7 volts, and a flux change in the inductor due to the trigger pulse of about $0{\cdot}16 \times 10^{-5}$ Wb in 1 millisec. This compares with the maximum rate of change of flux of about $7{\cdot}5 \times 10^{-5}$ Wb/millisec. This is sufficient confirmation that, for short trigger pulses, all the trigger current flows into the capacitor. In the recordings of inductor current (see Fig. 12, for example) a pulse appears when the trigger pulse is applied. This is because it is only the secondary current which is being measured and the pulse is the current pulse which flows into the capacitor, while its flux in the inductor core is cancelled by that of the pulse in the primary winding.

Using an analysis similar to that of eqn. (2) a rectangular trigger pulse lasting from t_a to t_b can be seen to add a ramp to the capacitor voltage beginning at time t_a and continuing with a slope I_T/C until it reaches a value $(I_T/C)(t_b - t_a)$ volts at time t_b.

In the voltage-integral analysis a ramp is therefore added to the curve of $(I_d/\omega C)(1 - \cos \omega t)$ at the appropriate time and the new curve of $\frac{1}{C}\int_0^t i_L dt$ is plotted as before. Hence the voltage waveform can be obtained during and after the trigger pulse, and the voltages and currents studied during the transition from the dissonant to the resonant state.

Using the same transformer and capacitor as before, the voltage equation, including the trigger current, is

$$V = 5(1 - \cos 400\pi t) - \frac{10^6}{31{\cdot}8}\int_0^t i_L dt + \frac{10^6}{31{\cdot}8} I_T(t_b - t_a) - 7{\cdot}0$$

The effective trigger current, I_T, is $-0{\cdot}27$ amp, so that the voltage ramp has a slope of

$$-\frac{0{\cdot}27 \times 10^6}{31{\cdot}8} = -8{\cdot}5 \text{ volts/millisec}$$

and its duration is 1 millisec starting slightly after the drive current has reached its positive peak [Fig. 12(*a*)].

In Fig. 6(*a*), the voltage-integral method has been used, and the difference between curve (i), $V = 5(1 - \cos 400\pi t)$, and curve (ii), $V = \frac{10^6}{31{\cdot}8}\int i_L dt$, gives the dissonant steady-state voltage over one cycle from 0 to 5 millisec. The drive current, $0{\cdot}2 \sin 400\pi t$ amperes, reaches its positive peak at 1·25 millisec, so that the trigger pulse ramp is applied at 1·5 millisec, slightly after the peak, and continues to 2·5 millisec, as shown by curve (iii). Continuing the construction of the curve of $\frac{1}{C}\int i_L dt$ then gives curves (iv) and (iv)′. It can be seen that, at the end of the trigger pulse, the inductor current is only slightly different from what it would have been if there had been no trigger pulse. The circuit voltage is now given by the difference between curve (i) and curves (iii) and (iv) (the trigger current is negative). The analysis is continued from Fig. 6(*a*) to Fig. 6(*b*), where curves (v)–(vii) show three consecutive cycles. The actual voltage waveform obtained from these curves is shown i Fig. 7(*a*) and the current waveform in Fig. 7(*b*).

The results obtained experimentally are shown in Fig. 1 oscillograms (*b*) and (*c*). Oscillogram (*a*) gives the pha relationship between the drive current and the trigger puls Comparing Figs. 12(*c*) and 7(*a*), it can be seen that the wav forms are virtually identical even to the distortion caused by t trigger pulse. From Fig. 7(*a*) the amplitudes of successi voltage peaks after triggering are −4·8, +12, −14·8, +1 −16·7, +15·7 and −14·8 volts, and from the oscillogra corresponding amplitudes are −4·5, +12, −13·5, +15, −1 +15 and −14 volts. The agreement is within experiment accuracy, and some of the residual error may be caused slight inaccuracy in the hysteresis loop at large inductor curren Fig. 12(*b*) gives the current waveform, which should be co pared with Fig. 7(*b*). The reason for the trigger pulse appear on the measured waveform is explained above. From Fig. 7(the amplitudes of successive current peaks are −0·32, +0·9 −1·4, +1·53 and −2·0 amp, and from Fig. 12 they are −0· +0·9, −1·1, +1·4 and −1·5 amp. Although the wavefor are very similar in shape there is a significant difference in t amplitudes, because again a slight error in the saturation cur of the hysteresis loop can cause a large error in the peak induc current. These results show that the voltage-integral method analysis can give a complete transient analysis of the non-lin resonant circuit.

Since the circuit voltage and current in the dissonant st are nearly sinusoidal, it may be assumed as a reasonable appro mation that the triggering pulse is being injected into a lin circuit; and knowing both the dissonant and resonant voltag as functions of time, and one of the trigger pulse parameters, s its duration, T_d, it is possible to calculate the amplitude I_T a the finishing time t_b required for instantaneous triggering. both the dissonant and resonant voltages are virtually sinusoid and of known phase difference, the calculation of the pu parameters is relatively simple. (The equations for the chan of voltage and current due to a pulse are given in Section 7.2.)

Since the pulse current is considered to flow entirely into t capacitor, immediately after the pulse has ended the capacit current is back to its dissonant value, but the voltage has be increased by an amount corresponding to the additional char on the capacitor. For instantaneous triggering both the curre and voltage must be at their resonant values immediately aft the pulse, which must therefore end at the time in the dri current cycle when the dissonant and resonant capacitor curre are equal. Since the r.m.s. resonant current is much larger th the r.m.s. dissonant current, this equality occurs close to the tir at which the resonant current passes through zero (and t voltage is at a maximum). In the resonant state the circ impedance is mainly resistive, so that the voltage maximu occurs at about the same time as the drive current maximum.

The effect of departures from appropriate pulse timing a pulse duration is illustrated in Figs. 12 and 13. Fig. 13(*a*) sho a pulse of the correct polarity which finishes just at the dri current maximum and triggering occurs with very slight d tortion of the voltage waveform. With the pulse finishi slightly later, Fig. 13(*b*), the result is virtually identical. Fig. shows a pulse advanced a quarter of a cycle so that it finishes a zero of the drive current. There is considerable wavefo distortion, and the circuit takes about twice as long to switch the resonant state as with correct timing of the trigger puls This has been confirmed by voltage-integral analysis as shown Figs. 7(*a*) and (*b*). If the pulse is delayed half a cycle so that is of incorrect polarity, Fig. 13(*c*), the circuit does not trigger in the resonant state.

Returning to the same starting-point for the trigger pulse

n (*a*), an increase of duration to 1·8 millisec gives an acceptable esult [Fig. 13(*d*)]. With a pulse of 2·5 millisec [Fig. 13(*e*)] here is considerable overshoot, showing that too much energy s fed into the circuit, and it takes one or two cycles for this xcess energy to be dissipated. During the latter part of this ·5 millisec pulse it is no longer true to say that the inductor urrent is unaffected by the trigger pulse, since the inductor is aturated and of sufficiently low impedance for a large propor- ion of the trigger current to flow through it. Hence there is a arge spike on the inductor current waveform during the latter art of the trigger pulse.

Although it is theoretically possible to trigger a ferroresonant ircuit on and off at the supply frequency, this is of no value in ractice, as virtually all the circuit energy would then be provided y the trigger pulse and none would be available for driving other ircuits. Usually it is desirable to draw a rectified output from ferroresonant circuit and store this voltage in an interstage apacitor. It can be arranged that when the capacitor has harged up to the peak resonant voltage, the stored charge is ufficient to trigger another ferroresonant circuit. A suitable ating pulse can be provided to discharge this capacitor through he trigger winding of the required circuit. The value of the apacitor, and the ferroresonant transformer ratio, must be djusted to give the correct trigger pulse. Since the triggering nergy is stored in the interstage capacitor, the ferroresonant ircuit connected to this capacitor must be in its resonant state ong enough to charge the capacitor fully. With appropriate ircuit design three or four cycles of the supply frequency should e adequate, and it would be expected that the maximum pulse ate attainable in practice would be about a quarter of the supply requency.

(5) ACKNOWLEDGMENTS

The paper is a sequel to earlier work[4] which was carried out the Electrical Engineering Department, University of Bir- ingham, under a Ministry of Supply Contract. The greater art of the present work was carried out while Dr. Newport eld an Assistantship in the Research Laboratory of Electronics, Massachusetts Institute of Technology, and he wishes to thank rofessor J. B. Wiesner for the facilities placed at his disposal.

(6) REFERENCES

) Isborn, C.: 'Ferroresonant Flip-Flops', *Electronics*, April, 1952, **25**, p. 121.
) Rutishauser, R. W.: 'Ferroresonant Flip-Flop Design', *ibid.*, May, 1954, **27**, p. 152.
) Cutler, P. H.: 'Ferroresonant Trigger Circuits', Ministry of Supply, S.R.D.E. Report No. 1083, September, 1955.
) Newport, C. B., and Bell, D. A.: 'Ferroresonant Circuits for Digital Computers', *Journal of the British Institution of Radio Engineers*, 1957, **17**, p. 619.
) Storm, H. F.: 'Magnetic Amplifiers' (Wiley, 1955).

(7) APPENDICES

(7.1) Phase-Plane Analysis

The principle of phase-plane analysis is that two variables hich are related functions of time are plotted against each her. In the present application the two variables are inductor rrent and voltage; and the relationship between them is sumed to be single-valued, i.e. hysteresis is ignored. First nsider the case of a parallel combination of a linear lossless ductor and capacitor fed from a step-function source. If a rve is plotted of the voltage v across the circuit as a function of the inductor current, an ellipse is obtained, and by normalizing the scales so that

$$v' = v\sqrt{C} \quad \text{and} \quad i' = i\sqrt{L}$$

it becomes a circle with its centre at

$$i' = I_{dc}\sqrt{L} = I'_{dc}$$

Now, if a resistor R_p (linear or non-linear) is placed in parallel with the LC combination it will shunt some of the current, I_{dc}, the amount depending upon the instantaneous value of the resistance and the instantaneous voltage across it, so that less will be available to drive the other elements. A curve of $-R_p$ can be plotted on the $v'i'$-plane (phase plane) as shown in Fig. 14,

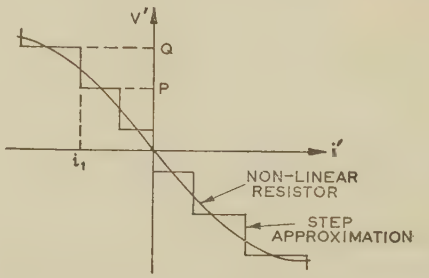

Fig. 14.—Approximation to current through non-linear resistor by sequence of constant-current steps.

and this can then be approximated by a series of current sinks each of which is operative only over a certain voltage range. For instance, over the voltage range P–Q the equivalent sink absorbs a current i_1, and thus over this range the current available to drive the LC combination is $I'_{dc} - i_1$. The way in which the resistance characteristic is approximated by current sinks is fairly arbitrary and non-critical; but the best arrangement is for a given sink to absorb as much current at the centre of its voltage range as the actual resistor does at the centre of the same range.

Now, to draw the phase-plane characteristic of the parallel LCR circuit, note that if a current step is applied to a linear LC circuit the currents and voltages in the circuit will be sinusoidal functions of time, and the corresponding trajectory in the $v'i'$-plane is a circle. The non-linear circuit may be approximated over successive small ranges by a linear circuit with different parameters for each range, and its trajectory built up from given initial conditions, say $v = 0$, $i_L = 0$, as a series of circular arcs. These arcs have their centres on the i'-axis, at a distance $I'_{dc} - i'_n$ from the origin, where i'_n is the equivalent current sink over the voltage range of any particular arc. Thus a piecewise circular approximation to the actual phase-plane characteristic is obtained, a simple example of which is shown in Fig. 15. With a rudimentary approximation to the resistor characteristic, something approaching slide-rule accuracy is possible.

To obtain the actual current or voltage waveform, note that the rate of rotation of the operating point about the centre of each arc is ω radians per second, where $\omega = 1/\sqrt{(LC)}$. Thus the time taken to traverse each arc can be calculated and timing marks plotted on the curve, from which the various waveforms can be obtained.

If the step-function source is now replaced by an arbitrarily varying current source, I_{dc} becomes I_{ac}. To take account of this variation the current waveform is approximated by a series of steps. Over any one of the steps the phase-plane characteristic can be constructed by the method described above, using the source current value dictated by the stepwise approximation to the actual current waveform. At the end of the time interval

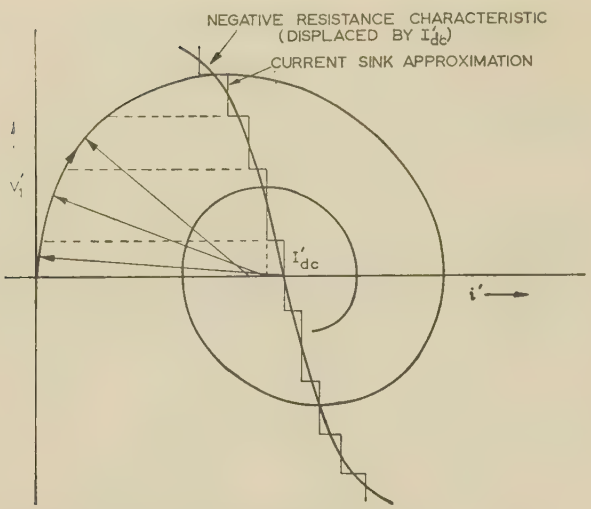

Fig. 15.—Simple example of phase-plane analysis of non-linear resonant circuit.

the source current changes and the construction is continued with this new current. To determine the point on the characteristic at which the source current is changed, note that the operating point is always rotating with constant angular velocity ω about the appropriate centre. Thus, for the time interval t_1 to t_2 the operating point rotates through an angle θ, where

$$\theta = \frac{t_2 - t_1}{\sqrt{(LC)}} \text{ radians}$$

Hence it is necessary to keep a check only on the angle of rotation of the compasses, and when this reaches θ, to make an appropriate step change in the value of the source current.

The inductance affects only two of the parameters in the phase plane, the scale of the current axis $i' = i\sqrt{L}$ and the angular velocity of the operating point, ω.

An approximate representation of the effect of a non-linear inductor is obtained by taking an approximation to the actual flux/current curve in the form of a sufficient number of straight lines (generally three or five). Each of these lines then represents a constant value of the incremental inductance. The flux/current curve is assumed to be single valued for simplicity, and the loss due to hysteresis is included by reducing the parallel resistance. A 3-line piecewise-linear approximation to the flux/current curve is indicated in Fig. 16. Up to the current i_K, the inductor

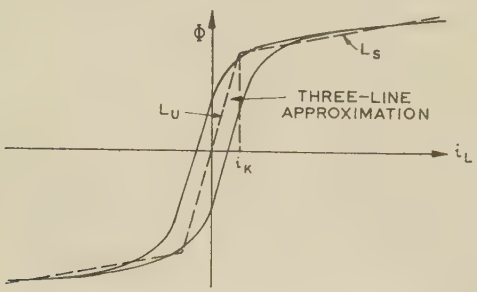

Fig. 16.—Piece-wise approximation to magnetization characteristic.

is considered to be in the unsaturated state and to have a constant inductance L_u; but for higher currents the inductor is assumed to be saturated and to have a smaller, constant value L_s. Thus two different scales are necessary for the normalized current, i', namely $i'_u = i\sqrt{L_u}$ and $i'_s = i\sqrt{L_s}$. The unsaturated scale, i'_u, starts with its origin coincident with the origin of the curre axis and extends for positive and negative currents up $|i'_u| = i_K\sqrt{L_u}$. When the trajectory has been plotted as far i_K the saturated scale of i'_s is adjusted along the current axis s that it coincides with the unsaturated scale at the curre corresponding to the inductance break point. It is, of cours necessary to plot the non-linear resistor characteristic to eac of the i'_s scales so that the appropriate current-sink approxima tions can be obtained.

The initial conditions are most conveniently expressed as th circuit voltage and the inductor current at some specified tim and, of course, the drive current must be known on the sam time scale.

Normally the object of the analysis is to determine the volta and current waveforms in the two steady states. With arbitra initial conditions, the voltage and current will probably chan

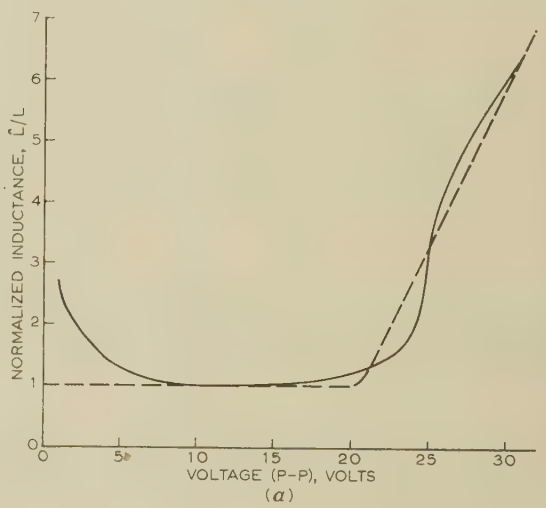

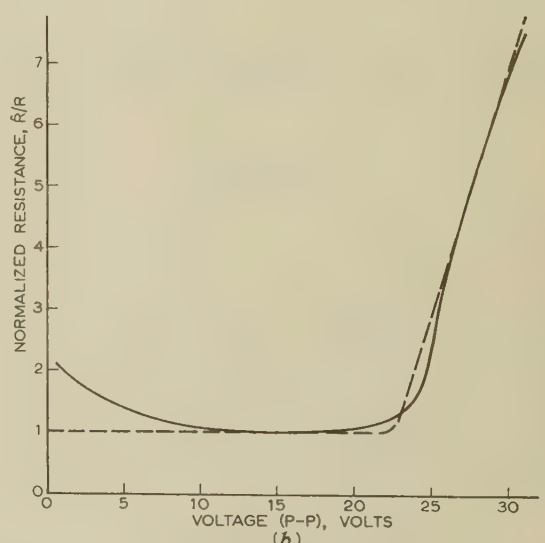

Fig. 17.—Approximation to characteristics of inductor as measure by resonant circuit.

(*a*) Inductance. $\hat{L} = 60$ mH.
—— Actual inductance characteristic.
---- Linear approximation.
$L_u = 60$ mH. $L_s = 2{\cdot}5$ mH.

(*b*) Resistance. $\hat{R} = 210$ ohms.
—— Actual resistance characteristic.
---- Linear approximation.
$R_u = 210$ ohms. $R_s = 5{\cdot}5$ ohms.

Curves are proportional to reciprocal inductance and reciprocal resistance.

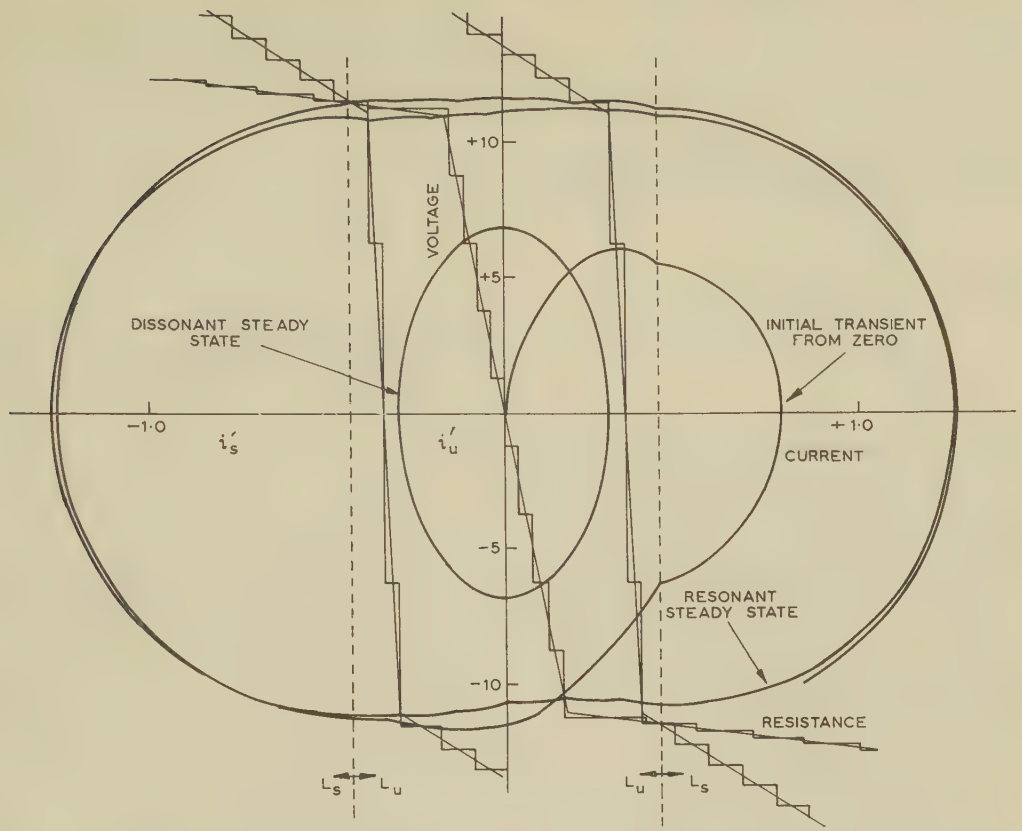

Fig. 18.—Phase-plane construction of dissonant and resonant steady states of experimental circuit, using values of inductor parameters from Fig. 17.

$L_s = 2{\cdot}5\,\text{mH}$ $L_u = 60\,\text{mH}$

or a few cycles, the number being dependent on the initial onditions and circuit damping, before steady-state oscillations re obtained. The number of transient cycles can be minimized y making an estimate of the initial conditions which lie close to he steady-state conditions, with the aid of the quasi-linear nalysis given in a previous paper.[4] The plot of reactive current gainst resistive current there described will give the current nplitude directly, and the phase angle between drive current nd circuit voltage as the angle between the drive-current vector the stable point and the resistive-current axis. The initial onditions determined in this way are usually closer to the steady ate for the dissonant condition than for the resonant condition ecause the non-linearities are more pronounced in the latter.

The phase-plane method requires instantaneous values of ductance and resistance, and approximate values can be btained by a synthetic method. The variation of mean ductance and resistance with applied voltage can be measured y means of either a bridge or a resonant circuit: the latter has e advantage of permitting the voltage applied to the inductor be measured directly, while the total drive current is measured th the aid of a small resistor in series with the resonant circuit. he values measured should be the fundamental components of e voltage and of the non-sinusoidal current. One then assumes approximation to the true non-linear characteristic, e.g. a ine approximation, and computes the slopes of the three parts the characteristic which will give the best fit to the experientally measured variation of mean inductance with voltage. gs. 17(*a*) and (*b*) show the estimation of inductance and sistance by this method. Using these approximate inductor aracteristics and a resonant 33 μF capacitor, the resultant phase-plane characteristic is obtained, as shown in Fig. 18. The corresponding voltage and current waveforms are compared with the measured waveforms in Fig. 19.

It can be seen that the phase-plane method of analysis yields

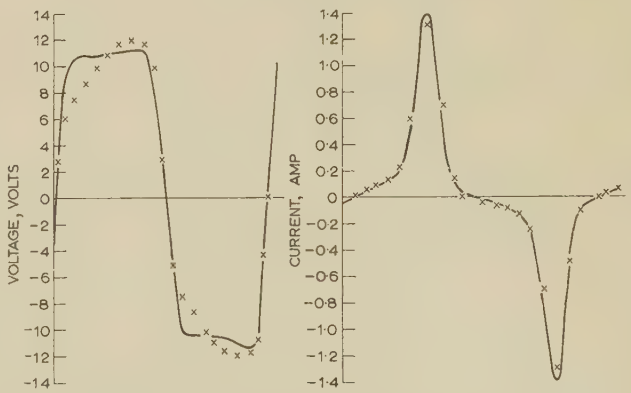

Fig. 19.—Comparison of voltages and current waveforms calculated by phase-plane analysis with experimental values.

——— Calculated × Measured.

reasonable results provided that the non-linearity is not too great. It has the advantage that it is not necessary to know the detailed non-linear characteristic of the reactor, a simply obtained mean characteristic being sufficient. Because less information is used the resultant waveforms are not as accurate as those obtained by the voltage-integral method.

(7.2) Equations for Instantaneous Triggering

By making the assumption that the ferroresonant circuit is linear when it is in the dissonant state, it is possible to calculate the equivalent circuit impedance, if the voltage and current waveforms and phases are given.

For a linear resonant circuit with a parallel combination of inductance, capacitance and resistance, it can easily be shown that

$$\omega L = \frac{1 \pm \left(\frac{|I_{ac}|}{|V_{ac}|\omega C\eta}\right)}{\left(1 - \frac{|I_{ac}|^2}{|V_{ac}|^2\omega^2C^2\eta^2}\right)\omega C}$$

where $$\eta^2 = 1 + \frac{1}{\tan^2\phi}$$

ϕ = Phase angle between I and V = arc tan $R[(1/\omega L) - \omega C]$.
ω = Drive-current angular frequency.

Thus the equivalent linear circuit can be calculated and its response to a trigger pulse obtained.

It is worth noting that, although the equivalent circuit assumed above is correct for sinusoidal voltages and currents at the drive-current frequency, it will be in error for pulse currents. The error increases as the circuit damping and the pulse length increase. In the subsequent analysis, it has been assumed that both the damping and the pulse length are small enough for this error to be neglected.

The total current includes the trigger pulse, which may be assumed to be constant-current of value I_T beginning at $t = t_a$ and ending at $t = t_b$. Since the circuit is linear, superposition can be applied, and it is necessary to consider only the effect of the trigger pulse. The trigger response must then be made equal to the difference between the resonant and the dissonant steady states, and if the trigger response is added to the dissonant steady state, the result will be the resonant steady state.

The basic equation is $V = IZ$, and, using Laplace transform notation,

$$V = \frac{pLI}{1 + p\frac{L}{R} + p^2LC}$$

Now $I = I_T[\mathrm{H}(t - t_a) - \mathrm{H}(t - t_b)]$, where $\mathrm{H}(t)$ is a unit step function. As I_T is constant,

$$I = \frac{I_T}{p}\left[\exp(-pt_a) - \exp(-pt_b)\right]$$

and it follows that

$$V(t) = \frac{I_T}{nC}[\varepsilon^{-\alpha}\sin n(t - t_a)]\mathrm{H}(t - t_a) - \frac{I_T}{nC}[\varepsilon^{-\beta}\sin n(t - t_b)]\mathrm{H}(t - t_b)$$

where $$n^2 = \frac{1}{LC} - \frac{1}{4C^2R^2}$$

$$\alpha = (t - t_a)/2CR$$

$$\beta = (t - t_b)/2CR$$

Thus, when $t = t_b$,

$$V_b = \frac{I_T}{nC}\varepsilon^{-T_d/2CR}\sin nT_d$$

where $T_d = t_b - t_a$, and for instantaneous triggering

$$(V_{res} - V_{dis})_b = \frac{I_T}{nC}\varepsilon^{-T_d/2CR}\sin nT_d \quad . \quad . \quad . \quad (4)$$

Similarly the circuit currents must be at their resonant valu just after the end of the trigger pulse. Since the sinusoidal dri current I equals $i_L + i_R + i_C$ after the pulse and $i_R = V/$ equating values of i_C will ensure that all currents have the resonant values. Thus

$$i_C = pCV = I_T\left[\frac{p}{\left(p + \frac{1}{2CR}\right)^2 + n^2}\right]\left[\exp(-pt_a) - \exp(-pt_b)\right]$$

Therefore it follows that at $t = t_{b+}$

$$i_C = I_T\varepsilon^{-T_d/2CR}\left(\cos nT_d - \frac{1}{2CRn}\sin nT_d\right) - I_T$$

and for instantaneous triggering the difference in capacit currents is

$$(i_{res} - i_{dis})_{b+} = I_T\varepsilon^{-T_d/2CR}\left(\cos nT_d - \frac{1}{2CRn}\sin nT_d\right) - I_T \quad (5)$$

Basically eqns. (4) and (5) give the change of voltage a current in a ferroresonant circuit caused by the application o fairly short trigger pulse of amplitude I_T and duration T Thus if the dissonant circuit voltage is known the circuit volta and current after the pulse can be calculated.

In principle, knowing both the dissonant and resonant voltag as functions of time, and one of the trigger pulse parameter say its duration T_d, it is possible to calculate the amplitude and the finishing time t_b required for instantaneous triggeri If both the dissonant and resonant voltages are virtually sinu soidal and of known phase difference, the calculation of t pulse parameters is relatively simple.

In the ferroresonant circuit used for all the previous tes the dissonant voltage is almost sinsuoidal, but the resona voltage contains a large proportion of higher harmonics, a the current waveforms are even more non-sinusoidal. To veri eqns. (4) and (5) the differences between the resonant and t dissonant voltages and currents after a given trigger pulse we obtained by the voltage-integral method. The parameters the pulse shown in Fig. 13(*d*) were used, since this is an examp of almost instantaneous triggering.

The pulse parameters are

$I_T = -0{\cdot}27$ amp, $t_a = 2{\cdot}5$ millisec, $t_b = 4{\cdot}3$ millisec, ($T_d = 1{\cdot}8$ millise

and Fig. 20 is the voltage-integral plot during the pulse.

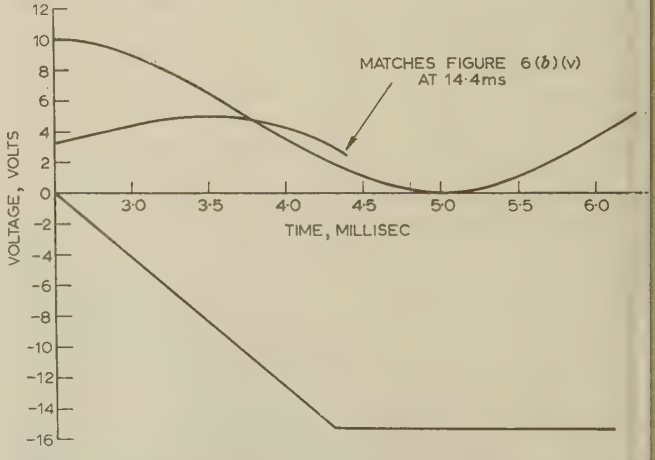

Fig. 20.—Calculation by voltage-integral method of the triggering process recorded in Fig. 13, oscillograms (*d*).

At the end of the pulse (4·3 millisec), the circuit voltage is −16·4 volts and the inductor current is −0·19 amp. These are the same as the voltages and currents at the points indicated by the two arrows at 19·3 millisec in Figs. 7(*a*) and (*b*), showing that the circuit is virtually resonant when the pulse ends. This is verified by Fig. 13(*d*).

The dissonant voltage and inductor current at an equivalent time in the cycle [say 4·3 millisec in Figs. 7(*a*) and (*b*)] are −5·7 volts and +0·05 amp.

Thus $(V_{res} - V_{dis})_b = -10{\cdot}7$ volts

and $(i_{res} - i_{dis})_b = +0{\cdot}24$ amp

Using the equivalent circuit values calculated in Section 4 with the aid of Figs. 9 and 10, the voltage and current changes due to the trigger pulse can be obtained:

$$V_b = \frac{I_T}{nC}\varepsilon^{-T_d/2CR}\sin nT_d$$

and $$i_b = I_T\varepsilon^{-T_d/2CR}\left(\cos nT_d - \frac{1}{2nCR}\sin nT_d\right) - I_T$$

where $$n = \left(\frac{1}{LC} - \frac{1}{4R^2C^2}\right)^{1/2}$$

and, putting $C = 31{\cdot}8\,\mu$F, $L = 68{\cdot}4$ mH, $R = 287$ ohms, and $T_d = 1{\cdot}8$ millisec, we obtain

$$V_b = 39{\cdot}55I_T \qquad i_b = -0{\cdot}754I_T$$

Thus, with $I_T = -0{\cdot}27$ amp,

$$V_b = -10{\cdot}66 \text{ volts} \qquad i_b = +0{\cdot}203 \text{ amp}$$

These compare well with the values of −10·7 volts and +0·24 amp obtained above.

It was previously stated that with a short trigger pulse virtually all the trigger current would flow into the capacitor. This result is also apparent from eqn. (4), where

$$V_b \to \frac{I_T}{nC}nT_d = \frac{I_TT_d}{C} \quad \text{as} \quad T_d \to 0$$

Thus for short pulses

$$V_b = \frac{I_TT_d}{C}$$

The maximum pulse duration, T_{dm}, for which this equation can be used can then be calculated, if the maximum tolerable error in V is defined.

Taking the maximum error to be 5%, T_{dm} is defined by

$$0{\cdot}95 \leqslant \varepsilon^{-T_d/2CR}\left(\frac{\sin nT_{dm}}{nT_{dm}}\right)$$

which, in the case examined above, gives a maximum pulse duration of about 0·5 millisec for the approximation to be valid.

621.372.826

The Institution of Electrical Engine
Monograph No. 43
Mar. 19

DESIGN OF CYLINDRICAL SURFACE WAVEGUIDES WITH DIELECTRIC AND MAGNETIC COATING

By T. BERCELI, Dr.Ing.

(*The paper was first received* 15*th December*, 1959, *in revised form* 3*rd September, and in final form* 29*th November*, 1960. *It was published as an* INSTITUTION MONOGRAPH *in March*, 1961.)

SUMMARY

The paper deals with wires whose coating has both dielectric and magnetic properties. Approximate formulae are given for the field concentration, propagation time, group velocity, power distribution, characteristic impedance, losses and maximum transmissible power for such coated wires.

The magnetic coat concentrates the field more strongly than does the dielectric one. The field concentration increases quickly with increase of permeability and hardly depends on permittivity.

The attenuation is due to the conductive, dielectric and magnetic losses of the guide. The dielectric loss depends also on permeability, and vice versa. The total loss of a given transmission line as a function of field concentration has a minimum, which can be achieved by a coating of appropriate thickness.

To determine the maximum transmissible power, two formulae can be used. One determines the maximum transmissible power from the highest permissible value of electric field strength, and the other from the highest permissible degree of overheating.

The paper concludes with a description of design procedure for surface waveguides, illustrated by an example.

LIST OF PRINCIPAL SYMBOLS

E_{z0}, E_{r0} = Components of external electric field.
$H_{\phi 0}$ = Component of external magnetic field.
E_{zi}, E_{ri} = Components of electric field in the coating.
$H_{\phi i}$ = Component of magnetic field in the coating.
γ = Propagation coefficient of surface-wave.
β = Phase-change coefficient of surface wave.
α = Attenuation coefficient of surface wave.
g_0 = Field-concentration factor (decay coefficient of external field).
g_i = Decay coefficient of the field in the coating.
K_0 = Propagation coefficient of free space.
ϵ = Permittivity.
μ = Permeability.
λ_0 = Wavelength in free space.
i = As subscript refers to the coating (insulation).
0 = As subscript refers to space outside the guide.
r = As subscript refers to relative values.
r, z, ϕ = Cylindrical co-ordinates.
t = Time co-ordinate.
ω = Angular frequency.

(1) INTRODUCTION

The question of surface-wave propagation has attracted considerable interest in recent years. Sommerfeld[1] showed theoretically as early as 1899 that surface-wave propagation is possible along a straight cylindrical conductor of finite conductivity and having a smooth surface. Recently, Goubau[2] drew attention to the comparatively low attenuation of surface-wave propagation. In some cases there may be an undesirably large spread of the field around a bare wire, and therefore t wave propagation is disturbed by nearby objects. For strong concentration of the field, Goubau coated the wire with dielectric layer. He made his theoretical and experimen investigations on such wires.[2, 3] The concentration of the fi may also be increased by a coat having magnetic properti Kaden[4] first dealt with such wires.

Barlow and Karbowiak[5] investigated surface-wave propag tion along dielectric-coated wires, and Barlow and Culle discussed the theoretical problems of different kinds of surfa waves. Barlow[7, 8] dealt with the power-carrying capacity bare-wire lines and also with the radiation of surface waveguid

The coating of the conductors to be dealt with in this pap has both dielectric and magnetic properties. The aim was determine approximate equations for calculation and practic design of such coated wires. The dependence of the chara teristics of wave propagation on the waveguide data is show by several diagrams. The results obtained may be applied the case of dielectric-coated wires when the relative permeabil is unity. The results may also be used in the case of wi coated with magnetic material when the relative permittivity unity.

The dependence of field-concentration on the permittivity a permeability of the coating was determined. Approxima formulae are given to calculate the phase velocity, group veloci propagation time, distribution of power around the guid power quota transferred in the coating and characteristic imp dance. Further, the calculation of attenuation, launching lo optimum field-concentration and maximum transmissible pow is discussed. The calculations led to the following remarkab results.

The magnetic coat concentrates the field more strongly th does the dielectric one. The field concentration increas rapidly with increase of permeability, and hardly depends permittivity.

The phase distortion of surface waveguides is small; its ser is opposite to that of the phase distortion of hollow guides a it may therefore be equalized by a short hollow guide.

The dielectric loss depends also on permeability and the ma netic loss on permittivity. If the loss factors are the same, t dielectric attenuation is less than the magnetic one.

The total loss of a given transmission line as a function field concentration has a minimum, i.e. there is an optimu field concentration. When designing surface waveguides t aim is to produce this optimum, and this can be done by t application of a coat of the correct thickness.

To determine the maximum transmissible power we have tw formulae. One determines the maximum transmissible pow from the highest permissible value of the electric field streng and the other from the highest permissible degree of overheatin The impulse peak power must not exceed the value given by t first formula, and the average power must not exceed that giv by the second.

At the end of the paper a procedure is described for t design of surface waveguides, illustrated by an example.

Correspondence on Monographs is invited for consideration with a view to publication.
Dr. Berceli is at the Research Institute for Telecommunication, Budapest, Hungary.

(2) FIELD EQUATIONS

The paper deals with a coated wire of infinite length, stretched in a homogeneous space of infinite extent. The coating of the wire has both dielectric and magnetic properties. Among the solutions of the Maxwell equations obtained for such boundary conditions we shall deal only with that which gives a radially-symmetric transverse magnetic wave. The attenuation of other modes is large and their excitation is unlikely on account of the symmetric arrangement. For this reason they will be excluded from further consideration.

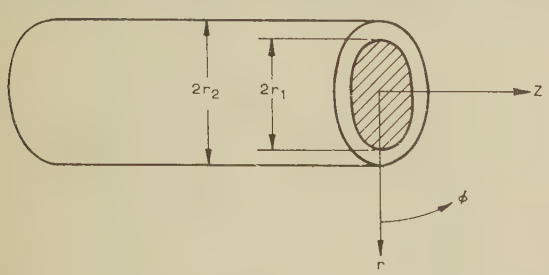

Fig. 1.—Cross-section of the coated wire, and the co-ordinate system.

Fig. 1 shows the cross-section of the coated wire and the co-ordinate system. The radius of the wire is r_1, and the outer radius of the coating is r_2. The z-axis is the direction of wave propagation. Excitation is sinusoidal as a function of time. The computations are based on the assumption of unattenuated wave propagation. The conductivity of the wire is taken as infinite and the coating is assumed to be loss-free.

(2.1) Field Components

The equations describing the field components in the coating are

$$\left.\begin{aligned} E_{ri} &= A_i\frac{\gamma}{g_i}[\mathrm{N}_0(g_ir_1)\mathrm{J}_1(g_ir) - \mathrm{J}_0(g_ir_1)\mathrm{N}_1(g_ir)]\varepsilon^{j\omega t}\varepsilon^{-\gamma z} \\ E_{zi} &= A_i[\mathrm{N}_0(g_ir_1)\mathrm{J}_0(g_ir) - \mathrm{J}_0(g_ir_1)\mathrm{N}_0(g_ir)]\varepsilon^{j\omega t}\varepsilon^{-\gamma z} \\ H_{\phi i} &= A_i\frac{K_i}{g_i}\sqrt{\left(\frac{\epsilon_i}{\mu_i}\right)}[\mathrm{N}_0(g_ir_1)\mathrm{J}_1(g_ir) - \mathrm{J}_0(g_ir_1)\mathrm{N}_1(g_ir)]\varepsilon^{j\omega t}\varepsilon^{-\gamma z} \end{aligned}\right\} \quad . \quad (1)$$

Coefficient A_i depends on the power of excitation. N_0 and N_1 indicate Neumann functions of zero and first order, respectively, and J_0 and J_1 indicate Bessel functions of zero and first order, respectively. K_i is the propagation coefficient of a free wave in the material of the coating:

$$K_i = j\omega\sqrt{(\epsilon_i\mu_i)} \quad . \quad . \quad . \quad . \quad . \quad . \quad (2)$$

The parameter g_i is defined as

$$g_i = \sqrt{(\gamma^2 - K_i^2)} \quad . \quad . \quad . \quad . \quad . \quad . \quad (3)$$

The propagation coefficient, γ, of the surface wave in general is complex:

$$\gamma = \alpha + j\beta \quad . \quad . \quad . \quad . \quad . \quad . \quad (4)$$

As we are examining unattenuated wave-propagation, γ is imaginary. Its value ranges between K_i and K_0, which is physically obvious, and therefore g_i is real.

The equations describing the external field are

$$\left.\begin{aligned} E_{r0} &= -jA_0\frac{\gamma}{g_0}\mathrm{H}_1^{(1)}(jg_0r)\varepsilon^{j\omega t}\varepsilon^{-\gamma z} \\ E_{z0} &= A_0\mathrm{H}_0^{(1)}(jg_0r)\varepsilon^{j\omega t}\varepsilon^{-\gamma z} \\ H_{\phi 0} &= -jA_0\frac{K_0}{g_0}\sqrt{\left(\frac{\epsilon_0}{\mu_0}\right)}\mathrm{H}_1^{(1)}(jg_0r)\varepsilon^{j\omega t}\varepsilon^{-\gamma z} \end{aligned}\right\} \quad . \quad (5)$$

Coefficient A_0 depends on the power of excitation. $\mathrm{H}_0^{(1)}$ and $\mathrm{H}_1^{(1)}$ are Hankel functions of the first kind, and of zero and first order, respectively. K_0, the free-space propagation coefficient is

$$K_0 = j\omega\sqrt{(\epsilon_0\mu_0)} \quad . \quad . \quad . \quad . \quad . \quad (6)$$

The parameter g_0 is

$$g_0 = \sqrt{(K_0^2 - \gamma^2)} \quad . \quad . \quad . \quad . \quad . \quad (7)$$

(2.2) Boundary Conditions

The field components parallel to the surface are continuous at the surface, and hence their quotient is continuous too:

$$\left(\frac{E_{zi}}{H_{\phi i}}\right)_{r=r_2} = \left(\frac{E_{z0}}{H_{\phi 0}}\right)_{r=r_2} \quad . \quad . \quad . \quad . \quad . \quad (8)$$

Substituting eqns. (1) and (5),

$$\sqrt{\left(\frac{\mu_i}{\epsilon_i}\right)}\frac{g_i}{K_i}\frac{\mathrm{N}_0(g_ir_1)\mathrm{J}_0(g_ir_2) - \mathrm{J}_0(g_ir_1)\mathrm{N}_0(g_ir_2)}{\mathrm{N}_0(g_ir_1)\mathrm{J}_1(g_ir_2) - \mathrm{J}_0(g_ir_1)\mathrm{N}_1(g_ir_2)} = j\sqrt{\left(\frac{\mu_0}{\epsilon_0}\right)}\frac{g_0}{K_0}\frac{\mathrm{H}_0^{(1)}(jg_0r_2)}{\mathrm{H}_1^{(1)}(jg_0r_2)} \quad (9)$$

Thus we have eliminated A_0, A_i and γ. Further, eliminating γ from eqns. (3) and (7) we get

$$g_i^2 = K_0^2 - K_i^2 - g_0^2 \quad . \quad . \quad . \quad . \quad (10)$$

We have two equations at our disposal for determining two unknowns, g_i and g_0. However, as calculation with eqn. (9) is rather cumbersome, we will make use of approximations.

(2.3) Limits of Approximate Calculations

In our approximations we shall assume that

$$g_ir_2 \ll 1 \quad \text{and} \quad g_0r_2 \ll 1 \quad . \quad . \quad . \quad . \quad (11)$$

Then we can use the zero representations of the cylinder functions in eqn. (9). Also, in eqn. (10) we shall ignore the value of g_0^2 compared with $K_i^2 - K_0^2$. The condition for this is

$$\left|\frac{g_0}{K_0}\right|^2 \ll \epsilon_{ir}\mu_{ir} - 1 \quad . \quad . \quad . \quad . \quad . \quad (12)$$

This condition, in conformity with eqn. (20), determines a minimum phase velocity, to the case of which the approximate calculation can no longer be applied. This phase velocity depends on ϵ_{ir} and μ_{ir} only, and it falls as they increase. When condition (12) is satisfied, g_i is approximately given by

$$g_i \simeq \sqrt{(K_0^2 - K_i^2)} \quad . \quad . \quad . \quad . \quad . \quad (13)$$

Substituting this in the first inequality of (11),

$$r_2 \ll \frac{\lambda_0}{2\pi\sqrt{(\epsilon_{ir}\mu_{ir} - 1)}} \quad . \quad . \quad . \quad . \quad (14)$$

As g_i is greater than g_0, if condition (14) is satisfied the second condition in (11) is also satisfied.

The approximate calculations will therefore be applicable to conductors with outer radii small compared with the wavelength, taking into account condition (14), and in cases when the phase velocity of wave propagation far exceeds the value determined by condition (12).

(3) CHARACTERISTICS OF WAVE PROPAGATION

(3.1) Field Concentration

If we use the zero representations of Bessel, Neumann and Hankel functions in eqn. (9), we get

$$\sqrt{\left(\frac{\mu_i}{\epsilon_i}\right)}\frac{g_i^2}{K_i}r_2 \log\frac{r_2}{r_1} = -\sqrt{\left(\frac{\mu_0}{\epsilon_0}\right)}\frac{g_0^2}{K_0}r_2 \log 0{\cdot}89 g_0 r_2 \quad (15)$$

In the course of deduction we made a further omission based on condition (11). We should now substitute for g_i^2 from eqn. (13) and rearrange:

$$\left(\mu_{ir} - \frac{1}{\epsilon_{ir}}\right)\left(\frac{r_2}{\lambda_0}\right)^2 \log\frac{r_2}{r_1} = -\left(\frac{g_0 r_2}{2\pi}\right)^2 \log 0{\cdot}89 g_0 r_2 \quad (16)$$

We introduce the designation $M(g_0 r_2)$, which is identical with the right-hand side of eqn. (16):

$$M(g_0 r_2) = -\left(\frac{g_0 r_2}{2\pi}\right)^2 \log 0{\cdot}89 g_0 r_2 \quad . \quad . \quad (17)$$

Thus eqn. (16) becomes

$$\left(\mu_{ir} - \frac{1}{\epsilon_i}\right)\left(\frac{r_2}{\lambda_0}\right)^2 \log\frac{r_2}{r_1} = M(g_0 r_2) \quad . \quad . \quad (18)$$

The factors on the left-hand side are given and $M(g_0 r_2)$ can be calculated; from this $g_0 r_2$ and therefore g_0 may be determined on the basis of eqn. (17). As this equation is unsuitable for computation, we have plotted $M(g_0 r_2)$ as a function of $g_0 r_2$ in Fig. 2.

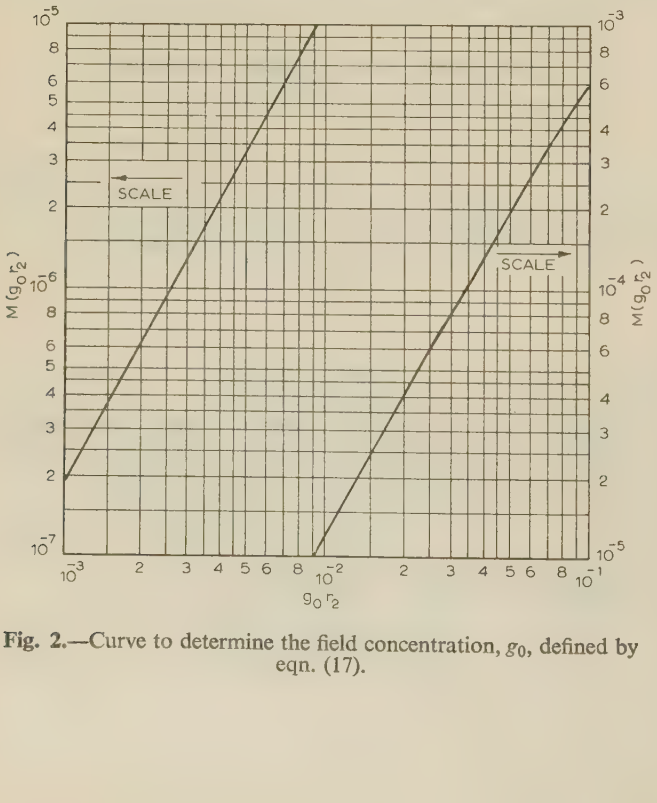

Fig. 2.—Curve to determine the field concentration, g_0, defined by eqn. (17).

The parameter g_0 gives the measure of field concentration which increases with g_0. This is the most important characteristic of the surface wave, and all the other characteristics are functions of it.

Field concentration, i.e. g_0, increases with increase of frequency, thickness of coating, permittivity and permeability. It decreases with increase of wire diameter. The variation of field concentration caused by the change of frequency is rather large.

The dependence of field concentration on material characteristics calls for special attention. The effect of permittivity on field concentration is shown in Fig. 3. The case represented is a guide, of outer radius 1·5 mm, inner radius 1·2 mm and frequency 3 Gc/s. We examine first the case of dielectric coating where μ_{ir} is equal to unity. Field concentration increases very rapidly with increase of ϵ_{ir} between 1 and 2. Above $\epsilon_{ir} = 2$ the increase of the field concentration is small. To increase the field concentration, it is not worth using material of high permittivity. If the coating has magnetic properties also the effect of permittivity on field concentration decreases rapidly with increasing permeability, as may be seen in Fig. 3.

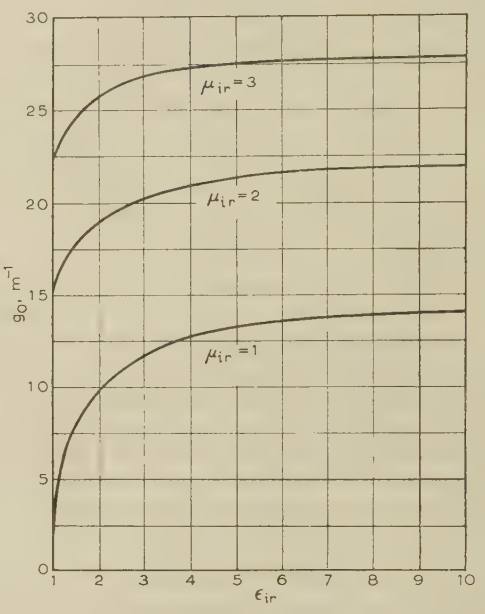

Fig. 3.—Dependence of field concentration on permittivity.
$r_1 = 1{\cdot}2$ mm.
$r_2 = 1{\cdot}5$ mm.
$f = 3$ Gc/s.

The effect of permeability on field concentration is shown in Fig. 4, for the same conductor dimensions and frequency as above. As can be seen, field concentration increases rapidly with permeability, and hardly depends on permittivity. Figs. 3 and 4 demonstrate that a higher field concentration may be achieved by magnetic coating than by a dielectric one. It therefore seems reasonable to increase field concentration by employing magnetic materials of high permeability. However this can be done only at the expense of increased attenuation since available magnetic materials have a higher loss than dielectric ones. As a matter of fact, magnetic coating offers design advantages in the upper part of the v.h.f. band (100–300 Mc/s), where the necessary field concentration could be achieved only by employing very thick dielectric coating.

* We suppose that we are not near to the cut-off frequency of the next mode TM_{02}, i.e. we are only concerned with cases where the attenuation of the waveguide is not great.

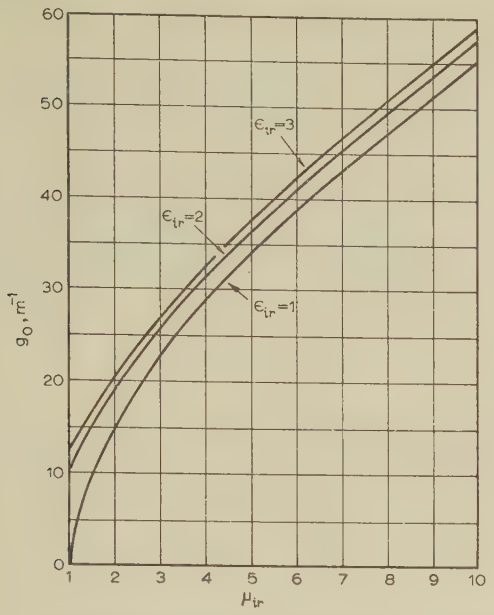

Fig. 4.—Dependence of field concentration on permeability.
$r_1 = 1{\cdot}2$ mm.
$r_2 = 1{\cdot}5$ mm.
$f = 3$ Gc/s.

(3.2) Phase Wavelength and Phase Velocity

With a knowledge of g_0, the propagation coefficient can be derived from eqn. (7). In the case of unattenuated wave propagation, γ is imaginary and its absolute value is the same as the phase-change coefficient. From this the phase wavelength is

$$\lambda_g = \frac{\lambda_0}{\sqrt{\left[1 + g_0^2\left(\frac{\lambda_0}{2\pi}\right)^2\right]}} \quad . \quad . \quad . \quad . \quad (19)$$

Phase wavelength is always less than the free-space wavelength. The length of the surface wave decreases as the field concentration and frequency increase.

Phase velocity may be obtained likewise:

$$v = \frac{c}{\sqrt{\left[1 + g_0^2\left(\frac{c}{\omega}\right)^2\right]}} \quad . \quad . \quad . \quad . \quad (20)$$

Phase velocity is always less than the velocity of light and it decreases with increase of field concentration and frequency. Phase velocity depends on frequency and the group velocity is therefore not equal to the phase velocity.

Fig. 5 shows the phase velocity compared with the velocity of light as a function of r_2/λ_0 for various values of r_2/r_1 (full-line curves). The curves relate to a conductor coated with polyethylene for which $\epsilon_{ir} = 2{\cdot}26$. The abscissae are proportional to the frequency if r_2 is kept constant. As can be seen, the phase velocity decreases as the frequency increases. Phase velocity likewise decreases as the thickness of coating increases.

(3.3) Propagation Time and Group Velocity

The propagation time for unit length is

$$\tau = \frac{1}{c}\left[1 + \frac{c^2}{2}\left(\frac{g_0}{\omega}\right)^2 \frac{\log 0{\cdot}89 g_0 r_2 - 0{\cdot}5}{\log 0{\cdot}89 g_0 r_2 + 0{\cdot}5}\right] \quad . \quad (21)$$

Propagation time exceeds the propagation time of light. Details of the computation are given in Section 12.1.

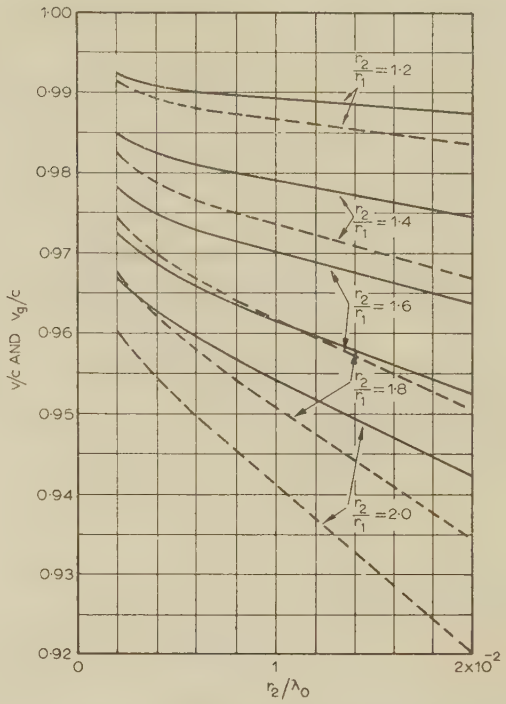

Fig. 5.—Phase and group velocities compared with the velocity of light as functions of r_2/λ_0.
—— Phase velocity.
---- Group velocity.
Permittivity = 2·26.

Group velocity is the reciprocal of the propagation time. The reciprocal of eqn. (21) gives, after transformations,

$$v_g = v - \frac{c^3}{2}\left(\frac{g_0}{\omega}\right)^2 \frac{1}{\log \frac{0{\cdot}68}{g_0 r_2}} \quad . \quad . \quad . \quad (22)$$

The group velocity as compared with the velocity of light may be seen in Fig. 5 as a function of r_2/λ_0, for various values of r_2/r_1 (curves in broken lines). The permittivity is again 2·26. As may be seen, group velocity is less than phase velocity and decreases with increase of frequency and thickness of coating.

The question arises, how does the frequency dependence of τ change? We obtain its derivative with respect to frequency, but as the full computation is lengthy we give only the final formula:

$$\frac{\partial \tau}{\partial \omega} = \frac{c}{2}\frac{g_0^2}{\omega^3}\left[-\frac{\log 0{\cdot}89 g_0 r_2 - 0{\cdot}5}{(\log 0{\cdot}89 g_0 r_2 + 0{\cdot}5)^2} + \frac{\log 0{\cdot}89 g_0 r_2}{(\log 0{\cdot}89 g_0 r_2 + 0{\cdot}5)^3}\right] \quad (23)$$

$\partial\tau/\partial\omega$ is positive. The propagation time thus increases with increase of frequency; in other words, the group velocity decreases as the frequency increases, as stated earlier. The group velocity of waves propagating in hollow guides increases with frequency and it does so much more rapidly than the group velocity of the waves propagating along a surface waveguide decreases. The phase distortion of the surface waveguide can therefore be equalized by a short hollow waveguide.

(4) DISTRIBUTION OF POWER

(4.1) Distribution of Power Around the Guide

We now examine the power distribution around the guide. To this end we determine the power transmitted outside a

cylinder of radius r. We should, therefore, write down the component of the Poynting vector in the z-direction:

$$S_z = \tfrac{1}{2}\mathscr{R}[E_{r0}H_{\phi 0}^*] = -\tfrac{1}{2}A_0A_0^*\sqrt{\left(\frac{\epsilon_0}{\mu_0}\right)}\frac{\gamma K_0}{g_0^2}[H_1^{(1)}(jg_0r)]^2 \quad (24)$$

The factor one-half results from applying the average of time. When forming the conjugate value, we have considered the behaviour of the Hankel function; i.e. since the $H_1^{(1)}$ Hankel function is negative and real in the case of a positive imaginary argument, its conjugate is equal to the original value.

Integrating eqn. (24) over the ring surface between r and ∞, we get the power transmitted outside the cylinder of radius r:

$$P_r = 2\pi\int_r^\infty S_z r dr = -\pi A_0A^*\sqrt{\left(\frac{\epsilon_0}{\mu_0}\right)}\frac{\gamma K_0}{g_0^2}\int_r^\infty [H_1^{(1)}(jg_0r)]^2 r dr \quad (25)$$

Solution of the integral will be found in Section 12.2. Substituting the result obtained there in eqn. (25),

$$P_r = -A_0A_0^*\frac{\pi}{2}\sqrt{\left(\frac{\epsilon_0}{\mu_0}\right)}\frac{\gamma K_0}{g_0^4}G(g_0r) \quad . \quad . \quad (26)$$

where

$$G(g_0r) = -(g_0r)^2\left\{\frac{2j}{g_0r}H_0^{(1)}(jg_0r)H_1^{(1)}(jg_0r) + [H_0^{(1)}(jg_0r)]^2 + [H_1^{(1)}(jg_0r)]^2\right\} \quad (27)$$

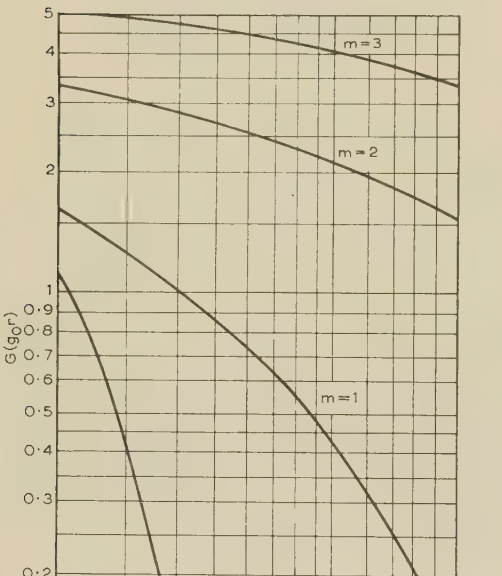

Fig. 6.—Curves determined by eqn. (27) for use in the calculation of power distribution around the guide.

The function $G(g_0r)$ is plotted in Fig. 6. The parameter m indicates the decades of g_0r. For the $m = 0$ curve, $10 \times G(g_0r)$ is plotted in order to get it on the diagram.

In the range $g_0r < 0{\cdot}1$, we can use the zero representations of Hankel functions. The value of $G(g_0r)$ will then be

$$G(g_0r) \simeq -\frac{8}{\pi^2}(\log 0{\cdot}89g_0r + 0{\cdot}5) \text{ if } g_0r < 0{\cdot}1 \quad (28)$$

In this case the power transmitted outside the cylinder of radius r is approximately

$$P_r \simeq A_0A_0^*\frac{4}{\pi}\sqrt{\left(\frac{\epsilon_0}{\mu_0}\right)}\frac{\gamma K_0}{g_0^4}(\log 0{\cdot}89g_0r + 0{\cdot}5) \quad \text{if } g_0r < 0{\cdot}1 \quad (29)$$

(4.2) Power Transmitted Around the Guide

The factor A_0 should be expressed in terms of the current I_0. With good approximation, according to the induction law $(H_{\phi 0})_{r=r_2} = I_0/(2\pi r_2)$. Here we have neglected the effect of displacement currents flowing in the coating. With the value of $H_{\phi 0}$ given in eqn. (5) we get

$$A_0A_0^* \simeq \frac{g_0^4}{16\omega^2\epsilon_0^2}I_0^2 \quad . \quad . \quad . \quad . \quad . \quad (30)$$

where I_0 is the peak value of the current.

The power transmitted around the guide is obtained from eqn. (29) with the substitution of $r = r_2$. Taking into account eqn. (30), the power transmitted around the guide is:

$$P_0 = \frac{j}{4\pi}I_0^2\frac{\gamma}{\omega\epsilon_0}(\log 0{\cdot}89g_0r_2 + 0{\cdot}5) \quad . \quad . \quad (31)$$

(4.3) Power Transferred in the Coating

The power transferred in the coating is determined by the values of E_{ri} and $H_{\phi i}$ provided by eqns. (1). As $g_ir_2 \ll 1$, we may use the zero representations of the Bessel and Neumann functions. In the following it is more convenient to express the field components in terms of the current. We therefore find the relationship between A_i and I_0. According to the induction law, the magnetic field intensity on the surface of the wire is $(H_{\phi i})_{r=r_1} = I_0/(2\pi r_1)$. Accordingly, with the value of $H_{\phi i}$ given in eqn. (1), we get

$$A_i = -j\frac{g_i^2}{4\omega\epsilon_i}I_0 \quad . \quad . \quad . \quad . \quad . \quad (32)$$

The magnetic field intensity is in phase with the current and the phase of A_i has been chosen with regard to that.

The approximate values of field components in the coating expressed in terms of the current are therefore

$$\left.\begin{aligned} E_{ri} &= -\frac{j}{2\pi}\frac{\gamma}{\omega\epsilon_i}I_0\frac{1}{r}\varepsilon^{j\omega t}\varepsilon^{-\gamma z} \\ E_{zi} &= \frac{j}{2\pi}\frac{g_i^2}{\omega\epsilon_i}I_0\log\frac{r}{r_1}\varepsilon^{j\omega t}\varepsilon^{-\gamma z} \\ H_{\phi i} &= \frac{1}{2\pi}I_0\frac{1}{r}\varepsilon^{j\omega t}\varepsilon^{-\gamma z} \end{aligned}\right\} \quad . \quad . \quad . \quad (33)$$

In making the substitution, there was also a term dependent on g_ir in the expressions for E_{ri} and $H_{\phi i}$. This, however, has been neglected compared with $1/g_ir$, since $g_ir \ll 1$.

The power transferred in the coating is given by the integral of the axial component of the Poynting vector over the cross-section of the coating. Integrating and taking into account eqn. (16), we get

$$P_i = -\frac{j}{4\pi}\frac{1}{\epsilon_{ir}\mu_{ir} - 1}\left(\frac{g_0}{K_0}\right)^2\frac{\gamma}{\omega\epsilon_0}I_0^2\log 0{\cdot}89g_0r_2 \quad (34)$$

Now we should establish what proportion of power is transferred in the coating compared with that transferred around the guide. To this end we find the quotient of eqns. (34) and (31), which is

$$\frac{P_i}{P_0} = -\frac{1}{\epsilon_{ir}\mu_{ir} - 1}\left(\frac{g_0}{K_0}\right)^2\frac{\log 0{\cdot}89g_0r_2}{\log 0{\cdot}89g_0r_2 + 0{\cdot}5} \quad (35)$$

This ratio decreases as the permittivity of the coating increases, i.e. a part of the energy goes into the outer medium. It is interesting to note that the permeability affects the ratio P_i/P_0 in the opposite sense. With increase of permeability g_0 increases in an almost direct ratio and so the ratio P_i/P_0 increases too. With increase of permittivity g_0 increases at a lower rate and so the ratio P_i/P_0 decreases. In the case of constant field concentration, as the permittivity and permeability increase, the power transferred in the coating decreases.

The ratio of the power transferred in the coating to the power transferred around the guide may be seen in Fig. 7 as a function

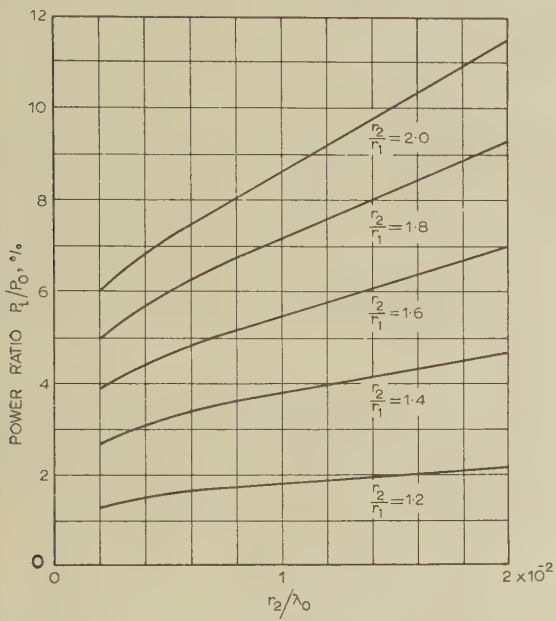

Fig. 7.—Power transmitted in the coating in relation to the power transmitted around the guide as a function of r_2/λ_0.
Permittivity = 2·26.

of r_2/λ_0 for various values of r_2/r_1. Here ϵ_{ir} is again 2·26 (polyethylene coating). As may be noticed, the power transferred in the coating increases with the increase of frequency.

Considering a reduction in the phase velocity of less than 3% and assuming that $\epsilon_{ir}\mu_{ir} > 2$, then in the range of g_0 examined, P_i/P_0 is smaller than 8%. Therefore we can neglect P_i compared with P_0 in most practical cases.

(5) CHARACTERISTIC IMPEDANCE

The relationship between the characteristic impedance, the power and the current is

$$P = \tfrac{1}{2}ZI_0^2 \quad . \quad . \quad . \quad . \quad . \quad . \quad (36)$$

Instead of the total power transmitted, we shall consider as an approximation only the power transmitted around the guide, and neglect the power transmitted in the coating. From eqns. (31) and (36), we get

$$Z = \frac{j}{2\pi}\frac{\gamma}{\omega\epsilon_0}(\log 0{\cdot}89g_0r_2 + 0{\cdot}5) \quad . \quad . \quad (37)$$

Using the approximation $\gamma \simeq K_0$ and common logarithms we obtain

$$Z = 138\log_{10}\frac{0{\cdot}68}{g_0r_2} \quad . \quad . \quad . \quad . \quad . \quad (38)$$

The characteristic impedance decreases with increase of field concentration, i.e. with increase of thickness of coating, frequency, permittivity and permeability, provided that the outer diameter is unchanged. Supposing that the thickness of the coating remains the same, the characteristic impedance also decreases with an increase of wire diameter.

The characteristic impedance may be seen in Fig. 8, as a

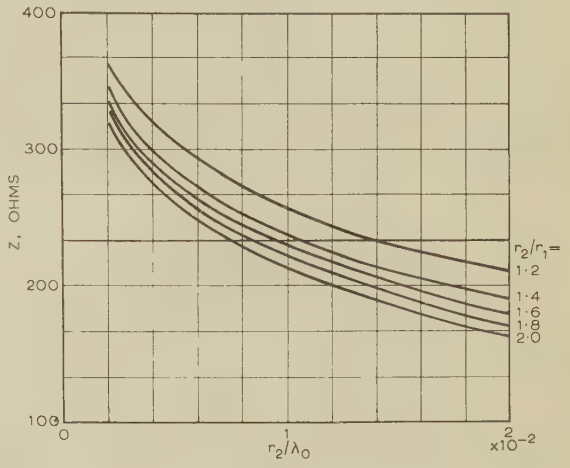

Fig. 8.—Characteristic impedance as a function of r_2/λ_0.
Permittivity = 2·26.

function of r_2/λ_0, for different values of r_2/r_1 (polyethylene coating, $\epsilon_{ir} = 2{\cdot}26$). As may be seen, characteristic impedance decreases with increase of frequency and thickness of the layer.

The characteristic impedance may be employed when designing surface-wave transmission lines, e.g. when analysing matching between the launching horns and the surface waveguide, or between surface waveguides of different parameters.

(6) LOSSES

(6.1) Losses in the Line

The effect of loss is calculated in the usual manner, assuming that the field distribution in an equiphase plane is approximately the same as in the lossless case.

The variation of the power in the z-direction is $P = P_1\varepsilon^{-2\alpha z}$ Differentiating this expression, we obtain

$$\alpha = -\frac{1}{2P}\frac{dP}{dz} \quad . \quad . \quad . \quad . \quad . \quad (39)$$

Here α is the attenuation coefficient in nepers per metre. The differential quotient dP/dz signifies the power lost per unit length.

The losses of the line consist of the conductive loss of the wire, and the dielectric and magnetic losses of the coating.

The I^2R loss per unit length is

$$\frac{dP_c}{dz} = -\frac{1}{4\pi r_1}\sqrt{\left(\frac{\omega\mu_c}{2\sigma_c}\right)}I_0^2 \quad . \quad . \quad . \quad (40)$$

where σ_c is the conductivity and μ_c is the permeability of the wire.

The dielectric loss in the coating is proportional to the total electric field strength, which is obtainable by vectorial addition of the components. As the radial component is much greater than the axial, we shall ignore the latter. Hence the power loss in a unit cube is $-\frac{1}{2}\omega\epsilon_i \tan\delta|E_{ri}|^2$, ($\tan\delta$ = dielectric-loss factor). Integrating this over the cross-section of the coating and taking into account eqn. (16), we get

$$\frac{dP_d}{dz} = \frac{1}{4\pi}\frac{\gamma^2}{\omega\epsilon_0}\left(\frac{g_0}{K_0}\right)^2\frac{1}{\epsilon_{ir}\mu_{ir}-1}\tan\delta I_0^2\log 0{\cdot}89g_0r_2 \quad (41)$$

The magnetic loss in a unit cube of the coating is $-\frac{1}{2}\omega\mu_l \tan\theta|H_{\phi l}|^2$, ($\tan\theta$ = magnetic-loss factor). Integrating over the cross-section of the coating and taking into account eqn. (16), we get

$$\frac{dP_m}{dz} = -\frac{1}{4\pi}\omega\mu_0 \frac{\epsilon_{ir}\mu_{ir}}{\epsilon_{ir}\mu_{ir}-1}\left(\frac{g_0}{K_0}\right)^2 \tan\theta I_0^2 \log 0{\cdot}89 g_0 r_2 \quad (42)$$

We now determine the value of the attenuation coefficient. In the course of our calculation, we shall ignore the power transmitted in the coating and take γ/K_0 as unity. Components of the attenuation coefficient on the basis of eqns. (31), (39)–(42), in nepers per metre, are

$$\left.\begin{aligned}
\alpha_c &= -\frac{1}{2}\frac{1}{r_1}\sqrt{\left(\frac{\omega\epsilon_0\mu_c}{2\sigma_c\mu_0}\right)}\frac{1}{\log 0{\cdot}89 g_0 r_2 + 0{\cdot}5} \\
\alpha_d &= \frac{j}{2}\frac{1}{\epsilon_{ir}\mu_{ir}-1}\frac{g_0^2}{K_0}\tan\delta\frac{\log 0{\cdot}89 g_0 r_2}{\log 0{\cdot}89 g_0 r_2 + 0{\cdot}5} \\
\alpha_m &= \frac{j}{2}\frac{\epsilon_{ir}\mu_{ir}}{\epsilon_{ir}\mu_{ir}-1}\frac{g_0^2}{K_0}\tan\theta\frac{\log 0{\cdot}89 g_0 r_2}{\log 0{\cdot}89 g_0 r_2 + 0{\cdot}5}
\end{aligned}\right\} \quad (43)$$

The total attenuation is the sum of these three components so that the attenuation coefficient in decibels per metre becomes

$$\alpha = \frac{R(g_0 r_2)}{r_1\sqrt{\lambda_0}} + \left(\frac{1}{\epsilon_{ir}\mu_{ir}-1}\tan\delta + \frac{\epsilon_{ir}\mu_{ir}}{\epsilon_{ir}\mu_{ir}-1}\tan\theta\right)\frac{\lambda_0}{r_2^2}B(g_0 r_2) \quad (44)$$

in which

$$R(g_0 r_2) = -0{\cdot}397\sqrt{\left(\frac{\mu_{cr}}{\sigma_c}\right)}\frac{1}{\log 0{\cdot}89 g_0 r_2 + 0{\cdot}5} \quad . \quad (45)$$

$$B(g_0 r_2) = 0{\cdot}69(g_0 r_2)^2\frac{\log 0{\cdot}89 g_0 r_2}{\log 0{\cdot}89 g_0 r_2 + 0{\cdot}5} \quad . \quad . \quad . \quad (46)$$

If the wire is of copper

$$R(g_0 r_2) = -5{\cdot}25 \times 10^{-5}\frac{1}{\log 0{\cdot}89 g_0 r_2 + 0{\cdot}5} \quad . \quad . \quad (47)$$

To make computation easier, the functions (46) and (47) are plotted in Fig. 9.

The conductive attenuation increases with the increase of field concentration, i.e. with increase of frequency, thickness of coating, permittivity and permeability. Conductive attenuation decreases with the increase of wire diameter and conductivity.

Dielectric attenuation increases with increase of frequency, thickness of coating and permeability. It decreases, however, with increase of permittivity, because the radial electric field strength in the coating is reduced by the increased permittivity. In the case of constant field concentration, a variation of the outer diameter hardly affects the dielectric attenuation.

Magnetic attenuation increases with increasing frequency, thickness of coating and permeability, but hardly depends on permittivity. If field concentration is constant, magnetic attenuation is not sensitive to a change in outer diameter.

A peculiar difference can be observed in the dependence of dielectric and magnetic attenuation on material properties. In the case of constant field concentration, the dielectric attenuation decreases rapidly with increasing permittivity and permeability, while the decrease of magnetic attenuation is small under similar conditions (provided that $\epsilon_{ir}\mu_{ir} > 2$). If the parameters of the transmission line, the frequency and the loss factors are the same, the dielectric attenuation is less than the magnetic one and the difference between them increases with $\epsilon_{ir}\mu_{ir}$. To decrease the attenuation, it is therefore worth while to employ dielectric coating of high permittivity.

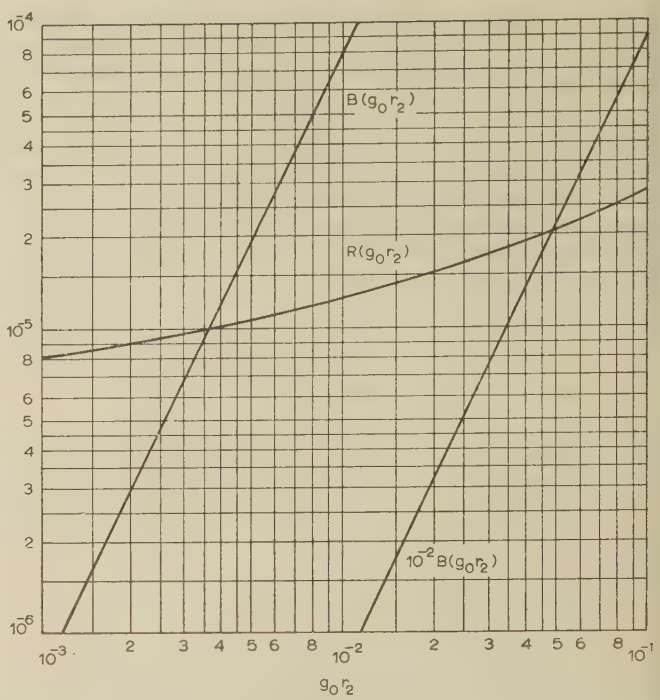

Fig. 9.—Curves for calculating attenuation [eqns. (46) and (47)].

(6.2) Launching Loss

The launching of the surface wave from a coaxial line is by means of a horn, as shown in Fig. 10. Only a part of the energy is transformed into surface-wave energy, the rest being radiated. The radiated energy constitutes loss.

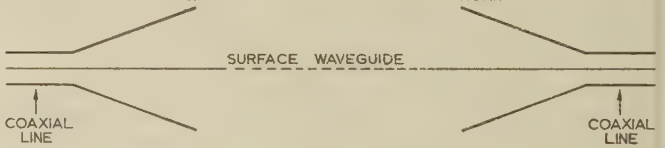

Fig. 10.—Launching of surface waves.

The horn loss can be calculated approximately. Considering the receiving end, the horn can collect only that portion of the field which falls within the area of the aperture. Thus, the efficiency of a horn is determined by the power transmitted within a cylindrical surface equal to the horn aperture, in proportion of the total power, which, using eqn. (26) is

$$\eta = 1 - \frac{G(g_0 r_h)}{G(g_0 r_2)} \quad . \quad . \quad . \quad . \quad . \quad . \quad (48)$$

The aperture radius of the horn is r_h. We have ignored the power transmitted in the coating.

By the reciprocity theorem, the efficiencies of the horns for transmission and reception must be the same. The combined efficiency of both horns, expressed in decibels, is called the launching loss:

$$L_g = -20\log_{10}\left[1 - \frac{G(g_0 r_h)}{G(g_0 r_2)}\right] \quad . \quad . \quad . \quad (49)$$

he larger the aperture of the horn and the greater the field ɔncentration, the smaller is the launching loss.

The launching loss is practically 1–2 dB above the figure ɛtermined by eqn. (49) and it cannot be decreased below 1 dB, ven by using very large horns. However, this increase of loss ınnot be calculated, and so it will be ignored.

(6.3) Total Loss

The total loss of a surface-wave transmission line is the sum of ıe line loss and the launching loss. The line loss is the product f the attenuation coefficient and the length of the line. The tenuation coefficient can be calculated from eqn. (44), the ngth of the line is given, and the launching loss can be obtained om eqn. (49).

(7) OPTIMUM FIELD CONCENTRATION

The total loss of a given surface-wave transmission line has minimum at a certain value of field concentration which is ılled the optimum field concentration. Below this optimum ılue, the launching loss increases faster than the rate at which ıe line loss falls. Thus the total loss of the transmission line ıcreases. In this range the launching loss is dominant. If field ɔncentration is increased above the optimum value, the line ɔss will be increasing quicker than the rate at which the ıunching loss decreases and the total loss of the transmission ne increases again. In this range the line loss is dominant.

As an illustration of the foregoing, the total losses of four ansmission lines of different lengths, but with otherwise lentical parameters, are plotted in Fig. 11 as functions of field

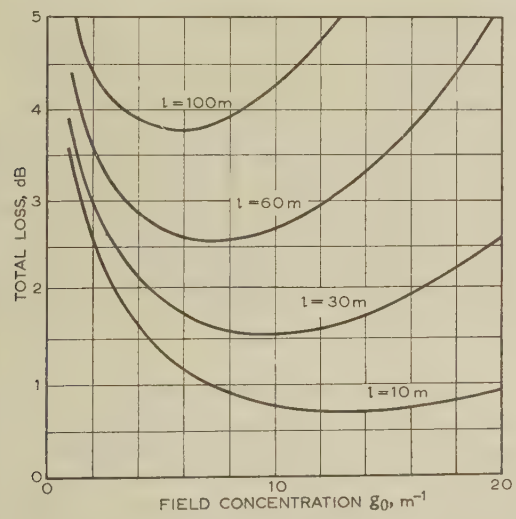

ig. 11.—Dependence of total loss of surface-wave transmission lines on field-concentration.

$r_h = 10$ cm.
$r_2 = 1{\cdot}5$ mm.
$f = 3$ Gc/s ($\lambda_0 = 10$ cm).
$\epsilon_{ir} = 2$.
$\tan\delta = 3 \times 10^{-4}$.

ɔncentration. To make the calculation quicker, we attribute to ıe coating dielectric properties only, i.e. $\mu_{ir} = 1$, $\tan\theta = 0$. his does not change the results qualitatively. It can be seen that ıe optimum field concentration shifts towards smaller values s the line length increases. This is because line loss increases ith length of line. By analogy, the effect of an alteration in the ther data of the transmission line on the optimum field con- ɛntration can be ascertained; it is only necessary to determine hether the alteration has increased or decreased the line loss.

The optimum field concentration increases as the horn aperture, line length, loss factors and permeability of the coating decrease, and as the permittivity of the coating and the diameter and conductivity of the wire increase. But optimum field concentration also depends on frequency. With increase of frequency, the optimum field concentration decreases.

It might be thought that optimum field concentration could be determined accurately by differentiating with respect to g_0 the formulae giving the total loss of the transmission line, and equating to zero. Unfortunately, the optimum value of g_0 cannot be given in an explicit form and so this procedure cannot be used; we should seek to find the optimum field concentration by trial and error.

The changes in the field concentration in the foregoing were equivalent to changes in the thickness of the coating. Therefore, to find the optimum field concentration meant finding the optimum thickness of coating. The abscissae of Fig. 11 could thus also indicate the thickness of the coating.

A variation of field concentration may also be effected by a change of frequency. All the data of the transmission line, including the thickness of the coating, are now constant, and so we get the frequency-dependence of the total loss in the transmission line. The optimum field concentration is at the frequency for which the total loss is minimum.

(8) MAXIMUM TRANSMISSIBLE POWER

(8.1) Maximum Transmissible Peak Power

First the maximum power-carrying capacity is determined from the maximum electric field strength allowable in air. Field strength is greatest on the surface of the coating and its components are obtained from eqns. (5). Here we are concerned with the real part of the expressions giving the field components and for this reason we must take into account the behaviour of the Hankel functions. In the case of a positive imaginary argument, $H_0^{(1)}$ is negative imaginary, whereas $H_1^{(1)}$ is negative real. In conformity with these, the values of the field components at the surface are

$$\left.\begin{aligned}(E_{r0})_{r=r_2} &= -jA_0\frac{\gamma}{g_0}H_1^{(1)}(jg_0r_2)\cos(\omega t-\beta z)\\ (E_{z0})_{r=r_2} &= jA_0H_0^{(1)}(jg_0r_2)\sin(\omega t-\beta z)\end{aligned}\right\} \quad . \quad (50)$$

There is a phase difference of $\pi/2$ between E_{z0} and E_{r0}. Since the amplitude of E_{z0} is smaller than that of E_{r0}, the maximum resultant field intensity is equal to the amplitude of E_{r0}:

$$E_{max} = -jA_0\frac{\gamma}{g_0}H_1^{(1)}(jg_0r_2) \simeq jA_0\frac{2}{\pi}\frac{\gamma}{g_0^2r_2} \quad . \quad (51)$$

Here we have used the zero representation of the Hankel function.

In the calculation of maximum transmissible power the power transferred in the coating is neglected. Using eqn. (51), let us express the value of $A_0A_0^*$ in terms of E_{max}^2 and substitute it in eqn. (29), putting $r = r_2$. Then

$$P_{max} = -\pi\sqrt{\left(\frac{\epsilon_0}{\mu_0}\right)}\frac{K_0}{\gamma}r_2^2E_{max}^2(\log 0{\cdot}89g_0r_2 + 0{\cdot}5) \quad (52)$$

In air the highest allowable value of electric field strength is 3×10^6 V/m. Substituting this and the values of ϵ_0 and μ_0, and the approximation $\gamma/K_0 = 1$ in eqn. (52) we get

$$P_{max} = 1{\cdot}73 \times 10^{11}r_2^2\log_{10}\frac{0{\cdot}68}{g_0r_2} \quad . \quad . \quad . \quad (53)$$

The maximum transmissible power decreases with increase of field concentration, i.e. with increase of frequency, thickness of coating, permittivity and permeability. Supposing that the field concentration is unchanged, as the outer diameter of the conductor increases, the power-carrying capacity increases.

(8.2) Maximum Transmissible Average Power

So far we have determined the maximum transmissible power on the basis of the highest allowable electric field strength. In designing surface waveguides, however, we must take into account the effect of heating since most coating materials are useless at high temperatures. The heating of the guide is due to losses and the power lost per unit length may be expressed from eqn. (39) as follows:

$$\left|\frac{dP}{dz}\right| = \frac{2}{8{\cdot}686}\alpha P \quad . \quad . \quad . \quad . \quad . \quad (54)$$

In this formula α should be substituted in decibels per metre.

The heat arising in the conductor flows to the outer surface by means of the thermal conductivity of the coat, from which it is transferred by convection to the sourroundings.

The general equation of heat conduction is

$$\frac{dQ}{dt} = \sigma_h \frac{F}{d}(T_1 - T_2) \text{ kilocalories per hour} \quad . \quad (55)$$

where dQ/dt = Rate of flow.
σ_h = Thermal conductivity.
F = Surface area at right angles to the flow.
d = Length of conducting path.
$T_1 - T_2$ = Temperature difference.

Consequently, the thermal resistance is $R_T = d/(\sigma_h F)$. We make our calculations for a unit length of the guide. Thus, $\frac{dQ}{dt} = \frac{1}{1{\cdot}16}\left|\frac{dP}{dz}\right|$ since 1 kcal/h = 1·16 watts.

The heat arising in the wire flows through the whole thickness of the coating. The thermal resistance of the coating is $R_T = \frac{1}{2\pi\sigma_h}\log\frac{r_2}{r_1}$. The temperature difference needed to remove the heat is

$$\Delta T_c = \frac{1}{1{\cdot}16}\frac{1}{2\pi\sigma_h}\left|\frac{dP_c}{dz}\right|\log\frac{r_2}{r_1} \quad . \quad . \quad . \quad (56)$$

The heat in the coat is distributed and so the temperature difference necessary for its removal will be smaller. A detailed calculation based on a knowledge of the field distribution (Section 12.3) gives

$$\Delta T_i = \frac{1}{2}\frac{1}{1{\cdot}16}\frac{1}{2\pi\sigma_h}\left|\frac{dP_i}{dz}\right|\log\frac{r_2}{r_1} \quad . \quad . \quad . \quad (57)$$

This is half the value required if the heat energy flows through the whole thickness of the coat.

The temperature difference needed to transfer the total heat energy to the outer surface is the sum of eqns. (56) and (57), and using eqn. (54), we get

$$T_1 - T_2 = 3{\cdot}16 \times 10^{-2}\frac{1}{\sigma_h}\left(\alpha_c + \frac{\alpha_d + \alpha_m}{2}\right)P\log\frac{r_2}{r_1} \quad (58)$$

Here T_1 and T_2 are the temperatures of the inner and outer surfaces of the coating, respectively.

The heat energy removed to the surface is transferred to the surrounding air by convection. The general equation of heat transfer by convection is

$$\frac{dQ}{dt} = aF(T_2 - T_3) \text{ kilocalories per hour} \quad . \quad . \quad (59)$$

where T_3 is the temperature of the surrounding air rem from the guide and a is the heat-transfer coefficient. Unf tunately, a is a function of many parameters. If the conduct are of small diameter and the temperature differences are very great,[9] a is given approximately by

$$a = 0{\cdot}169\frac{(T_2 - T_3)^{1/8}}{(r_2)^{5/8}} \quad . \quad . \quad . \quad . \quad (6$$

Taking into account eqns. (59), (60) and (54), the temperat difference necessary for the transfer of the heat energy per u length to the surrounding is

$$T_2 - T_3 = 0{\cdot}225\frac{\alpha^{8/9}}{(r_2)^{3/9}}P^{8/9} \quad . \quad . \quad . \quad (6$$

The total temperature difference, $T_1 - T_3$, is the sum eqns. (58) and (61). With these formulae we can determ the overheating of the guide when transmitting a given po and thus estimate the suitability of the guide.

However, the question that interests us more is to determ what power a guide can transmit with the maximum permissi overheating. To this end, we ought to find P from the sum eqns. (58) and (61). Unfortunately, this cannot be done. might find P by the method of repeated approximations, b instead we use a simple approximation. In the case of a t coat, $T_1 - T_2$ is, in general, much less than $T_2 - T_3$ and v be neglected in comparison. So the maximum transmissi power, from eqn. (61), is

$$P_{max} = 5{\cdot}35\frac{(r_2)^{3/8}}{\alpha}(T_2 - T_3)^{9/8}_{max} \quad . \quad . \quad . \quad (6$$

It increases with radius of conductor and permissible ov heating, and inversely as the attenuation of the guide.

Eqn. (53) determines the maximum transmissible po from the highest permissible electric field strength, wh eqn. (62) does so from the highest permissible degree of ov heating. The latter gives, in general, a value less by seve orders of magnitude and therefore in the case of continuc wave it is sufficient to calculate only by the latter formu However, in transmitting pulses of high power we need bo formulae. The average power must not exceed the value giv by eqn. (62) and the pulse peak-power the value given eqn. (53). In both cases the maximum transmissible powers a referred to the input of the guide, since the wave along the li is attenuated.

(9) METHOD OF DESIGN

In designing surface-wave transmission lines certain da such as length of line, frequency band and clearance area arou the guide, are given and in general cannot be changed. T clearance area determines the upper limit of the field extensi of the surface wave. The field extension of the surface wave c be characterized by the limit radius, which is the reciprocal of t field concentration:

$$r_0 = \frac{1}{g_0} \quad . \quad . \quad . \quad . \quad . \quad . \quad . \quad . \quad (6$$

The wave propagation is not disturbed by surrounding obj if they are at a distance at least three times the limit radius fr the guide. If the boundary of the clearance area has a radi r_a, then $r_a \geqslant 3r_0$, or

$$g_0 \geqslant \frac{3}{R_t} \quad . \quad . \quad . \quad . \quad . \quad . \quad . \quad (6$$

The minimum value of g_0 is thus determined by the radius the clearance area around the guide.

Other data are decided by the designer according to his o

dgment. Values are assumed for the outer radius of the ıide and the aperture radius of the horn, and the material of e coating is chosen. Then by trial and error the optimum ld concentration at the mid-frequency of the band is found ıd from this the necessary thickness of the coating is deter-ined. The suitability of the transmission line for the power quired is then checked and the phase distortion is determined. In order to reduce the attenuation, the outer radius of the ıide and the aperture radius of the horn should be as large as ssible. The material of the coating should have a high rmittivity, with small loss angle. The outer radius of the ıide should also be large, because thus rain, snow, ice and dirt cumulating on the surface will have less effect on the wave opagation.

We cannot produce the optimum field concentration in every se. On the one hand we cannot realize a smaller concentration an that of a bare wire,* and on the other hand the field concen-ıtion cannot be below the value given by eqn. (64) lest the wave opagation should be disturbed by surrounding objects. Con-quently, in the case of very long lines, when the optimum field ncentration is not realizable, the use of the smallest permissible ld concentration and the biggest permissible launching horns good engineering practice.

(10) EXAMPLE

Let us design a surface-wave transmission line for the band 5–3·5 Gc/s. The radius of the clearance area around the nductor is 1 m and the length of the line is 30 m.

We assume $r_2 = 1{\cdot}5$ mm, $r_h = 10$ cm, $\epsilon_{ir} = 2$ and $\tan\delta = \times 10^{-4}$.

The radius of the clearance area around the conductor termines the minimum value of g_0. From eqn. (64), $0)_{min} = 3\,\mathrm{m}^{-1}$. In the centre of the band, at $f = 3$ Gc/s $_0 = 10$ cm), we should find the value of the optimum field con-ntration. We should begin our calculation with $g_0 = 4\,\mathrm{m}^{-1}$, cause thus g_0 will not be less than $(g_0)_{min}$ at the lower edge of e band. Thus $g_0 r_2 = 0{\cdot}006$. From Fig. 2 we obtain the rresponding $\mathrm{M}(g_0 r_2) = 4{\cdot}77 \times 10^{-6}$. Then from eqn. (18) e determine the inner radius, $r_1 = 1{\cdot}44$ mm. The next thing to compute the attenuation factor. Fig. 9 gives the values $(g_0 r_2) = 1{\cdot}11 \times 10^{-5}$ and $\mathrm{B}(g_0 r_2) = 2{\cdot}75 \times 10^{-5}$. On intro-ıcing these into eqn. (44), $\alpha_c = 0{\cdot}024\,4$ dB/m and $\alpha_d =$ 000 36 dB/m. Hence $\alpha = 0{\cdot}024\,76$ dB/m. Thus, the line loss $L_v = \alpha l = 0{\cdot}743$ dB. We now look at the value of the unching loss. Taken from Fig. 6, $\mathrm{G}(g_0 r_h) = 0{\cdot}56$ and $(g_0 r_2) = 3{\cdot}85$. From eqn. (49) the launching loss is $L_g =$ 36 dB. The total loss is $L_t = L_g + L_v = 2{\cdot}1$ dB.

Next we calculate the total loss for $g_0 = 5\,\mathrm{m}^{-1}$, which is $= 1{\cdot}88$ dB. The total loss falls and therefore we are proaching the minimum. Continuing our trials, we shall find e optimum value of g_0. One of the curves in Fig. 11 just ustrates our example. According to this the minimum loss 1·5 dB. The optimum value of the field concentration from e curve is $(g_0)_{opt} = 10\,\mathrm{m}^{-1}$. The corresponding inner radius $r_1 = 1{\cdot}2$ mm. The optimum thickness of the coating is erefore 0·3 mm, and with this we have determined all the ıide dimensions.

Now we determine various characteristics of wave propaga-on along the guide. We are interested only in the extreme lues appearing in the unfavourable direction in the band. ese are obtained at the upper frequency of the band in respect every characteristic, and are as follows. The phase velocity, om eqn. (20), is $v/c = 98{\cdot}66\%$. The group velocity, from n. (22), is $v_g/c = 98{\cdot}3\%$. On the basis of eqn. (35), the

* Capacitive surfaces[10] are not taken into consideration.

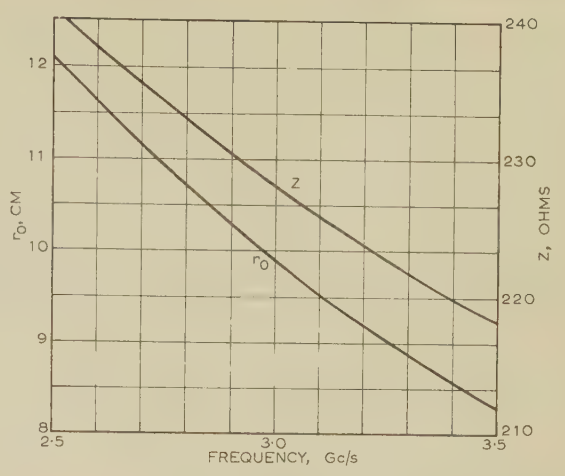

Fig. 12.—Frequency dependence of the limit radius and characteristic impedance.

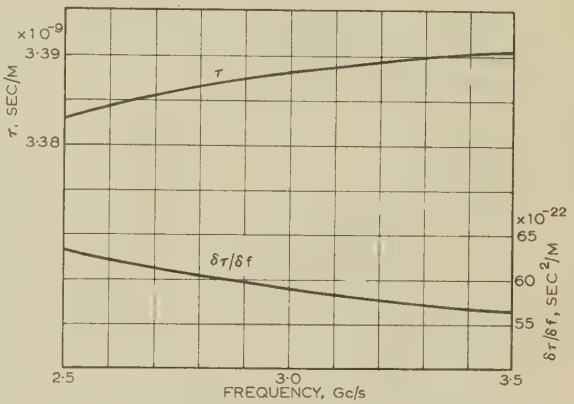

Fig. 13.—Propagation time per unit length (upper curve) and tangent of this curve (lower curve) as functions of frequency.

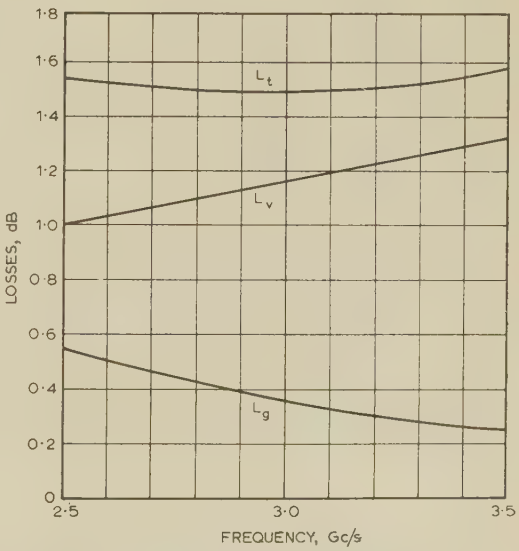

Fig. 14.—Frequency-dependence of losses.

L_t = Total loss.
L_v = Line loss.
L_g = Launching loss.

power quota transferred in the coating is $P_i/P_0 = 3{\cdot}1\%$. Characteristic impedance is obtained from eqn. (38): $Z = 217{\cdot}6$ ohms. The maximum transmissible pulse peak power, from eqn. (53), is 613 kW. The maximum transmissible average power, from eqn. (62), is 485 watts assuming a maximum temperature rise of 30° C. In both cases the maximum powers are referred to the input end.

We now deal with the frequency dependence of a few characteristics of the line. The frequency dependence of the limit radius and of the characteristic impedance is shown in Fig. 12. As the frequency rises, both of these decrease. Fig. 13 shows the propagation time per unit length as a function of frequency, giving at the same time the tangent of the curve $\partial\tau/\partial f$. As may be seen, the phase distortion is small and its sense is the opposite of the phase distortion of hollow waveguides. The frequency dependence of the losses may be seen in Fig. 14. The line loss grows as frequency increases but the launching loss decreases. The total loss, which is the sum of the two, has a minimum at the centre of the band.

(11) REFERENCES

(1) SOMMERFELD, A.: 'Über die Fortpflanzung elektrodynamischer Wellen längs eines Drahtes', *Annalen der Physik und Chemie*, 1899, **67**, p. 233.

(2) GOUBAU, G.: 'Surface Waves and their Application to Transmission Lines', *Journal of Applied Physics*, 1950, **21**, p. 1119.

(3) GOUBAU, G., and SHARP, C. E.: 'A U.H.F. Surface-Wave Transmission Line', *Proceedings of the Institute of Radio Engineers*, 1953, **41**, p. 107.

(4) KADEN, H.: 'Fortschritte in der Theorie der Drahtwellen', *Archiv der elektrischen Übertragung*, 1951, **5**, p. 399.

(5) BARLOW, H. E. M., and KARBOWIAK, A. E.: 'An Investigation of the Characteristics of Cylindrical Surface Waves', *Proceedings I.E.E.*, Paper No. 1462 R, April, 1953 (**100**, Part III, p. 321).

(6) BARLOW, H. E. M., and CULLEN, A. L.: 'Surface Waves', *ibid.*, Paper No. 1482 R, April, 1953 (**100**, Part III, p. 329).

(7) BARLOW, H. E. M.: 'The Relative Power-Carrying Capacity of High-Frequency Waveguides', *ibid.*, Paper No. 1225 R, January, 1952 (**99**, Part III, p. 21).

(8) BARLOW, H. E. M.: 'The Power Radiated by a Surface Wave Circulating around a Cylindrical Surface', *ibid.*, Paper No. 2771 E, March, 1959 (**106** B, p. 180).

(9) MICHEEV, M. A.: 'Principles of Thermic Convection' (in Russian) (State Publishing Company of Energetics, Moscow–Leningrad, 1949).

(10) BARLOW, H. E. M., and KARBOWIAK, A. E.: 'An Experimental Investigation of Axial Cylindrical Surface Waves Supported by Capacitive Surfaces', *Proceedings I.E.E.*, Paper No. 1786 R, May, 1955 (**102** B, p. 313).

(11) STRATTON, J. A.: 'Electromagnetic Theory' (McGraw-Hill, 1941), pp. 360–361.

(12) BERCELI, T.: 'Transmission Lines with Small Loss' (Manuscript in Hungarian), Candidate's dissertation, 1955. Available in the library of the Hungarian Academy of Sciences.

(12) APPENDICES

(12.1) Calculation of Propagation Time

The propagation time per unit length is the partial differential of phase-change coefficient with respect to ω, according to the definition. The phase-change coefficient can be expressed from eqn. (7). As $|g_0/K_0| \ll 1$, approximating the square root a taking into account $K_0 = j\omega/c$, the phase-change coefficient unattenuated wave propagation is

$$\beta = \frac{\omega}{c} + \frac{1}{2}\frac{c}{\omega}g_0^2 \quad . \quad . \quad . \quad . \quad . \quad (6$$

The propagation time per unit length is its derivative w respect to ω:

$$\tau = \frac{1}{c} - \frac{1}{2}\frac{c}{\omega^2}g_0^2 + \frac{c}{\omega}g_0\frac{\partial g_0}{\partial\omega}$$

$$= \frac{1}{c}\left[1 + \frac{c^2}{2}\left(\frac{g_0}{\omega}\right)^2\frac{\log 0{\cdot}89g_0r_2 - 0{\cdot}5}{\log 0{\cdot}89g_0r_2 + 0{\cdot}5}\right] . \quad . \quad (6$$

The value of $\partial g_0/\partial\omega$ can be obtained as follows. Le differentiate the function $M(g_0r_2)$, given in eqn. (17), w respect to ω:

$$\frac{\partial M(g_0r_2)}{\partial\omega} = \left(-\frac{g_0r_2}{2\pi^2}\log 0{\cdot}89g_0r_2 - \frac{g_0r_2}{4\pi^2}\right)\frac{\partial g_0r_2}{\partial\omega} \quad . \quad (6$$

The same differential may also be determined from eqn. (18

$$\frac{\partial M(g_0r_2)}{\partial\omega} = \frac{1}{2\pi^2}\left(\mu_{ir} - \frac{1}{\epsilon_{ir}}\right)\frac{r_2^2}{c^2}\omega\log\frac{r_2}{r_1} = \frac{2}{\omega}M(g_0r_2) \quad (6$$

From eqn. (17) we substitute for $M(g_0r_2)$:

$$\frac{\partial M(g_0r_2)}{\partial\omega} = -\frac{2}{\omega}\left(\frac{g_0r_2}{2\pi}\right)^2\log 0{\cdot}89g_0r_2 \quad . \quad . \quad (6$$

Expressing $\partial g_0r_2/\partial\omega$ from eqns. (67) and (69) and dividing r_2, we get

$$\frac{\partial g_0}{\partial\omega} = \frac{g_0}{\omega}\frac{\log 0{\cdot}89g_0r_2}{\log 0{\cdot}89g_0r_2 + 0{\cdot}5} \quad . \quad . \quad . \quad (6$$

(12.2) Calculation of Power Distribution around the Guide

The task is to define the integral contained in eqn. (25). T solution of integrals of this type is

$$\int_{r_1}^{r_2} r[Z_\nu(gr)]^2dr = \frac{1}{2}\left\{r^2\left[\frac{dZ_\nu(gr)}{d(gr)}\right]^2 + \left(r^2 - \frac{\nu^2}{g^2}\right)[Z_\nu(gr)]^2\right\}_{r_1}^{r_2}$$

. . . . (6

Here Z_ν designates a cylindrical function of the order ν.

Applying this to eqn. (25) and using the derivation formu for cylindrical functions, we obtain

$$\int_r^\infty r[H_1^{(1)}(jg_0r)]^2dr = -\frac{1}{2}r^2\left\{\frac{2j}{g_0r}H_0^{(1)}(jg_0r)H_1^{(1)}(jg_0r) + [H_0^{(1)}(jg_0r)]^2 + [H_1^{(1)}(jg_0r)]^2\right\} \quad (6$$

(12.3) Calculation of the Maximum Transmissible Power

The task is to determine the temperature difference needed remove the heat generated in the coating. The calculation for a unit length of the guide. The temperature differer necessary for the removal of the heat generated in the coat a tube of radius r and of thickness dr is obtained by analo with eqn. (56):

$$\Delta T_r = \frac{1}{1{\cdot}16}\frac{1}{2\pi\sigma_h}\left|\frac{dP_i}{dz}\right|_r\log\frac{r_2}{r} \quad . \quad . \quad . \quad (6$$

The heat generated in the elementary tube is the product

ıe heat per unit volume and of the volume of the elementary ıbe. We now take the heat power generated only as a conse-uence of the dielectric loss:

$$\left|\frac{dP_d}{dz}\right|_r = \pi\omega\epsilon_i \tan\delta |E_{ri}|^2 r dr \quad . \quad . \quad . \quad (74)$$

ubstituting this in eqn. (73) with the value of E_{ri} given in qn. (33) and integrating between r_1 and r_2, we get the necessary ɛmperature difference:

$$\Delta T_d = -\frac{1}{2}\frac{1}{1\cdot 16}\frac{1}{8\pi^2\sigma_h}\frac{\gamma^2}{\omega\epsilon_i}\tan\delta I_0^2\left(\log\frac{r_2}{r_1}\right)^2 \quad . \quad (75)$$

Let us express I_0^2 from eqn. (31) in terms of P_0 and the value of $\log r_2/r_1$ (not its square) from eqn. (16). By substituting these in eqn. (75) and taking into account eqns. (39) and (43),

$$\Delta T_d = \frac{1}{2}\frac{1}{1\cdot 16}\frac{1}{2\pi\sigma_h}\left|\frac{dP_d}{dz}\right|\log\frac{r_2}{r_1} \quad . \quad . \quad . \quad (76)$$

This is half the value which would result if the power lost per unit length, dP_d/dz, flowed through the whole thickness of the coating.

By a similar calculation we arrive at the same result for the removal of heat generated as a consequence of the magnetic loss.

621.372.833

The Institution of Electrical Engine
Monograph No. 43
Apr. 19

A BROAD-BAND WAVEGUIDE JUNCTION CONTAINING DIELECTRIC

By P. J. B. CLARRICOATS, B.Sc.(Eng.), Ph.D., Graduate.

(*The paper was first received* 11*th October, and in revised form* 1*st December*, 1960. *It was published as an* INSTITUTION MONOGRAPH *in April*, 1961.)

SUMMARY

A method is described for obtaining a broad-band impedance match between two joined waveguides of differing cross-section. The method involves the use of an axially mounted dielectric which partially fills the waveguide cross-section. With an appropriate choice of dielectric cross-sectional area and permittivity the electromagnetic field is mainly confined to the region of the rod. Under these conditions the waveguide cross-section may be abruptly changed without appreciable reflection. The case of two joined circular waveguides containing an axial dielectric rod is treated theoretically for H_{01}-mode propagation. A similar configuration is studied experimentally for the H_{11}-type mode of propagation. In both cases an appreciable reduction in reflection coefficient is demonstrated when the rod is present. The application of the principle to other waveguide cross-sections is briefly mentioned.

LIST OF SYMBOLS

$a = r_0'/r_1$.
a_m = Amplitude coefficient of mth normal mode field.
$b = r_0'/r_0$.
E_{tm}, E'_{tm} = Transverse electric fields of mth normal modes in waveguides of cross-sections S and S'.
E_t = Transverse electric field in junction aperture.
$F(x) = xJ_1'(x)/J_1(x)$.
$G(x) = J_0'(x)/xJ_0(x)$.
H_{tm}, H'_{tm} = Transverse magnetic fields of mth normal modes in waveguides of cross-sections S and S'.
$I_n(\bar{y})$ = Modified Bessel function of the first kind.
$J_n(x)$ = Bessel function of the first kind.
j_m = mth root of $J_n(x)$.
K, K_1 = Wavenumbers within and external to dielectric rod.
$\bar{K}_1$ = Value of K_1 appropriate to empty waveguide.
$k = -jK_1$.
$\bar{K}$, $\bar{k}$ = Values of K and k appropriate to unbounded rod.
$K_n(\bar{y})$ = Modified Bessel function of the second kind.
r, r_1, r_0, r_0' = Radius of point, rod and waveguide respectively.
t_1, t_2, t_2' = Functions defined for $\bar{\beta} < 1$ in eqn. (7)
$x_1 = Kr_1$.
$y_p = K_1 r_p$ $(p = 1, 0, 0')$.
$\bar{y}_p = k_1 r_p$ $(p = 1, 0, 0')$.
Y_0, Y_0' = Characteristic admittances of transmission lines representing waveguide junction.
Y_1, Y_1' = Wave admittances of H_{01} modes in waveguides of cross-sections S and S'.
Y_n = Bessel function of the second kind.
z = Longitudinal co-ordinate.
β, β', β_0, β_u = Phase-change coefficients corresponding to waveguides of cross-sections S and S', empty waveguide and unbounded rod respectively.
$\bar{\beta} = \beta\lambda_0/2\pi$ = Normalized phase-change coefficient.
$\delta_\beta = -(1 - \beta'/\beta)$.
$\delta_p = \left(1 - \frac{T_1 + t_2}{T_1 + t_2'}\right)$.
ϵ, ϵ_0 = Permittivities of rod and free space.
λ_0 = Free-space wavelength.
μ_0 = Permeability of free space.
ρ = Reflection coefficient.
ω = Angular frequency.

Correspondence on Monographs is invited for consideration with a view to publication.
Dr. Clarricoats is in the Department of Light Electrical Engineering, Queen's University of Belfast.

(1) INTRODUCTION

In a number of microwave systems there is a requirement i waveguides of differing cross-section to be joined. In orc that reflections occurring at such a junction be minimized o a wide frequency band, some form of distributed matchin usually employed. An example is found in the taper transiti of Fig. 1(*a*). In this, the waveguide cross-section is gradu

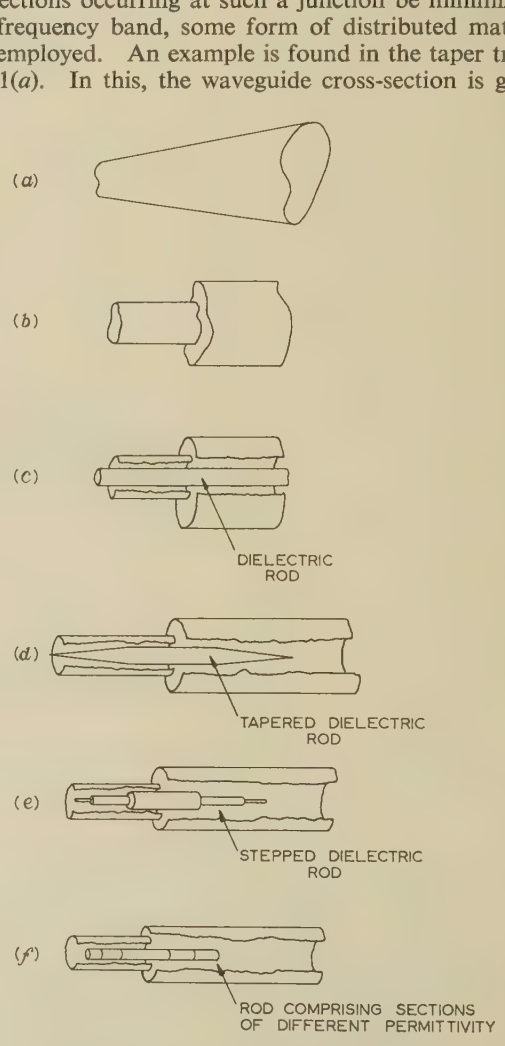

Fig. 1.—Junctions of waveguides having different cross-sections.
(*a*) Taper transition between waveguides of arbitrary cross-section.
(*b*) Abrupt junction of two waveguides.
(*c*) Junction of waveguides containing a dielectric rod.
(*d*) Tapered dielectric rod.
(*e*) Stepped dielectric rod.
(*f*) Multiple dielectric rod.

hanged between the limiting forms over an axial distance of everal guide wavelengths. The present paper describes a method f obtaining a broad-band impedance match at a junction where wo waveguides are joined abruptly as in Fig. 1(*b*). The method nvolves the use of an axial dielectric rod which partially fills he waveguides as in Fig. 1(*c*). Provided that the rod permittivity and radius are appropriately chosen the electromagnetic ield may be confined almost entirely to the rod. Under these onditions a reasonable change in waveguide cross-section can e made without causing appreciable reflection. If the method s to be of practical value, it is of course necessary to minimize eflections occurring at the junction between the waveguide ontaining dielectric and the empty waveguide. This may be ccomplished in a number of ways as illustrated in Figs. 1(*d*), *e*) and (*f*). It is evident that the present method dispenses vith the necessity for specially machined or electroformed wave- uide transitions. Furthermore, since it will transpire that the olerances on the dielectric rod dimensions are quite liberal, a iven rod design proves suitable for matching waveguides with range of differing cross-sections.

The first part of the paper is concerned with the theoretical valuation of the reflection coefficient at a junction of two ircular waveguides containing an axial dielectric rod. Each vaveguide supports an H_{01} mode. This particular configuration nd mode were chosen for study because of their mathematical implicity. It is to be expected that the main features of the esults obtained apply quite generally to other waveguide cross- ections and to other modes of propagation.

In the second part of the paper, experimental results are resented for a junction of circular waveguides containing a ielectric rod tapered at its ends, as illustrated in Fig. 1(*d*). An axial polystyrene rod supported by foamed polystyrene vas employed in the experiments, and the reflection coefficient f the H_{11} mode incident on the rod was measured over a requency band 8·75–9·7Gc/s. In Section 4 these results are avourably compared with those obtained in the absence of he rod.

(2) REFLECTION COEFFICIENT AT A JUNCTION OF CIRCULAR WAVEGUIDES CONTAINING A DIELECTRIC ROD

A method for determining the admittance at the junction of wo homogeneously filled waveguides of arbitrary cross-section as been described by Farmer.[1] An extension of this method o inhomogeneous waveguides is employed here in the derivation

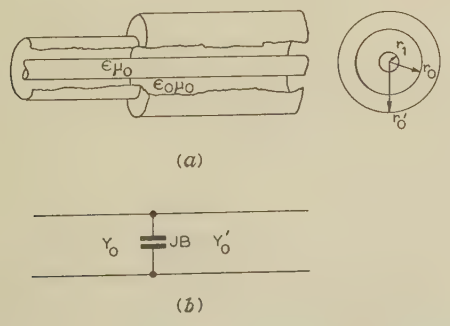

Fig. 2.—Circular waveguide junction and equivalent circuit.
(*a*) Junction of circular waveguides containing an axial dielectric rod.
(*b*) Equivalent-circuit representation of the junction of waveguides of arbitrary ross-section.

f the reflection coefficient at the waveguide junction depicted n Fig. 2(*a*). It is assumed that the waveguides and dielectric od have circular cross-section and that the region surrounding the rod has the permittivity and permeability of free space. It is also assumed that the waveguides are perfectly conducting and that the rod is lossless. The presence of slight loss in a practical structure will have negligible effect on the results.

Farmer[1] has shown that if two joined waveguides have cross-sections which differ only slightly in shape and area, the two-terminal equivalent circuit of Fig. 2(*b*) is a very good representation. Furthermore, the shunt susceptance is negligible and the junction may be regarded entirely as an impedance mismatch. Farmer has obtained a general expression for the admittance ratio Y_0'/Y_0 which is applicable to homogeneously filled waveguides. In deriving this expression use has been made of certain orthogonality relations which do not apply to inhomogeneously filled waveguides. For this reason, the following expression for Y_0'/Y_0, which is applicable to a certain class of inhomogeneous waveguides, has been derived.

$$\frac{Y_0'}{Y_0} = \frac{\int_s Y_1' E_{t1}' \cdot E_{t1} dS \int_s Y_1' E_{t1}' \cdot E_{t1}' dS}{\int_s Y_1 E_{t1}' \cdot E_{t1} dS \int_{s'} Y_1' E_{t1}' \cdot E_{t1}' dS} \quad . \quad . \quad . \quad (1)$$

Y_0 and Y_0' are the respective characteristic admittances of the transmission lines representing the incident and transmitted modes in the two waveguides, and Y_1 and Y_1' are the respective wave admittances of these modes. E_{t1} is the electric field of the mode in the waveguide of cross-section S while E_{t1}' is the electric field of the mode in the waveguide of cross-section S'.

Eqn. (1) applies when the mode incident on the junction of Fig. 2(*a*) possesses circular symmetry. Only circularly symmetric modes can propagate with either E_z or H_z zero in a circular waveguide containing an axial dielectric rod. If the dielectric rod has a permeability μ_0, eqn. (1) takes the more simple form of eqn. (2). For circularly symmetric H-modes,

$$\frac{Y_0'}{Y_0} = \frac{Y_1' \int_s E_{t1}' \cdot E_{t1}' dS}{Y_1 \int_{s'} E_{t1}' \cdot E_{t1}' dS} \quad . \quad . \quad . \quad . \quad . \quad (2)$$

Under the above conditions, Y_1' and Y_1 have the values $\beta'/\omega\mu_0$ and $\beta/\omega\mu_0$ in both the regions $r_0 > r > r_1$ and $r_1 > r > 0$. Furthermore, since in eqn. (1) Y_1' and Y_1 do not depend on position within either region, they can in this case be taken outside the integrals. When this is done eqn. (2) is obtained. The equation contains two principal terms. One is the ratio of the wave admittances in the two waveguides, the other is the ratio of the instantaneous power flow integrated over the cross-sections S and S' respectively, in the waveguide of radius r_0'.

For an H_{01} mode propagating in a waveguide of radius r_0',

$$E_{t1}' = E_\theta i_\theta = \frac{A\omega\mu_0}{K} J_0'(Kr) \varepsilon^{j(\omega t - \beta' z)} i_\theta \quad (r_1 > r > 0) \quad . \quad (3)$$

and

$$E_{t1}' = E_\theta i_\theta = \frac{A\omega\mu_0}{K_1} J_0(Kr) P_0(K_1 r, r_0') \varepsilon^{j(\omega t - \beta' z)} i_\theta \quad (r_0 > r > r_1)$$

$$. \quad . \quad . \quad . \quad (4)$$

where A is an arbitrary amplitude coefficient; $K^2 = \omega^2\epsilon_0\mu_0 - \beta'^2$; $K_1^2 = \omega^2\epsilon_0\mu_0 - \beta'^2$; $J_0(x)$ is a Bessel function of the first kind and of zero order; and

$$P_0(K_1 r, r_0') = \frac{J_0'(K_1 r) Y_0'(K_1 r_0') - Y_0'(K_1 r) J_0'(K_1 r_0')}{J_0(K_1 r_1) Y_0'(K_1 r_0') - Y_0(K_1 r_1) J_0'(K_1 r_0')}$$

The phase-change coefficient β' satisfies the characteristic equation

$$\frac{J_0'(Kr_1)}{Kr_1 J_0(Kr_1)} = \frac{P_0(K_1 r_1, r_0')}{K_1 r_1} \quad . \quad . \quad . \quad . \quad (5)$$

On substitution for E_{t1}', Y_1' and Y_1 in eqn. (2), the admittance ratio for an H_{01} mode at the junction of Fig. 2(*a*) is given by

$$\frac{Y_0'}{Y_0} = \frac{\beta'}{\beta} \frac{\int_0^{r_1} J_0'^2(Kr)rdr + \left(\frac{K}{K_1}\right)^2 J_0^2(Kr_1) \int_{r_1}^{r_0} P_0(K_1 r, r_0')rdr}{\int_0^{r_1} J_0'^2(Kr)rdr + \left(\frac{K}{K_1}\right)^2 J_0^2(Kr_1) \int_{r_1}^{r_0'} P_0(K_1 r, r_0')rdr} \quad . \quad (6)$$

which becomes, after integration,

$$\frac{Y_0'}{Y_0'} = \frac{\beta'}{\beta} \frac{t_1 + \left(\frac{K}{K_1}\right)^4 \left[\frac{J_0(Kr_1)}{J_1(Kr_1)}\right]^2 t_2}{t_1 + \left(\frac{K}{K_1}\right)^4 \left[\frac{J_0(Kr_1)}{J_1(Kr_1)}\right]^2 t_2'} \quad . \quad . \quad . \quad (7)$$

where $$t_1 = (Kr_1)^2 - 1 + F^2(Kr_1)$$

$$F(x) = xJ_1'(x)/J_1(x)$$

$$t_2 = \frac{(y_0^2-1)\psi_1^2(y_0', y_0) + y_0^2\psi_2^2(y_0', y_0) - (y_1^2-1)\psi_1^2(y_0', y_1) - y_1^2\psi_2^2(y_0', y_1)}{\psi_3^2(y_0', y_1)}$$

$$t_2' = \frac{(2/\pi)^2 - (y_1^2 - 1)\psi_1^2(y_0', y_1) - \psi_2^2(y_0', y_1)}{\psi_3^2(y_0', y_1)}$$

$$\psi_1(y_0', y) = Y_1(y_0')J_1(y) - J_1(y_0')Y_1(y)$$
$$\psi_2(y_0', y) = Y_1(y_0')J_1'(y) - J_1(y_0')Y_1'(y)$$
$$\psi_3(y_0', y_1) = J_1(y_0')Y_0(y_1) - Y_1(y_0')J_0(y_1)$$
$$y = K_1 r \quad y_1 = K_1 r_1 \quad y_0 = K_1 r_0 \quad y_0' = K_1 r_0'$$

The above expressions apply when $\bar{\beta}'$ is less than unity. Expressions for t_2 and t_2' which apply when $\bar{\beta} > 1$ can be obtained quite readily.

When the admittance ratio is determined from eqn. (7), the reflection coefficient ρ can be obtained from the equation

$$\rho = \frac{Y_0'/Y_0 - 1}{Y_0'/Y_0 + 1} \quad . \quad . \quad . \quad . \quad . \quad . \quad (8)$$

(3) EVALUATION OF REFLECTION COEFFICIENT

(3.1) Evaluation of β'/β

A first stage in the evaluation of the admittance ratio of eqn. (7), and hence the reflection coefficient, is the determination of the phase coefficients β and β'. These can be obtained by numerical solution of eqn. (5). However, it transpires that in cases of practical interest, β and β' are very nearly equal over quite a wide range of values of r_1/r_0 and r_1/r_0'. For this reason perturbation methods have been employed which enable the difference between β and β' to be determined more explicitly. For convenience a perturbation method has also been used when the rod is thin. The validity of a particular method depends on the actual values of β and β', which in turn depend on r_1/r_0 and r_1/r_0' respectively. Three methods have been used.

When $r_1/r_0 \ll 1$ and $r_1/\lambda_0 \ll 1$, β is determined by a perturbation method in which the empty waveguide represents the unperturbed state. β' is determined similarly in this range. When $\bar{\beta}$ and $\bar{\beta}'$ are approximately unity, a perturbation method is employed in which either of the conditions $\bar{\beta} = 1$ and $\bar{\beta}' = 1$ represents the unperturbed states. Finally, when either $\bar{\beta}$ or $\bar{\beta}'$ exceeds unity by an amount which renders the above methods invalid, a perturbation is employed in which the unbounded rod ($r_0 = r_0' = \infty$) is chosen as the unperturbed state. This method remains valid until the smaller waveguide is nearly filled. However, when $r_1 = r_0$, $\bar{\beta}$ is given by a simple expression since the waveguide is then homogeneously filled. Under this condition $\bar{\beta}'$ can still be obtained by the latter perturbation method until r_0 and r_0' are nearly equal. A brief description of each method now follows.

When $r_1/r_0 \ll 1$ and $r_1/\lambda_0 \ll 1$, the small change in phase coefficient $\delta\beta$ caused by introducing a dielectric rod into a circular waveguide propagating an H_{01} mode can be obtained by expanding the functions involving r_1 in eqn. (5) about the condition $r_1 = 0$. The function $J_1(K_1 r_0)$ must also be expanded since $J_1(K_1 r_0) = 0$ when $r_1 = 0$. $\delta\beta$ is then given by

$$\frac{\delta\beta}{\beta_0} = \frac{j_1^4}{32}\left[\frac{\pi Y_1(j_1)}{\beta_0}\right]^2 (\bar{\epsilon} - 1)\left(\frac{r_1}{r_0}\right)^4 \quad . \quad . \quad .$$

$\delta\beta'/\beta_0'$ is obtained on replacing r_0 by r_0'.

When $\bar{\beta} = 1$, $K_1 = 0$ and by expanding the right-hand side of eqn. (5) about that condition, the following equation is obtained

$$F(Kr_1) = -\left[1 + \frac{2}{(r_0/r_1)^2 - 1}\right] \quad . \quad . \quad . \quad (1$$

Eqn. (10) has been solved and Fig. 3 shows $2r_0/\lambda_0$ as a function

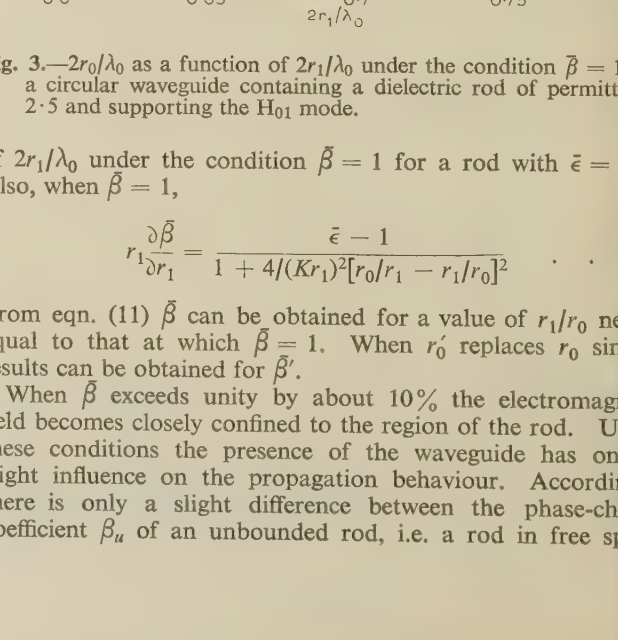

Fig. 3.—$2r_0/\lambda_0$ as a function of $2r_1/\lambda_0$ under the condition $\bar{\beta} = 1$ f a circular waveguide containing a dielectric rod of permittiv 2·5 and supporting the H_{01} mode.

of $2r_1/\lambda_0$ under the condition $\bar{\beta} = 1$ for a rod with $\bar{\epsilon} = 2$. Also, when $\bar{\beta} = 1$,

$$r_1 \frac{\partial\bar{\beta}}{\partial r_1} = \frac{\bar{\epsilon} - 1}{1 + 4/(Kr_1)^2[r_0/r_1 - r_1/r_0]^2} \quad . \quad . \quad (1$$

From eqn. (11) $\bar{\beta}$ can be obtained for a value of r_1/r_0 nea equal to that at which $\bar{\beta} = 1$. When r_0' replaces r_0 simi results can be obtained for $\bar{\beta}'$.

When $\bar{\beta}$ exceeds unity by about 10% the electromagne field becomes closely confined to the region of the rod. Und these conditions the presence of the waveguide has only slight influence on the propagation behaviour. According there is only a slight difference between the phase-char coefficient β_u of an unbounded rod, i.e. a rod in free spa

ıd the phase-change coefficient β of the corresponding mode
ı a waveguide containing a dielectric rod. β_u satisfies

$$\frac{J_0'(\bar{K}r_1)}{\bar{K}r_1 J_0(\bar{K}r_1)} = -\frac{K_0'(\bar{k}_1 r_1)}{\bar{k}_1 r_1 K_0(\bar{k}_1 r_1)} \quad . \quad . \quad . \quad (12)$$

here

$$\bar{K}^2 = \omega^2\epsilon\mu_0 - \beta_u^2$$

$$\bar{k}_1^2 = \beta_u^2 - \omega^2\epsilon_0\mu_0$$

satisfies the form of eqn. (5) appropriate to $\bar{\beta} > 1$, namely

$$\frac{J_0'(Kr_1)}{Kr_1 J_0(Kr_1)} = \frac{I_0'(kr_1)K_0'(k_1r_0) - K_0'(k_1r_1)I_0'(k_1r_0)}{k_1r_1[I_0(k_1r_1)K_0'(k_1r_0) - K_0(k_1r_1)I_0'(k_1r_0)]} \quad . \quad (13)$$

The right-hand side of eqn. (13) may be rewritten as

$$\frac{J_0'(Kr_1)}{Kr_1 J_0(Kr_1)} = -\frac{K_0'(k_1r_1)}{k_1r_1K_0(k_1r_1)} + \frac{K_0'(k_1r_0)}{(k_1r_1)^2K_0^2(k_1r_1)I_0'(k_1r_0)} \quad . \quad (14)$$

qn. (14) is valid provided that

$$-\frac{I_0(k_1r_1)K_0'(k_1r_0)}{I_0'(k_1r_0)K_0(k_1r_1)} \ll 1$$

)n comparing eqns. (12) and (14) it can be seen that they differ nly through the second term on the right-hand side of eqn. (14). lowever, this term is smaller than the first term by a factor pproximately equal to $\varepsilon^{-2k_1(r_0-r_1)}/(k_1r_1)^2$, which is very much ss than unity provided that the dielectric rod does not fill or early fill the waveguide. Under these conditions $\bar{\beta}$ and $\bar{\beta}_u$ re very nearly equal.

If $\bar{\beta} = \bar{\beta}_u + \delta\bar{\beta}$,

$$\bar{\beta} = \frac{-K_1(k_1r_0)/I_1(k_1r_0)}{(k_1r_1)^2K_0^2(k_1r_1)\bar{\beta}_u[2G(\bar{K}r_1) + 1]\left(\frac{1}{\bar{\epsilon} - \bar{\beta}_u^2} + \frac{1}{\bar{\beta}_u^2 - 1}\right)} \quad . \quad (15)$$

ı eqn. (15), k_1 may be replaced by $\bar{k}_1$, $\bar{k}_1$ being the wave-umber for the unbounded rod which satisfies eqn. (12). On ubstituting r_0' for r_0 in eqn. (15), $\delta\bar{\beta}'$ is similarly obtained. The atio in eqn. (7) is then given by

$$\frac{\bar{\beta}'}{\bar{\beta}} = 1 + \frac{\delta\bar{\beta}' - \delta\bar{\beta}}{\bar{\beta}_u} \quad . \quad . \quad . \quad . \quad (16)$$

When $r_1/r_0 = 0$, $\bar{\beta}$ is given by

$$\bar{\beta} = \left[1 - \left(\frac{j_1\lambda_0}{\pi 2r_0}\right)^2\right]^{1/2} \quad . \quad . \quad . \quad . \quad (17)$$

hile when $r_1/r_0 = 1$,

$$\bar{\beta} = \left[\bar{\epsilon} - \left(\frac{j_1\lambda_0}{\pi 2r_0}\right)^2\right]^{1/2} \quad . \quad . \quad . \quad . \quad (18)$$

Figs. 4 and 5 show $\bar{\beta}$, $\bar{\beta}'$ and $(\bar{\beta}'/\bar{\beta} - 1)$ as functions of r_1/λ_0 for a rod with $\bar{\epsilon} = 2{\cdot}5$ and with waveguides of diameter uch that $2r_0/\lambda_0 = 1{\cdot}6$ and $2r_0'/\lambda_0 = 2{\cdot}0$. As anticipated, when and $\bar{\beta}'$ exceed unity, there is only a very slight difference between ıeir values until the condition $r_1/r_0 = 1$ is approached. The bove results were obtained using the methods just outlined, upplemented in the range $\bar{\beta}$ and $\bar{\beta}'$ less than unity with values btained by a numerical method for the solution of eqn. (5). he latter values were required since there is a range in which either the thin-rod perturbation nor the $\bar{\beta} = 1$ perturbation is alid. However, in this range, the difference between $\bar{\beta}$ and $\bar{\beta}'$ sufficient for a high computational accuracy not to be emanded.

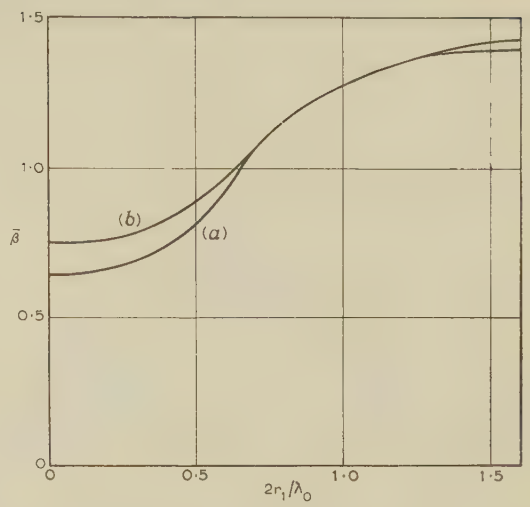

Fig. 4.—$\bar{\beta}$ and $\bar{\beta}'$ as functions of $2r_1/\lambda_0$.
$\bar{\epsilon} = 2{\cdot}5$; (a) $2r_0/\lambda_0 = 1{\cdot}6$; (b) $2r_0'/\lambda_0 = 2{\cdot}0$.

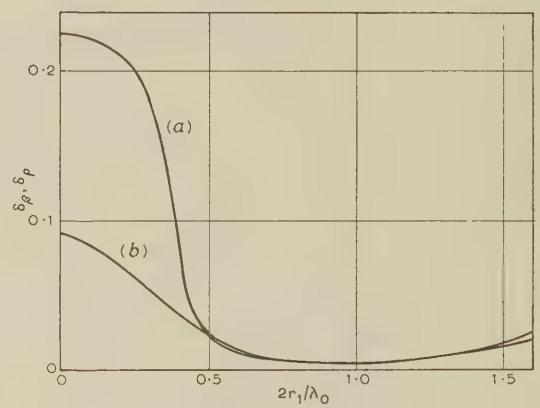

Fig. 5.—δ_β and δ_p as a function of $2r_1/\lambda_0$.
$\bar{\epsilon} = 2{\cdot}5$; $2r_0/\lambda_0 = 1{\cdot}6$; $2r_0'/\lambda_0 = 2{\cdot}0$.
(a) $\delta_\beta = \beta'/\beta - 1$
(b) $\delta_p = 1 - \frac{T_1 + t_2}{T_1 + t_2'}$

(3.2) Evaluation of Power Ratio

This Section is concerned with the evaluation of the second term in eqn. (7), which is here called the power ratio. As previously mentioned the term is equal to the ratio of the instantaneous power flow of the H_{01} mode integrated over the cross-sections S and S' respectively, in the waveguide of radius r_0'. Eqn. (7) can be conveniently rewritten so that terms involving K_1r_0 and K_1r_0' explicitly are separated from those involving only Kr_1 explicitly. Thus

$$\frac{Y_0'}{Y_0} = \frac{\beta'(T_1 + t_2)}{\beta(T_1 + t_2')} \quad . \quad . \quad . \quad . \quad . \quad (19)$$

where

$$T_1 = \left[\frac{J_1(Kr_1)}{J_0(Kr_1)}\right]^2\left(\frac{K_1}{K}\right)^4 t_1 \quad . \quad . \quad . \quad . \quad (20)$$

The evaluation of the power ratio may be simplified by the use of series expansions and approximations similar to those used in the evaluation of $\bar{\beta}'/\bar{\beta}$. Three particular cases are considered: $r_1/r_0' \ll 1$, $r_1/\lambda_0 \ll 1$; $\bar{\beta}' = 1$; and $\bar{\beta}' \simeq \bar{\beta}_u$.

When $r_1/r_0' \ll 1$ and $r_1/\lambda_0 \ll 1$, an expression for the power ratio which involves r_1/r_0' explicitly can be obtained by expanding

the functions appearing in the ratio about their values when $r_1 = 0$. Thus

$$\frac{T_1 + t_2}{T_1 + t_2'} = 1 + \frac{t_2 - t_2'}{T_1 + t_2'}$$

Now $T_1 = 0$ when $r_1 = 0$, whereby

$$\frac{T_1 + t_2}{T_1 + t_2'} = 1 + \frac{(t_2 - t_2')_{r_1=0}}{(t_2')_{r_1=0}} + O(r_1^4)$$

$$\frac{T_1 + t_2}{T_1 + t_2'} = \frac{[(y_0^2 - 1)J_1^2(y_0) + y_0^2 J_1'^2(y_0)]Y_1^2(y_0')}{(2/\pi)^2}$$

$$+ \frac{(y_0^2 - 1)J_1^2(y_0)Y_1^2(y_0')\delta_1}{(2/\pi)^2} + \frac{y_0^2 J_1'^2(y_0)Y_1^2(y_0')\delta_2}{(2/\pi)^2}$$

$$+ \frac{\{[(y_0^2 - 1)J_1^2(y_0) + y_0^2 J_1^2(y_0)]Y_1^2(y_0') - (2/\pi)^2\}\delta_3}{(2/\pi)^4} \quad . \quad . \quad . \quad . \quad (21)$$

δ_1, and δ_2 and δ_3 are each proportional to $\delta\beta'$, as given by eqn. (9) with r_0' and β_0' replacing r_0 and β_0, and thus depend on r_1 through a term in r_1^4.

When $\bar{\beta}' = 1$, $K_1 = 0$. By expanding the functions in t_2 and t_2' about the condition $K_1 = 0$, and putting $a = r_0'/r_1$ and $b = r_0'/r_0$,

$$t_2 = \left(\frac{a}{2}\right)^2 (K_1 r_1)^4 \left[2a^2 \log_\varepsilon \frac{a}{b} + \frac{a^2}{2b^4} - \frac{1}{2a^2} + 2\left(1 - \frac{a^2}{b^2}\right)\right]$$

$$t_2' = \left(\frac{a}{2}\right)^2 (K_1 r_1)^4 \left(2a^2 \log_\varepsilon a - \frac{3}{2}a^2 - \frac{1}{2a^2} + 2\right)$$

Since $J_1(Kr_1)/Kr_1 J_0(Kr_1) = 1/[1 + F(Kr_1)]$ when $\bar{\beta}' = 1$,

$$T_1 = \left[\frac{J_1(Kr_1)}{J_0(Kr_1)}\right]^2 \left(\frac{K_1}{K}\right)^4 t_1$$

$$= \frac{(Kr_1)^2 - 1 + F^2(Kr_1)}{(Kr_1)^2[1 + F(Kr_1)]^2}(K_1 r_1)^4$$

Thus $\dfrac{T_1 + t_2}{T_1 + t_2'} =$

$$\frac{\dfrac{(Kr_1)^2 - 1 + F^2(Kr_1)}{(Kr_1)^2[1 + F(Kr_1)]^2} + \left(\dfrac{a}{2}\right)^2 \left[2a^2 \log_\varepsilon \dfrac{a}{b} + \dfrac{a^2}{2b^4} - \dfrac{1}{2a^2} + 2\left(1 - \dfrac{a^2}{b^2}\right)\right]}{\dfrac{(Kr_1)^2 - 1 + F^2(Kr_1)}{(Kr_1)^2[1 + F(Kr_1)]^2} + \left(\dfrac{a}{2}\right)^2 \left[2a^2 \log_\varepsilon a - \dfrac{3}{2}a^2 - \dfrac{1}{2a^2} + 2\right]} \quad . \quad . \quad . \quad . \quad (22)$$

When $\bar{\beta}'$ exceeds unity by about 10%, most of the power flows through the rod. Under these conditions $t_2 \simeq t_2'$ and $t_2/T_1 \ll 1$. A good approximation for the ratio is then given by

$$\frac{T_1 + t_2}{T_1 + t_2'} \simeq 1 + \frac{t_2 - t_2'}{T_1} \quad . \quad . \quad . \quad . \quad (23)$$

Also, in evaluating $t_2 - t_2'$ and T_1 in eqn. (23), the values of k_1 and K appropriate to an unbounded rod may be used with negligible effect on the result.

Fig. 5(*b*) shows $(t_2 - t_2')/(T_1 + t_2')$ as a function of $2r_1/\lambda_0$ for the same rod and waveguide parameters as before. The above quantity represents the deviation of the power ratio from unity. It can be seen that when $\bar{\beta}' > 1$ the deviation is slight. Furthermore it is significant that the power ratio is then less than unity by almost exactly the same amount as the ratio $\bar{\beta}'/\bar{\beta}$ is greater than unity.

(3.3) Behaviour of Reflection Coefficient

If $$\bar{\beta}'/\bar{\beta} - 1 = \delta_\beta$$

and $$1 - \frac{T_1 + t_2}{T_1 + t_2'} = \delta_p \quad . \quad . \quad . \quad . \quad . \quad (2$$

then $$\frac{Y_0'}{Y_0} = 1 + \delta_\beta - \delta_p$$

assuming that $\delta_\beta \ll 1$ and $\delta_p \ll 1$.

From eqn. (8),

$$\rho = \tfrac{1}{2}(\delta_\beta - \delta_p) \quad . \quad . \quad . \quad . \quad . \quad (2$$

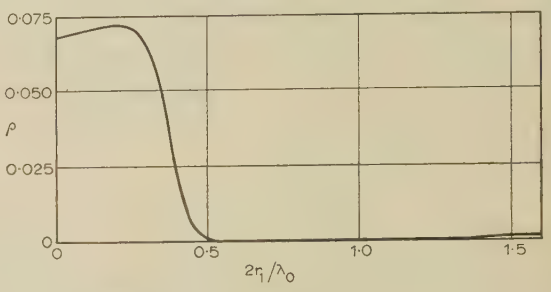

Fig. 6.—ρ as a function of $2r_1/\lambda_0$.
$\varepsilon = 2{\cdot}5$; $2r_0/\lambda_0 = 1{\cdot}6$; $2r_0'/\lambda_0 = 2{\cdot}0$.

Fig. 6 shows ρ as a function of $2r_1/\lambda_0$. It is evident that o a wide range of normalized rod radius the reflection coefficie due to the change in waveguide diameter is negligibly sm A better indication of the actual reflection coefficient is provid by Fig. 7, which shows a portion of Fig. 5 on an enlarged scal

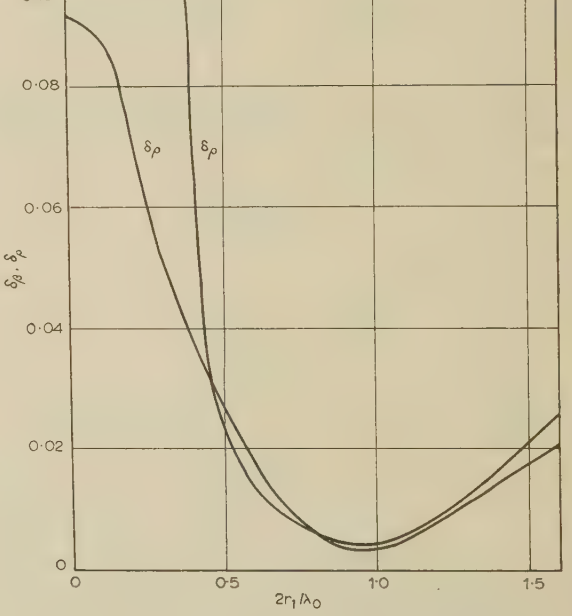

Fig. 7.—A portion of Fig. 5 on an enlarged scale.

One may therefore conclude that, in so far as the junctio in Fig. 2(*a*) can be regarded as an impedance mismatch, th reflection coefficient can for a representative junction be mad negligible by the introduction of a dielectric rod of appropria diameter. Clearly for maximum bandwidth a rod diamet should be chosen intermediate between r_0 and that renderin $\bar{\beta}' = 1$. It is also apparent that if the rod permittivity is increase

ıd the rod diameter appropriately decreased the reflection ɔefficient will remain unchanged. This follows since the rod ıdius required to produce the condition $\bar{\beta}' = 1$ decreases onotonically as permittivity increases (see Figs. 8 and 9).

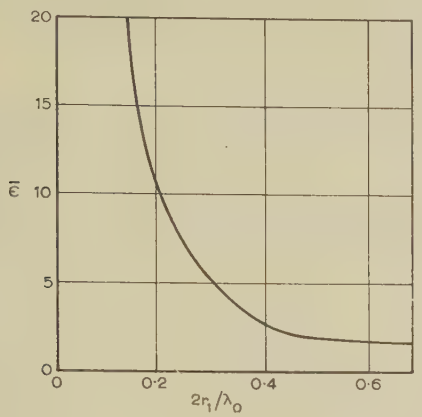

Fig. 8.—$2r_1/\lambda_0$ as a function of $\bar{\epsilon}$ under the condition $\bar{\beta} = 1$ in a circular waveguide supporting the H_{11}-type mode.
$2r_0/\lambda_0 = 0{\cdot}685$.

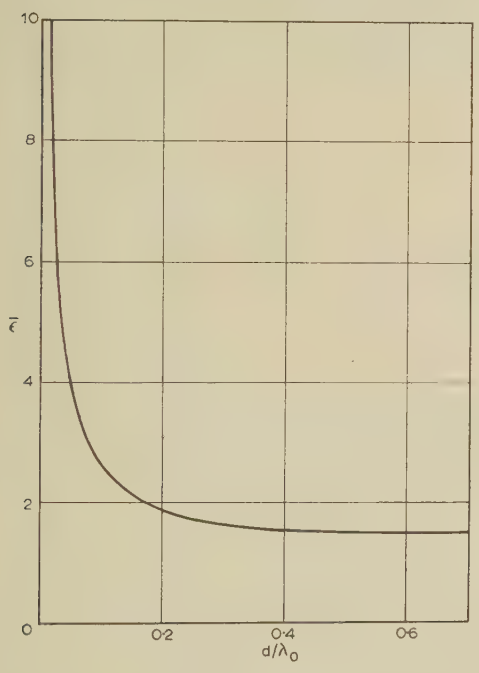

Fig. 9.—d/λ_0 as a function of $\bar{\epsilon}$ under the condition $\bar{\beta} = 1$ in a rectangular waveguide supporting the H_{01} mode.
$L/\lambda_0 = 0{\cdot}704$.

learly, if a considerable change in waveguide cross-section is quired to be made, a small-diameter rod of high permittivity ıould be used in order to reduce the junction reflection ɔefficient.

Although the above results apply specifically to a junction of rcular waveguides supporting an H_{01} mode, it seems reasonable expect that the principle by which the reflection coefficient is duced will hold more generally. For example, it has been ıown elsewhere for other modes[2] that when $\bar{\beta} > 1$ the fields a waveguide containing a dielectric rod are closely confined the rod region.

As a guide to the choice of rod or slab parameters for junctions involving respectively the H_{11}-type mode in circular waveguide and the H_{01} mode in rectangular waveguide, the appropriate characteristic equations under the condition $\bar{\beta} = 1$ are given below:

$$F(Kr_1) = \frac{1 + \bar{\epsilon} - (K_1 r_1)^2 \left[\dfrac{2\log_e (r_0/r_1)}{1 - (r_1/r_0)^4} + \dfrac{1}{2}\right]}{\dfrac{(r_1/r_0)^2 + 1}{(r_1/r_0)^2 - 1} + \dfrac{\bar{\epsilon}[(r_1/r_0)^2 - 1]}{(r_1/r_0)^2 + 1}} \quad . \quad (26)$$

for the H_{11}-type mode in circular waveguide, and

$$\cot \frac{Kd}{2} = \frac{K(L - d)}{2} \quad . \quad . \quad . \quad . \quad . \quad (27)$$

for the H_{01} mode in rectangular waveguide, where d is the thickness of the dielectric slab contained in a waveguide of width L.

Figs. 8 and 9 show $2r_1/\lambda_0$ and d/λ_0 as a function of $\bar{\epsilon}$ for typical values of $2r_0/\lambda_0$ and L/λ_0.

(4) EXPERIMENTAL STUDY OF CIRCULAR WAVEGUIDE JUNCTION

In this Section results are presented of an experimental study of a waveguide junction employing a tapered dielectric rod as in Fig. 1(*d*). Two circular waveguides of diameters 0·875 in and 1·026 in were joined abruptly. Each waveguide supported the H_{11} mode in the absence of the dielectric rod and the hybrid H_{11}-type mode in the presence of the rod. A polystyrene rod of diameter 0·5 in was used in the experiments. The length of the uniform section of the rod was 8 in while the tapers were each of length 6 in. The rod was supported by means of a polystyrene-foam tube so that the middle of the length of the rod approximately coincided with the waveguide junction. The choice of rod dimensions was made quite arbitrarily, apart from the following requirements, which were adequately met in the above design. These were that the rod diameter be sufficient for $\bar{\beta}'$ to exceed unity, that the length of the rod of uniform diameter be at least one guide wavelength and that the tapered portions be as long as could conveniently be made. The fact that the length of the uniform section of the rod was over six guide wavelengths enabled multiple reflection effects to be easily distinguished. In a device one would substantially reduce this length.

A precision standing-wave detector in rectangular waveguide was used for measurements. An electroformed taper transition was used to join the rectangular and circular waveguides. By using a 3-stub tuner in rectangular waveguide, the mismatch due to the transition was reduced before measurements of the junction properties were made.

Fig. 10 shows the v.s.w.r. measured in the frequency range 8·75–9·7 Gc/s. Curve (*a*) refers to the junction in the absence

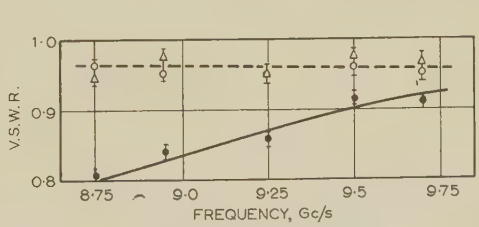

Fig. 10.—V.S.W.R. as a function of frequency for a junction of circular waveguides containing a polystyrene rod and supporting an H_{11}-type mode.
--△-- Junction with dielectric.
○ Dielectric alone.
——— Junction without dielectric.

of the dielectric, and curve (*b*) to that in the presence of the dielectric. The v.s.w.r. of the dielectric in the absence of the junction was also measured. It can be seen that, within the limits of experimental accuracy, estimated to be about 2½%, the v.s.w.r. of the junction in the presence of the dielectric can be entirely accounted for by the dielectric alone. The improved broad-band impedance match due to the presence of the dielectric is evident.

(5) CONCLUSIONS

A method of obtaining a broad-band impedance match between two joined waveguides of differing cross-section has been demonstrated. In the experimental model studied, the mismatch has been found to arise almost entirely from the transitions between the empty waveguide and the waveguide containing dielectric. Thus the problem of matching two waveguides of differing cross-section has been reduced to one of matching a dielectric-loaded waveguide.

If the overall length of the junction is unimportant, long tapers as depicted in Fig. 1(*d*) prove satisfactory. The design and fabrication of the complete dielectric insert is then a very straightforward matter. However, if a short junction is required alternative methods of matching the dielectric may be employed, as shown in Figs. 1(*e*) and (*f*). Reggia and Spencer[3] have satisfactorily used the latter arrangement to obtain a broad-band match between an empty rectangular waveguide and one containing an axial ferrite rod. Their results indicate that the total length of the additional dielectric matching transformers ne not exceed ½ in, in the frequency range 9–10 Gc/s. Also, if high-permittivity dielectric rod is chosen for the main trans section, its length need not exceed 1 in, while satisfying t requirement stated in Section 4. Thus, it would appear th the principle of matching waveguides of different cross-sectio as described in the paper, may also be used when a compa junction is desired.

Although in the previous Sections examples have been chos where circular waveguides are joined, there is reason to expe satisfactory results with waveguides of arbitrary cross-sectio The shape of the dielectric will not appreciably influence t performance, although, for convenience, account of the wa guide symmetry might be taken when making a choice.

(6) REFERENCES

(1) Farmer, E. D.: 'Junction Admittance between Waveguid of Arbitrary Cross-Sections', *Proceedings I.E.E.*, Mon graph No. 148 R, August, 1955 (**103** C, p. 145).

(2) Clarricoats, P. J. B.: 'Propagation Along Unbound and Bounded Dielectric Rods', *ibid.*, Monographs N 409E and 410E, October, 1960 (**108** C, pp. 170 and 177)

(3) Reggia, F., and Spencer, E. G.: 'A New Technique Ferrite Phase Shifting for Beam Scanning of Microwa Antennas', *Proceedings of the Institute of Radio Enginee* 1957, **45**, p. 1510.

1.313.1.013.2

The Institution of Electrical Engineers
Monograph No. 438 U
Apr. 1961

ERTAIN APPROACHES TO ELECTROMAGNETIC FIELD PROBLEMS PERTAINING TO DYNAMO-ELECTRIC MACHINES

By K. C. MUKHERJI, B.E., Ph.D., Graduate.

(*The paper was first received* 1*st September, and in revised form* 15*th December*, 1960. *It was published as an* INSTITUTION MONOGRAPH *in April*, 1961.)

SUMMARY

Current-carrying circuits in electrical rotating machines give rise electromagnetic fields which are modified by surface polarities duced in adjacent ferromagnetic media and by eddy currents induced neighbouring conducting media. The paper reviews certain proaches towards solving some of the electromagnetic problems volved and introduces a method for taking account of the reaction eddy currents induced in a ferromagnetic medium on their inducing id.

LIST OF PRINCIPAL SYMBOLS

B = Magnetic flux density.
d = Classical depth of penetration = $(\rho/\mu\omega)^{1/2}$.
f = Frequency.
h = Radial width.
H = Magnetic intensity.
k = π/τ.
l = Axial thickness.
n = Order of space harmonic.
p_e = Eddy-current loss per unit area.
J = Eddy-current density.
Ω = Scalar electromagnetic potential.
ω = Angular frequency.
μ = Permeability.
μ_0 = Permeability of free space.
μ_r = Relative permeability.
ρ = Resistivity.
τ = Pole-pitch at mean circumference of core end plate.
∇ = Hamilton's vector operator.

Bold-face symbols indicate vector quantities. The rationalized M.K.S. system of units is used throughout.

(1) INTRODUCTION

Fields in dynamo-electric machines originate from current-arrying sources and are thus essentially electromagnetic in ature. The sources are located in the vicinity of, and in fact re often embedded in, ferromagnetic media, the electromagnetic roperties of which are essentially non-linear. In most cases, owever, a redeeming feature of the ensuing field problems is hat the magnetic permeability of the iron, even though variable, s large compared with that of free space.

Fig. 1 shows an idealized example of a type of field encountered n machine problems; it is the field produced by a stationary nfinitely-long current-carrying conductor located in a region f free space lying between the plane parallel boundaries of wo semi-infinite ferromagnetic media having constant and nite but unequal permeabilities. With an unvarying current n the conductor it is possible, for all practical purposes, to distinguish three zones in the bounded region of free space, each zone being characterized by a distinctive field distribution:

(*a*) At large distances from the conductor.
(*b*) In the vicinity of the conductor.
(*c*) Inside the conductor itself.

It is well known that Poisson's equation holds good in zone (*c*), while Laplace's equation governs the field distribution in zones (*a*) and (*b*).

In the determination of the internal characteristics of a rotating machine, the problems confronting the designer can, in general, be classified as relating primarily to the magnetic fields in air and iron, to the reactances and losses in the windings,

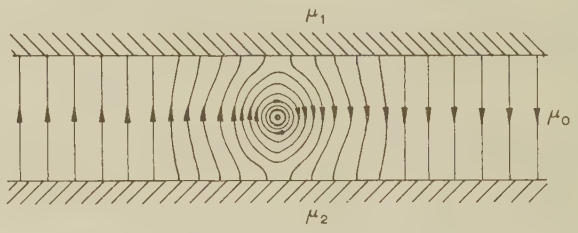

Fig. 1.—Idealized example of field distribution.

and to the losses in laminated iron, solid iron and other associated metal parts. The self- and mutual inductances, and also the effective resistances, of individual windings of the machine can be deduced from its dimensions. The determination of losses in machine parts are of importance primarily from the point of view of efficiency, but no less so from that of local heating which is governed by the specific loss, i.e. loss per unit volume of material; for example, in an alternator on leading reactive load under line-charging conditions the temperature rise of the stator end-teeth due to stray load losses has been known to set a sharp limit to the duration or magnitude of such loading.

The stray-load loss of a machine indicates the increase in its total losses on application or increase of load, after allowance for the changes in the I^2R losses in armature and field windings only. It undoubtedly is an aggregate of several component losses due to various factors and in different parts of the machine. Some of these losses are interrelated, but it is practicable to distinguish certain types of loss associated with particular regions in the machine which can be investigated individually and the results then synthesized to yield a practical design treatment.

A substantial part of stray-load loss is recognized as being associated with the two end regions of a machine. The field in these regions is 3-dimensional; further, the shape of the end-winding and also the various constructional features of the core ends influence the end losses considerably. However, a consideration of the sizes of machine end-parts and of the magnitudes of end losses points towards the core end-plates and to the teeth supports and the teeth ends of the core behind the core plates as the likely seats of bulk losses, while minor structural

Correspondence on Monographs is invited for consideration with a view to ublication.
Dr. Mukherji was formerly with Associated Electrical Industries (Manchester), td., and is now Associate Professor in Electrical Engineering, Indian Institute of echnology, Bombay.

parts, e.g. winding clamps and stay rings, fan baffles, etc., will give rise to some further losses. At any rate, the need is clearly indicated for an intensive study of the losses in laminated core-ends in the absence of an end-plate, in solid mild-steel end-plates, in solid non-magnetic materials of high resistivity such as non-magnetic cast iron, and in solid materials of low resistivity such as copper. The losses in some form of core end-plates might well prove to be lower than the reduction in the losses in cores shielded by such end-plates. But the specific utility of practical constructional innovations such as non-magnetic cast-iron end-plates and end-fingers, segmental subdivision of end-plates, setting back in steps of the teeth ends in a core, isolation of narrow packets of core end-stampings by means of ventilation ducts, or splitting the core teeth-ends by means of radial slits, can be assessed only on the basis of a detailed investigation of this kind.

Dynamo-electric machines possess circumferential symmetry so that the field distribution is periodic circumferentially. In polyphase machines the fundamental as well as the harmonic fields are rotating, and so are the parasitic tooth-ripple fields in any machine. Also, the stationary pulsating field in a single-phase machine can be represented by two rotating fields. Since the forms of the end-windings are complex and the determination of losses induced in masses of conducting materials is not straightforward, the entire problem is best attacked, first by a complete determination of the magnetic field of the stator and rotor end-windings at all points and its expression in the form of a series of harmonic rotating fields, the amplitudes of which would vary radially as well as axially, and next by a study of the losses occasioned in conducting masses by harmonic rotating fields of different wavelengths sweeping past these with different velocities.

Expressed in general terms, electromagnetic-field problems in rotating machines have two broad aspects:

(*a*) The determination of fields produced in different media by current-carrying sources.
(*b*) The investigation of mutual reaction between fields and material media.

The paper concentrates mainly on (*b*), or rather that part of it relating to eddy currents, following a brief discussion of (*a*).

(2) DETERMINATION OF FIELDS

Unlike the idealized example in Fig. 1, the sources of electromagnetic fields in actual machines are necessarily in the form of current-carrying circuits. Such fields can usually be determined by analogue or by analytical methods. Also, a third possibility, of direct measurement of the magnitude and direction of the field at all points in an actual machine by suitable detectors, need not be ruled out.

(2.1) Analogue Methods

A circuit, not necessarily planar, carrying an unvarying current can be replaced by an Ampère's equivalent shell. In the case of a planar circuit, this artifice renders the problem amenable to solution with the help of an electrolytic tank. For example, a plane circular loop of wire carrying a steady current can be replaced by a shell in the form of a disc in the plane of the loop. The two circular faces of the disc then become, from symmetry, two equipotentials which can be so maintained in an electrolytic tank.

A non-planar circuit, such as a multi-turn double-layer diamond coil of the pulled type, can still be replaced by a shell with the circuit as its boundary. But surfaces which are to be maintained as equipotentials in an electrolytic tank can no longer be easily determined. The question whether a circuit can be replaced by its projections on three orthogonal planes without altering the field distribution (at best, the field distances large compared with the dimensions of the circ itself) would merit investigation, although it appears that t field distribution in the immediate vicinity of the circuit wo still remain intractable by the analogue method.

Among other analogues of use in solving magnetic-fie distribution problems are the resistance-mesh or electric-circ analogue, and the soap-film or membrane analogue.

(2.2) Analytical Methods

Analogue methods prove to be of limited use in investigati the field distribution in machine problems where the operati permeabilities of the ferromagnetic media either undergo mark variations or are not too high (or infinite) compared with t permeability of free space. Analytical methods have to be us in these cases, which invariably necessitate restrictive simplify assumptions. Even so, one often has to fall back upon tim consuming numerical methods for solving most of these boundar value problems, though digital computers are fast coming to t rescue.

The method of images is a valuable mathematical tool f obtaining the field distribution (Searle's problems[1,2]) of curre carrying sources in the vicinity of ferromagnetic media. Sim as the method might appear to be, it becomes quite labori to apply it for solving the field problem, even in the ideali example in Fig. 1. The method originated in electrostatics b the better-known treatises[3,4] do not appear to have based t method directly on its underlying principle, namely the princi of Green's equivalent stratum as spoken of in electrosta potential theory.[5] It is only very recently that Hammond[6] h given a detailed formulation of the image problem for electr static, magnetostatic and electromagnetic fields and has co cluded that the image method in electromagnetics mu necessarily be confined to problems involving infinite conducting plane boundaries.

The technique of conformal transformation has been prof ably employed, notably by Carter[7] and also by Coe and Tayl and by Gibbs,[9] for solving important electromagnetic-fie problems arising in electrical machines. In most cases, fiel are obtained in terms of transcendental functions which a useful for field mapping but are difficult to manipulate for analytical investigation of the effects of the fields. The usu artifice is to plot the field and analyse it into space harmonic the effects of each harmonic are then investigated separate the principle of superposition being finally invoked for a sy thesis of the results on the assumption of linearity. Fiel plotting techniques have been discussed in detail in sever well-known treatises.[10–14]

An analytical treatment of the field of an idealized alternat end-winding has been given recently by Hammond.[15] In th the actual conductor currents are replaced by infinitely th axial and circumferential (tubular) current sheets; the effec of the shape of the coils or of the presence of iron in the vicini of the coils are ignored. With these simplifications, the magne field is obtained from the vector potential of the current shee in terms of double Fourier series of modified Bessel function More recentyl, Hammond[6] has indicated the possibility taking account of the contribution from the end-iron surfa of a machine to the magnetic field in the end regions in terms an image of the end-winding.

(3) EFFECT OF FIELDS

The phenomenon essential to the operation of a dynam electric machine is the motion of electromagnetic fields relati to certain material media; this, however, is invariably associate

ith other, normally undesirable, phenomena among which the duction of eddy currents in conducting media is of major portance. The problem involving eddy currents in conduct-g media that is encountered in dynamo-electric machines can e stated in general terms as follows.

Stationary or moving circuits carrying currents give rise to eady, pulsating or rotating electromagnetic fields which are fluenced by the presence of magnetic as well as non-magnetic nducting media in the neighbourhood. This influence arises om two factors:

(*a*) The polarization of the magnetic media and the ensuing field due to the surface polarities on their boundaries.
(*b*) The reaction of the eddy currents that are set up in those conducting media in which electric forces are induced by time-varying magnetic fields.

n (*b*), it is necessary to distinguish between two types of eddy rrents, resistance-limited and reactance-limited: the currents f the first type are so limited by the resistance of their paths, s in a finely-laminated medium, that their reaction on the ducing field is insignificant; the reaction of the currents of e second type, as in solid-copper or iron masses, is, however, n important factor in limiting their magnitudes.

In the more usual types of dynamo-electric machines, the roblem is considerably simplified because the dimensions of e media relative to the wavelengths of the field are such that hase-propagation effects could be ignored even if the media ere assumed to be perfect insulators. Factors (*a*) and (*b*) bove can then be considered separately, as indicated in the llowing Sections.

(3.1) Polarization Effect

3.1.1) General Considerations.

All media are first treated as perfectly non-conducting and hase-propagation effects are ignored. With these assumptions, calar electromagnetic potential fields satisfying Laplace's quation in free space as well as in all the media are fully deter-ined, except at spaces occupied by current-carrying conductors .e. 'sources') enclosed therein. It is sufficient for this purpose o determine the potential (or its normal derivative, i.e. the ormal magnetic intensity) on the bounding surfaces of each egion. This follows from the uniqueness theorem,[5] applicable o solutions of Laplace's equation. Such boundary data also uffice to determine the Laplacian potential outside the region, rovided that this potential, Ω, decreases at least as rapidly as $/r$ at large distances from the boundary surface (i.e. for large alues of r)—in other words, provided that $\Omega = \mathrm{O}(1/r)$ and rad $\Omega = \mathrm{O}(1/r^2)$ as $r \to \infty$.

3.1.2) Method of Potentials.

The potential field in free space intervening between a source nd a polarized medium can be readily expressed as the sum f two parts—one, A', increasing and the other, B', decreasing ith distance away from the boundary of the medium towards he source. Of these, A' is to be attributed directly to the source nd B' to the surface polarity induced on the boundary. In ther words, A' corresponds to the field that would have existed n that region of free space in the absence of the medium and ence may appropriately be called the *inducing field* while the m of A' and B' may be called the *total applied field.*

In order that A' can be distinguished from B' in this way, the rientation of the source, though not its actual location, with espect to the polarized medium needs to be known if the calar potential or the normal magnetic intensity on the boundary f the medium is taken as the starting-point of the analysis.

(3.2) Eddy-Current Effect

The field distribution in the absence of eddy currents having been determined as above, all the relevant media are next considered with their appropriate finite resistivities. This enables eddy currents to flow, subject to relevant boundary conditions, in those media that are linked by time-varying magnetic fields. The currents induced in any one medium give rise to a field of their own inside that medium, in the adjacent media and in free space; this secondary field also links the current-carrying circuit which is the source of the inducing field. The initial field distribution as determined in Section 3.1 thus gets modified. As a first approximation, each medium can be considered by itself, ignoring the presence of the adjacent media and of the source circuit, all of which may be considered as free space. Two alternative procedures then become available, as indicated in Sections 3.2.1 and 3.2.2.

(3.2.1) Carter's Method.

Carter[16] started from a feasible eddy-current-density distribution $\boldsymbol{J}$ inside the medium consistent with the boundary conditions and calculated the resultant field $\boldsymbol{H}_R$ required to induce the ohmic drop per unit length $\rho\boldsymbol{J}$ in the medium and also the field $\boldsymbol{H}_J$ produced in the medium by these eddy currents themselves. The difference between these two fields was equated to the total applied field $\boldsymbol{H}_A$ as evaluated or measured in the absence of the eddy currents, for $\boldsymbol{H}_R = \boldsymbol{H}_A + \boldsymbol{H}_J$; the values of the fields on the boundary of the medium were conveniently used for establishing this equation.

(3.2.2) Method of Potentials.

A parallel method will now be described, based on the potential fields obtaining in free space with and without the eddy currents in the medium. This method makes use of the fact that the secondary field due to the eddy currents decreases with distance away from the boundary of the medium towards the source and, as such, alters only the part B' of the total applied field; A', which is the inducing field, remains unaffected. As in Carter's method, the resultant field $\boldsymbol{H}_R$ is calculated from the eddy-current-density $\boldsymbol{J}$ sufficient to induce the ohmic drop per unit length $\rho\boldsymbol{J}$ in the medium (the reverse procedure of determining the resistance-limited eddy-current density $\boldsymbol{J}$ induced by the resultant field $\boldsymbol{H}_R$ is also feasible). Moreover, the Laplacian potential field obtaining in free space in the presence of these eddy currents in the medium can be determined in terms of the field $\boldsymbol{H}_R$ on its boundary, i.e. in terms of $\boldsymbol{J}$. In this resultant field also, two parts A and B can again be distinguished, having the same characteristics as the parts A' and B' of the total applied field. Noting that the part A of the resultant field represents the unaltered inducing field given by the part A' of the total applied field, the eddy-current density $\boldsymbol{J}$ is finally obtained in terms of the total applied field. The details of this procedure are illustrated in Section 8.1.

(4) ANALYSIS OF EDDY CURRENTS IN CORE END-PLATE BY THE METHOD OF POTENTIALS

The axial runs of conductors in a polyphase end-winding give rise on load to a rotating field, and the circumferential runs to a pulsating axial field. The problem of a ring, such as the core end-plate, placed in a pulsating axial field can be analysed by conventional methods.[17] The rotating-field problem is analysed in this Section; it is important from the point of view not only of end-plate losses but also of the reactance of the end-winding.

The starting-point of the analysis is a given distribution of radial magnetic flux density at the inner cylindrical surface of

the end-plate in the absence of eddy currents; this might be determined analytically, or with the help of analogues, or even by direct experiment. The cylindrical surfaces are developed into infinite plane surfaces and the rectangular Cartesian system of co-ordinates is used; the x-axis is taken as directed radially outwards, the y-axis along the periphery and the z-axis along the axis of the machine. The field and the eddy-current vectors are then treated as periodic functions of $\omega t - n(\pi/\tau)y$. The analysis is made in terms of the fundamental alone ($n = 1$), and k is used[18] for π/τ. The origin of x is taken on the inner periphery of the end-plate.

(4.1) Illustration of Procedure

To illustrate the procedure, the case of a semi-infinite medium (Fig. 2) of constant resistivity ρ and constant permeability

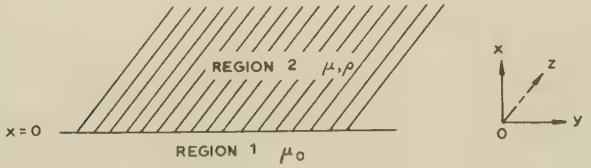

Fig. 2.—The problem of semi-infinite medium.

$\mu(= \mu_0 \mu_r)$ filling the entire region 2 ($x \geqslant 0$) is considered first; region 1 ($x < 0$) is free space. The boundary conditions are:

(*a*) All the field variables are independent of z, and $B_z = 0$.

(*b*) The source is located in region 1 ($x < 0$).

(*c*) $B_x = \hat{B} \cos(\omega t - ky) = \mathscr{R}\hat{B}\varepsilon^{j(\omega t - ky)}$ on $x = 0$.

(*d*) $\boldsymbol{B} \to 0$ as $x \to +\infty$ in region 2.

Expressions for the field-intensity components in region 2 are derived in Section 8.1, where it is also shown that the eddy currents in the medium (region 2) under these conditions are wholly axial, the axial current density being given by

$$(J_2)_z = \mathscr{R}\frac{\mu_r + 1}{k\mu_r + \left(k^2 + \frac{j}{d^2}\right)^{1/2}} \frac{\hat{B}}{\mu d^2} \exp\left[-x\left(k^2 + \frac{j}{d^2}\right)^{1/2} + j(\omega t - ky)\right] \quad (1)$$

$$x \geqslant 0$$

where d is the classical depth of penetration. Also, the resultant potential field Ω_1 in free space (region 1), as modified by the reaction of the eddy currents, is given by

$$\Omega_1 = \mathscr{R}(\mu_r + 1)\frac{\hat{B}}{2k\mu} \left[\varepsilon^{-kx} - \frac{k\mu_r - \left(k^2 + \frac{j}{d^2}\right)^{1/2}}{k\mu_r + \left(k^2 + \frac{j}{d^2}\right)^{1/2}} \varepsilon^{kx}\right] \varepsilon^{j(\omega t - ky)} \quad (2)$$

$$x < 0$$

and

$$\boldsymbol{B}_1 = -\mu_0 \operatorname{grad} \Omega_1 \quad . \quad . \quad . \quad . \quad . \quad (3)$$

The eddy-current loss per unit area of the boundary surface $x = 0$ is given by

$$p_e = \tfrac{1}{2}\rho \int_0^\infty |J_2|^2 dx = \frac{\rho \hat{B}^2}{4\mu^2 d^4 \alpha} \frac{(\mu_r + 1)^2}{\mu_r^2 k^2 + 2\mu_r k\alpha + \alpha^2 + \beta^2} \quad . \quad . \quad (4)$$

where

$$\alpha + j\beta = \left(k^2 + \frac{j}{d^2}\right)^{1/2} \quad . \quad . \quad . \quad .$$

The results indicated by eqns. (1), (4) and (5) are identical w those obtained by Carter,[11] but his work did not extend to t field in free space given by eqn. (2).

(4.2) The Core End-Plate Problem

Fig. 3 shows a part of a solid core end-plate of radial wid h and axial thickness l. The boundary conditions are:

(*a*) The source is located in region 1 ($x < 0$) which is fr space.

(*b*) $\boldsymbol{B} \to 0$ as $x \to +\infty$ in region 3, which is again fr space at the back of the end-plate rim.

(*c*) $B_x = \hat{B} \cos(\omega t - ky) = \mathscr{R}B\varepsilon^{j(\omega t - ky)}$ on $x = 0$, $-l/2$ $z < l/2$, with the origin of z at the middle of the axial thickn of the end-plate. This can be expressed in terms of a Four series:

$$B_x = \mathscr{R}\frac{4B}{\pi}\left[\sum_{p\ odd} \frac{(-1)^{(p-1)/2}}{p} \cos\frac{p\pi z}{l}\right] \varepsilon^{j(\omega t - ky)}$$

$$\text{on } x = 0,\ -l/2 < z < l/2$$

Expressions for the three components each of the fie intensity and the eddy-current-density vectors in the core en plate (region 2) are obtained by following a procedure identi with that in Section 8.1. The final results and also the result potential fields in free space (regions 1 and 3), as modified the reaction of the eddy currents, are given in Section 8.2. is to be expected, eqns. (1), (4) and (5) follow directly from th general results as both h and l tend to infinity. The resu are valid for all values of μ_r including unity, i.e. for magnetic well as non-magnetic core end-plates.

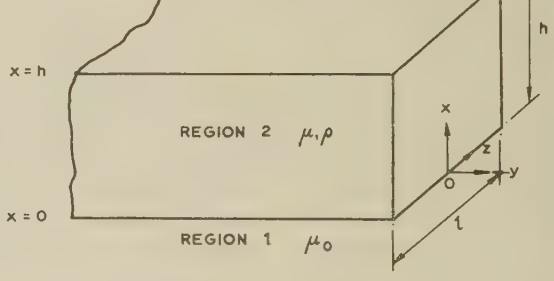

Fig. 3.—Solid core end-plate.

x Radial.
y Peripheral.
z Axial.

(5) CONCLUSIONS

Certain approaches to electromagnetic field problems dynamo-electric machines have been discussed and outline Both Carter's method and the method of potentials introduc here can, in principle, be used to determine the eddy curren induced in a ferromagnetic medium by a given field, taking f account of the reaction of these currents on the given field. T second method has the added advantage of providing an insig into the effects of surface polarities and also into the field outsi the medium as modified by the reaction of the eddy currents.

The method of potentials raises some associated problem chiefly regarding the possibility of extending this approach

ore general problems dealing with multiple sources and aterial media. Given field distributions on the boundaries of ie media in the static or non-conducting state appear to be a etter starting-point than given strengths and locations of the ources. But the development of a general procedure, if at all ossible, which could take account of any configurations of ources and of the effects of conducting and polarized media any shapes or sizes does not yet appear to be within sight.

(6) ACKNOWLEDGMENTS

The author thanks Dr. J. M. Dodds, Manager, Research epartment, Associated Electrical Industries (Manchester) Ltd., r his kind permission to include in the paper part of the work rried out by the author in his department. He is also indebted Mr. S. Neville of the same Company who was primarily sponsible for initiating him into the dissection of practical sign problems and into the electromagnetic-field approach wards solving the resulting part-problems.

(7) REFERENCES

(1) SEARLE, G. F. C.: 'On the Magnetic Field due to a Current in a Wire Placed Parallel to the Axis of a Cylinder of Iron', *Electrician*, 28th January, 1898, pp. 453 and 510.
(2) HAGUE, B.: 'Electromagnetic Problems in Electrical Engineering' (Oxford University Press, 1929), Chapter IV.
(3) MAXWELL, J. C.: 'Electricity and Magnetism', Vols. I and II (Clarendon Press, 1892), Articles 119, 155–181, 189, 318 and 662.
(4) JEANS, J. H.: 'The Mathematical Theory of Electricity and Magnetism' (Cambridge University Press, 1951), pp. 185–201.
(5) JEFFREYS, H., and JEFFREYS, B.: 'Methods of Mathematical Physics' (Cambridge University Press, 1956), pp. 215–221.
(6) HAMMOND, P.: 'Electric and Magnetic Images', *Proceedings I.E.E.*, Monograph No. 379, May, 1960 (**107** C, p. 306).
(7) CARTER, F. W.: 'The Magnetic Field of the Dynamo-Electric Machine'. *Journal I.E.E.*, 1926, **64**, p. 1115.
(8) COE, R. T., and TAYLOR, H. W.: 'Some Problems in Electrical Machine Design involving Elliptic Functions', *Philosophical Magazine*, 1928, **6**, p. 100.
(9) GIBBS, W. J.: 'Induction and Synchronous Motors with Unlaminated Rotors', *Journal I.E.E.*, 1948, **95**, Part II, p. 411.
(10) BEWLEY, L. V.: 'Two-dimensional Fields in Electrical Engineering' (Macmillan, 1948).
(11) ATTWOOD, S. S.: 'Electric and Magnetic Fields' (Chapman and Hall, 1949).
(12) WEBER, E.: 'Electromagnetic Fields: Theory and Application', Vol. I (Chapman and Hall, 1950).
(13) SHAW, F. S.: 'An Introduction to Relaxation Methods' (Dover Publications, 1953).
(14) SEELY, S.: 'Introduction to Electromagnetic Fields' (McGraw-Hill, 1958).
(15) HAMMOND, P.: 'The Calculation of the Magnetic Field of Rotating Machines', *Proceedings I.E.E.*, Monograph No. 333, May, 1959 (**106** C, p. 158).
(16) CARTER, F. W.: 'Pole-Face Losses', *Journal I.E.E.*, 1916, **54**, p. 168.
(17) MCLACHLAN, N. W.: 'Bessel Functions for Engineers' (Clarendon Press, 1955), pp. 162–165.
(18) BONDI, H., and MUKHERJI, K. C.: 'An Analysis of Tooth-Ripple Phenomena in Smooth Laminated Pole-Shoes', *Proceedings I.E.E.*, Monograph No. 225 S, February, 1957 (**104** C, p. 349).
(19) LIEBMANN, G.: 'Precise Solution of Partial Differential Equations by Resistance Networks', *Nature*, 1949, **164**, p. 149.
(20) LIEBMANN, G.: 'Solution of Partial Differential Equations with a Resistance Network Analogue', *British Journal of Applied Physics*, 1950, **1**, p. 92.
(21) LIEBMANN, G.: 'The Change of Air-Gap Flux in Electrical Machines due to the Displacement of Opposed Slots', *Proceedings I.E.E.*, Monograph No. 208 M, November, 1956 (**104** C, p. 204).

(8) APPENDICES

(8.1) Problem of Semi-infinite Medium in a Rotating Field

In the following, suffixes refer to the relevant regions of investigation as shown in Figs. 2 and 3.

(8.1.1) Medium Assumed Non-Conducting.

All field vectors relating to a non-conducting medium are indicated by a prime. In region 2 ($x \geqslant 0$), the field equations in this state are div $\boldsymbol{H}_2' = 0$ and curl $\boldsymbol{H}_2' = 0$, so that by putting $\boldsymbol{H}_2' = -$ grad Ω_2', we have

$$\nabla^2\Omega_2' = 0 \quad . \quad . \quad . \quad . \quad . \quad . \quad . \quad (6)$$

The solution of this equation, satisfying the condition $B_2' \to 0$ as $x \to +\infty$, is given by

$$\Omega_2' = A_2'\varepsilon^{-kx+j(\omega t - ky)}$$

To determine the arbitrary constant A_2', we note that at $x = 0$,

$$[(H_2')_x]_{x\to 0+} = \left[-\frac{\partial\Omega_2'}{\partial x}\right]_{x\to 0+} = kA_2'\varepsilon^{j(\omega t-ky)} = \frac{\hat{B}}{\mu}\varepsilon^{j(\omega t-ky)}$$

Therefore

$$\Omega_2' = \frac{\hat{B}}{k\mu}\varepsilon^{-kx+j(\omega t-ky)} \quad . \quad . \quad . \quad . \quad (7)$$

In region 1 ($x < 0$), the field equations are div $\boldsymbol{H}_1' = 0$ and curl $\boldsymbol{H}_1' = 0$, so that by putting $\boldsymbol{H}_1' = -$ grad Ω_1', we have

$$\nabla^2\Omega_1' = 0 \quad . \quad . \quad . \quad . \quad . \quad . \quad . \quad (8)$$

Also,

$$[\Omega_1']_{x\to 0-} = -\frac{j}{k}[(H_1')_y]_{x\to 0-} = -\frac{j}{k}[(H_2')_y]_{x\to 0+} = -\frac{j}{k}\left(-\frac{k}{j}\right)[\Omega_2']_{x\to 0+} = \frac{\hat{B}}{k\mu}\varepsilon^{j(\omega t-ky)}$$

Thus the required solution of eqn. (8) is

$$\Omega_1' = \left(\frac{\hat{B}}{k\mu}\cosh kx + A_1'\sinh kx\right)\varepsilon^{j(\omega t-ky)}$$

To determine the arbitrary constant A_1', we note that at $x = 0$

$$[(H_1')_x]_{x\to 0-} = \left[-\frac{\partial\Omega_1'}{\partial x}\right]_{x\to 0-} = -kA_1'\varepsilon^{j(\omega t-ky)} = \frac{\hat{B}}{\mu_0}\varepsilon^{j(\omega t-ky)}$$

Therefore

$$\Omega_1' = (\mu_r+1)\frac{\hat{B}}{2k\mu}\left[\varepsilon^{-kx} - \left(\frac{\mu_r-1}{\mu_r+1}\right)\varepsilon^{kx}\right]\varepsilon^{j(\omega t-ky)} \quad (9)$$
$$= A' + B'$$

(8.1.2) **Medium Assumed Conducting.**

In region 2 ($x \geqslant 0$), the field equations in the conducting state are div $H_2 = 0$, curl $H_2 = J_2$, ρ curl $J_2 = -\mu \partial H_2/\partial t$.

Therefore

$$\left.\begin{aligned} \nabla^2 H_2 &= \frac{j}{d^2} H_2 \\ \text{and} \qquad \nabla^2 J_2 &= \frac{j}{d^2} J_2 \end{aligned}\right\} \quad \ldots\ldots \quad (10)$$

where $$d = \left[\frac{\rho}{\mu\omega}\right]^{1/2} \quad \ldots\ldots \quad (11)$$

Since $B_2 \to 0$ as $x \to +\infty$, div $H_2 = 0$ and $(B_2)_z = 0$, the solutions of eqn. (9) are

$$(H_2)_x = A_2 \exp\left[-x\left(k^2 + \frac{j}{d^2}\right)^{1/2} + j(\omega t - ky)\right] \quad . \quad (12)$$

$$(H_2)_y = jA_2 \frac{\left[k^2 + \frac{j}{d^2}\right]^{1/2}}{k} \exp\left[-x\left(k^2 + \frac{j}{d^2}\right)^{1/2} + j(\omega t - ky)\right]$$

$$(H_2)_z = 0 \quad \ldots\ldots \quad (13)$$

Since $J_2 = \text{curl } H_2$, the solutions of eqn. (10) are

$$(J_2)_x = 0$$

$$(J_2)_y = 0$$

$$(J_2)_z = \frac{A_2}{kd^2} \exp\left[-x\left(k^2 + \frac{j}{d^2}\right)^{1/2} + j(\omega t - ky)\right]$$

A_2 is an arbitrary constant in the above solutions. In region 1 ($x < 0$), as in Section 8.1.1, $H_1 = -\text{grad}\,\Omega_1$ and $\nabla^2\Omega_1 = 0$. Also,

$$[\Omega_1]_{x\to 0-} = -\frac{j}{k}[(H_1)_y]_{x\to 0-} = -\frac{j}{k}[(H_2)_y]_{x\to 0+}$$

$$= \frac{A_2}{k^2}\left(k^2 + \frac{j}{d^2}\right)^{1/2} \varepsilon^{j(\omega t - ky)}$$

Therefore

$$\Omega_1 = \left[\frac{A_2}{k^2}\left(k^2 + \frac{j}{d^2}\right)^{1/2} \cosh kx + D_1 \sinh kx\right] \varepsilon^{j(\omega t - ky)}$$

But at $x = 0$, $\quad [(H_1)_x]_{x\to 0-} = \mu_r[(H_2)_x]_{x\to 0+}$

so that $$D_1 = -\frac{\mu_r}{k} A_2$$

Therefore in region 1 ($x < 0$),

$$\Omega_1 = \left[k\mu_r + \left(k^2 + \frac{j}{d^2}\right)^{1/2}\right] \frac{A_2}{2k^2}$$

$$\left[\varepsilon^{-kx} - \frac{k\mu_r - \left(k^2 + \frac{j}{d^2}\right)^{1/2}}{k\mu_r + \left(k^2 + \frac{j}{d^2}\right)^{1/2}} \varepsilon^{kx}\right] \varepsilon^{j(\omega t - ky)} \quad (14)$$

$$= A + B$$

Noting that the part A' of the total applied field Ω_1' is the same as the part A of the resultant field Ω_1, we equate the coefficients of ε^{-kx} in eqns. (9) and (14). This determines the arbitrary constant A_2 as

$$A_2 = \frac{k(\mu_r + 1)}{k\mu_r + \left(k^2 + \frac{j}{d^2}\right)^{1/2}} \frac{\hat{B}}{\mu} \quad \ldots \quad (15)$$

Substituting this value of A_2 in eqns. (12) and (13), we have in region 2 ($x \geqslant 0$),

$$(H_2)_x = \frac{k(\mu_r + 1)}{k\mu_r + \left(k^2 + \frac{j}{d^2}\right)^{1/2}}$$

$$\frac{\hat{B}}{\mu} \exp\left[-x\left(k^2 + \frac{j}{d^2}\right)^{1/2} + j(\omega t - ky)\right]$$

$$(H_2)_y = j\frac{\left(k^2 + \frac{j}{d^2}\right)^{1/2}(\mu_r + 1)}{k\mu_r + \left(k^2 + \frac{j}{d^2}\right)^{1/2}}$$

$$\frac{\hat{B}}{\mu} \exp\left[-x\left(k^2 + \frac{j}{d^2}\right)^{1/2} + j(\omega t - ky)\right]$$

$$(H_2)_z = 0$$

$(J_2)_z$ is given by eqn. (1) in Section 4 and the potential Ω_1 in region 1 ($x < 0$) is given by eqn. (2) in the same Section.

(8.2) Solid Core End-Plate in a Rotating Field

The procedure followed is exactly the same as in Section 8.1. Only the main results are indicated below.

With region 2 ($0 \leqslant x \leqslant h$) assumed to be non-conducting the relevant field equations are:

Region 1 ($x < 0$): $\quad H_1' = -\text{grad}\,\Omega_1', \quad \nabla^2\Omega_1' = 0$

Region 2 ($0 \leqslant x \leqslant h$): $\quad H_2' = -\text{grad}\,\Omega_2', \quad \nabla^2\Omega_2' = 0$

Region 3 ($x > h$): $\quad H_3' = -\text{grad}\,\Omega_3', \quad \nabla^2\Omega_3' = 0$

The potential field only in region 1 ($x < 0$) is of interest in the problem. This is

$$\Omega_1' = \frac{4\hat{B}}{\pi\mu}\left(\frac{\mu_r - 1}{\mu_r + 1}\right)\left[\sum_{p\,odd} \frac{(-1)^{(p-1)/2}}{p\gamma_p} \frac{\left(\frac{\mu_r + 1}{\mu_r - 1}\right)^2 \varepsilon^{2\gamma_p h} - 1}{\left(\frac{\mu_r + 1}{\mu_r - 1}\right)\varepsilon^{2\gamma_p h} - 1} \times\right.$$

$$\left. \times (\cosh \gamma_p x - \mu_r \sinh \gamma_p x) \cos\frac{p\pi z}{l}\right] \varepsilon^{j(\omega t - k}$$

$$= \frac{2\hat{B}}{\pi\mu}(\mu_r - 1)\left\{\sum_{p\,odd} \frac{(-1)^{(p-1)/2}}{p\gamma_p} \frac{\left(\frac{\mu_r + 1}{\mu_r - 1}\right)^2 \varepsilon^{2\gamma_p h} - 1}{\left(\frac{\mu_r + 1}{\mu_r - 1}\right)\varepsilon^{2\gamma_p h} - 1} \times\right.$$

$$\left. \times \left[\varepsilon^{-\gamma_p x} - \left(\frac{\mu_r - 1}{\mu_r + 1}\right)\varepsilon^{\gamma_p x}\right] \cos\frac{p\pi z}{l}\right\} \varepsilon^{j(\omega t - ky)} \quad (14$$

$$x < 0, \quad -\frac{l}{2} < z < \frac{l}{2}$$

where $$\gamma_p = \left(k^2 + \frac{p^2\pi^2}{l^2}\right)^{1/2} \quad \ldots \quad (11$$

* Throughout Sections 8.1 and 8.2, the magnetic-field intensity and eddy current density components, and also the potential, are to be taken as equal only to the real parts of the corresponding complex expressions obtained.

With region 2 ($0 \leqslant x \leqslant h$) assumed to be conducting, the relevant field equations are:

Region 1 ($x < 0$): $\quad \boldsymbol{H}_1 = -\operatorname{grad} \Omega_1, \quad \nabla^2 \Omega_1 = 0$

Region 2 ($0 \leqslant x \leqslant h$): $\nabla^2 \boldsymbol{H}_2 = \dfrac{j}{d^2} \boldsymbol{H}_2,$

$$\nabla^2 \boldsymbol{J}_2 = \frac{j}{d^2} \boldsymbol{J}_2, \quad \boldsymbol{J}_2 = \operatorname{curl} \boldsymbol{H}_2$$

Region 3 ($x > h$): $\quad \boldsymbol{H}_3 = -\operatorname{grad} \Omega_3, \quad \nabla^2 \Omega_3 = 0$

The solutions of these equations are as follows.

(*a*) Region 1 ($x < 0, \ -l/2 < z < l/2$):

$$\Omega_1 = \sum_{p\ odd} \frac{1}{\gamma_p^2} [\delta_p (a_{p-} - a_{p+}) \cosh \gamma_p x - \mu_r \gamma_p (a_{p-} + a_{p+}) \sinh \gamma_p x] \cos \frac{p\pi z}{l} \times \varepsilon^{j(\omega t - ky)}$$

$$= \left(\sum_{p\ odd} \frac{1}{2\gamma_p^2} \{ [(\mu_r \gamma_p + \delta_p) a_{p-} + (\mu_r \gamma_p - \delta_p) a_{p+}] \varepsilon^{-\gamma_p x} - [(\mu_r \gamma_p - \delta_p) a_{p-} + (\mu_r \gamma_p + \delta_p) a_{p+}] \varepsilon^{\gamma_p x} \} \cos \frac{p\pi z}{l} \right) \varepsilon^{j(\omega t - ky)} \quad (18)$$

(*b*) Region 2 ($0 \leqslant x \leqslant h, \ -l/2 < z < l/2$):

$$(H_2)_x = \left[\sum_{p\ odd} (a_{p-} \varepsilon^{-\delta_p x} + a_{p+} \varepsilon^{\delta_p x}) \cos \frac{p\pi z}{l} \right] \varepsilon^{j(\omega t - ky)}$$

$$(H_2)_y = jk \left[\sum_{p\ odd} \frac{\delta_p}{\gamma_p^2} (a_{p-} \varepsilon^{-\delta_p x} - a_{p+} \varepsilon^{\delta_p x}) \cos \frac{p\pi z}{l} \right] \varepsilon^{j(\omega t - ky)}$$

$$(H_2)_z = \frac{\pi}{l} \left[\sum_{p\ odd} \frac{p\delta_p}{\gamma_p^2} (a_{p-} \varepsilon^{-\delta_p x} - a_{p+} \varepsilon^{\delta_p x}) \sin \frac{p\pi z}{l} \right] \varepsilon^{j(\omega t - ky)}$$

$$(J_2)_x = 0$$

$$(J_2)_y = \frac{j\pi}{d^2 l} \left[\sum_{p\ odd} \frac{p}{\gamma_p^2} (a_{p-} \varepsilon^{-\delta_p x} + a_{p+} \varepsilon^{\delta_p x}) \sin \frac{p\pi z}{l} \right] \varepsilon^{j(\omega t - ky)}$$

$$(J_2)_z = \frac{k}{d^2} \left[\sum_{p\ odd} \frac{1}{\gamma_p^2} (a_{p-} \varepsilon^{-\delta_p x} + a_{p+} \varepsilon^{\delta_p x}) \cos \frac{p\pi z}{l} \right] \varepsilon^{j(\omega t - ky)} \quad . \ . \ . \ . \quad (19)$$

(*c*) Region 3 ($x > h, \ -l/2 < z < l/2$):

$$\Omega_3 = \sum_{p\ odd} \frac{\delta_p}{\gamma_p^2} [(a_{p-} - a_{p+}) \cosh \delta_p h - (a_{p-} + a_{p+}) \sinh \delta_p h] \varepsilon^{-\gamma_p (x-h)} \cos \frac{p\pi z}{l} \times \varepsilon^{j(\omega t - ky)}$$

$$= \left[\sum_{p\ odd} \frac{\delta_p}{\gamma_p^2} (a_{p-} \varepsilon^{-\delta_p h} - a_{p+} \varepsilon^{\delta_p h}) \varepsilon^{-\gamma_p (x-h)} \cos \frac{p\pi z}{l} \right] \varepsilon^{j(\omega t - ky)} \quad . \ . \ . \ . \quad (20)$$

where

$$\gamma_p = \left(k^2 + \frac{p^2 \pi^2}{l^2} \right)^{1/2}$$

$$\delta_p = \left(k^2 + \frac{p^2 \pi^2}{l^2} + \frac{j}{d^2} \right)^{1/2} \quad . \ . \ . \ . \ . \ . \ . \ . \ . \quad (21)$$

and

$$a_{p\pm} = \frac{4\hat{B}}{\pi \mu} (\mu_r - 1) \frac{(-1)^{(p-1)/2}}{p} \frac{\left(\dfrac{\mu_r + 1}{\mu_r - 1} \right)^2 \varepsilon^{2\gamma_p h} - 1}{\left(\dfrac{\mu_r + 1}{\mu_r - 1} \right) \varepsilon^{2\gamma_p h} - 1} \frac{\gamma_p}{\mu_r \gamma_p \mp \delta_p} \left[1 - \left(\frac{\mu_r \gamma_p \pm \delta_p}{\mu_r \gamma_p \mp \delta_p} \right)^2 \varepsilon^{\pm 2\delta_p h} \right]^{-1} \quad (22)$$

621.372.54

The Institution of Electrical Engineer
Monograph No. 439 M
Apr. 196

A NOTE ON OPTIMUM LINEAR MULTIVARIABLE FILTERS

By R. J. KAVANAGH, B.Sc., M.A.Sc., Ph.D., Graduate.

(*The paper was first received 8th August, and in revised form 16th December*, 1960. *It was published as an* INSTITUTION MONOGRAPH *in April*, 1961.)

SUMMARY

The explicit solution for the optimum linear physically realizable multivariable filter involves the factorization of a power-spectra matrix into two matrices, one having all its poles in the left-half p-plane and the other having all its poles in the right-half p-plane. No general method of accomplishing this factorization has previously been available.

This note contributes a method of factorizing any power-spectra matrix in the required manner. As a result, the explicit solution for the optimum filter is obtainable in a number of cases not previously solvable without resort to implicit methods. In the course of developing the factorization method it is shown that it is always possible to obtain a physically realizable multivariable system which will transform any given set of signals into an equal number of incoherent white-noise signals. Similarly it is shown that a physically realizable multivariable shaping filter may always be found to transform a set of incoherent white-noise signals into an equal number of signals with any desired power-spectra matrix.

LIST OF SYMBOLS

$A(p)$, $B(p)$, $C(p)$, $D(p)$, $E(p)$, $H(p)$, $S(p)$, $T(p)$ = System transfer matrices.
$\tilde{A}(u)$ = System weighting-function matrix.
$e_i(t)$ = ith error of optimum system.
I = Identity matrix.
$p = j\omega$.
$U(p)$ = Unitary transfer matrix.
$V(t)$ = Column matrix with $v_i(t)$ as ith element.
v_i = ith output of $A(p)$.
$X(t)$ = Column matrix with $x_i(t)$ as ith element.
x_i = ith input to optimum system.
y_i = ith output of optimum system.
z_i = ith desired output of optimum system.
$\Phi^{vv}(p), \Phi^{xv}(p), \Phi^{xx}(p), \Phi^{xz}(p), \Phi^{1}(p)$ = Power-spectra matrices.
$\Phi^{xx}_{+}(p)$, $\Phi^{xx}_{-}(p)$ = Factors of $\Phi^{xx}(p)$ whose elements have all poles in left-half and right-half p-plane, respectively.
$\Phi_{x_ix_j}(p)$, $\Phi_{v_iv_i}(p)$, $\Phi_1(p)$, $\Phi_2(p)$ = Power spectra.
$\Phi^{+}_{v_iv_i}(p)$ = Factor of $\Phi_{v_iv_i}(p)$ containing all its left-half p-plane poles and zeros.
$\phi^{vv}(\tau)$ = Matrix of correlation functions for the v_i's.
$\phi^{xv}(\tau)$ = Matrix of cross-correlation functions for the x_i's and v_i's.
τ = Time shift.
$[\ ]'$ = Transpose of a matrix.
$[\ ]_+$ = Those terms of a partial-fraction expansion of a matrix containing poles only in the left-half p-plane.

(1) INTRODUCTION

The problem with which the paper is concerned is that of determining the optimum physically realizable linear multivariable system whose inputs are a set of signals with know statistical properties and whose outputs are to approximate second set of signals. The optimum system will be that whic causes the sum of the mean-square errors between the syste outputs and the second set of signals to be minimized. Th situation is illustrated in Fig. 1, in which $H(p)$ is the desir

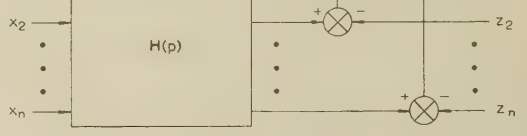

Fig. 1.—Optimum linear filter.

multivariable system and the x's and the z's are given sets o signals. $H(p)$ is to be chosen so as to minimize

$$\sum_{i=1}^{n} \overline{e_i^2(t)}$$

This problem has applications in the control of processes an systems having several inputs and outputs. Examples whic may be cited are the control of turbo-jet engines, steel rollin mills and chemical processes. The same mathematical proble arises in the field of the estimation of optimum linear mode for multivariable processes when use is made of typical operatin records of the variables. In this case the x's are the actu process inputs, the z's are the actual process outputs and $H($ is the desired linear model for the system. The optimum mod is taken to be that which minimizes the sum of the mean-squa errors between the process outputs and the corresponding mod outputs when both model and process have identical inputs.

The formal solution for this problem has been shown b Amara[1] to be

$$[H(p)]' = [\Phi^{xx}_{+}(p)]^{-1}\left[[\Phi^{xx}_{-}(p)]^{-1}\,\Phi^{xz}(p)\right]_{+} \quad . \quad (($$

For the simple case of x's with zero cross-correlation, $\Phi^{xx}(p)$ a diagonal matrix, and it may easily be factorized into tw diagonal matrices to give $\Phi^{xx}_{+}(p)$ and $\Phi^{xx}_{-}(p)$ having all the poles, respectively, in the left- and right-half p-plane. For th particular case it is also necessary for $\Phi^{xx}_{+}(p)$ to have all i zeros* in the left-half p-plane in order to obtain a realizab transfer matrix[2] $H(p)$. For the case where cross-correlatio exists between any of the x's, $\Phi^{xx}(p)$ is not a diagonal matri and it has not hitherto been possible to obtain the facto $\Phi^{xx}_{+}(p)$ and $\Phi^{xx}_{-}(p)$ except in certain special cases. It will b shown in this note that any $\Phi^{xx}(p)$ may be factorized into th required form and that the explicit solution for $H(p)$ given b eqn. (1) may be used for a wider range of cases than was pr viously possible.

Correspondence on Monographs is invited for consideration with a view to publication.

Dr. Kavanagh was formerly in the Department of Electrical Engineering, Imperial College of Science and Technology, University of London, and is now in the Department of Electrical Engineering, University of Toronto.

* The poles and zeros of a matrix refer to the poles and zeros of the individ matrix elements.

In the course of deriving the factorization method two interesting results will be developed. The first is a general method of converting a set of cross-correlated signals to an equal number of incoherent* white-noise signals. The second concerns the converse problem, i.e. that of converting a set of incoherent white-noise signals to an equal number of signals with a desired power-spectra matrix. In both cases it will be shown that the desired transformation may always be effected by means of a physically realizable linear multivariable system.

(2) CONVERSION OF ARBITRARY SIGNALS TO INCOHERENT WHITE-NOISE SIGNALS

A set of n signals, $x_1, x_2 \ldots x_n$, is assumed to be given and to have a known power-spectra matrix $\Phi^{xx}(p)$, which is assumed to be non-singular. It is desired to operate on these signals with a linear physically realizable system such that the n output signals, $y_1, y_2 \ldots y_n$, are all white-noise signals with zero cross-correlation. A system with transfer matrix $D(p)$ is therefore required such that $\Phi^{yy}(p) = I$. The determination of $D(p)$ will proceed in three stages. A system $A(p)$ will first be found which transforms the x's into a set of signals with zero cross-correlation. $A(p)$ will in general be physically unrealizable. A second system $B(p)$ will now transform these signals into incoherent white-noise signals. Finally a third system $C(p)$ will transform these white-noise signals into another set of white-noise signals with zero cross-correlation in such a way that the overall system $D(p) = C(p)B(p)A(p)$ will be physically realizable.

It is shown in Section 10 that $\Phi^{xx}(p)$, $\Phi^{vv}(p)$ and $A(p)$ are related by

$$\Phi^{vv}(p) = A(-p)\Phi^{xx}(p)[A(p)]' \quad . \quad . \quad . \quad (2)$$

where $\Phi^{vv}(p)$ is the power-spectra matrix of the outputs of $A(p)$. First, therefore, it is necessary to find a transfer matrix $A(p)$ such that when substituted in eqn. (2) a diagonal $\Phi^{vv}(p)$ is obtained.

Now $\Phi^{xx}(p)$ is, for example in the three-variable case, of the form

$$\Phi^{xx}(p) = \begin{bmatrix} \Phi_{x_1x_1}(p) & \Phi_{x_1x_2}(p) & \Phi_{x_1x_3}(p) \\ \Phi_{x_1x_2}(-p) & \Phi_{x_2x_2}(p) & \Phi_{x_2x_3}(p) \\ \Phi_{x_1x_3}(-p) & \Phi_{x_2x_3}(-p) & \Phi_{x_3x_3}(p) \end{bmatrix} \quad . \quad (3)$$

Since, because of the properties of power spectra, $\Phi^{xx}(p)$ is a Hermitian matrix[3] for $p = j\omega$. If $\Phi_{x_1x_2}(p)/\Phi_{x_1x_1}(p)$ times the first column of $\Phi^{xx}(p)$ is subtracted from its second column and then $\Phi_{x_1x_2}(-p)/\Phi_{x_1x_1}(p)$ times the first row of $\Phi^{xx}(p)$ is subtracted from its second row, a matrix of the following form results:

$$\Phi^1(p) = \begin{bmatrix} \Phi_{x_1x_1}(p) & 0 & \Phi_{x_1x_3}(p) \\ 0 & \Phi_1(p) & \Phi_2(p) \\ \Phi_{x_1x_3}(-p) & \Phi_2(-p) & \Phi_{x_3x_3}(p) \end{bmatrix} \quad . \quad . \quad (4)$$

In this matrix $\Phi_1(p)$ and $\Phi_2(p)$ are functions of the original elements of $\Phi^{xx}(p)$. Now these two operations on $\Phi^{xx}(p)$ may be written in matrix form as

$$\Phi^1(p) = A_1(-p)\Phi^{xx}(p)[A_1(p)]' \quad . \quad . \quad . \quad (5)$$

where

$$A_1(p) = \begin{bmatrix} 1 & 0 & 0 \\ -\dfrac{\Phi_{x_1x_2}(p)}{\Phi_{x_1x_1}(p)} & 1 & 0 \\ 0 & 0 & 1 \end{bmatrix} \quad . \quad . \quad . \quad (6)$$

* A set of signals with all cross-correlations zero is said to be incoherent.

Thus a system with transfer matrix $A_1(p)$ will transform the x's into a set of signals with power-spectra matrix $\Phi^1(p)$ as given by eqn. (4). Evidently this same procedure may be carried out twice more so that the resultant set of signals has a diagonal power-spectra matrix. The necessary transfer matrix $A(p)$ which accomplishes this diagonalization may therefore be easily determined. Since $A(p)$ has elements which are of the form of ratios of power spectra, it will in general have poles in the right-half of the p-plane and will therefore be physically unrealizable.

If the outputs of $A(p)$ are $v_1, v_2 \ldots v_n$, the power-spectra matrix for these signals will be of the form

$$\Phi^{vv}(p) = \begin{bmatrix} \Phi_{v_1v_1}(p) & 0 & 0 \\ 0 & \Phi_{v_2v_2}(p) & 0 \\ 0 & 0 & \Phi_{v_3v_3}(p) \end{bmatrix} \quad . \quad . \quad (7)$$

for a three-variable case. To convert the v's to white-noise signals with zero cross-correlation it is necessary to pass them through a system with transfer matrix $B(p)$, where

$$B(p) = \begin{bmatrix} \dfrac{1}{\Phi^+_{v_1v_1}(p)} & 0 & 0 \\ 0 & \dfrac{1}{\Phi^+_{v_2v_2}(p)} & 0 \\ 0 & 0 & \dfrac{1}{\Phi^+_{v_3v_3}(p)} \end{bmatrix} \quad . \quad . \quad (8)$$

and where $\Phi^+_{v_iv_i}(p)$ consists of a factor of $\Phi_{v_iv_i}(p)$ containing its left-half p-plane poles and zeros only. It is now apparent that a system with transfer matrix $B(p)A(p)$ will transform the x's to white-noise signals with zero cross-correlation. The matrix $B(p)A(p)$ is still unrealizable, in general, and some further transformation, $C(p)$, is required which will transform the outputs of $B(p)$ to another set of white-noise signals with zero cross-correlation such that $C(p)B(p)A(p)$ is realizable.

Such a system is obtainable in the following way. $C(p)$ is made a diagonal matrix such that the diagonal elements $c_{ii}(p)$ have zeros corresponding to all right-half p-plane poles appearing in the ith row of $B(p)A(p)$. These poles, which render $B(p)A(p)$ unrealizable, will now be cancelled by the zeros of $C(p)$. In order that the outputs of $C(p)$ shall still be white noises, the poles of $c_{ii}(p)$ must be equal in number to the number of zeros of $c_{ii}(p)$ and must be negative conjugate to the zeros. Thus $c_{ii}(p)$ are all-pass networks.

It now follows that the overall system $D(p) = C(p)B(p)A(p)$ is the required system. Since each of the three constituent systems may always be found it follows that a physically realizable $D(p)$ may always be determined for any given $\Phi^{xx}(p)$. It will be noticed that $D(p)$ usually has non-minimum phase elements.

(3) NON-UNIQUENESS OF DIAGONALIZING SYSTEM

It is now relevant to inquire whether the system $D(p)$ which transforms the x's to white-noise signals, $y_1, y_2 \ldots y_n$, with zero cross-correlation is unique. It is known that

$$D(-p)\Phi^{xx}(p)[D(p)]' = \Phi^{yy}(p) = I \quad . \quad . \quad . \quad (9)$$

Suppose that some other system with transfer matrix $E(p)$ also performs the required transformation. Then it follows that

$$E(-p)\Phi^{xx}(p)[E(p)]' = I \quad . \quad . \quad . \quad . \quad (10)$$

Let

$$E(p) = U(p)D(p) \quad . \quad . \quad . \quad . \quad . \quad (11)$$

Substitution for $E(p)$ in eqn. (10) gives

$$U(-p)D(-p)\Phi^{xx}(p)[D(p)]'[U(p)]' = I \quad . \quad . \quad (12)$$

Using eqn. (9), this yields

$$U(-p)[U(p)]' = I \quad . \quad . \quad . \quad . \quad . \quad (13)$$

Thus $E(p)$ will perform the required transformation provided that it can be written as $U(p)D(p)$, where $U(p)$ satisfies eqn. (13). A matrix which satisfies eqn. (13) for $p = j\omega$ is known as a unitary matrix.[3] Provided that $U(p)$ is physically realizable, $E(p)$ must be physically realizable. There is an infinite number of realizable unitary matrices, a particularly useful one being of the form

$$U(p) = \begin{bmatrix} \frac{a(p)}{a(-p)} & 0 & 0 \\ 0 & \frac{b(p)}{b(-p)} & 0 \\ 0 & 0 & \frac{c(p)}{c(-p)} \end{bmatrix} \quad . \quad . \quad . \quad (14)$$

where $a(p)$, $b(p)$ and $c(p)$ are polynomials with all zeros in the right-half p-plane. It may be concluded that, if a system $D(p)$ will convert a set of cross-correlated signals to white-noise signals with zero cross-correlation, any other system with a transfer matrix $E(p) = U(p)D(p)$, where $U(p)$ is unitary, will also accomplish this transformation.

The physical interpretation of eqn. (11) is that the outputs of $D(p)$, which are white-noise signals with zero cross-correlation, are applied as inputs to a system with transfer matrix $U(p)$. The outputs of $U(p)$ are again incoherent white-noise signals. It follows that a characteristic property of a unitary system is that it will transform a set of incoherent white-noise signals to another such set without introducing cross-correlation. This property and the particular class of unitary system given by eqn. (14) suggest that unitary systems may be regarded as multivariable generalizations of all-pass systems. It should be emphasized that unitary systems are not confined to the form given in eqn. (14). Unitary matrices with non-zero off-diagonal terms are also available. The transfer matrix

$$U(p) = \begin{bmatrix} \frac{1}{1+p} & \frac{-p}{1+p} \\ \frac{-p}{1+p} & \frac{1}{1+p} \end{bmatrix}$$

for example, represents a unitary system.

(4) MULTIVARIABLE SHAPING FILTERS

The converse problem of that considered in the previous Section will now be examined. A set of incoherent white-noise signals is given. It is desired to obtain, by some physically realizable transformation of the signals, a second set having a desired power-spectra matrix. This problem is readily solved using results obtained in the previous Section.

Let the required signals be $x_1, x_2 \ldots x_n$ with power-spectra matrix $\Phi^{xx}(p)$. If $D(p)$ is the transfer matrix of any system, realizable or unrealizable, which will convert the x's to incoherent white-noise signals, then

$$D(-p)\Phi^{xx}(p)[D(p)]' = I \quad . \quad . \quad . \quad . \quad (15)$$

It follows that

$$\Phi^{xx}(p) = [D(-p)]^{-1}I\{[D(p)]'\}^{-1} \quad . \quad . \quad . \quad (16)$$

or

$$\Phi^{xx}(p) = S(-p)I[S(p)]' \quad . \quad . \quad . \quad . \quad (1$$

where

$$S(p) = [D(p)]^{-1} \quad . \quad . \quad . \quad . \quad . \quad (1$$

Thus a system with transfer matrix $S(p) = [D(p)]^{-1}$ is a shapi filter which will convert the white-noise signals to a set of x with the required power-spectra matrix.

By a method analogous to that used in Section 3 it may shown that, in general, any system with a transfer matrix $T($ where

$$T(p) = S(p)U(p) \quad . \quad . \quad . \quad . \quad . \quad (1$$

will also be a desirable shaping filter, $U(p)$ again being a unita system. The physical interpretation of eqn. (19) is that t white-noise signals are first operated upon by $U(p)$ to give second set of incoherent white-noise signals. This second s of signals is then transformed by $S(p)$ to give the desired x's.

The system $S(p)$ will not necessarily be physically realizab By choosing $U(p)$ to have the form given by eqn. (14), whe the zeros of each diagonal term cancel all the right-half p-pla poles of the corresponding column of $S(p)$, $T(p)$ can always made physically realizable. Thus it may be concluded that t desired physically realizable shaping filter is always obtainab As an alternative to obtaining $T(p)$ from $D(p)$, a derivati similar to that used in Section 2 could have been used in wh a suitable set of matrix operations would be found to transfo the identity matrix into $\Phi^{xx}(p)$.

(5) FACTORIZATION OF $\Phi^{xx}(p)$

It is now possible to solve the basic problem with which t paper is concerned. It is required to find two matrices $\Phi_+^{xx}($ and $\Phi_-^{xx}(p)$ such that

$$\Phi^{xx}(p) = \Phi_-^{xx}(p)\Phi_+^{xx}(p) \quad . \quad . \quad . \quad . \quad (2$$

where $\Phi_+^{xx}(p)$ has all of its poles in the left-half p-plane a $\Phi_-^{xx}(p)$ has all of its poles in the right-half p-plane.

Suppose that a set of x's with the power-spectra matr $\Phi^{xx}(p)$ can be obtained from an equal number of white-noi signals with zero cross-correlation by means of a physica realizable system $T(p)$. Then it follows that

$$\Phi^{xx}(p) = T(-p)[T(p)]' \quad . \quad . \quad . \quad . \quad (2$$

But $T(p)$, being realizable, must have all of its poles in t left-half p-plane. Consequently $T(-p)$ must have all of poles in the right-half p-plane. Comparing eqns. (20) and (2 it may therefore be seen that the required factors are given by

$$\Phi_+^{xx}(p) = [T(p)]' \quad . \quad . \quad . \quad . \quad . \quad (2$$

$$\Phi_-^{xx}(p) = T(-p) \quad . \quad . \quad . \quad . \quad . \quad (2$$

Solution of the factorization problem therefore involves fi the determination of a physically realizable shaping filter cor sponding to the given $\Phi^{xx}(p)$ and then application of eqns. (2 and (23). Since $T(p)$ is not unique it also follows that t factorization is also non-unique.

This method of determining $\Phi_+^{xx}(p)$ and $\Phi_-^{xx}(p)$ now enab eqn. (1) to be used to determine the optimum realizable line multivariable filter for a wider range of cases than was pr viously possible. In a previous paper,[1] $\Phi^{xx}(p)$ was restrict to matrices having the property that $\Phi^{xx}(p) = \Phi^{xx}(-p)$ in orc that an explicit solution of eqn. (1) could be obtained. T method of the present paper extends the application of eqn. to include all cases in which $[\Phi_+^{xx}(p)]^{-1}$ is realizable.

(6) EXAMPLES

As a first example of the factorization method let it be supposed hat two signals are given with the following power spectra natrix:

$$\Phi^{xx}(p) = \begin{bmatrix} \frac{3}{4-p^2} & \frac{3p}{4-p^2} \\ \frac{-3p}{4-p^2} & \frac{4-4p^2}{4-p^2} \end{bmatrix} \quad . \quad . \quad . \quad (24)$$

: will be noted that $\Phi^{xx}(p) \neq \Phi^{xx}(-p)$. In determining $\Phi^{xx}_{+}(p)$ and $\Phi^{xx}_{-}(p)$, both the corresponding shaping filter and ne system which transforms the x's to white noise with zero ross-correlation will be found as an illustration of the method.

By inspection of eqn. (24), it will be seen that a system which ansforms the x's to two signals with zero cross-correlation is

$$A(p) = \begin{bmatrix} 1 & 0 \\ -p & 1 \end{bmatrix} \quad . \quad . \quad . \quad . \quad . \quad (25)$$

he power-spectra matrix of the outputs of $A(p)$ is

$$\Phi^{vv}(p) = \begin{bmatrix} \frac{3}{4-p^2} & 0 \\ 0 & 1 \end{bmatrix} \quad . \quad . \quad . \quad . \quad (26)$$

o obtain white-noise signals the outputs of $A(p)$ must be ansformed by a system with transfer matrix

$$B(p) = \begin{bmatrix} \frac{2+p}{\sqrt{3}} & 0 \\ 0 & 1 \end{bmatrix} \quad . \quad . \quad . \quad . \quad (27)$$

Now the overall transfer matrix of these two systems is

$$B(p)A(p) = \begin{bmatrix} \frac{2+p}{\sqrt{3}} & 0 \\ -p & 1 \end{bmatrix} = D(p) \quad . \quad . \quad . \quad (28)$$

$D(p)$ is seen to be physically realizable and so represents the esired system.

Without regard to realizability, a suitable shaping filter is iven by

$$S(p) = [D(p)]^{-1} \quad . \quad . \quad . \quad . \quad . \quad (29)$$

n this case

$$S(p) = \begin{bmatrix} \frac{\sqrt{3}}{2+p} & 0 \\ \frac{\sqrt{3}p}{2+p} & 1 \end{bmatrix} \quad . \quad . \quad . \quad . \quad . \quad (30)$$

or this example $S(p)$ is itself physically realizable and does not equire transformation by a unitary system in order to obtain a ealizable shaping filter.

Application of eqns. (22) and (23), where in this case $(p) = S(p)$, yields the required factors

$$\Phi^{xx}_{+}(p) = \begin{bmatrix} \frac{\sqrt{3}}{2+p} & \frac{\sqrt{3}p}{2+p} \\ 0 & 1 \end{bmatrix} \quad . \quad . \quad . \quad (31)$$

nd

$$\Phi^{xx}_{-}(p) = \begin{bmatrix} \frac{\sqrt{3}}{2-p} & 0 \\ \frac{-\sqrt{3}p}{2-p} & 1 \end{bmatrix} \quad . \quad . \quad . \quad . \quad (32)$$

If an optimum filtering operation is now to be performed on the x's, substitution of $\Phi^{xx}_{+}(p)$ and $\Phi^{xx}_{-}(p)$ from the above into eqn. (1) will yield a solution for any $\Phi^{xz}(p)$, since $[\Phi^{xx}_{+}(p)]^{-1}$ is readily verified to be realizable.

As a second example of the method, consider the power-spectra matrix

$$\Phi^{xx}(p) = \begin{bmatrix} \frac{4-p^2}{1-p^2} & \frac{4\cdot 9}{1-p^2} \\ \frac{4\cdot 9}{1-p^2} & \frac{9-p^2}{1-p^2} \end{bmatrix} \quad . \quad . \quad . \quad (33)$$

The system which transforms the x's to two signals with zero cross-correlation is

$$A(p) = \begin{bmatrix} 1 & 0 \\ \frac{-4\cdot 9}{4-p^2} & 1 \end{bmatrix} \quad . \quad . \quad . \quad . \quad (34)$$

The power-spectra matrix of the outputs of $A(p)$ is

$$\Phi^{vv}(p) = \begin{bmatrix} \frac{4-p^2}{1-p^2} & 0 \\ 0 & \frac{12-p^2}{4-p^2} \end{bmatrix} \quad . \quad . \quad . \quad (35)$$

To obtain incoherent white-noise signals, the v's must be transformed by a system with transfer matrix

$$B(p) = \begin{bmatrix} \frac{1+p}{2+p} & 0 \\ 0 & \frac{2+p}{\sqrt{12+p}} \end{bmatrix} \quad . \quad . \quad . \quad (36)$$

The overall transfer matrix of these two systems is

$$B(p)A(p) = \begin{bmatrix} \frac{1+p}{2+p} & 0 \\ \frac{-4\cdot 9}{(2-p)(\sqrt{12+p})} & \frac{2+p}{\sqrt{12+p}} \end{bmatrix} = D(p) \quad (37)$$

$D(p)$ is not physically realizable because of the pole at $p = 2$. To obtain a realizable diagonalizing system the outputs of $D(p)$ must be further transformed by a suitable unitary system. Thus, if $U_1(p)$ is given by

$$U_1(p) = \begin{bmatrix} 1 & 0 \\ 0 & \frac{2-p}{2+p} \end{bmatrix} \quad . \quad . \quad . \quad . \quad (38)$$

the final diagonalizing system $E(p) = U_1(p)D(p)$ is given by

$$E(p) = \begin{bmatrix} \frac{1+p}{2+p} & 0 \\ \frac{-4\cdot 9}{(2+p)(\sqrt{12+p})} & \frac{2-p}{\sqrt{12+p}} \end{bmatrix} \quad (39)$$

Without regard to realizability, a suitable shaping filter is given by

$$S(p) = [D(p)]^{-1} \quad . \quad . \quad . \quad . \quad . \quad (40)$$

In this case

$$S(p) = \begin{bmatrix} \frac{2+p}{1+p} & 0 \\ \frac{4\cdot 9}{(2-p)(1+p)} & \frac{\sqrt{12+p}}{2+p} \end{bmatrix} \quad . \quad . \quad (41)$$

$S(p)$ is not physically realizable. To obtain a realizable shaping filter the inputs of $S(p)$ must first be transformed by a suitable unitary system. Thus, if $U_2(p)$ is given by

$$U_2(p) = \begin{bmatrix} \frac{2-p}{2+p} & 0 \\ 0 & 1 \end{bmatrix} \quad . \quad . \quad . \quad . \quad (42)$$

the final shaping filter $T(p) = S(p)U(p)$ is given by

$$T(p) = \begin{bmatrix} \frac{2-p}{1+p} & 0 \\ \frac{4 \cdot 9}{(2+p)(1+p)} & \frac{\sqrt{12}+p}{2+p} \end{bmatrix} \quad . \quad . \quad (43)$$

Application of eqns. (22) and (23) now yields the required factors

$$\Phi_+^{xx}(p) = \begin{bmatrix} \frac{2-p}{1+p} & \frac{4 \cdot 9}{(2+p)(1+p)} \\ 0 & \frac{\sqrt{12}+p}{2+p} \end{bmatrix} \quad . \quad . \quad . \quad (44)$$

and

$$\Phi_-^{xx}(p) = \begin{bmatrix} \frac{2+p}{1-p} & 0 \\ \frac{4 \cdot 9}{(2-p)(1-p)} & \frac{\sqrt{12}-p}{2-p} \end{bmatrix} \quad . \quad (45)$$

If eqn. (44) is now used in eqn. (1) it will be found that $[\Phi_+^{xx}(p)]^{-1}$ is not realizable. Thus the particular factorization of $\Phi^{xx}(p)$ accomplished here is not suitable for the optimum filter problem. Since, however, $\Phi^{xx}(p) = \Phi^{xx}(-p)$, this factorization can be accomplished by a method involving the use of a modal matrix.[1, 3] Using the result obtained by the latter method it is possible to reason that if instead of the matrix used for $U_2(p)$ in eqn. (42) the following unitary matrix is employed,

$$U_2(p) = \begin{bmatrix} 0 \cdot 523\left[\frac{\sqrt{12}+p}{2+p}\right] & 0 \cdot 855\left(\frac{1+p}{2+p}\right) \\ 0 \cdot 855\left(\frac{1-p}{2-p}\right) & -0 \cdot 523\left[\frac{\sqrt{12}-p}{2-p}\right] \end{bmatrix} \quad (46)$$

then an alternative factorization is possible for which $[\Phi_+^{xx}(p)]^{-1}$ is realizable. The factors obtained by the use of eqn. (46) instead of eqn. (42) are

$$\Phi_+^{xx}(p) = \begin{bmatrix} 0 \cdot 523\left[\frac{\sqrt{12}+p}{1+p}\right] & 0 \cdot 855\left[\frac{\sqrt{12}+p}{1+p}\right] \\ 0 \cdot 855 & -0 \cdot 523 \end{bmatrix} \quad (47)$$

$$\Phi_-^{xx}(p) = \begin{bmatrix} 0 \cdot 523\left[\frac{\sqrt{12}-p}{1-p}\right] & 0 \cdot 855 \\ 0 \cdot 855\left[\frac{\sqrt{12}-p}{1-p}\right] & -0 \cdot 523 \end{bmatrix} \quad . \quad . \quad . \quad (48)$$

This example illustrates the non-uniqueness of the factorization of $\Phi^{xx}(p)$ and suggests that, in some cases at least, the use of a non-diagonal $U(p)$ in eqn. (19) instead of the diagonal type of eqn. (14) may lead to a realizable $[\Phi_+^{xx}(p)]^{-1}$ which is not obtainable by the method of the paper.

(7) DISCUSSION AND CONCLUSIONS

A method has been given which enables any power-spectr matrix $\Phi^{xx}(p)$ to be divided into two factors, one with all c its poles in the left-half p-plane and one with all its poles i the right-half p-plane. The derivation of the method involve a demonstration of the fact that it is always possible to find physically realizable multivariable system which will transfor a given set of signals to an equal number of incoherent white noise signals. It is also shown that a physically realizab multivariable shaping filter is always obtainable for trans formation of incoherent white-noise signals to an equal numbe of signals with any desired power-spectra matrix. The avai ability of the factors of $\Phi^{xx}(p)$ enables the solution of th optimum-multivariable-filter problem to be accomplished for range of cases which could not previously be solved by a explicit solution of eqn. (1).

In addition to solving some problems, the paper raises other In particular, there are some power-spectra matrices which when factored by the method described above, yield a $\Phi_+^{xx}(p)$ with a non-realizable inverse. At least some of these matrice are, however, known to be factorizable, leading to a realizab $[\Phi_+^{xx}(p)]^{-1}$, by a method involving the use of a modal matrix.* This desirable factorization must be obtainable by the methods c the paper and can apparently be brought about by suitable choic of a non-diagonal matrix $U(p)$ in eqn. (19). It is therefo pertinent to ask whether all $\Phi^{xx}(p)$ matrices may be factorize so that $[\Phi_+^{xx}(p)]^{-1}$ is realizable. If so, how is the necessa $U(p)$ in eqn. (19) chosen? If not all $\Phi^{xx}(p)$ matrices may b factorized in this way, what determines the class of $\Phi^{xx}(p)$ matrices which can be factorized to give a realizable $[\Phi_+^{xx}(p)]^{-1}$ and has this class any particular significance? Answers to thes questions could lead to a general explicit solution of eqn. (1 for the optimum physically realizable linear multivariable filter.

(8) ACKNOWLEDGMENTS

The results described in the paper were obtained during th tenure of a Postdoctoral Overseas Fellowship awarded by th National Research Council of Canada. The author is gratefu to the Council for permission to publish the paper.

(9) REFERENCES

(1) AMARA, R. C.: 'Application of Matrix Methods to th Linear Least Squares Synthesis of Multivariable Systems' *Journal of the Franklin Institute*, 1959, **268**, p. 1.

(2) KAVANAGH, R. J.: 'The Application of Matrix Methods t Multi-Variable Control Systems', *ibid.*, 1956, **262**, p. 34

(3) FERRAR, W. L.: 'Finite Matrices' (Oxford, 1951), pp. 1 147 and 145.

(4) YOULA, D. C.: 'On the Factorization of Rational Matrices' Polytechnic Institute of Brooklyn, Research Repo PIBMRI 855–60, September, 1960.

(10) APPENDIX

(10.1) Relationship Between Input and Output Power-Spectra Matrices

Consider a linear multivariable system with n inputs, x $x_2, \ldots x_n$ and n outputs, $v_1, v_2, \ldots v_n$. Let the system transf matrix be $A(p)$. The relationship between the x's, v's and $A(p)$ can be written in the form of a convolution integral involvin matrices:

$$V(t) = \int_0^\infty \tilde{A}(u)X(t-u)du \quad . \quad . \quad . \quad . \quad (49$$

* Since the paper was written, the author's attention has been drawn to a repor in which it is shown that all power spectra may be factorized so that $[\Phi_+^{xx}(p)]^{-1}$ is realizable.

ostmultiplying both sides of eqn. (49) by $[V(t+\tau)]'$ and king the time average yields

$$\lim_{R\to\infty}\frac{1}{2R}\int_{-R}^{R}V(t)[V(t+\tau)]'dt$$

$$=\lim_{R\to\infty}\frac{1}{2R}\int_{-R}^{R}dt\int_{0}^{\infty}\tilde{A}(u)X(t-u)[V(t+\tau)]'du \quad (50)$$

nterchanging the order of integration on the right-hand side f eqn. (50) leads to the result

$$\phi^{vv}(\tau)=\int_{0}^{\infty}\tilde{A}(u)\phi^{xv}(\tau+u)du \quad . \quad . \quad . \quad (51)$$

Fourier transformation of eqn. (51) yields

$$\Phi^{vv}(p)=A(-p)\Phi^{xv}(p) \quad . \quad . \quad . \quad . \quad (52)$$

If eqn. (49) is now postmultiplied by $[X(t-\tau)]'$ and a similar procedure followed, there results

$$\Phi^{vx}(-p)=A(p)\Phi^{xx}(-p) \quad . \quad . \quad . \quad . \quad (53)$$

Transposition of eqn. (53) yields

$$\Phi^{xv}(p)=\Phi^{xx}(p)[A(p)]' \quad . \quad . \quad . \quad . \quad (54)$$

Elimination of $\Phi^{xv}(p)$ between eqns. (52) and (54) gives the result

$$\Phi^{vv}(p)=A(-p)\Phi^{xx}(p)[A(p)]' \quad . \quad . \quad . \quad (55)$$

$\Phi^{xx}(p)$ and $\Phi^{vv}(p)$ are said to be related by a conjunctive transformation.[3]

621 3.014.31 : 621.387

The Institution of Electrical Engineer
Monograph No. 440
Apr. 196

FACTORS AFFECTING THE BEHAVIOUR OF AN ELECTRIC ARC UNDER TRANSIENT CONDITIONS

By I. A. BLACK, B.Sc.(Eng.), Ph.D., Graduate.

(*The paper was first received* 14*th December*, 1959, *in revised form* 18*th August, and in final form* 21*st December*, 1960. *It was published as an* INSTITUTION MONOGRAPH *in April*, 1961.)

SUMMARY

The paper describes an investigation into the relationship between voltage and current in an arc under transient conditions. It is shown theoretically that the arc resistance is a function of the energy in the arc column, while the power loss from the arc is a function of arc resistance.

The relationship between arc resistance and change of arc energy has been obtained by injecting pulses into a static arc. This relationship is valid for periods from 3 μs up to at least a millisecond. The relationship between power loss and arc resistance has also been derived experimentally. Measurement of the electrode voltage drop under transient conditions has enabled electrode and arc column effects to be separated.

It is shown how the relationship between resistance and energy, as well as between power loss and resistance, is affected by a change of arc length, initial arc current and electrode material.

Finally, the experimental results are compared with dynamic arc equations published in the literature.

LIST OF SYMBOLS

a = Distance from arc axis.
e = Electron charge.
g = Conductance per unit length of arc column.
l = Arc length.
p = Arc power loss per unit length.
q = Energy per unit volume of arc column.
r = Arc resistance per unit length = E/I.
t = Time.
w = Energy per unit length of arc.
E = Arc voltage per unit length = V/l.
I = Arc current at any instant, t.
I_0 = Initial (static) arc current.
J = Current density at any point in the arc column.
N = Number of molecules per unit volume of arc.
P = Power loss from an arc column of length l.
R = Resistance of arc column of length l.
V = Voltage across arc column of length l.
W = Energy contained in an arc of length l.
W_0 = Initial energy in an arc of length l.
θ = Temperature at given point in the arc column.
μ = Effective mobility of electrons and ions.
σ = Arc conductivity = J/E.
χ = Degree of ionization.

(1) INTRODUCTION

A considerable amount of information has been published on the static arc since the turn of the century, when the advent of the arc lamp caused many people to begin work in this field. Chief among these was Hertha Ayrton, who published her book on 'The Electric Arc' in 1902. It was not until very much late that investigations began on the properties of the arc unde transient conditions.

Norberg[1] in 1927 made a passing reference to a form dynamic arc equation, and Cassie[2] in 1939 was the first t publish a dynamic arc equation. His equation aims describing conditions in a circuit-breaker and is based on a arc model for which the temperature is constant throughout th arc column and is also independent of current; variations arc current result in a change of arc diameter. He also assume that the static arc voltage is independent of current. His dy equation may be written

$$r\frac{d}{dt}\left(\frac{1}{r}\right) = \frac{1}{I}\frac{dI}{dt} - \frac{1}{E}\frac{dE}{dt} = \frac{E^2/\rho_C - \eta_C}{q_C} \quad . \quad . \quad (2)$$

in which

ρ_C = Arc resistivity, assumed constant by Cassie.
η_C = Power loss per unit volume of arc, assumed constant.
q_C = Energy per unit volume, assumed constant.

The remaining symbols are defined in the list of symbols.

Mayr[3] proposed another arc model in 1943. He considered an arc with constant diameter whose temperature varies both throughout the arc column and also with current. His stati arc equation is hyperbolic. His assumptions lead to a dynam arc equation

$$r\frac{d}{dt}\left(\frac{1}{r}\right) = \frac{1}{I}\frac{dI}{dt} - \frac{1}{E}\frac{dE}{dt} = \frac{EI - p_M}{w_M} \quad . \quad . \quad (3)$$

in which

w_M = Energy required to change the resistance of an arc unit length by a factor ε (2·718 3); w_M is assume constant by Mayr.
p_M = Power loss per unit length of arc, assumed constant.

These expressions show that the two equations are simila in spite of the very different physical conditions assumed b Cassie and Mayr.

From theoretical considerations, Browne[4] has shown tha for most of the time a power-frequency arc is governed by a equation of the form developed by Cassie, whereas Mayr equation describes conditions in the high-resistance arc forme just after current zero. Experimental work by Browne an Strom[5] showed this to be true over a limited range of curren and time during that portion of the half-cycle near a curren zero. Yoon and Spindle[6] have also shown that the low-curren arc follows Mayr's equation during small changes in the a current.

In an attempt to form a single equation for the behaviour a dynamic arc, valid over a wide range of current and tim Bishop[7] assumed a general differential equation for the arc:

$$f\left(E, \frac{dE}{dt}, \ldots \frac{d^mE}{dt^m}, I, \frac{dI}{dt}, \ldots \frac{d^nI}{dt^n}, t\right) = 0 \quad . \quad . \quad (4)$$

Correspondence on Monographs is invited for consideration with a view to publication.

The paper forms part of a thesis submitted for the degree of Doctor of Philosophy at London University.

Dr. Black was formerly in the Electrical Engineering Department, Queen Mary College, University of London, and is now with Associated Electrical Industries (Rugby), Ltd.

here m and n are integers. This general equation obviously ncludes Cassie's and Mayr's equations. Using the method of oclinals, the graphical form of eqn. (3) may be solved with a rcuit equation to obtain voltage/time and current/time curves. ishop showed how, given these two curves, the method of oclinals may be applied in reverse to obtain the equation of the rc.

As a first approximation, Bishop assumed that only the first erivatives of voltage and current enter the equation. He nalysed voltage/time and current/time oscillograms taken from ynamic carbon and copper arcs on this basis, but his results ere inconclusive.

The author assumes more general physical conditions in the rc column than either Cassie or Mayr did. A relationship is btained which describes the behaviour of an arc subjected to a onsiderable range of transient currents. It is then shown how arious conditions in the arc affect this dynamic arc equation.

(2) THEORETICAL DISCUSSION OF THE PROPERTIES OF THE ARC COLUMN UNDER TRANSIENT CONDITIONS

This Section is devoted to a consideration of the variables overning the behaviour of a transient arc. It is shown that, nder most conditions, the arc-column resistance is a function f the energy stored in the column. A method of calculating ne rate of heat loss from the arc is then described, so that the tored energy may be calculated from voltage/time and current/ ime oscillograms.

The number of electrons available to carry current in unit olume of the arc plasma is χN. Both χ and N are functions f the arc temperature, θ, at the point considered. Most of the urrent is carried by electrons, but ionic current may be included y assuming an effective mobility, μ, which is also a function of emperature. Hence the current density is $J = 2\chi Ne\mu E$, and

$$\sigma = J/E = 2\chi Ne\mu = f_1(\theta) \quad . \quad . \quad . \quad . \quad (4)$$

The arc temperature at any point is a function of the energy ensity q there, so that eqn. (4) may be rewritten

$$\sigma = f_2(q) \quad . \quad . \quad . \quad . \quad . \quad . \quad (5)$$

he arc conductance per unit length of the arc column, g, is btained by integrating this equation with respect to the distance from the arc axis:

$$g = 2\pi \int_0^\infty a f_2(q) da \quad . \quad . \quad . \quad . \quad . \quad (6)$$

he energy per unit length of arc may be written

$$w = 2\pi \int_0^\infty aqda \quad . \quad . \quad . \quad . \quad . \quad . \quad (7)$$

oth g and w depend upon the radial temperature distribution. n general, the temperature distribution depends on the way in vhich the power supplied to the arc has varied with time. Iowever, at times which are long compared with the thermal ime-constant of the arc, the temperature distribution has tabilized itself; it is then dependent only on the total arc energy. his means that, for a given value of w, the relationship between and a is determined. It follows from eqn. (6) that g is also ixed for a particular value of w. Hence, at times much longer han the thermal time-constant of the arc,

$$r = \frac{1}{g} = F(w) \quad . \quad . \quad . \quad . \quad . \quad (8)$$

For an arc of length l eqn. (8) becomes

$$R = F(W) \quad . \quad . \quad . \quad . \quad . \quad (9)$$

If the energy in the arc column is initially W_0, then

$$R = F\left[W_0 + \int_0^t (VI - P)dt\right] \quad . \quad . \quad . \quad (10)$$

The experimental determination of the form of the function of eqn. (10) is described in Section 3.

It is now necessary to obtain the power loss from the arc. For the above conditions, the temperature distribution in the arc column is a function of W, so that the power loss from the column is also a function of W, and hence

$$P = \phi(R) \quad . \quad . \quad . \quad . \quad . \quad . \quad (11)$$

The experimental determination of the relationship between the power loss and the arc resistance is described in Section 3.4.

(3) EXPERIMENTAL DETERMINATION OF THE PROPERTIES OF THE 9 MM CARBON ARC UNDER TRANSIENT CONDITIONS

The object of the experimental work of this Section is first to verify that the arc-column resistance of a transient arc is a definite function of the arc energy, and then to obtain the form of this relationship.

(3.1) Experimental Procedure

A steady d.c. arc was formed by drawing apart two identical electrodes in the circuit shown in Fig. 1. The current was

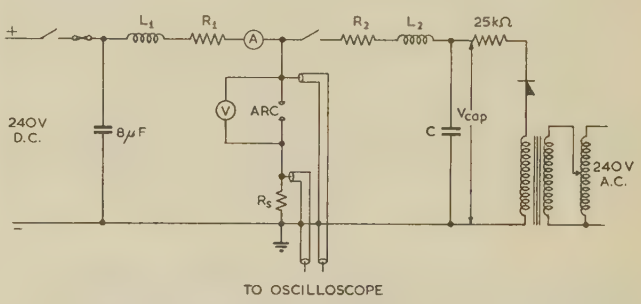

Fig. 1.—Test circuit.

controlled by the resistance R_1 and was stabilized by the inductance L_1. The arc length was adjusted to give the arc voltage and current of a particular point on the static characteristic. This static arc was then disturbed by discharging through it a capacitor, C. The magnitude and shape of the discharge current was controlled by the circuit parameters C, R_2, L_2 and V_{cap}.

For a certain initial arc current, I_0, and arc length, l, current pulses of varying magnitude, duration and shape were applied to the arc. The transient voltage across the arc and the arc current were recorded on two single-beam oscilloscopes having a common time-base. Carbon rods of 12 mm diameter were used in all tests on the carbon arc.

(3.2) Analysis of Experimental Results

Since the relationships derived in Section 2 apply to the arc column only, the electrode voltage must be subtracted from the measured transient arc voltage before analysing the results. Experimental values of the transient electrode voltage drop are given in Section 3.3.

In order to calculate changes of energy in the arc column, the power loss from the arc must be known. This is determined in Section 3.4 in terms of the arc-column resistance.

With this information, instantaneous values of R, and hence of P, may be evaluated from a pair of voltage/time and current/time oscillograms of a transient arc. This enables $VI - P$ to be computed as a function of time. The change in the arc-column energy may then be obtained by numerically calculating $\int_0^t (VI - P)dt$ in terms of t. The energy change is then plotted as a function of the arc resistance.

(3.3) Transient Electrode Voltage Drop

Little information has been published on the transient electrode voltage drop, and the author[8] has therefore measured this voltage under the same conditions as those used in studying the dynamic characteristics of the arc.

The transient electrode voltage was measured by injecting a current pulse into a very short arc and recording the resultant voltage. Fig. 2 gives the electrode voltage of both carbon and

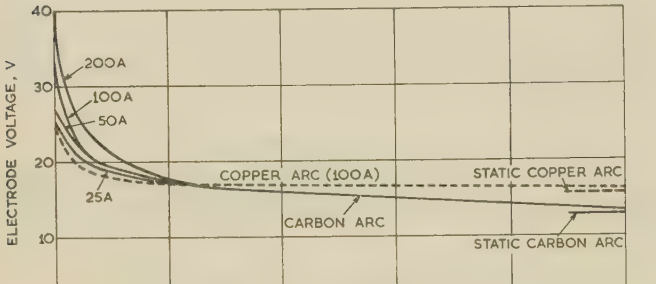

Fig. 2.—Electrode voltage when a current step is applied to carbon and copper arcs.
$I_0 = 6$ A
Figures refer to the instantaneous arc current.

copper after a current step has been applied to the arc. The voltage rises as soon as the current is applied, but drops to almost the static value within 200 μs. For carbon electrodes, the rise of electrode voltage is small compared with the transient voltage of the 9 mm arc and is affected little by the magnitude of the current. When considering current pulses of various shapes, a reasonable estimate of the electrode voltage may be obtained from Fig. 2 in terms of time and the instantaneous arc current.

(3.4) Measurement of Power Loss from the Arc Column

The method of calculating the power loss from the arc assumes that there is a relationship between the arc resistance and the arc energy but the form of this relationship cannot be established accurately until the power loss itself is known. Using an approximate value of power loss, determined from the static arc characteristic, the author[8] has shown that a definite relationship does, in fact, exist between W and R, as predicted in eqn. (9).

Differentiating eqn. (9) with respect to time,

$$\frac{dR}{dt} = \mathrm{F}'(W)\frac{dW}{dt}$$

Hence, when $dR/dt = 0$, dW/dt is also zero and no power is absorbed by the arc column. The power loss is therefore equal to the instantaneous power supplied to the arc column at times when dR/dt is zero.

The power loss has been measured at various values of ar resistance, using a variety of voltage/time and current/tim oscillograms. The curve of power loss against resistance plotted in Fig. 3 for a 9 mm carbon arc. Since there is only

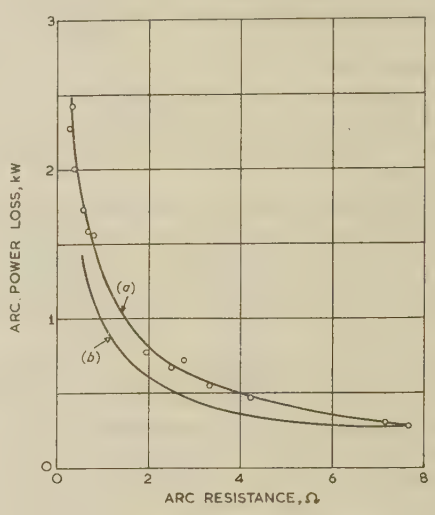

Fig. 3.—Power loss from carbon arc.
$I_0 = 6$ A
$l = 9$ mm
(*a*) Transient power loss.
(*b*) Power loss from static arc characteristic.

small scatter of the experimental points it follows that there is relationship between P and R of the form shown. The rate c heat loss determined from the static arc characteristic is als given in Fig. 3 as a comparison with the transient power loss When energy is added to the arc, the power loss is greater tha the static value until the electrode temperature has risen to it new value. The transient curve in Fig. 3 is valid for about th first millisecond (which covers the transient conditions cor sidered here), after which the power loss gradually falls to th static value.

(3.5) Experimental Determination of Relationship Between Ar Resistance and Arc Energy

Now that the rate of heat loss from the arc column can b estimated, the change of arc-column energy can be calculate for a corresponding change in the arc resistance. This ha been done for a wide range of voltage/time and current/tim oscillograms, taken on a 9 mm transient carbon arc which wa initially burning steadily at 6 A. The results are plotted i Fig. 4. In these tests, the initial rate of rise of current varie

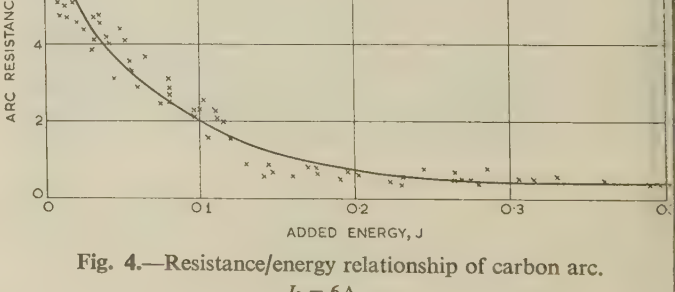

Fig. 4.—Resistance/energy relationship of carbon arc.
$I_0 = 6$ A
$l = 9$ mm

between 0·01 and 75 A/μs, the peak current was up to 136 A and the transient lasted between 3 μs and 1 ms. The transient voltage was occasionally as great as 500 V. The standard deviation of all the points about the mean curve of Fig. 4 is only 0·6 Ω, showing that there is a definite relationship between the arc-column resistance and the energy in the arc column, as was predicted in Section 2.

An exception occurs during the first three microseconds of a transient, when the current rises faster than about 100 A/μs. The arc resistance may then be as low as 50% of the value predicted from the R/W curve. The reason for this is that the temperature changes in the arc take place in a time comparable with the duration of the transients considered. This was foreseen in Section 2. Since the R/W curve is always obeyed 3 μs after the start of the transient, this is the time required for stabilization of the radial temperature distribution. This time is short compared with the duration of most transients considered here.

It is concluded that the energy-balance method of accounting for the transient characteristics of the arc is valid for times from 3 μs up to at least 1 ms after the start of the transient current, when the arc energy is raised above its static value.

(4) INVESTIGATION OF FURTHER FACTORS AFFECTING THE DYNAMIC ARC CHARACTERISTICS

(4.1) Effect of Variation of Arc Length

The power-loss/resistance and resistance/energy relationships have been investigated for carbon arcs of various lengths. The results are plotted in Figs. 5 and 6 in terms of unit length of arc column. In all cases the initial steady arc current was 6 A.

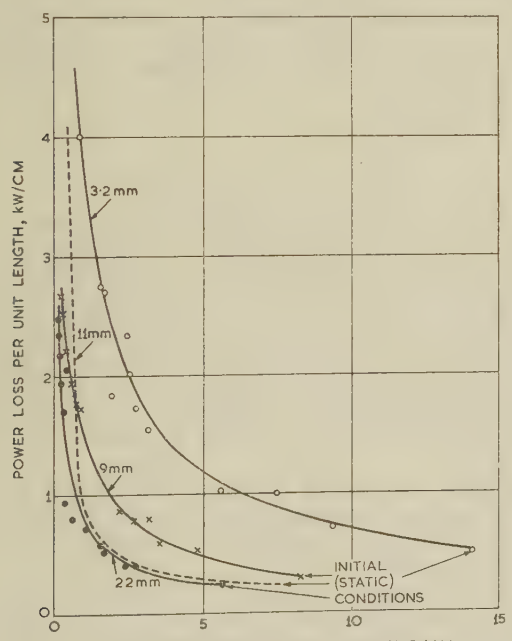

Fig. 5.—Power loss from arcs of various lengths with carbon and copper electrodes, in terms of unit length of column.
$I_0 = 6$ A
——— Carbon electrodes.
– – – Copper electrodes.

The power loss per unit length, p, is plotted in Fig. 5 and is greater for short arcs owing to the proximity of the electrodes. As the arc length is increased, p is affected progressively less by the electrodes.

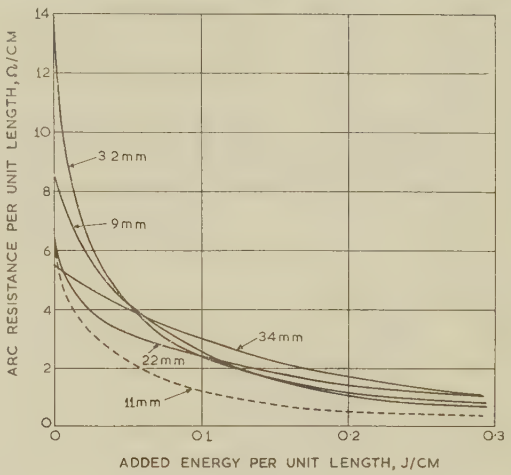

Fig. 6.—Resistance/energy curves for arcs of various lengths with carbon and copper electrodes, in terms of unit length of column.
$I_0 = 6$ A
——— Carbon electrodes.
– – – Copper electrodes.

In a static arc the resistance per unit length is greater for short arcs owing to the predominance of the higher voltage gradient near the electrodes. As the arc is lengthened, the static resistance per unit length approaches a limiting value. In spite of these initially different resistivities, Fig. 6 shows that the r/w curves for arcs of different lengths approach each other as the arc-column energy is increased. This follows from the fact that a greater proportion of the energy supplied to the arc is absorbed by the regions of high resistivity near the electrodes than by an equal length in the middle of the column. In consequence of this, the resistance per unit length becomes more uniform throughout the arc and r is then less dependent upon the arc length.

(4.2) Effect of Initial Arc Current in a 9 mm Carbon Arc

Fig. 7 gives the power-loss/resistance curves plotted for a 9 mm carbon arc with three initial arc currents, together with the static power-loss/resistance curve of the arc column. The power loss is very dependent upon the initial arc current, owing to the temperature of the electrodes and the immediate surroundings not following the change of arc temperature quickly enough. However, as the arc resistance falls, the change of arc temperature is so great that the initial electrode temperature has progressively less effect upon the rate of heat loss.

Eqn. 10 predicts that the arc resistance depends upon the sum of the initial energy, W_0, and the added energy during the transient. Curves of resistance against added energy for arcs having different initial resistances may therefore be superimposed, as shown in Fig. 8. The curves do not differ greatly, indicating that the resistance/energy relationship is valid for static arcs as well as for those under transient conditions.

(4.3) Effect of Electrode Material as Shown by the Dynamic Characteristics of a Copper Arc

Tests have been made to investigate the transient characteristics of arcs between 1 in-diameter copper electrodes. An initial static arc current of 6 A was used, with an electrode spacing of 11 mm.

Measurements show that the electrode voltage drop of copper electrodes is affected very little by the magnitude of the current. For clean copper electrodes, the electrode voltage is the same

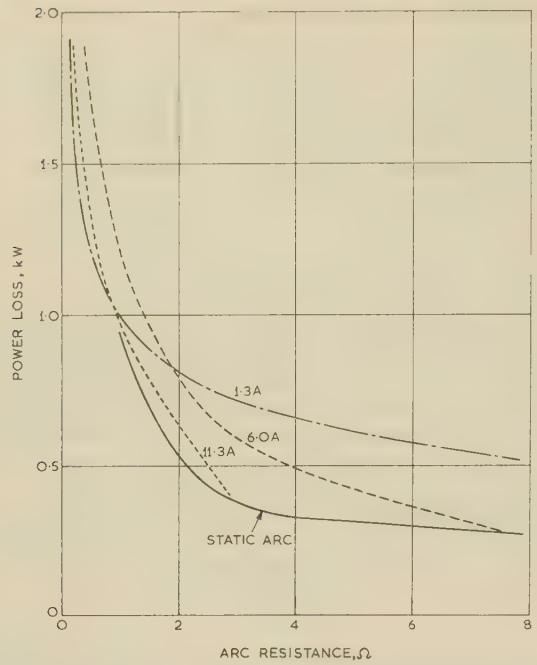

Fig. 7.—Power loss from carbon arc with various initial arc currents.

$l = 9$ mm
——— Static arc
—·—· $I_0 = 1{\cdot}3$ A
— — $I_0 = 6{\cdot}0$ A
- - - - - $I_0 = 11{\cdot}3$ A

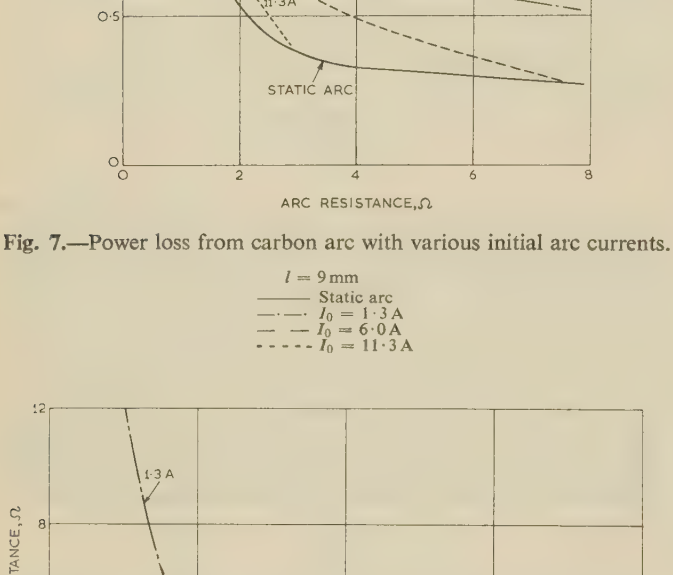

Fig. 8.—Resistance/energy curves of carbon arc with various initial arc currents.

$l = 9$ mm
—·—·—·— $I_0 = 1{\cdot}3$ A
— — — — $I_0 = 6{\cdot}0$ A
- - - - - - - - - $I_0 = 11{\cdot}3$ A

for static and transient conditions, but when the electrodes are well oxidized the transient electrode voltage increases slightly. This variation is shown in Fig. 2 and is smaller than that of the carbon arc.

The characteristics of a copper arc are given in terms of a unit length arc and are plotted in Figs. 5 and 6. The power loss is approximately the same as that of the equivalent carbon arc except at low arc resistance, where the loss is greater owing to the higher thermal conductivity of the electrodes. The r/w curve of the copper arc is of the same form as that for the carbon arc, but the copper arc requires less energy to bring it to a low resistivity.

(5) CONCLUSIONS

The paper shows, both theoretically and by experiment, tha under transient conditions the instantaneous arc-column resi tance is a function of the instantaneous energy stored in the ar This relationship has been obtained experimentally for carbo arcs having lengths between 1 and 34 mm as well as for an 11 m copper arc. It is not valid during the first three microsecon of a current pulse owing to a lack of thermal equilibrium in th arc column. Apart from this, the relationship holds for tim up to at least 1 ms.

Because of the considerable heat flow along the electrode the power loss from the arc is dependent upon the electro material, temperature and spacing. The effect of these par meters has been investigated experimentally.

Although the transient electrode voltage drop is usual small compared with the voltage across the arc column, th separation of arc column and electrode effects has resulted i a more accurate analysis of the experimental results.

The arc models proposed by Cassie and Mayr each imply unique resistance/energy relationship, although their results a not expressed in terms of this quantity. Cassie's resi tance/energy curve is hyperbolic, while that due to Mayr is negative exponential curve. These relationships approxima to the author's experimental resistance/energy curve only ov small ranges of energy. A similar result was obtained b Browne and Strom, who showed each equation to be va during part of a half cycle of a power-frequency arc. As oppos to Browne and Strom, the comparison of the author's resul with Cassie's and Mayr's equations is not confined to any or test but considers results taken over a wide range of voltag current and time.

The present investigation also shows that a differential a equation (as proposed by Bishop) cannot describe conditio in the arc, since dynamic arc characteristics depend on th energy in the arc rather than on instantaneous values of voltag and current derivatives.

(6) ACKNOWLEDGMENTS

The author expresses his sincere thanks to Professor W. . John, Professor Emeritus at Queen Mary College, Universit of London, under whose guidance this work was carried ou for his help and interest throughout. He also thanks Dr. A. E Guile of Queen Mary College for many useful discussion Dr. C. E. R. Bruce of the Electrical Research Association, wh made many valuable suggestions, and Dr. D. O. Bishop, fo merly Head of the Electrical Engineering Department, Rege Street Polytechnic, whose study of the arc led up to the prese work.

The author also wishes to thank the Central Electricit Authority for their financial assistance for the year 1952–53 an the Governors of Queen Mary College for grants for the yea 1953–54 and 1954–55.

He also thanks the Governors of Queen Mary College an the Directors of Associated Electrical Industries (Rugby), Ltd. for permission to publish the paper and the firm for assistanc in its presentation.

(7) REFERENCES

(1) Norberg, S.: 'Arc Formation and Breaking Characteristic of Switches', *Journal of Allmanna Svenska Elektriska A.B* 1927, **4**, p. 28.

(2) Cassie, A. M.: 'Arc Rupture and Circuit Severity—A Ne Theory' (E.R.A. Report Ref. G/XT 79; 1939).

(3) MAYR, O.: 'Beitrage zur Theorie des Statischen und des Dynamischen Lichtbogens', *Archiv für Elektrotechnik*, 1943, **37**, p. 588.

(4) BROWNE, T. E.: 'A Study of A.C. Arc Behaviour near Current Zero by Means of Mathematical Models', *Transactions of the American I.E.E.*, 1948, **67**, p. 141.

(5) BROWNE, T. E., and STROM, A. P.: 'A Study of Conduction Phenomena near Current Zero for an A.C. Arc Adjacent to Refractory Surfaces', *ibid.*, 1951, **70**, p. 398.

(6) YOON, K. H., and SPINDLE, H. E.: 'A Study of the Dynamic Response of Arcs in Various Gases', *ibid.*, 1958, **77**, Part III, p. 1634.

(7) BISHOP, D. O.: 'A Method of Determining the Dynamic Characteristics of Electric Arcs', *Proceedings I.E.E.*, Monograph No. 72 M, August, 1953 (**101**, Part IV, p. 18).

(8) BLACK, I. A.: 'Factors Affecting the Behaviour of an Electric Arc Under Transient Conditions', Ph.D. Thesis, University of London, 1956.

621.384.62

The Institution of Electrical Engineers
Monograph No. 441 M
Apr. 196

AN EXPERIMENTAL PROTON LINEAR ACCELERATOR USING A HELIX STRUCTURE

By D. P. R. PETRIE, M.Sc., R. BAILEY, B.Sc., Associate Member, D. G. KEITH-WALKER, B.Sc.(Eng.), Associate Member, H. LONGLEY, B.Sc., and D. R. CHICK, D.Sc., Member.

(*The paper was first received 28th June*, 1960, *and in revised form 5th January*, 1961. *It was published as an* INSTITUTION MONOGRAPH *in April*, 1961.)

SUMMARY

The paper describes the design and construction of a short experimental length of linear accelerator using a helical waveguide as the slow-wave structure to accelerate protons from 2·5 MeV to 4 MeV.

Factors influencing the design of the helix structure are considered; these include the maximum voltage between turns which can be tolerated and the available power and frequency of the r.f. supply. The theory of a helix supported on a dielectric tube is given, and from the results the variations of pitch are determined to give the required acceleration.

The accelerator was driven by a push-pull triode oscillator operating under 6μs pulsed conditions at 300 Mc/s with a peak output of 600 kW. The oscillator and r.f. components are described in detail.

The beam-energy spectrum at the output of the accelerator was measured for a variety of working conditions, changes being made in beam-energy input and power and frequency of the r.f. supply. The results obtained confirm the theory and show that with certain restrictions a helix slow-wave structure of the type described provides a convenient me hod of proton acceleration.

LIST OF SYMBOLS

a = Helix radius.
b = Helix shield radius.
E = Electric field.
E_0 = E_z field on axis.
K = Helix coupling factor.
l_c = Critical coupling length.
m_e = Electron mass.
m_p = Proton mass.
P = Power flux.
P_L = Power loss per unit length.
P_0 = Power flux along a free-space helix.
r = Radial co-ordinate.
T = Kinetic energy.
u = Particle velocity.
v = Wave phase velocity.
v_g = Wave group velocity.
V_0 = Beam voltage.
z = Axial co-ordinate.
$Z_0 = \sqrt{(\mu/\epsilon)}$ = Wave impedance of free space.
Z_n = Characteristic impedance of relevant helix.
α = Axial attenuation coefficient.
β = Axial phase-change coefficient.
γ = Radial distribution coefficient.
ϵ = Permittivity.
η_B = Beam collection efficiency.
λ = Wavelength.
μ = Permeability.
$\xi = v/c$ = Relative phase velocity.
ρ = Reflection coefficient.
ϕ = Helix pitch angle.
ψ = Particle phase angle with respect to accelerating field.
ψ_0 = Phase stable angle.
$\Delta\psi$ = Acceptance angle.

Correspondence on Monographs is invited for consideration with a view to publication.
Messrs. Petrie, Keith-Walker and Chick are with Associated Electrical Industries, Ltd.
Mr. Bailey was formerly with Associated Electrical Industries, Ltd., and is now at the U.K.A.E.A. Atomic Energy Research Establishment.
Mr. Longley was formerly with Associated Electrical Industries, Ltd., and is now with the Hawker Siddeley Nuclear Power Company.

(1) INTRODUCTION

The use of a helix to provide the slow-wave structure necessary for the acceleration of protons was first suggested by Walkinshaw and Wyllie[1] in 1948. This was followed in 1949 by a more detailed appraisal of a practical helix accelerator by Chick and Petrie;[2] this report provided the basis for the work described herein. In 1951 Johnsen and Dahl[3] published an article putting forward the idea of a helix as a linear accelerator, and later Johnsen[4] made an appraisal of the losses of a helix as compared with an Alvarez type accelerator, presumably as part of a design study in a linear accelerator for C.E.R.N. At about the same time, Servranckx[5] started on the design of an accelerator using a helical waveguide.

Chick and Petrie in their paper covered the design of an accelerator for 4–20 MeV, but they recommended that a short length be constructed initially for test purposes. It was decided to carry out a pilot experiment using a 1 m length of accelerator with an injection energy of 2·5 MeV and a power flux of 500 kW. These rather low values were chosen so that a comparatively large and reliable proton current could be obtained from the existing Van de Graaff accelerator, and to reduce the time required to develop the r.f. power supply. The objects of the experiment were to check the theoretical basis of the helix design, to develop practical methods of construction of the helix and associated equipment and finally to assess the merits of the helix against other accelerators in the range 5–30 MeV. The experimental helix accelerator was completed[6] and tested in 1957.

In addition to an experimental helix proton accelerator, an electron model was made using the same helix design. To obtain the same velocity and acceleration the 2·5 MeV input beam energy and the 500 kW power flux were scaled by factors m_e/m_p and $(m_e/m_p)^2$, respectively. The input electron beam energy required was then 1·36 keV, and the r.f. power required was 150 mW. A standard cathode-ray-tube gun assembly was used for the injected beam, and a signal generator of high output power was used as a source of r.f. power.

Under these conditions the particle motions in the electron model should be identical with those in the proton accelerator. Results obtained from the model tended to confirm the theoretical predictions for particle acceleration.

(2) HELIX DESIGN CONSIDERATIONS

(2.1) Optimum Dimensions

The choice of the accelerator parameters—helix radius, r.f. power and frequency—depends upon a number of factors. These include particle velocity and the ratio of the square of the

xial accelerating field to power flow and power losses. The ecessary relations were obtained from the theory of Pierce,[7] who nalysed the field distribution of an idealized helical sheath, i.e. metal cylinder conducting only in the helical direction.

The average particle velocity over the accelerator length can e taken as $0{\cdot}085c$. Under this condition the theory shows that he quantity $E_0^2\lambda^{1/2}/P_i$ is a maximum when $a/\lambda = 0{\cdot}01$. The heory also shows [see eqn. (7)] that $E_0^2 \propto 1/\lambda a$.

For a given accelerating field, therefore, it is advantageous, vhether designing for minimum power loss or minimum power low, to make both a and λ as small as possible, with the condi- ion $a/\lambda = 0{\cdot}01$. From considerations of helix construction nd availability of high powers at high frequencies it was decided o make the helix radius, a, equal to 1 cm and the power fre- uency, f, 300 Mc/s. With an input beam energy of 2·5 MeV ixing the initial relative phase velocity at 0·072 5, the pitch of a ree-space helix would be 0·35 cm.

It was felt that a trial length of accelerator should be con- ervatively rated, and one of the main considerations in the esign would be the power flux which could be carried by the elix without voltage breakdown between turns. It was decided hat the maximum field, which will occur at the surface of the vire, should not exceed 50 kV/cm. For 16 s.w.g. wire—a con- enient size for a partially self-supporting helix—this field epresents 8·75 kV between turns. Hence the axial field averaged ver a complete pitch is 25 kV/cm. This can be taken as the xial field E_z at the surface $r = a$ of a helical sheath, and hence he axial field $\hat{E}_0$ on the axis can be obtained from the theoretical elation

$$\hat{E}_0 = \frac{(E_z)_{r=a}}{I_0(\gamma a)}$$

The values $(E_z)_{r=a} = 25$ kV/cm and $\gamma a = 0{\cdot}862$ yield $\hat{E}_0 =$ 21 kV/cm.

The relation between E_0 and the power flux P is given in eqn. (7), and is plotted in Fig. 1 for $a/\lambda = 0{\cdot}01$. For $v/c =$ 0·072 5 the curve gives $E_0\lambda/\sqrt{P} = 2750$, whence the power lux, P, is 580 kW.

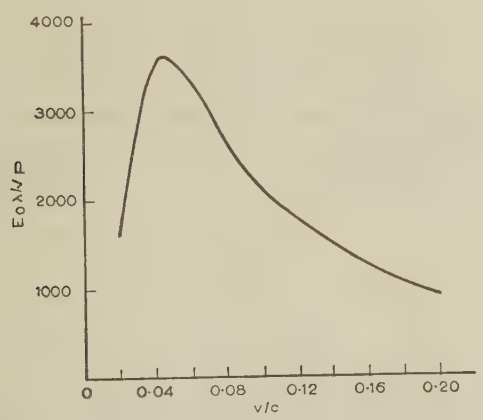

Fig. 1.—Plot of $E_0\lambda/\sqrt{P}$ against v/c for $a/\lambda = 0{\cdot}01$.
[Reproduced from Walkinshaw's results.]

It was decided to restrict the power flux to a nominal 500 kW. The phase-stable position was fixed at the arbitrary angle of 30° as being a suitable working value, though with all other parameters fixed this may be changed with suitable change in power flux to provide variations in acceptance angle.

The gradation in pitch along the helix was calculated, for the given values of power flux and phase-stable position, by the method described in Section 3.1.

(2.2) Feedback Considerations

For a given axial accelerating field the r.f. power input required by an accelerator may be reduced by the application of positive feedback. This can conveniently be achieved either by the use of an external coaxial system between the r.f. input and output or by resonating the helix.

The disadvantages of feedback are that the build-up time of the fields on the helix is increased, the device becomes more frequency sensitive, and, in the case of a resonated system, the peak field between the helix turns is increased at the antinodes. In view of the disadvantages, and as the r.f. power required for a non-feedback system was fairly easily obtainable, it was decided that, for the trial length of accelerator, feedback would not be attempted.

(2.3) Focusing Considerations

In the helix structure, as in other r.f. accelerating structures, the accelerated particles in the vicinity of the phase-stable position are in a defocusing field. The effect of this field can be determined approximately as follows:

Considering only the radial forces acting on the particle, the radial energy equation is

$$\tfrac{1}{2}m\left(\frac{dr}{dt}\right)^2 = e\int_{r_1}^{r} E_r dr \quad . \quad . \quad . \quad . \quad . \quad (1)$$

where

$$E_r = jE_0\frac{\beta}{\gamma}I_1(\gamma r)\varepsilon^{j(\omega t-\beta z)} \quad . \quad . \quad . \quad . \quad (2)$$

For a particle remaining in the phase-stable position ψ_0, and $\gamma r \ll 1$, as it will be, eqn. (2) simplifies to

$$E_r = \tfrac{1}{2}E_0\beta r \sin\psi_0 \quad . \quad . \quad . \quad . \quad . \quad . \quad (3)$$

Substituting this expression for E_r in eqn. (1), and replacing dt by dz/u and using $\frac{1}{2}mu^2 = eV_0$, we obtain the differential equation for the path of a particle entering parallel to the axis:

$$\left(\frac{dr}{dz}\right)^2 = \frac{1}{4}\frac{E_0\beta\sin\psi_0}{V_0}(r^2 - r_1^2)$$

The integration of this equation over the helix length l yields

$$\frac{r_2}{r_1} = \cosh\tfrac{1}{2}l\sqrt{\frac{E_0\beta\sin\psi_0}{V_0}} \quad . \quad . \quad . \quad . \quad (4)$$

where r_1 and r_2 are the initial and final radial positions.

The values of β and E_0 change along the helix, but a good approximation may be obtained by taking the following average values:

$$\beta = 78{\cdot}5\,\mathrm{m}^{-1}.$$
$$E_0 = 2{\cdot}10^6\,\mathrm{V/m}.$$
$$V_0 = 2{\cdot}5 \times 10^6\,\mathrm{V}.$$
$$\sin\psi_0 = 0{\cdot}5.$$
$$l = 1\,\mathrm{m}.$$

These yield $r_2/r_1 = 8{\cdot}25$, implying that for a 1 m length of helix very few particles will be lost to the walls if the input beam is constrained to within a 2 mm diameter, though the output beam will be diverging. This analysis, though approximate, represents the worst case, i.e. for particles entering in the phase stable position. Particles entering or oscillating into a negative phase angle will experience a focusing field which will tend to compensate for the defocusing effect when they are at a positive phase angle. As the losses due to defocusing over 1 m appear to be small, it was decided not to incorporate any form of focusing.

(2.4) Helix Construction and Support

The helix structure (Fig. 2) consists of a 0·060 in-diameter solid copper wire wound on a glass tube, the wire diameter being chosen to give minimum peak field between the turns. The choice of support for the helix was influenced largely by the necessity to insulate the wire electrically, and at the same time to ensure adequate cooling of the structure; heat dissipation could approach 500 W under certain circumstances. The use of a glass tube inside the helix enables the structure to be operated

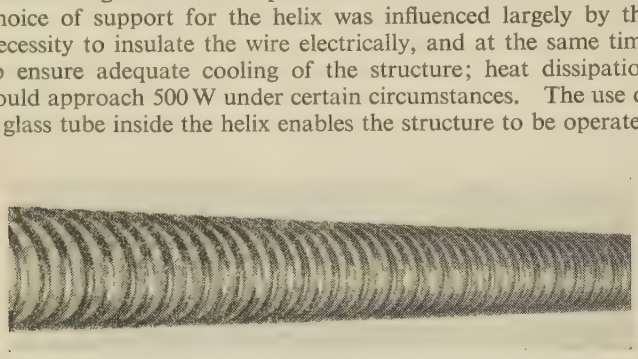

Fig. 2.—Helix accelerator structure.

in a pressurized gas, which increases the breakdown potential between the turns and convects heat away from the wire. It also has other advantages. If the wire is fixed to the glass tube at frequent intervals a very rigid structure is obtained and the helix may be wound to close tolerances; the construction is comparatively cheap and versatile, and, if necessary, several helices may be made up either as replacements or as test structures with different parameters. A further unexpected advantage is that in the 2·5–4 MeV region the series impedance is slightly increased.

The disadvantages of this type of support are that the dielectric losses are rather higher than with other types, and there is a possibility of wall charges being set up on the inner wall of the glass tube when a proton beam is present. This latter effect could be a very serious limitation, but tests carried out on a plain glass tube, 1 m long, with a 2·5 MeV proton beam injected through it showed no signs of wall charging.

To determine accurately the helix pitch at all points on the structure it was necessary to ensure that the wire was held firmly by the supporting tube. This was achieved by soldering the helix wire to spots of silver, previously baked on to the surface of the glass tube. The accelerating part of the helix was made 1·05 m long, but at each end a constant pitch section was wound, 0·11 m in length. The pitch of these sections corresponded to the pitch of the accelerating section adjoining them. These end-sections were for coupling power in and out, and are described in detail in Section 4.3.1.

Metal tubes were attached to the ends of the glass supporting tube to facilitate connection to the proton beam tube and vacuum pumping system, the connection between glass and metal being made with Araldite, which was found quite satisfactory as a pressure/vacuum seal even at temperatures up to 100° C.

By this method of helix construction the maximum turn-to-turn error in spacing was kept below 0·3 mm and the maximum cumulative error below 0·5 mm. Thus over the length of the helix a phase-change error of less than 3° was expected.

(3) THE HELIX PARAMETERS

(3.1) Determination of the Pitch Angle

The pitch and its variation along the length is the most important parameter determining the phase velocity along the helix, and therefore has to be calculated as accurately as possible to ensure that the particles will keep in step with the wave throughout the length. The pitch determination depends on two calculations; first, the differential equation of motion of particle in the phase-stable position has to be solved, in orde to obtain the particle velocity throughout the helix; secondly the pitch has to be determined to make the phase velocity equa to the particle velocity at every point. Both calculations deman a knowledge of the complete field distribution inside and outsid the helix, in terms of helix parameters. The field distributio provides the power flux P, and hence the accelerating field E_0 which enters the differential equation of motion; it also provide the relation between pitch and phase velocity.

Pierce[7] has derived the field distribution for an idealize sheath helix in free space. For the present work his analysi was extended to take account of the dielectric tube within th helix. No attempt was made to allow for the finite wir diameter.

The analysis consisted in solving Maxwell's equations for th boundary conditions shown in Fig. 3, where medium 2 is th dielectrically-filled region, and a_2 is the helix radius. As th

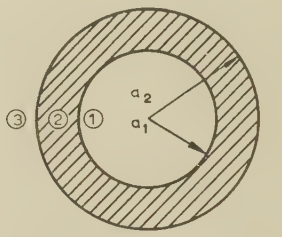

Fig. 3.—Cross-section of helix and supporting tube.

solution is long and tedious, only the final expressions used wi be quoted here. The approximation was made that $\gamma_1 = \gamma_2 = \gamma$ which is true within 1% for a medium 2 of permittivity 5; γ i the radial propagation coefficient, related to the axial propagatio coefficient β by

$$\gamma^2 = \beta^2 - \frac{\omega^2}{c^2} = \frac{\omega^2}{c^2}\,\frac{1-\xi^2}{\xi^2} \quad . \quad . \quad . \quad . \quad (5$$

It was further assumed for power-flux calculations that th wall thickness of the glass tube was small, by putting $a_1 = a_2(1-\delta$ and expanding all Bessel functions as far as first-order terms in δ This approximation was not made in calculating the pitch angle

The expression obtained for the power flux in terms of peal accelerating field was

$$P = P_0 + \frac{\delta \hat{E}_0^2 \pi \beta \omega \epsilon_1 a_2^3 (1-\epsilon_1/\epsilon_2) I_0^2}{2\gamma} \left[\left(\frac{K_0}{K_1} - \frac{I_0}{I_1}\right)\left(\frac{\epsilon_2}{\epsilon_1} - \frac{I_1^2}{I_0^2} - \frac{2I_1K_1}{I_0K_0}\right) - \frac{2I_1}{I_0}\left(1 - \frac{K_1^2}{K_0^2}\right) + \frac{2}{\gamma a_2}\left(\frac{\epsilon_2}{\epsilon_1} - \frac{2I_1^2}{I_0^2} - \frac{4I_1K_1}{I_0K_0}\right)\right] \quad . \quad (6$$

where P_0 represents the expression obtained by Pierce in the absence of the dielectric:

$$P_0 = \frac{\hat{E}_0^2}{Z_0}\,\frac{\lambda a_2}{2}\,\frac{\xi^2}{(1-\xi^2)^{3/2}}\,\frac{I_0}{K_0}\left(\frac{I_1}{I_0} - \frac{I_0}{I_1} + \frac{K_0}{K_1} - \frac{K_1}{K_0} + \frac{4}{\gamma a_2}\right) \quad . \quad . \quad . \quad . \quad (7$$

The argument of the Bessel functions I_0, I_1, K_0 and K_1 is γa_2 throughout.

The term in δ in eqn. (6) is numerically negative, and amount to 2·83% of P at the beginning of the helix, and 2·04% at the end. For ease of calculation, therefore, P_0 was calculated from eqn. (7), and P was adjusted to be 2·43% lower than P_0. This

nakes P correct to within 0·4% at any point along the helix, nd hence E_0 correct to within 0·2%, for a given input power nd attenuation.

If P' is the input power and α the attenuation coefficient, the ower flux at any point z is

$$P = P' \exp\left(-2\int_0^z \alpha dz\right) \quad . \quad . \quad . \quad . \quad (8)$$

nd hence, with the approximation just mentioned,

$$P_0 = 1{\cdot}0243\ P' \exp\left(-2\int_0^z \alpha dz\right) \quad . \quad . \quad . \quad (9)$$

The values of α used in the computation were obtained from neasurements of attenuation of uniformly wound helices of arious pitch. Eqns. (7) and (9) determine the field E_0 in terms f the function $\xi(z)$, the input power, and the known constants f the helix.

The phase velocity is to be the same as the velocity of a article at the phase-stable position, throughout the length of he helix, and can therefore be determined, as a function of z, rom the particle dynamics. The energy equation for a phase-table particle is

$$mc^2\left[\frac{1}{(1-\xi^2)^{1/2}} - \frac{1}{(1-\xi_0^2)^{1/2}}\right] = e\int_0^z E_0 dz$$

where $E_0 = \hat{E}_0 \cos\psi_0$ is the axial field at the phase-stable osition. Therefore

$$\frac{d\xi}{dz} = \frac{e\cos\psi_0}{mc^2}\,\frac{(1-\xi^2)^{3/2}}{\xi}\hat{E}_0$$

ntroducing the expression for $\hat{E}_0$ obtained from eqns. (7) and (9), we obtain the differential equation for $\xi(z)$:

$$\frac{d\xi}{dz} = \frac{2e\cos\psi_0}{mc^2}\left(\frac{1{\cdot}0243P'Z_0}{\lambda a_2}\right)^{1/2}\frac{(1-\xi^2)^{9/4}}{\xi^2}B\exp\left(-\int_0^z \alpha dz\right)$$

. . . . . (10)

where B, introduced for brevity, is defined by

$$\frac{1}{B^2} = \frac{I_0}{K_0}\left(\frac{I_1}{I_0} - \frac{I_0}{I_1} + \frac{K_0}{K_1} - \frac{K_1}{K_0} + \frac{4}{\gamma a_2}\right) \quad . \quad . \quad (11)$$

Eqn. (10) can be integrated by conventional numerical step-by-tep methods. As ξ is small compared with unity, most of the ariation on the right-hand side is due to $1/\xi^2$; it is therefore an dvantage to take ξ^3 as the dependent variable:

$$\frac{d(\xi^3)}{dz} = \frac{6e\cos\psi_0}{mc^2}\left(\frac{1{\cdot}0243P'Z_0}{\lambda a_2}\right)^{1/2} B(1-\xi^2)^{9/4}\exp\left(-\int_0^z \alpha dz\right)$$

. . . . . (12)

The right-hand side now changes slowly with z, and the inte-ration can be carried out with relatively few large steps in z.

Finally, the pitch angle ϕ, and hence the pitch itself, was valuated as a function of z from the following expression btained from the field analysis:

$$\tan^2\phi = \tan^2\phi'\left\{1 + \left(\frac{\epsilon_2}{\epsilon_1} - 1\right)\frac{K_0(\gamma a_2)}{I_0(\gamma a_2)}\left[\gamma a_2 I_1(\gamma a_2)I_0(\gamma a_2) - \frac{\gamma a_1 I_1(\gamma a_1)I_0(\gamma a_1)}{1 + \left(1 - \frac{\epsilon_1}{\epsilon_2}\right)\gamma a_1 \frac{I_1(\gamma a_1)}{I_0(\gamma a_2)}\left[I_0(\gamma a_1)K_0(\gamma a_2) - I_0(\gamma a_2)K_0(\gamma a_1)\right]}\right]\right\}$$

. . . . . (13)

where $\tan^2\phi'$ represents Pierce's expression for a sheath helix without dielectric:

$$\tan^2\phi' = \frac{\omega^2}{\gamma^2 c^2}\,\frac{I_1(\gamma a_2)K_1(\gamma a_2)}{I_0(\gamma a_2)K_0(\gamma a_2)} \quad . \quad . \quad . \quad (14)$$

(3.2) Acceptance Angle and Beam-Collection Efficiency

The acceptance angle can be calculated to a high degree of accuracy for a short accelerator by ignoring phase damping effects.

Fig. 4 shows the field pattern, where the acceptance angle $\Delta\psi = \psi_2 - \psi_1$ and $\psi_1 = -\psi_0$.

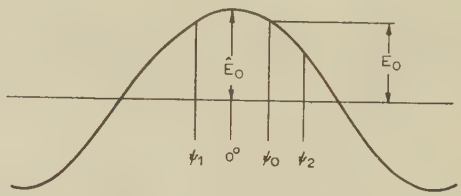

Fig. 4.—Axial field pattern.

Assuming undamped oscillatory motion of the particle about ψ_0, then ψ_2 can be determined by equating the incremental potential energy at ψ_1 and ψ_2:

$$\hat{E}_0\int_{\psi_1}^{\psi_0}(\cos\psi - \cos\psi_0)d\psi = \hat{E}_0\int_{\psi_2}^{\psi_0}(\cos\psi - \cos\psi_0)d\psi \quad . \quad (15)$$

Hence $$\sin\psi_2 = (\psi_0 + \psi_2)\cos\psi_0 - \sin\psi_0 \quad . \quad . \quad (16)$$

from which $\Delta\psi$ may be evaluated as a function of ψ_0.

The beam-collection efficiency is defined as the ratio

$$\eta_B = \frac{\text{Accelerated beam current}}{\text{Input beam current}}$$

Excluding defocusing effects and other beam losses this ratio becomes

$$\eta_B = \frac{\Delta\psi}{2\pi}$$

It is convenient to know how the phase-stable angle, ψ_0, and beam collection efficiency, η_B, change with power input. These are shown plotted in Fig. 5, the value of ψ_0 as a function of power flux P being evaluated from eqn. (7).

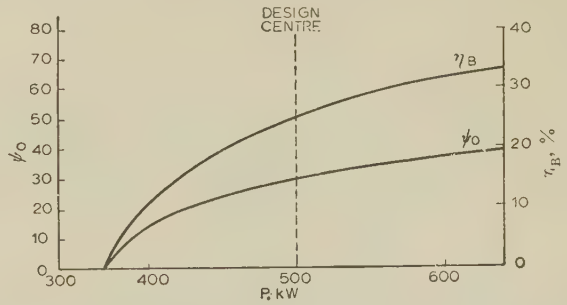

Fig. 5.—Plot of phase-stable angle ψ_0 and beam-collection efficiency η_B against r.f. power flux, P.

(3.3) Energy Spread of Proton Beam

There will be an energy spread in the accelerated beam due to particles which have not entered the structure at the phase-stable position. The limit of possible energy spread can be

estimated by considering a particle which initially entered the helix at the limit of the acceptance angle, say ψ_1, and has reached the phase-stable angle ψ_0 at the exit. Such a particle gains kinetic energy ΔT relative to the wave, given by:

$$\Delta T = \frac{\lambda_g e\hat{E}_0}{2\pi}\int_{\psi_1}^{\psi_0}(\cos\psi - \cos\psi_0)d\psi \quad . \quad . \quad . \quad (17)$$

(see Section 3.2).

The corresponding gain in kinetic energy δT, relative to the laboratory frame of reference, is given by

$$\frac{\delta T}{T_0} = \frac{\lambda_g eE_0}{\pi T_0}(\tan\psi_0 - \psi_0) + 2\left[\frac{\lambda_g eE_0}{\pi T_0}(\tan\psi_0 - \psi_0)\right]^{1/2} \quad . \quad (18)$$

This represents the relative energy spread on one side of the mean output energy assuming negligible phase damping; the total energy spread will be twice this. The resulting energy spread on taking average values $E_0 = 1{\cdot}5$ MV/m, $T_0 = 4$ MeV,

$$\lambda_g = 0{\cdot}085\,\text{m and } \psi_0 = 30° \text{ is } \pm 4{\cdot}75\%.$$

(4) ACCELERATOR AND ASSOCIATED EQUIPMENT

(4.1) Accelerator

A diagram of the accelerator is shown in Fig. 6. The whole of the accelerating structure was enclosed by a steel pressure casing whose diameter was large compared with the helix to ensure that it did not influence the phase velocity and loss. Pure nitrogen was maintained at 150 lb/in^2 in the casing to inhibit voltage breakdown and to assist in cooling. Several ports were provided in the pressure casing to allow for monitoring, r.f. power transfer and inspection.

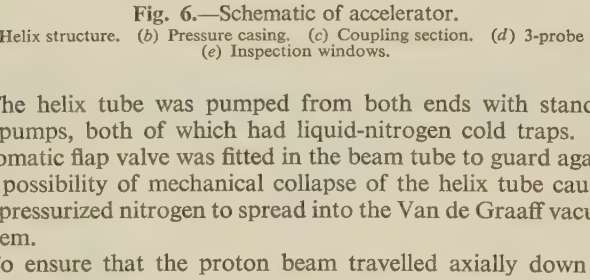

Fig. 6.—Schematic of accelerator.
(*a*) Helix structure. (*b*) Pressure casing. (*c*) Coupling section. (*d*) 3-probe unit. (*e*) Inspection windows.

The helix tube was pumped from both ends with standard oil pumps, both of which had liquid-nitrogen cold traps. An automatic flap valve was fitted in the beam tube to guard against the possibility of mechanical collapse of the helix tube causing the pressurized nitrogen to spread into the Van de Graaff vacuum system.

To ensure that the proton beam travelled axially down the helix tube the helix assembly had to be accurately aligned. This was achieved by fitting irises at either end of the tube and lining up initially with a light beam. After alignment had been achieved the input iris was enlarged to a 4 mm-diameter hole, while the output iris was removed entirely.

(4.2) R.F. Oscillator

The frequency and power-stability requirements of an oscillator can be predicted by considering their effect on the change of phase angle of the particle and change of acceptance angle in the accelerator. The two expressions for frequency and power stability are given by

$$\frac{\delta f}{f_0} = -\frac{\delta\psi}{2\pi f_0(l-z)\left(\frac{1}{v_g} - \frac{1}{u_z}\right)} \quad . \quad . \quad . \quad (19)$$

and

$$\frac{\delta P}{P} = \frac{2}{3}\delta(\Delta\psi)\tan\psi_0 \quad . \quad . \quad . \quad . \quad . \quad (20$$

If a maximum change of 5° is allowable in the phase ang or acceptance angle, a frequency stability of about 0·2% and power stability of about 3% will be required. These requir ments are obtainable with comparatively conventional oscillat design.

The oscillator consisted of two CV 2163 triodes operated i push pull with two separate 3λ/4 coaxial cavities in the gri cathode circuit and a common λ/4 twin line screened anod circuit. Feedback was achieved by coaxial-line couplin between the anode and separate cathode cavities. The outpu of 600 kW maximum at 300 Mc/s when modulated with a 6 μ pulse was coupled out by a single coaxial line.

(4.3) R.F. Components

(4.3.1) Coupling Sections.

The problem of coupling to a helical structure is essentiall one of matching the boundary conditions for a plane wave a the end of a coaxial line with the complicated boundary co ditions for the wave associated with the termination of the heli This may be achieved if the helix wave is transferred to esse tially a plane wave form, albeit travelling in a helical directio before connection to a coaxial line. If a helix is surrounded b a conducting sheath, where the distance between the walls o the sheath and the helix wires are considerably closer than th distance between adjacent wires, propagation is virtually o plane wave form, in the direction of the wire.

The transition between a helix with large or infinite shiel diameter, and a closely shielded helix can be achieved by th following methods:

(*a*) Gradually tapering the diameter of the sheath over severa wavelengths. This tapering distance can be considerably reduce by 'stepping' the transition in λ/4 steps.
(*b*) Gradually or by λ/4 steps increasing the pitch of the helix.
(*c*) Gradually or by λ/4 steps increasing the diameter of the heli
(*d*) Coupling to a larger concentric helix which is closely shielde

Method (*d*) has two advantages: the length of the couplin sections is smaller than for the other methods, and there is n physical connection between the coupling helix and the propa gating helix. The latter factor is of considerable importance a it would enable the helix assembly to be installed or replace with ease, and in fact the radial and longitudinal position of th helix is not critical between certain comparatively broad limit The coupling helix system was therefore adopted for use with th accelerator.

The theory of coupling between helices has been covered i the literature.[8–10]

For complete power transfer from one helix to the other th coupling helix must be of a critical length, and the phas velocities of the two helices considered separately must b slightly different. Lichtenburg[9] gives the expression for critica coupling length as

$$l_c = \frac{\pi}{2K\beta_2} \quad . \quad . \quad . \quad . \quad . \quad . \quad . \quad (21$$

and the ratio of the two phase-change coefficients as

$$\frac{\beta_1}{\beta_2} = \left[1 - \frac{2K(Z_1 - Z_2)}{(Z_1 + Z_2)}\right]^{1/2} \quad . \quad . \quad . \quad . \quad (22$$

The coupling factor K for a closely shielded coupling helix i given to a good approximation by:

$$K^2 \simeq \frac{K_0(\gamma b)/I_0(\gamma b) - K_0(\gamma a_2)/I_0(\gamma a_2)}{K_0(\gamma b)/I_0(\gamma b) - K_0(\gamma a_1)/I_0(\gamma a_1)} \quad . \quad . \quad (23$$

In practice, the coupling helix and shield radii were 2·4 and 3 cm, respectively; the pitch and critical-length dimensions obtained from eqns. (21) and (22), but modified by the presence of a polythene insulating liner between the shield and the helix, are as follows:

Input coupler $l_c = 9{\cdot}9$ cm
Pitch $= 1{\cdot}33$ cm

Output coupler $l_c = 7{\cdot}3$ cm
Pitch $= 1{\cdot}55$ cm

The dimensions of the coupling helix were such as to make its characteristic impedance 100 Ω. As it was fed by a 50 Ω coaxial line a $\lambda/4$ transformer was inserted between them. To ensure complete matching a double-stub matching section was included in the input and output coaxial line.

(4.3.2) **R.F. Load.**

The output coaxial line from the accelerator was terminated in a water-cooled r.f. load. The load itself consisted of a lossy dielectric coaxial line containing butyl alcohol as the lossy element. Power input was measured by monitoring the change in temperature and the rate of flow of the cooling water through the load.

(5) MEASUREMENTS

(5.1) Phase and Group Velocity

The phase velocity was measured by plotting nodes of the standing wave along the helix using an external probe; this gives values of average phase velocity at $\lambda/2$ intervals. By changing the impedance at the helix termination it was possible to shift the standing-wave pattern, and phase-velocity measurements were obtained at $\lambda/10$ intervals. Fig. 7 shows the plot of theoretical and measured relative phase velocity along the helix at 290 and 300 Mc/s. A deviation between measured and theoretical values is apparent at the output

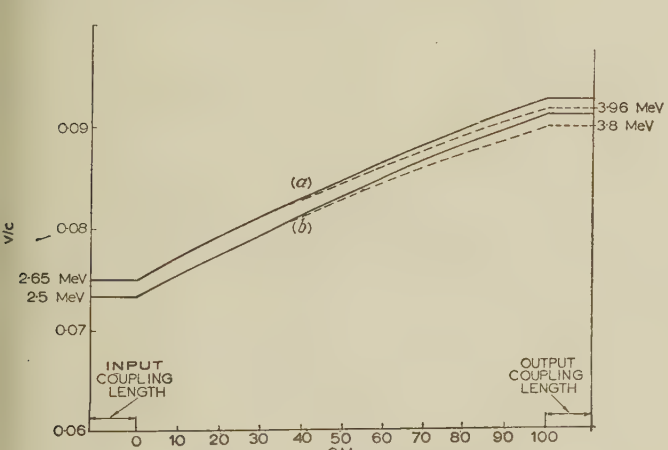

Fig. 7.—Relative phase velocity along structure.
(*a*) At 290 Mc/s. (*b*) At 300 Mc/s.
Theoretical ----
Measured ——

end of the helix, but as this amounts to about 1% it may be concluded that the accuracy of the theoretical analysis is confirmed. From the results for v/c at two frequencies, corresponding values of relative group velocity may be obtained remembering that $v_g = d\omega/d\beta$:

At $Z = 20$ cm $\quad v_g/c = 0{\cdot}047$
At $Z = 80$ cm $\quad v_g/c = 0{\cdot}055$

(5.2) Loss Measurements

Helix losses were determined by measuring the Q-factor of a resonant length. The difficulty of obtaining an efficient short-circuit at the ends of the helix was overcome by the use of a high/low-impedance quarter-wave stepped end shield. A Q-factor of 450 was obtained from measurements; this value is an average for the whole helix, and the actual Q-factor would change along the helix as the parameters changed. However, the change will be small and the average value can conveniently be used to a good degree of approximation. The field attenuation coefficient is given by the expression:

$$\alpha = \frac{\omega}{2v_g Q} \quad . \quad . \quad . \quad . \quad . \quad . \quad . \quad (24)$$

Taking an average value of v_g from the two values obtained in Section 5.1:

$$\alpha = 0{\cdot}137 \text{ N/m}$$

The attenuation length of the accelerator, defined as the length of accelerator at which the field drops to $1/\varepsilon$ of its initial value is:

$$L = \frac{1}{\alpha} = 7{\cdot}3 \text{ m}$$

(5.3) High-Power R.F. Measurements

The main high-power r.f. measurements which have to be made are the monitoring of power both at the output and the input of the accelerator, and the determination of the standing-wave pattern at various points in the circuit.

The power monitoring was achieved by the use of coaxial directional couplers, as described by Morrison and Younker.[11] These were initially calibrated using the r.f. load as a standard. They were then used at the input and output of the accelerator; being directional couplers they could also be used to check that the system at these points was matched.

As it is possible to have a matched line into the input coupler with a mismatch on the helix structure, it was necessary to have some method of determining the standing-wave pattern on the helix. This was achieved by the use of a 3-probe unit; the 3-probe method of measuring the amplitude and phase of the standing-wave pattern in a coaxial line or a waveguide is described in Reference 12. The method is equally applicable in the case of a slow-wave structure provided that the distances between the probes are the correct electrical length, and the probes are far enough away from the helix wires for the effect of the longitudinal discontinuities to be negligible.

(6) ACCELERATOR PERFORMANCE

Since the accelerator is only operative for the duration of the r.f. pulse, the input proton beam was pulsed to reduce the mean beam current and thus the probability of excessive wall charges. This was achieved by deflecting the beam by means of electrostatic deflecting plates driven from a high-voltage pulse generator, which was synchronized with the r.f. modulator.

The output beam energy from the helix was measured by means of a magnetic analyser, consisting of a deflecting magnet followed by 4 mm slits and a Faraday-cage collector. The collector current was measured by the rise of voltage across the collector capacitance, the triangular voltage waveform being amplified in a completely screened head amplifier and presented on an oscilloscope. The magnetic field was monitored with a magnetic fluxmeter, and this was calibrated against beam energy by means of the direct beam from the electrostatic generator. For energies higher than 2·5 MeV, particles of mass 2 and 3 were used for calibration.

Initially considerable difficulty was experienced in obtaining a steady output beam, the movement of the beam suggesting charging of the tube wall; this effect was investigated further. If a beam was passed through the helix tube with no r.f. power present, the output beam was perfectly steady; similarly if the beam pulse was made to follow immediately after the r.f. pulse, no appreciable beam deflection took place. Only when beam and r.f. power were coincident did serious deflection occur, and thus it must be assumed that the defocusing effect of the field must cause wall charges to be set up. However, by using a low modulator p.r.f. this effect was minimized.

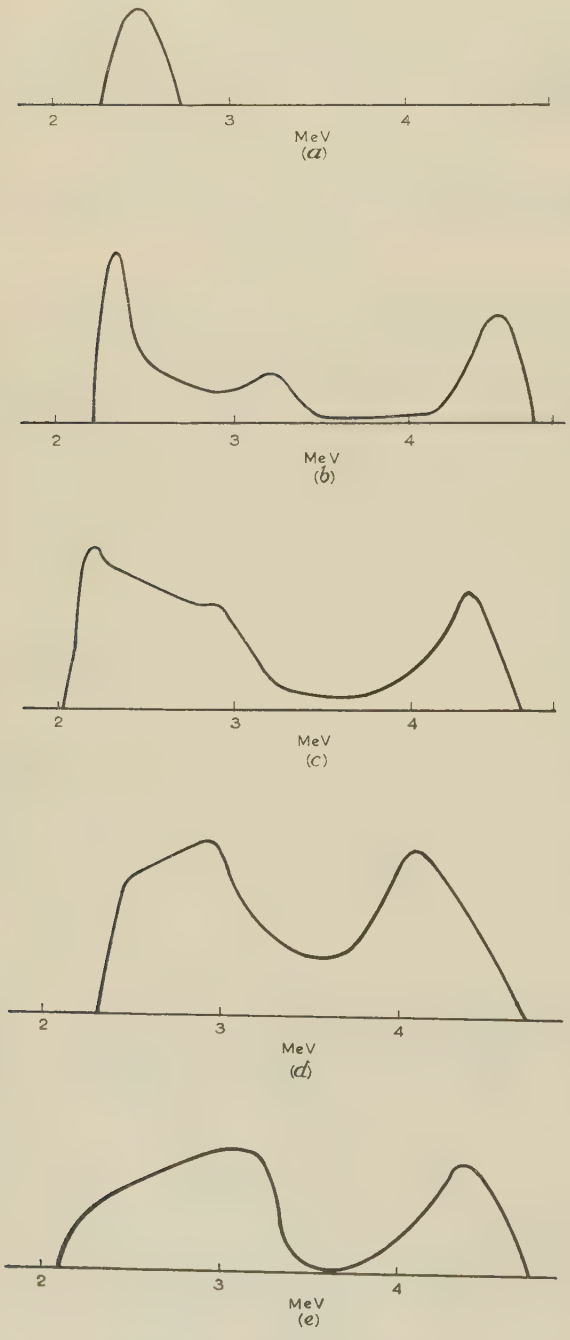

Fig. 8.—Output beam energy spectra with variation of r.f. power flux.

Input beam energy = 2·5 Mev. f = 300 Mc/s.
(*a*) 418 kW. (*b*) 465 kW. (*c*) 510 kW. (*d*) 558 kW. (*e*) 605 kW.

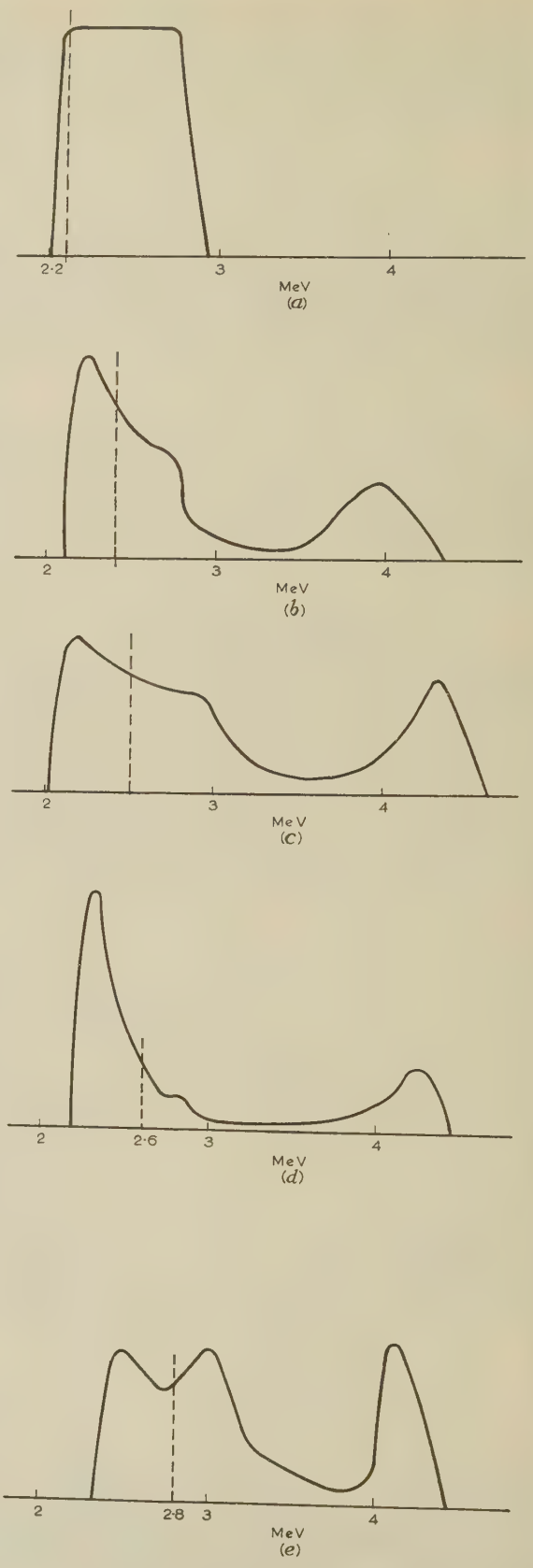

Fig. 9.—Output beam energy spectra with variation of input beam energy.

Power flux = 510 kW. f = 300 Mc/s.
(*a*) 2·2 MeV. (*b*) 2·4 MeV. (*c*) 2·5 MeV. (*d*) 2·6 MeV. (*e*) 2·8 MeV.

Measurement of the output energy spectrum was made for arious r.f. power inputs to the helix, for various input beam nergies, and for a change in radio frequency to 290 Mc/s.

The results obtained are shown in the form of output beam nergy spectra in Figs. 8, 9, and 10. The r.f. power shown is he power flux at the input of the accelerating section of the elix, an allowance of 7% having been made for losses in the oupling and matching sections.

Fig. 8 shows the beam output spectra for r.f. power fluxes rogressively increasing from 418 to 605 kW. The absence of ccelerated output at 418 kW is predicted from Fig. 5 which gives value of η_B of about 5%, which would be difficult to detect. he change in shape of the spectra, both for low and high nergies, may be expected for short lengths of helix, although o detailed theoretical calculation of the output spectrum was arried out.

Fig. 9 shows the spectra for a change of input beam energies. t is to be expected that some acceleration will take place for nput energies slightly lower than the design rating; in fact, the lowest beam which can be accelerated can be computed by onsidering the energy range acceptable from consideration of he acceptance angle. This gives a lower limit of input energy f 2·35 MeV, although between 2·35 and 2·5 MeV the effective cceptance angle will increase from zero to 30°. The energy pectra of Figs. 9(*a*), (*b*) and (*c*) bear out this result, acceleration aking place at an input of 2·4 MeV, with reduced beam effi-iency. Above 2·5 MeV the tendency will be for the particles o travel down the helix suffering small positive and negative energy changes until they reach a point where the phase velocity corresponds to their energy, when, if they are within the acceptance angle, they will be accelerated to 4·3 MeV.

Figs. 10(*a*) and (*b*) show the effect of reducing the radio frequency to 290 Mc/s. From Fig. 7 it can be seen that at 290 Mc/s the correct input energy is 2·65 MeV, and thus little or no acceleration is to be expected. No explanation of the unusual shape of the spectrum of Fig. 10(*b*) can be advanced. Fig. 10(*c*) shows the spectrum as in Fig. 10(*b*), but with a 2·6 MeV input beam. In this case particles were accelerated up to 5 MeV, an enhanced output energy being expected owing to the overall increase in phase velocity.

On account of the wall-charging effect the beam losses are much greater than are predicted by the beam-collection efficiency curve of Fig. 5; at the best, values of $\eta_B = 8\%$ were obtained. However, a comparison with the theory can be made if it is assumed that deflection due to wall charges causes equal losses for all beam energies. Then the beam efficiency, η'_B, may be defined as the ratio of accelerated beam current to total output beam current.

The standard spectrum of Fig. 8(*c*) yields $\eta'_B = 20\%$, which may be compared with the theoretical $\eta_B = 27\%$ for an r.f. input of 510 kW and an acceptance angle of 96°.

Thus it must be supposed that the difference of 7% represents the beam losses due to the defocusing effects of the r.f. field. As this defocusing field acts only upon the accelerated particles, particle loss due to it should be expressed relative to the accelerated current, in which case the beam defocusing losses amount to 35%.

This was not an unreasonable value, because the input beam diameter was made twice that stipulated as the maximum in Section 2.3 in order to improve the detection and energy analysis of output beam current.

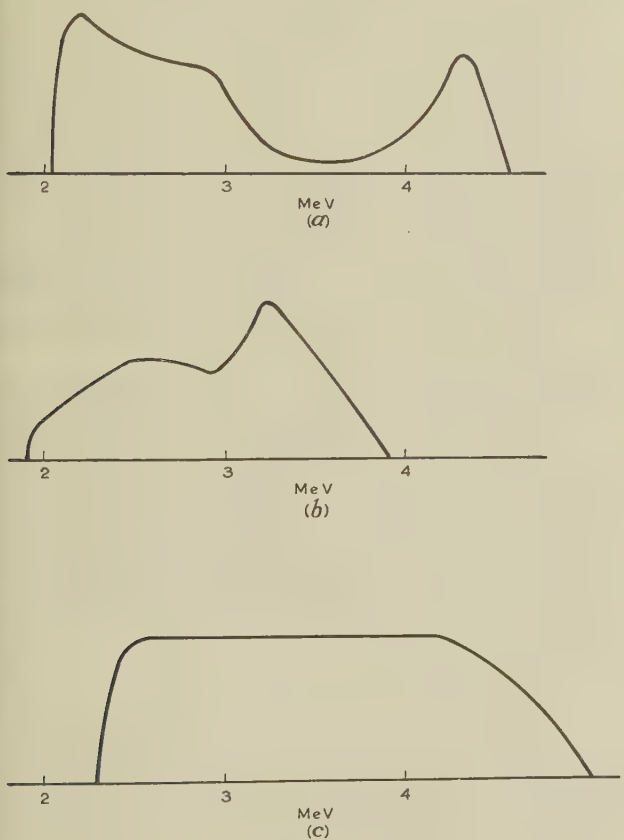

Fig. 10.—Output beam spectra with variation of both frequency and input beam energy.

Power flux = 510 kW.
(*a*) 2·5 MeV; f = 300 Mc/s.
(*b*) 2·5 MeV; f = 290 Mc/s.
(*c*) 2·6 MeV; f = 290 Mc/s.

(7) CONCLUSIONS

The results of the theoretical analysis of an internally supported helix structure indicate that the series impedance is superior to a small degree over an unsupported structure. The shunt impedance is reduced, however, but no more than may be expected for external supports. The results show that the theoretical design parameters are reasonable, and considerable agreement with theoretical expectations has been obtained. The main deviation of the measured results from the theoretical results is in respect of beam efficiency. Heavy beam losses are experienced in the helix tube, owing to beam deflection caused by wall charging, and this may limit the usefulness of an internally supported helix. It would be possible to remove wall charging by using a conducting glass tube, or by severely coating the inside of the tube with a conducting film; both these solutions would cause comparatively heavy r.f. power losses and reduce the advantage of the helix over other types of accelerator. Another alternative would be to use an externally supported helix; this would introduce difficulties associated with cooling the helix, and possibly with voltage breakdown, although measurements made on voltage breakdown *in vacuo* indicate that, with care, this latter difficulty could be overcome.

No attempt was made in this investigation to focus the beam; however, some thought was given to methods of focusing, and these are outlined here. The method which has been used for travelling-wave tubes, of introducing an axial magnetic field by means of a long solenoid, is not really applicable, owing to the very large fields required for a proton beam; however, focusing by an electron-beam space-charge effect has been suggested.[13] The use of magnetic strong focusing is a possibility, and the difficulty of introducing the magnet poles very near the beam may be overcome by building an accelerator up

in sections of 1 m or less, and incorporating the strong focusing in the drift tubes between the sections. Another possibility is the use of electrostatic strong focusing continuously along the helix tube. This would entail using conducting films inside the helix tube, which would introduce additional r.f. power losses; however, as this system would inhibit wall charges, it is worthy of consideration. Phase focusing has been investigated by Servranckx,[5] in which use is made of the fact that particles travelling within the acceptance angle at $\psi < 0$ are accelerated and focused. It would be possible to operate a helix under these conditions with considerably reduced effective acceptance angle, but beam efficiency would be low unless very efficient particle bunching could be achieved.

It would be advantageous if the accelerated beam current could be increased; at present, for 10μA input current, the mean accelerated beam current has a maximum theoretical possible value of less than 0·1μA. The use of a pulsed ion source for the electrostatic generator could give a considerable increase of peak current input, while, with an efficient beam bunching system, a theoretically maximum increase of about four times the output current may be obtained.

Some thought has been given to the problem of devising a method for varying continuously the output beam energy. Chick and Petrie[2] have suggested varying physically the point on the helix at which power is removed. Another method which would be somewhat easier to devise mechanically could consist of a power-absorbing sleeve, which could be moved along the outside of the helix, and could be tapered in diameter to provide a reflectionless attenuator. To ensure no further acceleration it is only necessary to reduce the acceptance angle to zero, i.e. to reduce the phase-stable angle to zero, and as this angle is a function of power it would be necessary to reduce the power by a factor given by $\Delta P/P = \cos^2 \psi_0$, where ΔP is power absorbed in the attenuating sleeve. This would be approximately 400 W maximum for a modulator duty ratio of 300 and $\psi_0 = 30°$. The same effect could be achieved without loss of power if a semi-resonant system were used, and the attenuating sleeve were replaced by a reflecting element which caused a power reflection coefficient:

$$|\rho|^2 = \cos^2 \psi_0$$

This would set up a standing-wave pattern which would periodically increase the electric field strength to 1·5 times its previous value; voltage-breakdown difficulties would be increased, but, on the other hand, an input power reduction of 25% would be achieved.

Another method for obtaining small continuous changes of output power has been suggested by Chick and Petrie[2] and Gallup[14] independently. This consists in changing frequency and input beam energy by interrelated values, thus making use of the constant change of phase velocity along the structure; this effect has been measured and is presented in the results (see Section 7). A nearly constant change of phase velocity along the helix is only obtained for small frequency changes, and thus the method will only produce a limited output energy change.

(8) ACKNOWLEDGMENTS

The authors wish to thank Dr. S. E. Hunt for many helpful discussions and Mr. E. D. Taylor, Mrs. J. Shaw and Mr. W. W. Evans, for their efforts in connection with this work. We are also indebted to Dr. T. E. Allibone, F.R.S., Director of the Laboratory, for permission to publish the paper.

(9) REFERENCES

(1) WALKINSHAW, W., and WYLIE, K.: 'Helix as Linear Proton Accelerator', Atomic Energy Research Establishment Mathematics Memo/57/WW.

(2) CHICK, D. R., and PETRIE, D. P. R.: 'The Helix as a Accelerator of Protons to Energies in the Region of 3 to 20 MeV', Associated Electrical Industries Research Report No. A.65, 1949.

(3) JOHNSEN, K., and DAHL, H.: 'An Investigation of a Helix as a Linear Accelerator', *Christian Michelsens Institutt Beretminger*, 1951, **14**, p. 4.

(4) JOHNSEN, K.: 'Theoretical Losses in a Helix with Shield and Support', Centre d'Études et Recherches Nucléaires PS/KJ, 27, 1954.

(5) DOME, G., and SERVRANCKX, R.: 'On the Helix Linear Proton Accelerator at the Brussels Military Academy', *L'Onde Électrique*, 1957, **367**, p. 1.

(6) CHICK, D. R., PETRIE, D. P. R., KEITH-WALKER, D. G. and LONGLEY, H.: 'An Experimental Proton Linear Accelerator using a Helical Waveguide', *Nature*, 1957, **180**, p. 432.

(7) PIERCE, J. R.: 'Theory of the Beam-Type Travelling Wave Tube', *Proceedings of the Institute of Radio Engineers*, 1947, **35**, p. 111.

(8) WADE, G., and RYNN, N.: 'Coupled Helices for use in Travelling Wave Tubes', *Transactions of the Institute of Radio Engineers*, 1955, **15ED**, No. 3.

(9) LICHTENBURG, A.: 'Helical Coupling System', Massachusetts Institute of Technology, Electronics Research Laboratory Technical Report No. 290, 1954.

(10) COOKE, J. S., *et al.*: 'Coupled Helices', *Bell System Technical Journal*, 1957, **35**, p. 127.

(11) MORRISON, J. F., and YOUNKER, E. L.: 'A Method of Determining and Monitoring Power and Impedance at High Frequencies', *Proceedings of the Institute of Radio Engineers*, 1948, **36**, p. 212.

(12) DUFFIN, W. J.: 'Three Probe Method of Impedance Measurement', *Wireless Engineer*, 1952, **29**, p. 317.

(13) CHICK, D. R., and PETRIE, D. P. R.: 'The Helix as a Linear Accelerator for Protons', *Nature*, 1951, **168**, p. 782.

(14) GALLUP, J. W.: 'Variable-Energy Particle Accelerators', *ibid.*, 1957, **179**, p. 492.

621.372.833

The Institution of Electrical Engineers
Monograph No. 442 E
May 1961

WIDE-BAND COUPLING SYSTEMS BETWEEN A WAVEGUIDE AND A TRANSMISSION LINE

By B. ROGAL, B.Sc.(Eng.), Associate Member, and Professor A. L. CULLEN, O.B.E., Ph.D., Member.

(*The paper was first received 9th August, and in revised form 14th December*, 1960. *It was published as an* INSTITUTION MONOGRAPH *in May*, 1961)

SUMMARY

The paper describes a wide-band microwave system suitable for coupling power between a coaxial line and a waveguide or between two waveguides. Such a system can be applied to normal matched transmission as well as, for example, to coupling power between a coaxial klystron cavity and a waveguide. An appreciable improvement in performance over other schemes results in an almost constant power transfer over a bandwidth in the region of 25%. A practical example of the system in X-band is described.

LIST OF PRINCIPAL SYMBOLS

f_c, f_1, f_2 = Cut-off frequencies of waveguides.
f_m = Mid-band frequency.
ϵ_r = Relative permittivity.
α_c, α_1, α_2 = Coefficients of linear frequency dependence.
β = Phase-change coefficient of coupling guide.
ϵ_0 = Permittivity of free space.
μ_0 = Permeability of free space.

(1) INTRODUCTION

In some microwave systems it is necessary to couple power between a coaxial line and a waveguide, or between two waveguides, in such a way that the coupling factor does not vary appreciably over a wide band of wavelengths. The term 'transmission line' signifies any means for guiding electromagnetic waves and includes a coaxial line and a waveguide as special cases. The problem of obtaining a wide band usually arises because the characteristic impedance of the two transmission lines to be coupled may not vary in the same manner with a change of frequency.

(2) COAXIAL-TO-WAVEGUIDE COUPLING METHODS

One such system comprises a coaxial klystron cavity to be coupled to a rectangular waveguide. General methods in dealing with such a coupling are:

(*a*) To use a coaxial cable with an inductive-loop probe inserted into the klystron cavity and a capacitive probe launching the required wave in the rectangular guide. The adjustment of such a coupling system over a wide band of frequencies is purely experimental and is difficult, and, in general, the variation in power transferred is about 4 : 1 over the bandwidth of 15%.

(*b*) To couple the power into the waveguide by means of an aperture. In such cases a trial-and-error method is employed and this usually results in a system which is very frequency sensitive (dependent on the fourth power of the wavelength). In order to obtain the best power transfer, considerable matching manipulation is necessary at each frequency.

(*c*) To use short sections of 'guide-below-cut-off' as a coupling element. This system is successful if only a small fraction of the power available in the klystron cavity is to be fed into the waveguide, which is rather inefficient. To make this system satisfactory, even for narrow-band operation, a variable matching system, which can be adjusted experimentally, is usually provided.

These methods have two drawbacks: they are difficult to set up, and they fail to provide the constant loading which, with modern klystrons such as the CV.2346, enables a uniform power output to be produced over a considerable band of frequencies.

Quarter-wave sections have been proposed by Reed[1] as a coupling technique, and show much more promise than the other methods. A new design principle for such couplers is described below.

(3) NEW PRINCIPLE

(3.1) Single-Element Coupling using Special Waveguide

The system described here was designed to meet a requirement for coupling a coaxial klystron cavity operating in X-band to a rectangular guide.[2] Before discussing this specific application, however, we shall first consider the simple configuration of Fig. 1.

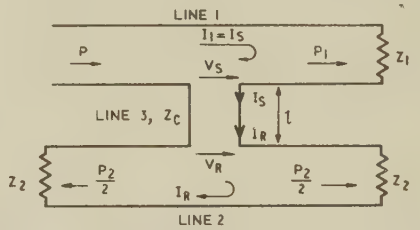

Fig. 1.—Coupling system between a transmission line (line 1) and a waveguide (line 2).

Line 1 is a transmission line, which can be either a coaxial line carrying a TEM wave or a waveguide of uniform cross-section carrying an E- or H-mode wave. In the latter cases its characteristic impedance will be a function of frequency.

Line 2 is a waveguide of uniform cross-section and as such its characteristic impedance will in general be a fixed function of frequency.

Line 3 is the coupling guide of characteristic impedance Z_c, dependent again on frequency, and forming a series T-junction at each end with lines 1 and 2.

Let P be the total incident power in line 1; P_1, the power delivered to Z_1; and P_2, the total power transferred to line 2, both ends of which are terminated by reflectionless loads, Z_2. If the currents and voltages at the receiving and sending ends of the coupling guide are as shown, and assuming that the coupling is weak and the lines are loss-free, we can write the following equations:

$$I_R = \frac{V_R}{2Z_2} \quad . \quad . \quad . \quad . \quad . \quad . \quad . \quad . \quad . \quad . \quad (1)$$

$$V_s = V_R \cos \beta l + jI_R Z_c \sin \beta l$$
$$= V_R\left(\cos \beta l + j\frac{Z_c}{2Z_2} \sin \beta l\right) \quad . \quad . \quad . \quad (2)$$

$$I_s = I_R \cos \beta l + j\frac{V_R}{Z_c} \sin \beta l$$
$$= V_R\left(\frac{\cos \beta l}{2Z_2} + j\frac{1}{Z_c} \sin \beta l\right) \quad . \quad . \quad . \quad (3)$$

where $\beta = 2\pi/\lambda_{gc}$ and l is the length of the coupling guide.

Correspondence on Monographs is invited for consideration with a view to publication.
Mr. Rogal is with Research and Engineering Controls Ltd., and was formerly with the Wayne Kerr Laboratories Ltd. Prof. Cullen is Professor of Electrical Engineering, University of Sheffield.

The input impedance, Z_s, at the upper junction is given by

$$Z_s = \frac{V_s}{I_s} = \frac{\cot \beta l + jZ_c/2Z_2}{\cot \beta l/2Z_2 + j/Z_c} \quad . \quad . \quad . \quad (4)$$

If the coupling factor is defined as the ratio P_2/P_1, which is equal to $\mathscr{R} Z_s/Z_1$, it is easily shown that

$$\frac{P_2}{P_1} = \frac{Z_c^2}{2Z_1Z_2} \frac{1}{\sin^2 \beta l + (4Z_c^2/Z_2^2) \cos^2 \beta l} \quad . \quad . \quad (5)$$

If $Z_c \ll Z_2$, the term $(4Z_c^2/Z_2^2) \cos^2 \beta l$ is small in comparison with $\sin^2 \beta l$ for a wide range of values of βl centred on $\beta l = \pi/2$. Thus the coupling guide should be made a quarter guide-wavelength long at the desired mid-band frequency.

At mid-band the coupling factor is

$$\frac{P_2}{P_1} = \frac{Z_c^2}{2Z_1Z_2} \quad . \quad . \quad . \quad . \quad . \quad . \quad . \quad (6)$$

To a close approximation for weak coupling, we find

$$\frac{P_2}{P_1} \simeq \frac{Z_c^2}{2Z_1Z_2} \frac{1}{\sin^2 \beta l} \quad . \quad . \quad . \quad . \quad . \quad (7)$$

The change in coupling due to the factor $1/\sin^2 \beta l$ for a total 25% band is less than 0·3 dB and can usually be neglected. The remaining factor is Z_c^2/Z_1Z_2, in which Z_c is usually much smaller than either Z_1 or Z_2.

A change of Δf_m from the mid-band frequency f_m will alter Z_1 to a new value which can be written $Z_1(1+\alpha_1\Delta f_m+\gamma_1\Delta f_m^2+\ldots)$, with similar expressions for Z_2 and Z_c. Neglecting terms in Δf_m^2, Δf_m^3, etc., it can be seen that, for the coupling to be independent of frequency, the required condition (to the first order of approximation) is that

$$2\alpha_c = \alpha_1 + \alpha_2 \quad . \quad . \quad . \quad . \quad . \quad (8)$$

As shown in Section 7, for a waveguide employing either H or E mode and having a cut-off frequency f_c, the coefficient α_c is found to be equal to $\frac{1}{f_m} \frac{1}{(f_m/f_c)^2 - 1}$ with corresponding results for α_1 and α_2, namely

$$\frac{1}{f_m} \frac{1}{(f_m/f_1)^2 - 1} \text{ and } \frac{1}{f_m} \frac{1}{(f_m/f_2)^2 - 1}$$

The relationship $2\alpha_c = \alpha_1 + \alpha_2$ then yields the following formula for f_c in terms of the cut-off frequencies, f_1 and f_2, of the two transmission lines to be coupled:

$$\frac{2}{(f_m/f_c)^2 - 1} = \frac{1}{(f_m/f_1)^2 - 1} + \frac{1}{(f_m/f_2)^2 - 1} \quad . \quad (9)$$

It may be of interest that when $f_1 = f_2$ this formula gives $f_c = f_1 = f_2$, so that the known result for similar-guide coupling is obtained.

3.1.1) Coupling between a Coaxial Line and a Waveguide.

For a coaxial line, $f_1 = 0$, i.e. the characteristic impedance is independent of the frequency and eqn. (9) simplifies to

$$(f_m/f_c)^2 = 2(f_m/f_2)^2 - 1$$

or, in terms of the corresponding cut-off wavelengths, to

$$\lambda_c = \sqrt{[2\lambda_2^2 - \lambda_m^2]} \quad . \quad . \quad . \quad . \quad . \quad (10)$$

Thus a broad-band coupling can be achieved if a waveguide of suitable dimensions is used as a coupling element. If a rectangular waveguide is used for one of the lines to be coupled, it may be found that the required coupling guide is wider than one of the coupled lines. In this case the width of the required coupling waveguide may be reduced by making this a rectangular waveguide containing a dielectric material having a permittivity greater than that of the material in either or both of the lines which are coupled, as shown in Fig. 2. Alternatively, or in addition, the coupling may be a ridge waveguide.

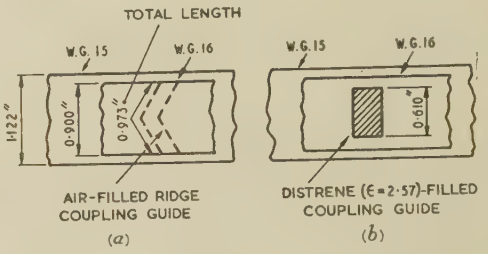

Fig. 2.—Coupling system between two rectangular guides of different sizes.

As an example of this principle, in Fig. 3 the relative power coupling is shown plotted against frequency for a single element coupler between a coaxial transmission line and waveguide W.G.16. In the case of curve (*a*) the coupling guide is c

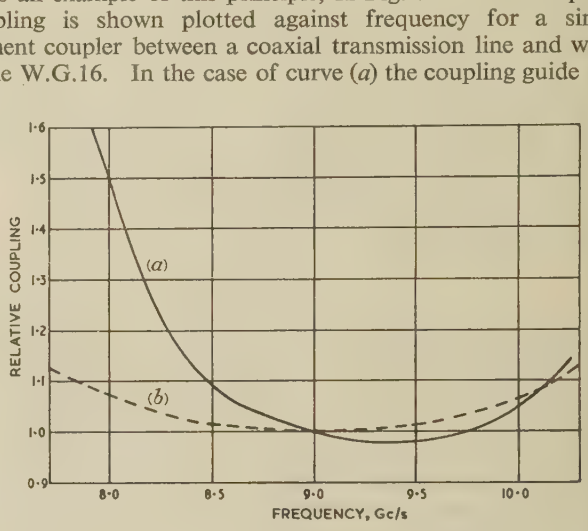

Fig. 3.—Relative power coupled between transmission line and waveguide.

—— $\lambda_c = 4{\cdot}57$ cm.
---- $\lambda_c = 5{\cdot}52$ cm.

the same width as W.G.16 and its length is $\lambda_g/4$ at 9 Gc/s. Curve (*b*) shows an improved performance of the coupling system using a waveguide with a cut-off wavelength of 5·54 cm. As would be expected, the main improvement results at the lower frequencies.

(3.1.2) Coupling between Two Waveguides Operating in H_{01} Mode.

As a practical example employing the system described, consider the coupling of W.G.16 (internal dimensions 0·9 × 0·4 in) to W.G.15 (1·12 × 0·595 in) at X-band. The cut-off frequencies of these guides are 6·57 and 5·27 Gc/s respectively.

Assuming the centre of the band to be 9 Gc/s, it is found from eqn. (9) that the cut-off frequency for the coupling guide should be 6·06 Gc/s. This value is neither a geometric nor an algebraic mean of the first two cut-off frequencies. The broad dimension of the coupling guide should be 0·973 in. This is greater than the width of W.G.16 and either of the arrangements shown in Fig. 2 can be used.

With the arrangement shown in Fig. 2(*a*), in calculating the coupling coefficient, allowance must be made for the fact that the coupling guide does not extend across the whole width o

W.G.15. The same applies to the arrangement shown in Fig. 2(*b*), where the coupling is now affected by the reduced width of the coupling guide with respect to the two waveguides as well as by the reduced characteristic impedance of the coupling guide, which is given by

$$\frac{\frac{a}{b}\sqrt{\frac{\mu_0}{\epsilon_0}}}{\sqrt{\left[\epsilon_r - \left(\frac{\lambda_0}{\lambda_c}\right)^2\right]}}$$

Allowance for the reduced width of the coupling is automatically made to the first order by using voltage/current characteristic impedances for all the waveguides involved, as is done in the above expression for Z_c, in which b is the broad dimension of the guide.

(3.1.3) Coupling Range.

The technique described above is suitable for a coupling range of 10–20 dB, in which case the coupling can be easily calculated from eqn. (6), modified as necessary to deal with the systems shown in Fig. 2. Tighter coupling involves a wider coupling aperture, and junction reactance effects become important. If unidirectional coupling, or a coupling tighter than 10 dB is required, or if the best match in either line is to be secured, then two or more branches can be used to achieve this, but, for the best frequency performance, the width of the coupling guide should still obey the relationship given by eqn. (9).

(3.2) System for Weak Coupling

If very weak coupling is required, it may be difficult to obtain a sufficiently low characteristic impedance in the coupling guide merely by choice of its dimensions, and it may be modified by using an inductive diaphragm at one end and a capacitive diaphragm at the other. If the susceptances of both these diaphragms are large in comparison with the characteristic admittances of the waveguides concerned, very weak coupling can be obtained and there will be very little change with frequency. In general, the frequency variations of susceptance of the diaphragms may be offset against one another and/or against the frequency variation of the characteristic impedance of the waveguides in such a way as to produce a broad-band performance. In this case, it is sometimes preferable to use a coupling guide of length different from a quarter guide-wavelength, the precise length depending on the values of the susceptances employed.

(3.2.1) Principle of Broad-Band Coupling using Reactive Elements of Opposite Sign.

Consider the system shown in Fig. 4, where line 1 is frequency independent. Shunt decoupling reactances, X_1 and X_2, of

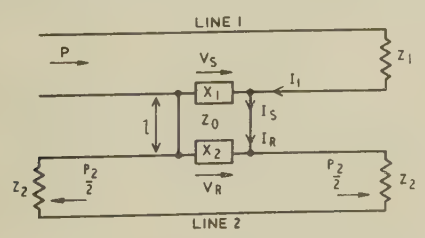

Fig. 4.—Equivalent circuit for weak coupling.

opposite sign are placed at either end of the coupling line. If X_1 and X_2 are small compared with Z_c, and Z_2 is greater than $2Z_0$, then the receiving-end voltage, V_R, at the far end of the coupling line will be given, to the first order, by the product of the receiving-end current, I_R, and the reactance, X_2, of the shunting element.

Equations can now be written for the sending-end voltage, V_s, and current, I_s, and for the total current, I_1, flowing into the junction:

$$V_s = V_R\left(\cos\beta l + \frac{Z_0}{X_2}\sin\beta l\right) \quad . \quad . \quad . \quad (11)$$

$$I_s = -j\frac{V_R}{Z_0}\left(\frac{Z_0}{X_2}\cos\beta l - \sin\beta l\right) \quad . \quad . \quad . \quad (12)$$

$$I_1 = I_s + V_s/jX_1 \quad . \quad . \quad . \quad . \quad . \quad . \quad . \quad (13)$$

Thus

$$\frac{I_1}{V_R} = -j\frac{1}{Z_0}\left[\left(\frac{Z_0^2}{X_1X_2}\right)\sin\beta l + \left(\frac{Z_0}{X_2} + \frac{Z_0}{X_1}\right)\cos\beta l\right] \quad (14)$$

Eqn. (14) is quite general and is symmetrical in X_1 and X_2, so that an interchange of decoupling reactances does not affect the result. For constant power transfer between lines 1 and 2, V_R should remain approximately constant over the required band. Under weak-coupling conditions, the current I_1 should be dependent primarily on the value of Z_1, the input impedance of the coupling guide being very small in comparison with Z_1. Thus, the right-hand side of eqn. (14) should be independent of frequency.

In a waveguide, normalized capacitive reactance varies as $\lambda_g(=2\pi/\beta)$, normalized inductive reactance as $1/\lambda_g(=\beta/2\pi)$.

At a T-junction the situation is much more complicated, and the reactance of a capacitive or inductive diaphragm at such a position will depend on both the guide wavelengths. For simplicity of analysis we take the junction-guide wavelength as the variable on which the reactances depend, but a more accurate analysis would involve the coupled-guide wavelength also. Short of carrying out an accurate analysis, it is impossible to justify our choice except on grounds of simplicity, and on the experimental evidence given later which tends to support the results of our approximate analysis. For convenience $\beta l = \theta$ is taken as a frequency variable and $|X_1|$ and $|X_2|$ are made equal to $|X_0|$ when the frequency is such that $\beta_g l$ is equal to $\pi/2$. If X_1 is made capacitive and X_2 inductive then $X_1 = -X_0\pi/2\theta$ and $X_2 = +X_0 2\theta/\pi$.

Substituting these values in eqn. (14) and rearranging it slightly,

$$\frac{I_1}{V_R} = -j\frac{1}{X_0}\left[\left(\frac{Z_0}{X_0} - \frac{X_0}{Z_0}\right)\sin\theta + \left(\frac{\pi}{2\theta} - \frac{2\theta}{\pi}\right)\cos\theta\right] \quad (15)$$

Since X_0 is a constant,

$$\frac{I_1}{V_R} = -j\frac{1}{X_0}F(\theta) \quad . \quad . \quad . \quad . \quad . \quad (16)$$

The function F(θ) for various values of θ can now be plotted choosing a controlling parameter to be the ratio $n = Z_0/X_0$. The computed values of F(θ) are plotted in Fig. 5. For a 2 : 1 change in λ_g (θ changing from 60° to 120°) the function F(θ), and hence the receiving-end voltage, V_R, will remain constant to within 13·5%, 4% and 5% respectively for $n = 2$, 3 and 4. The curves show that the coupled power can now be controlled to very close limits, especially if the change in λ_g is smaller (as it usually is) in practical cases.

If an impedance of $4Z_0$ is in parallel with X_2, the curves obtained for $n \geqslant 2$ are practically indistinguishable from those in Fig. 5.

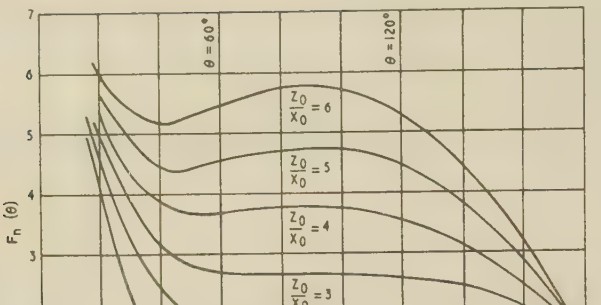

Fig. 5.—Plot of $F_n(\theta)$ against θ with Z_0/X_0 as a parameter.

For the sake of completeness, consider a conductance $G_2 = m/Z_0$ in parallel with X_2. In this case the full equation, similar to eqn. (15), would be

$$\frac{I_1}{V_R} = -j\frac{1}{X_0}\left\{\left[\left(\frac{Z_0}{X_0} - \frac{X_0}{Z_0}\right)\sin\theta + \left(\frac{\pi}{2\theta} - \frac{2\theta}{\pi}\right)\cos\theta\right] + jm\left(\frac{X_0}{Z_0}\cos\theta + \frac{2\theta}{\pi}\sin\theta\right)\right\} \quad (17)$$

or

$$\frac{I_1}{V_R} = -j\frac{1}{X_0}[F(\theta) + jG(\theta)] \quad . \quad . \quad . \quad (18)$$

When the coupling is weak the usual condition is $|F(\theta)| \gg |G(\theta)|$.

(3.2.2) Coupling Waveguide not $\lambda_g/4$ in Length.

It was assumed previously that the coupling guide was exactly a quarter-guide-wavelength long at mid-band, and that the values of the two reactances were the same. Neither of these conditions need be adhered to, and in fact any desired value of coupling, and a wide range of behaviour with change of frequency, can be produced by altering the conditions. An example of this is shown in Fig. 6 for a design of a coupling section

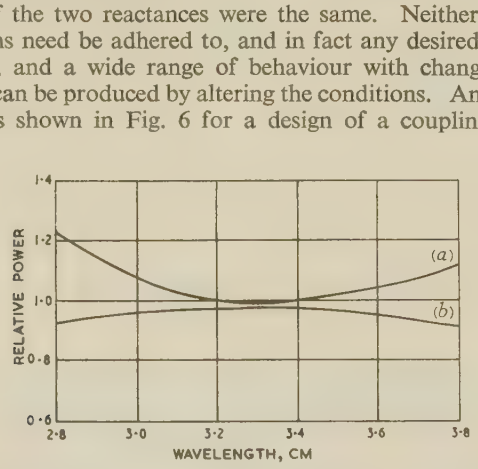

Fig. 6.—Coupling of W.G.16 waveguide in 3·3 cm band.
Curve (a): $l = \lambda_g/4 = 1{\cdot}12$ cm.
Curve (b): $l = \lambda_g/9 = 0{\cdot}53$ cm.
$B_1 = -j6Y_0$; $B_2 = +j6Y_0$

consisting of waveguide W.G.16 in the band 3–3·6 cm. In curve (a), ($l = \lambda_g/4$) the relative power coupled increases towards the ends of the band, in (b), ($l = \lambda_g/9$) it decreases.

(3.3) Combination of the Two Coupling Systems

The two methods discussed above may be used separately o jointly to produce any desired rate of change of coupling wit frequency. The actual reactances and the equivalent circuit of the T-junctions can be obtained from published data.[3] I general these can be taken as giving only approximate values the final adjustment of the coupling being confirmed experi mentally.

(3.3.1) Practical Design of X-Band Oscillator coupled to Waveguid W.G.16.

A combination of the two systems has been used in th practical design of a coupling between a klystron coaxial cavit and waveguide W.G. 16 in the range 8·5–10 Gc/s. The klystro used was a low-voltage plug-in type (CV.2346) capable of givin an output in excess of 30 mW, constant to within 3 dB over th whole frequency band, provided a suitable coupling is employe The schematic of the coaxial cavity is shown in Fig. 7. Th

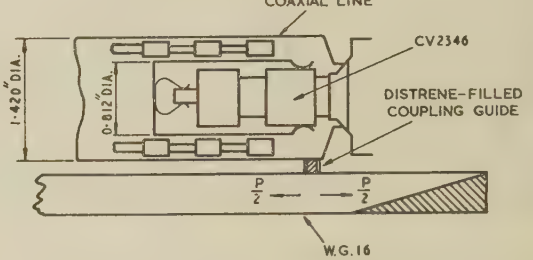

Fig. 7.—Coaxial-line X-band oscillator.

characteristic impedance of the line is approximately 24 Ω, an the theoretical length of the cavity is 5λ/4, the practical leng being reduced to just above 3λ/4 owing to the klystron grid-ga capacitance and the inductance of the cavity corner. Th operating mode of the oscillator corresponded to 4¾ cycles o the reflector transit time. The chosen dimensions of the coaxia line gave freedom from interference of the TE_{11}, TE_{21} and an of the TM modes in the coaxial line. Interference from th possible klystron operation in the 3λ/4, 2¾ cycles mode, wa avoided by employing suitably shaped contacts on the inne conductor of the coaxial line. The capacitance of these contact to the outer conductor separated the wanted and unwante modes. The tuning of the cavity was provided by a micrometer head operating an anodized-aluminium piston, which wa designed in the form of multiple low- and high-impedance filte sections and gave a very effective short-circuit over the whol frequency band.

Fig. 8 shows the dimensions of the coupling guide and th susceptance elements. For convenience, an inductive elemen was used at the coaxial-line end and a capacitive element at th

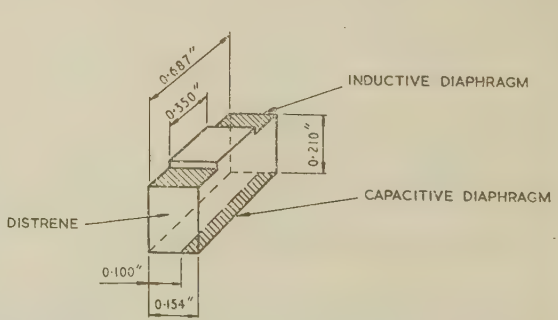

Fig. 8.—Details of coupling guide.

waveguide end. The coupling is a combination of the two systems described and uses a coupling waveguide filled with Distrene ($\epsilon = 2 \cdot 57$) and having a cut-off wavelength of 5·56 cm. The length of the coupling guide was made equal to $\lambda_g/9$ at mid-band and its characteristic impedance was one-half of that of W.G.16.

It is not immediately obvious that the analysis in Sections 3.1 and 3.2 of the systems of Figs. 1 and 4 has any relevance to the klystron coupling problem in which line 1 is a coaxial resonator of characteristic impedance Z_1 terminated in a short-circuit. For constant output from the klystron, the loaded Q-factor of its resonator should remain approximately constant over the whole frequency band. If the coupling point were located at a current maximum in line 1, this condition would be satisfied if $\mathscr{R} Z_s/Z_1$ remained constant. This is exactly the condition studied in Sections 3.1 and 3.2 and so that analysis can be applied.

There is, however, a complicating factor. As the klystron is tuned over the frequency range, the positions of the current maxima in the resonator move. The coupling guide must therefore be situated at the correct position for the mid-band frequency, and some attempt must be made to compensate for the falling-off of the coupling at the ends of the frequency range when a current maximum no longer coincides with the coupling point. To allow for this, the inductive and capacitive reactances were made equal to one-third and one-sixth respectively of the characteristic impedance of the coupling guide. This combination gave a coupling which increased at the ends of the X-band by approximately 15%. This rise in coupling compensated for the fall of power due to the coupling guide not being placed at the current maximum when the oscillator was tuned to either the lowest or the highest frequency.

The klystron cavity has been tested subsequently with a very large number of CV.2346 valves, with 85% of which the output remained constant to well within 2 dB, the maximum output being achieved at mid-band, i.e. near 9·1 Gc/s. With the remainder of the valves the power never fell below 3 dB of the maximum value. No adjustment was necessary during subsequent large-scale production, and the power obtainable from any one klystron approached 70% of the maximum available. It should perhaps be explained that the system must suit *any* klystron without overloading. Hence the system was designed to undercouple even the weakest valve, provided that it came within the CV specification.) It was not possible to achieve such consistent results with either of the other methods of coupling mentioned at the beginning of the paper.

Although the experimental results quoted cannot be regarded as a detailed study of the theory, they do give support to it and have the merit of illustrating an important practical situation in which the new principle has been successfully applied.

Finally, it may be worth while to mention the advantages of the present coupling scheme which offset the obvious disadvantage that half the power is wasted in a matched load:

(*a*) The power output is uniform over the frequency band, so that the oscillator is suitable as a wide-band local oscillator for a search receiver.

(*b*) The source impedance is closely matched to the waveguide.

(*c*) The effects of varying the load impedance on the power output and the frequency of oscillation are greatly reduced.

(*d*) If more power is needed at any given wavelength, the matched load can be replaced by a properly located piston, thus doubling the power.

(4) CONCLUSIONS

The methods of coupling described in this paper can be applied to a variety of systems, but as proved in practice they are specifically suitable for the difficult case of coupling a coaxial-line klystron cavity to a waveguide over a 17% frequency band.

(5) ACKNOWLEDGMENT

The authors wish to thank the Directors of the Wayne Kerr Laboratories Ltd. for permission to publish the paper.

(6) REFERENCES

(1) REED, E. D.: 'A Tunable Low-Voltage Reflex Klystron for Operation in the 50–60 Gc/s Band', *Bell System Technical Journal*, 1955, **34**, p. 563.

(2) British Patent No. 745 701.

(3) MARCUVITZ, N.: 'Waveguide Handbook' (M.I.T. Radiation Laboratory Series, McGraw-Hill, New York, 1951).

(7) APPENDIX

(7.1) Value of Coefficient α

In any air-filled waveguide of uniform cross-section, the characteristic impedance for an H wave is given by

$$Z_0 = \frac{\lambda_g}{\lambda}\sqrt{\frac{\mu_0}{\epsilon_0}} = \sqrt{\frac{\mu_0}{\epsilon_0}}\frac{1}{\sqrt{[1-(f_c/f)^2]}} \quad . \quad . \quad (20)$$

At mid-band frequency f_m, we can denote the impedance by

$$Z_{0m} = \sqrt{\frac{\mu_0}{\epsilon_0}}\frac{1}{\sqrt{[1-(f_c/f_m)^2]}} \quad . \quad . \quad . \quad (21)$$

At a frequency differing from f_m by Δf_m we can write

$$Z_{0m} + \Delta f_m = Z_{0m}(1 + \alpha_c \Delta f_m + \gamma_c \Delta f_m^2 + \ldots) \quad (22)$$

For small values of Δf_m:

$$Z_{0m} + \Delta f_m = Z_{0m} + \Delta Z_{0m} = Z_{0m}(1 + \Delta Z_{0m}/Z_{0m}) \quad (23)$$

To a first approximation we can neglect terms higher than Δf_m in eqn. (22) and equate this with eqn. (23). This provides the relationship

$$\alpha_c = \frac{1}{\Delta f_m}\frac{\Delta Z_{0m}}{Z_{0m}} \quad . \quad . \quad . \quad . \quad . \quad (24)$$

Differentiating Z_{0m} with respect to f_m [from eqn. (21)] and dividing by Z_{0m} we obtain

$$\frac{\Delta Z_m}{Z_m} = -\frac{1}{(f_m/f_c)^2 - 1}\frac{\Delta f_m}{f_m} \quad . \quad . \quad . \quad (25)$$

and hence the value of α_c is given by

$$\alpha_c = -\frac{1}{f_m}\frac{1}{(f_m/f_c)^2 - 1} \quad . \quad . \quad . \quad . \quad (26)$$

Similarly it can be shown that for E waves this value is given by

$$\alpha_c = \frac{1}{f_m}\frac{1}{(f_m/f_c)^2 - 1} \quad . \quad . \quad . \quad . \quad (27)$$

621.385.032.213.13

The Institution of Electrical Engineers
Monograph No. 443 [illegible]
May 196[illegible]

THE CONDUCTIVITY OF OXIDE CATHODES

Part 10.—Spontaneous Generation of Negative Ions

By G. H. METSON, M.C., D.Sc., Ph.D., M.Sc., B.Sc.(Eng.), Member.

(*The paper was first received* 30*th September*, 1960, *and in revised form* 6*th January*, 1961. *It was published as an* INSTITUTION MONOGRAPH *in May*, 1961.)

SUMMARY

The experimental work described here proves that a barium-strontium-oxide matrix is thermally unstable at 1 020° K and continuously generates negative ions of oxygen in its hollow pore system. The barium-oxide component of the matrix is essentially stable and the strontium-oxide component is the oxygen-ion generator. The action is a fundamental one and proceeds at constant and unalterable rate. Factors determining the equilibrium concentration of free oxygen ions in the pores are examined and described. One conclusion reached is that donor concentration of a thermally-activated barium-strontium-oxide matrix is almost wholly strontium metal.

(1) INTRODUCTION

It was confirmed in Part 8 that the passage of a current through an oxide cathode results in a dissociation of the oxide molecule. The particular experimental circumstances of this unexceptional finding led to the rather novel conclusion that the dissociative action was thermal rather than electrolytic. The action involved was imagined to take the following course. Isolated particles of oxide are raised above the 1 020° K ambient temperature of the matrix by repeated inelastic collisions of electrons flying freely through the hollow pores. This increase of thermal energy causes the molecule to dissociate into its constituent ions which then drift apart in the applied electric field. The essence of the hypothesis is that the molecular dissociation results from the accession of thermal energy to the particle and that the manner in which this thermal energy is acquired is quite incidental. If, for example, no electric field exists across the matrix but a particular particle is raised in temperature by any means whatever, the particle will dissociate into its constituent ions. The two types of ion will then diffuse to a cooler environment and there recombine to form the oxide. The passage of current is therefore visualized as having two quite separate actions: inelastic collisions by the electrons raise the temperature of a particle to the point at which it dissociates thermally, and then the two types of ion are permanently separated by the electric field.

It is the purpose of the present Part to examine this thermal dissociation in some detail. In the course of the work it will be shown that dissociation occurs at the conventional working temperature of 1 020° K in the absence of current flow, and is mainly associated with the strontium-oxide component of the barium-strontium-oxide matrix.

Perhaps the easiest way of introducing the experimental approach is to describe the manner in which the phenomenon was first observed. The test vehicle used throughout the work was the standard S-type assembly* which is shown diagrammatically in Fig. 1. Two similar S-type assemblies, one with platinum cores and the other with active O-nickel cores, were taken from the pump and found to have resistances at 1 020° K in the range 30–50 Ω. Both samples were then given therm[illegible]

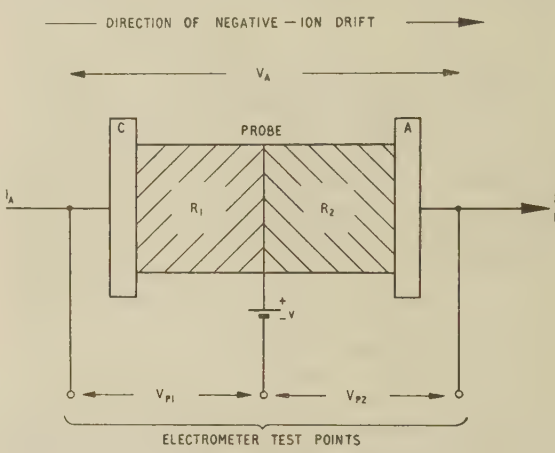

Fig. 1.—Potentiometric arrangements.

treatment at 1 250° K until the resistance of each had levelled out in the characteristic resistance, R_0, range of 16 ± 3 Ω. The valves were next set up on test at 1 020° K, carrying zero current, and their resistances were measured periodically. It was found that the resistance of the active-nickel system remained constant at the R_0 value of about 15 Ω, whereas that of the platinum system increased steadily up to about 30 Ω, thereafter remaining relatively constant. After a further minute at 1 250° K, the resistance of the platinum system returned to the familiar value of 15 Ω at 1 020° K, but subsequent zero-current running produced a slow climb back to about 30 Ω. This action was repeated over a number of cycles and reproduced on a number of individual samples. The phenomenon therefore seemed to be a general one and to indicate that the platinum-cored barium-strontium-oxide system tends to collect gas within its hollow pores during zero-current running at 1 020° K. From such rather casual observations the present work originated.

(2) EXPERIMENTAL ARRANGEMENTS

(2.1) Oxygen Action in an S-Type Assembly

The S-type assemblies were fitted with a 1 mil-diameter pure platinum probe wire situated centrally in the oxide matrix, as shown in Fig. 1, the two equal halves of the matrix being

* Specification of standard S-type assembly:
Cores: Active nickel, 4% tungsten-nickel or pure platinum.
Matrix: Co-precipitated equimolar barium-strontium oxide.
Matrix density: About 1·0.
Matrix thickness: 150 μm.
Matrix area: 0·25 cm².
Vacuum processing is as described in Part 1.

The paper is a continuation of Monographs Nos. 221 R and 243 R, published in February and June, 1957 (see 104 C, pp. 316 and 496), Nos. 268 R, 269 R and 289 R, published in December, 1957, and February, 1958 (see 105 C, pp. 183, 189 and 374), No. 317 R, published in November, 1958 (see 106 C, p. 55), No. 347 E, published in October, 1959 (see 107 C, p. 91). No. 357 E, published in February, 1960 (see 107 C, p. 158), and No. 397 E, published in September, 1960 (see 108 C, p. 83).
Correspondence on Monographs is invited for consideration with a view to publication.
Dr. Metson is at the Post Office Research Station.

stinguishable by their positioning relative to the direction of ssage of an electron flow I_A. The half-section of resistance $_1$ adjacent to the cathodic core C is termed the 'leading' ction and the other section of resistance R_2 adjacent to the odic core A is the 'trailing' section. These resistances can e measured by observing the potentials V_{P1} and V_{P2} (Fig. 1) ising from the passage of I_A. A refinement of this measure- ent is derived from the existence of a small thermo-electric m.f., v, which is always found to be in the probe wire in the nse* shown in Fig. 1. Thus

$$R_1 = \frac{V_{P1} - v}{I_A} \text{ and } R_2 = \frac{V_{P2} + v}{I_A}$$

suming always that no temperature difference exists across the o core faces.

It was shown in Part 1 that, in a well-activated system with -nickel cores† at 1 020° K, the two resistances are always equal; us, $R_1 = R_2 \simeq 7\Omega$ or $R_2/R_1 = 1$.

If a trace of oxygen gas is now injected into such a system the ity value of R_2/R_1 is upset. Both resistances increase, but $_2$ much more rapidly than R_1, i.e. the system moves into the ndition $R_2/R_1 > 1$. This reaction is simply explained. As xygen atoms enter the hollow pores of the matrix, they become gatively ionized and drift under the applied electric field into e trailing half of the matrix. Congregation therefore occurs d the electron-cloud density in the hollow pores is more avily suppressed in the trailing half than in the leading half of e matrix. The condition $R_2/R_1 > 1$ consequently arises.

The S-type assembly with a central probe wire is thus well ited to detect, and to some extent measure, the free oxygen ns within its hollow pore structure. Extensive use of this as been made in the present work.

(2.2) Practical Arrangements

The main physical dimensions of the standard S-type assembly ill be maintained throughout the work, but the following ariations of a chemical nature will be introduced:

(*a*) *Core Metals.*—In any one assembly the two cores will always be identical but may be prepared from pure platinum, O-nickel or pure nickel alloyed with 4% tungsten.

(*b*) *Probe Wire.*—This may be pure platinum or pure nickel.

(*c*) *Matrix.*—This may be the usual co-precipitated equimolar double barium-strontium oxide, single barium oxide or single strontium oxide. The density is approximately 1 g/cm^3.

The measurement of potentials is made by a vibrating- apacitor electrometer of effectively infinite internal impedance. he thermo-electric potential, v, is determined by measuring e cathode-probe and probe-anode potentials with the S-type ssembly on open-circuit ($I_A = 0$). The two observed values ould be of equal magnitude but opposite sense. The magni- ude of v is usually small compared with V_{P1} and V_{P2} and may e ignored without introducing sensible error. Where it is nportant it will be used and reference made in the text.

(2.3) Experimental Plan

The main object of the work is to prove that the barium rontium oxide at the conventional working temperature of 020° K is subject to spontaneous thermal dissociation. This issociation involves the evolution of negative ions of oxygen nto the hollow pores, and these ions are to be detected and easured by observation of the unbalance condition $R_2/R_1 > 1$.

It is, of course, possible to observe the unbalance only by passing a current through the device, and this at once poses a question of some apparent difficulty. How can a current be passed through the matrix to observe the unbalance condition without at the same time causing doubt that the act of current passage has not in itself produced the unbalance? At 1 020° K it is, in fact, well proven that dissociation occurs rapidly at high current densities and can reasonably be expected to occur slowly at low current densities. The answer to this seemingly difficult situation turns out to be quite simple. If free negative ions are present in a matrix they can be caused to drift under an electric field from leading to trailing section at any matrix temperature sufficiently high to permit ion movement. It will be shown that the free negative ion of oxygen has a detectable mobility at 400° K in the barium-strontium-oxide matrix, and at 550° K the drift is rapid enough for practical routine measurements. It will furthermore be proved that the passage of an adequate current for the measurement of R_2/R_1 at these low temperatures produces no detectable dissociation of the matrix.

The broad experimental plan will now be clear. The S-type assembly in some form or other is run at zero current and 1 020° K for some test period. At suitably spaced intervals of time the matrix temperature is lowered to 550° K and a spot measurement of R_2/R_1 is made. That this value of R_2/R_1 reflects the free ion concentration in the matrix at 1 020° K will become apparent as the work progresses.

This brief preamble may assist the reader in appreciating the overall trend of a rather complex sequence of individual experiments.

(3) BEHAVIOUR OF THE BARIUM-STRONTIUM-OXIDE SYSTEM ON PLATINUM CORES

(3.1) Correlation of R_2/R_1 at 1020 and 550° K

Our first task is to show that measurements of R_2/R_1 made at 550° K faithfully reflect the ionic state of the matrix at 1 020° K. A standard S-type assembly fitted with platinum cores and a platinum probe wire in the centre of the barium-strontium-oxide matrix is given 5 min of thermal treatment at 1 250° K for initial activation. The valve is now set up for a test run of 500 hours' duration at 1 020° K and with zero current. At appropriate intervals of time it is temporarily removed from test and subjected to the following two measurements:

(*a*) At 1 020° K a current of 20 mA is passed through the device for 1 min, during which time the leading and trailing resistances, R_1 and R_2, are measured potentiometrically. At this temperature the thermo-electric e.m.f. is an appreciable fraction of V_{P1} and V_{P2} and must therefore be taken into account.

(*b*) The temperature of the device is next lowered to 550° K and a potential $V_A = 0{\cdot}50$ V applied across the core faces. Potentiometric measurements of V_{P1} and V_{P2} are now made over a period of 30 min, during which time the negative ions, moving relatively slowly at 550° K, have all drifted into the trailing section. R_1 and R_2 are derived once this steady state has been reached; v is negligible at 550° K and can be ignored.

After these two measurements have been completed, the valve is returned to its test rack and left at 1 020° K until the next measurement is due.

The characteristics of R_1 and R_2 measured at 1 020 and 500° K are shown in Fig. 2. Comparison of the two sets shows the same qualitative features. Both sets of R_1 show a small initial increase over the first 100 hours of the test run, after which they are essentially constant. Both sets of R_2 show a much greater rise in the first 100 hours, after which they are also effectively constant. One interesting difference is that the R_2 excursion at 550° K is much greater than that at 1 020° K. This is a strong point in favour of the low-temperature method of measurement,

* The e.m.f. is thought to be a thermo-electric phenomenon arising from the eration of the probe wire at a temperature slightly lower than that of the two metal re pieces.

† O-nickel contains about 0·05 % magnesium and such cores have an inherent ndency to activate the matrix by the reaction $Mg + BaO \rightarrow MgO + Ba$.

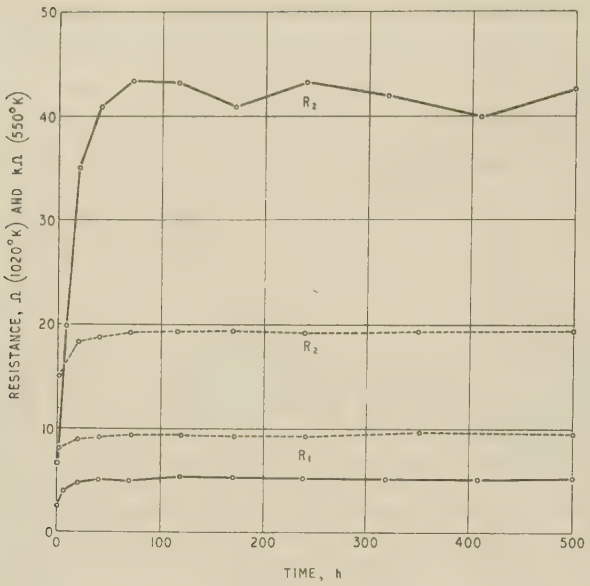

Fig. 2.—R_1 and R_2.
----- At 1 020° K.
—— At 550° K.

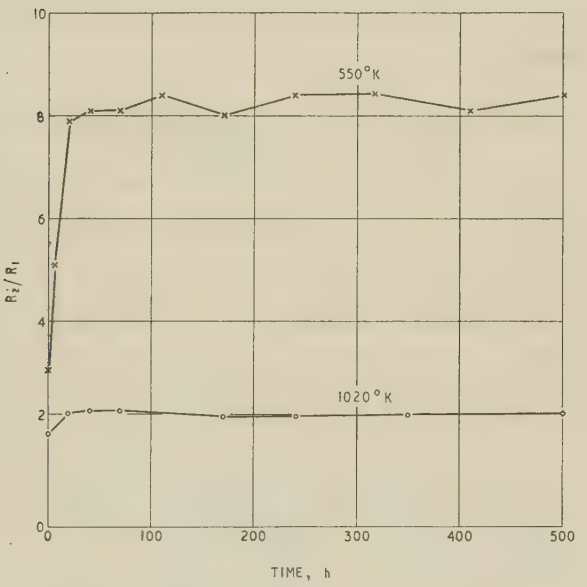

Fig. 3.—Comparison of R_2/R_1 at 1 020 and 550° K.

i.e. the 550° K technique is several times more sensitive than the 1 020° K one.

Fig. 3 shows R_2/R_1 for the 550 and 1 020° K measurements, and here the greater sensitivity of the low-temperature measurement is very apparent.

The conclusion drawn from the experiment is that exploration of the free negative-ion content of the matrix can be made at 550° K with perhaps greater accuracy than at 1 020° K. The low-temperature method will now be presumed to be valid and it becomes possible to measure changes of free ion content of a matrix which has carried no current at all during its lifetime at 1 020° K. There still remains the possibility that the low-temperature test for R_2/R_1 may introduce free ions into the system, but this possibility will be excluded by the experiment recorded in Section 3.4. We have thus arrived at the point where we can study the generation of free ions within the matr under conditions which formally exclude the known dissociati action of current flow.

(3.2) Variation of R_1/R_2 with Operating Time at 1020° K

It is now proposed to examine in greater detail the ion mov ments at 550° K and to establish the generality of the characte istic set out in Fig. 2. Standard S-type assemblies with platinu cores and a double-oxide matrix will be employed, and t samples will be run for their entire test life at 1 020° K witho the passage of current.

Suppose a sample is taken and given thermal treatment 1 250° K to reduce its resistance to something approaching t characteristic R_0 value. The valve is then placed on life test 1 020° K with zero current and removed periodically for dete mination of R_2/R_1 at 550° K. A voltage of 0·50 V is now appli and maintained constant across the matrix, and time charact istics are taken of I_A, V_{P1} and V_{P2}. The thermo-electric pow between the probe and the cores is negligible and can be ignore From these measurements the changes of R_1 and R_2 are derive

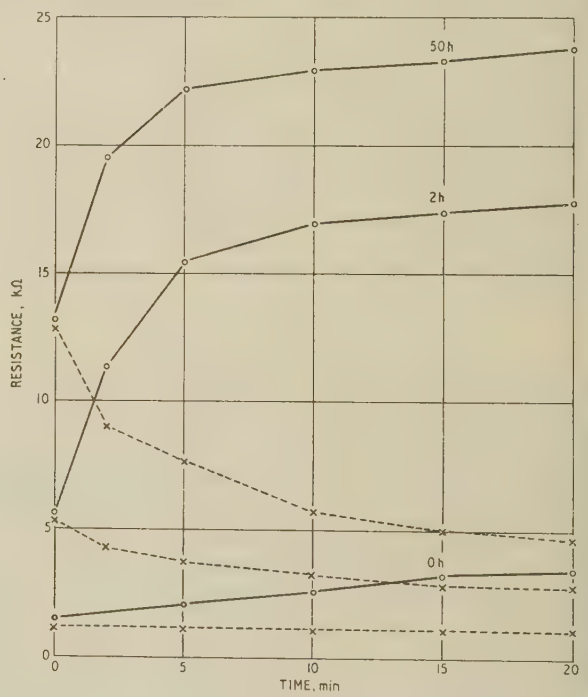

Fig. 4.—Ion migrations at 550° K as functions of operating time at 1 020° K.
---- R_1
—— R_2

Results are shown in Fig. 4. At zero time the free negati ions are uniformly distributed throughout the matrix and t initial potentials, V_{P1} and V_{P2}, are equal. As the negative io drift from the leading to the trailing section R_1 falls and R_2 increases. After 30 min both R_1 and R_2 have reached near constant values and it can be assumed that all the ions are the trailing section. The leading section has thus fallen to t lowest resistance compatible with its temperature and state activation; R_2/R_1 has therefore increased from unity at zero tim to a maximum value after about 30 min. This maximum valu is a measure of the free ion content of the matrix and is that use in the compilation of Fig. 3.

Fig. 4 shows three pairs of R_1/R_2 characteristics taken at 0, and 50 hours of zero-current operation at 1 020° K. Characte

tics taken after 50 hours' operation show no further significant ariation, i.e. the free negative-ion build-up has by then reached a onstant concentration. Points arising from Fig. 4 are

(*a*) The final steady values of R_1, R_2 and R_2/R_1 increase from 1·0 to 4·6kΩ, from 3·5 to 23·8kΩ and from 3·5 to 5·2, respectively.

(*b*) At zero test time at 550°K where $R_1 = R_2$, the resistance increases from 1·5 to 13·0kΩ.

Any one of these four functional changes could, of course, be sed as a measure of the build-up of free ion concentration, but $_2/R_1$ has been chosen on the grounds that it is a dimensionless umber with a special significance attached to its unity value .e. $R_1 = R_2$) which defines a gas-free matrix in a steady ectric field.

From Fig. 3 it is observed that R_2/R_1 climbs from 2 to 8 in out 20 hours. If at this time the matrix temperature is raised om 1 020°K to 1 250°K for 1 min a retest at 550°K will show at the system has reverted to the condition $R_2/R_1 = 2$. A rther 20 hours at 1 020°K with zero current sees the ratio turning to a steady value of 8, and this cyclic state can pparently be indefinitely maintained. In short, gas is expelled om the matrix at 1 250°K but builds up to a constant concen- ation again at 1 020°K.

To sum up, it might be said that the platinum-cored barium- rontium-oxide system is in equilibrium with a fixed concentra- on of free negative ions at 1 020°K. The rate of build-up of is concentration and its steady-state magnitude are curiously onstant among individual samples.

(3.3) A Technical Attempt to Influence the Steady-State Magnitude of R_2/R_1

The build-up of free ion concentration may be due to some ndamental property of the oxide matrix or to some trivial chnical cause, such as the long-term outgassing of a piece part. Much effort was put into examining the latter possibility, and is will be given very brief mention. The S-type assembly onsists only of two metal cores with insulated heaters, two upporting tungsten springs and the surrounding glass envelope. ach of these items was given increasingly rigorous thermal eatment in an endeavour to eliminate occluded gas. The rgest metal mass is the platinum core itself, and this was ubjected to three different thermal treatments in a vacuum etter than 10^{-6} torr, namely (*a*) 12 min at 1 200°C, (*b*) 2 hours t 1 200°C and (*c*) 18 hours at 1 200°C.

Treatment (*a*) is the normal one given to the cores before they re sprayed. Samples made up from each pre-processing varia- on gave stable levels of R_2/R_1 which were statistically indis- nguishable from each other. Substantial alterations in the lass-envelope treatment likewise gave negative results.

From such experiments it was concluded that the build-up and table level of free ion concentration cannot be influenced by ny reasonable variation of piece-part processing. It would eem probable then that the phenomenon is a fundamental one nvolving the thermal dissociation of the barium-strontium xide. It is hoped to prove this notion by formal experiment in ection 4, but a number of matters concerning the free ion will e discussed first.

(3.4) Matrix Stability under Current Load at 550°K

An essential link in the chain of argument is to prove that the ct of measuring R_2/R_1 at 550°K does not itself introduce free ons into the system. The measurement necessarily involves he passage of current through the matrix under an applied otential of 0·50V. The current employed is frequently of the rder of 10μA, and at 550°K the total core heater power is 430mW and the testing power, $V_A I_A$, is 5μW, i.e. 0·001% of the power applied to the core heater to maintain the system at 550°K.

Suppose now that a platinum-cored S-type assembly with barium-strontium-oxide matrix is given thermal treatment at 1 250°K to reduce the resistance to something approaching R_0. The valve is set up for a zero-current run at 1 020°K for a period of 3 hours, during which time R_1 and R_2 at 550°K are measured six times at appropriate intervals. Results are set out on the left-hand side of Fig. 5. The behaviour is qualitatively identical with the results in Fig. 2 showing only the early stages of increase of both resistances.

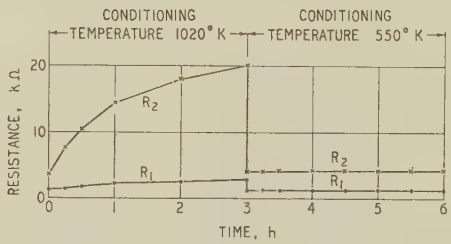

Fig. 5.—Matrix stability under load at 550°K with envelope maintained at 49°C.

At the end of this first 3-hour period the valve is given 1 min at 1 250°K and its temperature reduced to 550°K for the measurement of R_1 and R_2. The ions have been driven from the matrix by the high-temperature treatment and the resistances have regained their low initial values as at time $t = 0$. The valve is next run for a further 3 hours with zero current at 550°K with regular measurements of R_1 and R_2 at 550°K at suitable intervals of time. Eight measurements in all have been made and these are shown on the right-hand side of Fig. 5. It will be clear that these eight measurements have contributed nothing to the free-ion content of the matrix.

One experimental precaution may be worth mention. During the first 3-hour run with the oxide system at 1 020°K the glass-envelope temperature was 49°C. This temperature would fall to 31°C during the second 3-hour run with the oxide system at 550°K. Steps were taken, however, to maintain the glass temperature constant at 49°C throughout the whole experiment. This precaution eliminates the glass envelope as a source of supply of free ions to the matrix during the first 3-hour run.

The conclusion drawn from the exercise is that the growth of free-ion content during the first 3 hours is due wholly to thermal dissociation of the matrix at 1 020°K and not in any way to the 550°K testing procedure.

(3.5) Mobility of the Free Negative Ions as a Function of Temperature

In the determinations of the R_2/R_1 ratio at 550°K it was observed in Fig. 4 that R_1 and R_2 reach a steady value after about 20 min. Continuation of the testing beyond this time results in little further change in the resistances and it can be assumed that all the negative ions have passed into the trailing half of the matrix. It is now proposed to establish the influence of matrix temperature on the time taken to move all the ions into the trailing section at some constant field strength. This movement under electric force will be described as 'mobility.'

A platinum-cored S-type assembly with double-oxide matrix is run with zero current at 1 020°K for 100 hours to establish the equilibrium concentration of free negative ions in the pore system. The matrix is then set at 550°K, a constant potential

of 0·50 V is applied and regular measurements of R_2 are taken over a test period of about 3 hours. The result is shown in the lowest curve of Fig. 6, from which it appears that all the negative ions have drifted into the trailing section in about 30 min, i.e. the characteristic has become flat in that time.

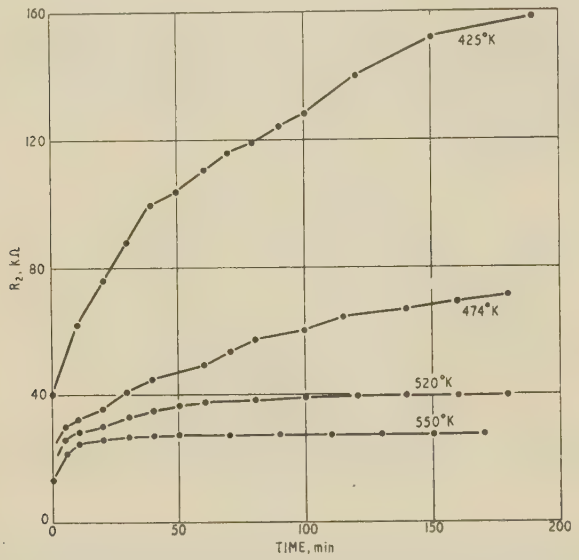

Fig. 6.—Negative-ion mobility as function of temperature.

The matrix is next run with zero current for an hour at 1 020° K to permit the re-establishment of a uniform ion density by a process of diffusion. The temperature is now set at 520° K, the applied potential being 0·5 V, and a further 3-hour run is recorded in respect of R_2. This procedure is continued until the family of four characteristics shown in Fig. 6 is established.

Examination of the curves shows that the time taken at constant field strength for R_2 to achieve a steady value increases as the temperature is decreased. In other words, the mobility of the free ions increases with temperature. At 425° K the mobility is so small that there is no stability achieved in a 6-hour test, while at 1 020° K the stable condition for R_2 is reached in a few seconds.

The reason for choosing 550° K as the measuring temperature for R_2/R_1 will now be apparent—the mobility of negative ions at 550° K is just about right for a convenient speed of testing.

(3.6) Diffusion Rates of the Free Negative Ions

Suppose an S-type assembly is in possession of its equilibrium concentration of free negative ions at 1 020° K. The temperature is reduced to 550° K, a potential of 0·50 V is applied and the system is run for 30 min to drift the ions into the trailing section. The left-hand side of Fig. 7 shows the course of this operation. At this stage all the free ions are pressed against the anodic core face, off which there now exists a steep concentration gradient. The applied potential $V_A = 0{\cdot}50$ V is next removed, whereupon the negative ions begin to drift away from the anodic core toward the leading section. After 5 min V_A is applied pulse-wise for just sufficient time to enable V_{P1} to be read on the electrometer, i.e. the R_1 and R_2 states of the matrix are explored without exposing the ions to other than a momentary electric force. This pulse technique is repeated every 5 min for a total of 30 min run. The resulting resistive states, R_1 and R_2, are plotted on the right-hand side of Fig. 7. The curves show that diffusion at 550° K under a concentration gradient is quite rapid and that uniform distribution of ions is re-established in about 30 min.

The experiment has been exactly repeated at 425° K and t results are shown in Fig. 8 which corresponds to the right-ha half of Fig. 7. At 550° K a uniform free negative-ion distributi is re-established in about 30 min, whereas the time taken 425° K is probably about 300 min. Diffusion of the free negati ions is thus dependent on temperature in a similar manner mobility.

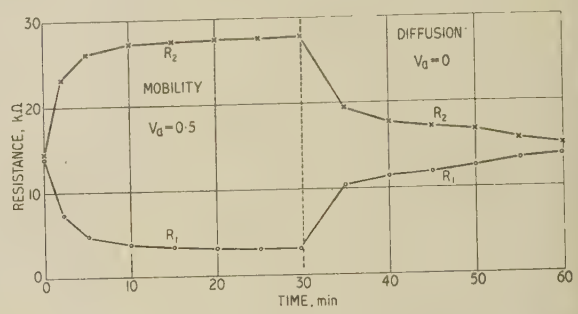

Fig. 7.—Diffusion of negative ions in a concentration gradient at 550° K.

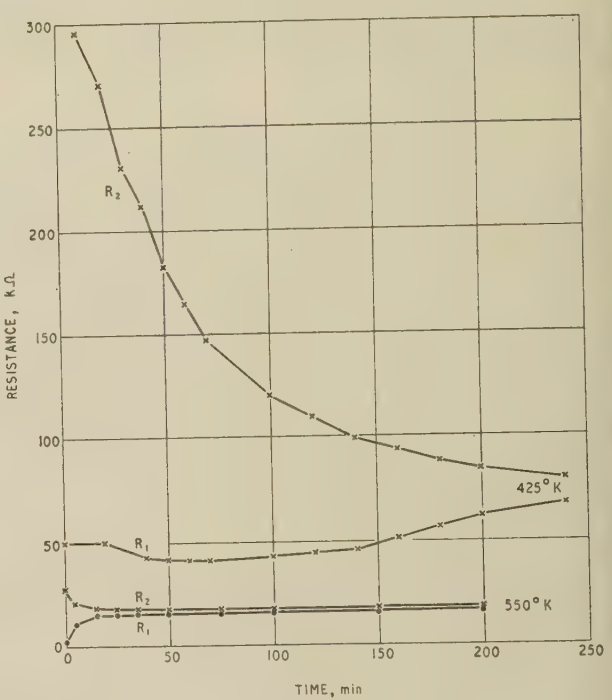

Fig. 8.—Negative-ion diffusion as a function of temperature.

(3.7) Reversibility of R_1 and R_2

The mobility of the negative ions is most effectively demo strated by a rhythmical reversal of direction of the appl electric field. Fig. 9 shows the second, third and fourth cyc of a system running at 580° K. The first cycle is different fr subsequent ones, since it starts with a uniform distribution free ions, i.e. $R_1 = R_2$ at $t = 0$. Succeeding cycles are appro mately similar without any systematic changes of magnitu over 10 cycles. One physical half-section—which is, of cour alternately in the leading and trailing positions—is drawn a broken-line characteristic, and the other physical half-section a solid line, in Fig. 9.

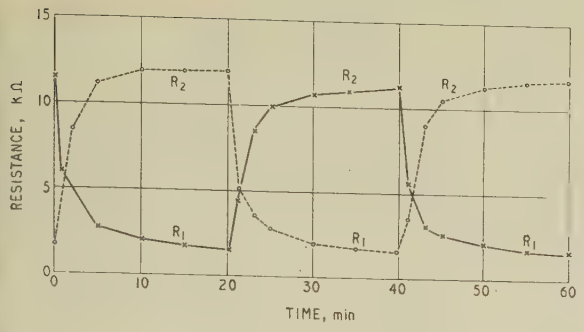

Fig. 9.—R_1 and R_2 in a cyclic state.
$T = 580°K$, $V_A = \pm 0{\cdot}5V$.
The graph shows the second, third and fourth cycles.

(3.8) Storage of Negative Ions in Anodic Sink

The levelling off of the R_2 characteristic with time in Fig. 9 is ıpposed to indicate that all the free negative ions have been riven to the trailing section and are now pressed against the nodic core face of pure platinum. If such an R_2/time character- tic is extended, as in curve (*a*) of Fig. 10, R_2 continues to rise

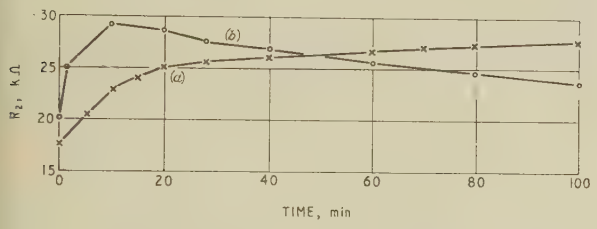

Fig. 10.—Storage of negative ions in an anodic sink at 550°K.
(*a*) Normal state.
(*b*) Provided with anodic sink.

t a decreasing rate and ultimately flattens out to an apparently onstant value. Such a result might be expected, since no hemical action is likely to occur which might remove the ions. he only avenue of escape for the ion is, in fact, by thermionic mission from the matrix edge into the surrounding vacuum. his emission may occur, but evidence seems to show that, if it oes, it is a very slow process.

Suppose now that we employ the two alternative arrangements f the matrix shown in Fig. 11. In (*a*) the matrix is limited trictly to the space between the inner faces of the two cores, and ıis is the standard arrangement used throughout the present ork. If an electron current flows from X to Y, the ions will e pressed up against the inner face of Y and their only possible scape path is by thermionic emission in the direction of the rrows.

In (*b*), each core is sprayed on all sides and in the finished evice each core is completely surrounded by oxide matrix. If n electron flow passes from X to Y the negative ions are first ressed against the anodic core face and then diffuse under a oncentration gradient round to the back of the core. The path f the diffusing ions is shown by the arrows. The ions pass apidly under electric force from leading to trailing section and R_2 increases to a maximum value. As the concentration builds p the diffusive flow starts and the ions leak away to the ion sink n the outer face of Y. The result of this leak is to cause R_2 to ecay slowly as shown by curve (*b*) of Fig. 10.

The experiment brings out clearly the reluctance of the ions o escape from the device at 550°K by thermionic emission, in ıarked contradistinction to their ease of movement within the matrix itself. It might be supposed that the negative ions travel mainly over the surfaces of the solid particles rather than by a vacuum flight across the hollow pores.

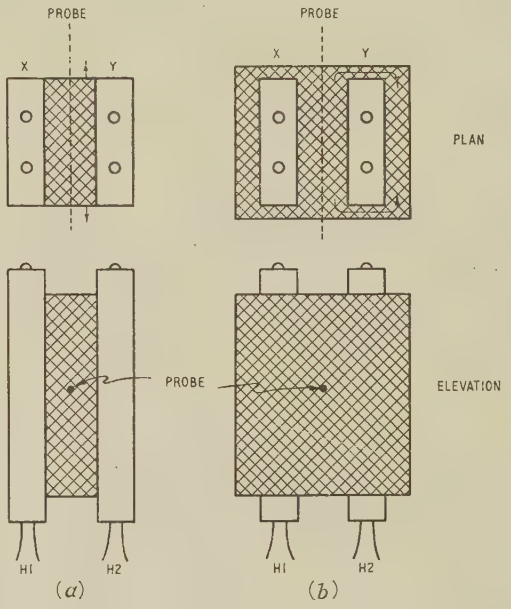

Fig. 11.—Alternative arrangements of the barium-strontium-oxide matrix.

(3.9) Movement of Negative Ions in a Temperature Gradient

The direction of movement of the free negative ions in a matrix subjected to a temperature gradient can be easily demonstrated. A standard platinum-cored S-type assembly with double-oxide matrix is allowed to run at 1 020°K with zero current for 100 hours to acquire its equilibrium concentration of free negative ions. With the tube still passing zero current and at a uniform temperature of 1 020°K the power to the X-core heater (H_1 in Fig. 12) is switched off. The X-core thereupon cools and a temperature gradient of about 250° is set up. At this stage power to the Y-core heater, H_2, is also switched off and the two cores cool under a constantly decreasing temperature gradient to room temperature. It now remains to discover the whereabouts of the free ions, and this is achieved in the following manner. Equal power is supplied to both heaters to raise the

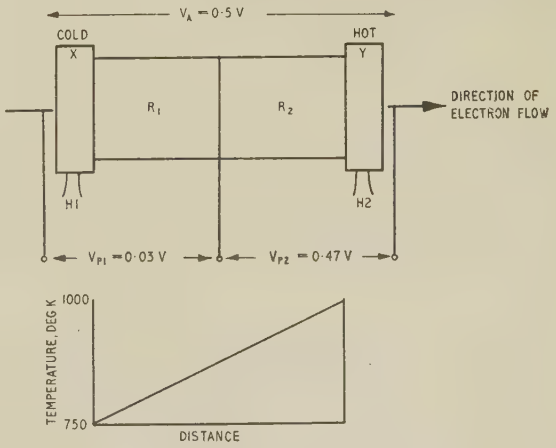

Fig. 12.—Movement of negative ions in a temperature gradient.

matrix temperature to 450° K, where both mobility and diffusion are very slow. A potential of 0·50 V is applied across the device and an electron flow is set up in the direction XY. Potentiometric measurements of V_{P1} and V_{P2} are then recorded and show that $R_2/R_1 = 15{\cdot}6$. In other words, the great bulk of the negative ions are close to the Y-core and have migrated to and settled in the hotter half of the matrix.

It had, of course, been expected that the free ions would congregate in the cooler half and the opposite result calls for some explanation. This probably lies in the thermo-electric power action of the electrons during the cooling of the matrix under a temperature gradient. If the electrometer is placed across the cores during the cooling phase, a maximum potential of 0·72 V is recorded with the hotter core, Y, at a positive potential with reference to the cooler core, X. This is simply a thermo-electric e.m.f. due to the movement of electrons, but the consequent electric field is of apparently sufficient magnitude and duration to drive almost all of the free negative ions to the positive or hotter core.

(3.10) Physical Mechanism of the $R_2/R_1 > 1$ State

At 1 020° K the congregation of negative ions in the trailing section is supposed to suppress the surface emission of electrons from the pore walls and to decrease the density of the pore electron cloud. Since the resistance of each section is a function of the electron-cloud density therein the condition $R_2/R_1 > 1$ obviously follows. Such matters were considered in Parts 2 and 5.

This simple explanation of R_2/R_1 action at 1 020° K cannot be directly applied at 550° K, since vacuum conductivity has virtually ceased and solid conductivity is paramount. No difficulty need arise, however, for it was shown in Part 7 that a trace of oxygen admitted to an S-type assembly operating at 420° K destroys the solid conductivity. It was further shown that this destructive action occurs even with the matrix operating at room temperature. Provided that the negative ions have adequate mobility, it follows that the $R_2/R_1 > 1$ condition should be applicable to the solid state.

One further point of interest arises from Part 7, where it was shown that the conductivity at 1 020° K has a property akin to space-charge limitation. Thus conductivity at first increases rapidly as the concentration of alkaline-earth metal increases in the oxide matrix, but then slows down to a nearly constant value as donor concentration is further increased. Suppression of emission at 1 020° K is therefore likely to be an insensitive process, since many donor centres must be extinguished for a small change in conductivity. This phenomenon may well explain the greater sensitivity of the $R_2/R_1 > 1$ technique when used in the solid rather than the vacuum phase.

(3.11) First Hypothesis

A first tentive hypothesis will now be set down in the following terms:

> A platinum-cored S-type assembly with barium-strontium-oxide matrix running with zero current at 1 020° K spontaneously generates oxygen in negative-ion form. These ions congregate in the hollow matrix pore system through which they move freely under electric force or concentration gradient. The concentration increases up to an equilibrium level which is indefinitely maintained.

At present the hypothesis stands on the very tenuous evidence that the observer is unable to alter the equilibrium concentration of free ions by any improvement in technological processing of the piece parts of the S-type assembly. This is slender ground for confidence, but a quick move will now be made to put the hypothesis on an altogether sounder basis.

(4) BEHAVIOUR OF THE SINGLE-OXIDE SYSTEMS ON PLATINUM CORES

(4.1) Comparative Behaviour of the Single-Oxide Systems

The single-oxide systems of barium and strontium platinum-cored S-type assemblies are made up in precisely t same way as the standard equimolar double-oxide syste Care is taken to ensure the maintenance of the standard 150 μ thickness and the densities are kept at about 1·0, i.e. about on fifth of the volume of each type of matrix is occupied by so matter. After removal from the pump both the barium- and t strontium-oxide systems are given a 10 min activation run w zero current at 1 250° K in a manner similar to that describ for the double-oxide system.

A sample of each single-oxide system is now set up for a zer current run at 1 020° K and both are measured at appropri intervals of time for the ratio R_2/R_1 at 650° K. The reason the change from the usual 550° K will become apparent fr Section 4.2, but implies no significant alteration in testi method or principle.

The behaviour of the barium-oxide system is at once remar able and revealing in that it shows no separation of R_1 and R_2 the zero-time test in the 1 020° K life run. In other words, ov the whole test period at 650° K, R_1 and R_2 remain the same, i $R_2/R_1 = 1$.

In marked contrast, the strontium-oxide system shows even larger resistance separation than a double-oxide syste and starts life with $R_2/R_1 = 3{\cdot}3$. Results of a typical test ov an extended zero-current run at 1 020° K are shown in Fig. 1

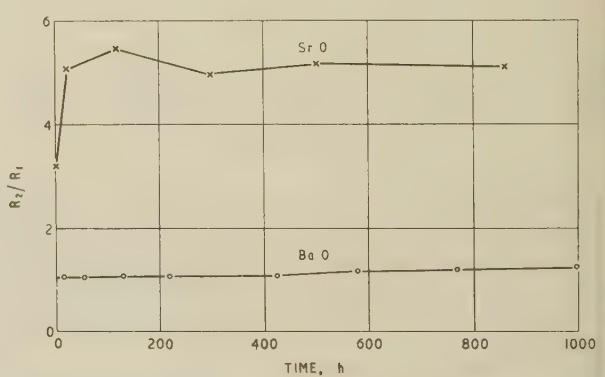

Fig. 13.—R_2/R_1 for single oxides on platinum cores plotted again operating time at 1 020° K.

from which it will be seen that the strontium-oxide case sta life with a considerable free-ion concentration which increas in the first 100 hours to an equilibrium level. It behaves, fact, in very similar fashion to the double-oxide case. T barium-oxide system is entirely different, starting life with free-ion content and effectively acquiring none during 1 000 hou of zero-load operation at 1 020° K.

A typical example of a test measurement at 650° K is sho in Fig. 14 as a continuous line. The test has been extended 80 min, in contrast to the usual 20–30 min for the double-oxi case at 550° K, and this point will be discussed in Section 4 The lack of any free negative-ion content in the barium oxide clearly apparent.

A number of firm conclusions can now be set out in t following terms:

> (*a*) The barium-oxide matrix on platinum at 1 020° K is a sta system undergoing no dissociation into free ions.
> (*b*) The strontium-oxide matrix on platinum at 1 020° K is unstable system spontaneously generating free negative ions.

(*c*) The double-oxide matrix on platinum at 1 020° K is an unstable system arising from the spontaneous dissociation of the strontium-oxide component accompanied by the appearance of free negative ions.

(*d*) The free negative ions are those of oxygen.

(*e*) For every free negative ion of oxygen liberated into the hollow pore system, one positive ion of stronium must be dissolved in the solid particle system.

(*f*) The possibility of some undetected residual gas action causing the $R_2/R_1 > 1$ phenomenon, as suggested in Section 3.11, is now rigorously excluded by the $R_2/R_1 =$ constant $\simeq 1$ result for the barium-oxide case.

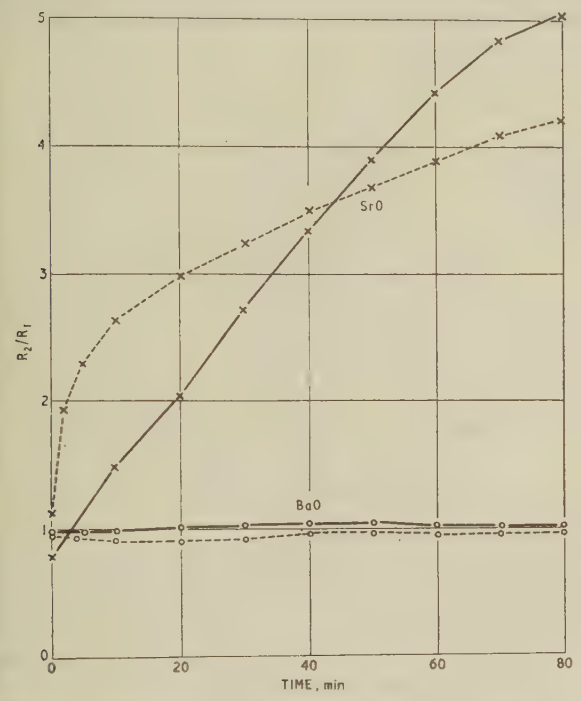

Fig. 14.—Stability of R_2/R_1 at 650° K for single oxides.
—— On platinum.
---- On O-nickel.

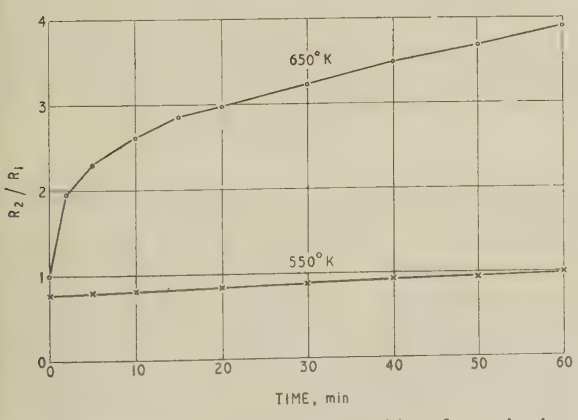

Fig. 15.—Temperature dependence of mobility of negative ions on strontium oxide.

(4.2) Mobility and Diffusion of the Free Negative Ion on Strontium Oxide

For the double oxide at 550° K under a constant applied potential $V_A = 0{\cdot}50$ V the two resistances have separated from equality to the steady condition $R_2/R_1 = 6$ in about 30 min. Re-establishment of a uniform ion distribution by diffusion takes about the same time.

Mobility of the free negative ion on strontium oxide is much slower, and Fig. 15 shows that 550° K would be a quite impracticable measuring temperature for R_2/R_1. It is for this reason that 650° K has been chosen, and even here the test time must be extended to 90 min. For comparison of the barium and strontium oxide cases in Fig. 13 all R_2/R_1 measurements were made with $V_A = 0{\cdot}50$ V at 650° K with a test time of 90 min.

Diffusion of the free ion under a concentration gradient in strontium oxide can be shown by the method of Section 3.6 to be very much slower than that in the double oxide.

(4.3) Behaviour of the Barium-Oxide System under prolonged Current Loading

Close scrutiny of Fig. 13 will show that R_2/R_1 for barium oxide is almost constant at unity for the 1 000 hour test run, but not absolutely so. There is therefore the probability of a free ion generation by barium oxide, but at incomparably slower rate than by strontium oxide.

Suppose now that the barium-oxide system is given a current loading of 20 mA at 1 020° K for 100 hours. It was stated as a hypothesis in Part 8 that the electrons pass vacuum-wise through the matrix, making repeated inelastic collisions with the solid particles and so raising their temperature. Owing to their random arrangement, a few particles are raised to a temperature much higher than the ambient of 1 020° K, and these tend to dissociate thermally. The negligibly slow dissociation rate of Fig. 13 may therefore be greatly accelerated by the passage of current. This proved in practice to be the case, and a load of 20 mA for 100 hours leaves the barium-oxide system with a measurable concentration of free negative ions. These ions show all the properties described in Section 3, except that the mobility on barium oxide is less than on the double oxide but greater than on strontium oxide, i.e. the order of increasing mobility is

$$\text{SrO} < \text{BaO} < \text{BaSrO}$$

If, after the generation of a free-ion concentration by current loading, the barium-oxide system is heated to 1 250° K for 1 min, the free ions are driven out of the system into the surrounding vacuum. The system now reverts to the basically ion-free state shown in Fig. 13. For the remainder of the present Part it will suffice to consider barium oxide as essentially stable in comparison with strontium oxide, which is essentially unstable.

(4.4) Second Hypothesis

The first hypothesis set out in Section 3.12 can now be rewritten in more definite form:

> A platinum-cored S-type assembly with barium-strontium-oxide matrix running with zero current at 1 020° K generates oxygen in negative-ion form. These oxygen ions arise from a spontaneous dissociation of the strontium-oxide component of the matrix.

A question which arises at this stage concerns the nature of the dissociation of the strontium oxide. Is it a spontaneous thermal dissociation or is it associated in some way with the platinum cores of the assembly? It will be recalled that strontium metal is readily soluble in platinum at 1 020° K and the dissociation might conceivably be associated with this property at the platinum/strontium-oxide interface. This question will be answered in the next Section.

(5) BEHAVIOUR OF SINGLE-OXIDE SYSTEMS ON NICKEL CORES

(5.1) Comparative Behaviour of Single-Oxide Systems

The standard S-type assembly with nickel cores is made up in exactly the same form as the platinum-cored assemblies used in

Sections 4 and 5. The only point calling for comment concerns the nature of the core metals and the probe wire. Two kinds of core metal were used—active O-nickel containing small amounts of magnesium and silicon,* and a very pure nickel containing 4% tungsten. The first variant is a chemically active one and the second can be regarded as very mildly active. In both cases the 1-mil probe wire was of pure nickel.

The valves were processed in the same way as the platinum systems and given an initial zero-current activation run at 1 250° K for 10 min. Thereafter both types were set up for life test with zero current at 1 020° K and removed from time to time for measurement of the R_2/R_1 ratio at 650° K. A typical set of measurements at the 100-hour test point is set out as the broken lines in Fig. 14.

The results are exactly comparable with those obtained with platinum cores. With a barium-oxide matrix R_2/R_1 remains at about unity, and with strontium oxide R_2/R_1 increases from unity to 4·3 in the 80 min test.

Another case with O-nickel cores is set out in Fig. 16 and shows both systems at 650° K tested for 30 min in each direction in turn. The barium-oxide case is typical in that it is constant but rather greater than unity in one direction and constant but rather less than unity in the other. The strontium-oxide case is an obvious time-dependent function in both directions.

Work on cores of 4% tungsten-nickel gave similar results.

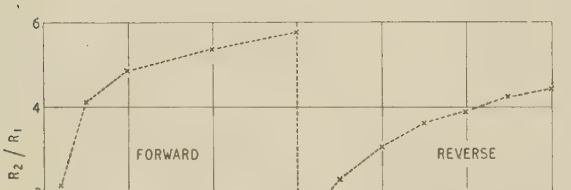

Fig. 16.—R_2/R_1 for active-nickel-cored S-type assemblies in forward and reverse directions.

—— Barium oxide.
---- Strontium oxide.

(5.2) Third Hypothesis

The results obtained on nickel-core systems show clearly that the dissociation of the strontium-oxide molecule is independent of the type of core metal employed. It is therefore concluded that the dissociative action is purely thermal.

The hypothesis in Section 4.4 can thus be simplified into the following terms, which omit any reference to the nature of the core metal:

> A barium-strontium-oxide matrix running with zero current at 1 020° K generates oxygen in negative-ion form. These oxygen ions arise from a spontaneous thermal dissociation of the strontium-oxide component of the matrix.

(6) WORKING MODEL OF THE DISSOCIATION PROCESS

It has been observed that the concentration of free negative ions in a platinum-cored barium-strontium-oxide system at 1 020° K rises to an equilibrium level which is apparently maintained unchanged over 1 000 hours or more. An attempt will now be made to develop a working model which will explain this equilibrium concentration. The model will then be further developed to predict the effect of changing the chemical characteristics of the core metals.

* The British Valve Manufacturers' Association's specification for O-nickel limits magnesium to 0·05–0·10% and silicon to a maximum of 0·05%. Typical concentrations are 0·07% and 0·03% respectively.

(6.1) Equilibrium Pressure in a Closed System

Consider a barium-strontium-oxide matrix at 1 020° K of the usual density and completely filling a closed box whose walls are neutral to both oxygen and strontium ions.

It will be assumed that at zero time the matrix is stoichiometric and the hollow pores are devoid of free ions. Our object is to determine the increase of gas content of the pores as a function of time. The closed system is represented diagrammatically in Fig. 17(*a*).

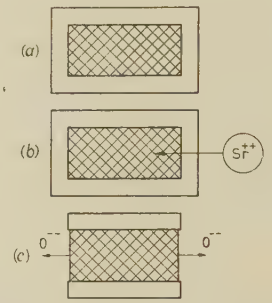

Fig. 17.—Various matrix arrangements.

(*a*) Closed system.
(*b*) Closed system with strontium injection.
(*c*) Open system.

The strontium-oxide component of the matrix is subject to thermal dissociation. The energy of the molecules follows a Maxwellian probability distribution and the rate of dissociation, n, will therefore be proportional to the total number of strontium oxide molecules in the system. The number of free negative ions of oxygen liberated into the hollow pores in time t is therefore nt. This rate of liberation is shown in Fig. 18(*a*) as the straight broken line of slope n.

As the number of free ions of both types increases, they begin to encounter each other during their diffusive travels and to recombine. The probability of such recombination increases in proportion to the number of ions present, and we have therefore superimposed on a constant and unchanging dissociation rate n, a time-dependent recombination rate, q_t, where

$$q_t = kN_t$$

where k is a constant of proportionality and N_t is the number of free oxygen ions present in the pores at time t.

The recombination rate increases with time but cannot exceed in magnitude the constant dissociation rate n. The system therefore moves to an equilibrium condition where $q_e = n$. The total free-ion concentration, N_t, of the matrix therefore takes the shape of the solid line in Fig. 18(*a*), levelling out at an equilibrium value N_e.

Since N_t is the number of free oxygen ions present in the hollow pores at time t, the total gain of ions in time dt is dN_t, and

$$dN_t = ndt - kN_t dt$$

or

$$\frac{dN_t}{dt} + kN_t = n$$

The solution of this first-order differential equation is

$$N_t = A\varepsilon^{-kt} + n/k$$

At $t = 0$ and $N_t = 0$, $A = -n/k$

nd therefore

$$N_t = \frac{n}{k}(1 - \varepsilon^{-kt})$$

nd $N_e = n/k$

The concentration of oxygen ions in the system is therefore irectly proportional to the dissociation rate and inversely roportional to the recombination rate. At any one temperature he dissociation rate, n, is inalterably fixed by the total number f strontium-oxide molecules in the system, but practical means re available for altering the recombination rate, q_t. The ffects of such an alteration are shown in Fig. 18(*b*).

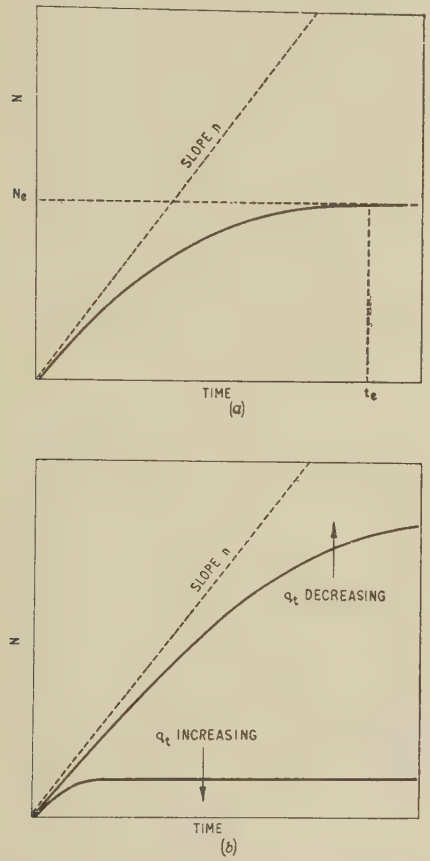

Fig. 18.—Characteristics of N/t in a closed system.

(6.2) Injection of Barium or Strontium Ions

Suppose now that we elaborate the simple closed-box system f Fig. 17(*a*) to the closed system (*b*), which has the ability to ject ions of barium or strontium metal. As the concentration alkaline-earth metal increases in the matrix the migrating xygen ions will find their partners more easily, the recombina- on rate increases and the oxygen concentration, N_t, falls. When e injection of metal ceases, a new and lower equilibrium level, $_e$, is established. If, however, the injection process is taken r enough, the oxygen concentration becomes vanishingly small, though the rate of oxygen generation, n, remains unaltered.

The thermionic activity of the matrix measured by its con- ntration of excess alkaline-earth metal is therefore an inverse nction of the free oxygen-ion equilibrium concentration, N_e. other words, although n oxygen ions are generated per second respective of the activity state of the matrix, their lifetime is intimately connected with the activity state. In a highly active matrix the lifetime is short and in an inactive matrix it is long.

Suppose now we apply an electric field across a barium-strontium-oxide system at 1 020° K. The free oxygen ions possessing mobility tend to drift into the trailing section and develop the condition $R_2/R_1 > 1$. The time taken to make the journey from leading to trailing section is appreciable, and the lifetime of an oxygen ion must be greater than this if the journey is to be successfully completed. If the ion lifetime is much smaller than the essential travel time, there will be no arrivals and the condition of the matrix will remain that of $R_2/R_1 = 1$. A sufficiently active matrix should therefore hold the condition $R_2/R_1 = 1$ despite the fact that oxygen-ion generation is continuing at an unchanging rate, n. In short, if the oxygen-ion lifetime is sufficiently small, the matrix should exhibit the 'gas-free' condition $R_2/R_1 = 1$. The term 'gas-free' is therefore a misnomer.

Methods of injecting barium and strontium ions into the matrix will be examined in Section 7.

(6.3) Oxygen Ion Loss from an Open System

Suppose the closed double-oxide system in Fig. 17(*a*) is run at 1 020° K to reach its equilibrium oxygen concentration, N_e. In each of the hollow pores there will exist a gaseous pressure, P_e, with the oxygen ions distributing themselves partly within the vacuum and partly on the solid particle walls. The fraction, θ, of the particle walls covered with adsorbed oxygen ions might be imagined to follow Langmuir's isotherm,

$$\theta = \frac{P_e}{1 + aP_e}$$

where a is a term involving temperature, here regarded as constant.

If the closed box is itself enveloped in a vacuum and its narrow sides are removed, as in Fig. 17(*c*), the following action will occur. The edge-wise pores are now exposed to a vacuum and P_e falls to zero. The ion coverage, θ, of these particular pores likewise tends to zero, thereby creating a concentration gradient and a diffusive flow of ions from the interior. The system therefore leaks oxygen ions into the surrounding vacuum, and this action is equivalent to an increase in the recombination rate q_e.

The rate of ion leakage is quite unknown, of course, but it may be very slow. At a vacuum boundary the oxide surface is covered by a space-charge cloud of electrons, and this will tend to hinder the escape of the negative ions. A further inhibiting action will be the image force set up by an ion as it leaves the surface.

(7) ACHIEVEMENT OF THE $R_2/R_1 = 1$ CONDITION IN BARIUM-STRONTIUM-OXIDE SYSTEMS

(7.1) Active-Nickel-Core System

The obvious way of injecting barium or strontium ions into the system is to use an active-nickel core metal containing some such reducing agent as magnesium, i.e.

$$\mathrm{Mg} + \mathrm{XO} \rightarrow \mathrm{MgO} + \mathrm{X}$$

where X is barium or strontium.

Fig. 19 shows a typical life-test characteristic at 1 020° K of a standard double oxide S-type assembly with O-nickel cores. Initially the R_2/R_1 ratio is large but it decreases steadily to a value approaching unity after a few hundred hours. At the end of this 600-hour activating run the tube was kept on life test at 1 020° K with zero current for 1 000 hours. During this period R_2/R_1 was measured periodically at 550° K. The ratio remained

constant and the resistances at 550° K showed no separation. In other words, the assembly has achieved a high state of activation wherein the recombination rate q_t is too great to permit movement of negative ions from leading to trailing section.

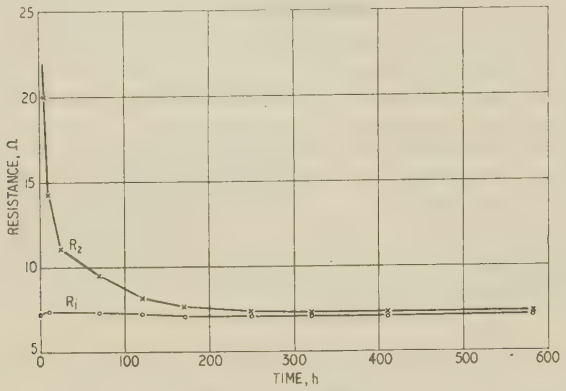

Fig. 19.—Characteristics of R/t for an active nickel core S-type assembly.

The cause* of the $R_2/R_1 > 1$ state during the first 100 hours or so of Fig. 19 is obviously the thermal dissociation of the strontium-oxide component in a matrix of low initial activity and a consequent low recombination rate q_t.

(7.2) Platinum-Core System

The active-nickel-cored double-oxide system achieves the $R_2/R_1 = 1$ state by virtue of its chemical ability to generate free alkaline-earth metal at 1 020° K. The equivalent platinum-cored system possesses no such ability, but it has one interesting physical property which does, in fact, enable it to achieve the $R_2/R_1 = 1$ state.

Suppose a standard S-type assembly with a double-oxide matrix is heated for a short time at 1 450° K. At this relatively high temperature the rate of dissociation of the strontium oxide is high. The free oxygen ions leak rapidly from the system into the surrounding vacuum, as described in Section 6.4, and the strontium metal ions dissolve in the matrix. As the concentration of Sr^{++} in the matrix increases, the metal commences to flow towards the platinum cores and a solid solution of strontium builds up in the platinum. The concentration of this solid solution increases with the time of action. If the system is now set at the usual 1 020° K, there occurs a back diffusion of strontium metal from its solid solution in the core into the oxide matrix. We have, in fact, built a strontium-metal generator into the platinum system and this produces an effect similar to that of an active nickel core.

The whole action is demonstrated in the following way. A standard barium-strontium-oxide assembly with platinum cores and probe wire is heated with zero current flowing at 1 450° K for 1 min. The system is then run for 20 hours with zero current at 1 020° K to permit the free-ion build-up from the dissociation of strontium oxide, and R_2/R_1 is measured at 550° K in the usual manner. This sequence of operations is then repeated until R_2/R_1 has been measured over a total range of time, t_{con}, of operation at 1 450° K; $t_{con} = 12$ min is adequate to bring the ratio to a constant value.

* In Part 2 of the paper this initial fall of R_1 was thought to be due to the gradual removal of a residual gas (carbon monoxide) by getter action. The presence of the residual gas was considered due to inadequate technical processing of the S-type assembly. The constancy of R_2/R_1 at unity for barium-oxide systems throughout life has now shown the earlier view to be false.

Fig. 20 shows R_1 and R_2, measured after the standard 30 mi operation at 550° K, plotted against units of 1 min of time t_{co} at 1 450° K. It will be clear that the more significant paramete R_2 decreases steadily until it coincides with R_1 after $t_{con} = 10$ mi The changes of R_2 under the constant potential $V_A = 0{\cdot}5$ V fo the 30 min of the assessment test at 550° K are shown in Fig. 21 After about 9 min of the high-temperature treatment R_2 i virtually constant and coincident with R_1 over the whole 30 mi of the test.

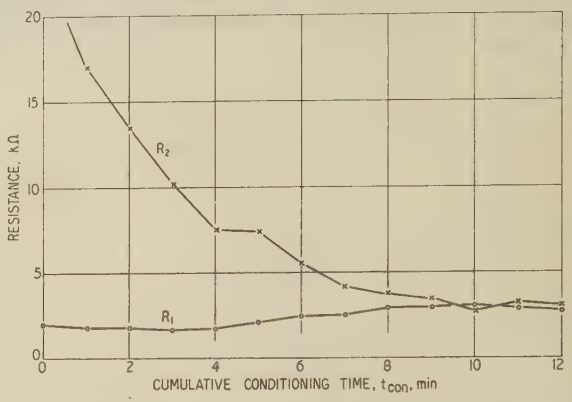

Fig. 20.—Characteristics of R_1 and R_2 against cumulative conditionin time, t_{con} at 550° K.

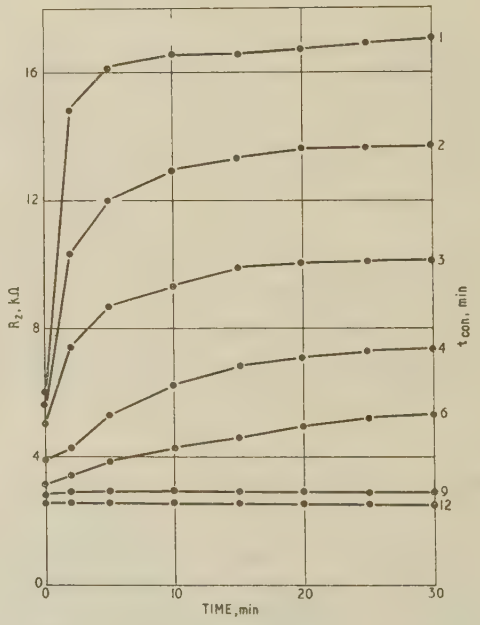

Fig. 21.—Characteristics of R_2 at 550° K.

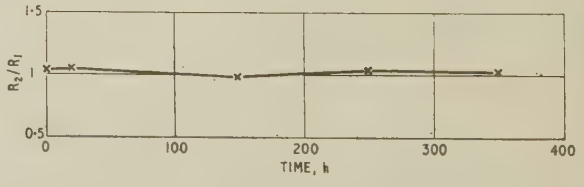

Fig. 22.—Stability of R_2/R_1 for S-type assembly with strontium dissolved in the platinum cores.

The assembly is operated at 1 020° K with zero current, and R_2/R_1 is measured a 550° K.

After attainment of the $R_2/R_1 = 1$ state, the assembly was run t 1020° K with zero current for a test period of 400 hours. eriodical measurements of R_2/R_1 were made at 550° K (see ig. 22). It is apparent that the strontium-in-platinum cores are cting as effective strontium generators over a long period of me and the system is behaving in identical fashion to one with ctive nickel cores.

(8) CONCLUSIONS

The following conclusions can now be drawn from the work:

(*a*) A barium-strontium-oxide matrix operating at 1020° K ith zero current passing is subject to thermal dissociation volving negative ions of oxygen at a constant and inalterable ate n.

(*b*) The component of the matrix subject to thermal dissocia- ion is strontium oxide. By comparison the barium oxide is ssentially stable and contributes only a negligible fraction of he free oxygen ions.

(*c*) Positive ions of strontium metal are generated at a constant nd inalterable rate n.

(*d*) The free oxygen ions remain in the hollow matrix pores where they move easily under electric force or concentration gradient.

(*e*) Recombination of the oxygen and strontium ions occurs at an increasing rate q_t until the system comes into equilibrium, when $q_e = n$.

(*f*) The equilibrium concentration, N_e, of free oxygen ions in the pores of the matrix is proportional to the dissociation rate and inversely proportional to the recombination rate.

(*g*) The recombination rate q_t increases in proportion to the n-type activity of the matrix, i.e. to its total concentration of alkaline-earth metals.

(*h*) In a thermally-activated barium-strontium-oxide matrix the donor is almost wholly strontium metal.

(9) ACKNOWLEDGMENTS

Acknowledgment is made to the Engineer-in-Chief of the Post Office for permission to use the information contained in the paper. The author also wishes to thank Mr. H. Batey for skilled assistance throughout the work.

621.385.032.213.13

The Institution of Electrical Engineers
Monograph No. 444
May 196

THE CONDUCTIVITY OF OXIDE CATHODES

Part 11.—Thermal Stability of the Alkaline-Earth Oxides

By G. H. METSON, M.C., D.Sc., Ph.D., M.Sc., B.Sc.(Eng.), Member, and H. BATEY

(*The paper was first received* 18*th November*, 1960, *and in revised form* 12*th January*, 1961. *It was published as an* INSTITUTION MONOGRAPH *in May*, 1961)

SUMMARY

The three common alkaline-earth oxides are examined for thermal stability at 1 200° C. In an experimental arrangement involving a massive evaporation from a platinum substrate it is shown that barium oxide is removed in the form of unchanged molecules while strontium and calcium oxides leave the substrate in elemental form as metal and oxygen. It is concluded that the dissociation is a thermal one and not concerned with the nature of the substrate.

(1) INTRODUCTION

It was shown in Part 10 that the standard S-type assembly with platinum cores tends to accumulate free negative ions within the hollow pores of the matrix. This growth of pore gas pressure was traced to a thermal dissociation of the strontium-oxide component, although the barium-oxide component was found to be essentially stable. The supporting evidence was based wholly on the resistive effects produced by moving the ion cloud in the matrix under an electric field. It is proposed here to examine the relative thermal stability of the two oxides by a method using a more direct experimental approach. The main conclusions of the previous Part are amply confirmed.

(2) EXPERIMENTAL ARRANGEMENTS

The experimental valve used is shown in Fig. 1. A rectangular-box core A, of pure platinum and fitted internally with an insulated heater, is fixed by metal supports in an evacuated glass envelope. The core has the same dimensions as that used in the standard S-type assembly; one side of it is covered with alkaline-earth oxide, and to the other, uncoated, side is welded a thermocouple, T_1T_2. Opposite the oxide coating of the core is a small lead-glass cylinder with nickel-iron wires fused to its extremities, which are coated with graphite to ensure good contact between the connecting wires and the sides. One electrode of the cylinder is led out of the envelope by way of a top-cap seal and the other by way of the pinch at the bottom of the assembly. Both pinch and envelope are of lead glass. Barium-metal getters are fitted in the recess of the pinch.

The core is sprayed in the usual way with alkaline-earth carbonate using a poly-*n*-butyl methacrylate binder. After assembly, the valve is mounted on a bench pump and its pressure reduced to 10^{-5} torr. The envelope is then baked at 400° C for 1 hour and allowed to cool. Power is finally applied to the core heater to decompose the carbonate at about 1 000° C and the temperature is reduced to 700° C when the pressure has fallen to 5×10^{-6} torr. The getters are then flashed and the tube is sealed off from the pump.

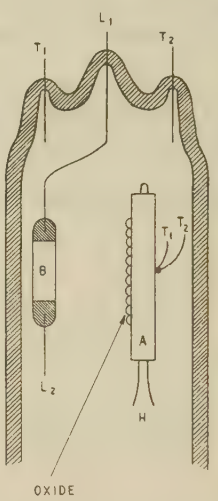

Fig. 1.—Layout of experimental valve.

The manner of electrical operation is shown in Fig. 2. Th glass cylinder, of resistance R, is arranged in series with a 1 M resistor and an accurate potential of 1·00 V is maintained acro them. This potential is observed by a multi-range vibratin capacitor electrometer measuring from 0·1 to 1 000 mV. Wit the overall voltage constant at 1 V, the potential, v, across th resistor is measured as a function of core testing time. Thu

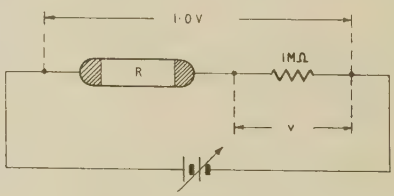

Fig. 2.—Electrical circuit.

when $R \gg 1\,M\Omega$, v is zero and, when $R \ll 1M\Omega$, v approach its maximum value of 1 000 mV. In other words, v is a co venient measure of the electrical *conductivity* of the glass cylinde The actual conductivity of the cylinder can be readily comput from v but is of little practical importance. After pump proces ing the valve is ready for testing and in all cases has a resistanc R, greater than 1 000 MΩ.

The conduct of the experiment is simple. Power is appli to the core heater until the core temperature has reached a pr determined value, T degrees Celsius as indicated by the therm couple. This temperature is accurately maintained througho the test run, which may last several hundred hours. During th period the following observations are made:

(*a*) The visual appearance of the evaporated films on the gla cylinder and on the walls of the envelope is noted, with the aid the 'shadow' cast by the cylinder on the envelope.

The paper is a continuation of Monographs Nos. 221 R and 243 E, published in February and June, 1957 (see 104 C, pp. 316 and 496), Nos. 268 R, 269 R and 289 R, published in December, 1957, and February, 1958 (see 105 C, pp. 183, 189 and 374), No. 317 R, published in November, 1958 (see 106 C, p. 55), Nos. 347 E and 357 E, published in October, 1959, and February, 1960 (see 107 C, pp. 91 and 158), No. 397 E, published in September, 1960 (see 108 C, p. 83) and No. 443 E, published in May, 1961 (see p. 438).

Correspondence on Monographs is invited for consideration with a view to publication.

Dr. Metson and Mr. Batey are at the Post Office Research Station.

(*b*) The value of the potential, v, is observed.
(*c*) The heater power required to maintain the core at the constant temperature T is measured.
(*d*) The 'cold' resistance of the heater is recorded.

Core temperatures of 1 100 and 1 200° C were found to be convenient. A preliminary experiment conducted with a pure platinum core with no oxide coating confirmed the calculated prediction that evaporation of platinum would have no measurable effect on the resistance of the cylinder under the conditions of the experiments.

The cold resistance of the insulated tungsten heater showed no significant change in any experiment and will receive little further attention.

(3) EXPERIMENTAL RESULTS

(3.1) Barium-Strontium Oxide

The barium-strontium oxide is arranged to be 150 μm thick with a specific density of 0·7. It is derived from the usual co-precipitated equimolar carbonates.

In the first experiment the core is maintained at a constant temperature of 1 100° C, while v is observed over a period of 500 hours. The result (Fig. 3) shows a slow and irregular increase in conductivity over the first 250 hours followed by a rapid increase up to a steady high level approaching the maximum possible value, $v = 1\,000$ mV. During the whole of this constant-temperature run the core heater power shows a slow but significant increase, although the cold resistance of the insulated tungsten heater remains substantially constant.

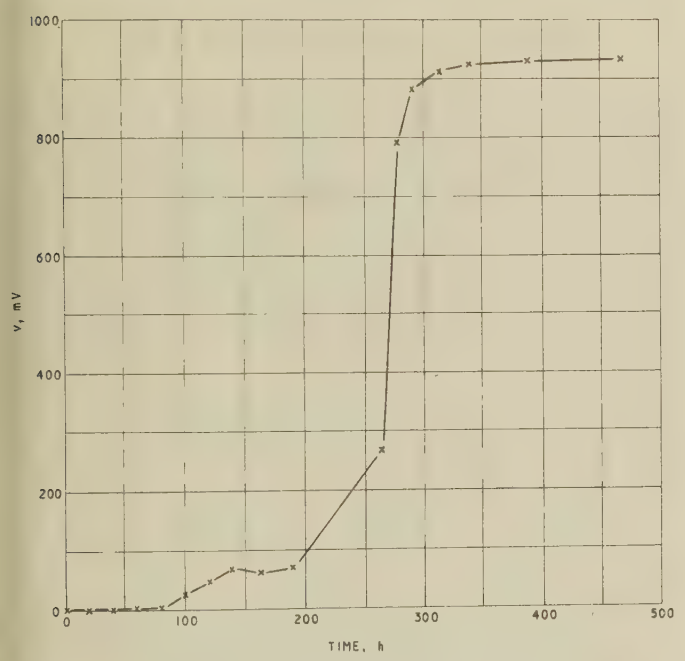

Fig. 3.—Characteristic of v/time for barium-strontium oxide at 1 100° C.

At zero time the glass envelope opposite the hot oxide is quite clear and shows no trace of evaporated film. After about 100 hours, however, a film is clearly visible in the form of concentrically arranged bands of colour (Newton's rings). At this stage the film, although exhibiting clear colour bands, is quite transparent. With time, the bands become more pronounced until at about 250 hours they begin to lose their clear transparency and become increasingly grey. This trend quickens after the steep rise of conductivity at 250 hours until the film approaches a state which might be described as black. The density of this black film may be sufficiently great to obscure the interior of the tube. If the tube is opened to the atmosphere the black film disappears instantly, leaving a white film of varying opacity. The conductivity of the cylinder also falls to zero.

The results of a similar experiment carried out at $T = 1\,200$° C are shown in Fig. 4. All the same qualitative features are observed, although the irregular plateau before the steep rise of v is much more pronounced.

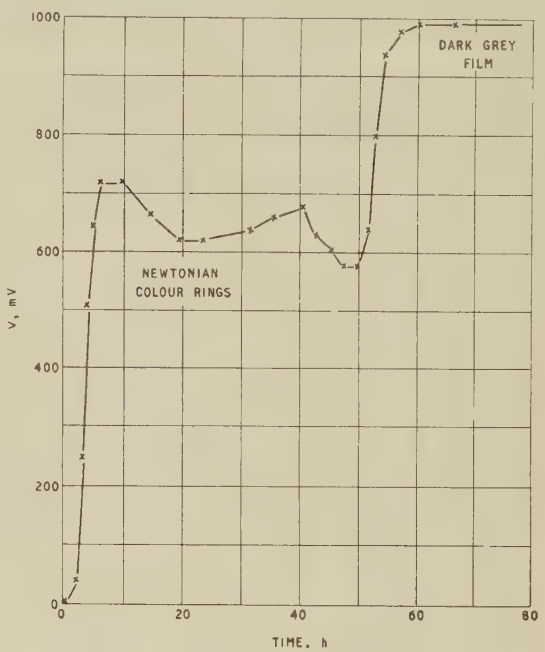

Fig. 4.—Characteristic of v/time for barium-strontium oxide at 1 200° C.

(3.2) Barium Oxide

The barium oxide is arranged to have a thickness of 150μm with a specific gravity of 0·7 and is derived from analytically pure barium carbonate. Two experiments were undertaken: at 1 100° C for 500 hours and at 1 200° C for 200 hours. Qualitatively identical results, differing only in the time scale, were obtained for both runs.

At 1 200° C the initial resistance of the glass cylinder was greater than 1 000 MΩ and it showed no measurable change in 200 hours. Similarly the core-heater power showed no significant change during the test run, in marked contrast to the double-oxide case.

The circumstances of the film growth on the glass envelope are significant in that the strongly demarked Newtonian colour rings remained quite transparent and unchanged after the first 10 hours of the whole run, and no sign of grey deposit appeared during the experiment.

Observation of the platinum core itself showed that after the first 10 hours the whole of the barium oxide had evaporated leaving the platinum surface quite clean. (This differs from the double-oxide case, where some oxide coating remained at the end of the experiment.) The test was continued for a further 190 hours to prove that platinum evaporation had no measurable effect on v—a result which is used in the next Section.

(3.3) Strontium Oxide

The strontium-oxide layer was 180 μm thick, with a specific gravity of 0·7, but thinner coatings have been used and will be

mentioned in the text. The temperature of the tests has been limited to 1 200° C.

Typical results for two thicknesses of strontium oxide are shown in Fig. 5 with one for barium oxide for reference purposes. Extension of these characteristics to 200 hours shows no measurable change from those noted at 100 hours. In marked contradistinction to the barium-oxide case, the value of v for the strontium-oxide system rises in a smooth regular curve from zero to the maximum value, $v \simeq 1\,000$ mV. There is, moreover, no plateau effect, such as occurs in the double-oxide case. Much of the oxide still remained on the platinum core at the end of the experiment.

The influence of spray thickness was investigated and it was found that the rate of rise of v to its maximum value increased with decrease of thickness. (See Fig. 5.)

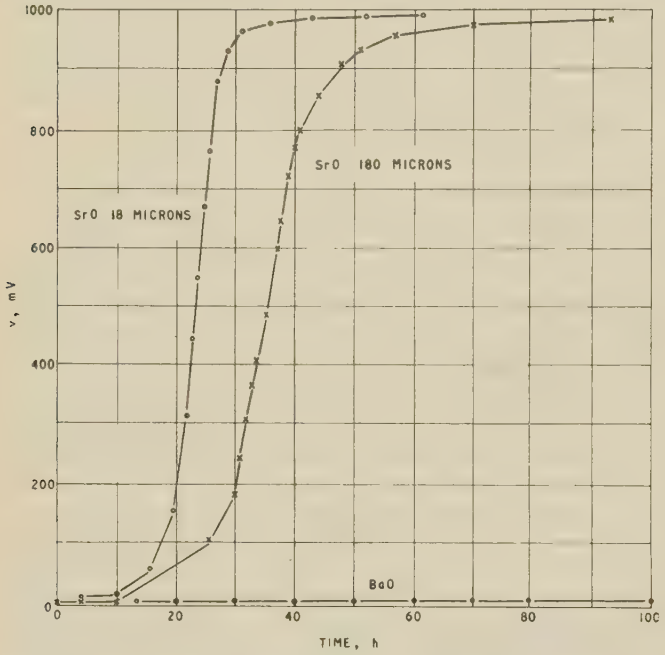

Fig. 5.—Characteristic of v/time for strontium oxide and barium oxide at 1 200° C.

The circumstances of visible film growth on the glass envelope were particularly interesting in the case of strontium oxide. Careful observation revealed no trace of the coloured Newtonian rings. The shadow edge on the glass envelope behind the glass cylinder was a uniform grey when it first became visible, and the only change with time was a steady increase in density. Films of almost black opacity were obtained. On opening the envelope to the atmosphere such films instantly turned white.

(3.4) Mechanism of the Strontium-Oxide Dissociation

If two systems of barium oxide and strontium oxide respectively are run at 1 200° C and the core heater powers are measured as functions of time, it is found that the heater power required for the barium oxide falls slightly as the oxide evaporates from the core and then remains substantially constant. In the strontium-oxide case, however, the required core-heater power rises sharply to a maximum value, where it remains roughly constant for a time which is dependent on the thickness of the coating. If the strontium-oxide coating is sufficiently thin this maximum is soon passed and the heater power declines slowly to a value rather lower than the initial value. A comparative example of two thin coatings of about 5 μm thickness is shown in Fig. 6 for a run of 100 hours at 1 200° C. For a thicker coating (e.g. 180 μm), the heater power required for strontium oxide rises to a higher value and then remains substantially constant for 200 hours or more.

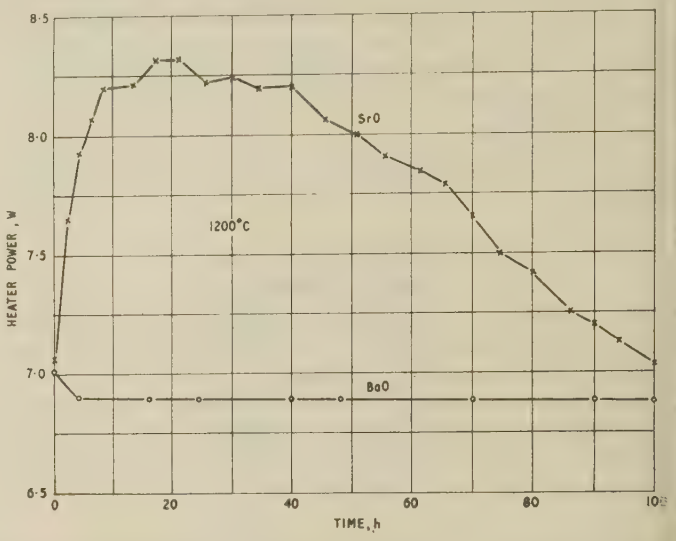

Fig. 6.—Characteristic of heater power/time for barium-oxide and strontium-oxide systems maintained at 1 200° C.
Initial thickness is about 5 μm.

The experimental process can now be taken a step further. Two systems with 150 μm thick coatings are run for 100 hours at 1 200° C. Both envelopes are then cracked open and the platinum cores recovered. The barium oxide has evaporated from its core, which is bright and shining with the platinum crystal boundaries clearly defined. The other core, still covered with the more involatile strontium oxide, is cleaned with dilute acid, thoroughly washed and dried for microscopic examination. That part of the core previously covered by strontium oxide is seen to be deeply etched, of a dull matt grey colour, and showing no sign of the platinum crystal boundaries. The reclaimed core is now fitted with a new heater, remounted in the standard assembly shown in Fig. 1, and run at 1 200° C for 100 hours. The observed relationship, v/time (Fig. 7), shows that the measurable conductivity of the test cylinder has risen from zero to a maximum. At the same time, the glass envelope has been coated with a dense black deposit. At zero time the core-heater power was 9·6 W and this has decayed only to 9·0 W after 100 hours; thus the thermal emissivity of the core is still high and the strontium reservoir is not yet exhausted.

Assuming that the matt-grey core surface is an alloy of platinum and strontium metal, the experiment proves:

(*a*) That after thermal dissociation the oxygen element is the first to leave the system, followed later by the strontium element.

(*b*) That the increase in core-heater power required to maintain a constant core temperature is due to the high thermal emissivity of the platinum-strontium alloy.

The reclaimed core, which had originally been coated with barium oxide, showed no evidence of the evaporation of any dissolved barium metal.

Both barium and strontium dissolve readily in platinum at red heat, and the constancy of the core-heater power and absence of dissolved barium in the barium-oxide case are strong evidence in support of the thermal stability of barium oxide.

(3.5) Nature of the Films

Some information concerning the nature of the films can be obtained from their temperature characteristics. In the strontium-oxide cases shown in Fig. 5 and the special case in

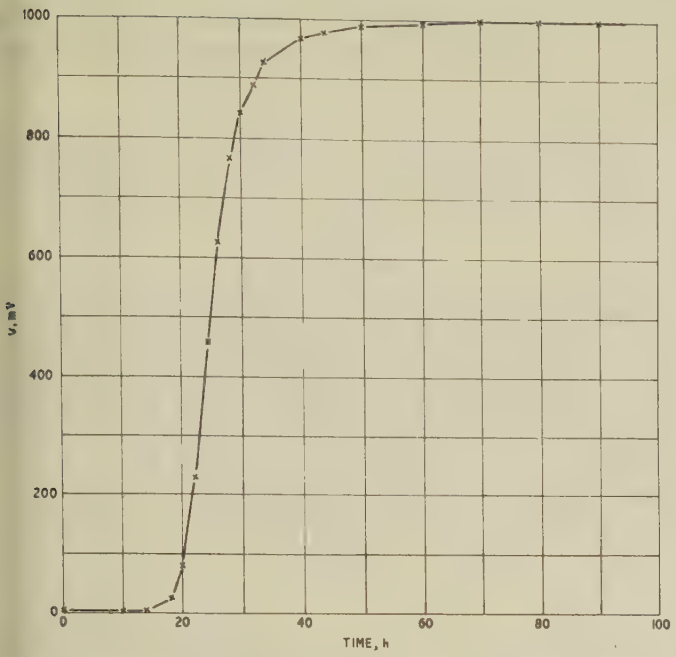

Fig. 7.—Evaporation of strontium metal from a reclaimed platinum core at 1 200° C.

Fig. 7 the films have virtually no temperature dependence and are represented by the upper characteristic in Fig. 8. The data have been presented in the conventional form of a plot of the logarithm of the conductivity against the reciprocal of the glass-cylinder temperature. The latter is measured by a thermocouple fixed to the cylinder which receives its heat by radiation from the heated platinum core.

The double-oxide case has been measured in the plateau condition shown in Fig. 4 after 30 hours' running, and its characteristic is shown in the lower half of Fig. 8. Clearly the characteristic is that of a semiconductor and must be interpreted as that of barium oxide activated by strontium metal. As the evaporation proceeds for 80 hours or more, a layer of metallic strontium overlays the activated barium oxide and the conductivity/temperature characteristic gradually levels off to approach the 'metal' form of the upper graph.

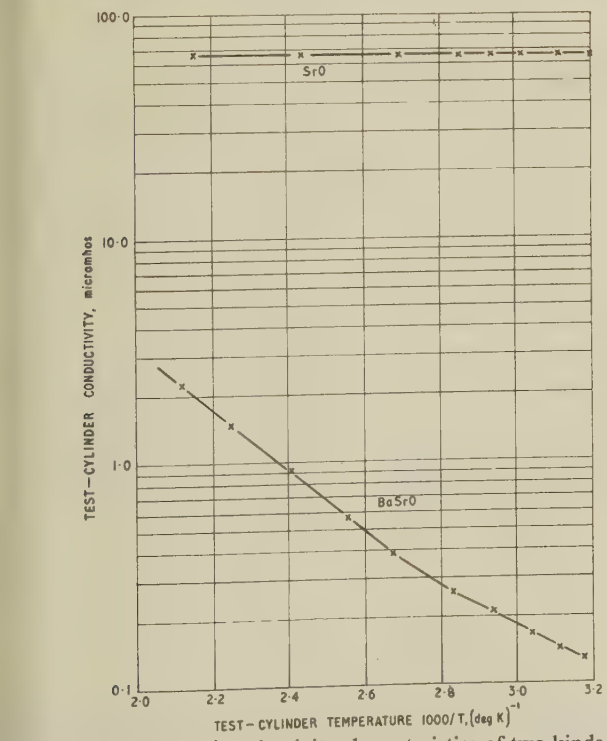

Fig. 8.—Temperature/conductivity characteristics of two kinds of film.

The pure barium-oxide case has not been examined, since the conductivity is always too small to measure with the available apparatus. It probably evaporates and condenses in something approaching stoichiometric form.

(3.6) Calcium Oxide

So far it has become clear that barium oxide evaporates as a molecule from a platinum substrate while strontium oxide dissociates with a loss of oxygen to the surrounding vacuum and a storage of strontium metal as a solution in the platinum core. This confirms the findings of Part 10, where it was further shown that the initial dissociation is a thermal phenomenon and independent of the nature of the core metal. The two oxides have therefore a marked difference in thermal stability. The two metals belong to Group 2 of the periodic system and it might therefore be predicted that calcium oxide would be unstable, like strontium oxide. For this reason it was decided to include calcium oxide in the experimental sequence and the result is shown in Fig. 9. It can be seen that the variation of v with time at 1 200° C is similar to that of strontium oxide. The growth of v is, moreover, accompanied by the formation of a black film of calcium metal, by an absence of Newtonian colour bands, and by a steady rise of the power required to maintain a constant core temperature. In short, the qualitative behaviour of calcium oxide is identical with that of strontium oxide.

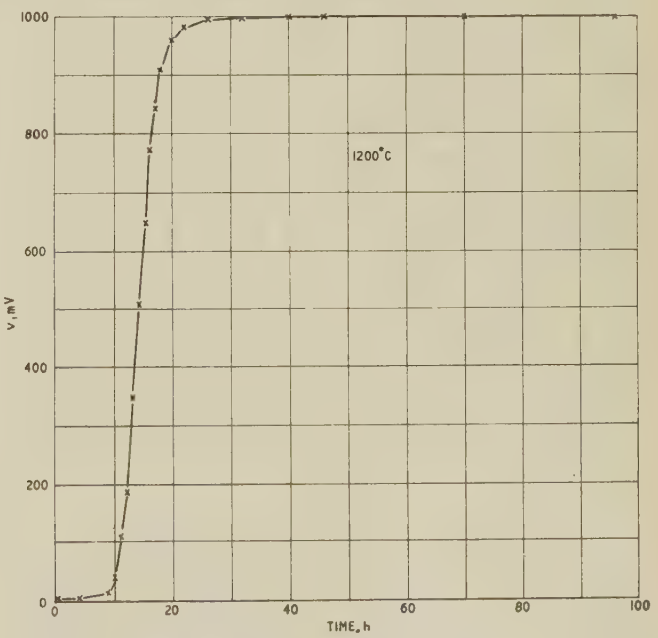

Fig. 9.—Characteristic of v/time for calcium oxide at 1 200° C.

(3.7) Previous Work

The products of evaporation from the oxide cathode have been examined by three different workers[1, 2, 3] using the mass-spectrometer. The most recent and systematic contribution is from Pelchowitch,[3] who finds that barium oxide evaporates in the unchanged molecular form. Using platinum as a substrate in the temperature range 1 400–1 500° C, Pelchowitch further observes the evolution of strontium metal, oxygen and strontium-

oxide molecules from a strontium-oxide matrix. Analogous results are obtained with calcium oxide. Work on a nickel substrate in a mass-spectrometer is difficult because of the relatively high evaporation rate of nickel.

(4) CONCLUSION

From the negative-ion movements in platinum- and nickel-cored S-type assemblies recorded in Part 10, from the direct macroscopic observations of the present Part and from the mass-spectrometric measurements of previous workers, the following conclusion can now be confidently written:

> It is a fundamental property of the common barium-strontium-oxide cathode operating at 1 000° K that it maintains an atmosphere of free negative ions of oxygen within its hollow pore system. These ions arise from the thermal dissociation of the strontium-oxide component and are generated at a constant rate throughout the life of the cathode. The concentration of free ions in the pore system rises to an equilibrium level where the constant rate of dissociation is balanced by an equal rate of recombination.

A corollary of the conclusion is that a barium-strontium-oxide cathode has an inherent tendency towards self-activation under any operating condition favouring the escape of the free oxygen ion.

(5) ACKNOWLEDGMENT

Acknowledgment is made to the Engineer-in-Chief of the Post Office for permission to use the information contained in this paper.

(6) REFERENCES

(1) ALDRICH, L. T.: 'The Evaporation Products of Barium Oxide from Various Base Metals and of Strontium Oxide from Platinum', *Journal of Applied Physics*, 1951, **22**, p. 1168.

(2) PLUMLEE, R. H., and SMITH, L. P.: 'Mass Spectrometric Study of Solids: I.—Preliminary Study of Sublimation Characteristics of Oxide Cathode Materials', *ibid.*, 1951, **21**, p. 811.

(3) PELCHOWITCH, I.: 'A Study of the Evaporation Products of Alkaline Earth Oxides', *Philips Research Reports*, 1954, 9, p. 42.

621.3.011

The Institution of Electrical Engineers
Monograph No. 445
May 1961

TRANSITIONAL ELECTRICAL UNITS

By LEO YOUNG, Dr. Eng., M.A., M.S., Member.

(*The paper was first received 4th November, and in revised form 29th December*, 1960. *It was published as an* INSTITUTION MONOGRAPH *in May*, 1961.)

SUMMARY

The paper is concerned with the six metric systems of electrical units in common use. The equations of each system differ by constants involving 4π and (approximately) 3×10^{10}. Although this is well understood and accepted, difficulties sometimes arise when a comparison is made between the units or quantities of different systems. The paper endeavours to show that these difficulties are largely semantic, and that they can be overcome with 'transitional electrical units' by converting a given unit into its transitional counterpart, and thence into the unit of the desired system.

LIST OF PRINCIPAL SYMBOLS

$\boldsymbol{D}$ = Electric displacement.
$\boldsymbol{B}$ = Magnetic induction.
$\boldsymbol{E}$ = Electric field strength.
$\boldsymbol{H}$ = Magnetic field strength.
ρ = Charge density.
$\boldsymbol{J}$ = Current density.
$\boldsymbol{F}$ = Force.
Q = Charge.
S = Constant of proportionality, later associated with solid angle.
U = Constant of proportionality, later associated with plane angle.
γ = Dimensionless constant numerically equal to the velocity of light expressed in centimetres per second. (The symbol c is reserved for the velocity of light, and has dimensions LT^{-1}.)

(1) INTRODUCTION

The electromagnetic equations of the six metric systems in common use differ by two constants of proportionality, namely 4π and (approximately) 3×10^{10}. As a result, difficulties sometimes arise when comparing the quantities of different systems, which are often measured in units having the same name but different magnitudes. This is a semantic problem, which can be overcome by suitable choice of terminology. The purpose of the paper is to show that this can be done rigorously and that a consistent system of 'transitional electrical units' can be set up. Difficulties of conversion between either quantities or equations expressed in different systems can be overcome by converting a given quantity or equation into its transitional counterpart and thence into that of the desired system. The full transitional name or equation need be retained only when a comparison between different systems is contemplated.

The electric and magnetic field quantities may be defined by Maxwell's equations, which can be written in generalized form[1, 2]

$$\text{div } \boldsymbol{D} = S\rho \quad . \quad . \quad . \quad . \quad . \quad . \quad (1)$$

$$\text{div } \boldsymbol{B} = 0 \quad . \quad . \quad . \quad . \quad . \quad . \quad (2)$$

$$U^{-1} \text{ curl } \boldsymbol{E} = -\dot{\boldsymbol{B}} \quad . \quad . \quad . \quad . \quad . \quad . \quad (3)$$

$$U^{-1} \text{ curl } \boldsymbol{H} = S\boldsymbol{J} + \dot{\boldsymbol{D}} \quad . \quad . \quad . \quad . \quad . \quad . \quad (4)$$

and one force equation such as

$$EQ = F \quad . \quad . \quad . \quad . \quad . \quad . \quad . \quad . \quad (5)$$

By assigning the appropriate numerical values to S and U, the systems shown in Table 1 are obtained.

Table 1

NUMERICAL VALUES OF S AND U

	S	U
M.K.S. rationalized	1	1
M.K.S. unrationalized	4π	1
e.s.u.	4π	1
e.m.u.	4π	1
Gaussian	4π	$1/\gamma$
Heaviside–Lorentz	1	$1/\gamma$

where γ is a dimensionless number, approximately equal to 3×10^{10}.

(2) FUNDAMENTAL AND DERIVED QUANTITIES

Every physical quantity has to be defined by one of two alternative methods, namely (*a*) in terms of an arbitrary unit by direct comparison, or (*b*) in terms of other quantities by some arbitrary process. If the former, it is referred to as a fundamental (or primary) quantity; if the latter, as a derived (or secondary) quantity.[3] For a derived quantity the definition takes the form of an equation, and involves an arbitrary constant of proportionality. It is largely a matter of choice whether we decide to take a given physical quantity as fundamental or derived. However, there is a minimum number of fundamental quantities required. In mechanics there are three, in electromagnetism there is also a fourth.

The unit of a derived quantity changes whenever we change the units of the fundamental quantities on which it depends through its defining equation, and whenever we change the constant of proportionality in that equation.

The equations do not change with the fundamental units, but only with the constants of proportionality.

(3) PRIMARY AND SECONDARY DIMENSIONS

With any electrical quantity there are associated four primary dimensions, which will be taken* as force, F, length, L, time, T, and charge, Q. These dimensions are assigned to a quantity through its defining equation. The process may be summarized as follows. Strip the defining equation of its constant of proportionality and all operator symbols (such as differential or integral operators), leaving only the symbols F, L, T and Q. If necessary, first reduce all previously defined derived quantities to their primary dimensions in F, L, T and Q. This turns the defining equation into the dimensional formula of the quantity

Correspondence on Monographs is invited for consideration with a view to publication.
Dr. Young was formerly with Westinghouse Electric Corporation, Baltimore, Maryland, and is now with the Stanford Research Institute, California, U.S.A.

* Force rather than mass is chosen for convenience in dimensionless computations. Charge rather than μ_0 or ϵ_0 is chosen for the electrical dimension to avoid fractional indices. Current I was adopted as the fourth fundamental quantity by the Tenth General Conference of Weights and Measures, 1954. If this is used in place of charge Q, replace [Q] by [IT].

defined. It tells how the unit of the derived quantity changes when the units of the fundamental quantities are changed.

In the process of obtaining the dimensional formula, the information carried by the constant of proportionality in the defining equation has been lost. For most equations and in most systems this constant is unity, and the information is of no consequence. Sometimes, however, this information is worth preserving.

Consider, for instance, eqn. (1), which defines electric displacement $\boldsymbol{D}$. When div is replaced by its dimensional value, and S is dropped, it gives the dimensional formula of $\boldsymbol{D}$ as

$$[\mathrm{D}] = [\mathrm{L}^{-2}\mathrm{Q}] \quad . \quad . \quad . \quad . \quad . \quad . \quad (6)$$

Suppose, however, that S had been left in, so that

$$[\mathrm{D}] = [\mathrm{L}^{-2}\mathrm{Q\,S}] \quad . \quad . \quad . \quad . \quad . \quad (7)$$

where [S] is kept as a fifth dimension. We shall speak of [S] as a secondary dimension, to distinguish it from the minimum number of (four) primary dimensions. Its usefulness lies in the possibility of treating a change of equations as a change of units, since the generalized equations remain the same.

(4) ANGLE DIMENSIONS

Since [S] appears in the dimensional formula for $\boldsymbol{D}$, it will appear also in the dimensional formula of any quantity (such as ϵ_0) involving $\boldsymbol{D}$ in its definition. S also appears in eqn. (4) which defines $\boldsymbol{H}$, and will therefore appear in the dimensional formula of $\boldsymbol{H}$ and any quantity (such as wave impedance) derived from $\boldsymbol{H}$.

Similarly [U] appears in the dimensional formulae of $\boldsymbol{B}$ and $\boldsymbol{H}$, and any quantities derived from them.

The introduction of the secondary dimensions [S] and [U] to correspond to the constants of proportionality in Maxwell's equations is thus a uniquely defined process.

With every dimension there goes a unit, and any physical quantity which involves that dimension has also to be expressed in terms which involve that unit. For example, the dimensional equation for electric displacement $\boldsymbol{D}$ is given by eqn. (6) or (7). In the M.K.S. rationalized system, the unit of $\boldsymbol{D}$ is then the coulomb per meter squared, by eqn. (6); or if S is to be retained, it is the coulomb (S) per meter squared, by eqn. (7), where (S) stands for the appropriate unit of S. This becomes easier to apply and to memorize when a name is found for that unit of S. It was shown in another paper[1] that a natural choice for that name is 'sphere'. Electric displacement $\boldsymbol{D}$ is then measured in transitional units of coulomb-sphere per meter squared in the M.K.S. rationalized system. The units of S in the six common metric systems are reproduced[1] in Table 2.

Table 2

UNITS OF S

M.K.S. rationalized	Sphere
M.K.S. unrationalized	Steradian
e.s.u.	Steradian
e.m.u.	Steradian
Gaussian	Steradian
Heaviside–Lorentz	Sphere

For example, the transitional unit of $\boldsymbol{D}$ in the M.K.S. unrationalized system is coulomb-steradian per meter squared, from which it follows at once that one M.K.S. rationalized unit of $\boldsymbol{D}$ equals 4π M.K.S. unrationalized units.

A similar convenient terminology for the units of U in the six common metric systems is reproduced[1] in Table 3.

The units of S and U in the selected terminology are all angles.

Table 3

UNITS OF U

M.K.S. rationalized	Turn
M.K.S. unrationalized	Turn
e.s.u.	Turn
e.m.u.	Turn
Gaussian	γ turns
Heaviside–Lorentz	γ turns

Although angles have some of the attributes of dimensions,[4–6] the present argument in no way depends on this claim. It is S and U which have (secondary) dimensions. In looking for a name for the corresponding unit quantities, the choice of units of solid angle and (plane) angle for the units of S and U, respectively, is a natural one,[1] and a convenient solution to a semantic problem.

(5) DISCUSSION

In the past, various paradoxes and dilemmas have been pointed out from time to time as arising from the process of rationalization.[7–10] These can all be resolved by making any comparisons or conversions between different unit systems through transitional units.

For example, the relation between the oersted and the M.K.S. units of magnetic field is discussed at some length in Reference 10. We note that, since

$$[\mathrm{H}] = [\mathrm{Q\,S\,U\,L^{-1}\,T^{-1}}] \quad . \quad . \quad . \quad . \quad (8)$$

it follows that

$$1 \text{ oersted} = 1 \text{ e.m.u. of magnetic field}$$

$$= \frac{10 \times \frac{1}{4\pi} \times 1}{10^{-2} \times 1} \text{ M.K.S. rationalized units}$$

$$= \frac{1\,000}{4\pi} \text{ ampere-sphere-turns per meter (M.K.S. rationalized units)}$$

$$= 1\,000 \text{ ampere-steradian turns per meter (M.K.S. unrationalized units)}$$

These equations sum up many otherwise longer discussions.[7, 10]

(6) ACKNOWLEDGMENT

The author wishes to thank Mr. J. A. Ratcliffe who took an early interest in the paper and suggested the present method of approach.

(7) REFERENCES

(1) YOUNG, L.: 'Electrical Units and Dimensions', *Transactions of the American I.E.E.*, Part I, 1956, **75**, p. 767.

(2) HESSLER, V. P., and ROBB, D. D.: 'Generalized Electrical Formulas', *Electrical Engineering*, 1951, **70**, p. 332.

(3) BRIDGMAN, P. W.: 'Dimensional Analysis' (Yale University Press, New Haven, 1931).

(4) YOUNG, L.: 'Units and Terminology', *Journal I.E.E.*, 1955, **1**, p. 652; and 'The Theory of Dimensions', *ibid.*, 1956, **2**, p. 218.

(5) CHAPMAN, F. T., and DOVER, A. T.: 'Electrical Engineering (General)', Appendix C (Longmans, Green and Co., 1956).

(6) MICHELS, W. C., and PATTERSON, A. L.: 'Elements of Modern Physics' (Van Nostrand, 1951), pp. 265–8 and 629–30.

(7) SILSBEE, F. S.: 'Does Rationalization Change Units?' *Electrical Engineering*, 1957, **76**, p. 296.

(8) KAPP, R. O.: 'Differences of Opinion about Dimensions', *Proceedings I.E.E.*, Paper No. 2167, September, 1956 (**104** B, p. 198).
(9) YOUNG, L.: 'Rationalization of Units', *Electrical Engineering*, 1957, **76**, p. 760.
(10) AVČIN, F.: 'Some Multihorned Dilemmas in the Magnetic Field', *Transactions of the American I.E.E.*, Part I, 1959, **78**, p. 1087.

(8) APPENDICES

(8.1) Relations between Fundamental Units

1 m = 100 cm
1 kg = 1 000 g
1 coulomb = 0·1 e.m.u. of charge
= 3×10^9 e.s.u.s (approximately)
= 3×10^9 Gaussian units
= $3 \times \sqrt{(4\pi)} \times 10^9$ Heaviside–Lorentz units.

(8.3) Example of Conversion Between Equations

Given that the energy density of the electric field in e.s.u. is $ED/8\pi$, what is the expression in M.K.S. rationalized units? The missing dimension is assumed to be S^x. Then

$$[E]\,[D]\,[S^x] = [\text{energy}]\,[L^{-3}]$$

From the Table in Section 8.2, $x = -1$. Since $S = 4\pi$ e.s.u., the transitional expression for the energy density of the electric field is

$$\frac{ED}{8\pi} \times \frac{4\pi}{S} = \frac{ED}{2S}$$

In the M.K.S. rationalized system $S = 1$ and this then reduces to $E\,D/2$.

(8.2) Dimensions of some Common Physical Quantities and their Name in Transitional M.K.S. Rationalized Units

Quantity	Symbol	Dimensions in F	L	T	Q	S	U	Transitional M.K.S. rationalized unit
Charge	Q				1			Coulomb
Electric field intensity	E	1			−1			Volt/meter
Electric displacement	D		−2		1	1		Coulomb-sphere/meter^2
Permittivity	ϵ_0	−1	−2		2	1		Farad-sphere/meter
Polarization	P		−2		1			Coulomb/meter^2
Current	I			−1	1			Ampere
Magnetic field intensity	H		−1	−1	1	1	1	Ampere-turn-sphere/meter
Magnetic induction	B	1	−1	1	−1		−1	Weber/meter^2
Wave impedance	Z_w	1	1	1	−2	−1	−1	Ohm/turn-sphere
Permeability	μ_0	1		2	−2	−1	−2	Henry/meter-sphere-turn^2
Magnetic flux	Φ	1	1	1	−1		−1	Weber
Pole strength*	p	1	1	1	−1	−1	−1	Weber/sphere
Intensity of magnetization†	M or $\mathscr{M}$	1	−1	1	−1	−1	−1	Weber/sphere-meter^2
Electric potential (e.m.f.)	V	1	1		−1			Volt
Resistance	R	1	1	1	−2			Ohm
Capacitance	C	−1	−1		2			Farad
Inductance†	L or $\mathscr{L}$	1	1	2	−2			Henry
Conductivity	σ	−1	−2	−1	2			Mho/meter
Resistivity†	ρ or r	1	2	1	−2			Ohm meter
Magnetomotive force† (m.m.f.)	F or $\mathscr{F}$			−1	1	1	1	Ampere-turn sphere
Reluctance†	S or $\mathscr{S}$	−1	−1	−2	2	1	2	Ampere-turn-sphere/weber

Note especially the difference in dimensions between such quantities as D and P, I and H, B and M, R and Z_w, Φ and p.

* Defined by $pH = F$.
† The first symbol is the British Standard. Since there are more quantities than letters, these conflict in turn with the symbols for mass, length, charge density, force and the dimensional constant S. The second symbol is suggested as an alternative in dimensional equations to avoid using the same symbol twice.

621.318.13.017:621.3.018.7

The Institution of Electrical Engineer
Monograph No. 446 M
May 196

INTERNAL WAVEFORM DISTORTION IN SILICON-IRON LAMINATIONS FOR MAGNETIZATION AT 50 c/s

By Professor F. BRAILSFORD, Ph.D., Member, and J. M. BURGESS, B.Sc.(Eng.).

(*The paper was received* 14*th October*, 1960, *and in revised form* 13*th January*, 1961. *It was published as an* INSTITUTION MONOGRAPH *in May*, 1961.)

SUMMARY

The internal distribution of magnetic flux and eddy currents to be expected in a homogeneous magnetic lamination having a sinusoidal total flux has been investigated experimentally using an analogue. It is concluded that the anomalous loss in laminations found to occur in practice cannot be accounted for by waveform distortions within the lamination.

LIST OF SYMBOLS

b_0, b_1, b, etc. = Instantaneous flux density in the lamination and in the cores.
J_{01}, J_{12}, J, etc. = Instantaneous current density in the lamination.
i_{01}, i_{12}, i, etc. = Instantaneous current in the lamination.
I_{01}, I_{12}, I, etc. = Instantaneous current in the analogue with N turns.
l = Length of sheet and of magnetic path in cores.
d = Width of sheet.
d' = Width of core laminations.
a = Half-thickness of sheet.
a' = Total thickness over all cores.
n = Number of imaginary layers in sheet.
r = Resistance of one layer.
r' = Resistance in analogue with one turn.
R = Resistance in analogue with N turns.
N = Number of turns on each eddy-current winding in analogue.
ρ = Electrical resistivity of material of simulated lamination.
N_1 = Number of turns on each eddy-current winding in analogue per unit length of magnetic path.
v = Total volume of cores in analogue.

(1) INTRODUCTION

An account is given of an experimental investigation on an analogue which was constructed to simulate a single ferromagnetic lamination. It was a purpose of the work to determine the internal magnetic-flux and eddy-current waveforms to be expected in silicon-iron laminations carrying a sinusoidal total flux, and to find if waveform distortions might account for extra or anomalous losses in the material. The subject of anomalous losses has been discussed in a previous paper.[1]

The waveform distortions considered in this investigation are those which would arise from the non-linear relationship between flux density, B, and field strength, H, in a supposedly homogeneous material. No account is taken of local internal discontinuities due to the ferromagnetic domain structure of the crystals of the polycrystalline material, or due to any other non-uniformity. The possibility that the extra losses are associated with the size of the domains has recently been investigated theoretically.[2, 3, 4] Mathematical work is, however, made difficult by the non-linearities mentioned, or entails the use of simplifying assumptions. It was therefore thought worth while to carry out the detailed experimental work described here.

(2) CONSTRUCTION OF THE ANALOGUE

Fig. 1 shows how an analogue may be devised to simulate a single lamination. In Fig. 1(*b*) the half-thickness of part of

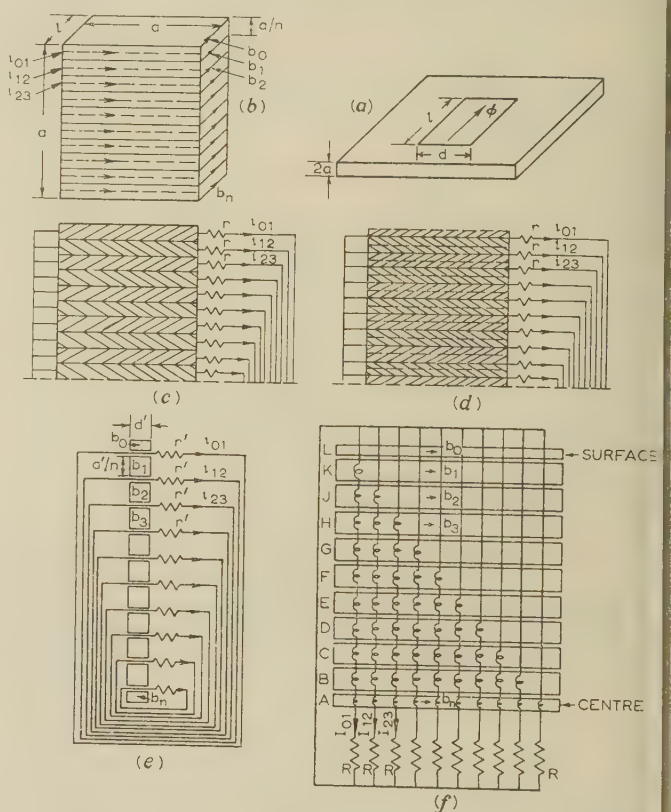

Fig. 1.—Development of an analogue to simulate a single lamination.
(*a*) Lamination to be simulated.
(*b*), (*c*) and (*d*) Half-thickness of lamination subdivided into n layers.
(*e*) Analogue with artificial eddy-current paths.
(*f*) Eddy-current circuits in analogue.

lamination carrying a sinusoidal total flux is shown. Th half-thickness is divided into n equal layers, and the instantaneou induced eddy currents appropriate to the layers are shown a i_{01}, i_{12} . . . etc., while the flux densities are represented b b_0, b_1 . . . b_n. In Fig. 1(*c*) the resistance r of each layer assumed to be brought outside the lamination and in (*d*) th resistors r are included in circuits threaded through the lamina tion. In Fig. 1(*e*) equal packets of laminations are now subst tuted for the individual layers of the original lamination, bu with the outer packets halved. The cross-sectional area of eac

Correspondence on Monographs is invited for consideration with a view to publication.
Prof. Brailsford is Professor of Electrical Engineering, University College London, and Mr. Burgess is with the London Transport Executive.
The paper is based on Report Ref. N/T89 of the British Electrical and Allied Industries Research Association.

packet may be made for convenience much greater than that of the simulated layer and r now becomes r' where $r' = a'd'r/ad$.

In the analogue each packet was made up of thin insulated rings and the eddy-current windings were not restricted to a single turn. The final arrangement of the component packets of rings and of the eddy-current windings is shown in Fig. 1(f). It will be seen that separate equal eddy-current windings were put on each packet, and these windings were connected in series. It is easy to show that, if ρ is the electrical resistivity and a is the half-thickness of the simulated lamination, the resistors to be used in the analogue each have resistance $R = \rho n v N_1^2/a^2$, where v is the total volume of the cores in the analogue and N_1 is the number of eddy-current winding turns per unit length of the magnetic path in the rings.

In addition to the windings shown in Fig. 1(f), equal magnetizing windings were put on each packet. These windings were connected in series to a sinusoidal source of supply at a frequency of 50 c/s, so that the total flux in the whole analogue was sinusoidal. Each packet was also provided with a search coil.

Ideally the core material of the analogue should have the same dynamic hysteresis characteristics as the material of the lamination being simulated. Eddy currents in the ring laminations themselves should also be kept negligibly small, either by stamping the rings from very thin sheets or using material of high electrical resistivity, or both. n should also be large. Under these circumstances, for the same mean flux density in the simulated lamination and in the analogue, the flux density, in magnitude and waveform, is the same at any depth in the lamination and in the corresponding core of the analogue. The current density at any point in the lamination is obtainable from observation of the currents I_{01}, I_{12} . . ., etc., and the iron losses per unit volume are the same in the lamination and in the analogue.

(3) APPARATUS

In constructing the analogue, n was made equal to 10. Each tenth of the half-section of the simulated lamination was represented by a packet of laminations built up from 0·003 in varnished rings of inside diameter 8 cm and outside diameter 12 cm, the material being 2·8% silicon-iron. Because of the thinness of the laminations and the relatively high silicon content, the eddy-loss component of this material itself was small compared with its hysteresis component at 50 c/s. To make up the analogue as represented in Fig. 1(f), nine packets of rings were assembled of cross-sectional area 5·26 cm^2 and mean length of magnetic path 31·4 cm. To represent the outermost and innermost layers, two packets, each of half the cross-sectional area, were used. Each packet had a magnetizing winding of 100 turns and a search coil winding of 25 turns. The eddy-current windings, depicted in Fig. 1(f), each had 20 turns of 26 s.w.g. copper wire.

Flux waveforms were determined by using a synchronous commutator and moving-coil reflecting galvanometer, eddy-current waveforms were obtained from a cathode-ray oscilloscope, iron-loss measurements at 50 c/s were made by a reflecting electrodynamic wattmeter and static hysteresis loops by using a ballistic galvanometer.

Two thicknesses of dynamo-iron laminations were simulated and investigated in detail, namely 0·021 in and 0·080 in.

(4) RESULTS FOR A 0·021 IN LAMINATION

A lamination of 0·021 in-thickness of dynamo iron was first simulated in order to compare the results, in the present investigation using a more refined analogue, with those previously published using a cruder model.[1]

If the resistivity of dynamo iron is taken as $\rho = 14 \times 10^{-8}\,\Omega$-m and $2a = 0{\cdot}021$ in $= 0{\cdot}054$ cm, then $R = 128\,\Omega$. Each eddy-current circuit in the analogue was made up to this value using external resistors of constantan wire.

Flux waveforms corresponding to a flux density $B_{max} = 1{\cdot}12$ Wb/m^2 (11 200 G) for the whole lamination are shown in Fig. 2, where the letters A, B, C, . . . correspond to those given

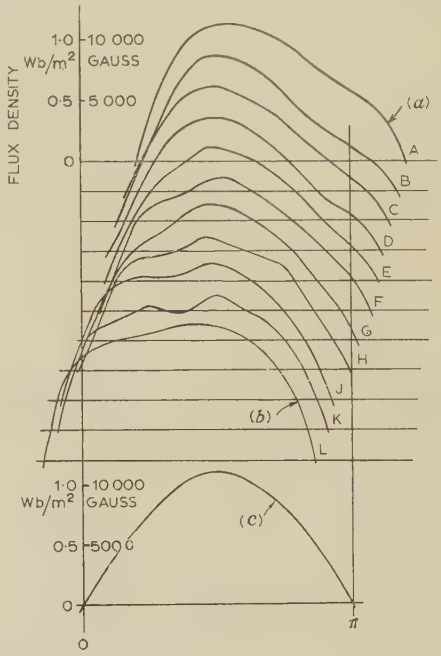

Fig. 2.—Flux waveforms observed for 0·021 in dynamo iron.

(*a*) Centre of lamination.
(*b*) Surface of lamination.
(*c*) Mean flux density.

in Fig. 1(f). The mean waveform for the sum of all the cores is very nearly a sine wave, as shown, but the internal flux waveform tends to be triangular at the centre, varying to a more flat-topped shape at the surface. The harmonic contents of these waves are given in Table 1.

The observed peak flux density at any point in the sheet as derived from the analogue and the phase angle of the fundamental components in relation to the total flux are plotted as the full lines in Fig. 3 for this case. The broken lines given the theoretical values calculated from the classical formulae* assuming linear conditions with a constant relative permeability of 2 500 for the material. The observed phase angles are a little less than those previously reported by Brailsford,[1] while the variation in B_{max} across the section is negligible, although using a cruder model it was previously suggested that a flux-density variation of the order of about $\pm 15\%$ might occur.

From these results it was clear that there would be no increase in hysteresis loss in the lamination arising from non-uniformity of B_{max} across the section. Estimates also showed that distortion produced no significant increase in eddy-current loss above the calculated classical value. It was therefore decided to investigate the case of a lamination of greater thickness in which distortion and non-uniformity would be accentuated. As already mentioned, a thickness of 0·080 in was chosen.

(5) RESULTS FOR A 0·080 IN LAMINATION

To simulate a dynamo-iron sheet of 0·080 in thickness the resistance in each eddy-current circuit was reduced to $R = 9{\cdot}0\,\Omega$.

* See, for example, RUSSELL, A.: 'Alternating Currents', Vol. 1 (Cambridge, 1914), p. 490.

Table 1

HARMONICS IN FLUX DENSITY EXPRESSED AS A PERCENTAGE OF EACH FUNDAMENTAL FOR 0·021 IN LAMINATIONS AT A MEAN B_{max} OF 1·12 WB/M²

Harmonic	Harmonic content in cores										
	A	B	C	D	E	F	G	H	J	K	L
3rd	% 16	% 17	% 14	% 11	% 8	% 8	% 5	% 10	% 16	% 18	% 19
5th	5	4	4	3	4	5	5	4	5	5	7
7th	1	—	—	—	3	3	3	4	—	3	3
9th	—	—	—	—	—	—	—	—	—	2	2

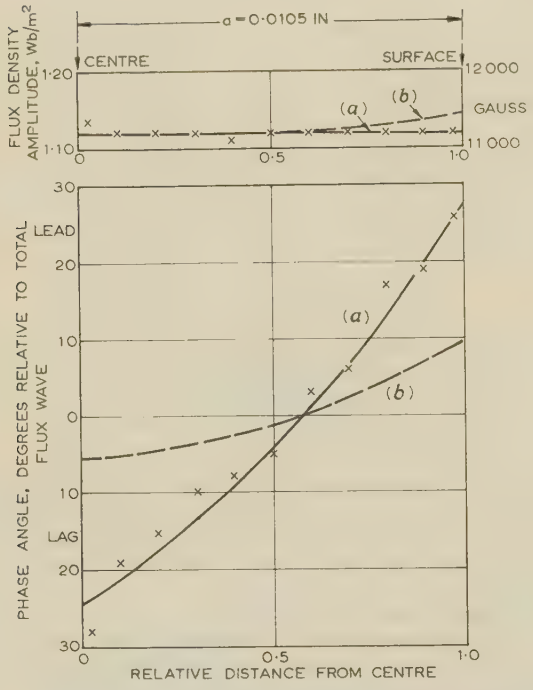

Fig. 3.—Amplitude of internal flux density and phase angle of internal flux fundamentals relative to total flux wave.

Dynamo iron 0·021 in thick. Mean flux density B_{max} = 1·12 Wb/m².
(*a*) Observed.
(*b*) Theoretical (μ_r = 2500).

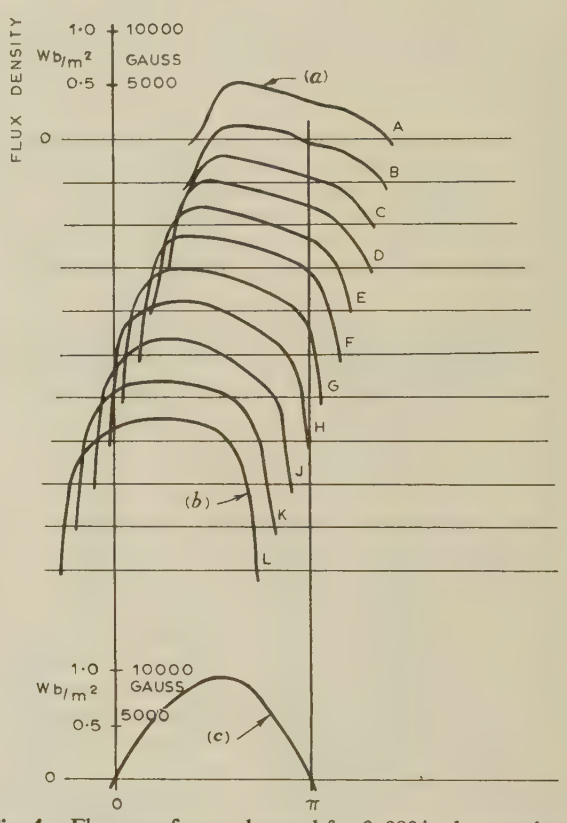

Fig. 4.—Flux waveforms observed for 0·080 in dynamo iron.

(*a*) Centre of lamination.
(*b*) Surface of lamination.
(*c*) Mean flux density.

Table 2

HARMONICS IN FLUX DENSITY EXPRESSED AS A PERCENTAGE OF EACH FUNDAMENTAL FOR 0·080 IN LAMINATION AT A MEAN B_{max} OF 0·95 WB/M²

Harmonic	Harmonic content in cores										
	A	B	C	D	E	F	G	H	J	K	L
3rd	% 20	% 21	% 23	% 25	% 25	% 26	% 25	% 23	% 23	% 23	% 24
5th	9	9	9	12	10	12	12	12	11	10	11
7th	4	4	5	7	6	6	7	7	6	5	5
9th	2	2	2	5	4	4	4	4	4	4	3

he mean value of B_{max} for the lamination was limited in this ase to 0·95 Wb/m² (9 500 G) to avoid overheating the windings n the analogue.

Fig. 4 shows the flux waveforms obtained in the successive ores in magnitude and in the correct phase relation with the ean flux density for the whole lamination. The harmonic mponents of these waves are given in Table 2.

The observed values of B_{max} and the theoretical values at any oint in the lamination are shown in Fig. 5, and the phase angles f the fundamental components of the flux are shown in Fig. 6.

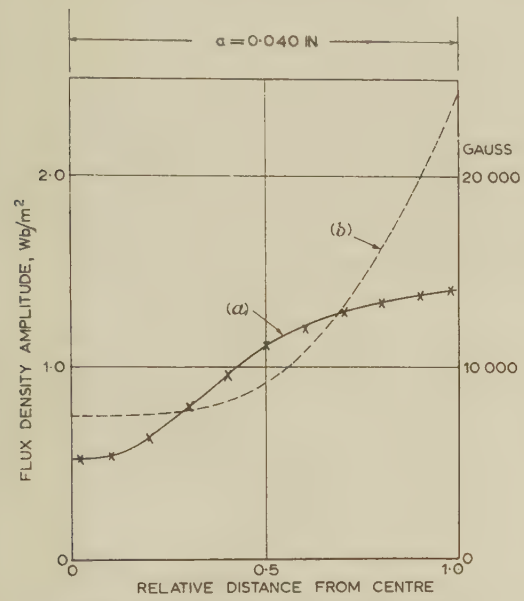

Fig. 5.—Amplitude of internal flux density.
Dynamo iron 0·080 in thick. Mean flux density B_{max} = 0·95 Wb/m².
(*a*) Observed.
(*b*) Theoretical (μ_r = 2500).

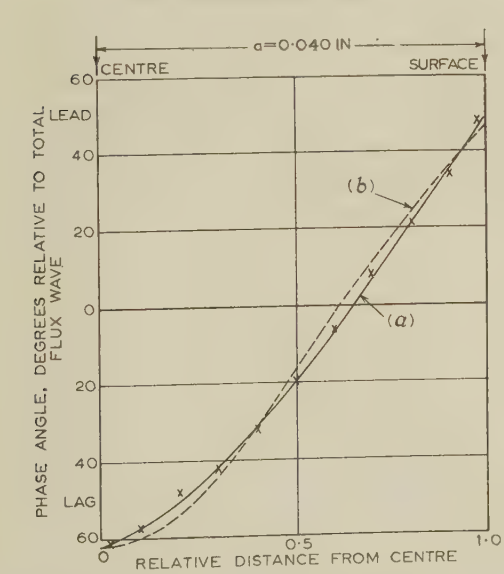

Fig. 6.—Phase angle of internal flux fundamentals relative to total flux wave.
Dynamo iron 0·080 in thick. Mean flux density B_{max} = 0·95 Wb/m².
(*a*) Observed.
(*b*) Theoretical (μ_r = 2500).

Fig. 7(*a*) is a vector polygon showing the fundamental compo- ent of the fluxes in magnitude and direction in the successive ores, and Fig. 7(*b*) is a similar diagram for the third harmonics.

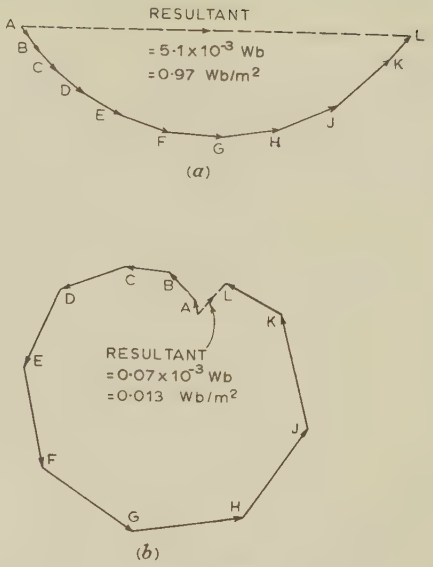

Fig. 7.—Vector polygons of components of flux in 0·080 in dynamo iron.
(*a*) Fundamenta lcomponents.
(*b*) Third harmonic components.

This latter polygon does not quite close on itself since there is a resultant third-harmonic component corresponding to a flux density of 0·013 Wb/m² (130 G). The total flux was therefore not quite sinusoidal but contained a third harmonic of about 1·4%. The phase angles appropriate to the fifth and seventh harmonics were also determined, but the results do not appear to be of particular interest and are not reproduced.

The currents I_{01}, I_{12}, etc. [see Fig. 1(*f*)] were observed oscillographically and their r.m.s. values measured. From these values the corresponding values of J_{01}, J_{12}, etc., were found. The observed r.m.s. values of J are plotted in Fig. 8 as the full line, in relation to distance from the centre of the sheet. The current densities, calculated from the classical theory based on a constant relative permeability of μ_r = 2 500, i.e. for theoretical sinusoidal

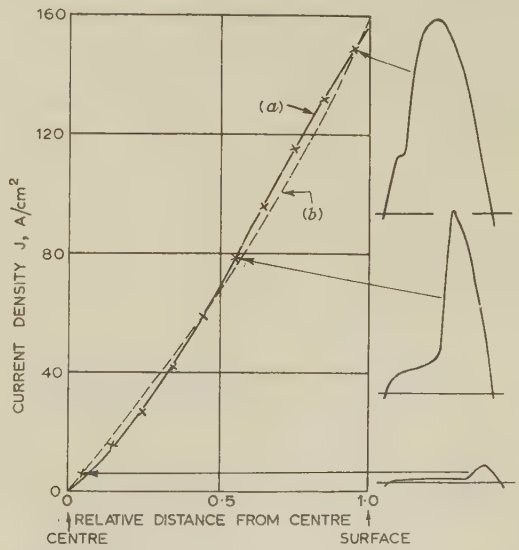

Fig. 8.—Current density at any point in 0·080 in lamination as observed from analogue, and the observed current waveforms at three points.
(*a*) Observed.
(*b*) Calculated from classical theory.

conditions, are given by the broken line. The agreement between observation and theory is so close that there can be no substantial discrepancy between the calculated eddy-current loss using the classical formula and the actual loss for a homogeneous material with distorted eddy-current waveforms. The eddy-current waveforms corresponding to three points of the curve in Fig. 8 are also shown.

Finally, Fig. 9 shows measurements of hysteresis loss under

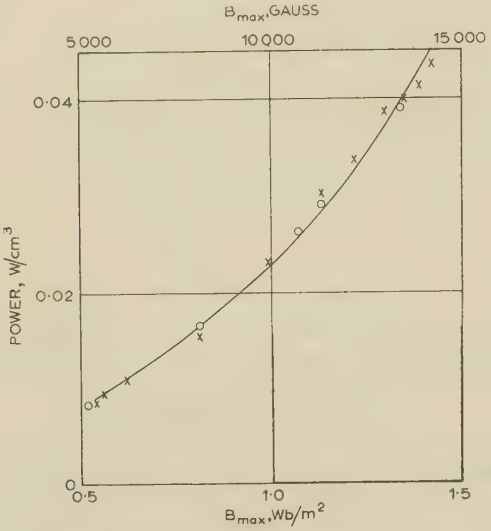

Fig. 9.—Hysteresis loss in relation to sinusoidal total flux density; analogue simulating 0·080 in lamination.

—— No eddy current, sinusoidal flux in every packet.
× Observed hysteresis loss with eddy current; distorted flux waveforms.
○ Calculated hysteresis loss from observed B_{max} values and static hysteresis loops.

three conditions over a range of flux densities for the analogue. The full line gives the losses in the analogue when the eddy-current circuits were disconnected, i.e. with a sinusoidal flux of amplitude B_{max} in every section of the analogue. The crosses are the measured losses in the analogue, with the eddy currents corresponding to a simulated thickness of 0·080 in after subtracting the eddy-current losses. That is to say, the crosses represent the total hysteresis loss in relation to the mean value of B_{max} in the whole analogue when the flux waveforms are distorted. The circles represent the losses measured from static hysteresis loops of the material in relation to B_{max}. It is not possible to say from a comparison of these results that there any difference between them within the limits of experiment error.

(6) CONCLUSIONS

Measurements of waveforms of flux and currents on th analogue of a lamination show that severe waveform distortio of the internal eddy current and flux density will occur in lamination carrying a sinusoidal flux at 50 c/s.

For the thicknesses of lamination simulated, that is up t 0·080 in, the eddy-current losses due to the distorted edd currents will not differ by more than a few per cent from th losses calculated from the classical formula.

Although the flux-density waveforms are distorted and th distribution of B_{max} differs somewhat from the theoretical value the total hysteresis loss was not appreciably affected thereby fo the particular material of which this analogue was made.

It is concluded that the anomalous loss found to occur i laminations of iron or silicon-iron cannot be accounted for b the internal flux waveform distortions which would occur in lamination having a supposed small domain size.

(7) ACKNOWLEDGMENTS

The authors wish to acknowledge, with thanks, a grant fro the University of London, assistance received in the form of supplementary maintenance grant from the Department Scientific and Industrial Research, a financial contribution fo equipment from the Electrical Research Association, and th gift, by the G.K.N. Group Research Laboratory, of the silico iron rings used in the investigation.

(8) REFERENCES

(1) Brailsford, F.: 'Investigation of the Eddy-Current Anoma in Electrical Sheet Steels', *Journal I.E.E.*, 1948, **95**, Part I p. 38.

(2) Williams, H. J., Shockley, W., and Kittel, C.: 'Studies the Propagation Velocity of a Ferromagnetic Doma Boundary', *Physical Review*, 1950, **80**, p. 1090.

(3) Pry, R. H., and Bean, C. P.: 'Calculation of the Energy Lo in Magnetic Sheet Materials using a Domain Model *Journal of Applied Physics*, 1958, **29**, p. 532.

(4) Lee, E. W.: 'Eddy-Current Losses in Thin Ferromagnet Sheets', *Proceedings I.E.E.*, Monograph No. 284 M February, 1958 (**105** C, p. 337).

621.387.014.31 : 537.52

The Institution of Electrical Engineers
Monograph No. 447 S
May 1961

THE MOTION OF COLD-CATHODE ARCS IN MAGNETIC FIELDS

By A. E. GUILE, Ph.D., B.Sc.(Eng.), T. J. LEWIS, Ph.D., M.Sc., B.Sc.(Eng.), Associate Members, and P. E. SECKER, Ph.D., B.Sc.(Eng.), Graduate.

(*The paper was first received* 17*th November*, 1960, *and in revised form* 25*th January*, 1961. *It was published as an* INSTITUTION MONOGRAPH *in May*, 1961.)

SUMMARY

The paper first discusses the way in which theories concerning the motion of cold-cathode arcs when acted upon by a magnetic field have ranged from proposing cathode-fall mechanisms for retrograde motion to column processes for forward motion. A very recent mechanism proposed by Ecker for retrograde motion is then examined and found to be capable of extension to higher pressures where forward motion occurs.

Previously published experimental results for forward motion are viewed in the light of this mechanism, which is found to be consistent with them, and some features which had hitherto been anomalous may now be explained. Thus there emerges a unified model for the cathode spot and fall region which appears to be valid for both forward and retrograde movements of the arc. It is suggested that this provides a vital step in the approach to the development of certain devices in which arc discharges take place.

(1) INTRODUCTION

It was discovered at a very early date[1] that the application of a magnetic field to an electric arc transverse to the axis of the arc current caused movement of the arc in a direction mutually perpendicular to the magnetic field and the arc axis. At atmospheric pressure the direction of movement in a transverse magnetic field (t.m.f.) is given by Ampère's law, and it therefore seemed natural at first to consider the arc as a flexible conductor, perhaps experiencing an aerodynamic drag as it moved and acted on by a force proportional to the t.m.f., and the arc current.[2–5] The fact that reduction of pressure caused the arc to decrease in velocity and eventually to move in the opposite or retrograde direction[6, 7] was unfortunate since such behaviour would not be explained in terms of the forces acting on a simple conductor. Evidence accumulated in recent years shows that the arc movement is actually controlled by conditions in the cathode-fall space and on the cathode surface, and that in most cases the rest of the arc (which still has an Ampèrian force on it[8]) can have little effect on the velocity. Conditions for maintaining the arc in the anode and column regions are easily realized, but in the cathode region the maintenance conditions are critical and influence the whole discharge. The arc current is carried mainly by electrons, since these have a far greater mobility than positive ions, and these electrons are emitted from the cathode spot and accelerated in the cathode-fall space.

The movement of ions across the fall region and the possibility of electron–gas-molecule collisions are of great importance in the description of arc motion given below, but an equally important process is that of electron emission from the cathode spot. A single dominant emission mechanism has not been established for cold-cathode arcs in which the current densities exceed 10^5 A/cm^2. Field emission and field-aided thermionic emission can occur, and it is probable that other processes such as Auger and resonance ejection by positive ions and ejection by metastable excited atoms and incident photons are important. For all these processes the effective work function of the cathode spot will be important, and this parameter will depend strongly on surface conditions.

It has been suggested that a number of processes occurring in the cathode-fall region and in the cathode spot are capable of inducing retrograde motion,[7, 9–12] but none of these theories has received general acceptance. A new theory of this type which explains the experimental results more adequately has recently been given by Ecker,[13] and this will be discussed in Section 2. It will be shown that it may be extended to agree with the experiments of Guile and Secker,[14] who have stressed the unsoundness of considering the column as the predominant seat of motion in the case of forward movement. Their evidence indicates that, while an Ampèrian force on the column does exist, it plays a minor role and the arc velocity is, in fact, controlled by conditions in the cathode-fall space and on the cathode surface. For example, in experiments at atmospheric pressure, using parallel horizontal electrodes of 1 cm diameter situated in a vertical plane with the anode uppermost and current connection made at one end of the electrodes, the results shown in Fig. 1 were obtained.[14] The t.m.f. which moved the arc along the electrodes was the self-field set up by the current in the anode and cathode. Leaving until later the discussion of a discontinuous mode of motion which occurred under certain conditions, the arc

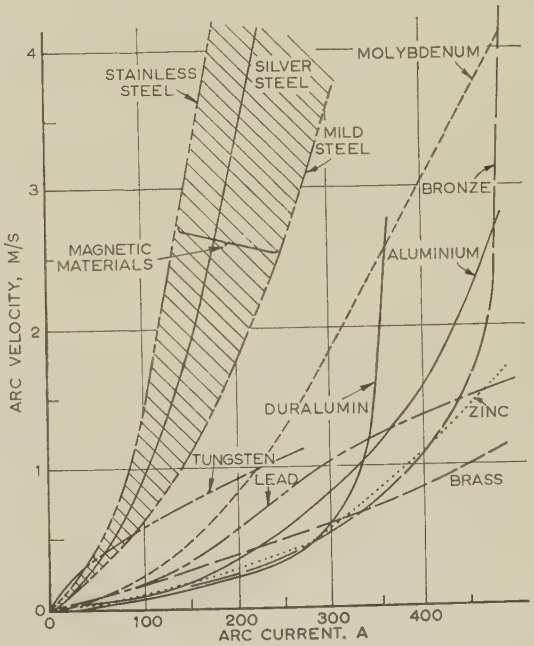

Fig. 1.—Arc velocity as a function of material and current.[13]
Current feed to one end of electrodes only.
Inter-electrode gap = 3·2 cm.

Correspondence on Monographs is invited for consideration with a view to publication.
The authors are in the Electrical Engineering Department, Queen Mary College, University of London.

moved continuously with a velocity which depended on the material of the electrodes, and it is significant that the velocity was very much greater for magnetic than for non-magnetic materials. From Fig. 1 alone it is clear that phenomena in the neighbourhood of the cathode must be important, because for any given current and therefore t.m.f. the motive force on the column should not be very different for different electrodes.

Further experiments[15] were designed to eliminate the self-field by feeding balanced currents to both ends of each electrode and supplying the t.m.f. by an external solenoid. The arc velocity in the continuous mode was then proportional to the t.m.f. but independent of arc current above 40 A. These results were not entirely in agreement with those of previous investigators, but this was attributed to less accurate measuring techniques in the earlier work. A most surprising effect was that the velocity on non-magnetic materials was now greater than on steel (see Fig. 2), whereas when the t.m.f. had been supplied by the current itself the reverse had been true (Fig. 1). More detailed analysis[15] of the situation shows, however, that, for the electrode configuration which yielded the results in Fig. 2, the field in the immediate vicinity of a magnetic electrode where the arc roots operated would be very small, although it would increase progressively to the normal value further out in the inter-electrode space. If the velocity depends on the field in the cathode neighbourhood, the low value for a magnetic electrode in this configuration is explained. Furthermore, in the configuration for Fig. 1 it has been shown[16] that a significant skin effect occurs as the arc moves on the magnetic electrodes, owing to the rapidly changing paths of the current in the electrode near the cathode spot. This forces the current paths to an outer sheath of the electrode, and the increase in the magnetic field just outside the electrode is of the correct order to give the increased velocity observed. Thus both situations emphasize the significance of the magnetic field in the cathode-fall space and the lack of importance of forces on the column.

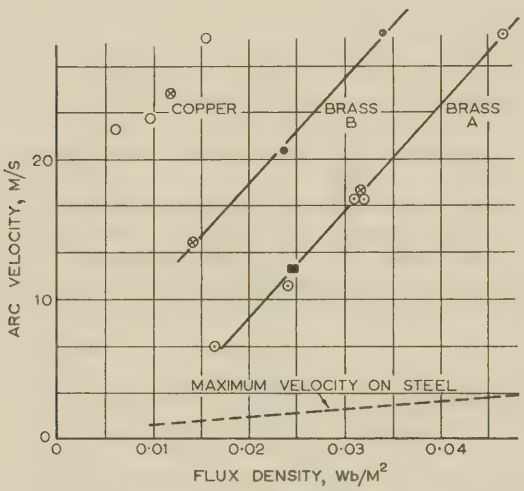

Fig. 2.—Arc velocity on copper, steel and brass of two compositions.
Balanced current feed to both ends of the electrodes.
Inter-electrode gap = 3·2 cm.
Arc currents
○○ 500 A.
×× 170 A.
●● 108 A.
■■ 40 A.

The discussion of further experiments which indicate that motion is associated with the cathode is best facilitated by postulating a general model which, it is suggested, represents the major processes controlling arc motion in the Ampèrian and retrograde directions.

(2) MODEL FOR THE MOVEMENT OF THE ARC CATHODE

It is clear that a moving arc must establish a succession of cathode spots in its travel, and the ease with which this can occur will depend on the emission properties of the cathode surface. Furthermore, as demonstrated by the random motion of the spot when a t.m.f. is absent, the arc prefers not to anchor at a given point, suggesting that sufficient emission from a given spot cannot be maintained indefinitely. The randomness is removed when a t.m.f. is imposed, and the spot then moves at a rate determined by the magnitude of the t.m.f. and the cathode conditions. It is therefore necessary to study the emission properties of the cathode spot, especially the factors which lead to random wandering and the processes by which a t.m.f. can lead to a preferred direction of motion.

(2.1) Cathode Emission

The cold-cathode arc spot is believed to consist of several small emitting sites each of limited current capacity.[17, 18] For an arc in air at atmospheric pressure the limit is about 45 A but it decreases to about 1 or 2 A at 25 torr. The tendency to form separate sites can be expected from considerations of stability[18] and from the fact that electrons will not be emitted uniformly from the cathode.

While the nature of the emission process for cold-cathode arcs will be important in determining arc motion, it is likely that no single mechanism is operative but that several processes are combined to give the required magnitude of emission current. It is clear that the temperature of the cathode spot is not sufficient to give the necessary electron current by a purely thermionic (T) emission, nor is the local surface field high enough to induce simple field (F) emission when the effective work function of the surface is taken to be that of the pure metal. A better starting-point is to consider that the emission is caused simultaneously by the field and temperature (T–F)[19] and to acknowledge that the effective work function may be appreciably less than that of the clean metal because of the surface films present on the cathode. In addition, it has been shown that to gain an accurate assessment of the total emission current it is necessary to consider microscopic local fields due to impinging ions, and to employ stochastic methods of computation.[20]

The cathode field will be set up by positive ions in the fall space and particularly by an ion layer established on the cathode films. The ions will be statistically distributed, and the field at the surface will undergo spatial and temporal changes about a mean value determined by the rate of incidence of ions and their neutralization on the surface layer. Because the emission will generally increase rapidly with field strength, these fluctuations will be important in determining the emission. T–F emission will be sensitive to the nature of the insulating surface film (which is likely to be oxide layer in most cases) and to the presence of any gas layers, dust particles or surface irregularities. As will be demonstrated below, these surface conditions appear to be all-important in determining the arc velocity.

Apart from T–F emission, additional electrons will arise as the result of the incidence of uncharged particles. The yield from photons is likely to be small, but that from excited metastable molecules produced in the discharge may be large. Transferred resonance radiation from these can finally cause emission at the cathode; the possible efficiency of this has been discussed by Hagstrum[21] and by von Engel and Robson.[22] It is clear that the process is important. However, in establishing a cathode site, the incidence of positive ions which lower the potential barrier will be, for any mechanism, a necessary first stage. The strong influence of surface layers in causing glow–arc transitions has been well demonstrated by Edels[23] and co-workers,

nd it is known that low-current arcs cannot be maintained on oxide-free surfaces. If the arc causes removal of any insulating urface film at the cathode spot, a lowering of the strength of the on layer and an increase in the potential barrier may be expected. The wandering normally observed with cold-cathode arcs etween solid electrodes in air is thus due to a search for new oxidized sites which can act as more efficient emitters, and is lso affected by the temperature difference between new and xisting sites.

Thus, if an arc is initiated on an oxidized surface, emission will be established at suitable sites within the cathode spot. These will immediately tend to become less suitable as the oxide s removed and the arc will be forced to seek new sites, the election of which will depend on the surface potential barrier n the vicinity at the moment of transfer. The resulting random vandering may be turned into a directed motion of the spot by he application of a t.m.f. To understand this, the behaviour of positive ions and electrons in the cathode-fall space must be considered.

(2.2) Effect of T.M.F.

Both the electrons emitted from the cathode spot and the positive ions created at the top of the fall region will experience a deflecting force in the Ampèrian direction when a t.m.f. is applied. The ions produced by an electron stream from a given emission site will be constrained to travel towards the cathode n the form of a beam or tube of ions, owing to the self-magnetic pinch force. This tube is deflected in the Ampèrian direction, as shown in Fig. 3. Ecker has shown that [13] this ion tube appears

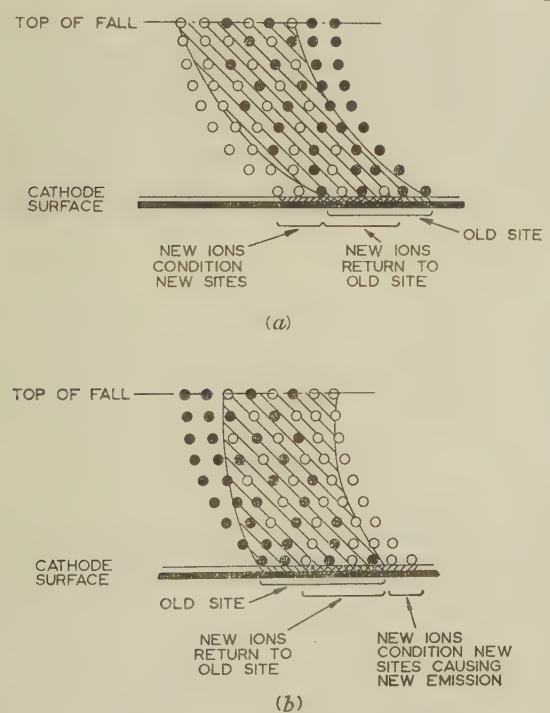

Fig. 3.—Idealized model of cathode fall and root of an arc.
●● Original ion tube.
○○ New ion tube.
▨ Main electron stream.
(*a*) Retrograde motion.
(*b*) Ampèrian motion.

to the emitted electrons as a trough of low potential, such that any electron would require a kinetic energy of several electron-volts to escape from the boundary of the ion tube. Thus although electrons will be emitted with arbitrary initial directions of motion, they will be constrained to move in the ion tube, because of the positive ion field, which is greatest near the cathode.[24] The coupling between the electrons and ions in the tube increases the bending beyond that which would occur for ions alone.[25] At low pressure and in the presence of a t.m.f., Ecker postulates that retrograde motion occurs basically as follows. The emitted electrons are accelerated in the ion tube, and because this is deflected in the Ampèrian direction the electrons are given a retrograde component of velocity [Fig. 3(*b*)]. As the electrons move up the ion tube they gain an amount of kinetic energy such that they may be able to leave the tube. The initial component of retrograde velocity causes the electrons to break out from the tube on the retrograde side, thus giving rise to fresh ionization and to a new tube on that side of the existing system. The theory proposed by Ecker is confined to the behaviour at low pressures, since it is implicitly assumed that the electrons do not suffer collisions with gas molecules during their passage through the fall region.

If this model is now extended to higher pressures, electron–molecule and ion–molecule collisions must now be considered. At atmospheric pressure the initial retrograde velocity of the electrons will quickly be lost because of many elastic scattering collisions with gas molecules. The electrons will thus acquire only a drift motion in the Ampèrian direction due to the t.m.f. and will tend to reach the top of the fall region on the Ampèrian side [Fig. 3(*a*)]. Ions produced by these electrons will create a new ion tube directed to regions on the Ampèrain side of the existing spot, which will be conditioned to form new emitting sites. Thus according to the pressure we may expect either a forward or a retrograde shift of the region of new ion production relative to that in which the ions causing the initial site were created. For some intermediate pressure the two opposing processes can cancel, and an immobility then arises.[7] Thus the new ionization zone and new ion tube are formed in the same region as the existing system, and the arc remains stationary until the local emission efficiency of the cathode becomes so poor that the arc root is forced to move.

Suppose we consider a particular emitting site at a given instant. The t.m.f. will cause a shift in the region of ion production, and consequently the axis of the ion tube and the sites for subsequent electron emission will also be shifted. Ultimately, a continuation of this process would lead to no further ions returning to the original site, but there will be an intervening period in which ions continue to return to the original site in decreasing numbers. As a consequence of the shift of ion and electron tubes there will also be a shift of the region in which excited molecules reach the cathode, but this will not be well defined. The original site, receiving less positive ions and excited molecules, is likely to decline in emission efficiency, especially if there is erosion of the insulating surface layer on which the ions exist. On the other hand, sites in the adjacent region to which the ions have been directed will increase in emission efficiency as a result of the ion layer built up and the heat energy transferred to the surface. Eventually, emission ceases at the old site and the new site (or sites) will produce the required emission, only to die out in turn. If new sites are not sufficiently prepared before the old site dies, this part of the cathode spot is extinguished and the current must transfer to other trains of sites. If this is not possible the arc as a whole will tend to extinguish.

The arc velocity (in the continuous mode) will depend, therefore, on the rates of decline of emission from the old sites and growth on the new. These are determined by surface conditions, arc current, gas pressure, etc., as well as by the t.m.f. in the cathode-fall space. The observed motion under various conditions may now be discussed in the light of the mechanisms suggested above.

(3) COMPARISON OF EXPERIMENTAL RESULTS AND MODEL PREDICTIONS

(3.1) Effect of Pressure

As already described, the model predicts that as the pressure is reduced the Ampèrian velocity should decrease, and after it has passed through an immobility range, retrograde motion should set in. This has been demonstrated by Yamamura[7] (see Fig. 4) for aluminium electrodes in air and by Gallagher[26] for

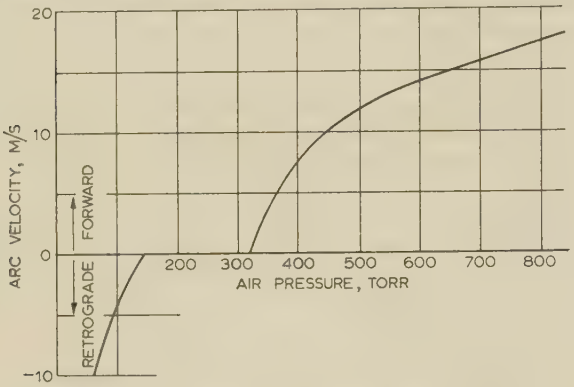

Fig. 4.—Arc velocity as a function of pressure.[7]

Arc current = 10 A.
Magnetic flux density = 0·075 Wb/m².
Inter-electrode gap = 2·5 mm.
Aluminium electrodes.

several different cathode materials in helium, argon, nitrogen, oxygen and carbon dioxide. The cathode root controlled the behaviour and the reversal pressure was approximately proportional to the first excitation potential of the gas. At any given pressure the excitation potential will determine the dimensions of the cathode-fall space and therefore the curvature of the ion tube. An increase in the curvature of the tube will increase the reversal pressure as found.

Sometimes, as reported by many investigators, the cathode spot moves in the retrograde direction while the column and anode spot tend to continue in the Ampèrian direction. This leads to discontinuous jumping of the cathode spot in the forward direction to prevent extinction.

(3.2) Influence of T.M.F.

The experiments already described (Figs. 1 and 2) show the importance of the magnitude of the t.m.f. in the fall region. According to the mechanism suggested, relatively simple relationships between t.m.f. and velocity could be expected for both Ampèrian and retrograde motion. This has been confirmed for Ampèrian motion on brass electrodes in air (Fig. 2). Fig. 5 shows that when a mercury arc moves under the action of a t.m.f. in argon at 150 torr, a progressive reduction in the magnetic flux density causes the retrograde arc velocity to decrease to zero, and subsequently causes the forward velocity to increase. An explanation based upon the model is that as the t.m.f. weakens the ion tube is deflected less and the initial retrograde electron velocity is reduced. Consequently, new ion production occurs in a region not so far to the retrograde side of the ionization zone as before, and thus the retrograde arc velocity is reduced. Continued reduction in the t.m.f. will then lead to immobility, and this will be followed by Ampèrian motion due to the diminishing initial component of retrograde velocity. Finally, as the field decreases further, the velocity in the Ampèrian direction might be expected to pass through a maximum and then tend to zero, because the weakening field is no longer able to cause marked deflection in the Ampèrian

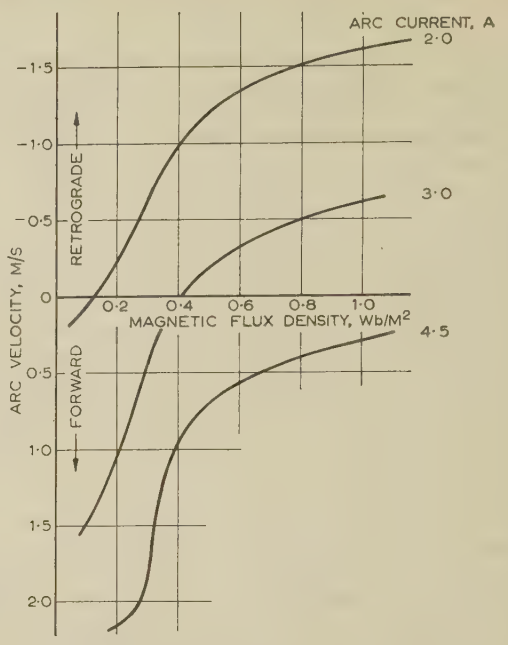

Fig. 5.—Arc velocity as a function of magnetic field strength for constant arc currents.[10]

Argon pressure = 150 torr.
Mercury-molybdenum cathode.

sense of the emitted electrons, which by this stage receive a negligible initial retrograde component of velocity. The curve for an arc of 4·5 A in Fig. 5 tends to confirm this.

In a high-vacuum arc the electrons will have a small probability of collision on their passage in the ion tube, so that they do not lose their initial retrograde component of velocity. Thus, as the t.m.f. decreases, the probability of forward motion occurring is much less, and Fig. 6 shows that the retrograde velocity merely decreases to zero.

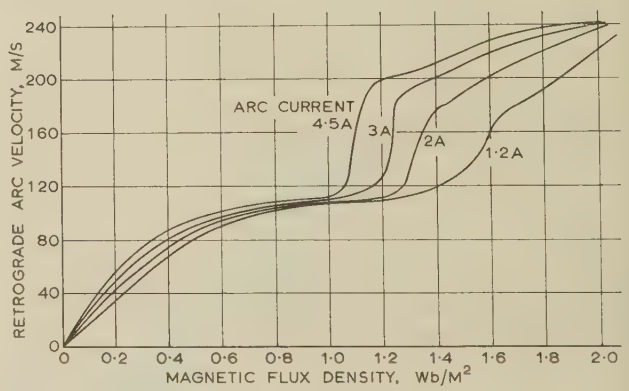

Fig. 6.—Arc velocity as a function of magnetic field strength for constant arc currents in vacuum.[10]

Mercury-molybdenum cathode.

Fig. 6 also shows another important phenomenon, namely a rapid increase in retrograde velocity when the t.m.f. exceeds 0·9 Wb/m², so that two velocity plateaux appear. Spectral analysis indicated that, above the first plateau, Hg^{2+} ions were being produced in the discharge, and further that another increase in velocity observed above the second plateau was associated with the production of Hg^{3+}. The effects disappeared on the addition of argon to the system. These results have been the downfall of most of the theories of retrograde motion, but as

cker[13] has already shown, the present model can explain them mply. Hg^{2+} ions will be deflected more in the Ampèrian irection than Hg^{+} ions, and thus the initial retrograde com- onent of velocity imparted to the emitted electrons will be ncreased. The new region of ionization consequently will be isplaced more in the retrograde direction and increased arc elocity will result. The production Hg^{3+} at even higher fields ill cause a further increase in velocity for the same reason.

(3.3) Multiple Sites and the Influence of the Arc Current

The arc current affects the motion by changing the conditions n the cathode spot. If the spot consists of several independent mitting sites, each of limited current capacity, it is possible to xplain why the arc velocity should increase with current up to certain value and then show no further increase. In air at tmospheric pressure the limit[14] is about 45 A, and below this alue only one site would exist in the spot. A change in current elow about 45 A might be expected to alter the site charac- eristics by changing the electron emission density and the degree f ion bombardment. According to the proposed model these hanges will affect the rates of decay and growth of emission fficiency of the site and thus will change the arc velocity. If he current exceeds 45 A more than one site will exist and change f current in this range will have less effect on the velocity, ecause the majority of sites will exist and move independently ith a current at the limit of about 45 A for each. The results btained by Winsor and Lee[27] with copper electrodes tend to onfirm this. Up to 49 A the velocity increased rapidly with urrent, but above this value the increase was less than 20% ven when the current was more than doubled. The measure- nents[7] displayed in Fig. 7 are even more striking in this respect,

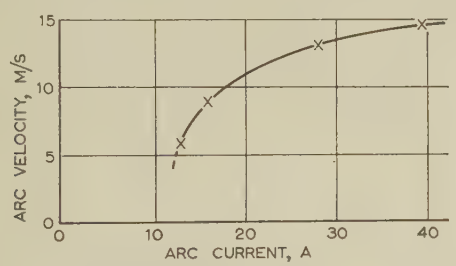

Fig. 7.—Dependence of forward cathode-root velocity[14] on arc current below 40 A.

Inter-electrode gap = 3·2 mm.
Transverse flux density = 0·027 Wb/m².
Brass electrodes.

while recent experiments with brass electrodes in hydrogen at 25 torr indicated that multiple sites occurred when the current in the retrograde-moving arc[28] exceeded about 1 A.

A secondary effect of the arc current is particularly obvious at low pressures. As the current increases there is an increased tendency for Ampèrian motion,[10] so that at pressures in the range 50–125 torr the t.m.f. needs to be increased linearly with arc current in order to maintain the immobility condition. The probable explanation is that the current influences the local pressure in the cathode-fall space by determining the density of metal vapour present. An increase in current would increase the pressure and so encourage Ampèrian motion.

The tracks left on electrodes after passage of the arc afford further evidence for multiple emission sites and the influence of current on the motion. Fig. 8 shows tracks left on polished brass electrodes[29] for Ampèrian motion at both atmospheric and low pressures. In both cases branched filamentary tracks indicate the existence of multiple emission sites. At low pres- sures, however, the overall motion is only just in the Ampèrian

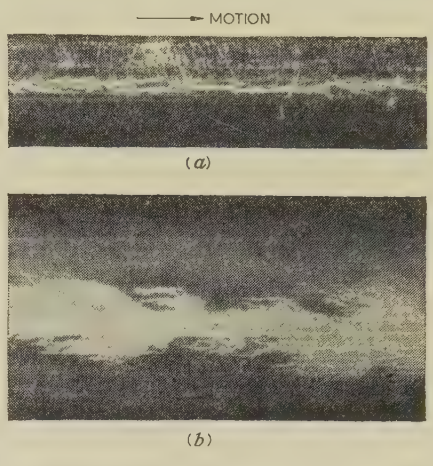

Fig. 8.—Cathode-root tracks.
(*a*) At atmospheric pressure.
(*b*) At reduced pressure.

sense, and it will be seen that many of the filamentary tracks turn back from the main track, thus showing that some emission sites travel in the retrograde direction for a short time just before dying out. This shows that when the pressure is reduced almost to the range of immobility, some sites can move forward while others move retrogradely, depending on local conditions such as surface state, site current and local variations of t.m.f. (due possibly to self-field effects). This seems to offer further support for a unified model of forward and retrograde motion. It can be seen in Fig. 8 that those emitting sites which move outwards and decay, while moving forward at the higher pressure, do so while moving retrogradely at the lower pressure, despite the overall forward movement of the cathode spot. Sites to the edge of the main track will tend to move outwards, owing to repulsive forces in both cases, and the current carried by each marginal emitting site will tend to decrease as a result of the sites being inadequately conditioned by ion bombardment. At the lower pressure, however, reduction in current will give a tendency towards retrograde motion (Fig. 5), so that these sites will lag behind the majority of the emitting sites. The current carried by the latter will set up a self-field (pinch field) which will augment the t.m.f. and further increase the retrograde tendency of the lagging sites (see Fig. 5). At the higher pressure there is no tendency for retrograde motion, and Fig. 7 shows that a reduction in current may reduce the forward velocity of the marginal emitting sites so that they lag behind the main discharge and eventually extinguish.

(3.4) Cathode Effects

The model proposed suggests that the nature of the cathode surface should have a strong influence on the velocity and particularly that insulating oxide or other tarnishing surface layers will be important. It has been shown by many workers that an arc prefers to operate on an oxidized surface, and recent measurements in this laboratory have clearly demonstrated these effects.[29] It might be expected that the growth of emission at a new site to which the arc is to transfer will depend critically on the thickness and insulating properties of the oxide layer there. For thin layers the positive charge will be neutralized easily by electrons tunnelling from the base metal, but this neutralization will decrease as the oxide layer increases, so that a site will condition more rapidly to a suitable emission efficiency for arc transfer. However, for thick oxide layers the electrons emitted are likely to come from the oxide itself rather than from

the base metal, and the emission and thus the arc velocity may decrease again. It is interesting to note that Hancox has recently shown[30] that insulating inclusions in the cathode surface encourage the initiation of new cathode spots, owing to their being charged by incident positive ions. The reasoning here considers processes at new sites only, but the behaviour of the old sites from which the arc has to transfer will be equally important in determining arc velocity. These sites will ultimately become poor emitters, first because of reduced ion bombardment, and secondly because of the removal of the oxide layer. The arguments ignore the temperature dependence of the T–F emission, which may also be important and depend on oxide thickness. Site transfer might occur when the temperature of the new site bears some relation to that of the old, depending on the T–F process. The temperatures of both old and new sites may be determined by the rate of heat flow through the oxide layers involved, and again a simple thermodynamic treatment[28] shows that the arc velocity should go through a maximum as the oxide layer increases. Fig. 9 shows results of this

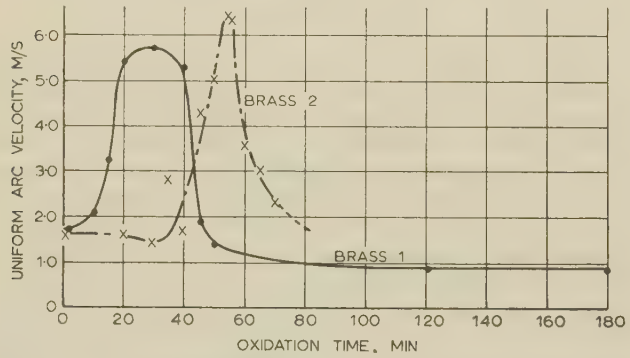

Fig. 9.—Variation of uniform arc velocity with time of cathode oxidation.

Current = 70 A.
Pressure = 25 torr.
Flux density = 0·024 Wb/m².
Inter-electrode gap = 6·4 mm.

nature for Ampèrian motion on brass electrodes which were initially etched and then allowed to oxidize for fixed times before testing. Many other results for both Ampèrian and retrograde motion indicating the great influence of cathode-surface conditions have been reported recently.[29] In particular, arcs on oxidized annular brass electrodes initiated in nitrogen or hydrogen and allowed to move for some minutes changed in velocity continuously as the oxide layer was gradually reduced by the arc. If air was admitted to the system the velocity gradually changed back again, corresponding to the re-formation of the oxide layer.

Other electrode materials also exhibited the same general cathode phenomena. Thus an arc in air on stainless-steel electrodes with some surface oxidation moved steadily, but when the electrodes were polished and a hydrogen atmosphere substituted an arc could not be maintained. With polished platinum an arc could be initiated in air only with considerable difficulty, and the small change in velocity with arc running time was probably due to surface roughening rather than oxidation effects.

Contrary to the results of earlier investigations, it was found difficult to maintain arcs on copper electrodes at low pressures, even when these had been allowed to oxidize freely for several days. At atmospheric pressure the arc was stable, but even then it could not be made to function in a reproducible manner. It has been suggested[29] that this behaviour is due to the oxide layer on copper being mainly the semiconducting cuprous oxide, Cu_2O, with an extremely thin surface film of insulating cupric oxide, CuO. At low pressures the cupric oxide could be quickly removed by the arc, so exposing the cuprous oxide, which is not efficient in maintaining the arc. At atmospheric pressure, in the presence of a greater amount of oxygen, the cupric oxide could be continuously regenerated and the arc attain a constant velocity. The failure of previous workers to appreciate the significance of the oxide layer and their use of well-conditioned (i.e. well arced) electrodes in many cases may be partly responsible for the lack of agreement in their experimental results.

(4) HELICAL MOTION

The discussion so far has concerned arc tracks which are straight, since they are influenced only by a t.m.f. When the cylindrical electrodes used in obtaining the results shown in Fig. 1 were magnetized in an axial direction, either permanently or by the application of an external magnetizing coil, the arc moved helically along the cathode in the Ampèrian direction. It was found possible for the cathode spot to make several complete turns of the electrode without the column short-circuiting back to the electrode.[31] It was observed that the direction of the helix motion was determined by the direction of the combined axial and circumferential fields, the axial direction being that of the field inside the cathode. This discovery appears at first sight to be at variance with the concept that motion is determined by the t.m.f. in the cathode-fall space. However, a perfect gas–electrode interface with abrupt reversal of the field does not exist for permanently magnetized electrodes. The interface will have many irregularities due to roughness and crystal boundaries, and between irregularities the field direction could be that of the interior of the electrodes.

The circumferential field acting is the self-field of the current in the electrodes, whereas the applied axial field is independent of current, so that it might be expected that an increase in arc current with constant axial field would cause the helix angle between the arc track and the electrode axis to decrease, i.e. the helix would open out. Fig. 10 shows[14] that the opposite

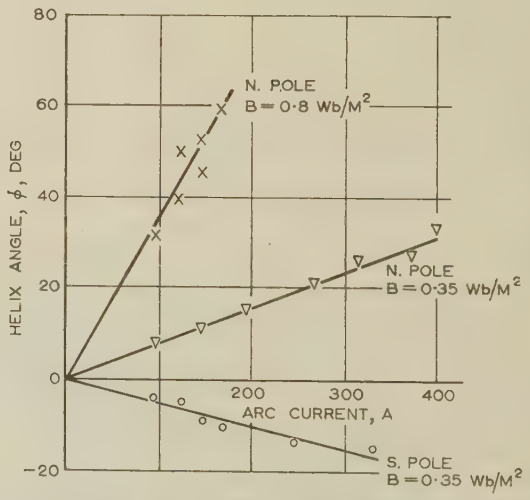

Fig. 10.—Variation of cathode-track helix angle with arc current for various axial magnetic fields.[14]

Current feed to one end of electrodes only.
Inter-electrode gap = 3·2 cm.
Steel electrodes.

actually occurs and is well defined. A possible explanation for this can be advanced in terms of the model.

The variation in helix angle in Fig. 10 is due to the effective axial field being influenced by the current in the electrodes, and this may be aided by the circumferential field, which does not

rise in proportion to the current. Moreover, at high currents the increase in skin effect[28] may further distort the pattern of current flow near the cathode spot in such a way that the circumferential field does not increase at the rate predicted by simple considerations.

The axial field is likely to be modified by the current flowing from the cathode spot, because this is not uniform and axial until some distance from the spot. In the immediate neighbourhood of the spot there will be components of current along the surface at right angles to the axis of the electrode. This results in the effective axial field being non-uniform along this circumference, since the component on one side of the spot augments the applied axial field, while on the other side the current tends to reduce it. Examination of the relative field directions shows that the axial field is reduced on the leading side of the cathode spot and increases on the trailing side. For the arc currents of the magnitudes shown in Fig. 10 the cathode spot will be composed of a number of emission sites. Those on the leading side of the spot, which are in the process of being established, experience the weaker axial magnetic field. Their rate of growth will be increased because their positive-ion tubes will not be so sharply deflected ahead of them, and thus they will receive positive ions at a greater rate. Moreover, sites on the trailing edge, which experience the increased axial field, will have their ion tubes more sharply deflected, and this will speed up their extinction and the growth of new emitting sites ahead.

The gradient of axial field across the cathode spot will increase with current, so that on the basis of the mechanism suggested above the circumferential component of velocity might increase, as has been observed.[31] Although the explanation is tentative, it is supported to a certain extent by the results of Kesaev.[32] He observed that, when an arc was established in an asymmetric magnetic field at low pressure, retrograde movement occurred towards the region of maximum field strength. Robson[33] has reported arc motion for retrograde conditions which seems to be related to this helix motion. An arc of 10 A was struck between flat parallel electrodes in air at pressures in the range 0·05–0·5 torr and a uniform magnetic field was applied, inclined at an angle θ to the cathode surface. The resultant arc motion was found to have a component in the direction of the acute angle θ as well as the expected retrograde component along the longitudinal axis of the cathode. The arc track was thus formed at an angle ϕ (see Fig. 11) to the axis, and ϕ increased with θ,

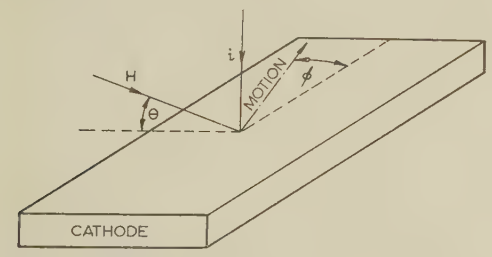

Fig. 11.—Inclined direction of magnetic field used by Robson.[33]

magnetic field strength and arc current. When the pressure was increased to above that for normal retrograde motion the arc movement became erratic, the tracks left being a series of close spirals and randomly directed interconnecting paths.

Robson has sought to explain the movement in terms of the theory of Robson and von Engel[9] already discussed, but the present model is also capable of explaining it adequately. The component of the field parallel to the cathode is a t.m.f. deflecting the ions of the fall region in the Ampèrian sense and producing an ion velocity parallel to the cathode. The normal component of the magnetic field is perpendicular to the direction of this velocity and so a force will arise to cause further deflection of the ion tube in a direction perpendicular to the axis of the electrode. Although the ions are deflected in the Ampèrian direction, the electrons emitted will move in a retrograde sense, as described in Section 2.2, having both axial and transverse components. The observed effects of changing θ, magnetic field and arc current are consistent with the above description. If the pressure is raised to the immobility range, consistent retrograde deflection will cease and secondary forces will set up the random motion observed.

(5) DISCONTINUOUS MODE

So far, discussion has been limited to the continuous mode of arc motion for which the model is valid, but a discontinuous mode can also be found in which the arc moving in the Ampèrian direction proceeds by a series of irregular steps of the cathode spot, leaving the cathode unmarked in between.[15] In general, the discontinuous mode occurred when the t.m.f. was large (greater than 0·05 Wb/m^2). A mechanism for this mode has been proposed by Dunkerley and Schaefer[34] which basically depends on factors similar to those governing continuous motion. They suggest that the arc column is caused to bow out ahead of the existing spot and to come close to the cathode surface. Ions can then come from the column itself rather than from the top of the fall region to condition the surface and cause emission well ahead of the original spot. Both cathode and column processes will operate, as has been demonstrated.[15] A change of cathode material altered the velocity (measured as the overall distance moved in unit time) by a factor of four, while a change in time-constant of the external circuit (keeping the current constant) resulted in a fivefold velocity change. While the change of electrode would affect only the cathode processes, a change in time-constant would alter the flexibility of the column through the transient voltage which could be impressed. It is surprising that the velocity in this mode is independent of current, because although the cathode processes may be independent of current, the column deflection would not be if it were considered as being similar to a metallic conductor. This result further stresses the fallacy of the conductor concept and suggests that deflection of the column arises from forces on the individual ions and not from some collective action of the current considered as a circuit parameter.

It should be noted that, while in nearly every case the overall velocity of movement is greater for discontinuous rather than for continuous motion, the surface damage from the former may be far more serious. It usually consists of a series of raised and roughened areas where the arc has dwelt which may, for instance, easily prevent satisfactory mating of contacts.

(6) CONCLUSIONS

All the evidence summarized here indicates the important part played by cathode processes in determining arc motion. The presence of insulating layers, which are likely to be the oxides of the base metal in most situations, is seen to be vital in determining the velocity and degree of damage. This is of more than academic interest and has direct application to industrial equipment in which an arc is required to traverse a surface many times. If the arc operates in air, the arc track will tend to become more heavily oxidized and the arc will follow the same path in subsequent operation of the device. In hydrogen or nitrogen the opposite will tend to occur, and so there are advantages in operating arcing devices in non-oxidizing atmospheres, since the wear will be reduced. Even when operating in air, however, the damage can be greatly reduced by suitable electrode design and treatment.

It now appears that a single model of the operation of cold-cathode arcs can be given which applies to both Ampèrian and retrograde motion and to the immobility region.

It should be emphasized that his model requires further experimental confirmation, but at present it seems to offer a reasonable basis for the planning of further work.

(7) ACKNOWLEDGMENTS

The authors wish to thank Professor M. W. Humphrey Davies for his encouragement and the British Electrical and Allied Industries Research Association for the use of certain equipment built for an earlier investigation on behalf of the Association.

One author (P. E. S.) gratefully acknowledges the award of an I.M.E.A. Scholarship by The Institution.

(8) REFERENCES

(1) DAVY, H.: 'Further Researches on the Magnetic Phenomena produced by Electricity, with some new Experiments on the Properties of Electrified Bodies in their relations to Conducting Powers and Temperature', *Philosophical Transactions of the Royal Society*, A, 1821, p. 425.

(2) BABAKOV, N. A.: 'Speed of Motion of Short Electric Arcs', *Elektrichestvo*, 1948, **7**, p. 74.

(3) EIDINGER, A., and RIEDER, W.: 'Verhalten des Lichtbogens in transversalen Magnetfeld', *Archiv für Elektrotechnik*, 1957, **63**, p. 94.

(4) FECHANT, M. D.: 'Vitesse de déplacement d'arcs électriques dans l'air', *Revue Générale de l'Électricité*, 1959, **68**, p. 519.

(5) HESSE, D.: 'Über den Einfluss des Lautshienenfeldes auf die Ausbildung und Bewegung von Lichtbogenfusspunkten', *Archiv für Electrotechnik*, 1960, **45**, p. 188.

(6) WEINTRAUB, E.: 'Investigation of the Arc in Metallic Vapours in an Exhausted Space', *Philosophical Magazine*, 1904, **7**, p. 95.

(7) YAMAMURA, S. J.: 'Immobility Phenomena and Reverse Driving Phenomena of the Electric Arc, Driven by Magnetic Field', *Journal of the Faculty of Engineering* (University of Tokyo), 1957, **25**, p. 59.

(8) SMITH, C. G.: 'Motion of the Copper Arc in a Transverse Magnetic Field', *Physical Review*, 1943, **63**, p. 217.

(9) ROBSON, A. E., and VON ENGEL, A.: 'Origin of Retrograde Motion of Arc Cathode Spots', *ibid.*, 1945, **93**, p. 1121.

(10) ST. JOHN, R. M., and WINANS, J. G.: 'Motion and Spectrum of Arc Cathode Spot in a Magnetic Field', *ibid.*, 1955, **98**, p. 1664.

(11) HIMLER, G. J., and COHN, G. I.: 'The Reverse Blowout Effect', *Electrical Engineering*, 1948, **67**, p. 1148.

(12) HERNQVIST, K. G.: 'Emission Mechanism of Cold-Cathode Arcs', *Physical Review*, 1958, **109**, p. 636.

(13) ECKER, G., and MULLER, K. E.: 'Theorie der "Retrograde Motion" ', *Zeitschrift für Physik*, 1958, **151**, p. 577.

(14) GUILE, A. E., and SECKER, P. E.: 'Arc Cathode Movement in a Magnetic Field', *Journal of Applied Physics*, 1958, **29**, p. 1662.

(15) SECKER, P. E., and GUILE, A. E.: 'Arc Movement in a Transverse Magnetic Field at Atmospheric Pressure', *Proceedings I.E.E.*, Paper No. 3044 S, August, 1959 (**106** A, p. 311).

(16) SECKER, P. E.: 'Explanation of the Enhanced Arc Velocity on Magnetic Electrodes', *British Journal of Applied Physics*, 1960, **11**, p. 385.

(17) FROOME, K. D.: 'Current Densities of Free-Moving Cathode Spots on Mercury', *ibid.*, 1953, **4**, p. 91.

(18) ROBSON, A. E.: 'The Concentration of Current at Arc Cathodes'. E.R.A. Report Ref. L/T330.

(19) LEE, T. H.: 'On the Discussion of the T–F Theory by Robson and von Engel', *Journal of Applied Physics*, 1958, **29**, p. 734.

(20) ECKER, G., and MULLER, K. G.: 'Der Einfluss der individuellen Feldcomponente auf die Elektronenemission der Metalle', *Zeitschrift für Naturforschung*, 1959, **14a**, p. 511.

(21) HAGSTRUM, H. D.: 'Auger Ejection of Electrons from Tungsten by Noble Gas Atoms', *Physical Review*, 1956, **104**, p. 317.

(22) VON ENGEL, A., and ROBSON, A. E.: 'The Excitation Theory of Arcs with Evaporating Cathodes', *Proceedings of the Royal Society*, 1957, **242**, p. 217.

(23) PRICE, W. L., GAMBLING, W. A., and EDELS, H.: 'High-Pressure Glow-to-Arc Transitions with Tungsten and Copper Cathodes'. *Nature*, 1955, **176**, p. 28.

(24) BRAGG, J. K., SHARBAUGH, A. H., and CROWE, R. W.: 'Cathode Effects in the Dielectric Breakdown of Liquids', *Journal of Applied Physics*, 1954, **25**, p. 382.

(25) ECKER, G.: 'Current Transition Gas—Metal. 1. Electrode Discharge Components of the Arc', Technical Report for U.S. Dept. of Navy, FTR 1, 1959.

(26) GALLAGHER, C. J.: 'The Retrograde Motion of the Arc Cathode Spot', *Journal of Applied Physics*, 1950, **21**, p. 768.

(27) WINSOR, L. P., and LEE, T. H.: 'Properties of a D.C. Arc in a Magnetic Field', *Transactions of the American I.E.E.*, 1956, **75**, p. 143.

(28) SECKER, P. E.: 'The Dependence of Arc-Root Mobility on Electrode Conditions', Ph.D. Thesis, University of London, 1960.

(29) LEWIS, T. J., and SECKER, P. E.: 'The Influence of the Cathode Surface on Arc Velocity', *Journal of Applied Physics*, 1961, **32**, p. 54.

(30) HANCOX, R.: 'Importance of Insulating Inclusions in Arc Initiation', *British Journal of Applied Physics*, 1960, **10**, p. 468.

(31) GUILE, A. E., LEWIS, T. J., and MEHTA, S. F.: 'Arc Motion with Magnetised Electrodes', *ibid.*, 1957, **8**, p. 444.

(32) KESAEV, I. G.: 'On the Causes of Retrograde Arc Cathode Spot Motion in a Magnetic Field', *Soviet Physics 'Doklady'*, 1957, **2**, p. 60.

(33) ROBSON, A. E.: 'The Motion of an Arc in a Magnetic Field', *Proceedings of the Fourth International Conference on Gas Discharges*, 1959, **1**, p. 346.

(34) DUNKERLEY, N. S., and SCHAEFER, D. C.: 'Observations of Cathode Arc Tracks', *Journal of Applied Physics*, 1955, **26**, p. 1384.

621.316.728:621.311.153.2

The Institution of Electrical Engineers
Monograph No. 448 S
May 1961

FREQUENCY-RESPONSE ANALYSIS OF DISPLACEMENT GOVERNING IN SYNCHRONOUS POWER SYSTEMS

By P. A. W. WALKER, B.Eng., Graduate, and A. S. ALDRED, M.Sc., Ph.D., Associate Member.

(*The paper was first received* 21*st November*, 1960, *and in revised form* 28*th January*, 1961. *It was published as an* INSTITUTION MONOGRAPH *in May*, 1961.)

SUMMARY

The paper describes the application of the frequency-response concept to the analysis of displacement governing in a synchronous machine system. The governor loop is shown to combine with the basic closed-loop pattern of the generator and modifies only the feedback element in the original basic loop. The analysis is used to compare stability boundaries for different governor conditions, these boundaries being derived by the application of the Nyquist stability criterion. The results obtained by this method, although based on small-displacement theory, were found to be in agreement with those obtained from a power-system simulator.

The effects of phase lags, arising in the steam header of the turbine and the servo mechanism operating the throttle valve, on the stability of the system are considered together with that of a second-derivative stabilizer. An examination is also made of the damping in the system, as this provides a useful appraisement when comparing the relative stability of different configurations in the governor loop.

LIST OF SYMBOLS

δ = Rotor angle.
α = Time error or displacement angle.
β = Angle between busbar voltage and control vector.
ω = Frequency of small oscillations of rotor, rad/s.
f', ω' = System frequency, c/s and rad/s.
H = Inertia constant, kWs/kVA.
$M = H/180f'$.
T_i = Turbine torque.
T_u = Torque output.
g = Governor gain.
$g(p)$ = Transfer function of governed turbine.
g_b = Gain of governor stabilizer.
τ_1 = Steam header or penstock time-constant.
τ_2 = Servo mechanism time-constant.
τ_{d0} = Generator field time-constant.
K_D = Mechanical damping-torque coefficient.
v = Busbar voltage.
v_{fd} = Generator field voltage.
$V_{fd} = v_{fd}X_{ad}/R_{fd}$ = Open-circuit terminal voltage at normal speed.
Φ_d = Direct-axis armature flux linkage.
Φ_q = Quadrature-axis armature flux linkage.
v_d = Direct-axis busbar voltage.
v_q = Quadrature-axis busbar voltage.
i_d = Direct-axis armature current.
i_q = Quadrature-axis armature current.
X_{ad} = Mutual reactance between generator field and direct-axis armature winding.
X_d, X_q = Total direct- and quadrature-axis reactances.
X'_d = Total direct-axis transient reactance.
R_{fd} = Field resistance.

Correspondence on Monographs is invited for consideration with a view to publication.
Mr. Walker and Dr. Aldred are in the Department of Electrical Engineering, University of Liverpool.

(1) INTRODUCTION

The present trend in the design of turbo-alternators is towards larger machine ratings. This concentration of generated power in individual machines emphasizes the necessity for improved methods of load and frequency control and for increasing the margin of stability. The conventional method of control is by means of a centrifugal governor that detects a change in speed from a fixed reference, and thereby operates the throttle valve on the turbine to compensate for load fluctuations. This technique has the disadvantages of relatively inefficient control of frequency and load sharing, and contributes very little to ensuring stability. The introduction of fast-acting voltage regulators helps to improve the stability of the generator, but this is partially offset by the inclusion of current feedback in the regulator. It is pertinent, therefore, to examine alternative supplementary control techniques. One such technique that has been proposed[1,2] is known as displacement governing (alternatively known as synchronous or time-error governing). Here the characteristic of the governor causes the turbine torque to be proportional to the time error or angle by which the rotor lags a vector (rotating at 50 c/s) that represents standard time, the constant of proportionality being the governor gain.

Consider a single machine connected to an infinite busbar. The busbar voltage, in general, lags the standard vector by an angle that is fixed owing to the infinite nature of the system. The machine rotor is displaced from the busbar vector by the rotor angle δ. A third rotating vector is proposed and defined here as the control vector. This is illustrated in Fig. 1(*a*), and its space position may be varied with respect to the standard reference vector or, because the system is infinite, the busbar vector, from which it is displaced by an angle β. The time-error angle is then the angle between the rotor and control vector. It is apparent that for correct operation of this type of governing the frequency of the infinite busbar must be exactly 50 c/s. It follows that the machines feeding the busbar must themselves be controlled by displacement governors. A block diagram representing the method of control for a single machine is shown in Fig. 1(*b*). To supply a given load, T_u, requires a certain rotor angle δ. The necessary value of β is determined when it is realized that the displacement-governed set will operate in the steady state only when the turbine torque $T_i = g(\beta - \delta) = T_u$, assuming that the governor gain is fixed. If the load tends to decrease, the rotor angle will tend to increase as a result of an accelerating torque acting on the rotor. In so doing the difference between the controlling quantity β and the rotor angle will decrease, consequently reducing the turbine torque to create a decelerating torque on the rotor. Provided that there is sufficient damping in the system the rotor oscillations will decay until the machine is stable at the original load. Thus a change in load can be met only by a suitable rotation of the control vector position, i.e. of β. From the foregoing description, it should be evident that the governor, because of its negative torque/angle characteristic, contributes to the stiffness of the system.

It has been suggested[3] that this phenomenon might be used to

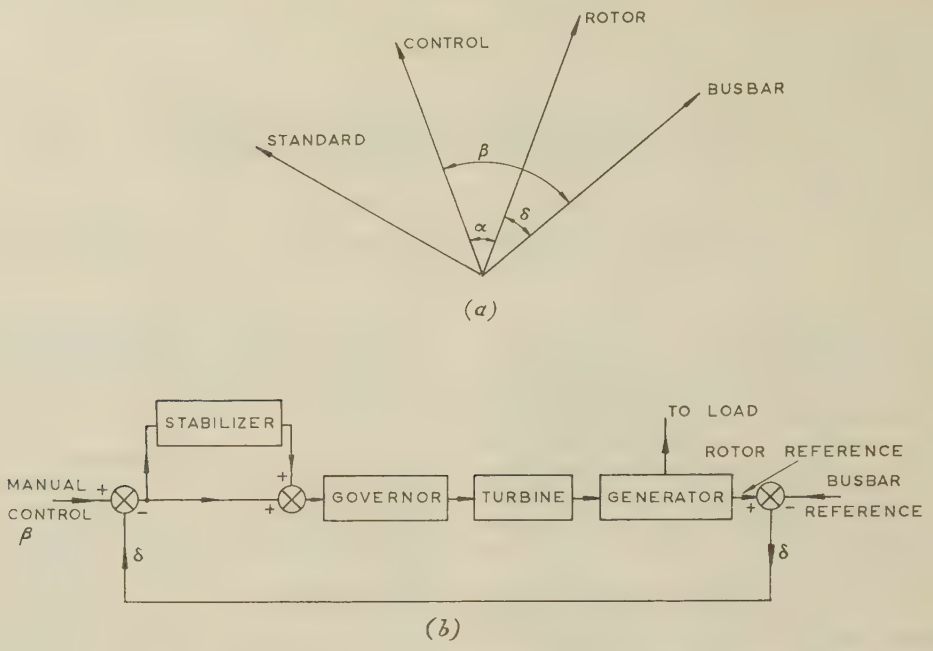

Fig. 1.—Synchronous-machine system with displacement governor.
(*a*) Principal rotating-vector quantities.
(*b*) Complete block diagram.

extend the region of stable operation of the machine into the dynamic-stability region. It is also necessary to take into account the effect of the phase lags in the governor loop. This is because the movement of the rotor subsequent to a small disturbance is dependent upon the damping in the system and the net synchronizing torque acting upon it. The existence of phase lags in the governor loop modifies both these quantities. The occurrence of a small disturbance would then give rise to a response from the system that might be considerably different from the response with no phase lags.

The object of the paper is to examine the influence on the steady-state stability boundary of the governor gain and, in particular, of phase lags in the governor loop. The improvement in stability of the machine, to be expected from the inclusion of a stabilizer, is dealt with. An examination is also made of the damping in the system, as this provides a useful appraisement for comparing the relative stability of different configurations in the governor loop.

(2) ANALYSIS OF A SYNCHRONOUS MACHINE WITH A DISPLACEMENT GOVERNOR

(2.1) Operation of Governor

When the prime mover is controlled by a displacement governor the stiffness of the set is increased by an amount equal to the gain of the governor, if there are no phase lags in the governor loop. This allows of operation in the dynamic-stability region where the synchronizing-torque coefficient of the machine itself is negative. To operate at the point P in Fig. 2, the minimum governor gain, necessary for stable operation, is the slope of the torque/angle curve at that point. The corresponding governor characteristic line is MN. It is tangential to the curve at P and is described by the equation

$$T_i = g\alpha \quad . \quad . \quad . \quad . \quad . \quad . \quad . \quad . \quad (1)$$

in which the error angle α equals $\beta - \delta$. This represents a stability boundary because the net synchronizing-torque coefficient of the system is zero at this point. It might be noted that, if the governor characteristic intersects the torque-angle curve twice,

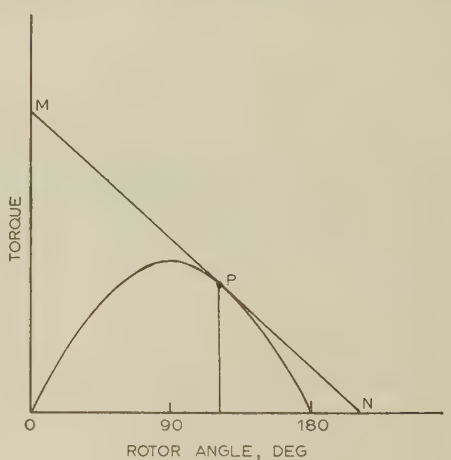

Fig. 2.—Governor characteristic line imposed on the torque-angle curve.

the machine will be stable only at the intercept corresponding to the smaller rotor angle. It is evident that for stable operation at a specific load three conditions must be satisfied, namely

(*a*) The resultant torque acting on the alternator must be zero.
(*b*) The net synchronizing-torque coefficient must be positive.
(*c*) The damping coefficient must be positive.

The provision of (*a*) amounts to the proper adjustment of the angle by the control vector, whilst that of (*b*) and (*c*) is more difficult since, in practice, there are phase lags associated with the operation of the steam-head valve of the turbine.

It is envisaged that there are two principal phase lags in the governed turbine. These arise from the steam in the turbine header and the hydraulic servo mechanism actuating the steam head valve. Broadbent[1] has, to some extent, compensated for these by the use of a second-derivative stabilizer, which provides phase advance for the electrical signal representing the time error angle. It consisted of a tachometer feeding an *RC* network. The attenuation and phase lag of this network could

be minimized by gain compensation. The complete torque/angle transfer function of the turbine operating with a stabilized governor and including phase lags is

$$\frac{T_i}{\alpha} = g(p) = \frac{1}{(1+\tau_1 p)(1+\tau_2 p)}(g + g_b p^2) \quad . \quad . \quad (2)$$

It is evident from eqn. (2) that stability cannot be determined from absolute steady-state analysis and that an operational method or frequency-response approach is necessary. The method adopted by the authors, to determine whether or not conditions (*b*) and (*c*) obtain, is the technique of frequency-response analysis, which is based on the linearization of the machine equations using small-displacement theory. This has been fully described elsewhere.[5]

(2.2) Small-Displacement Theory

The system that is analysed is shown in block-schematic form in Fig. 1(*b*). The operational equations, together with the assumptions implicit in them, for a machine connected through a transmission line to a busbar without any governor, are derived in Section 8·1 of Reference 5. For convenience the equations are restated here in per-unit notation.

Direct axis $$v_d = -\Phi_q = v \sin\delta \quad . \quad . \quad . \quad . \quad . \quad . \quad (3)$$

Quadrature axis $$v_q = \Phi_d = v \cos\delta \quad . \quad . \quad . \quad . \quad . \quad . \quad (4)$$

where $$\Phi_q = -X_q i_q \quad . \quad . \quad . \quad . \quad . \quad . \quad . \quad . \quad (5)$$

$$\Phi_d = G(p)V_{fd} - X_d(p) i_d \quad . \quad . \quad . \quad . \quad . \quad (6)$$

and $$G(p) = \frac{1}{1+\tau_{d0}p} \qquad X_d(p) = \frac{X_d + X_d'\tau_{d0}p}{1+\tau_{d0}p}$$

The equation of motion of the system is

$$T_i = M\frac{d^2\delta}{dt^2} + k_D\frac{d\delta}{dt} + T_D\frac{d\delta}{dt} + \Phi_d i_q - \Phi_q i_d \quad . \quad (7)$$

Here T_D is the damping-torque coefficient arising from the presence of either damper windings in a salient-pole machine or rotor eddy currents in a round-rotor machine. To the above equations we now add that for the output torque of the governed turbine, namely

$$T_i = g(p)\alpha \quad . \quad . \quad . \quad . \quad . \quad . \quad . \quad (8)$$

where $$\alpha = \beta - \delta.$$

The small-displacement equations for the system are obtained by allowing all the variables in eqns. (3)–(8) to change by small amounts from the initial operating conditions. Steady-state initial-condition voltages and angles are denoted by the subscript 0. It will be sufficient here to quote the results of this technique which is set out in detail in Reference 5.

When these equations are solved for the ratio $\Delta T_i/\Delta\delta$ they yield:

$$\frac{\Delta T_i}{\Delta\delta} = \frac{g(p)\Delta\beta}{\Delta\delta}$$

$$= Mp^2 + K_D p + T_D p + \frac{vV_{fd}}{X_d}\cos\delta_0 + \frac{v^2(X_d - X_q)}{X_d X_q}\cos 2\delta_0 + \frac{v^2 \sin^2\delta_0 (X_d - X_d')\tau_{d0}p}{X_d(X_d + X_d'\tau_{d0}p)} + g(p) \quad . \quad . \quad . \quad . \quad (9)$$

It is of interest to examine the conditions necessary for a continuous sinusoidal oscillation to exist in the system when there is no disturbing force, i.e. when $\Delta T_i = \Delta\beta = 0$. By writing $p = j\omega$ and extending this equality to eqn. (9), it is evident that the latter will reduce to a real and an imaginary quantity. To obtain the proper solution each of these terms must be zero. Equating the real part to zero gives an equation which may be solved to determine the natural undamped frequency of oscillation of the system. The imaginary part reveals the amount of damping, $K_D p\Delta\delta$ (either positive or negative), required to cancel that in the system. The latter is taken to include positive damping due to the load and damper windings or round-rotor eddy currents and negative damping due to phase lags in the governor loop.

(3) FREQUENCY-RESPONSE ANALYSIS

(3.1) Closed-Loop Representation

It has been shown[5] that a synchronous machine can be considered as a basic closed-loop pattern, amenable to analysis by the normal frequency-response method developed by Nyquist. The addition of a regulator to the machine alters only the form of the feedback function but in no way modifies the basic closed-loop pattern. The addition of a displacement governor to operate the steam-head valve of the turbine introduces a second closed loop into the system, and it is now shown that these two loops can be conveniently combined.

The small-displacement equation (9) of the machine driven by a turbine having a displacement governor may be written

$$\frac{g(p)\Delta\beta}{\Delta\delta} = Mp^2 + f(p) + g(p) \quad . \quad . \quad . \quad (10)$$

where $$f(p) = \phi(\delta_0) + \phi(p) \quad . \quad . \quad . \quad . \quad (11)$$

From eqn. (9),

$$\phi(\delta_0) = \frac{vV_{fd}}{X_d}\cos\delta_0 + \frac{v^2(X_d - X_q)}{X_d X_q}\cos 2\delta_0 \quad . \quad (12)$$

and $$\phi(p) = K_D p + T_D p + \frac{v^2 \sin^2\delta_0 (X_d - X_d')\tau_{d0}p}{X_d(X_d + X_d'\tau_{d0}p)} \quad . \quad (13)$$

Rewriting eqn. (10),

$$\frac{\Delta\delta}{g(p)\Delta\beta} = \frac{1/Mp^2}{1 + [f(p) + g(p)]/Mp^2} \quad . \quad . \quad . \quad (14)$$

The simple block diagram which represents eqn. (14) is shown in Fig. 3, and this is the basic closed-loop pattern for the synchronous-generator system for small displacements from the initial conditions. The function $[f(p) + g(p)]/Mp^2$ is the open-loop transfer function in operational form of the governed system. The term $g(p)\Delta\beta$ represents a small change in the prime-mover torque produced by a small rotation, $\Delta\beta$, of the

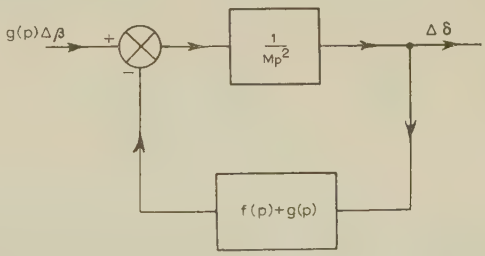

Fig. 3.—Basic closed-loop pattern for a synchronous machine operating with a displacement governor, derived from small-displacement theory.

control vector. This has the effect of slightly moving the governor characteristic line in a direction parallel to the torque axis in Fig. 2.

The Nyquist diagram is constructed by plotting the open-loop transfer function of Fig. 3, i.e. $[f(p) + g(p)]/Mp^2$, for $p = j\omega$ over a range of ω. The Nyquist criterion may be stated as follows. When the function is plotted for values of p between $-j\infty$ and $+j\infty$ the number of encirclements of the $(-1, 0)$ point must equal the number of poles of the transfer function with positive real parts minus the number of zeros. Since, in the present instance for the system under analysis, there are no such poles there must be no net encirclement of the $(-1, 0)$ point if the machine is to remain stable.

(3.2) Determination of Dynamic-Stability Boundaries

The frequency-response method is illustrated by consideration of both a turbo-alternator and a salient-pole alternator. Their principal parameters in per-unit notation have the values indicated in Table 1.

Table 1

Turbo-alternator

$X_d = 1{\cdot}7$	$X_q = 1{\cdot}7$	$X'_d = 0{\cdot}65$	$v = 1{\cdot}0$
$V_{fd0} = 1{\cdot}0$	$\tau_{d0} = 5$ sec	$H = 5$ kWs/kVA	$T_D = 3$ p.u.

Salient-pole alternator

$X_d = 1{\cdot}5$	$X_q = 1{\cdot}2$	$X'_d = 0{\cdot}7$	$v = 1{\cdot}0$
$V_{fd0} = 1{\cdot}0$	$\tau_{d0} = 5$ sec	$H = 3$ kWs/kVA	

Stability boundaries are determined by calculating and plotting the open-loop frequency response. Different values of governor gain are then chosen until, by application of the Nyquist stability criterion, the system is on the point of being unstable. Experimental results were obtained from an electronic power-system simulator[6] to which the analogue of the governor equations had been added. The stability boundaries for the turbo-alternator were calculated, whilst those for the salient-pole alternator were obtained both by calculation, based on small-displacement theory, and from the analogue computer. As the differences between these two are small only the theoretical results are shown in this Section.

(3.2.1) Synchronous Machine with Ideal Conditions in the Governor Loop.

The performance of the governor will be affected by the two principal time-constants τ_1 and τ_2, and it is clear that the optimum governor response will be obtained if these are both zero. For this condition the governor may be defined as ideal, and in consequence it will be useful if the stability boundary for this ideal case is derived initially. The open-loop frequency response is obtained from the open-loop transfer function

$$\frac{f(p) + g(p)}{Mp^2} = \frac{1}{Mp^2}\left[\phi(\delta_0) + \frac{v^2 \sin^2 \delta_0 (X_d - X'_d)\tau_{d0}p}{X_d(X_d + X'_d\tau_{d0}p)} + g + T_D p + g + T_D p\right] \quad . \quad . \quad . \quad . \quad (15)$$

by writing $p = j\omega$, and putting in values for the load angle δ_0 and the governor gain g. For example, turbo-alternator responses are plotted in Fig. 4 for an initial load angle of 150° for three different values of governor gain. It is seen that in the region of the $(-1, 0)$ point the curves are all similar. The difference between stable and unstable operation will be determined by the closure of the graphs in the region $p = j0$. This will depend on the sign of $[\phi(\delta_0) + g]/M(j\omega)^2$, which will undergo an inflection when the negative slope of the torque/angle curve, $\phi(\delta_0)$, becomes greater than the governor gain, i.e. when

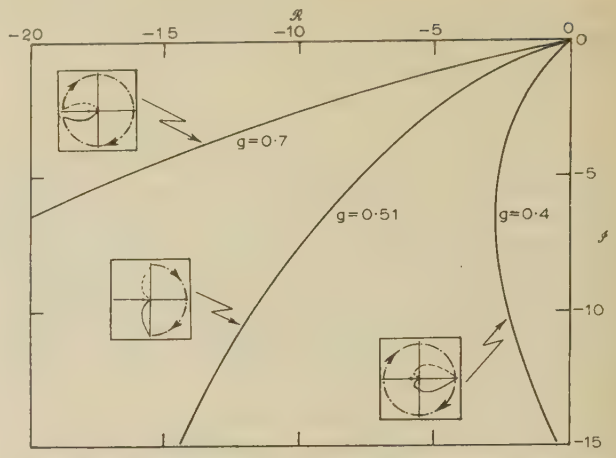

Fig. 4.—Frequency response of a turbo-alternator with ideal steam and governor conditions showing effect of governor gain.
$\delta_0 = 150°$. $T_D = 3$ p.u.

the net synchronizing-torque coefficient becomes negative. The locus of the steady-state stability limit as a function of governor gain and rotor angle is shown in Fig. 5(*a*), where it is compared with the unregulated rotor-angle limit. This locus divides the

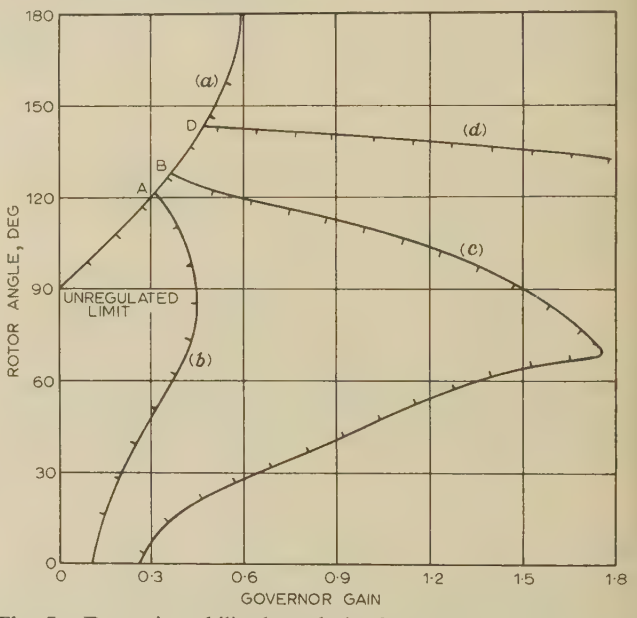

Fig. 5.—Dynamic stability boundaries for a turbo-alternator with a displacement governor.

Unstable | | | Stable

(*a*) $\tau_1 = 0$	$\tau_2 = 0$	$g_b = 0$	$T_D = 3$ p.u.
(*b*) $\tau_1 = 0{\cdot}5$ sec	$\tau_2 = 0$	$g_b = 0$	$T_D = 3$ p.u.
(*c*) $\tau_1 = 0{\cdot}5$ sec	$\tau_2 = 0{\cdot}5$ sec	$g_b = 0$	$T_D = 3$ p.u.
(*d*) $\tau_1 = 0{\cdot}5$ sec	$\tau_2 = 0{\cdot}5$ sec	$g_b = 1{\cdot}0$	$T_D = 3$ p.u.

two regions, namely the unstable region on the left of the boundary and the stable region on the right. Fig. 6(*a*) shows the corresponding boundary for a salient-pole alternator which is seen to be of a similar nature.

(3.2.2) Synchronous Machine with Displacement Governor—Effect of Phase Lags.

In Fig. 7, the function $[f(j\omega) + g(j\omega)]/M(j\omega)^2$ is plotted for the turbo-alternator with two phase lags in the governor loop. When $g = 1{\cdot}75$ the graph passes through the $(-1, 0)$ point. When $g > 1{\cdot}75$ there are two net encirclements of the critical

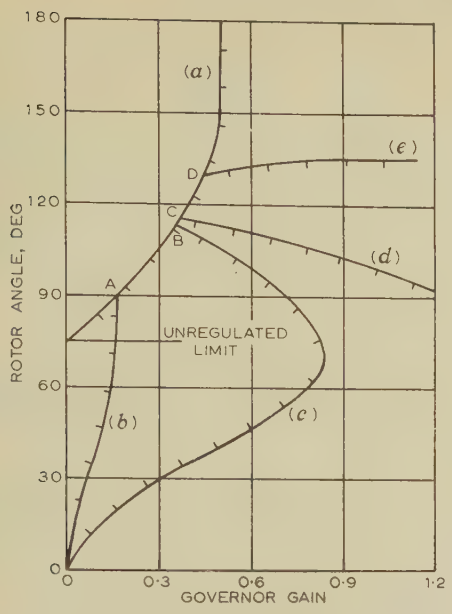

Fig. 6.—Dynamic-stability boundaries for a salient-pole alternator with a displacement governor.

Unstable | Stable

(*a*) $\tau_1 = 0$ $\tau_2 = 0$ $g_b = 0$
(*b*) $\tau_1 = 0$ $\tau_2 = 0{\cdot}5$ sec $g_b = 0$
(*c*) $\tau_1 = 0{\cdot}5$ sec $\tau_2 = 0{\cdot}5$ sec $g_b = 0$
(*d*) $\tau_1 = 0{\cdot}5$ sec $\tau_2 = 0{\cdot}5$ sec $g_b = 0$ $T_D = 3$ p.u.
(*e*) $\tau_1 = 0{\cdot}5$ sec $\tau_2 = 0{\cdot}5$ sec $g_b = 1{\cdot}0$ $T_D = 3$ p.u.

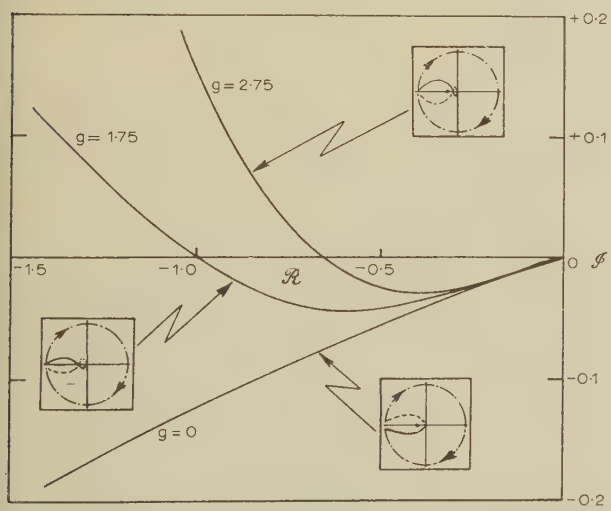

Fig. 7.—Frequency response of turbo-alternator with two phase lags in governor loop.

$\tau_1 = 0{\cdot}5$ sec $\tau_2 = 0{\cdot}5$ sec $\delta_0 = 70°$ $g_b = 0$ $T_D = 3$ p.u.

point, and since there are no poles of the function with positive real parts, self-excited oscillations will occur. Fig. 5(*c*) shows the locus of the boundary, as a function of rotor angle and governor gain, which has two distinct parts. The first, up to the break-point B at a rotor angle of 128°, is coincident with the ideal stability boundary where instability arises from lack of synchronizing torque. On the second part of the curve, which starts at the point B, instability will arise from the presence of negative damping. If it were assumed that the servo mechanism of the governor had no associated phase lags, i.e. if there were only one phase lag in the governor loop, the stability boundary would have the form shown in Fig. 5(*b*). Again this has two distinct parts separated by a break-point A, which is now at a rotor angle of 121°.

The salient-pole machine, which initially is assumed to have no damper windings, is now considered. Fig. 6(*b*) shows the locus of the boundary when it is assumed that the only phase lag in the governor loop is in the servo mechanism operating the water gate of the turbine. When account is taken of the inertia of the water in the penstock and the tailrace, by assuming that these have a time-constant of half a second, the stability boundary takes the form shown in Fig. 6(*c*), where the break-point has now increased from 90° to 113°. Whilst, in practice, the penstock time-constant might be considerably larger, it is apparent that increasing the time-constant would make the system more stable as a result of reducing the negative damping in the governor loop. These results appertain to a machine without damping other than that introduced by the field. Thus, in particular, boundary (*c*) in Fig. 6 does not represent a true picture of the operating conditions. A more realistic result is obtained when the damping supplied by the damper windings is taken into account. This may be done in one of two ways: first by introducing damper equations into the analysis and secondly by introducing a constant damping coefficient T_D. The authors have observed, by frequency-response analysis, that the results of applying both these methods are virtually identical over a restricted range of δ_0. Therefore a constant damping-torque coefficient T_D of 3 p.u. was introduced into the mechanical equation of motion (7). This value was computed by frequency-response analysis from typical values of damper parameters.[7] The resulting stability boundary of Fig. 6(*d*) shows a very considerable increase in stability, and the break-point is now at 117·5°. This improvement is gratifying since boundary (*c*) would appear to practically inhibit operation of the system.

Figs. 5(*b*) and (*c*) and Figs. 6(*b*), (*c*) and (*d*) all exhibit the break-point characteristic arising from the fact that the cause of system instability changes from lack of positive synchronizing torque to the presence of negative damping at the break-points. They also indicate that at certain rotor angles the systems are conditionally stable. For example, in Fig. 6, consider the machine operating at a load angle of 90° for system conditions described by boundary (*c*). If $0 < g < 0{\cdot}16$ the system will be unstable, whilst for $0{\cdot}16 < g < 0{\cdot}71$ it will be stable, but will become unstable again when $g > 0{\cdot}71$. Thus by steadily increasing the governor gain from zero to 1·2 the system is progressively unstable, stable and again unstable. Curve (*c*) in Fig. 6, together with curves (*b*) and (*d*), therefore represents a control system which is conditionally stable at certain rotor angles.

(3.2.3) Influence of Stabilizer on Dynamic-Stability Boundary.

Fig. 8 shows the open-loop frequency-response plot for the governed salient-pole alternator when the second-derivative phase-advance circuit suggested in Reference 1 is included. The complete stability boundary is drawn in Fig. 6(*e*), where it can be seen that the stabilizer effects a considerable improvement on the stability boundary when two phase lags are present. The inclusion of the dampers now has a negligible effect on the boundary, because the second-derivative stabilizer introduces a damping-torque coefficient of the order of 19 p.u. compared with 3 p.u. from the damper. Fig. 5(*d*) illustrates a similar effect when a stabilizer is added to the turbo-alternator governor.

It is of some interest to note that, by examination of Figs. 7 and 8, where the open-loop frequency-response plots are concave to the $(-1, 0)$ point, the effect of increasing the inertia of the

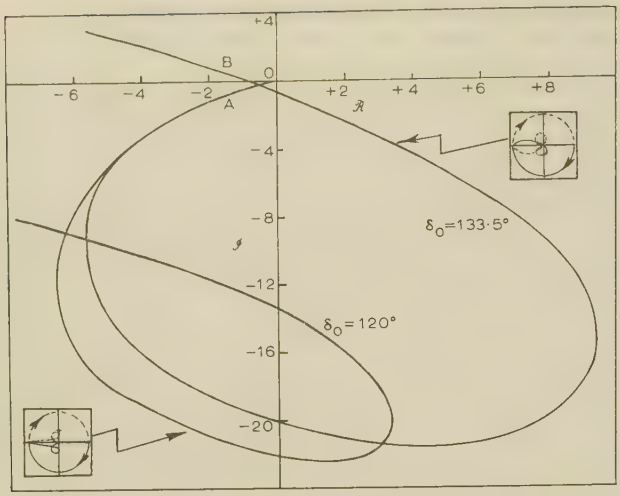

Fig. 8.—Frequency response of salient-pole alternator with second-derivative stabilizer in the governor loop.
$\tau_1 = 0{\cdot}5$ sec $\tau_2 = 0{\cdot}5$ sec $g = 1{\cdot}0$ $g_b = 1{\cdot}0$

rotor is to make the machine less stable. This is in contradistinction to the more usual case illustrated, for example, in Fig. 4. Here the plot is convex to the $(-1, 0)$ point and increasing the inertia of the rotor makes the machine more stable.

(4) DAMPING CHARACTERISTICS OF THE GOVERNED SYSTEM

It was indicated in Section 2.2 that the damping inherent in the system might be cancelled in the small-displacement eqn. (9) by including an equal and opposite damping torque $K_D p\Delta\delta$ in the mechanical equations of motion. The value of K_D required to make the system oscillate with constant amplitude gives a measure of the damping in the system corresponding to the undamped natural frequency for the given operating conditions. An examination of the system damping not only helps to elucidate the mechanism of stability but also provides a useful appraisement when comparing the relative stability of different configurations in the governor loop. The damping-torque coefficients may be calculated from the expressions obtained from the imaginary part of eqn. (9) after the substitution $p = j\omega$ has been made. Alternatively, the values of K_D required for small oscillations to exist may be obtained from an electronic power-system simulator, both methods being employed by the authors. All the results in this Section will refer to a salient-pole alternator. As might be expected, however, the turbo-alternator has been shown, by calculation, to have similar characteristics.

(4.1) Generator with Ideal Conditions in Governor Loop

In Fig. 9(*a*) the damping-torque coefficient is plotted as a function of rotor angle, the results being obtained from the analogue computer. At $\delta_0 = 0$ and 180° the damping is zero and the machine will hunt continuously. Between these two points the damping is positive. There is a close correlation between the above curve and that calculated from the expression for the damping coefficient derived from eqn. (9) assuming that dampers are absent, i.e.

$$K_D = \frac{v^2 \sin^2 \delta_0 (X_d - X_d')\tau_{d0}}{X_d^2 + \omega^2 \tau_{d0}^2 X_d'^2} \quad . \quad . \quad . \quad (16)$$

This formula indicates that the damping, under idealized governor conditions, is always positive. Thus provided that the

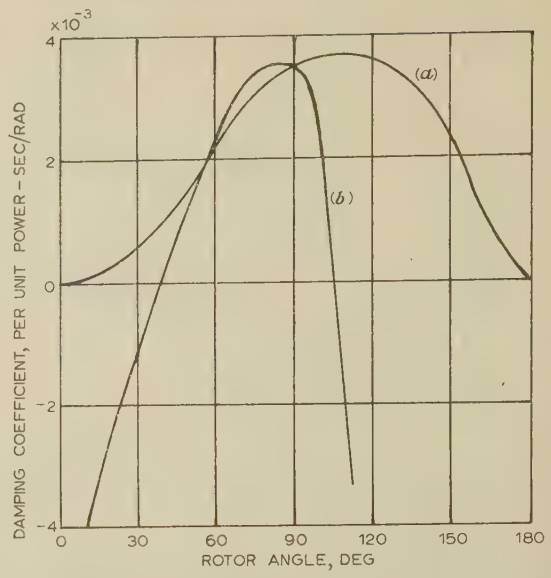

Fig. 9.—Damping coefficient of salient-pole alternator as a function of rotor angle derived experimentally.
(*a*) Idealized conditions: $\tau_1 = 0$ $\tau_2 = 0$ $g = 1{\cdot}0$ $T_D = 0$
(*b*) Two phase lags in governor loop: $\tau_1 = 0{\cdot}5$ sec $\tau_2 = 0{\cdot}5$ sec $g = 0{\cdot}5$ $T_D = 9$

synchronizing-torque coefficient is positive, as shown by boundary (*a*) in Fig. 6, the system will always be stable under steady-state conditions.

(4.2) Generator with Displacement Governor—Effect of Phase Lags

The expression for the damping coefficient from eqn. (9), after substituting

$$g(p) = \frac{1}{(1 + \tau_1 p)(1 + \tau_2 p)} g$$

and again neglecting the effect of dampers is given by

$$K_D = \frac{v^2 \sin^2 \delta_0 (X_d - X_d')\tau_{d0}}{X_d^2 + \omega^2 \tau_{d0}^2 X_d'^2} - g\frac{(\tau_1 + \tau_2)}{(1 + \omega^2\tau_1^2)(1 + \omega^2\tau_2^2)} \quad . \quad (17)$$

Fig. 9(*b*) shows the behaviour of the damping coefficient, as a function of rotor angle, derived from the analogue computer. Comparison of this curve with boundary (*c*) in Fig. 6 indicates that inside the boundary the damping is positive. Outside the boundary the damping coefficient is negative, so precluding stable operation. It is evident from eqn. (17) that with the value of 0·5 sec for the time-constants τ_1 and τ_2 and with natural system frequencies of the order of 1 c/s, putting $\tau_2 = 0$ will increase the negative damping introduced by the governor. As a consequence the system becomes less stable and the break-point A in Fig. 6(*b*) will be considerably lower down the ideal characteristic than that for boundary (*c*) where there are two phase lags. The effect of the dampers on the damping coefficient is to transport the curve in Fig. 9(*b*) in a positive direction by an amount equal to $9{\cdot}6 \times 10^{-3}$ p.u. power-second/rad (=3 p.u.). This makes the net damping coefficient positive up to a rotor angle of about 112°.

(4.3) Generator with Displacement Governor—Effect of Stabilizer

The effect of the second-derivative stabilizer on the damping coefficient for various rotor angles is shown in Fig. 10. If this curve is compared with those of Figs. 9(*a*) and (*b*), the stabilizer

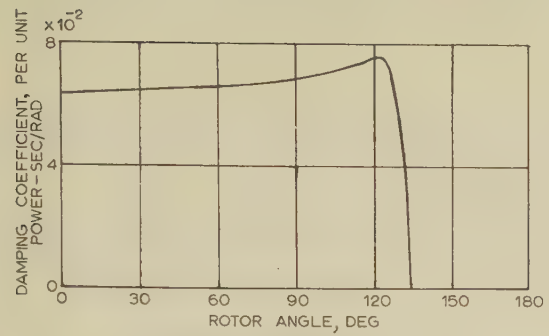

Fig. 10.—Damping coefficient of salient-pole alternator as a function of rotor angle for the stabilized governor, calculated from small-displacement theory.

$\tau_1 = 0{\cdot}5$ sec $\tau_2 = 0{\cdot}5$ sec $g = 1{\cdot}0$ $g_b = 1{\cdot}0$ $T_D = 0$

oop is seen to increase the damping coefficient by a factor of en to give a damping coefficient of about 19 p.u. The effect of dampers in the machine would therefore be negligible compared with the stabilizer. The rather sharp cut-off displayed in Fig. 10 is due to a change in the mode of operation of the machine. This can be best explained with reference to the frequency-response plot of Fig. 8. For rotor angles less than 130° he machine operates in the region A having a natural frequency of the order 2·9 c/s. When the machine approaches close to he stability limit, i.e. as region B approaches more closely the −1, 0) point, the mode of oscillation changes and the machine will operate with a natural frequency of about 0·135 c/s. For a slight increase of rotor angle above the stability limit, this region, from Fig. 8, rises above the real axis, indicating that the damping is negative and therefore unstable operation will ensue.

(5) CONCLUSIONS

Reference has been made to the need for improved methods of load and frequency control, and it appears that this need would, to some extent, be satisfied by the use of displacement governing. Once the governor gain and the space position of the control vector have been fixed, steady-state operation can occur only at one rotor angle corresponding to the intersection of the governor characteristic line and the torque/angle curve of the machine. The load may be changed only by a suitable rotation of the control vector. The alternator frequency is determined absolutely by the speed of rotation of the control vector to which the machine rotor is 'locked', provided that the machine is stable. It should be realized that this single mode of operation occurs only in the case of one machine connected to an infinite system that is governed in a similar manner.

The paper shows quite clearly that, by employing a displacement governor with a suitable gain in conjunction with a subsidiary stabilizer, a very substantial improvement should be effected in the steady-state stability limit of a synchronous alternator. Up to the present, displacement governors have been used in an actual system only by Électricité de France. This has been described[2] under the title of 'load-phase regulation' using the very low gain of 0·00032 p.u. power/rad. Broadbent[1] has described a model system using gains up to 0·16 p.u. power/rad. Thus the maximum gain used in the present paper represents an increase of six times above that used elsewhere.

The governor gain having been fixed, the most important factor in the system would appear to be the damping-torque coefficient. When the gain becomes, as in the present paper, of the same order as the synchronizing-torque coefficient, the amount of damping in the system is considerably altered by the presence of phase lags in the governor loop. This effect is only partially mollified by the damper windings in the alternator. The addition of a stabilizer in the governor loop such as the second-derivative type used here is essential for satisfactory operation, since it not only increases the 'steady-state' stability limit but also introduces heavy damping of the order of 19 p.u. It should, however, be possible to improve the design of the stabilizer to increase the stability limit further.

The small-displacement study reveals how the phase lags and the stabilizer in the governor loop affect the damping in the synchronous generator. The open-loop frequency-response method for predetermining whether or not the system will be stable after a small perturbation is shown to give results that correlate very well with those from a power-system simulator which represents the complete system equations.

(6) ACKNOWLEDGMENTS

The authors are grateful to Professor J. M. Meek for his interest in the work and for facilities provided in the laboratories of the Electrical Engineering Department of Liverpool University. They are indebted to the Central Electricity Generating Board for financial support, and in Mr. Walker's case to the Leverhulme Trust for similar assistance.

(7) REFERENCES

(1) Broadbent, D.: 'Governing in Power Systems by Time-Error', *Proceedings I.E.E.*, Monograph No. 200, September, 1956 (**104** C, p. 130).

(2) Cahen, F., and Chevallier, A.: 'Automatic Frequency Regulation in Large Networks', C.I.G.R.É., Paris, 1954, Paper No. 339.

(3) Prescott, J. C., and El-Kharashi, A. K.: 'The Performance of Displacement Governors under Steady-State Conditions', *Proceedings I.E.E.*, Paper No. 3179 S, February, 1960 (**107**A, p. 85).

(4) Broadbent, D. Discussion on Reference 3, *ibid.* (**107**A, p. 399).

(5) Aldred, A. S., and Shackshaft, G.: 'A Frequency-Response Method for the Predetermination of Synchronous-Machine Stability', *ibid.*, Monograph No. 340 S, August, 1959 (**107** C, p. 2).

(6) Corless, K. G., and Aldred, A. S.: 'An Experimental Electronic Power-System Simulator', *ibid.*, Paper No. 2673 S, October, 1958 (**105** A, p. 503).

(7) Aldred, A. S., and Shackshaft, G.: 'Frequency Response Analysis of the Stabilizing Effect of a Synchronous Machine Damper', *ibid.*, Monograph No. 393 S, July, 1960 (**108** C, p. 58).

621.316.923.9:681.142

The Institution of Electrical Engineers
Monograph No. 449 S
June 1961

ANALYTICAL DETERMINATION OF THE CHARACTERISTICS OF ENCLOSED AND OIL-IMMERSED FUSES

By COLIN ADAMSON, D.Sc., M.Sc.(Eng.), Associate Member, and M. VISESHAKUL, M.Sc.Tech., Ph.D.

(*The paper was first received 23rd September*, 1960, *and in revised form 6th February*, 1961. *It was published as an* INSTITUTION MONOGRAPH *in June*, 1961.)

SUMMARY

In a previous paper the authors dealt with the case of semi-enclosed fuses, manufactured from uniform thin strip or with single or double discontinuities in their cross-sections. An analytical solution for the time/current characteristic of such fuses was shown to exist, which was in very close correlation with experimental derivations of the same characteristics.

This work has now been extended in two ways. First, the analytical derivation of fuse characteristic has been extended to cases of fuses with n discontinuities in their cross-sections, where $n > 2$; this work was carried out with the aim of investigating the full range of alternative characteristics available from such fuses. Secondly, and the most important part of the work, has been the extension of the solution obtained for a semi-enclosed fuse to fuses of similar metallic construction but immersed in oil or enclosed in a silica-type filler.

Having established a method and form of solution, a substantial amount of computation is necessary in any one case; in order to facilitate computation, a simple form of transient analogue computer has been used, and is described in the paper. In the case of fuses immersed in oil or enclosed in silica-type filler, the main problems have been to establish the parameters of heat transfer prior to finding a form of solution of the relevant equations.

The Appendices contain representative Tables of results in the form in which they were obtained from the analogue computer, and an analysis showing the feasibility of establishing a single series of Tables of analogue-computer results for fuses with multiple discontinuities in cross-section.

LIST OF PRINCIPAL SYMBOLS

t = Time, sec.
x = Axial distance measured along the fuse from one end, cm.
$\theta - \theta_0$ = Temperature rise, deg C.
θ_0 = Initial ambient temperature, deg C.
T = Temperature of fuse at distance x along the fuse axis independent of time.
ψ = Transient temperature, a function of x and t.
A_1, A_2 = Fuse cross-sectional areas, cm^2.
p = Perimeter of fuse, cm.
l = Length of fuse, cm.
H = Coefficient of thermal transfer between fuse surface and medium surrounding the fuse.
k = Mean thermal conductivity.
c = Specific heat, cal/g.
J = Joule's equivalent.
ρ = Density, g/cm^3.
σ = Mean electrical conductivity between room temperature and the melting temperature of the fuse, mhos/cm.

Correspondence on Monographs is invited for consideration with a view to publication.
Dr. Adamson is in the Power Systems Laboratory, Department of Electrical Engineering, Manchester College of Science and Technology.
Dr. Viseshakul was formerly in the Power Systems Laboratory, and is now with Public and Municipal Works Department, Bangkok, Thailand.

(1) INTRODUCTION

Earlier work[1] established the validity of a method for predicting the characteristics of semi-enclosed fuses. The supposition on which this work rested was that discontinuities in cross-section, which are used by most manufacturers as shown in Fig. 1, were subject to analytical treatment and could thus be

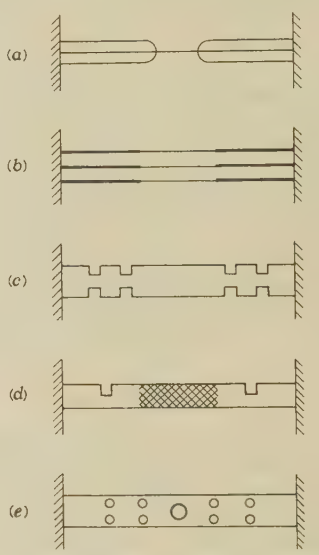

Fig. 1.—Common forms of fuse-element construction with discontinuities in cross-section.
(*a*) British type.*
(*b*) U.S. type.†
(*c*) U.S. type.‡
(*d*) 'Hi-cap' fuse (U.S. type).§
(*e*) German-type h.r.c. fuse.||

* English Electric publication FG/131.
† *General Electric Review*, May, 1951.
‡ *Electrical Engineering*, 1953, 72.
§ *Transactions of the American I.E.E.*, 1952, **72**, p. 77.
|| Bulletin Association Suisse, 1954, 45.

introduced in a controlled fashion to give particular desired characteristics. Apart from the formulation and solution of the thermo-electric equations involving discontinuities, the work took into account surface heat losses and was applicable both to round wires and the more difficult case of flat strip. Close correlation was obtained between predicted characteristics and those obtained by experiment on a large number of laboratory-manufactured samples, and it was thus logical to attempt to extend the work to fuses enclosed in more complicated media. The paper describes the way in which the original method has been successfully applied to fuses immersed in oil and short-length fuses enclosed in silica/quartz filler.

(2) THERMAL EQUATIONS OF FUSES

For a constant current flowing in a fuse, heat is generated; either the temperature rises and reaches equilibrium or the fuse element melts and interrupts the current.

The equation[2] for the temperature rise $(\theta - \theta_0)$ in a thin wire eated by electric current was given by Verdet in 1872 as

$$\frac{\partial\theta}{\partial t} = K\frac{\partial^2\theta}{\partial x^2} - \lambda(\theta - \theta_0) + a \quad . \quad . \quad . \quad (1)$$

here $K = \dfrac{kA}{\rho Ac} \qquad \lambda = \dfrac{Hp}{Ac\rho} \qquad a = \dfrac{I^2}{JA^2\rho c\sigma}$

The problem is divided into one of steady temperature and ne of variable temperature,

e. $$\theta = T + \psi$$

The solution obtained from eqn. (1) for a fuse of uniform ross-section is:

$$_x = \frac{4b}{\pi}\sum_{n=1}^{\infty}\frac{\mu^2 l^2 \sin\dfrac{(2n-1)\pi}{l}x}{(2n-1)[(2n-1)^2\pi^2 + \mu^2 l^2]} \times \left\{1 - \exp\left[-\frac{\lambda t}{2} - \frac{Kt}{2}(2n-1)^2\frac{\pi^2}{2}\right]\right\} \quad (2)$$

here $\mu = \sqrt{\dfrac{\lambda}{K}} \qquad b = \dfrac{a}{\lambda}$

This solution has been extended to fuses with single and double iscontinuities in their cross-section by applying the appropriate oundary conditions (see Fig. 2) at each point of discontinuity,

e. $$A_1\frac{d\theta_1}{dx_1} = A_2\frac{d\theta_2}{dx_2}$$

hus the solution for a single discontinuity of section l_1 is iven as

$$_{x1t} = \sum_{n=1}^{\infty}\frac{4b_1\mu_1^2 l_1^2 \sin(2n-1)\dfrac{\pi x_1}{l_1}}{\pi(2n-1)[(2n-1)^2\pi^2 + l_1^2\mu_1^2]} \times \left\{1 - \exp\left[-\frac{\lambda t}{2} - \frac{Kt}{2}(2n-1)^2\frac{\pi^2}{l_1^2}\right]\right\}$$

$$+ \sum_{n=1}^{\infty}\frac{8}{\pi^2}\frac{T_s(-1)^{n+1}}{(2n-1)^2}\sin\frac{(2n-1)\pi x_1}{2l_1} \times \left\{1 - \exp\left[-\frac{\lambda_1 t'}{2} - \frac{Kt'}{2}(2n-1)^2\frac{\pi^2}{4l_1^2}\right]\right\} \quad (3)$$

nd the solution[1] for a double discontinuity of section length l_1 niddle section) is

$$_{c1t} = \sum_{n=1}^{\infty}\frac{4b_1\mu_1^2 l_1^2 \sin\dfrac{(2n-1)\pi x_1}{l_1}}{\pi(2n-1)[(2n-1)^2\pi^2 + \mu_1^2 l_1^2]} \left\{1 - \exp\left[-\frac{\lambda_1 t}{2} - \frac{Kt}{2}(2n-1)^2\frac{\pi^2}{l_1^2}\right]\right\}$$

$$+ \sum_{n=1}^{\infty}\frac{8T_sC_1\mu_1 l_1(-1)^{n+1}}{(2n-1)^2\pi^2 + 4\mu_1^2 l_1^2}\left[\sin\frac{(2n-1)\pi(l_1 - x_1)}{2l_1} + \sin\frac{(2n-1)\pi x_1}{2l_1}\right]\left\{1 - \exp\left[-\frac{\lambda_1 t'}{2} - \frac{Kt'}{2}(2n-1)^2\frac{\pi^2}{4l_1^2}\right]\right\} \quad . \quad . \quad . \quad . \quad (4)$$

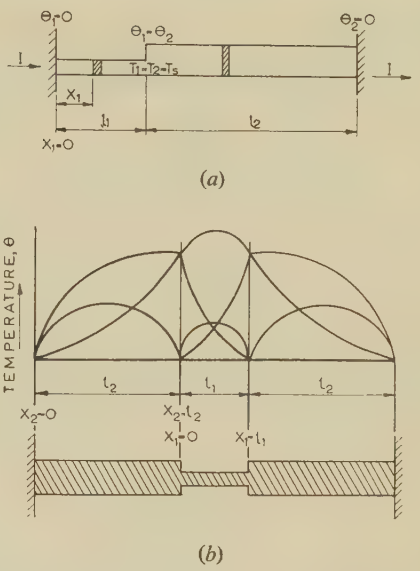

Fig. 2.—Experimental fuse elements with discontinuities in cross-section.
(*a*) Single discontinuity.
(*b*) Double discontinuity, with pattern of temperature distribution along the fuse.

where $C_1 = \dfrac{1}{\tanh\mu_1 l_1}$; T_s is the steady-state temperature at the point of discontinuity and t' is the apparent time.

The solutions for T_s and t' have been given and illustrated.[1]

(3) FUSE ELEMENTS WITH MULTIPLE DISCONTINUITIES IN THEIR CROSS-SECTIONS

Fuses with more than two discontinuities (see Fig. 3) in their cross-sections are not commonly in industrial use, although one

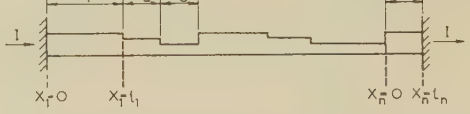

Fig. 3.—Generalized case of a fuse with multiple discontinuities.

that is commercially available is shown in Fig. 1(*c*). The forms of solution above may, however, be applied to fuses which have this particular form of metallic element and are included here for analytical completeness. The general solution is of interest in that it indicates the full extent to which fuse characteristics may be controlled by adjusting the geometrical shape or arrangement of the fuse element.

(3.1) Formulation of Equations and Their Solution

For steady-state conditions, rewriting eqn. (1) we have

$$0 = K\frac{\partial^2 T_n}{\partial x^2} - \lambda T_n + a \quad . \quad . \quad . \quad . \quad (5)$$

where
$$\left.\begin{aligned} &T_1 = 0 \text{ at } x_1 = 0 \qquad T_1 = T_{s12} \text{ at } x_1 = l_1 \\ &T_2 = T_{s12} \text{ at } x_2 = 0 \qquad T_2 = T_{s23} \text{ at } x_2 = l_2 \\ &\quad . \quad . \quad . \quad . \quad . \quad . \quad . \quad . \quad . \quad . \quad . \quad . \\ &\quad . \quad . \quad . \quad . \quad . \quad . \quad . \quad . \quad . \quad . \quad . \quad . \\ &T_n = T_{s(n-1)n} \text{ at } x_n = 0 \qquad T_n = 0 \text{ at } x_n = l_n \end{aligned}\right\} \quad . \quad (6)$$

With conditions

$$\left.\begin{aligned} A_1\frac{dT_1}{dx_1} &= A_2\frac{dT_2}{dx_2} \text{ at } x_1 = l_1 \text{ and } x_2 = 0 \\ A_2\frac{dT_2}{dx_2} &= A_3\frac{dT_3}{dx_3} \text{ at } x_2 = l_2 \text{ and } x_3 = 0 \\ &\cdots\cdots\cdots\cdots \\ &\cdots\cdots\cdots\cdots \\ A_{(n-1)}\frac{dT_{(n-1)}}{dx_{(n-1)}} &= A_n\frac{dT_n}{dx_n} \text{ at } x_{(n-1)} = l_{(n-1)} \text{ and } x_n = 0 \end{aligned}\right\} \quad (7)$$

Eqn. (5) may be solved with the conditions stated in eqns. (6) and (7) to give

$$T_{s(n-2)(n-1)}\frac{-A_{(n-1)}\mu_{(n-1)}}{\sinh \mu_{(n-1)}l_{(n-1)}} + T_{s(n-1)n}\left[\frac{A_{(n-1)}\mu_{(n-1)}}{\tanh \mu_{(n-1)}l_{(n-1)}} + \frac{A_n\mu_n}{\tanh \mu_n l_n}\right] + T_{sn(n+1)}\left(\frac{-A_n\mu_n}{\sinh \mu_n l_n}\right)$$

$$= A_{(n-1)}\left[\frac{\mu_{(n-1)}b_{(n-1)}}{\tanh \mu_{(n-1)}l_{(n-1)}} - \frac{\mu_{(n-1)}b_{(n-1)}}{\sinh \mu_{(n-1)}l_{(n-1)}}\right] + A_n\left(\frac{\mu_n b_n}{\tanh \mu_n l_n} - \frac{\mu_n b_n}{\sinh \mu_n l_n}\right) \quad (8)$$

Following the same method indicated in the authors' earlier work,[1] the final temperature at the rth section from the starting end will be

$$\theta_r = \sum_{n=1}^{\infty}\frac{4b_r\mu_r^2 l_r^2 \sin\frac{(2n-1)\pi x_r}{l_r}}{\pi(2n-1)[(2n-1)^2\pi^2 + l_r^2\mu_r^2]} \times \left\{1 - \exp\left[-\frac{\lambda_r t}{2} - \frac{Kt}{2}(2n-1)^2\frac{\pi^2}{l_r^2}\right]\right\}$$

$$+ \sum_{n=1}^{\infty}\frac{8T_{s(r-1)r}C_r\mu_r l_r}{(2n-1)^2\pi^2 + 4\mu_r^2 l_r^2}(-1)^{n+1}\sin\frac{(2n-1)\pi(l_r - x_r)}{2l_r} \times \left\{1 - \exp\left[-\frac{\lambda_r t'}{2} - \frac{Kt'}{2}\frac{(2n-1)^2\pi^2}{4l_r^2}\right]\right\}$$

$$+ \sum_{n=1}^{\infty}\frac{8T_{sr(r+1)}C_r\mu_r l_r}{(2n-1)^2\pi^2 + 4\mu_r^2 l_r^2}(-1)^{n+1}\sin\frac{(2n-1)\pi x_r}{2l_r} \times \left\{1 - \exp\left[-\frac{\lambda_r t''}{2} - \frac{Kt''}{2}\frac{(2n-1)^2\pi^2}{4l_r^2}\right]\right\} \quad (9)$$

(3.2) Application to a Fuse Element with 3 Discontinuities in its Cross-Section

To illustrate the application to a multiple cross-section fuse, the minimum fusing current of the element shown in Fig. 4 will be calculated.

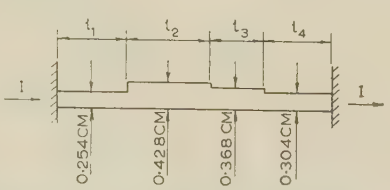

Fig. 4.—Particular illustrative case of a fuse with three discontinuities in cross-section.

$l_1 = 1{\cdot}14$ cm $\quad l_2 = 1{\cdot}4$ cm
$l_3 = 0{\cdot}889$ cm $\quad l_4 = 1{\cdot}14$ cm

Thickness $= 0{\cdot}0165$ cm

$a_1 = 0{\cdot}59I^2$	$a_2 = 0{\cdot}204I^2$	$a_3 = 0{\cdot}281I^2$
$\mu_1 = 0{\cdot}2175$	$\mu_2 = 0{\cdot}2150$	$\mu_3 = 0{\cdot}2150$
$b_1 = 34{\cdot}6I^2$	$b_2 = 12{\cdot}26I^2$	$b_3 = 16{\cdot}75I^2$
$\lambda_1 = 0{\cdot}01707$	$\lambda_2 = 0{\cdot}01667$	$\lambda_3 = 0{\cdot}01677$
$l_1 = 1{\cdot}14$ cm	$l_2 = 1{\cdot}4$ cm	$l_3 = 0{\cdot}89$ cm
$A_1 = 0{\cdot}0042$ cm^2	$A_2 = 0{\cdot}0071$ cm^2	$A_3 = 0{\cdot}0061$ cm^2

$a_4 = 0{\cdot}310I^2$
$\mu_4 = 0{\cdot}2167$
$b_4 = 24{\cdot}25I^2$
$\lambda_4 = 0{\cdot}0191I^2$
$l_4 = 1{\cdot}14$ cm
$A_4 = 0{\cdot}0050$ cm^2

From eqn. (8), and substituting values, we have

$$\begin{aligned} 0 + 90T_{s12} - 50{\cdot}27T_{s23} &= 67{\cdot}09I^2 \\ -50{\cdot}27T_{s12} + 121{\cdot}81T_{s23} + 67{\cdot}99T_{s34} &= 49{\cdot}11I^2 \\ -67{\cdot}99T_{s23} + 114{\cdot}14T_{s34} + 0 &= 53{\cdot}73I^2 \end{aligned}$$

Evaluating, $T_{s12} = 1{\cdot}98I^2$, $T_{s23} = 2{\cdot}22I^2$, $T_{s34} = 1{\cdot}79I^2$. By adding the first part of eqn. (9)

at $\frac{l_1}{2}$, $T_s = 0{\cdot}257I^2$

at $\frac{l_2}{2}$, $T_s = 0{\cdot}137I^2$

at $\frac{l_3}{2}$, $T_s = 0{\cdot}077I^2$

at $\frac{l_4}{2}$, $T_s = 0{\cdot}185I^2$

By graphical means, as indicated in Fig. 5, the maximum temperature occurs at

$$T_{s23} = 2{\cdot}22I^2$$

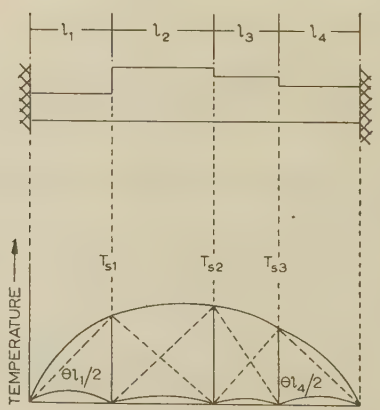

Fig. 5.—Temperature-distribution pattern for fuse element shown in Fig. 4.

Hence the melting point $= 232 = 2{\cdot}22I^2$ and thus $I = 10{\cdot}2$ A, compared with $I = 10{\cdot}4$ A obtained by experimental testing.

A complete calculation of a less complicated fuse element with double discontinuities has already been published.[1]

(4) ELECTRICAL ANALOGUE OF A FUSE

An electrical network can be set up for most simple sets of second-order differential equations, thereby enabling them to be solved by analogy. Guile and Carne[3] have attempted a solution of the cartridge-fuse equation which involved the inclusion of terms for radial heat transfer in the surrounding silica powder as well as the axial heat transfer in the fuse element. The form of analogue adopted by those authors is shown in Fig. 6(*a*); it is complex and difficult to set up and manipulate.

The authors have found that a simpler form of analogue [see Fig. 6(*b*)] is quite satisfactory and may be used with greater facility; much less manipulation of circuit parameters is necessary when changing from one form of fuse element to another, including such marked changes as from a uniform section to one with multiple discontinuities. This simplification follows from the analytical approach previously examined. The new analogue includes the terms for both radial and axial heat transfer for the fuse element and the radial heat transfer through the surrounding medium; the axial heat transfer from any point in the surrounding medium to, and through, adjacent points in the medium in an axial direction is neglected.

(4.1) Mathematical Analogue

Considering the electrical circuit of Fig. 6(*b*), the equation of the circuit is

$$\frac{1}{R_1}\frac{\partial^2 V}{\partial x^2} - \frac{V}{R_2} + i_g = C\frac{\partial V}{\partial t} \quad . \quad . \quad . \quad (10)$$

Comparison of eqn. (10) with eqn. (1) shows that they are analogous; thus the equivalent circuit of Fig. 6(*b*) and eqn. (10) can represent the performance of a fuse of uniform cross-section.

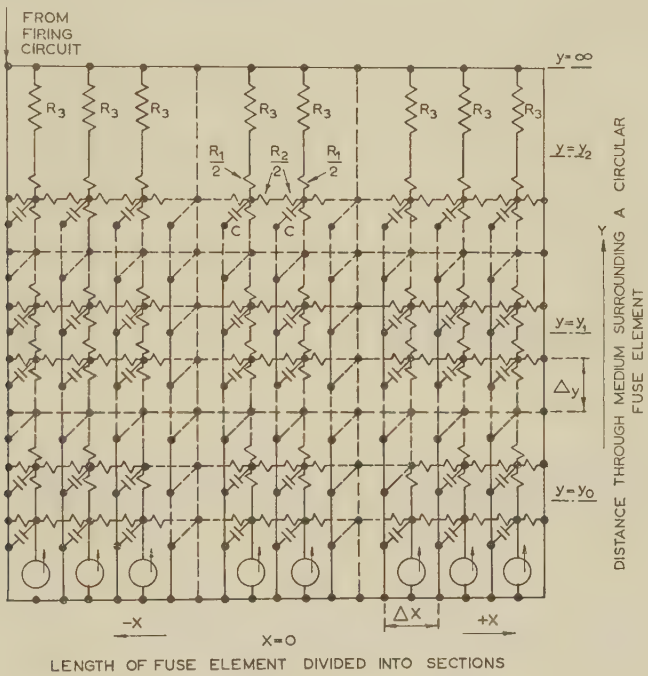

(*a*)

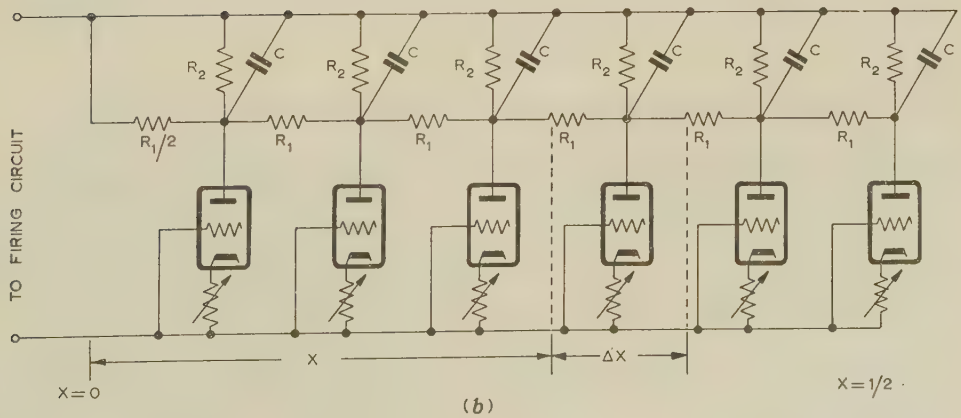

(*b*)

Fig. 6.—Electrical circuit analogues of a fuse.

(*a*) Fuse analogue allowing for heat transfer in an axial direction through the medium surrounding the fuse element.
(*b*) Simplified analogue adopted by the authors.

(4.2) Analogue for a Strip Fuse with Discontinuities in its Cross-Section

For a wire with n discontinuities in its cross-section, the general heat equation is of the form given by eqn. (1), but the boundary conditions are different.

$$\frac{\partial\theta_n}{\partial t} = K\frac{\partial^2\theta_n}{\partial x_n^2} - \lambda_n\theta_n + a_n \quad . \quad . \quad . \quad (11)$$

with
$$\theta_n = T_{(n-1)} \text{ at } x_n = 0$$
$$\theta_n = T_n \text{ at } x_n = l_n$$
$$\theta_n = 0 \text{ when } t = 0$$

In order to deal with any particular fuse sections, as in previous cases when using a purely mathematical approach, eqn. (11) will be broken up to form three equations:

(i) $$\frac{\partial\theta}{\partial t} = K\frac{\partial^2\theta}{\partial x^2} - \lambda\theta + a \quad \text{with } \theta = 0 \text{ at } x = 0 \text{ and } x = l, \ \theta = 0 \text{ when } t = 0 \quad . \quad (11a)$$

(ii) $$\frac{\partial\theta}{\partial t} = K\frac{\partial^2\theta}{\partial x^2} - \lambda\theta \quad \text{with } \theta = 0 \text{ at } x = 0, \ \theta = \theta_1 \text{ at } x = l, \ \theta = 0 \text{ when } t = 0 \quad . \quad (11b)$$

(iii) $$\frac{\partial\theta}{\partial t} = K\frac{\partial^2\theta}{\partial x^2} - \lambda\theta \quad \text{with } \theta = \theta_2 \text{ at } x = 0, \ \theta = 0 \text{ at } x = l, \ \theta = 0 \text{ when } t = 0 \quad . \quad (11c)$$

Any nth section of a fuse with multiple discontinuities in its cross-section will then be described by the conditions in eqns. (11a), (11b) and (11c).

The instantaneous temperature will then be

$$\theta_1 = \theta_{1a} + \theta_{1b} + \theta_{1c} \quad . \quad . \quad . \quad . \quad . \quad (12)$$

Eqn. (11a) will describe the analogue circuit of Fig. 6(b).

Comparing eqns. (11), (11a), (11b) and (11c) with eqns. (10) and (13),

$$\left.\begin{aligned} i &= i_q\Delta xm = m\Delta x a_n \\ C &= 2C_0\Delta xm = 2m\Delta x \\ R_1 &= R\Delta x\frac{1}{m} = \frac{\Delta x}{Km} \\ R_2 &= \frac{1}{\lambda\Delta x}\frac{1}{m} = \frac{1}{\Delta x\lambda m} \end{aligned}\right\} \quad . \quad . \quad . \quad (14)$$

(4.4) Procedure for Solution

(4.4.1) To Find a Current/Time Characteristic of a Single Wire.

(a) The maximum temperature of a single wire heated by an electric current will be at its centre.

(b) Convert the analogue current in terms of a_n [eqn. (14) first part].

(c) $a_n = pI^2$; the corresponding current for that recorded voltage will be $I = \left[\frac{a_n}{p}\right]^{1/2}$.

(d) From the recorded voltage and corresponding current, find N; $V = NI^2 = Na_n/p$.

(e) Find the fusing current at time t:

$$\theta = \text{melting-point temperature} = NI^2$$

or
$$I = \left[\frac{\theta}{N}\right]^{1/2} = \left[\frac{\theta a_n}{Vp}\right]^{1/2}$$

N is the temperature per current squared at distance x from the origin.

$$p = \frac{1}{JA^2\rho c\sigma} \text{ or } a = \frac{I^2}{JA^2\rho c\sigma} = pI^2$$

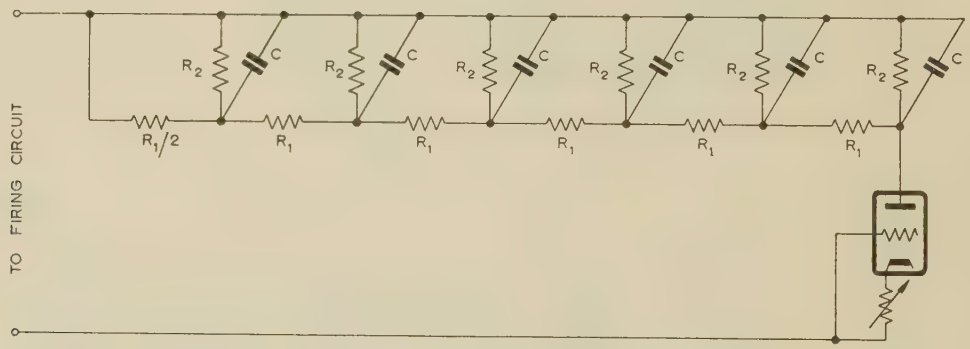

Fig. 7.—Subsidiary analogue circuit for a fuse with multiple discontinuities in cross-section.

For eqns. (11b) and (11c), consider the electrical circuit shown in Fig. 7; when the switch is closed at $t = 0$ the instantaneous voltage will be

$$C\frac{\partial V}{\partial t} = \frac{1}{R_1}\frac{\partial^2 V}{\partial x^2} - \frac{V}{R_2} \quad . \quad . \quad . \quad . \quad (13)$$

Inspection shows that eqn. (13) is analogous to eqns. (11b) and (11c).

The difference between them lies only in the limiting boundary conditions.

(4.3) General Parameters

For accurate results the overall length of the fuse should be divided into as large a number of sections as possible.

(4.4.2) To Find the Minimum Fusing Current of a Fuse with n Discontinuities in Cross-Section.

(a) Find the value of N as shown in Section 4.4.1 throughout the fuse element of n sections, using Tables of the form shown in Appendix 12.1. These are obtained from the analogue computer illustrated in Fig. 6(b).

(b) From Tables 11 and 12 in Appendix 12.1 find $d\theta/dx$ at every point where there are changes in cross-section.

(c) Assume the steady-state value T_{s12}, T_{s23}, etc., at the points of discontinuity.

(d) Find the approximate value of $d\theta/dx$ due to T_{s12}, T_{s23}, etc. (approximately a straight line function), or find the accurate

value of $d\theta/dx$ due to T_{s12}, T_{s23}, etc., by the represented circuit as in Fig. 7.

(*e*) Compute and evaluate T_{s12}, T_{s23}, etc., by

$$A_1\frac{d\theta_1}{dx_1} = A_2\frac{d\theta_2}{dx_2} \text{ at } x_1 = l_1,\ x_2 = 0$$

$$A_2\frac{d\theta_2}{dx_2} = A_3\frac{d\theta_3}{dx_3} \text{ at } x_2 = l_2,\ x_3 = 0$$

. . . etc.

(*f*) Add the result of (*e*) to the value of N obtained from (*a*).

(*g*) Find the accurate maximum value of NI^2 and its location.

(*h*) Minimum fusing current, $I = \left[\dfrac{\text{(melting temperature)}}{N}\right]^{1/2}$.

(4.4.3) To Find the Time/Current Characteristic of a Multiple-Cross-Section Fuse Element.

(*a*) Find the steady-state distribution as shown in Section 4.4.2.

(*b*) Find θl_1, θl_2, etc., at various points along the length of the multiple-cross-section fuse from the electrical analogue as shown in Section 5.2 in terms of T_{s12}, T_{s23}, etc.

(*c*) Find $\theta l_n' = \dfrac{A_{(n-1)}l_{(n-1)}\theta_{(n-1)t} + A_n l_n \theta_{nt}}{A_{(n-1)}l_{(n-1)} + A_n l_n}$

for time t.

(*d*) Plot the pattern of distribution at time t.

(*e*) Find the maximum value of NI^2 and its location.

(*f*) Find the corresponding current at time t,

$$I = \left(\frac{\text{melting temperature}}{N}\right)^{/2}$$

(5) RATE OF HEAT TRANSFER IN OIL

When a heated vertical plate has been set up in a liquid, natural convection occurs, and the equations of motion and heat flow[5] are

$$u\frac{\partial u}{\partial x} + v\frac{\partial u}{\partial y} = \alpha_k\frac{\partial^2 u}{\partial y^2} + g\beta\theta \quad . \quad . \quad . \quad (15)$$

$$u\frac{\partial \theta}{\partial x} + v\frac{\partial \theta}{\partial y} = \frac{k}{c}\frac{\partial^2\theta}{\partial y^2} \quad . \quad . \quad . \quad . \quad . \quad (16)$$

where u and v are the velocity components in the x and y directions, the x-axis being vertical, the y-axis horizontal and at right angles to the heated vertical plate; α_k is the kinematic viscosity, and β is the coefficient of change of density ρ with temperature as defined by $\rho = \rho_0(1 + \beta\theta)$, where ρ_0 is the density at temperature $\theta = 0$.

If the horizontal motion is ignored,

$$\frac{\partial u}{\partial x} + \frac{\partial v}{\partial y} = 0 \quad . \quad . \quad . \quad . \quad . \quad . \quad (17)$$

where $u = v = 0$ and $\theta = \theta_0$ when $y = 0$ for all values of x.

By putting G_r (the Grashof number) $\equiv \dfrac{g\beta\theta_{(0)}l^3}{\alpha_k^3}$

and P_r (the Prandtl number) $\equiv \dfrac{c\alpha_k}{k}$, the unit velocity may be taken as k/cl.

Also put

$$z = (3/4G_rP_r)^{1/4}\frac{y}{x^{1/4}}$$

From eqns. (15), (16) and (17) the solution for the mean rate of heat transfer per unit area[5] H, for a plate of length l, is given by

$$H = -\frac{k\theta_{(0)}}{l}\int_0^1 \left|\frac{\partial\theta}{\partial y}\right|_{y=0} dx$$

$$= \frac{k\theta_{(0)}}{l}\left(\frac{64G_rP_r}{27}\right)^{1/4}\left|\frac{\partial\theta}{\partial z}\right|_{z=0}$$

or $$\frac{Hl}{k\theta_{(0)}} = \omega(G_rP_r)^{1/4} \quad . \quad . \quad . \quad . \quad . \quad . \quad . \quad (18)$$

Saunders[4] has given an approximate theoretical value of ω, derived from eqns. (15), (16) and (17), as $\omega = 0{\cdot}54$; Lorenz[5] has obtained results by measurement, and gives $\omega = 0{\cdot}56$ for switchgear oil.

(6) HEAT TRANSFER THROUGH POWDERED MATERIAL

(6.1) General Conduction Equation

When heat is conducted through powdered solid, it can be shown that

$$\frac{\partial^2\theta}{\partial x^2} + \frac{\partial^2\theta}{\partial y^2} + \frac{\partial^2\theta}{\partial z^2} = \frac{\rho c}{k}\frac{\partial\theta}{\partial t} \quad . \quad . \quad . \quad . \quad (19)$$

Eqn. (19) may be transformed readily into a cylindrical system of co-ordinates,

$$z = r\cos\gamma \text{ and } y = r\sin\gamma$$

Eqn. (19) for θ becomes

$$\frac{\partial\theta}{\partial t} = \frac{k}{c\rho}\left(\frac{\partial^2\theta}{\partial r^2} + \frac{1}{r}\frac{\partial\theta}{\partial r} + \frac{1}{r^2}\frac{\partial^2\theta}{\partial y^2} + \frac{\partial^2\theta}{\partial x^2}\right) \quad . \quad (20)$$

Again when the initial and boundary conditions do not contain γ, the flow of heat takes place in planes through the axis, and the equation of conduction through powdered solid becomes

$$\frac{\partial\theta}{\partial t} = \frac{k}{c\rho}\left(\frac{\partial^2\theta}{\partial r^2} + \frac{1}{r}\frac{\partial\theta}{\partial r} + \frac{\partial^2\theta}{\partial x^2}\right) \quad . \quad . \quad . \quad (21)$$

Eqn. (21) has been confirmed by other authors.[2, 3]

The cartridge-fuse equation will thus be

$$\frac{\partial\theta_1}{\partial t} = K_1\frac{\partial^2\theta_1}{\partial x^2} + \frac{(2\pi r_1)k_2}{A_1c_1\rho_1}\left(\frac{\partial\theta_2}{\partial r}\right)_{r=r_1} + a_1 \quad . \quad (22)$$

and from eqn. (21) by neglecting the axial heat transfer from any point in the surrounding powder to, and through, adjacent points,

$$c_2\rho_2\frac{\partial\theta_2}{\partial t} = k_2\left(\frac{\partial^2\theta_2}{\partial r^2} + \frac{1}{r}\frac{\partial\theta}{\partial r}\right) \quad . \quad . \quad . \quad (23)$$

For a steady rate of heat dissipation, the inside radius r (of the fuse-element) remains at a temperature θ_1 and the outside radius r_2 (of the cartridge) is at room temperature.

Then the rate of heat transfer per unit length is[2]

$$2\pi r_1k_2\frac{\partial\theta}{\partial r}\Big|_{r_2}^{r_1} = \frac{2\pi k_2(\theta_1 - \theta_2)}{\log\dfrac{r_2}{r_1}} \quad . \quad . \quad . \quad . \quad (24)$$

Eqn. (22) can then be put into approximate form as follows:

$$\frac{\partial\theta_1}{\partial t} = K_1\frac{\partial^2\theta_1}{\partial x^2} + \lambda\theta_1 + a \quad . \quad . \quad . \quad . \quad (25)$$

where
$$K_1 = \frac{k_1}{c_1\rho_1}$$
$$\lambda = \frac{2\pi k_2}{A_1 c_1 \rho_1 \log\left(\frac{r_2}{r_1}\right)}$$
$$a = \frac{I^2}{JA_1^2 c_1 \rho_1 \sigma}$$

(6.2) Elliptical Field of a Strip Fuse with Rectangular Cross-Section

(6.2.1) Basic Relationships.

Assume that the thermal field, under specified conditions, is analogous to the electric field: then

$$C_0 = \frac{q}{V_1 - V_2} = \frac{2\pi\epsilon}{\log\frac{r_2}{r_1}}$$

where q = Charge.

V = Voltage, representing a line of equipotential.

ϵ = Permittivity.

and
$$\frac{H_i}{J(\theta_1 - \theta_2)} = \frac{2\pi k}{\log\frac{r_2}{r_1}}$$

where θ = Temperature.

k = Thermal conductivity.

H_i = Heat in the inner cylinder per unit length per unit time.

From Fig. 8 of Reference 6

$$C_0 = \frac{\epsilon\int du}{V_2 - V_1}$$

Consider the ellipse (Fig. 9). If $2d$ (width of the strip) $\gg$ the thickness of the strip, $2g$ (cartridge diameter) $\gg 2d$ and $2b \gg 2d$,

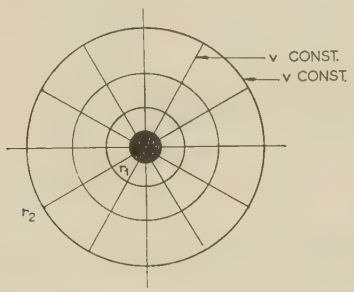

Fig. 8.—Field between two cylindrical surfaces.

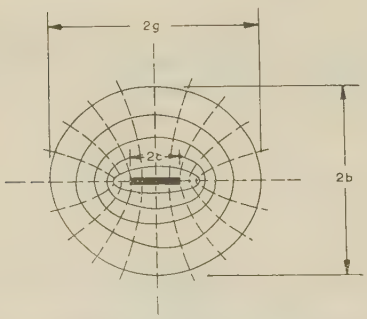

Fig. 9.—Elliptical field pattern surrounding a strip of rectangular cross-section.

by conformal transformation it may be shown that the flat strip is given by the degenerate ellipse $V = 0$, so that $V_1 = 0$. The ellipse is given by

$$\cosh V = \frac{g}{d}$$

i.e.
$$V_2 = \cosh^{-1} g/d$$

When $g \simeq b$ the ellipse becomes a circle of diameter $D = 2g$. Then

$$V_2 = \cosh^{-1}\frac{D}{2d}$$

$$C_0 = \frac{\epsilon\int du}{V_2 - V_1} = \frac{2\pi\epsilon}{\cosh^{-1}\frac{D}{2d}}$$

If the fuse element is circular

$$H_{i1} = \frac{2\pi k}{\log\frac{r_2}{r_1}} J(\theta_1 - \theta_2) \quad . \quad . \quad . \quad . \quad (26)$$

If the fuse element is a strip

$$H_{i1} = \frac{2\pi k}{\cosh^{-1}\frac{2r_2}{2d}} J(\theta_1 - \theta_2) \quad . \quad . \quad . \quad (27)$$

The strip of width $2d$ will have surface dissipation equivalent to a circular element of surface $2\pi r_1$ by the relation:

$$\log\frac{r_2}{r_1} = \cosh^{-1}\frac{2r_2}{2d}$$

or
$$r_1 = \frac{r_2}{\exp\left(\cosh^{-1}\frac{2r_2}{2d}\right)} \quad . \quad . \quad . \quad (28)$$

(6.2.2) Electrical Analogue Parameters.

The analogous electric circuit representing eqn. (25) will then be the same as that given in Section 4.3, i.e.

$$K = 0{\cdot}359; \quad R_1 = \frac{\Delta x}{Km}; \quad R_2 = \frac{1}{\Delta x \lambda m}$$

(7) DETERMINATION OF ACTUAL FUSE CHARACTERISTICS

(7.1) Example for a Uniform-Cross-Section Semi-Enclosed Fuse

Material: tin sheet; $K = \frac{k}{c\rho} = 0{\cdot}359$; $\lambda = 0{\cdot}022$ (in air).

From Section 4.4 Table 1 is obtained.

Table 1

ANALOGUE PARAMETERS

Elemental length of fuse element of any cross-section a_n	R_1	R_2	C	$i_g = 5$ mA
cm	kΩ	kΩ	μF	
0·508	3·48	228	400	$\frac{2a}{10^4}$
0·254	0·870	228	400	$\frac{2a}{10^4}$
0 127	0·218	228	400	$\frac{2a}{10^4}$
0·064	0·218	228	100	$\frac{2a}{10^4}$

Table 2

CURRENT/TIME CHARACTERISTIC OF STRIP FUSE

Time	Voltage for length 0·889 cm (from Appendix 12.1)	Voltage for length 1·14 cm (from Appendix 12.1)	Average voltage for length 1·02 cm	$N = \frac{0{\cdot}58\,V}{25}$	$I^2 = \frac{232}{N}$	I (from analogue)	I (from calculation confirmed by test)
sec	V	V	V			A	A
50	33	51·5	42·25	0·98	236·7	15·4	16·55
20	33	52·0	42·0	0·974	238·2	15·4	16·55
10	32	47	39·5	0·916	253·3	15·9	16·6
5	28·5	37	32·75	0·76	305·3	17·57	17·5
2	18	20	19	0·441	326·07	22·9	21·8
1	10·3	11	10·65	0·247	939·3	30·6	28·75
0·5	5·5	5·6	5·55	0·129	1 798·4	42·35	39·25
0·2	2·4	2·4	2·4	0·057	4 165·2	64·55	64·2
0·1	1·15	1·17	1·16	0·026 9	8 624·5	92·9	87
0·05	0·58	0·59	0·589	0·013 6	17 058·8	130·6	129·2
0·02	0·235	0·245	0·24	0·005 7	40 701·7	201·8	
0·01	0·11	0·11	0·11	0·002 55	90 980·4	301·6	
0·005	0·05	0·05	0·05	0·001 16	200,000	447·21	

The material dimensions of the tin strip used in the analytical and experimental derivations were 2·03 cm long, 0·013 cm thick and 0·343 cm wide. Taking sections of 0·254 cm length, the maximum temperature will be at $l/2$ or $2{\cdot}03/2 = 1{\cdot}016$ cm; this is the average between points 0·889 cm and 1·143 cm in a section of 0·254 cm length.

$$i_g = 5\,\text{mA} = \frac{2a}{10^4}$$

$$\text{or } a = 25 = \frac{I^2}{JA\rho c\sigma} = 0{\cdot}58I^2$$

$$\text{or } I^2 = \frac{25}{0{\cdot}58}$$

$$V\,(\text{the recorded voltage}) = NI^2$$

$$N = \frac{V}{I^2} = \frac{0{\cdot}58}{25}V$$

whence Table 2 is obtained.

(7.2) Example. To Find the Current/Time Characteristic of a Fuse 0·241 cm Wide, 2·03 cm Long and 0·165 cm Thick, Immersed in Switchgear Oil (to B.S. 148: 1959)

$$a = \frac{I^2}{JA^2\rho c\sigma} = 0{\cdot}655I^2$$

To find H_{oil}

In order to find the average kinematic viscosity between 10° C (ambient) to 230° C (melting point of the fuse), the scale has been divided into 14 ranges, 13·9° C apart.

The average of the integrated kinematic viscosity from 10° C to 204° C is thus $\frac{66{\cdot}3}{14} = 4{\cdot}73$ units, corresponding to the kinematic viscosity at 81° C.

To find G_rP_r for a temperature variation of 1° C and 1 cm length of metal plate at the average viscosity (81° C), the results in Table 4 are based on those of Lorenz,[5] who used a metal plate, 0·119 m in length, immersed in switchgear oil.

Extrapolating from Table 4, G_rP_r at 81° C is 145×10^4.

From eqn. (18),

$$\frac{H}{k_{oil}} = \omega(G_rP_r)^{1/4} = 0{\cdot}55\,(145 \times 10^4)^{1/4} = 19$$

$$k_{oil} = 0{\cdot}000\,317 \text{ C.G.S. units}^7$$

$$H_{oil} = 19 \times 0{\cdot}000\,317 = 0{\cdot}006\,02$$

$$H_{air} = 5{\cdot}15 \times 10^{-5} \text{ or } H_{oil} = 114{\cdot}6H_{air}$$

Table 3

AVERAGE KINEMATIC VISCOSITY OF SWITCHGEAR OIL

Temperature	Viscosity	Average viscosity
°C		
10	40	
24·5	21	30·5
37·2	12·2	16·6
51·6	8·0	10·1
65·5	5·5	6·75
79·3	4·1	4·8
93·3	3·2	3·65
107·1	2·55	
122·1	2·1	
135·0	1·78	
149·0	1·54	
163·0	1·35	
176·8	1·18	
190·5	1·07	
204·2	0·96	$\sum_1^{14} = 66{\cdot}3$

Table 4

DETERMINATION OF G_rP_r

θ	Temperature difference between plate and liquid	GrP_r (for specimen 0·119 m long[5])	G_rP_r (unit/cm unit/deg C)
°C	°C		
18·4	7·7	$2{\cdot}001 \times 10^7$	$15{\cdot}4 \times 10^4$
25·1	12·1	$4{\cdot}45 \times 10^7$	$21{\cdot}8 \times 10^4$
33·1	18·0	$9{\cdot}638 \times 10^7$	$31{\cdot}6 \times 10^4$
37·5	21·7	$1{\cdot}432 \times 10^8$	39×10^4
54·0	32·7	$3{\cdot}88 \times 10^8$	70×10^4
70·2	44·5	$8{\cdot}595 \times 10^8$	114×10^4

Therefore,

$$R_2 \text{ for oil} = \frac{228}{114{\cdot}6} = 2\,\text{k}\Omega.$$

From Table 1, with $R_2 = 2\,\text{k}\Omega$, similar to the case of Table 2, the complete solution with comparison of experimental results is tabulated in Table 5.

Table 5

CURRENT/TIME CHARACTERISTIC OF FUSE IMMERSED IN OIL

Analogue computation					Experimental determination	
Time	Voltage at 2·28 cm	Voltage at 1·78 cm	Average voltage V' at 2·03 cm	$I = \left(\frac{232 \times 25}{0{\cdot}655\,V'}\right)^{1/2}$	Current	Time
sec	V	V	V	A	A	sec
0·01	0·11	0·11	0·11	284	122	0·040 5
0·02	0·24	0·23	0·235	194	90	0·072
0·05	0·57	0·56	0·569	125	65	0·185
0·1	1·07	1·06	1·065	91·2	50	0·47
0·2	2·05	2·0	2·02	66·3	41·5	0·70
0·5	4·2	4·2	4·2	45·9	34	1·15
1	7·0	6·9	6·95	35·7	30	2·0
2	9·1	9·0	9·05	31·3	28	8·2
5	10·4	10·4	10·4	29·2	27	time
Time	10·6	10·5	10·55	29·0		to
to						m.f.c.
m.f.c.						

Table 6

CHARACTERISTIC OF FUSE ENCLOSED IN SILICA FILLER

Time	Voltage at $l/2 = 1{\cdot}14$ cm	Voltage at $l/2 = 0{\cdot}889$ cm	Average voltage V' at $l/2 = 1{\cdot}015$ cm	$I = 89\,\frac{1}{\sqrt{V'}}$	By experiment	
					I	t
sec	V	V	V	A	A	sec
0·02	0·22	0·22	0·22	191	205	0·015
0·05	0·58	0·58	0·58	117	102	0·044
0·1	1·2	1·18	1·19	81·1	70	0·09
0·2	2·4	2·3	2·95	58·2	52	0·20
0·5	5·1	5·0	5·1	39·5	41	0·4
1	8·8	8·5	8·65	30·3	35·5	0·8
2	13·5	12·0	12·7	25	31	1·82
5	18·2	14·5	16·3	22·1	26	2·8
10	18·5	15·0	16·7	22	24	4·8
50	19·0	15·3	17·15	21·55	18·5	345

(7.3) Cases of Fuse Elements Enclosed in Quartz Filler

(7.3.1) Example. To Find the Current/Time Characteristic of a Strip Fuse 2·03 cm Long, 0·0165 cm Thick, 0·228 cm Wide, the Filler being $k_2 = 5{\cdot}9 \times 10^{-4}$ c.g.s.u. and the Cartridge Diameter 1·27 cm.

From eqn. (28),

$$r_1 = \frac{r_2}{\exp\left(\cosh^{-1}\frac{2r_2}{2d}\right)} = \frac{0{\cdot}635}{\exp\left(\cosh^{-1}\frac{0{\cdot}5}{0{\cdot}09}\right)} = 0{\cdot}057\,\text{cm}$$

$$\lambda_1 = \frac{2\pi k_2}{A_1 c_1 \rho_1 \log\frac{r_2}{r_1}} = 1{\cdot}05$$

$$R_2 = \frac{5 \times 10^3}{1{\cdot}05} = 4{\cdot}75\,\text{k}\Omega$$

with 5 mA current, Table 6 may be assembled, again with comparison of experimentally derived results.

(7.3.2.) Example.

As a further example in this category, the current/time characteristic of a fuse 0·508 cm wide and 2·79 cm long, embedded in quartz powder, will be found.

Table 7

CHARACTERISTIC OF A FUSE OF DIFFERENT DIMENSIONS FROM THOSE GIVEN IN TABLE 6

By analogue (i_g = 5 mA)			By experiment	
Time	Voltage	$I = \left(\frac{232 \times 25}{Va}\right)^{1/2}$	Current	Time
sec	V	A	A	sec
0·02	0·22	423	250	0·0385
0·05	0·545	269	151	0·095
0·1	1·25	177	98	0·343
0·2	2·35	129·6	74·5	0·82
0·5	5·25	86·6	59	2·0
1·0	9·8	63·35	45·5	6·6
2·0	16·0	49·6	49	13·5
10	25	39·6	49	13·5

The tin sheet from which the fuses were manufactured was 0·178 cm thick, and $r_{cartridge} = 0{\cdot}635$ cm.

$$a = 0{\cdot}147\,5I^2$$

$$r_1 = \frac{0{\cdot}635}{\exp\left(\cosh^{-1}\dfrac{0{\cdot}5}{0{\cdot}2}\right)} = 0{\cdot}133\,\text{cm}$$

$$\lambda_1 = \frac{2\pi k_2}{A_1 c_1 \rho_1 \log \dfrac{r_2}{r_1}} = 0{\cdot}777$$

Therefore $R_2 = \dfrac{5 \times 10^3}{0{\cdot}777} = 6{\cdot}44 \simeq 6{\cdot}5\,\text{k}\Omega.$

As before, constructing a tabular comparison of results we have Table 7.

(8) EXAMPLE OF A FUSE WITH DOUBLE DISCONTINUITY IN ITS CROSS-SECTION

A double-discontinuity fuse (3·04 cm long, 0·013 cm thick, 0·38 cm wide and 0·137 cm neck width with 0·508 cm neck length) is immersed in oil in accordance with B.S. 148: 1959.

$$a_1 = 4{\cdot}234 I^2 \qquad a_2 = 0{\cdot}471 I^2$$

$$b_1 = 1{\cdot}6 I^2 \qquad b_2 = 0{\cdot}19 I^2$$

$$H_{oil} = 0{\cdot}006\,02 \quad \text{and} \quad R_2 = 2\,\text{k}\Omega$$

To find T_s, substitute in eqn. (8); alternatively, and more simply, T_s may be obtained from eqn. (12) of Reference 1.

$$T_s = 0{\cdot}417 I^2$$

Table 8

TEMPERATURE FROM THE FIRST PART OF EQN. (9) FOR THE DISTANCE $l_1/2$, WHERE $l_1 = 0{\cdot}508$ CM, AND USING THE ANALOGUE FOR SECTIONS OF ELEMENTAL LENGTH 0·064 CM

Time	Voltage from analogue, corresponding to $i_g = 5$ mA			$NI^2 = \frac{Va}{100}$
	at $l/2$ where $l = 0{\cdot}508$ cm	at $l/2$ where $l = 0{\cdot}444$ cm	at $l/2$ where $l = 0{\cdot}571$ cm	
sec	V	V	V	
0·005	0·22	0·22	0·22	$0{\cdot}009\,3I^2$
0·01	0·46	0·46	0·46	$0{\cdot}019I^2$
0·02	0·9	0·9	0·9	$0{\cdot}038I^2$
0·05	2·22	2·05	2·13	$0{\cdot}09I^2$
0·1	3·95	3·3	3·62	$0{\cdot}153I^2$
0·2	6·3	4·45	5·37	$0{\cdot}227I^2$
0·5	8·1	5·05	6·57	$0{\cdot}278I^2$
1	8·7	5·2	6·95	$0{\cdot}294I^2$
2	8·7	5·2	6·95	$0{\cdot}294I^2$

(8.1) Minimum Fusing Current

At $l_1/2$ the temperature [second and third part of eqn. (9)] is $0{\cdot}79T_s$ (from Table 9) $= 0{\cdot}79 \times 0{\cdot}417 I^2 = 0{\cdot}329 I^2$.

At $l_1/2$ the temperature [first part of eqn. (9)] is $0{\cdot}294I^2$ (from Table 8). Therefore the total temperature is $0{\cdot}623I^2 = NI^2$, and the melting temperature is 232° C. The minimum fusing current is $[232/0{\cdot}623]^{1/2} = 19{\cdot}4$ A and from experiment it is 19·0 A.

From Tables 8 and 9 and Fig. 10, and the experimental results, Table 10 is obtained.

Table 9

DETERMINATION[1] OF θ'

Time	θl_2				θl_1 and $\frac{\theta l_1}{2}$				$\theta l' = \frac{A_1 l_1 \theta l_1 + A_2 l_2 \theta l_2}{A_1 l_1 + A_2 l_2}$
	at $l_2 = 1{\cdot}4$ cm	at $l_2 = 1{\cdot}14$ cm	at $l_2 = 1{\cdot}27$ cm	θl_2 in terms of T_s	θl_1 at $l_1 = 0{\cdot}444$ cm	θl_1 at $x_1 = 0{\cdot}317$ cm	θl_1 at $x_1 = 0{\cdot}571$ cm	θl_1 at $x_1 = 0{\cdot}19$ cm	θl_1 at $l_1 = 0{\cdot}508$ cm	$\frac{\theta l_1}{2}$ at $\frac{l_1}{2} = 0{\cdot}254$ cm	$2\theta\frac{l_1}{2}$	
sec	V	V	V	V	V	V	V	V	V	V	V	V
0·02	0·23	0·22	0·225	$0{\cdot}047T_s$	$0{\cdot}21 = 0{\cdot}097T_s$	$0{\cdot}001 = 0{\cdot}000\,387T_s$	$0{\cdot}21 = 0{\cdot}081T_s$	$0{\cdot}001 = 0{\cdot}000\,437T_s$	$0{\cdot}085T_s$	$0{\cdot}000\,4T_s$	$0{\cdot}000\,8T_s$	$0{\cdot}051T_s$
0·05	0·55	0·54	0·545	$0{\cdot}115T_s$	$0{\cdot}45 = 0{\cdot}197T_s$	$0{\cdot}015 = 0{\cdot}005\,77T_s$	$0{\cdot}45 = 0{\cdot}157T_s$	$0{\cdot}015 = 0{\cdot}006\,47T_s$	$0{\cdot}18T_s$	$0{\cdot}006\,05T_s$	$0{\cdot}012\,1T_s$	$0{\cdot}123T_s$
0·1	1·04	1·04	1·04	$0{\cdot}219T_s$	$0{\cdot}76 = 0{\cdot}32T_s$	$0{\cdot}061 = 0{\cdot}023T_s$	$0{\cdot}77 = 0{\cdot}30T_s$	$0{\cdot}06 = 0{\cdot}256T_s$	$0{\cdot}31T_s$	$0{\cdot}024\,3T_s$	$0{\cdot}048\,6T_s$	$0{\cdot}23T_s$
0·2	1·8	1·8	1·8	$0{\cdot}379T_s$	$1{\cdot}2 = 0{\cdot}31T_s$	$0{\cdot}20 = 0{\cdot}077T_s$	$1{\cdot}2 = 0{\cdot}46T_s$	$0{\cdot}215 = 0{\cdot}092T_s$	$0{\cdot}485T_s$	$0{\cdot}084\,5T_s$	$0{\cdot}169T_s$	$0{\cdot}39T_s$
0·5	2·95	2·95	2·95	$0{\cdot}621T_s$	$1{\cdot}88 = 0{\cdot}807T_s$	$0{\cdot}625 = 0{\cdot}24T_s$	$1{\cdot}87 = 0{\cdot}72T_s$	$0{\cdot}55 = 0{\cdot}235T_s$	$0{\cdot}76T_s$	$0{\cdot}237T_s$	$0{\cdot}475T_s$	$0{\cdot}637T_s$
1	3·95	3·95	3·95	$0{\cdot}832T_s$	$2{\cdot}25 = 0{\cdot}967T_s$	$0{\cdot}95 = 0{\cdot}36T_s$	$2{\cdot}38 = 0{\cdot}915T_s$	$0{\cdot}75 = 0{\cdot}32T_s$	$0{\cdot}94T_s$	$0{\cdot}34T_s$	$0{\cdot}68T_s$	$0{\cdot}845T_s$
2	4·55	4·5	4·52	$0{\cdot}947T_s$	$2{\cdot}3 = 0{\cdot}987T_s$	$1{\cdot}1 = 0{\cdot}42T_s$	$2{\cdot}55 = 0{\cdot}98T_s$	$0{\cdot}80 = 0{\cdot}34T_s$	$0{\cdot}98T_s$	$0{\cdot}38T_s$	$0{\cdot}76T_s$	$0{\cdot}951T_s$
5	4·75	4·75	4·75	$1{\cdot}0T_s$	$2{\cdot}34 = 1{\cdot}0T_s$	$1{\cdot}13 = 0{\cdot}43T_s$	$2{\cdot}6 = 1{\cdot}0T_s$	$0{\cdot}85 = 0{\cdot}36T_s$	$1{\cdot}0T_s$	$0{\cdot}395T_s$	$0{\cdot}79T_s$	$1{\cdot}0T_s$
10	4·75	4·75	4·75	$1{\cdot}0T_s$	$2{\cdot}34 = 1{\cdot}0T_s$	$1{\cdot}13 = 0{\cdot}43T_s$	$2{\cdot}6 = 1{\cdot}0T_s$	$0{\cdot}85 = 0{\cdot}36T_s$	$1{\cdot}0T_s$	$0{\cdot}395T_s$	$0{\cdot}79T_s$	$1{\cdot}0T_s$

The values of θl_2 and θl_1 were obtained from the analogue computer expressed as voltages or in terms of T_s; sections of elemental length 0·254 cm were used for l_2, and sections of elemental length 0·127 cm for l_1.

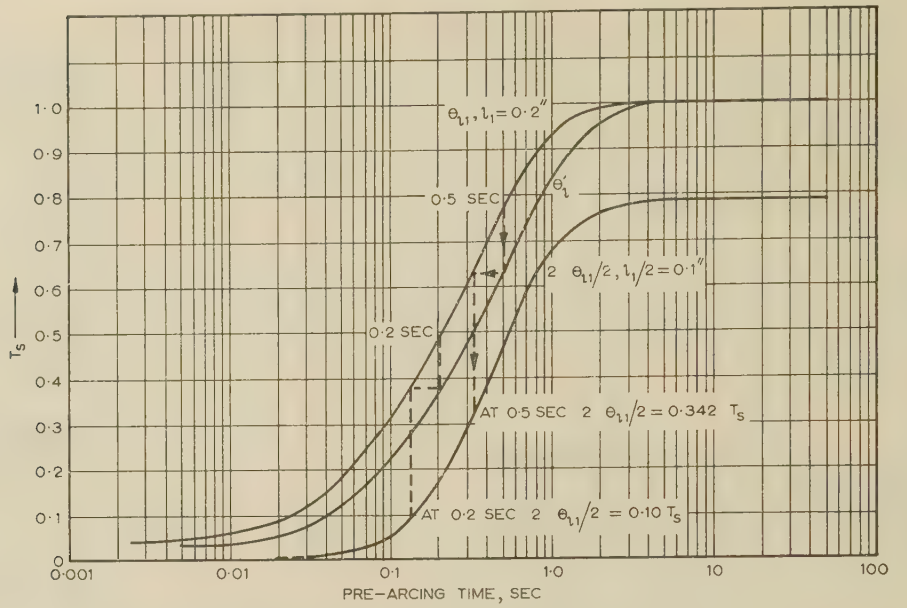

Fig. 10.—Graphical determination of temperature rise at a discontinuity.
Fuse with double discontinuity immersed in oil.

Table 10

CURRENT/TIME CHARACTERISTIC OF A FUSE WITH A DOUBLE DISCONTINUITY IN ITS CROSS-SECTION, AND IMMERSED IN OIL

Analogue computation						Experimental results	
Time	at $\frac{I_1}{2}$ [1st part of eqn. (9)] Table 8	at $\frac{I_1}{2}$ [2nd and 3rd parts of eqn. (9)] Table 9	$T_s = 0{\cdot}417\ I^2$ (substituting)	Total temperature	Current = $\left[\frac{232}{H}\right]^{1/2}$	Current	Time
sec.					A	A	sec
0·005	$0{\cdot}009I^2$	—	—	$0{\cdot}009I^2$	160·5	78	0·021
0·01	$0{\cdot}019I^2$	—	—	$0{\cdot}019I^2$	110·5	58·5	0·045
0·02	$0{\cdot}038I^2$	—	—	$0{\cdot}038I^2$	78·15	45	0·086
0·05	$0{\cdot}09I^2$	$0{\cdot}005T_s$	$0{\cdot}002I^2$	$0{\cdot}092I^2$	50·25	35	0·16
0·1	$0{\cdot}153I^2$	$0{\cdot}02T_s$	$0{\cdot}008I^2$	$0{\cdot}161I^2$	37·96	26	0·43
0·2	$0{\cdot}227I^2$	$0{\cdot}1T_s$	$0{\cdot}042I^2$	$0{\cdot}269I^2$	29·36	22·2	1·1
0·5	$0{\cdot}278I^2$	$0{\cdot}342T_s$	$0{\cdot}143I^2$	$0{\cdot}421I^2$	23·5		
1	$0{\cdot}294I^2$	$0{\cdot}56T_s$	$0{\cdot}234I^2$	$0{\cdot}528I^2$	20·97	20	2·1
2	$0{\cdot}294I^2$	$0{\cdot}71T_s$	$0{\cdot}296I^2$	$0{\cdot}59I^2$	19·8		time
5	$0{\cdot}294I^2$	$0{\cdot}79T_s$	$0{\cdot}33I^2$	$0{\cdot}624I^2$	19·4	19	for
m.f.c.	$0{\cdot}294I^2$	$0{\cdot}79T_s$	$0{\cdot}33I^2$	$0{\cdot}624I^2$	19·4		m.f.c.

(9) CONCLUSIONS

The paper describes an extension of previous work[1] to fuses with multiple discontinuities, fuses immersed in oil and fuses in silica or quartz filler. The analysis has thus been made more general; furthermore, an analogue computer has been developed for practical fuse-equation solution, and its mode of use is emphasized by means of a number of examples. Very close correlation has been obtained between theoretical results obtained by the methods described in the paper and the experimental results obtained in the laboratory under controlled conditions; these sets of results are given in Tables 2 and 5 for semi-enclosed and oil-immersed fuses, respectively. Close correlation was also obtained for the example given in Section 8 where the fuse had a doubly discontinuous cross-section similar to those of many fuses in common use, e.g. Fig. 1(*a*); the experimental and analytically determined results in this case are given in Table 10.

To reduce computational labour, an electrical-analogue computer has been built to facilitate the mathematical approach used in the analysis of a uniform fuse element, as well as that of a fuse with multiple discontinuities in its cross-section. The analogue includes elements for representing the axial heat transfer, the radial heat transfer, the heat energy from the initiating current and the radial heat transfer of the surrounding medium. The axial heat of the surrounded medium has been neglected, thereby enabling a reduction in the size of the analogue, thus making it more economical and easy to use. The results obtained are very satisfactory and thoroughly justify the approximation.

Fuses immersed in a liquid, such as the oil-immersed fuse, required special considerations. A satisfactory solution for a liquid-immersed fuse was formulated through the application of the mathematical theory of the natural convection of liquids, an experiment to investigate the natural convection of switch-

gear oil, and with a modified application of the analogue computer to the solution of the thermo-electric fuse equation.

Consideration has also been given in the paper to the thermal performance of the conducting medium in powder-filled cartridge fuses. The problem of a uniform-cross-section single-wire fuse of this class has been treated by Guile and Carne,[3] and the work above has been concentrated on non-uniform sections (rectangular cross-section strip), the radial heat transfer from the element being taken into account. This treatment led to application of the analogy between electric and thermal fields for obtaining a solution of the strip fuse enclosed in quartz/silica filler; the mathematical process adopted once the analogy has been established is the same as in the previous cases. From the two examples quoted in Section 7.3, the results of which are given in Tables 6 and 7, respectively, it can be seen that the results show reasonable accuracy for cases of fuses which are not very long compared with their width, e.g. length : width $\geqslant 10$. For longer fuses in this class, it is clear that more accurate computational methods should be used, e.g. extension of the analogue computer to permit the fuse length to be represented by a greater number of elemental sections, together with improvements in the method of measurement on the analogue computer; the logical step would be to adopt the equivalent of this in the form of solution by digital computer. Alternatively, a different approach could be made to the problem of the long fuse element enclosed in heat-conducting filler; one possibility is application of the methods of Jaeger and Newstead[8] in their work on the transient heating of buried cables.

(10) REFERENCES

(1) Adamson, C., and Viseshakul, M.: 'An Analytical Method for Predicting the Performance of Semi-enclosed Fuses', *Proceedings I.E.E.*, Monograph No. 387 S, June, 1960 (**108** C, p. 2).

(2) Carslaw, H. S., and Jaeger, J. C.: 'Conduction of Heat in Solids' (Clarendon Press, Oxford, 1947).

(3) Guile, A. E., and Carne, E. B.: 'An Analysis of an Analogue Solution Applied to the Heat Conduction Problem in a Cartridge Fuse', *Transactions of the American I.E.E.*, 1954, **72**, Part I, p. 861.

(4) Saunders, O. A.: 'Natural Convention in Liquids', *Proceedings of the Royal Society*, A, 1939, **172**, p. 55.

(5) Lorenz, W.: 'Natural Convention in Oil', *Zeitschrift für Technische Physik*, 1951, **22**.

(6) Pipes, L. A.: 'Applied Mathematics for Engineers and Physicists' (McGraw-Hill, 1946).

(7) Manchester Oil Refinery: 'Physical Properties of Switchgear Oil—B.S. 148', Technical Literature, Manchester Oil Refinery, Manchester, 1958.

(8) Jaeger, J. C., and Newstead, G. H.: 'Transient Heating of Buried Cables', *Proceedings I.E.E.*, Monograph No. 253 S, August 1957 (**105** C, p. 57).

(11) ACKNOWLEDGMENTS

The authors wish to express their gratitude for the facilities provided by the Electrical Engineering Department (Prof. Bradshaw) of the Manchester College of Science and Technology, for carrying out the work described in the paper. They are also indebted to their colleague, Mr. A. Efthymiadis, and their former colleague, Dr. E. A. Talkhan, for editorial assistance.

(12) APPENDICES

(12.1) Tables of Fuse Data Derived from Analogue-Computer Studies

The following Tables have been assembled from results of analogue studies carried out on the computer described in Section 4. The complete set of Tables were of fuse data for fuses varying in length from 0·445 cm to 2·79 cm. The columns marked 'length' refer to the distance of the nodes from the origin, as in Fig. 6(*b*), and correspond to the elemental lengths into which the fuse has been divided. In all cases, $C = 400\,\mu$F and $i_g = 5$ mA. Average values from Tables 11 and 12 were taken for fuse lengths of 2·03 cm used in the experiments.

Table 11

FUSE DATA

Length x	Voltage corresponding to time t, sec												
cm	V	V	V	V	V	V	V	V	V	V	V	V	V
1·14	0·05	0·11	0·25	0·59	1·17	2·40	5·60	11·0	20·0	37·0	47·0	51·0	51·5
0·89	0·05	0·11	0·24	0·585	1·17	2·40	5·50	10·5	19·0	34·5	42·0	46·0	46·5
0·64	0·05	0·11	0·24	0·58	1·15	2·35	5·30	9·5	16·5	27·0	34·0	38·0	38·5
0·38	0·05	0·105	0·235	0·58	1·15	2·28	4·65	7·5	11·7	20·5	23·0	26·3	26·5
0·128	0·05	0·105	0·130	0·535	0·92	1·54	2·50	3·70	5·4	8·4	9·2	10·3	10·4
	0·005	0·01	0·02	0·5	0·1	0·2	0·5	1·0	2·0	5·0	10·0	20·0	50·0

Total length = 2·28 cm

Table 12

FUSE DATA

Length x	Voltage corresponding to time t, sec												
cm	V	V	V	V	V	V	V	V	V	V	V	V	V
0·89	0·05	0·11	0·235	0·58	1·15	2·40	5·50	10·3	18·0	28·5	32·0	33·0	33·0
0·64	0·05	0·11	0·235	0·58	1·15	2·35	5·40	9·5	16·1	25·0	28·0	29·0	29·0
0·38	0·05	0·105	0·235	0·57	1·15	2·30	4·70	7·5	12·0	18·7	20·3	21·0	21·0
0·128	0·05	0·105	0·228	0·53	0·90	1·57	2·50	3·50	5·40	7·20	8·30	8·47	8·47
	0·005	0·01	0·02	0·05	0·1	0·2	0·5	1·0	2·0	5·0	10·0	20·0	50·0

Total length = 1·78 cm

(22.2) Feasibility of Establishing a Single Series of Tables for Predicting the Current/Time Characteristic of a Fuse with Multiple Discontinuities in its Cross-Section

According to the method previously established for a fuse of doubly discontinuous cross-section, seven sets of Tables are generally required; two are required for each outer section and three for the middle section in each case in order to compute the current/time characteristic. Thus the analogue computer will have to be used to perform seven series of operations. However, if a mathematical solution for such a fuse shows that the seven series of operating solutions can be replaced by a single series, it is likely that the seven series of analogue-computer operations which follow the mathematical approach can be reduced to a single series also, thereby introducing economy.

To prove the possibility of a single series of electrical analogue operations is to prove the possibility of a single series of Tables of data for a multiple-cross-section fuse in general; the discussion here is restricted to three sections for simplicity. This method uses Laplace transformations to reduce the partial differential equation to the subsidiary differential equation. When the subsidiary equation has been solved with the appropriate boundary conditions, the Laplace transform of the problem will be given by the subsidiary equation's solution, and the procedure then involves methods of finding the final temperature by a contour integral. To illustrate this mathematical approach, a double-discontinuity fuse has been chosen, i.e. three sections.

From Fig. 2(*b*), the general equations, as before, are

$$\frac{\partial\theta_1}{\partial t} = K\frac{\partial^2\theta_1}{\partial x_1^2} - \lambda_1\theta_1 + a_1 \quad . \quad . \quad . \quad (29)$$

$$\frac{\partial\theta_2}{\partial t} = K\frac{\partial^2\theta_2}{\partial x_2^2} - \lambda_2\theta_2 + a_2 \quad . \quad . \quad . \quad . \quad (30)$$

Reduce the partial differential equations to subsidiary equations.

Eqn. (29) gives

$$0 = K\frac{\partial^2\bar{\theta}_1}{\partial x_1^2} - (\lambda_1 + p)\bar{\theta}_1 + \frac{a_1}{p} \quad . \quad . \quad . \quad (31)$$

Eqn. (30) gives:

$$0 = K\frac{\partial^2\bar{\theta}_2}{\partial x_2^2} - (\lambda_2 + p)\bar{\theta}_2 + \frac{a_2}{p} \quad . \quad . \quad . \quad (32)$$

With boundary conditions

(i) $A_1\dfrac{d\bar{\theta}_1}{dx_1} = A_2\dfrac{d\bar{\theta}_2}{dx_2}$ at $x_1 = 0$ and $x_2 = l_2$ . . . (33)

(ii) $\bar{\theta}_1 = \bar{\theta}_2 = \bar{\theta}_s$ at $x_1 = 0$, $x_2 = l_2$ and at $x_1 = l_2$ (34)

(iii) $\bar{\theta}_2 = 0$ at $x_2 = 0$ . . . . . (35)

Subsidiary equation (31) with eqn. (34) gives

$$\theta_{1x}(p) = \frac{a_1}{p(\lambda_1 + p)}\left[1 - \frac{\sinh\left(\frac{\lambda_1+p}{K}\right)^{1/2}x_1 + \sinh\left(\frac{\lambda_1+p}{K}\right)^{1/2}(l_1 - x_1)}{\sinh\left(\frac{\lambda_1+p}{K}\right)^{1/2}l_1}\right] + \bar{\theta}_s\frac{\sinh\left(\frac{\lambda_1+p}{K}\right)^{1/2}x_1 + \sinh\left(\frac{\lambda_1+p}{K}\right)^{1/2}(l_1 - x_1)}{\sinh\left(\frac{\lambda_1+p}{K}\right)^{1/2}l_1} \quad (36)$$

Subsidiary equation (32) with eqns. (34) and (35) gives

$$\bar{\theta}_{2x}(p) = \frac{a_2}{p(\lambda_2 + p)}\left[1 - \frac{\sinh\left(\frac{\lambda_2+p}{K}\right)^{1/2}x_2 + \sinh\left(\frac{\lambda_2+p}{K}\right)^{1/2}(l_2 - x_2)}{\sinh\left(\frac{\lambda_2+p}{K}\right)^{1/2}l_2}\right] + \bar{\theta}_s\frac{\sinh\left(\frac{\lambda_2+p}{K}\right)^{1/2}x_2}{\sinh\left(\frac{\lambda_2+p}{K}\right)^{1/2}l_2} \quad (37)$$

Differentiate eqns. (36) and (37) and equate with the condition in eqn. (33) giving

$$\bar{\theta}_s(p) = \frac{\dfrac{qa_1\left(\frac{\lambda_1+p}{K}\right)^{1/2}\left[1 - \cosh\left(\frac{\lambda_1+p}{K}\right)^{1/2}l_1\right]}{p(\lambda_1+p)\sinh\left(\frac{\lambda_1+p}{K}\right)^{1/2}l_1} + \dfrac{a_2\left(\frac{\lambda_2+p}{K}\right)^{1/2}\left[1 - \cosh\left(\frac{\lambda_2+p}{K}\right)^{1/2}l_2\right]}{p(\lambda_2+p)\sinh\left(\frac{\lambda_2+p}{K}\right)^{1/2}l_2}}{\dfrac{q\left(\frac{\lambda_1+p}{K}\right)^{1/2}\left[1 - \cosh\left(\frac{\lambda_1+p}{K}\right)^{1/2}\right]l_1}{\sinh\left(\frac{\lambda_1+p}{K}\right)^{1/2}l_1} + \dfrac{\left(\frac{\lambda_2+p}{K}\right)^{1/2}\cosh\left(\frac{\lambda_2+p}{K}\right)^{1/2}l_2}{\sinh\left(\frac{\lambda_2+p}{K}\right)^{1/2}l_2}}$$

where $q = \dfrac{A_1}{A_2}$.

For this type of fuse, the fuse breaks at $x_1 = l_1/2$,

$$\theta_{1x1}(p) = \frac{a_1}{p(\lambda_1+p)} + \frac{1}{p\cosh\left(\frac{\lambda_1+p}{K}\right)^{1/2}\frac{l_1}{2}}\left\{\frac{\frac{a_2}{(\lambda_2+p)} - \left[\frac{a_2}{(\lambda_2+p)} + \frac{a_1}{(\lambda_1+p)}\right]\cosh\left(\frac{\lambda_2+p}{K}\right)^{1/2}l_2}{q\left(\frac{\lambda_1+p}{\lambda_2+p}\right)^{1/2}\sinh\left(\frac{\lambda_2+p}{K}\right)^{1/2}l_2\frac{1 - \cosh\left(\frac{\lambda_1+p}{K}\right)^{1/2}l_1}{\sinh\left(\frac{\lambda_1+p}{K}\right)^{1/2}l_1} + \cosh\left(\frac{\lambda_2+p}{K}\right)^{1/2}l_2}\right\}$$

This can be solved by the expansion method or by the inversion theorem on the contour integral.

Using the inversion theorem:

$$\theta_{1(t)} = \frac{a_1}{\lambda_1}(1 - \exp(-\lambda_1 t)$$

$$+ \frac{1}{2\pi j}\int_{\gamma - j\infty}^{\gamma + j\infty} \frac{\exp yt}{y \cosh\left(\frac{\lambda_1 + y}{K}\right)^{1/2} \frac{l_1}{2}} \frac{\frac{a_2}{\lambda_2 + y} - \left(\frac{a_2}{\lambda_2 + y} + \frac{a_1}{\lambda_1 + y}\right) \cosh\left(\frac{\lambda_2 + y}{K}\right)^{1/2} l_2}{q\left(\frac{\lambda_1 + y}{\lambda_2 + y}\right)^{1/2} \sinh\left(\frac{\lambda_2 + y}{K}\right)^{1/2} l_2 \frac{1 - \cosh\left(\frac{\lambda_1 + y}{K}\right)^{1/2} l_1}{\sinh\left(\frac{\lambda_1 + y}{K}\right)^{1/2} l_1} + \cosh\left(\frac{\lambda_2 + y}{K}\right)^{1/2} l_2} dy$$

$$x_1 = \frac{l_1}{2}$$

The above solution can be calculated in one series of Tables. Therefore, for a multiple-cross-section fuse, it is likely that the electrical analogue can compute also in one series of Tables instead of $(3n - 2)$ series, where n is the number of cross-sections.

621.396.677.32:621.372.826

The Institution of Electrical Engineers
Monograph No. 450 E
June 1961

THE LAUNCHING OF SURFACE WAVES BY AN END-FIRE ARRAY OF SLOTS

By Prof. A. L. CULLEN, O.B.E., Ph.D., Member, and J. A. STANIFORTH, Ph.D., Graduate.

(*The paper was first received* 12*th August*, 1960, *and in revised form* 15*th February*, 1961. *It was published as an* INSTITUTION MONOGRAPH *in June*, 1961.)

SUMMARY

An end-fire array of slots suitable for launching a surface wave on a dielectric-coated metal sheet is described and analysed. The analysis is based on the representation of the slots as magnetic dipoles in the plane of the sheet, their axes being perpendicular to the line of the array.

In a practical embodiment of the scheme the elements take the form of slots fed by quarter-wavelength branch guides series fed from a waveguide partially filled with dielectric mounted beneath the metal sheet. Experimental results are given which support the theoretical conclusion that a high launching efficiency is possible. A launching efficiency of 95% is obtained theoretically for a 12-slot array launching a surface wave on a metal sheet coated with dielectric of relative permittivity 2·56 and of thickness 0·125 in at a frequency of 9·38 Gc/s.

LIST OF SYMBOLS

x, y, z = Cartesian co-ordinates.
r, ϕ, z = Cylindrical co-ordinates.
R, θ, ϕ = Spherical co-ordinates.
H, E = Magnetic and electric vectors.
k = z-axis unit vector.
U, V = Magnetic and electric scalar potentials.
β = Phase-change coefficient used in the analysis.
k = Phase-change coefficient of free space.
u, m = Surface-wave constants.
μ_0, ϵ_0 = Constants of free space.
ϵ_r = Relative permittivity of dielectric sheet.
$2a$ = Dielectric thickness.
h = Height of dipole from centre of dielectric sheet.
$J_0(x), J_1(x)$ = Bessel functions of order zero and one, respectively.
K = Magnetic surface current density of single sheet.
c = Radius of magnetic-current sheet.
M = Magnetic-current moment of dipole.
S, R = Suffixes for the surface wave and radiation field respectively.
λ_s = Surface-wave wavelength.
λ_g = Rectangular-guide wavelength.
p = Phase-change coefficient used in the calculation of the radiation pattern of the array.

(1) INTRODUCTION

The investigation described in the paper arose from an experimental study of the diffraction of plane surface waves by cylindrical obstacles. A narrow-beam launcher of surface waves was necessary in order to reduce reflections from the sides of the surface-wave-supporting surface. It was also desirable that the launcher should have as high a launching efficiency as possible. Moreover, in the earlier stages of the experimental investigations, the launcher was required to be flush with the metal surface on which the dielectric sheet required for surface-wave propagation was placed. A linear end-fire array of waveguide-fed slots (Fig. 6) was expected to meet these requirements. It is reasonable to suppose that a theoretical treatment in which the slots are idealized as infinitesimal dipoles parallel to, and in the plane of, the metal surface will be adequate for predicting the launching efficiency of the device.

Formulae for the radiation and surface-wave fields produced by a magnetic dipole lying parallel to a plane capable of supporting surface waves (we shall refer to such a dipole as a horizontal dipole) do not appear to be given in the literature. Tai[1] and Whitmer[2] have considered the fields produced by a long horizontal wire carrying an electric current, and Cullen[3] has considered the corresponding dual problem for a long horizontal magnetic-current filament. These are essentially 2-dimensional problems. On the other hand, vertical electric dipoles have been studied by Fernando and Barlow,[4] and by Brick,[5] and vertical magnetic dipoles also by Brick.[5] The present analysis first considers the fields produced by a single horizontal magnetic dipole situated within a dielectric sheet.

From the solution of this problem we can deduce the solution of the less general case where the sheet has been replaced by a sheet of half the thickness backed by a perfectly conducting plane. It is this last case which is of interest so far as the experimental work referred to earlier is concerned. An end-fire array of magnetic-current dipoles can then be analysed in terms of the solution for a single magnetic-current dipole. It is found that the surface-wave launching efficiency for the array is much higher than that for a single dipole.

(2) SINGLE DIPOLE SOLUTION

In solving the case of a long magnetic-current filament parallel to a surface-wave-supporting plane, Cullen employed Fourier analysis to synthesize a magnetic-line source, at a height h above the supporting surface, from magnetic-current sheets parallel to the surface and also at height h above the surface. A similar approach is used in the present paper, in which the magnetic-current dipole is synthesized from magnetic-current sheets lying in the plane containing the dipole. Referring to Fig. 1, the

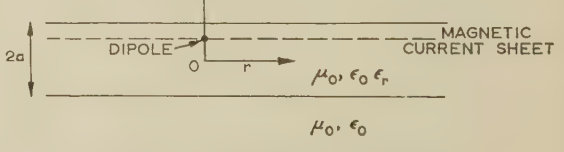

Fig. 1.—Dipole and current sheet.

direction of current flow in each sheet is assumed to be parallel to the y-axis, and it is further shown that the current flow varies with radial distance from the origin as $J_0(\beta r)$. The total field associated with any one of these current sheets can be calculated quite easily, and from this the field of the dipole can be obtained by summing fields associated with the individual

Correspondence on Monographs is invited for consideration with a view to publication.
Prof. Cullen is Professor of Electrical Engineering, University of Sheffield.
Dr. Staniforth is at the Royal Technical College, Salford, and was formerly in the Department of Electrical Engineering, University of Sheffield.

current sheets into which the dipole can be analysed. Fig. 1 shows a dielectric sheet of thickness $2a$ with a dipole situated at height h above its mid-plane. The field set up by a single magnetic-current sheet can be represented as the sum of two partial fields, one partial field having $E_z = 0$ and the other partial field having $H_z = 0$. These two partial fields can be obtained through scalar potentials V and U, respectively, from the following equations:

$$\left.\begin{aligned} E_v &= \operatorname{curl} kV \\ H_u &= \operatorname{curl} kU \end{aligned}\right\} \quad . \quad . \quad . \quad . \quad . \quad . \quad (1)$$

The potentials U and V must satisfy the scalar wave equation in cylindrical co-ordinates, they must be finite at the origin, and must also have an angular ϕ-dependence appropriate to a dipole field. In the free-space region above the dielectric sheet the appropriate forms are as follows:

$$U = j\omega\epsilon_0 D_1 \varepsilon^{-u(z-h)} \mathrm{J}_1(\beta r) \cos\phi \quad . \quad . \quad . \quad (2)$$

$$V = C_1 \varepsilon^{-u(z-h)} \mathrm{J}_1(\beta r) \sin\phi \quad . \quad . \quad . \quad . \quad . \quad (3)$$

Within the dielectric the exponential factors in these formulae are replaced by factor of the form $A \cos m(z-h) + B \sin m(z-h)$, where

$$\beta^2 = k^2 + u^2 = \epsilon_r k^2 - m^2 \quad . \quad . \quad . \quad . \quad (4)$$

Below the dielectric-sheet formulae of types (2) and (3) apply but with the sign of the exponent chosen so that the fields decay away from the surface if the exponent is real.

It is now necessary to express the arbitrary constants in terms of a magnetic surface current density $K(r)$. The dipole is analysed by summing the fields associated with this current, which always flows parallel to the dipole. At $z = h$, the discontinuity of E_r and E_ϕ together determines the magnetic surface current density. For the current to flow parallel to the dipole, E_r and E_ϕ, each of which has terms involving $\mathrm{J}_1(\beta r)$ and $\mathrm{J}_1'(\beta r)$, must have the same r-dependence. After simplification, this gives for the components of the magnetic surface current density

$$\left.\begin{aligned} K_y(r) &= K_0 \beta \mathrm{J}_0(\beta r) \\ \text{and} \quad K_x(r) &= 0 \end{aligned}\right\} \quad . \quad . \quad . \quad . \quad . \quad (5)$$

where K_0 is related to some of the foregoing arbitrary constants. It is a straightforward though somewhat laborious matter to determine the remaining arbitrary constants in terms of K_0 by making use of the boundary condition that tangential electric and magnetic fields must match on both sides of the free-space/dielectric interfaces and that the tangential magnetic field and the y-component of the tangential electric field must be continuous in the plane of the current sheet, whilst the x-component of the electric field must have a discontinuity appropriate to the magnetic current density. The next stage in the calculation is to represent the dipole in terms of magnetic-current sheets.

(2.1) Representation of the Magnetic Current Dipole

Referring to Fig. 2, the infinitesimal dipole can be regarded as the limit as $c \to 0$ of a circular patch of constant magnetic current density K of radius c polarized parallel to the dipole. The magnetic-current moment of a strip of current of thickness dx and length $2y$ is $K2ydx$, and hence the moment of the whole patch is $\pi c^2 K$, where c is the radius of the patch. It is assumed, of course, that c is small in comparison with the surface wavelength. As $c \to 0$ we assume that $K \to \infty$, so that $\pi c^2 K = M$, say, remains finite. The amplitudes of the magnetic-current sheets into which we analyse the dipole can be obtained

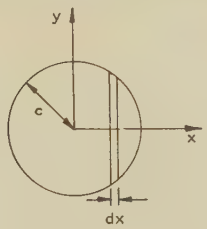

Fig. 2.—Magnetic current patch.

with the help of the Fourier–Bessel transform pair, when it is found that the sheets have the amplitude $M\beta/2\pi$.

(2.2) Image-Plane Solution with $h = 0$

In the problem of immediate interest the dipole is situated at the origin so that $h = 0$. The region below the plane $z = 0$ is assumed to be perfectly conducting. This, of course, limits the number of surface-wave modes which can be supported, but amongst these the dominant surface wave can still be supported. This wave has a component of electric field in the direction of propagation and a component of electric field perpendicular to the dielectric interface. Applying eqns. (2), (3) and similar equations, within the dielectric and outside, U and V can be found in terms of K_0. The potentials of the dipole can then be found by integrating over β from zero to infinity. The resulting integrals can be solved in the far field by contour integration in the complex β-plane; the contour being essentially that employed by Sommerfeld. The surface-wave field is obtained from the residues at the poles, and the radiation field is contributed by the branch cuts.

The poles occurring in the integral for U are given by

$$\tan ma = \frac{\epsilon_r u}{m} \quad . \quad . \quad . \quad . \quad . \quad . \quad (6)$$

If the thickness of the dielectric sheet is not too great there is only one solution of eqn. (6). The value of β corresponding to the particular value of m which satisfied eqn. (6) will be denoted by β_1. The poles arising in the integral representation of V exist only if the dielectric thickness is great enough. In what follows we shall assume that there are no poles contributed by the integral for V. In this case the surface-wave potentials for large values of r are given by

$$U_s = -\omega\epsilon_0 \frac{M}{2\sqrt{(2\pi)}} \frac{\varepsilon^{-j\pi/4}}{\sqrt{(\beta_1 r)}} \frac{\cos\phi \varepsilon^{-u(z-a)} \varepsilon^{-j\beta_1 r}}{\mathrm{F}'(\beta_1)} \quad . \quad (7)$$

$$V_s = 0$$

where $\mathrm{F}'(\beta_1) =$

$$-\beta_1 \left\{ \left[\frac{1}{\epsilon_r(\epsilon_r k^2 - \beta_1^2)^{1/2}} + \frac{a(\beta_1^2 - k^2)^{1/2}}{(\epsilon_r k^2 - \beta_1^2)^{1/2}} \right] \sin a(\epsilon_r k^2 - \beta_1^2)^{1/2} + \left[\frac{a}{\epsilon_r} + \frac{1}{(\beta_1^2 - k^2)^{1/2}} \right] \cos a(\epsilon_r k^2 - \beta_1^2)^{1/2} \right\}$$

The radiation field is found more conveniently by changing to spherical co-ordinates (G, θ, ϕ), as shown in Fig. 3. The method of steepest descent or the method of stationary phase can then be used to evaluate the resulting integral for large values of R. The potentials representing the radiation field under these conditions are

$$\left.\begin{aligned} U_R &= j\omega\epsilon_0 \frac{M}{4\pi} \frac{\cos\phi}{\mathrm{F}(k\sin\theta)} \frac{\cos\theta}{\sin\theta} \frac{\varepsilon^{-jkr}}{R} \\ V_R &= \frac{M}{4\pi} \frac{k\sin\phi\cos\theta(\epsilon_r - \sin^2\theta)^{1/2}}{\mathrm{G}(k\sin\theta)\sin\theta} \frac{\varepsilon^{-jkR}}{R} \end{aligned}\right\} \quad . \quad (8)$$

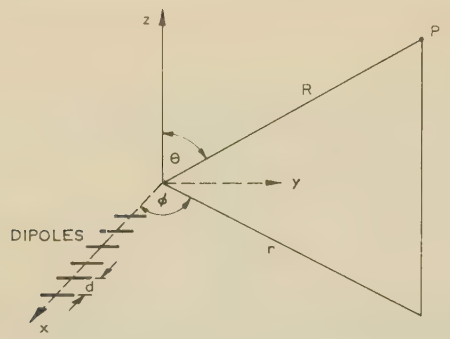

Fig. 3.—Spherical co-ordinate system and linear array.

where

$$F(k\sin\theta) = \frac{k}{\epsilon_r}(\epsilon_r - \sin^2\theta)^{1/2}\sin\left[ka(\epsilon_r - \sin^2\theta)^{1/2}\right] - jk\cos\theta\cos\left[ka(\epsilon_r - \sin^2\theta)^{1/2}\right] \quad . \quad (8a)$$

and

$$G(k\sin\theta) = jk\cos\theta\sin\left[ka(\epsilon_r - \sin^2\theta)^{1/2}\right] + k(\epsilon_r - \sin^2\theta)^{1/2}\cos\left[ka(\epsilon_r - \sin^2\theta)^{1/2}\right]$$

The surface-wave and radiation fields can be obtained from eqns. (7) and (8) using eqn. (1).

(2.3) Extension to a Linear Array of Dipoles

Knowing the field set up by a single magnetic dipole it is relatively simple to compute the surface-wave and radiation fields set up by a linear array of such dipoles, as shown in Fig. 3. The array consists of n dipoles, spaced a quarter surface-wavelength apart. There is a progressive phase delay along the line of dipoles corresponding to the phase velocity of the surface waves. Uniform excitation along the array is assumed. Under these conditions the array factor is given by

$$A = \frac{\sin n\xi/2}{\sin \xi/2} \quad . \quad . \quad . \quad . \quad . \quad . \quad . \quad (9)$$

where $$\xi = \frac{p\lambda_s}{4}\cos\phi\sin\theta - \pi/2$$

and p is the phase-change coefficient of the field considered.

Thus the fields produced by the array are as given by eqns. (7) and (8) through eqn. (1), but with a multiplication factor given by eqn. (9).

The total surface-wave power can be expressed as

$$P_s = \frac{M^2}{16\pi^2}\omega\epsilon_0\frac{\beta_1^2}{[F'(\beta_1)]^2}\left(\frac{1}{u_1} + \frac{2m_1a + \sin 2m_1a}{2m_1\epsilon_r\cos^2 m_1a}\right) \times \int_0^{\pi}\cos^2\phi\left\{\frac{\sin\left[\frac{n\pi}{4}(\cos\phi - 1)\right]}{\sin\left[\frac{\pi}{4}(\cos\phi - 1)\right]}\right\}^2 d\phi \quad . \quad (10)$$

Similarly the total radiation power is given by

$$P_R = \frac{M^2}{16\pi^2}k\omega\epsilon_0\int_0^{\pi}\int_0^{\pi/2}\cos^2\theta\sin\theta\left(\frac{\sin\frac{n\pi}{4}\xi'}{\sin\frac{\pi}{4}\xi'}\right)^2 \left[\frac{\cos^2\phi}{|F|^2} + \frac{\sin^2\phi(\epsilon_r - \sin^2\theta)}{|G|^2}\right]d\theta d\phi \quad . \quad (11)$$

where $$\xi' = \lambda_s/\lambda_0\cos\phi\sin\theta - 1$$

and F and G are given by eqn. (8a).

The integrals in eqns. (10) and (11) are quite complicated and are solved numerically for specific values of a and ϵ_r.

(2.4) Launching Efficiency

The launching efficiency, η, is defined by

$$\eta = \frac{P_s}{P_R + P_s} = \frac{1}{1 + P_R/P_s} \quad . \quad . \quad . \quad (12)$$

The launching efficiency of an end-fire array of horizontal magnetic dipoles was calculated from eqns. (10) and (11) using eqn. (12), for a dielectric of relative permittivity 2·56 and thickness 0·125 in; the frequency was taken as 9·38 Gc/s. In Fig. 4 the launching efficiency for such a linear array is plotted

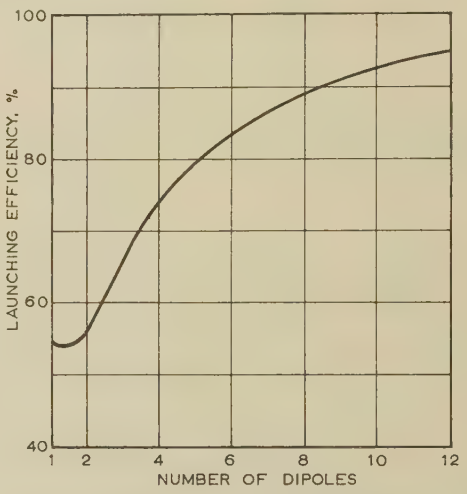

Fig. 4.—Launching efficiency plotted against number of dipoles.
The points were calculated for 1, 2, 4, 6, 9 and 12 dipoles. A smooth curve is drawn to aid interpolation.

as a function of the number of dipoles. With 12 dipoles a launching efficiency of 95% can be obtained.

In comparing this figure with experimental results, however, it must be borne in mind that the simplifications of the uniform aperture distribution, and of a phase difference between adjacent elements corresponding to the surface-wave velocity, may be quite inaccurate, if substantial coupling effects exist between the slots.

(3) EXPERIMENTAL

In the initial experiments of surface-wave diffraction referred to at the beginning of the paper, the surface-wave table was covered with a 0·125 in-thick Distrene sheet of relative permittivity 2·56. Subsequently this was replaced by the same thickness of Perspex of permittivity 2·61. In the experiments to be described the permittivity of 2·61 is appropriate, but it was felt that the 2% change did not justify recalculating the launching efficiency curve of Fig. 4. The Perspex was backed by an aluminium sheet 6 ft × 3 ft. The slotted array was positioned at the centre of one of the short sides of this sheet and the main beam was directed parallel to the long sides. The 12 slots were each 0·900 in × 0·050 in in size and were fed by stub waveguides, one-quarter guide-wavelength long, which in turn were excited by a travelling wave in waveguide No. 16 (of dimensions 0·900 in × 0·400 in), the frequency being 9·38 Gc/s. The arrangement is shown in Figs. 5 and 6. The stub guides were placed one-quarter surface-wavelength apart and the travelling wave in the feeding waveguide was retarded by partially filling

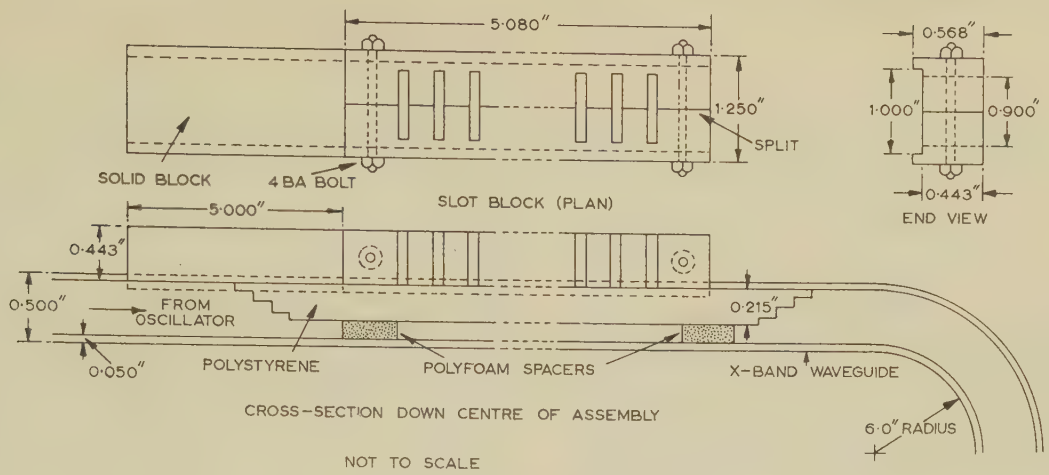

Fig. 5.—Arrangement of the launcher.

he guide with polystyrene of relative permittivity 2·56. The correct thickness of polystyrene was checked by experiment. Binomial step transformers at the ends of the polystyrene were provided in order to reduce reflection, following the method of Halford.[6] Reflections from the edges of the surface-wave table were reduced by tapered sections of carbon-loaded expanded polystyrene.

The launching efficiency was estimated from measurements of the radiation and surface-wave field strengths. The field probe of the same dimensions as that used by Fernando and Barlow[4] was used. Scattering from the probe was reduced by surrounding it with graphite-coated cards. The radiation pattern of the radiation field was measured in the plane $\phi = 0$ and on the cone $\theta = 70°$, this latter angle being obtained from the previous measurement in the plane $\phi = 0$ and corresponding to the main lobe direction.

The power in the radiation field was estimated by taking the product of the two principal-plane patterns. Similarly the surface-wave pattern was measured in the plane $\theta = 90°$ and the surface-wave power was estimated.

Correlation of the radiation and surface-wave pattern levels was achieved in the way described by Fernando and Barlow.[4] The launching efficiency was estimated from these measurements as 98%. This compares with the theoretical value for 12 slots of 95%. The agreement is entirely satisfactory in view of the approximations employed in calculating the radiated power from the experimental observations and in view of the probable departure of the aperture distribution from the assumed simple form. A further small contribution to the discrepancy would arise from the permittivity of 2·61 employed in the experiments, compared with the theoretical value of 2·56.

(4) CONCLUSIONS

Formulae for the radiation and surface-wave fields produced by a horizontal magnetic dipole embedded in a horizontal sheet of dielectric have been obtained. These formulae have been applied to the case of practical interest of a dielectric sheet backed by a metal plate, and have been used to represent the surface-wave and radiation fields set up by a linear end-fire array of slots. The theoretical dependence of launching efficiency on the number of slots has been calculated, and the high launching efficiency predicted for 12 slots has been verified experimentally.

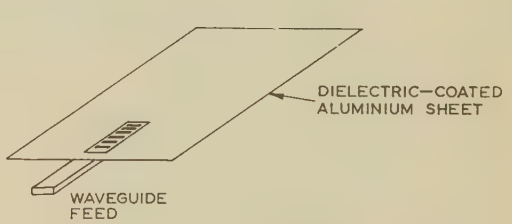

Fig. 6.—Launching area.

(5) ACKNOWLEDGMENTS

The authors are grateful for help received from the Plessey Co. in providing the carbon-loaded expanded polystyrene employed. One of the authors (J. A. S.) wishes to acknowledge with gratitude the receipt of a grant from the Department of Scientific and Industrial Research which made the work possible.

(6) REFERENCES

(1) TAI, C. T.: 'The Effect of a Grounded Slab on the Radiation from a Line Source', *Journal of Applied Physics*, 1951, **22**, p. 405.

(2) WHITMER, R. M.: 'Fields in Non-Metallic Waveguides', *Proceedings of the Institute of Radio Engineers*, 1948, **36**, p. 1105.

(3) CULLEN, A. L.: 'The Excitation of Plane Surface Waves', *Proceedings I.E.E.*, Monograph No. 93, February, 1954 (**101**, Part IV, p. 225).

(4) FERNANDO, W. M. G., and BARLOW, H. E. M.: 'An Investigation of the Properties of Radial Cylindrical Surface Waves Launched over Flat Reactive Surfaces', *ibid.*, Paper No. 2009, May, 1956 (**103** B, p. 307).

(5) BRICK, D. B.: 'The Radiation of a Hertzian Dipole Over a Coated Conductor', *ibid.*, Monograph No. 113, December, 1954 (**102** C, p. 104).

(6) HALFORD, G. J.: 'A Wide-Band Phase-Shifter', *ibid.*, Paper No. 1466, May, 1953 (**100**, Part III, p. 117).

621.372.853.1.

The Institution of Electrical Engineers
Monograph No. 451 E
June 1961

BACKWARD WAVES IN WAVEGUIDES CONTAINING DIELECTRIC

By P. J. B. CLARRICOATS, B.Sc.(Eng.), Ph.D., Graduate.

(*The paper was first received* 14*th November*, 1960, *and in revised form* 2*nd February*, 1961. *It was published as an* INSTITUTION MONOGRAPH *in June*, 1961.)

SUMMARY

A method is described for determining the conditions which ensure backward-wave propagation in dielectric-loaded inhomogeneous waveguide structures. It is established that backward-wave propagation can be ensured for the hybrid H_{11}-mode in a circular waveguide containing an axial dielectric rod whose relative permittivity exceeds approximately 9·4. The possibility of other inhomogeneous-waveguide modes exhibiting backward-wave properties is also examined.

LIST OF SYMBOLS

d = Dielectric slab thickness.
$F_n(x) = xJ_n'(x)/J_n(x)$.
$J_n(x)$ = Bessel function of the first kind and order n.
j_m = mth root of $J_n(x) = 0$.
K, K_1 = Transverse wavenumbers in dielectric and air respectively.
n = Azimuthal wavenumber.

$$R_n(K_1, r_1, r_0) = (K_1r_1)\frac{J_n'(K_1r_1)Y_n'(K_1r_0) - J_n'(K_1r_0)Y_n'(K_1r_1)}{J_n(K_1r_1)Y_n'(K_1r_0) - J_n'(K_1r_0)Y_n(K_1r_1)}.$$

r_1, r_0 = Radius of rod and waveguide respectively.

$$S_n(K_1, r_1, r_0) = (K_1r_1)\frac{J_n'(K_1r_1)Y_n(K_1r_0) - J_n(K_1r_0)Y_n'(K_1r_0)}{J_n(K_1r_1)Y_n(K_1r_0) - J_n(K_1r_0)Y_n(K_1r_1)}.$$

$$U(K_1, r_1, r_0) = (K_1r_1)\frac{J_0(K_1r_1)Y_1(K_1r_0) - J_1(K_1r_0)Y_0(K_1r_1)}{J_1(K_1r_1)Y_1(K_1r_0) - J_1(K_1r_0)Y_1(K_1r_1)}.$$

u_m = mth root of $J_n'(x) = 0$.

$$V(r_1, r_0) = -2/[(r_0/r_1)^2 - 1].$$

$$W(K, r_1, r_0) = \frac{\bar{\epsilon}\bar{\mu} + 1 - (Kr_1)^2\left\{2\log_\epsilon (r_0/r_1)/[1-(r_1/r_0)^4] + \frac{1}{2}\right\}}{\bar{\epsilon}\nu + \bar{\mu}/\nu}.$$

$Y_n(x)$ = Bessel function of the second kind and order n.
β = Phase-change coefficient.
ϵ, ϵ_0 = Permittivity of dielectric and free space respectively.
$\lambda_0 = 2\pi/\omega(\epsilon_0\mu_0)^{1/2}$ = free-space wavelength.
$\nu = [(r_1/r_0)^2 - 1]/[(r_1/r_0)^2 + 1]$.
μ, μ_0 = Permeability of dielectric and free space respectively.
ω = Angular frequency.

In the case of the symbols $F_n(Kr_1)$, $R_n(K_1, r_1, r_0)$ and $S_n(K_1, r_1, r_0)$ the suffix n is omitted when $n = 1$.

(1) INTRODUCTION

Although examples of periodic waveguide structures which support backward waves* are well known,[1] the existence of uniform isotropic waveguide structures which support backward waves has only recently been demonstrated.[2] A specific case has been studied by Waldron and the present author, who have found that a circular waveguide partially filled with an axial dielectric rod can support backward waves. In particular, the existence of a phase-coefficient/frequency characteristic of the kind shown in Fig. 1, curve (*b*), has been theoretically demonstrated in the case of the H_{11}-limit mode.* It can be seen that, in the frequency band $\omega_2 - \omega_1$, the group velocity $\partial\omega/\partial\beta$ is negative. Also, when $\omega = \omega_1$, $\partial\omega/\partial\beta = 0$.

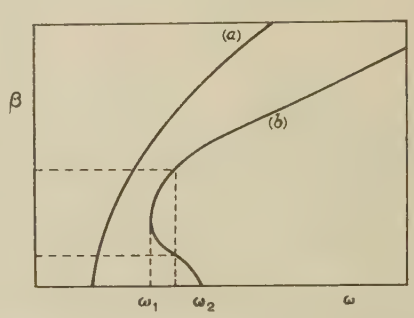

Fig. 1.—Phase-change coefficient as a function of frequency for a structure capable of supporting forward and backward waves.
(*a*) Homogeneous waveguide.
(*b*) Inhomogeneous waveguide with negative and positive group velocity.

In the present paper, the general conditions are determined which ensure the existence of backward waves in a circular waveguide containing an axial dielectric rod. It is found, for the H_{11}-limit mode of propagation, that the group velocity can be negative if the relative permittivity of the rod exceeds approximately 9·4. The possibility of backward-wave propagation for other modes in a circular waveguide containing dielectric and for the H_{01}-mode in a rectangular waveguide containing dielectric is also investigated.

(2) METHODS OF ESTABLISHING CONDITIONS FOR NEGATIVE GROUP VELOCITY

It can be readily shown[3] that uniform homogeneously-filled waveguides cannot support normal modes with negative group velocities. For such structures, the phase-change coefficient, β, is a monotonic increasing function of frequency, as illustrated in Fig. 1, curve (*a*). However, under appropriate conditions certain inhomogeneous waveguide structures can support normal modes with negative group velocities. A direct method for establishing these conditions will now be described.

From the characteristic equation of the particular inhomogeneous waveguide under consideration, β can be determined as a function of ω for constant values of dielectric and waveguide transverse dimensions and dielectric permittivity. Sets of curves of β as a function of ω for different values of the three parameters can then, in principle, be prepared and the conditions for negative group velocity precisely established. Unfortu-

* The term 'backward wave' describes an electromagnetic wave possessing phase and group velocities with opposing signs. Under these conditions the direction of flow of the total transmitted power and the direction of propagation of the field are opposed.

* The term 'H_{11}-limit mode' refers to that mode of an inhomogeneous circular waveguide which, in the homogeneous limit, corresponds to the H_{11}-mode. A similar nomenclature applies to other modes.

Correspondence on Monographs is invited for consideration with a view to publication.
Dr. Clarricoats is in the Department of Light Electrical Engineering, Queen's University of Belfast.

ıately, for a number of waveguide structures of interest, the haracteristic equation is quite formidable and much effort would ıave to be expended in following the above method. An ılternative approach will now be considered.

With reference to Fig. 1 curve (*b*), it is apparent that a region of negative group velocity is implied when, for a given value of ω, two different values of β can be found which satisfy the same characteristic equation.

The principal advantage of the present method springs from he relative simplicity of two specialized forms of the charac-eristic equation for inhomogeneous waveguides which arise when either $\beta = 0$ or $\beta = \omega(\epsilon_1\mu_1)^{1/2}$, where ϵ_1 and μ_1 are the permittivity and permeability of the medium which surrounds he dielectric; in the present study $\epsilon_1 = \epsilon_0$ and $\mu_1 = \mu_0$. Because of the simplifying features mentioned, the above two values of β are selected in the following investigation.

In Section 3, the specialized forms of the characteristic equation for a circular waveguide containing an axial dielectric rod are solved graphically for the H_{11}-limit mode. From this analysis, the minimum rod permittivity is determined in order to ensure backward-wave propagation. In particular, curves are obtained which show how the frequency at which $\beta = 0$ and $\beta = \omega(\epsilon_0\mu_0)^{1/2}$ depends on the dielectric-rod and waveguide parameters. It is found that, for sufficiently large values of rod permittivity, there exists a range of rod and waveguide parameters in which the frequency corresponding to $\beta = 0$ exceeds that for $\beta = \omega(\epsilon_0\mu_0)^{1/2}$. Within this range of parameters, a mode can propagate with negative group velocity. Although a region of negative group velocity may still exist even if $\omega_{\beta=\omega\sqrt{(\epsilon_0\mu_0)}} > \omega_{\beta=0}$, once the above range has been found the absolute limits should not be so difficult to determine. In Section 4, the above method is applied to investigate the possibility of backward-wave propagation for other modes of inhomogeneous circular waveguide and for the dominant mode of an inhomogeneous rectangular waveguide.

(3) CONDITIONS FOR THE PROPAGATION OF AN H_{11}-LIMIT MODE WITH NEGATIVE GROUP VELOCITY

The waveguide structure under consideration is shown in Fig. 2. The general form of the characteristic equation for the

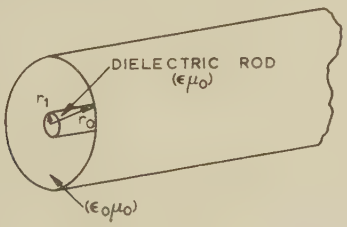

Fig. 2.—Circular waveguide containing an axial dielectric rod.

phase-change coefficient has been derived previously[4, 5] and shown to be given by

$$\left[\frac{\mu F_n(Kr_1)}{(Kr_1)^2} - \frac{\mu_0 R_n(K_1, r_1, r_0)}{(K_1 r_1)^2}\right]\left[\frac{\epsilon F_n(Kr_1)}{(Kr_1)^2} - \frac{\epsilon_0 S_n(K_1, r_1, r_0)}{(K_1 r_1)^2}\right] = \frac{n^2\beta^2}{\omega^2}\,\frac{[(K_1 r_1)^2 - (Kr_1)^2]^2}{[(K_1 r_1)^2 (Kr_1)^2]^2} \quad . \quad (1)$$

where

$$K^2 = \omega^2\epsilon\mu - \beta^2$$
$$K_1^2 = \omega^2\epsilon_0\mu_0 - \beta^2$$

When $\beta = 0$, eqn. (1) reduced, in the case of H-modes, to the form

$$F_n(Kr_1) = \bar{\epsilon} R_n(K_1, r_1, r_0) \quad . \quad . \quad . \quad . \quad (2)$$

where $\bar{\epsilon} = \epsilon/\epsilon_0$

while for E-modes,

$$F_n(Kr_1) = \bar{\mu} S_n(K_1, r_1, r_0) \quad . \quad . \quad . \quad . \quad . \quad (3)$$

where $\bar{\mu} = \mu/\mu_0$.

When $\beta = \omega(\epsilon_0\mu_0)^{1/2}$, it has been shown[5] that eqn. (1) reduces, in the case of H-modes, to the form

$$F_n(Kr_1) = W(K, r_1, r_0) \quad . \quad . \quad . \quad . \quad . \quad (4)$$

while for E-modes,

$$F_n(Kr_1) = \infty \quad . \quad . \quad . \quad . \quad . \quad . \quad (5)$$

The behaviour of eqns. (2) and (4) in the case of the H_{11}-limit mode ($n = 1$) will now be considered, subject to the assumption $\mu = \mu_0$.

A convenient method for investigating the possibility of backward-wave propagation is to obtain, in the range $0 < r_1/r_0 < 1$, curves showing $2r_0/\lambda_0$ as a function of r_1/r_0 under the conditions $\beta = 0$ and $\beta = \omega(\epsilon_0\mu_0)^{1/2}$. If these curves intersect, a region of backward-wave propagation is ensured. Figs. 3(*a*) and (*b*) show the results of investigations with rods possessing relative permittivities $\bar{\epsilon} = 15$ and $\bar{\epsilon} = 9$. The production of such curves will now be discussed.

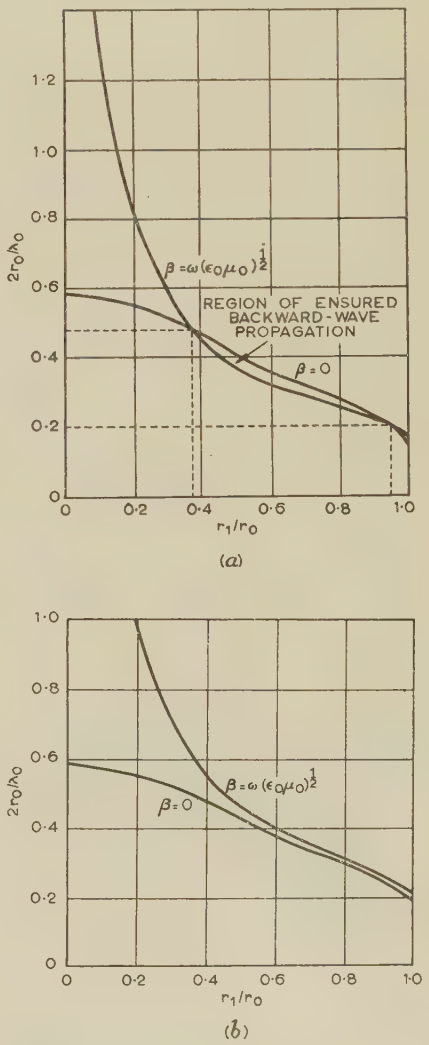

Fig. 3.—Graphs showing $2r_0/\lambda_0$ as a function of r_1/r_0 under the conditions $\beta = 0$ and $\beta = \omega(\epsilon_0\mu_0)^{1/2}$.
(*a*) $\bar{\epsilon} = 15$, (*b*) $\epsilon = 9$.

The range of $2r_0/\lambda_0$ will first be established. When $r_1/r_0 = 0$, the waveguide is empty, and if $\beta = 0$

$$K_1 r_0 = 2\pi r_0/\lambda_0 = u_1 \quad . \quad . \quad . \quad . \quad . \quad (6)$$

Thus
$$2r_0/\lambda_0 = u_1/\pi = 0{\cdot}586 \quad . \quad . \quad . \quad . \quad . \quad (7)$$

where u_1 is the first root of $J_1'(x) = 0$, while if $\beta = \omega(\epsilon_0\mu_0)^{1/2}$, since $K_1 = 0$,

$$2r_0/\lambda_0 = \infty \quad . \quad . \quad . \quad . \quad . \quad . \quad (8)$$

When $r_1/r_0 = 1$, the waveguide is filled with a medium of relative permittivity $\bar{\epsilon}$. If $\beta = 0$,

$$Kr_0 = (2\pi r_0/\lambda_0)\bar{\epsilon}^{1/2} = u_1 \quad . \quad . \quad . \quad . \quad (9)$$

Thus
$$2r_0/\lambda_0 = u_1/\pi\bar{\epsilon}^{1/2} \quad . \quad . \quad . \quad . \quad . \quad (10)$$

while if $\beta = \omega(\epsilon_0\mu_0)^{1/2}$,

$$Kr_0 = (2\pi r_0/\lambda_0)(\bar{\epsilon} - 1)^{1/2} = u_1 \quad . \quad . \quad . \quad (11)$$

Thus
$$2r_0/\lambda_0 = u_1/\pi(\bar{\epsilon} - 1)^{1/2} \quad . \quad . \quad . \quad . \quad (12)$$

It is apparent that when r_1/r_0 is equal to either zero or unity, the value of $2r_0/\lambda_0$ for $\beta = 0$ is less than that for $\beta = \omega(\epsilon_0\mu_0)^{1/2}$. Thus, consistent with earlier remarks, it follows that backward-wave propagation can only occur when $0 < r_1/r_0 < 1$.

The curves shown in Fig. 3 were obtained from graphical solutions of eqns. (2) and (4). The procedure adopted can be seen in Fig. 4. The functions $F(Kr_1)_{\beta=0}$, $F(Kr_1)_{\beta=\omega\sqrt{(\epsilon_0\mu_0)}}$, $\bar{\epsilon}R(K_1, r_1, r_0)$ and $W(K, r_1, r_0)$ are shown plotted against $2r_1/\lambda_0$ for different values of $2r_0/\lambda_0$. Intersections of the respective pairs of curves provide the values required for Fig. 3. It can also be seen that, when respective curves of $\bar{\epsilon}R$ and W intersect to the right of the curve $F(Kr_1)_{\beta=\omega\sqrt{(\epsilon_0\mu_0)}}$, a region of backward-wave propagation is ensured. This observation provides a means of readily establishing the general conditions under which backward waves can occur. In order to appreciate the effect of changes in permittivity and dimensions, the essential properties of the above functions must be studied.

The functions

$$F(Kr_1)_{\beta=0} = F\left(2\pi\frac{r_1}{\lambda_0}\bar{\epsilon}^{1/2}\right)$$

and
$$F(Kr_1)_{\beta=\omega\sqrt{(\epsilon_0\mu_0)}} = F\left[2\pi\frac{r_1}{\lambda_0}(\bar{\epsilon} - 1)^{1/2}\right]$$

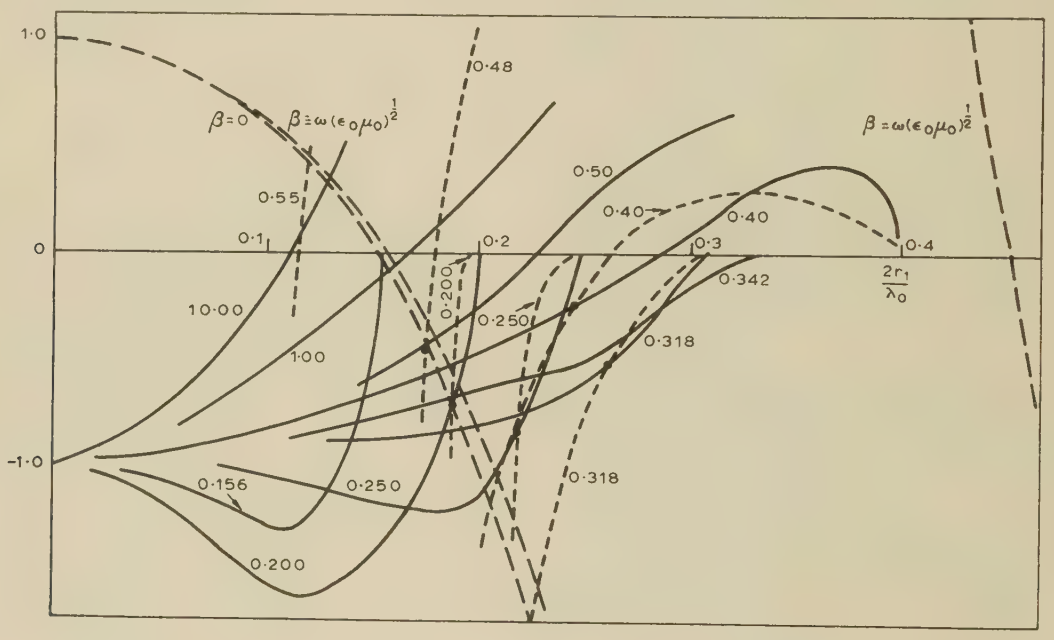

(a)

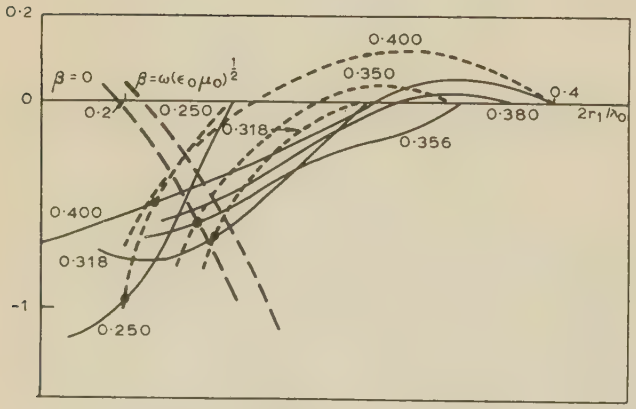

(b)

Fig. 4.—Various functions plotted against $2r_1/\lambda_0$ for different values of $2r_0/\lambda_0$.

- -------- $\bar{\epsilon}R(K, r_1, r_0)$
- ———— $W(K, r_1, r_0)$
- — — — $F(Kr_1)_{\beta=0}$, $F(Kr_1)_{\beta=\omega\sqrt{(\epsilon_0\mu_0)}}$
- • $\bar{\epsilon}R$ – W intersections

(a) $\bar{\epsilon} = 15$; (b) $\bar{\epsilon} = 9$.

Table 1

PROPERTIES OF $F(Kr_1)_{\beta=0}$, $F(Kr_1)_{\beta=\omega\sqrt{(\epsilon_0\mu_0)}}$, $\bar{\epsilon}R(K_1, r_1, r_0)$ AND $W(K, r_1, r_0)$

$2r_1/\lambda_0$	$2r_0/\lambda_0$	$F(Kr_1)_{\beta=0}$	$F(Kr_1)_{\beta=\omega\sqrt{(\epsilon_0\mu_0)}}$	$\bar{\epsilon}R(K_1, r_1, r_0)$	$W(K, r_1, r_0)$
0	a.v.*	1	1	$-\bar{\epsilon}$	-1
$u_1/\pi(\bar{\epsilon})^{1/2}$	a.v.	0	positive		
$u_1/\pi(\bar{\epsilon}-1)^{1/2}$	a.v.	negative	0		
$j_1/\pi(\bar{\epsilon})^{1/2}$	a.v.	$-\infty$	negative		
$j_1/\pi(\bar{\epsilon}-1)^{1/2}$	a.v.	positive	$-\infty$		
$2r_0/\lambda_0$	$2r_1/\lambda_0$			0	0
$<2r_0/\lambda_0$	$<1/\pi$			negative	negative
$<2r_0/\lambda_0$	$<\left(\frac{\bar{\epsilon}+1}{\bar{\epsilon}-1}\right)^{1/2}\frac{1}{\pi}$				negative

* a.v. = all values.

are monotonic decreasing functions of $2r_1/\lambda_0$ for all values of $\bar{\epsilon}$ and are clearly independent of $2r_0/\lambda_0$. As $\bar{\epsilon}$ increases, the zeros of the functions occur for smaller values of $2r_1/\lambda_0$. Two special points are listed in Table 1.

The behaviour of the function $R(K_1, r_1, r_0)$, which is independent of $\bar{\epsilon}$, is best visualized by considering the numerator R_N and denominator R_D separately. R_N is zero when $2r_1/\lambda_0 = 0$, and again when

$$\frac{J_1'(K_1r_1)}{Y_1'(K_1r_1)} = \frac{J_1'(K_1r_0)}{Y_1'(K_1r_0)} \quad . \quad . \quad . \quad . \quad . \quad (13)$$

One solution of eqn. (13) is evidently $r_1/r_0 = 1$; a further solution exists in the range $0 < r_1/r_0 < 1$ provided that $2r_0/\lambda_0 > 1/\pi$. R_D is a positive function throughout the range $0 < 2r_0/\lambda_0 < u_1/\pi$ with a zero at $2r_1/\lambda_0 = 0$. The function $R(K_1, r_1, r_0)$ behaves as $K_1r_1Y_1'(K_1r_1)/Y_1(K_1r_1)$ when $2r_1/\lambda_0 \to 0$, and has the value -1 in the limit.

Similarly, the function W will be considered in terms of the numerator W_N and the denominator W_D. W_N is a monotonic decreasing function of $2r_1/\lambda_0$ for all values of $\bar{\epsilon}$ and $2r_0/\lambda_0$. When $2r_1/\lambda_0$, $W_N = (\bar{\epsilon}+1)$. W_N is zero when

$$\frac{\bar{\epsilon}+1}{\bar{\epsilon}-1}\frac{1}{\pi^2} = (2r_1/\lambda_0)^2\left\{(2\log_\epsilon r_0/r_1)/[1-(r_1/r_0)^4] + \tfrac{1}{2}\right\} \quad . \quad (14)$$

When $r_1/r_0 = 1$, eqn. (14) becomes

$$\frac{\bar{\epsilon}+1}{\bar{\epsilon}-1}\frac{1}{\pi^2} = \left(\frac{2r_0}{\lambda_0}\right)^2 \quad . \quad . \quad . \quad . \quad . \quad (15)$$

It follows quite readily that a zero value of W_N will occur in the range $0 < r_1/r_0 < 1$ only if $(2r_0/\lambda_0)^2 > (\bar{\epsilon}+1)/\pi^2(\bar{\epsilon}-1)$. As $\bar{\epsilon} \to \infty$, this condition becomes $2r_0/\lambda_0 > 1/\pi$ which is just the same as the condition for R to be zero in the range $0 < r_1/r_0 < 1$. The behaviour of the zero values of R and W, and in particular the above observation, has an important bearing on the conditions for backward-wave propagation.

W_D is a negative quantity throughout the range $0 < r_1/r_0 < 1$, with the value $-(\bar{\epsilon}+1)$ when $r_1/r_0 = 0$ and $-\infty$ when $r_1/r_0 = 1$. The maximum value of W_D, $-2\bar{\epsilon}^{1/2}$, occurs when

$$\left(\frac{r_1}{r_0}\right)^2 = \frac{\bar{\epsilon}^{1/2}-1}{\bar{\epsilon}^{1/2}+1} \quad . \quad . \quad . \quad . \quad . \quad (16)$$

Table 1 summarizes some of the special properties of the above functions. Table 2 lists particular values of some essential points for two values of permittivity, $\bar{\epsilon} = 15$ and $\bar{\epsilon} = 9$.

The importance of the position of an intersection of $\bar{\epsilon}R$ and W for given $2r_0/\lambda_0$ has previously been mentioned. The essential part of the locus of such intersections is plotted in Fig. 5 together with the two F functions; results are given for two values of rod

Table 2

VALUES OF ESSENTIAL POINTS FOR $\bar{\epsilon} = 15$ AND $\bar{\epsilon} = 9$

$\bar{\epsilon}$	$u_1/\pi(\bar{\epsilon})^{1/2}$	$u_1/\pi(\bar{\epsilon}-1)^{1/2}$	$j_1/\pi(\bar{\epsilon})^{1/2}$	$j_1/\pi(\bar{\epsilon}-1)^{1/2}$	$\left[\frac{\bar{\epsilon}+1}{\bar{\epsilon}-1}\right]^{1/2}\frac{1}{\pi}$
15	0·151	0·156	0·314	0·324	0·342
9	0·195	0·207	0·406	0·431	0·356

permittivity, $\bar{\epsilon} = 15$ and $\bar{\epsilon} = 9$. It is apparent that the maximum value of $2r_1/\lambda_0$ associated with a point on either locus occurs for a value of $2r_0/\lambda_0 = 0{\cdot}3185 = 1/\pi$. This follows directly from the behaviour of the zeros of R and W. It will be recalled that, if $2r_0/\lambda_0 > 1/\pi$, R possesses a zero in the range $0 < r_1/r_0 < 1$, while if $2r_0/\lambda_0 > 1/\pi[(\bar{\epsilon}+1)/(\bar{\epsilon}-1)]^{1/2}$, W possesses a zero in that range. Thus, as $\bar{\epsilon}$ increases, a condition for the existence of backward waves is first established for a value of $2r_0/\lambda_0 = 0{\cdot}3185$. From Fig. 5 it can be seen that, as $\bar{\epsilon}$ increases, the value of $2r_1/\lambda_0$ corresponding to a point on the locus for $2r_0/\lambda_0 = 0{\cdot}3185$ also increases. The F curves shift to smaller values of $2r_1/\lambda_0$. Calculation shows that the critical relative permittivity is approximately 9·37. For a rod with this permit-

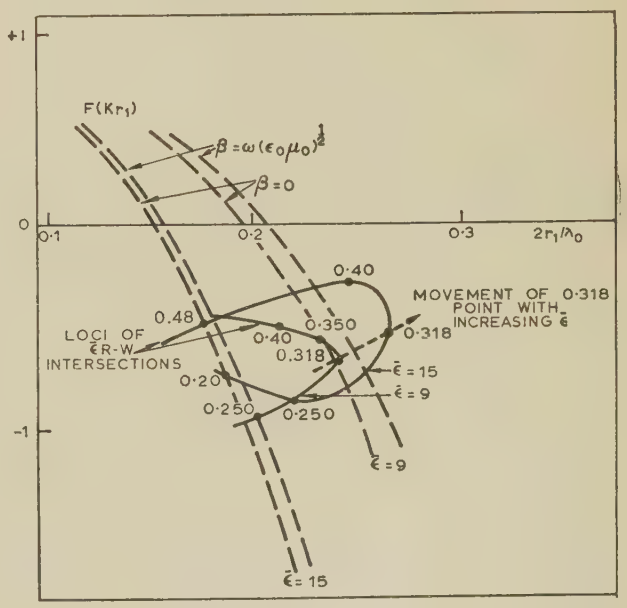

Fig. 5.—Loci of the intersection of $\bar{\epsilon}R(K_1, r_1, r_0)$ and $W(K_1, r_1, r_0)$ curves for $\bar{\epsilon} = 15$ and $\bar{\epsilon} = 9$.

tivity, backward-wave propagation is ensured when $2r_0/\lambda_0 = 0{\cdot}3185$ and $2r_1/\lambda_0 = 0{\cdot}244$ ($r_1/r_0 = 0{\cdot}766$). As $\bar{\epsilon}$ increases above this value, the range of values of r_1/r_0 over which backward waves are ensured also increases until in the limit, as $\bar{\epsilon} \to \infty$, the entire range $0 + \delta < r_1/r_0 < 1 - \Delta$ would be covered, where δ and Δ are vanishingly small quantities.

In a previous publication,[2] curves of β as a function ω were obtained directly from the characteristic equation using the electronic digital computer Deuce. The case of a rod when $\bar{\epsilon} = 15$ was investigated and curves were obtained corresponding to $2r_0/\lambda_0 = 0{\cdot}44$, $0{\cdot}42$, $0{\cdot}40$ and $0{\cdot}38$. Comparison of values of r_1/r_0 when $\beta = 0$ and $\beta = \omega(\epsilon_0\mu_0)^{1/2}$, between the above results and those given in Fig. 3, shows precise agreement.

The above analysis has established that backward waves associated with the H_{11}-limit mode can occur when $\bar{\epsilon} > 9{\cdot}37$. To investigate the possibility of backward-wave propagation for lower values of $\bar{\epsilon}$, a solution is required of the characteristic equation in its general form. However, this would not be quite such a formidable task as before, since permittivities in excess of $9{\cdot}37$ need not be chosen and the range of β, for which $\partial\beta/\partial\omega$ might be negative, is restricted to $0 < \beta < \omega(\epsilon_0\mu_0)^{1/2}$. Although it might be thought that the slope of the propagation curve at cut-off might provide some indication of the existence of backward waves, this is in fact not so, since it has been shown elsewhere[5] that $|\partial\beta/\partial\omega| = \infty$ when $\beta = 0$. While it seems probable that the sign of this gradient might provide the necessary information, the labour involved in calculating it would be very considerable.

(4) POSSIBILITY OF PROPAGATION WITH NEGATIVE GROUP VELOCITY FOR OTHER WAVEGUIDE MODES

(4.1) H_{01}-, H_{1m}- and E_{1m}-Modes in a Circular Waveguide containing a Dielectric Rod

In the case of the H_{01}-mode of propagation in a circular waveguide containing a dielectric rod, as shown in Fig. 2, the characteristic equation reduces to the following forms.[6]

When $\beta = 0$,

$$F(Kr_1) + 1 = U(K_1, r_1, r_0) \quad . \quad . \quad . \quad . \quad (17)$$

When $\beta = \omega(\epsilon_0\mu_0)^{1/2}$,

$$F(Kr_1) + 1 = V(r_1, r_0) \quad . \quad . \quad . \quad . \quad (18$$

There is an essential difference between these two equations and the corresponding equations, (2) and (4), for the H_{11}-limit mode. In neither of the above does the permittivity enter the right-hand side of the equation. This considerably simplifies the study of a condition which ensures backward-wave propagation. In a manner similar to that previously employed, the range of $2r_0/\lambda_0$ for $\beta = 0$ can be shown to lie between $j_1/\pi\bar{\epsilon}^{1/2}$ and j_1/π. Fig. 6 shows curves corresponding to $2r_0/\lambda_0 = 0{\cdot}318$ and $2r_0/\lambda_0 = 0{\cdot}954$, when $\bar{\epsilon} = 15$. With this permittivity the limits of $(2r_0/\lambda_0)_{\beta=0}$ are respectively $0{\cdot}315$ and $1{\cdot}22$.

The behaviour of U and V for other values of $2r_0/\lambda_0$ is easily visualized from Fig. 6. For backward-wave propagation to be ensured it would be necessary for the U and V curves to intersect to the left of the curve $F(Kr_1)_{\beta=0} + 1$. However, it is readily shown that the curves, in fact, do *not* intersect for any value of $2r_0/\lambda_0$ in the range $0 < 2r_0/\lambda_0 < j_1/\pi$ or for any value of r_1/r_0 in the range $0 < r_1/r_0 < 1$. Thus, in contrast with the H_{11}-limit mode, no condition can be found which ensures backward-wave propagation.

An analysis has not yet been performed for H_{1m}-limit modes in general, although it is clear that a condition for negative group velocity could be established. In Fig. 4, a branch of

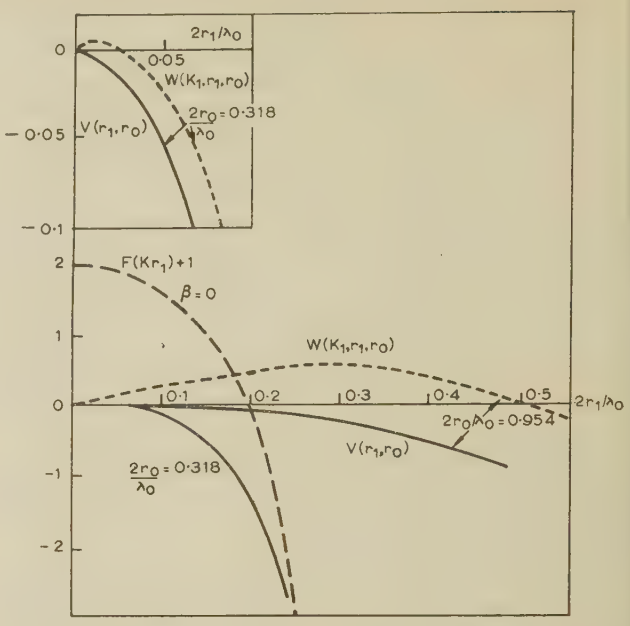

Fig. 6.—$F(Kr_1)_{\beta=0}$, $F(Kr_1)_{\beta=\omega(\epsilon_0\mu_0)^{1/2}}$, $U(K_1, r_1, r_0)$ and $V(r_1, r_0)$ as functions of $2r_1/\lambda_0$ for two values of $2r_0/\lambda_0$; $\bar{\epsilon} = 15$.

$F(Kr_1)_{\beta=\omega(\epsilon_0\mu_0)^{1/2}}$ is shown corresponding to part of the range $j_1 < Kr_1 < j_2$. Intersections between this branch and the $\bar{\epsilon}$R and W curves of Fig. 4 give solutions of eqns. (2) and (4) corresponding to the H_{12}-limit mode. If $\bar{\epsilon} = 15$, all $\bar{\epsilon}$R and W curves shown in Fig. 4 intersect to the left of the branch, and for these values of $2r_0/\lambda_0$ no region of backward-wave propagation exists for the H_{12}-limit mode. However, it is evident that a sufficient increase in $\bar{\epsilon}$ will shift the branch to the left so that a region of backward-wave propagation might be ensured. It must be noted that in a detailed investigation the upper limit of $2r_0/\lambda_0$ must be increased to the value j_m/π when the conditions for the H_{1m}-limit mode are being studied.

In the case of E_{1m}-limit modes, it can be seen that no such condition exists. Eqn. (5) shows that, independent of $2r_0/\lambda_0$, $\beta = \omega(\epsilon_0\mu_0)^{1/2}$ for the E_{1m}-limit mode when $2r_1/\lambda_0 = j_m/\pi(\bar{\epsilon}-1)^{1/2}$. However, any solution of eqn. (3) corresponding to the E_{1m}-limit mode must occur for a value of $2r_1/\lambda_0 < j_m/\pi\bar{\epsilon}^{1/2}$, i.e. for a value of $2r_1/\lambda_0$ less than that at which $\beta = \omega(\epsilon_0\mu_0)^{1/2}$.

(4.2) H_{01}-Modes in a Rectangular Waveguide containing a Dielectric

The possibility of backward-wave propagation with an H_{01}-mode in a rectangular waveguide containing dielectric will now be considered. The two configurations studied are shown in Fig. 7(*a*) and (*b*). For that in Fig. 7(*a*), the specialized forms of the characteristic equation for the H_{01}-mode[7] are as follows:

When $\beta = 0$

$$\cot Kd = \bar{\epsilon}^{1/2} \tan K_1(L - d) \quad . \quad . \quad . \quad (19)$$

When $\beta = \omega(\epsilon_0\mu_0)^{1/2}$

$$\cot Kd = K(L - d) \quad . \quad . \quad . \quad . \quad (20)$$

For the above mode, L/λ_0 lies in the range $\frac{1}{4}\bar{\epsilon}^{1/2} < L/\lambda_0 < \frac{1}{2}$ if $\beta = 0$, and $\frac{1}{4}(\bar{\epsilon} - 1)^{1/2} < L/\lambda_0 < \infty$ if $\beta = \omega(\epsilon_0\mu_0)^{1/2}$. The lower and upper limits correspond to the conditions $d/L = 1$ and $d/L = 0$ respectively. Suppose that, within the range for which $\beta = 0$, eqns. (19) and (20) were simultaneously satisfied

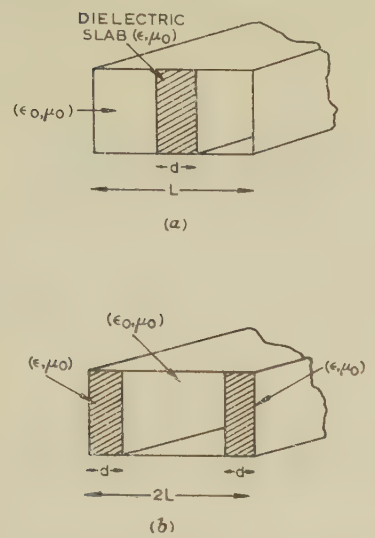

Fig. 7.—Rectangular waveguides.

(*a*) Containing dielectric slab located on waveguide axis (L = waveguide width).
(*b*) Containing dielectric slabs in contact with side walls (L = waveguide half-width).

for a given pair of values of L/λ_0 and d/L; the following equation would then apply:

$$\frac{\cot\left[\frac{2\pi d}{\lambda_0}(\bar{\epsilon}-1)^{1/2}\right]}{\cot\left[\frac{2\pi d}{\lambda_0}(\bar{\epsilon})^{1/2}\right]} = \frac{\frac{2\pi}{\lambda_0}(\bar{\epsilon}-1)^{1/2}(L-d)}{\bar{\epsilon}^{1/2}\tan\left[\frac{2\pi}{\lambda_0}(L-d)\right]} \quad . \quad (21)$$

However, in the above range, the right-hand side of eqn. (21) is always less than unity, while the left-hand side is always greater than unity. Thus a condition cannot exist whereby $\beta = 0$ and $\beta = \omega(\epsilon_0\mu_0)^{1/2}$ are satisfied by an identical configuration, and therefore a condition of the kind previously described does not apply.

For the configuration of Fig. 7(*b*) the specialized forms of the characteristic equation for the H_{01}-mode[7] are as follows:

When $\beta = 0$

$$\bar{\epsilon}^{1/2}\cot Kd = \tan K_1(L-d) \quad . \quad . \quad . \quad (22)$$

When $\beta = \omega(\epsilon_0\mu_0)^{1/2}$

$$\cot Kd = 0 \quad . \quad . \quad . \quad . \quad . \quad . \quad (23)$$

On substitution from eqn. (23) into eqn. (22), an inequality is obtained in the range for which $\beta = 0$ and, as before, it follows that a condition cannot exist whereby $\beta = 0$ and $\beta = \omega(\epsilon_0\mu_0)^{1/2}$ are satisfied by an identical configuration of the type shown in Fig. 7(*b*).

(5) CONCLUSIONS

The conditions under which backward-wave propagation is ensured have been theoretically established for the H_{11}-limit mode in a circular waveguide containing an axial dielectric rod. It has also been shown that backward-wave propagation is to be expected under appropriate conditions with all H_{11}-limit modes. However, no conditions have been found which ensure backward-wave propagation with H_{01}- or E_{1m}-limit modes in a dielectric-loaded circular waveguide, or with an H_{01}-mode in a dielectric-loaded rectangular waveguide. Further study might be devoted to the possibility that backward-wave propagation in passive uniform isotropic waveguides can only occur with H_{11}-limit modes in dielectric-loaded circular waveguides. Certainly the behaviour of such waveguides offers scope for further research and development.

The simultaneous presence in an inhomogeneous waveguide of backward and forward propagating waves with different phase velocities appears to offer a basis for a microwave filter. With periodic coupling to a homogeneous waveguide, it is envisaged that, at two different frequencies, a forward wave and a backward wave, respectively, could be excited in the inhomogeneous waveguide. The possible application of the low group-velocity properties of the structure of Fig. 2 have been previously mentioned in relation to travelling-wave devices.[2] An experimental programme in support of the above theoretical studies has been initiated.

(6) REFERENCES

(1) Beck, A. H. W.: 'Space Charge Waves' (Cambridge University Press, 1953).
(2) Clarricoats, P. J. B., and Waldron, R. A.: 'Non-Periodic Slow-Wave and Backward-Wave Structures', *Journal of Electronics and Control*, 1960, **8**, p. 455.
(3) Adler, R. B.: 'Properties of Guided Waves on Inhomogeneous Structures' (M.I.T. Technical Report 102, 1949).
(4) Beam, R. E., and Wachowski, H. M.: 'Shielded Dielectric Rod Waveguides', *Transactions of the American I.E.E.*, 1951, **70**, Part 1, p. 874.
(5) Clarricoats, P. J. B.: 'Propagation along Unbounded and Bounded Dielectric Rods, Part 2', *Proceedings I.E.E.*, Monograph No. 410 E, October, 1960 (**108** C, p. 177).
(6) Clarricoats, P. J. B.: 'A Broad-Band Waveguide Junction Containing Dielectric' (see page 398).
(7) Marcuvitz, N.: 'Waveguide Handbook' (McGraw-Hill, 1951), p. 389.
(8) Gillespie, E. F. F.: 'Power Flow and Negative Wave Impedance in the Dielectric-Rod Waveguide', *Proceedings I.E.E.*, Monograph No. 362 E, February, 1960 (**107** C, p. 198).

621—526: 621.372.6

The Institution of Electrical Engineers
Monograph No. 452 M
June 1961

THE RELATION BETWEEN DISCRETE PERIODIC INPUTS, THE TRANSFER FUNCTION AND THE TRANSIENT RESPONSE OF A SYSTEM

By T. GLUCHAROFF, M.E.

(*The paper was first received 4th October*, 1960, *and in revised form 4th March*, 1961. *It was published as an* INSTITUTION MONOGRAPH *in June* 1961.)

SUMMARY

Sampled-data systems are characterized by the presence of discrete signals at some point of the system, but the overall output is usually a continuous function of time. It is shown that the pulse sequence of discrete periodic signals, which result in a finite-settling-time response when applied to the input of a system, can be determined directly from the system transient response. Such a pulse sequence can be used to design a discrete controller to compensate the system, when its transfer function is not known. Further, it is shown that the transfer function of a system can be found once an input pulse sequence has been determined, with an accuracy limited only by the accuracy of the given transient response.

LIST OF SYMBOLS

$b_1, b_2 \ldots$ = Real or complex poles in a system transfer function.
k, n, q, r = Integers.
p = Laplace complex variable.
$z = \varepsilon^{pT}$.
$c(t)$ = Output time function.
$h(t)$ = Unit pulse response of a system.
$h(z)$ = Pulse sequence of $h(t)$.
$r(t)$ = Input time function.
$w(t)$ = Unit step response of a system.
$w(z)$ = Pulse sequence of $w(t)$.
K = Steady-state or low-frequency gain of a system.
$K_1, K_2 \ldots$ = Constants.
R_k = Magnitude of a step input applied at $t = kT$.
$R(k)$ = Magnitude of a pulse input applied at $t = kT$.
T = Time period.
$G(p)$ = Transfer function of the plant or of a system.
$C(z)$ = Pulse sequence of the output of a system.
$D(z)$ = Pulse transfer function of the discrete controller.
$E(z)$ = Pulse sequence of the error function.
$F(z)$ = Pulse sequence of the forcing function.
$R(z)$ = Pulse sequence of the input to a system.

(1) INTRODUCTION

The determination of a pulse sequence of discrete periodic signals, which yield finite-settling-time responses when applied to the input of a system, has been investigated in conjunction with the discrete compensation of saturating sampled-data control systems.[1,2] If the transfer function $G(p)$ of the plant to be controlled in the feedback system shown in Fig. 1 is known, the pulse sequence of the forcing function $F(z)$ can be determined from simultaneous equations which meet the steady-state and the transient requirements of the output for a given input to the overall feedback system. Once this pulse sequence has been found, the pulse transfer function of the discrete controller $D(z)$ can be obtained in a straightforward manner.

Correspondence on Monographs is invited for consideration with a view to publication.
Mr. Glucharoff is at Newcastle University College, University of New South Wales, Australia.

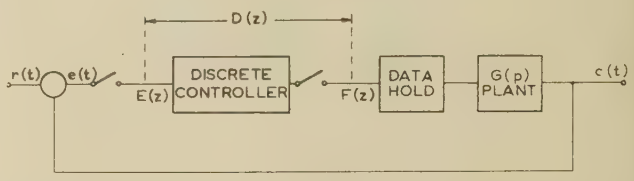

Fig. 1.—Sampled-data feedback control system with discrete controller.

Thus, the only point of interest is the relation between the input pulse sequence and the output of the plant. In the paper this relation is examined in greater detail and some general conclusions are deduced. This has led to the development of a method which permits the determination of an input pulse sequence for finite-settling-time responses directly from the transient response of the plant to be controlled. Finally, the combination of the above two methods allows the determination of the transfer function of a system from its transient response.

(2) INPUT PULSE SEQUENCE FROM THE TRANSFER FUNCTION OF A SYSTEM

(2.1) Input–Output Specifications

The discrete signals to be considered are constant between two consecutive time instants, as shown in Fig. 2, and can change

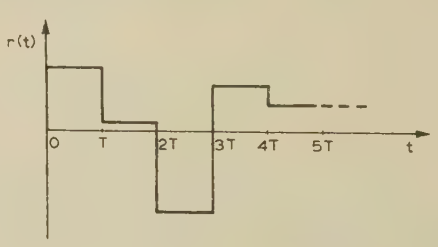

Fig. 2.—Discrete periodic signals.

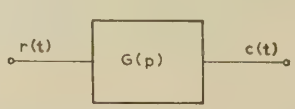

Fig. 3.—Linear continuous system.

only at the periodic instants of time $t = kT$. When such discrete signals are applied to the input of a system (Fig. 3), finite-settling-time responses may result, i.e. the output $c(t)$ of the system may remain constant or may continue to change at a fixed rate for all time after a finite number of time periods T. Such responses are frequently used as design criteria for control systems, and are the only type of responses considered in the paper.

Owing to the discrete nature of the input signals, finite-settling-time responses can be obtained only if the input to the system is zero or constant in the steady state. Thus, a system without integration can have only outputs which are constant after a finite number of time periods T, and a system with one integration can have only outputs which are constant or linearly increasing with time under the same conditions. Generally, the highest order of the output time function in the steady state is equal to the number of integrations in the system.

The discrete periodic signals shown in Fig. 2 can be made up of a series of step functions or a series of pulse functions. Each approach has advantages in certain cases, and both are considered in some detail in the following Sections.

(2.2) Periodic Step Inputs

If the system $G(p)$ in Fig. 3 is subjected to discrete periodic inputs and a finite-settling-time response is required, the output $c(t)$ can be written as a sum of delayed step response functions as

$$c(t) = \sum_{k=0}^{q} R_k w(t - kT) \quad . \quad . \quad . \quad . \quad (1)$$

where $(q + 1)$ is the number of step inputs for a finite-settling-time of $t = qT$ seconds.

(2.2.1) System without Integration.

The unit step response of a system with a finite number of poles but no integration is given by

$$w(t) = K + K_1\varepsilon^{b_1 t} + K_2\varepsilon^{b_2 t} + \ldots + K_n\varepsilon^{b_n t} \quad . \quad (2)$$

where $b_1, b_2 \ldots b_n$ are the poles and K is the low-frequency gain of the system.

Thus, from eqn. (1) the output of the system becomes

$$c(t) = \sum_{k=0}^{q} KR_k + \sum_{k=0}^{q} K_1 R_k \varepsilon^{b_1(t-kT)} + \ldots + \sum_{k=0}^{q} K_n R_k \varepsilon^{b_n(t-kT)} \quad . \quad . \quad . \quad . \quad (3)$$

If the output is required to remain constant at $c(t) = C$ for all time after $t = qT$, the sum of the time-independent terms should be made equal to C and the sum of the time-dependent terms should be equated to zero.

The application of these conditions yields the simultaneous equations

$$K \sum_{k-0}^{q} R_k = C \quad . \quad . \quad . \quad . \quad . \quad (4a)$$

$$\left.\begin{aligned} \sum_{k=0}^{q} R_k \varepsilon^{-b_1 kT} &= 0 \\ . \quad . \quad . \quad . \quad . \quad . \quad . \quad . \\ \sum_{k=0}^{q} R_k \varepsilon^{-b_n kT} &= 0 \end{aligned}\right\} \quad . \quad . \quad . \quad . \quad . \quad (4b)$$

which may be solved to obtain the magnitudes of the input steps R_k. The magnitudes of the input pulses $R(k)$ are then determined from the foll owing equations:

$$\left.\begin{aligned} R(0) &= R_0 \\ R(1) &= R_0 + R_1 \\ R(2) &= R_0 + R_1 + R_2 \\ . \quad . \quad . \quad . \quad . \quad . \quad . \quad . \quad . \quad . \quad . \quad . \quad . \quad . \\ R(q) &= R(q+1) = R(q+2) = \ldots \\ &= R_0 + R_1 + R_2 + \ldots + R_q = \frac{C}{K} \end{aligned}\right\} \quad . \quad . \quad (5)$$

(2.2.2) System with One Integration.

The unit step response of a system with one integration and a finite number of poles is given by

$$w(t) = Kt + K_0 + K_1\varepsilon^{b_1 t} + K_2\varepsilon^{b_2 t} + \ldots + K_n\varepsilon^{b_n t} \quad (6)$$

and the system output becomes

$$c(t) = \sum_{k=0}^{q} KR_k t - \sum_{k=0}^{q} KR_k kT + \sum_{k=0}^{q} K_0 R_k + \sum_{k=0}^{q} K_1 R_k \varepsilon^{b_1(t-kT)} + \ldots + \sum_{k=0}^{q} K_n R_k \varepsilon^{b_n(t-kT)} \quad (7)$$

For a constant output $c(t) = C$ after $t = qT$, the steady state and the transient conditions yield the equations

$$\sum_{k=0}^{q} R_k = 0 \quad . \quad . \quad . \quad . \quad (8a)$$

$$K_0 \sum_{k=0}^{q} R_k - KT \sum_{k=0}^{q} R_k k = C \quad . \quad . \quad . \quad (8b)$$

$$\left.\begin{aligned} \sum_{k=0}^{q} R_k \varepsilon^{-b_1 kT} &= 0 \\ . \quad . \quad . \quad . \quad . \quad . \\ \sum_{k=0}^{q} R_k \varepsilon^{-b_n kT} &= 0 \end{aligned}\right\} \quad . \quad . \quad . \quad (8c)$$

If the output is required to be linearly increasing with time in the steady state, i.e. for $c(t) = St$ after $t = qT$, the equations become

$$K \sum_{k=0}^{q} R_k = S \quad . \quad . \quad . \quad . \quad (9a)$$

$$K_0 \sum_{k=0}^{q} R_k - KT \sum_{k=0}^{q} R_k k = 0 \quad . \quad . \quad . \quad . \quad (9b)$$

$$\left.\begin{aligned} \sum_{k=0}^{q} R_k \varepsilon^{-b_1 kT} &= 0 \\ . \quad . \quad . \quad . \quad . \quad . \\ \sum_{k=0}^{q} R_k \varepsilon^{-b_n kT} &= 0 \end{aligned}\right\} \quad . \quad . \quad . \quad (9c)$$

Systems with more than one integration can also be considered, but the above results are sufficient to conclude that:

(*a*) The number of simultaneous equations to be solved, and hence the minimum number of input steps, is one more than the number of poles in the system transfer function.

(*b*) All poles, except those at the origin, yield transient equations of the same form.

(2.3) Periodic Pulse Inputs

When discrete periodic signals are applied to the input of a system, its output can also be written as a sum of delayed pulse response functions as

$$c(t) = \sum_{k=0}^{q-1} R(k)h(t - kT) + \sum_{k=q}^{\infty} R(k)h(t - kT) \quad . \quad (10)$$

where $h(t)$ is the unit pulse response of the system, i.e. the response of the system to an input pulse of unit height and width equal to one time period T, and q is the number of input pulses required for a finite-settling-time of $t = qT$ seconds.

(2.3.1) System without Integration.

Consider a system having a single pole at $p = b_r$ and low-

frequency gain K. The unit step response of this system is $w(t) = K + K_r\varepsilon^{b_r t}$, and the unit pulse response is given by

$$h(t) = w(t) - w(t - T) = K_r[\varepsilon^{b_r t} - \varepsilon^{b_r(t-T)}] \quad . \quad (11)$$

Thus, from eqn. (10), the output of the system becomes

$$c(t) = K_r \sum_{k=0}^{q-1} R(k)[\varepsilon^{b_r(t-kT)} - \varepsilon^{b_r(t-T-kT)}] + K_r \sum_{k=q}^{\infty} R(k)[\varepsilon^{b_r(t-kT)} - \varepsilon^{b_r(t-T-kT)}] \quad (12)$$

Since there is no integration in the system, the input and output must be constant in the steady state, and for a finite-settling-time response one has $R(k \geqslant q) = R(q) = C/K$. Thus, the second term can be replaced by the step response of the system due to a step input of magnitude $R(q)$ applied at time $t = qT$, and the output for all time after $t = qT$ becomes

$$c(t) = K_r \sum_{k=0}^{q-1} R(k)[\varepsilon^{b_r(t-kT)} - \varepsilon^{b_r(t-T-kT)}] + R(q)[K + K_r\varepsilon^{b_r(t-qT)}] \quad (13)$$

The time-independent term determines the value of the output in the steady state, giving $KR(q) = C$, as it should be, and application of the transient condition yields

$$K_r \sum_{k=0}^{q-1} R(k)[\varepsilon^{b_r(t-kT)} - \varepsilon^{b_r(t-T-kT)}] + K_r R(q)\varepsilon^{b_r(t-qT)} = 0$$

or
$$(\varepsilon^{-b_r T} - 1) \sum_{k=0}^{q-1} R(k)\varepsilon^{-b_r kT} = R(q)\varepsilon^{-b_r qT} \quad . \quad . \quad (14)$$

When a larger number of poles are present, each pole must satisfy this transient equation, and it is clearly seen that the number of simultaneous equations to be solved is equal to the number of poles contained in the system transfer function.

(2.3.2) **System with One Integration.**

Consider now a system with one integration and a pole at $p = b_r$. The unit step response of such a system is $w(t) = Kt + K_0 + K_r\varepsilon^{b_r t}$, and the unit pulse response is given by

$$h(t) = w(t) - w(t - T) = KT + K_r[\varepsilon^{b_r t} - \varepsilon^{b_r(t-T)}] \quad (15)$$

Substitution in eqn. (10) yields the output as

$$c(t) = \sum_{k=0}^{q-1} KTR(k) + K_r \sum_{k=0}^{q-1} R(k)[\varepsilon^{b_r(t-kT)} - \varepsilon^{b_r(t-T-kT)}] + \sum_{k=q}^{\infty} KTR(k) + K_r \sum_{k=q}^{\infty} R(k)[\varepsilon^{b_r(t-kT)} - \varepsilon^{b_r(t-T-kT)}] \quad (16)$$

If a constant output is required after q time periods, the integration in the system requires that $R(k \geqslant q) = 0$, and application of the steady-state and transient conditions yields

$$KT \sum_{k=0}^{q-1} R(k) = C \quad . \quad . \quad . \quad . \quad (17a)$$

$$\sum_{k=0}^{q-1} R(k)\varepsilon^{-b_r kT} = 0 \quad . \quad . \quad . \quad . \quad (17b)$$

If the output is required to be linearly increasing at the rate of S units per second in the steady state, the integration requires that $R(k \geqslant q) = R(q) = S/K$. Thus, the infinite terms in eqn. (16) can be replaced by the step response of the system due to a step input of magnitude $R(q)$ applied at time $t = qT$, and the output for all time after $t = qT$ becomes

$$c(t) = \sum_{k=0}^{q-1} KTR(k) + K_r \sum_{k=0}^{q-1} R(k)[\varepsilon^{b_r(t-kT)} - \varepsilon^{b_r(t-T-kT)}] + R(q)[K(t - qT) + K_0 + K_r\varepsilon^{b_r(t-qT)}] \quad (18)$$

The steady-state and transient conditions require that the sums of all time-independent terms and of all transient terms be zero, respectively, giving

$$KT \sum_{k=0}^{q-1} R(k) - qKTR(q) + K_0 R(q) = 0 \quad . \quad (19a)$$

$$(\varepsilon^{-b_r T} - 1) \sum_{k=0}^{q-1} R(k)\varepsilon^{-b_r kT} = R(q)\varepsilon^{-b_r qT} \quad . \quad (19b)$$

where $R(q) = S/K$.

The remaining term $R(q)Kt = St$ gives the output for all time after q time periods, and again it is noted that, if more poles are present, the transient equation must be satisfied by all poles except that at the origin.

It is now evident that when the equations are written in terms of the magnitudes of the input pulses $R(k)$, the following applies:

(*a*) The number of simultaneous equations to be solved, and hence the minimum number of input pulses, is equal to the number of poles in the system transfer function.

(*b*) All poles, except that at the origin, yield transient equations of the same form.

It is of interest to note that the link between the step method and the pulse method is given by eqns. (5). This can be readily verified by substituting in a set of step equations, from which the corresponding set of pulse equations can be obtained, or vice versa.

Example 1.—The transfer function of a system is $G(p) = 1/(p + 1)(p + 2)$, and it is required to determine the input pulse sequence which results in a constant output of 10 units in the minimum number of time periods. The time period T is 1 sec.

There are two poles in the transfer function, $b_1 = -1$ and $b_2 = -2$, and the low-frequency gain is 0·5. Hence the minimum number of input steps is three, and from eqn. (4) the simultaneous equations to be solved become

$$0{\cdot}5(R_0 + R_1 + R_2) = 10$$
$$R_0\varepsilon^0 + R_1\varepsilon^1 + R_2\varepsilon^2 = 0$$
$$R_0\varepsilon^0 + R_1\varepsilon^2 + R_2\varepsilon^4 = 0$$

Solving these equations yields $R_0 = 36{\cdot}56$, $R_1 = -18{\cdot}38$ and $R_2 = 1{\cdot}82$. The magnitudes of the input pulses are then found from eqns. (5) to be $R(0) = 36{\cdot}56$, $R(1) = 18{\cdot}18$ and $R(2) = R(3) = \ldots = 20$.

The same result can be obtained if eqn. (14) is used, which gives the simultaneous equations directly in terms of the input pulses as

$$(\varepsilon^1 - 1)[R(0)\varepsilon^0 + R(1)\varepsilon^1] = R(q)\varepsilon^2$$
$$(\varepsilon^2 - 1)[R(0)\varepsilon^0 + R(1)\varepsilon^2] = R(q)\varepsilon^4$$

where
$$R(q) = C/K = 10/0{\cdot}5 = 20.$$

The resulting input time function is shown in Fig. 4(*a*) and the output of the system is shown in Fig. 4(*b*). It is seen that after two time periods the output remains constant at the specified value of 10 units.

The minimum number of time periods for a finite-settling-time response is fixed by the number of poles in the system, but a larger number of time periods can be used if desired. In such cases the magnitudes of the excess pulses may be chosen arbitrarily, or they may be used to meet additional constraints on the magnitudes of the input pulses,[1,2] or to minimize the error in a feedback system, as will be shown in the next Section.

(2.3.3) ***z*-Transform Analysis.**

When the transfer function of a system is known, the corresponding pulse transfer function (z transfer function) can be

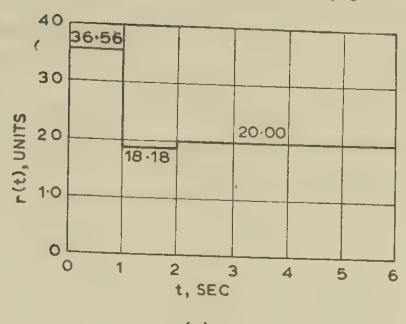

(a)

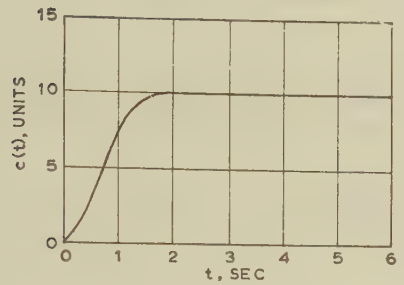

(b)

Fig. 4.—Finite-settling-time response of the system in example 1.
(*a*) Input.
(*b*) Output.

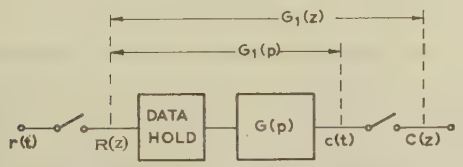

Fig. 5.—A linear system with zero-order data hold and periodic samplers.

obtained from Tables or calculated by well-known mathematical methods.[3] If a zero-order data hold is employed, as shown in Fig. 5, the input to the system, $G(p)$, consists of discrete periodic signals (Fig. 2), and the total transfer function becomes

$$G_1(p) = \frac{1 - \varepsilon^{-pT}}{p} G(p) \quad . \quad . \quad . \quad . \quad (20)$$

Considering the system in example 1, for which $G_1(p) = (1-\varepsilon^{-pT})/p(p+1)(p+2)$, the pulse transfer function is given by

$$G_1(z) = \frac{0{\cdot}200z^{-1} + 0{\cdot}07z^{-2}}{(1 - 0{\cdot}368z^{-1})(1 - 0{\cdot}135z^{-1})} \quad . \quad . \quad (21)$$

and the sequence of input pulses to this system for a finite-settling-time response is found to be

$$R(z) = 36{\cdot}56 + 18{\cdot}18z^{-1} + 20{\cdot}00z^{-2} + 20{\cdot}00z^{-3} + \ldots$$

$$= \frac{36{\cdot}56 - 18{\cdot}38z^{-1} + 1{\cdot}82z^{-2}}{1 - z^{-1}}$$

$$= \frac{36{\cdot}56(1 - 0{\cdot}368z^{-1})(1 - 0{\cdot}135z^{-1})}{1 - z^{-1}} \quad (22)$$

Examination of $G_1(z)$ and $R(z)$ reveals that the poles of the pulse transfer function are contained as zeros in the z-transform of the input signal, and after cancellation of poles and zeros the output becomes

$$C(z) = R(z)G_1(z) = \frac{36{\cdot}56(0{\cdot}200z^{-1} + 0{\cdot}07z^{-2})}{1 - z^{-1}}$$

$$= 7{\cdot}30z^{-1} + 10{\cdot}00z^{-2} + 10{\cdot}00z^{-3} + \ldots \quad (23)$$

It is evident that the z-transform of the input signal $R(z)$ which results in a finite-settling-time response can be easily determined if the pulse transfer function of a system is known. However, this method can be applied directly only if the minimum number of pulses is used and if a constant output is required. When a larger number of input pulses or a ramp output is required, additional zeros appear in the z-transform of the input signal and the method becomes difficult or impossible to use. A more general approach for determining the input pulse sequence from the z-transform of a system has been indicated recently in a discussion by Brown.[2]

(3) INPUT PULSE SEQUENCE FROM THE TRANSIENT RESPONSE OF A SYSTEM

(3.1) Periodic Step Inputs

When a series of periodic steps are applied to the input of a system, the output as a function of time is given by eqn. (1). However, if the output is considered only at the time instants $t = kT$, the z-transform technique can be used to express the output of the system as a function of the variable $z = \varepsilon^{pT}$. The inverse of this variable, z^{-1}, represents a time delay of one time period T, and the pulse sequence of the output can be written as

$$C(z) = w(z) \sum_{k=0}^{\infty} R_k z^{-k} = \sum_{k=0}^{\infty} C(k) z^{-k} \quad . \quad . \quad (24)$$

where $w(z) = w(0) + w(1)z^{-1} + w(2)z^{-2} + \ldots$ is the pulse sequence of the unit step response function $w(t)$.

The output of the system at the time instants $t = kT$ is simply given by the coefficients $C(k)$, which are the sum of all terms containing z^{-1} to the kth power in the above infinite summation. Thus, if the output is required to remain constant after q time periods, the sum of all terms with equal powers in z^{-k} should be made equal to this output for $k \geqslant q$. Application of this condition results in simultaneous equations which contain the step inputs satisfying the equations derived in Section 2, and can now be used to determine the magnitudes of the input steps.

It was shown that the number of simultaneous equations for finite-settling-time responses is one more than the number of poles in the system transfer function. Thus, the number of independent equations that can be obtained from the coefficients of the output $C(z)$ is also one more than the number of poles in the system transfer function. However, the number of equations required from the coefficients of $C(z)$ can be reduced if some of the equations from Section 2 are employed; for example, eqns. (4*a*), (8*a*) and (9*a*) can be used if desired. In cases where the number of poles in the system is not known, the number of equations should be increased until an input pulse sequence is obtained which results in a finite-settling-time response. The number of poles in the system is then one less than the number of equations used.

Example 2.—The unit step response of a system is shown in Fig. 6, and it is required to determine the input pulse sequence which results in a constant output of 10 units in the minimum number of time periods. The time period T is 1 sec.

It is evident from the given transient response that there is no integration in the system, and it is seen that the steady-state gain is 0·5. The number of poles is not immediately apparent,

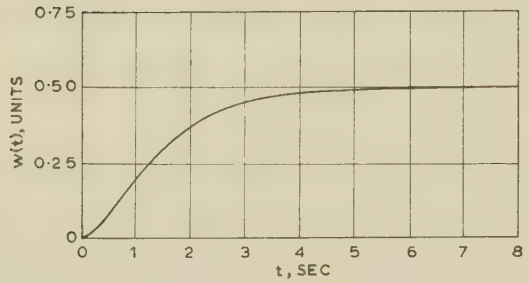

Fig. 6.—Unit step response of a system.

but assuming that two poles are present, the minimum finite-settling-time is $2T$ and three equations are required.

The pulse sequence of the unit step response is obtained by noting its values at the time instants $t = kT$, giving

$$w(z) = 0 + 0{\cdot}200z^{-1} + 0{\cdot}374z^{-2} + 0{\cdot}451z^{-3} + 0{\cdot}481z^{-4} + 0{\cdot}493z^{-5} + \ldots$$

Thus, the pulse sequence of the output of the system due to an input step sequence R_k is given by

$$C(z) = \sum_{k=0}^{2} R_k w(z) z^{-k} = R_0(0{\cdot}200z^{-1} + 0{\cdot}374z^{-2} + \ldots) + R_1(0{\cdot}200z^{-2} + 0{\cdot}374z^{-3} + \ldots) + R_2(0{\cdot}200z^{-3} + 0{\cdot}374z^{-4} \ldots)$$

and combining terms of equal powers in z^{-1} yields

$$C(z) = 0{\cdot}200R_0z^{-1} + (0{\cdot}374R_0 + 0{\cdot}200R_1)z^{-2} + (0{\cdot}451R_0 + 0{\cdot}374R_1 + 0{\cdot}200R_2)z^{-3} + (0{\cdot}481R_0 + 0{\cdot}451R_1 + 0{\cdot}374R_2)z^{-4} + \ldots$$

For a finite-settling-time of two time periods the equations to be solved are

$$0{\cdot}374R_0 + 0{\cdot}200R_1 = 10{\cdot}00 \quad \text{(coefficient of } z^{-2})$$
$$0{\cdot}451R_0 + 0{\cdot}374R_1 + 0{\cdot}200R_2 = 10{\cdot}00 \quad \text{(coefficient of } z^{-3})$$
$$0{\cdot}481R_0 + 0{\cdot}451R_1 + 0{\cdot}374R_2 = 10{\cdot}00 \quad \text{(coefficient of } z^{-4})$$

but any one of these equations can be replaced by the equation $K\sum_{k=0}^{2} R_k = 0{\cdot}5(R_0 + R_1 + R_2) = 10$, derived in Section 2.

Solving the simultaneous equations yields $R_0 = 36{\cdot}56$, $R_1 = -18{\cdot}38$ and $R_2 = 1{\cdot}82$, and comparison with the results in example 1 reveals that the input steps are identical. A plot of the output $c(t)$ shows that this input pulse sequence results in a finite-settling-time response which is also identical with the response in Fig. 4(*b*) of example 1. This indicates that the unit step response in Fig. 6 is that of the system in example 1.

The practical significance of the method should now be evident. This procedure is not only computationally simpler, but also it permits the determination of the input pulse sequence without a knowledge of the system transfer function.

(3.2) Periodic Pulse Inputs

When periodic pulses are applied to the input of a system, the pulse sequence of the output is given by

$$C(z) = h(z)\sum_{k=0}^{\infty} R(k)z^{-k} = \sum_{k=0}^{\infty} C(k)z^{-k} \quad . \quad . \quad (25)$$

where $h(z) = w(z) - w(z)z^{-1} = h(0) + h(1)z^{-1} + h(2)z^{-2} + \ldots$ is the pulse sequence of the unit pulse response function $h(t)$.

The coefficients $C(k)$ of the output pulse sequence may be restricted in exactly the same manner as before, and the magnitudes of the input pulses can be found by solving the simultaneous equations. The number of independent equations is equal to the number of poles in the system, and again, some equations from Section 2 may be used if desired. It should be noted that when the input pulse sequence in the steady state is not zero, it is constant, and its value can be found from the steady-state gain of the system and the desired output.

The periodic-pulse-input approach can frequently be employed to advantage, particularly when restrictions are to be imposed on the magnitudes of the input pulses. Another interesting application is the minimization of the error in a feedback system, and the following example serves to illustrate the design procedure.

Example 3.—The unit step response of the plant to be controlled in a feedback system, as shown in Fig. 1, is given in Fig. 7. The plant transfer function is not known and it is

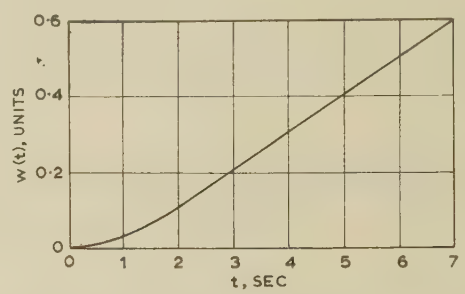

Fig. 7.—Unit step response of the plant in a feedback system.

required to determine the pulse transfer function of the discrete controller $D(z)$ which will minimize the error $E(z)$ when step inputs are applied to the input of the overall system. In addition, the output is required to equal the input for all time 3 sec after the application of a step input. The time period of the discrete periodic signals is 1 sec.

It is seen from the given unit step response that the plant contains one integration, and a test revealed that the total number of poles is two. Thus, a minimum of two pulses and two simultaneous equations are required for a finite-settling-time response.

The pulse sequence of the unit step response is $w(z) = 0{\cdot}368z^{-1} + 1{\cdot}135z^{-2} + 2{\cdot}050z^{-3} + 3{\cdot}018z^{-4} + 4{\cdot}007z^{-5} + \ldots$ and the pulse sequence of the unit pulse response becomes

$$h(z) = w(z) - w(z)z^{-1} = 0{\cdot}368z^{-1} + 0{\cdot}767z^{-2} + 0{\cdot}915z^{-3} + 0{\cdot}968z^{-4} + 0{\cdot}989z^{-5} + \ldots$$

Hence the output of the system is given by

$$C(z) = h(z)\sum_{k=0}^{\infty} F(k)z^{-k} = 0{\cdot}368F(0)z^{-1} + [0{\cdot}767F(0) + 0{\cdot}368F(1)]z^{-2} + [0{\cdot}915F(0) + 0{\cdot}767F(1) + 0{\cdot}368F(2)]z^{-3} + [0{\cdot}968F(0) + 0{\cdot}915F(1) + 0{\cdot}767F(2) + 0{\cdot}368F(3)]z^{-4} + \ldots$$

Assuming that the input to the overall system is $R = 2$ units, and noting that $F(3)$ is zero, since the system contains the

necessary integration for zero steady-state error, the equations to be solved become

$$0{\cdot}915F(0) + 0{\cdot}767F(1) + 0{\cdot}368F(2) = 2{\cdot}00$$

$$0{\cdot}968F(0) + 0{\cdot}915F(1) + 0{\cdot}767F(2) = 2{\cdot}00$$

One pulse can be chosen arbitrarily or can be used to minimize the error in the system. The integral squared error, based upon the values of the error at the sampling instants only, is given by

$$\begin{aligned}\sum_{k=0}^{2} E^2(k) &= [R - C(0)]^2 + [R - C(1)]^2 + [R - C(2)]^2 \\ &= [2{\cdot}00 - 0]^2 + [2{\cdot}00 - 0{\cdot}368F(0)]^2 \\ &\quad + [2{\cdot}00 - 0{\cdot}767F(0) - 0{\cdot}368F(1)]^2 \\ &= 12 - 4{\cdot}545F(0) + 0{\cdot}726F^2(0) \\ &\quad + 0{\cdot}566F(0)F(1) - 1{\cdot}472F(1) + 0{\cdot}135F^2(1)\end{aligned}$$

Differentiation with respect to $F(0)$ yields

$$-4{\cdot}545 + 1{\cdot}452F(0) + 0{\cdot}566F(1) = 0$$

The solution of this equation, together with the equations obtained from the coefficients of the system output, gives the magnitudes of the periodic pulses as $F(0) = 4{\cdot}06$, $F(1) = -2{\cdot}38$ and $F(2) = 0{\cdot}32$. The pulse sequence of the forcing function is thus $F(z) = 4{\cdot}06 - 2{\cdot}38z^{-1} + 0{\cdot}32z^{-2}$, and the pulse sequence of the error function is given by $E(z) = R(z) - C(z) = 2{\cdot}00 + 0{\cdot}50z^{-1} - 0{\cdot}24z^{-2}$.

Finally, the pulse transfer function of the discrete controller is obtained as

$$D(z) = \frac{F(z)}{E(z)} = \frac{4{\cdot}06 - 2{\cdot}38z^{-1} + 0{\cdot}32z^{-2}}{2{\cdot}00 + 0{\cdot}50z^{-1} - 0{\cdot}24z^{-2}}$$

The step responses of the compensated system with the controller designed for minimum error, and with the controller designed when $F(0)$ is chosen arbitrarily at 1 unit, are shown in Fig. 8. It is seen that in both cases the output remains

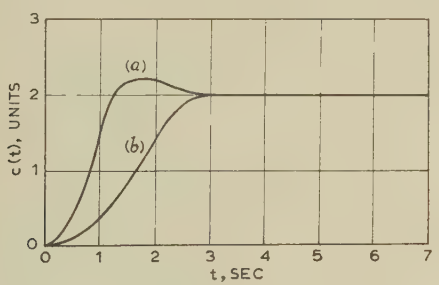

Fig. 8.—Step responses of the compensated system in example 3.
(*a*) Controller designed for minimum error.
(*b*) Controller designed with one arbitrary pulse.

constant after 3 sec, but during the transient periods the output is much closer to the desired value of 2 units when the system is designed for minimum error. Obviously, not only does the design method result in finite-settling-time responses, but it is also possible to control the behaviour of the output function during the transient periods. If more than one free pulse is available and a minimum error is desired, the squared-error function should be differentiated with respect to each free pulse to obtain as many equations as required.

(4) TRANSFER FUNCTION FROM TRANSIENT RESPONSE OF A SYSTEM

The transfer function of a system contains all the information required to determine its response for all possible inputs if the system is initially quiescent. In the design of control systems, the transfer function is usually the starting-point and should be known with sufficient accuracy.

The frequency-response method of determining the transfer function of a system is well known and its accuracy is acceptable for many applications. Sinusoidal measurements, however, involve lengthy tests, and some systems are quite unsuitable for sinusoidal excitations.

These disadvantages can be overcome by the application of a step or pulse input and measurement of the corresponding transient response, which can yield all the information contained in an extensive frequency analysis. Unfortunately, direct evaluation of the transfer function from the transient response of a system is possible only in very simple cases, and usually approximation methods are used, the response being approximated by triangular pulses or a broken line.[4] Another approach is to apply sampling techniques and, by the use of a recurring relation, to approximate the numerator and the denominator of the transfer function.[5] In the following, however, a method of determining the transfer function of a system from its transient response is presented which makes use of no approximations.

It was shown in Section 3 that the required input pulse sequence for finite-settling-time response can be determined from the step response or from the pulse response of a system. It was also shown in Section 2 that the same pulse sequence can be obtained from the system transfer function, the magnitudes of the discrete inputs and the poles of the transfer function being related by equations of known form. Thus, if an input pulse sequence has been found from the transient response of a system, these equations can now be used to determine the poles of the system transfer function. Alternatively, the poles of the transfer function can be obtained from those of the pulse transfer function, which, as pointed out in Section 2.3, appear as zeros in the z-transform of the input pulse sequence.

Generally, when determining a sequence of discrete inputs, in order to obtain the transfer function from a given transient response, the minimum number of discrete inputs for a constant output should be used. This results in the simplest possible procedure, and the appearance of zeros in the z-transform of the input signal, which are not contained as poles in the pulse transfer function of the system, is also avoided.

Example 4.—For the purpose of this example the step response of the system in example 2 is used (Fig. 6), for which the input steps for a constant output of 10 units in two time periods were found to be $R_0 = 36{\cdot}56$, $R_1 = -18{\cdot}38$ and $R_2 = 1{\cdot}82$. Next, in determining the transfer function from the transient response, it is necessary to find the poles of the system.

The system has two poles and both must satisfy the transient equation (4*b*), which is of the form $\sum_{k=0}^{2} R_k\varepsilon^{-b_r kT} = 0$. Substituting numerical values yields the equation

$$36{\cdot}56 - 18{\cdot}38\varepsilon^{-b_r} + 1{\cdot}82\varepsilon^{-2b_r} = 0$$

or $$36{\cdot}56 - 18{\cdot}38x + 1{\cdot}82x^2 = 0 \quad \text{where } x = \varepsilon^{-b_r}.$$

This quadratic equation has roots at $x_1 = 2{\cdot}72$ and $x_2 = 7{\cdot}38$, and the corresponding poles are $b_1 = -1$ and $b_2 = -2$.

To obtain the complete transfer function it is noted that the unit step response of a system with two poles is given by $w(t) = K + K_1\varepsilon^{b_1 t} + K_2\varepsilon^{b_2 t}$, where K is the steady-state gain of the system. In this case $K = 0{\cdot}5$, and the constants K_1 and K_2 are determined by considering the step response at two instants of time, giving

$$w(t) = 0{\cdot}5 + K_1 + K_2 = 0 \qquad \text{at } t = 0$$

$$w(t) = 0{\cdot}5 + K_1\varepsilon^{-1} + K_2\varepsilon^{-2} = 0{\cdot}2 \qquad \text{at } t = 1 \text{ sec.}$$

Solving the equations yields $K_1 = -1$ and $K_2 = 0{\cdot}5$, and the Laplace transform of the unit step response becomes

$$w(p) = \frac{0{\cdot}5}{p} + \frac{-1}{(p+1)} + \frac{0{\cdot}5}{(p+2)} = \frac{1}{p(p+1)(p+2)}$$

Thus, since the Laplace transform of the unit step input is $1/p$, the transfer function of the system is given by

$$G(p) = \frac{1}{(p+1)(p+2)}$$

Example 5.—The response of a system due to an input pulse of 1 sec duration and unit magnitude is given in Fig. 9. No

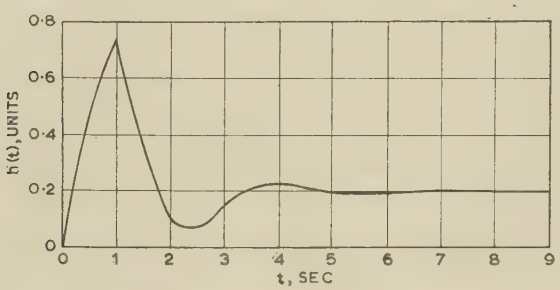

Fig. 9.—Unit pulse response of a system.

other information is available and it is desired to determine the transfer function of the system.

From the given unit pulse response it is seen that

(*a*) The system has one integration.

(*b*) The steady-state gain is 0·2.

(*c*) The system is oscillatory, indicating that complex poles are present, and care should be taken to ensure that the time period T is not equal to or a multiple of the natural period of oscillation of the system.

(*d*) The pulse sequence for a time period of 1 sec is

$$h(z) = 0{\cdot}75z^{-1} + 0{\cdot}09z^{-2} + 0{\cdot}16z^{-3} + 0{\cdot}23z^{-4} + 0{\cdot}20z^{-5} + \ldots$$

Since one integration and a pair of complex-conjugate poles are definitely present in the system, the minimum number of poles is three, and as a first attempt three equations will be used. The integration in the system requires the pulses $R(3)$, $R(4)\ldots$ to be zero if the output is to remain constant in the steady state, and the output pulse sequence becomes

$$\begin{aligned} C(z) = \sum_{k=0}^{2} R(k)h(z)z^{-k} &= 0{\cdot}75R(0)z^{-1} + [0{\cdot}09R(0) + 0{\cdot}75R(1)]z^{-2} \\ &+ [0{\cdot}16R(0) + 0{\cdot}09R(1) + 0{\cdot}75R(2)]z^{-3} \\ &+ [0{\cdot}23R(0) + 0{\cdot}16R(1) + 0{\cdot}09R(2)]z^{-4} \\ &+ [0{\cdot}20R(0) + 0{\cdot}23R(1) + 0{\cdot}16R(2)]z^{-5} \\ &+ \ldots \end{aligned}$$

Thus the equations for a constant output of one unit are

$$\begin{aligned} 0{\cdot}16R(0) + 0{\cdot}09R(1) + 0{\cdot}75R(2) &= 1{\cdot}00 \\ 0{\cdot}23R(0) + 0{\cdot}16R(1) + 0{\cdot}09R(2) &= 1{\cdot}00 \\ 0{\cdot}20R(0) + 0{\cdot}23R(1) + 0{\cdot}16R(2) &= 1{\cdot}00 \end{aligned}$$

and the solution yields $R(0) = 3{\cdot}45$, $R(1) = 1{\cdot}06$ and $R(2) = 0{\cdot}47$. If the output $C(z)$ is computed at any other time in the steady state, it will be seen that this pulse sequence results in a finite-settling-time response, indicating that the system has only three poles. To find these poles the transient equation (17*b*) is used, which becomes

$$\begin{aligned} \sum_{k=0}^{2} R(k)\varepsilon^{-b_r kT} &= R(0)\varepsilon^{0} + R(1)\varepsilon^{-b_r T} + R(2)\varepsilon^{-2b_r T} \\ &= 3{\cdot}45 + 1{\cdot}06\varepsilon^{-b_r} + 0{\cdot}47\varepsilon^{-2b_r} = 0 \end{aligned}$$

or

$$3{\cdot}45 + 1{\cdot}06x + 0{\cdot}47x^2 = 0$$

The roots of this equation are $x_1 = -1{\cdot}13 + j2{\cdot}47$ and $x_2 = -1{\cdot}13 - j2{\cdot}47$, and the corresponding poles are found to be very nearly $b_1 = -1 - j2$ and $b_2 = -1 + j2$.

Alternatively, the z-transform technique may be used to determine the poles of the transfer function from the input pulse sequence. In this case the z-transform of the input has only zeros, which are defined by the equation $R(z) = 3{\cdot}45 + 1{\cdot}06z^{-1} + 0{\cdot}47z^{-2} = 0$. The roots of this equation are the same as before, i.e. $(z^{-1})_1 = -1{\cdot}13 + j2{\cdot}47$ and $(z^{-1})_2 = -1{\cdot}13 - j2{\cdot}47$, and noting that $z^{-1} = \varepsilon^{-pT} = \varepsilon^{-b_r T}$ it is seen that the same values for the poles of the transfer function are obtained as above.

The determination of the complete transfer function is more easily conducted if the pulse sequence of the unit step response is obtained as follows:

$$\begin{aligned} w(z) &= \frac{h(z)}{1 - z^{-1}} \\ &= h(0) + [h(0) + h(1)]z^{-1} + [h(0) + h(1) + h(2)]z^{-2} + \ldots \\ &= 0{\cdot}75z^{-1} + 0{\cdot}84z^{-2} + 1{\cdot}00z^{-3} + 1{\cdot}23z^{-4} + 1{\cdot}43z^{-5} + \ldots \end{aligned}$$

and using the same approach as in example 4, the transfer function is found to be

$$G(p) = \frac{p^2 + 2{\cdot}5p + 1}{p(p^2 + 2p + 5)}$$

(5) CONCLUSIONS

The relation between certain discrete periodic inputs, the transfer function and the transient response of a system has been investigated. It has been shown that the step response or the pulse response of a system can be used to determine the input pulse sequence which results in a finite-settling-time response. The method is computationally very simple, and should be of considerable practical interest in the design of discrete controllers for compensation of feedback systems, particularly when the plant transfer function is not known. Further, by making use of some general relations between the poles of a transfer function and the discrete periodic inputs, a novel procedure for determining the transfer function of a system from its transient response has been developed. The procedure involves no approximations and can be applied to systems with any number of poles.

(6) REFERENCES

(1) MULLIN, F. J.: 'Stability and Compensation of Saturating Sampled-Data Systems', *Transactions of the American I.E.E.*, 1959, **78**, Part I, p. 270.

(2) GLUCHAROFF, T.: 'Discrete Analogue-Computer Compensation of Sampled-Data Control Systems', *Proceedings I.E.E.*, Paper No. 3341 M, November, 1960 (**108** B, p. 167).

(3) BARKER, R. H.: 'The Pulse Transfer Function and its Application to Sampling Servo Systems', *ibid.*, Monograph No. 43 M, July, 1952 (**99**, Part IV, p. 302).

(4) TRUXAL, J. G.: 'Automatic Feedback Control Systems' (McGraw-Hill, 1958).

(5) KOCHANOV, N. S.: 'On Connection of Transient Functions of Linear Systems with their Laplace Representation', *Avtomatika i Telemekhanika*, 1959, **21**, p. 20.

621.317.79.017.39: 621.313.042.143

The Institution of Electrical Engineers
Monograph No. 453 U
June 1961

A THEORETICAL AND ANALOGUE APPROACH TO STRAY EDDY-CURRENT LOSS IN LAMINATED MAGNETIC CORES

By D. A. JONES, B.Sc., Ph.D., Associate Member, and W. S. LEUNG, B.Sc.(Eng.), Ph.D., Graduate.

(*The paper was first received 8th December, 1960, and in revised form 17th March, 1961. It was published as an* INSTITUTION MONOGRAPH *in June, 1961.*)

SUMMARY

A method of obtaining the interlaminar eddy-current loss in laminated magnetic cores is devised by using a resistance-network analogy. It is assumed that in a laminated-core section the flux distribution is uniform, that there is a uniform resistivity in the direction across the laminations and that the *IR* drops in the direction along the planes of the laminations are negligible compared with those in the perpendicular direction. The stray eddy-current loss is derived as a function of the resistivity ratio between the two directions. The network analogy leads to the subsequent estimation of the effect on core loss of any short-circuiting paths in the section.

An experimental technique was developed to investigate the eddy-current distribution in any conductive network through which a uniform alternating magnetic flux passes. The eddy-current distribution for an isotropic section was first obtained. An analogy to the laminated-core section from the point of view of conductivity was effected using a differential wire network whose resistivity in one direction was of the order of 10^4 times that in the perpendicular direction. The eddy-current distribution in such a network under an alternating magnetic field was found to confirm the theoretical calculations for core sections with and without interlaminar short-circuits.

LIST OF SYMBOLS

P = Sum of eddy-current loss in individual laminations per unit length of core.
P_λ = Interlaminar eddy-current loss per unit length of core.
B_0 = Maximum flux density assumed uniform in the section.
Φ_0 = Flux corresponding to B_0.
ω = Angular frequency.
J = Interlaminar eddy-current density.
ρ = Resistivity of magnetic material.
γ = Interlaminar resistivity.
γ/ρ = Resistivity ratio.
t = Thickness of lamination.
b = Width of lamination.
h = Depth of core section.
l = Length of core.
n = Number of laminations in core.
(The above are in M.K.S. units unless otherwise stated.)

(1) INTRODUCTION

When a rotating (or alternating) magnetic field is applied to a laminated core, core losses are set up consisting of hysteresis loss and the sum of eddy-current losses in individual laminations. On the assumption that the insulation resistance between adjacent laminations is infinite, it is generally considered that there is no interlaminar eddy current present in the core. In practice, it is often found that this is not the case and the interlaminar resistance mainly depends on the type of insulation on the laminations. The interlaminar resistance for any particular type of insulation was successively investigated by Franklin,[1] Beiler and Schmidt[2] and Taylor.[3] Using different methods of measuring interlaminar resistance, all these investigators came to the conclusion that it was essentially a statistical problem. Taylor also discovered that, for the same laminated core, the interlaminar resistance varied with a change of either pressure or temperature. It is reasonable to assume, however, that with a uniform coating of insulation and uniform distribution of pressure of considerable magnitude, the interlaminar resistivity can be taken as reasonably constant for any particular core which is free from burrs. It was on this assumption that Bewley and Poritsky[4] in 1937 presented their rigorous solution for the stray eddy-current loss derived from Maxwell equations. Barton[5] in 1944, on the other hand, derived an approximate expression for the interlaminar resistance in ohms per square centimetre per lamination for a given ratio of stray eddy-current loss to core loss. His main consideration was the effect of the size of core section on the stray eddy-current loss. In the case of f.h.p. motor cores whose lamination insulation often depends on a coat of oxide, the comparatively low interlaminar resistivity becomes the dominating factor. A preliminary investigation on the interlaminar resistance of various cores led the authors to make a more thorough study of the nature of stray eddy currents in a laminated motor core which may also be subjected to interlaminar short-circuiting paths.

(2) THEORETICAL CONSIDERATIONS

(2.1) Eddy-Current Loss in Individual Laminations

To compare the magnitude of the stray eddy-current loss with the eddy-current loss in individual laminations, it is necessary to state the latter in M.K.S. units, as derived by Carter:[6]

$$P = \frac{nbt^3 B_0^2 \omega^2}{24\rho} \text{ watts} \quad . \quad . \quad . \quad . \quad . \quad (1)$$

on the following assumptions:

(*a*) The flux varies sinusoidally.
(*b*) The width of the plate is very great compared with its thickness.
(*c*) The effect of the eddy currents in modifying the distribution of magnetic flux may be neglected.

(2.2) Network Analogy of Core Section

The cross-section of practically all parts of any magnetic circuit of an electrical machine can be represented by a rectangle as in Fig. 1. Taking the axis YY at the mid-point and perpendicular to each lamination, and assuming that $\gamma \gg \rho$, we see that the *IR* drops in the x-direction can be neglected compared with those in the y-direction. Also, as a result of symmetry,

Correspondence on Monographs is invited for consideration with a view to publication.
The paper is Report Ref. Z/T127 of the British Electrical and Allied Industries Research Association.
Dr. Jones and Dr. Leung were in the Department of Electrical Engineering, University of Leeds. Dr. Jones is now with the Brush Electrical Engineering Co. Ltd., and Dr. Leung is in the Electrical Engineering Department, University of Hong Kong.

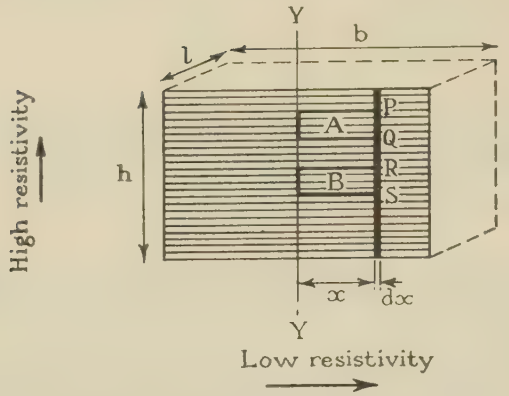

Fig. 1.—Laminated core section.

there is no current along the axis YY. To investigate the variation of current density along a column parallel to, and at a distance x from, YY, let us consider the induced e.m.f. and *IR* drops in two chosen identical rectangular loops A and B. With equal areas and uniform flux distribution, the induced e.m.f. of loop A must be equal to that of loop B. Since the *IR* drops of three sides in each loop are negligible, the *IR* drops in PQ (loop A) and in RS (loop B) must each be equal to the induced e.m.f. of either loop.

It follows that the current density along any column parallel to the YY axis is constant. Hence, it can be deduced that no current is accumulated at (or taken away from) the column, and therefore only the top and the bottom wires will carry any horizontal current.

(2.3) Interlaminar Eddy-Current Density

Consider a single vertical column at x_1 and another at x_2, connected at their ends by two wires as shown in Fig. 2. The

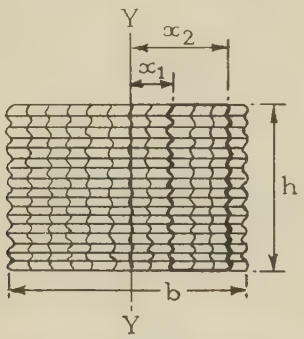

Fig. 2.—Resistance network.

r.m.s. value of the e.m.f. induced in the circuit is given by $[(x_2 - x_1)/b][\omega\Phi_0/\sqrt{2}]$, but the *IR* drops in high-resistance columns at x_1 and x_2 are respectively $\gamma h J_1$ and $\gamma h J_2$, where J_1 and J_2 are the current densities at column x_1 and column x_2.

Hence we have

$$\frac{x_2 - x_1}{b}\frac{\omega\Phi_0}{\sqrt{2}} = \gamma h(J_2 - J_1) \quad . \quad . \quad . \quad . \quad (2)$$

or

$$\frac{J_2 - J_1}{x_2 - x_1} = \frac{\omega\Phi_0}{\sqrt{2}}\frac{l}{bh\gamma} \quad . \quad . \quad . \quad . \quad . \quad (3)$$

Eqn. (3) shows that the variation of current density is linear across the width of the section. It follows that, at any instant of time, the interlaminar eddy-current density varies linearly

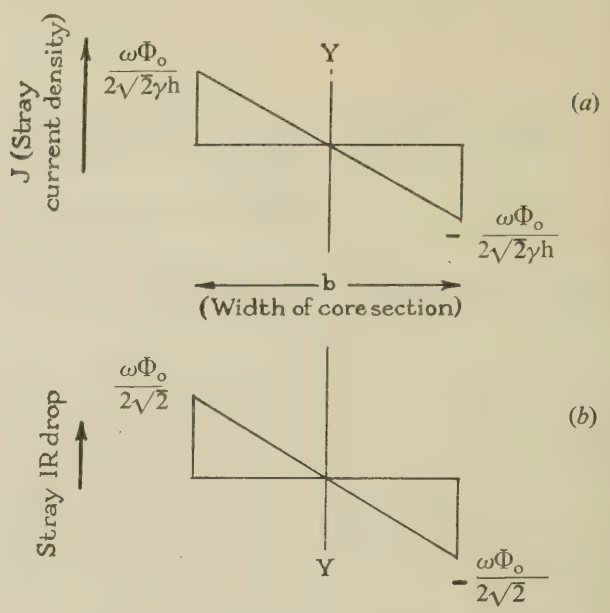

Fig. 3.—Variation of interlaminar current density.
(*a*) Stray eddy-current density across width of section.
(*b*) Stray *IR* drop across width of section.

with x so that its magnitude increases from zero at $x = 0$ to a positive maximum at $x = b/2$ and a negative maximum at $x = -b/2$. The linear variation of interlaminar current density across the width of the core section is illustrated in Fig. 3.

(2.4) Interlaminar Eddy-Current Loss

Referring to Fig. 1, the *IR* drop of an interlaminar column at a distance x from the centre-line is $(\omega\Phi_0/2\sqrt{2})(x/b\sqrt{2})$.

$$\text{Loss in column} = \left(\frac{\omega\Phi_0 x}{\sqrt{2}b}\right)^2 \frac{\delta x}{\gamma h}$$

$$\text{Total loss in core of unit length} = 2\int_0^{b/2} \frac{\omega^2\Phi_0^2}{2b^2\gamma h}x^2 dx$$

$$= \frac{\omega^2\Phi_0^2 b}{24\gamma h} \quad . \quad . \quad . \quad . \quad . \quad (4)$$

(2.5) Additional Eddy-Current Loss in End Laminations

The current distribution in the top (or bottom) lamination is shown in Fig. 4. At any instant, consider that current is

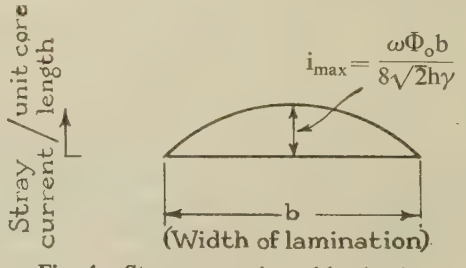

Fig. 4.—Stray current in end lamination.

collected by the lamination along the left-hand half and emitted from it along the right-hand half. The distribution of inter-laminar current density shows that the rate of collection (or emission) of current by the lamination is proportional to the

distance from the centre of the lamination, i.e. current in an end lamination is given by

$$\frac{di}{dx} = kx \quad . \quad . \quad . \quad . \quad . \quad . \quad . \quad . \quad (5)$$

When $x = 0$, $di/dx = 0$ and $i = \omega\Phi_0 b/8\sqrt{2\gamma h}$ (i.e. the summation of all interlaminar currents on either side of the centre-line of section). When $x = b/2$, $i = 0$.

Solving eqn. (5) we get,

$$i = \frac{\omega\Phi_0}{2\sqrt{2h\gamma}}\left(\frac{b}{4} - \frac{x^2}{b}\right) \quad . \quad . \quad . \quad . \quad . \quad . \quad . \quad (6)$$

$$i^2 = \frac{\omega^2\Phi_0^2}{8h^2\gamma^2}\left(\frac{b^2}{16} - \frac{x^2}{2} + \frac{x^4}{b^2}\right)$$

The I^2R loss in the top lamination is thus

$$2\int_0^{b/2} \frac{\omega^2\Phi_0^2\rho}{8h^2\gamma^2 t}\left(\frac{b^2}{16} - \frac{x^2}{2} + \frac{x^4}{b^2}\right)dx = \frac{\omega^2\Phi_0^2\rho b^3}{240\gamma^2h^2t}$$

and the total loss in both end laminations $= \dfrac{\omega^2\Phi_0^2\rho b^3}{120\gamma^2h^2t}$ . . (7)

Comparing the eddy-current losses in each lamination with the stray eddy-current loss obtained above:

$$\text{Total stray loss, } P_\lambda = \frac{\omega^2\Phi_0^2 b}{24\gamma h}\left(1 + \frac{\rho b^2}{5\gamma ht}\right).$$

From eqn. (1), legitimate eddy-current loss

$$P = \frac{nbt^3B_0^2\omega^2}{24\rho} \text{ or } \frac{\omega^2\Phi_0^2 t}{24\rho bn}$$

Therefore, the ratio of stray eddy-current loss to legitimate eddy-current loss is given by

$$\frac{P_\lambda}{P} = \frac{nb^2}{ht}\left[\frac{\rho}{\gamma} + \frac{b^2}{5ht}\left(\frac{\rho}{\gamma}\right)^2\right] \quad . \quad . \quad . \quad . \quad (8)$$

It can be seen that the ratio of stray eddy-current loss to the legitimate eddy-current loss in a laminated core is in the form of a quadratic equation with the inverse resistivity ratio, ρ/γ, as the independent variable. In the simplified form we can write

$$\frac{P_\lambda}{P} = m\left(\frac{\rho}{\gamma}\right) + n\left(\frac{\rho}{\gamma}\right)^2$$

where m and n are constants whose values depend on the dimensions of the core section. The term containing the square of the inverse resistivity ratio is relatively small since the ratio is usually not less than 10^{-4}.

It can be seen from the derived expressions that the stray eddy-current loss is critically affected by both the width of the core section and the resistivity ratio. In general, the resistivity ratio for fractional-horsepower-motor cores is much less than that encountered in large electrical machinery or transformer cores. Hence an appreciable amount of stray eddy-current loss could well be present in small motor cores despite the fact that the width of sections of magnetic paths in such cores is generally small.

Unlike the lamination eddy-current loss (and the hysteresis loss), which is evenly distributed over the entire core, the interlaminar eddy-current loss varies directly as the square of the distance from the centre plane of a magnetic path, reaching a maximum at the two sides. It is therefore less undesirable from the point of view of heat dissipation. Under adverse conditions with either low interlaminar resistance or large width of core section, the stray loss on the two end laminations may become several times that on each of the intermediate laminations.

(2.6) Limitation of Analogy

The expressions and equations so far obtained are valid on the basis of negligible IR drop in the direction along the planes of the laminations. In fact, we have found that a current flows in each of the two end laminations, thus producing an IR drop. The validity of the derived formulae on stray eddy current and its loss will hold good as long as the IR drops in the direction along the planes of the laminations do not exceed a small percentage of the maximum IR drop in the perpendicular direction.

From eqn. (6), the current in each end lamination is

$$i = \frac{\omega\Phi_0}{2\sqrt{2\gamma h}}\left(\frac{b}{4} - \frac{x^2}{b}\right)$$

and the IR drop across a small length, δx, at any position along the lamination is

$$\frac{\omega\Phi_0}{2\sqrt{2\gamma h}}\left(\frac{b}{4} - \frac{x^2}{b}\right)\frac{\rho}{t}\delta x$$

The total IR drop along half a lamination is

$$\int_0^{b/2} \frac{\rho}{t}\,\frac{\omega\Phi_0}{2\sqrt{2\gamma h}}\left(\frac{b}{4} - \frac{x^2}{b}\right)dx = \frac{\omega\Phi_0\rho b^2}{24\sqrt{2\gamma ht}} \quad . \quad . \quad (9)$$

The IR drop in one end lamination is

$$\frac{\omega\Phi_0\rho b^2}{12\sqrt{2\gamma ht}}$$

The percentage of end-lamination IR drop to maximum interlaminar IR drop at one edge is

$$\frac{b^2}{6ht}\,\frac{\rho}{\gamma} \times 100$$

Taking the worst case encountered in f.h.p. motors to be $b^2/6ht = 10$, the resistivity ratio can have a value as low as 1 000 for the IR drop in an end lamination to be equal to 1% of the interlaminar IR drop at the edge of the core section.

(2.7) Consideration of Interlaminar Short-Circuits

The short-circuits now considered are those formed by conductors such as rivets, welds, frames, shafts, etc., which are in contact with the laminated cores. Another type of interlaminar short-circuit is caused by a layer of burrs on the edges of the laminations caused by machining or punching. The core section which is short-circuited by the former type of interlaminar conductive path may be represented by a network of resistances [Fig. 5(*a*)]. Here the contact resistance between the conductor and the laminations is assumed to be negligible.[10] Similarly, it can be shown that the interlaminar IR drop and interlaminar current density, J, are as shown in Fig. 5(*b*) and (*c*). The distribution of interlaminar current density is such that the total current on the left of the short-circuit is equal to the sum of the current on the right of the short-circuit and that in the short-circuit.

(2.8) Stray Eddy-Current Loss in a Short-Circuited Section

It is assumed that the resistance of the short-circuit is negligible compared with that of the rest of the circuits in the interlaminar direction. Hence the loss in the short-circuit is not taken into account.

Let x_1 be the distance of the short-circuit from the centre-line of the core section as shown in Fig. 5(*a*).

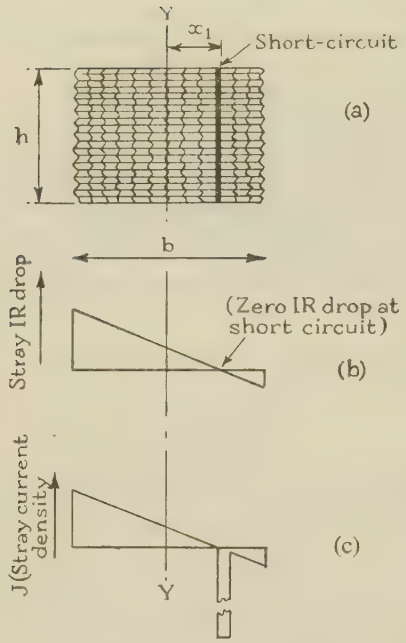

Fig. 5.—Network resistances, interlaminar *IR* drop and current density.

(*a*) Short-circuited core section.
(*b*) Stray *IR* drop across width of section.
(*c*) Stray current density across width of section.

By reasoning similar to that in Section 2.4, it can be shown that the eddy-current loss

$$P_\lambda = \frac{(\omega\Phi_0)^2}{6hb^2\gamma}\left[\left(\frac{b}{2}+x_1\right)^3+\left(\frac{b}{2}-x_1\right)^3\right] \quad . \quad . \quad (10)$$

When the short-circuit is at the edge of the section i.e. $x_1 = \pm b/2$,

$$P_\lambda = \frac{(\omega\Phi_0)^2 b}{6h\gamma} \quad . \quad . \quad . \quad . \quad . \quad (11)$$

The stray eddy-current loss is here at its maximum value, being four times what it was when there was no short-circuit in the section.

(3) EXPERIMENTAL INVESTIGATIONS

The object of the following experiments was to obtain the eddy-current distribution (both in magnitude and in direction) in a conductive section which was traversed by uniform alternating magnetic flux. The magnetic field was provided by an electromagnet constructed with an air-gap sufficiently large and regular for the purpose. The conductive section, which was in the form of a sheet, was placed in the air-gap and the uniformity of the magnetic field checked. Since any measured voltage from the conductive sheet was the difference between the induced e.m.f. and the eddy *IR* drop between the two points, it is necessary to interpret the voltage readings in terms of the eddy *IR* drops from which eddy-current densities may be deduced. This is explained in Section 7.

(3.1) Eddy Current in an Isotropic Section

The first investigation of the distribution of eddy-current density was carried out on an isotropic section, which was in the form of a thin sheet of aluminium. Since this was the first experiment on the measurement of *IR* drops using the new technique, it was felt that some means of checking the results was desirable. The authors have shown elsewhere[9] that the eddy-current densities in the two perpendicular directions of an isotropic section are given by

$$\left.\begin{aligned} J_x &= \frac{j\omega}{\pi\rho}\sum_{m=1,3,5..}^{\infty}\sum_{n=1,3,5..}^{\infty}\frac{\frac{n}{h}a_{mn}}{\left(\frac{m}{b}\right)^2+\left(\frac{n}{h}\right)^2} \times \cos\frac{m\pi x}{b}\sin\frac{n\pi y}{h} \\ J_y &= \frac{-j\omega}{\pi\rho}\sum_{m=1,3,5..}^{\infty}\sum_{n=1,3,5..}^{\infty}\frac{\frac{m}{b}a_{mn}}{\left(\frac{m}{b}\right)^2+\left(\frac{n}{h}\right)^2} \times \sin\frac{m\pi x}{b}\cos\frac{n\pi y}{h} \end{aligned}\right\} \quad . \quad (12)$$

(3.1.1) Apparatus and Measurement Technique.

Briefly, the apparatus consisted of an electromagnet with a square cross-section (4 × 4 in) and a ¾ in air-gap. The aluminium sheet was secured against one side of the air-gap in a central position. The *IR* drops of the aluminium sheet were measured by a special voltage-measurement probe (Fig. 6)

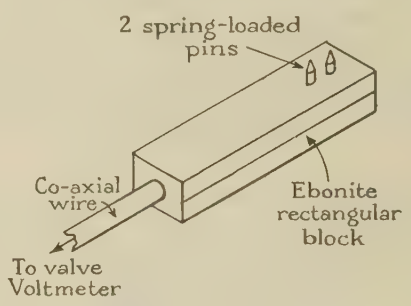

Fig. 6.—Probe.

which was connected to a precision valve voltmeter through coaxial wires. The magnitude and direction of the eddy-current density at any given point could be deduced from the measurement of *IR* drops at two points (represented by the pins) placed equidistant on either side of the particular point, and in two perpendicular directions in turn.

A graphical representation of the results is given in Fig. 7(*a*). From the relation $V = Jh\rho$, and taking the resistivity of aluminium at the prevailing temperature as $3 \times 10^{-8}\,\Omega$-m, the eddy-current density distribution of the isotropic conductive section is deduced and given in Fig. 7(*b*). It can readily be seen from eqn. (12) that the experimental eddy-current density distribution confirms the theory.

(3.2) Eddy Current in an Anisotropic Section

To investigate the stray eddy current in a laminated core section, it was proposed to perform an experiment using the apparatus and method of the preceding investigation. In order to show that the theoretical assumptions were justified for the worst case, i.e. oxide-coated cores, a conductive sheet with a resistivity ratio of the order of 10^4 was required.

(3.2.1) Differential Network.

Preliminary attempts were made to construct a rectangular wire-mesh network with two types of wire, of different resistivities, in two perpendicular directions. The first difficulty

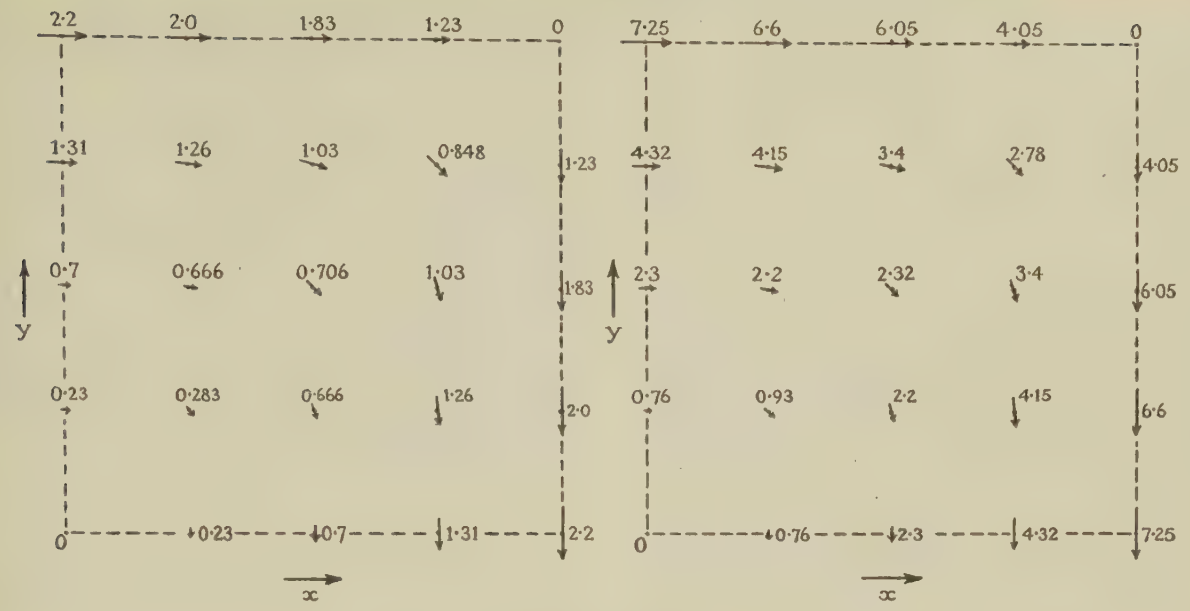

Fig. 7.—Isotropic section.
(*a*) Distribution of *IR* drop/cm in first quadrant (mV).
(*b*) Distribution of eddy-current density in first quadrant (A/mm²).

was to weave metal wires by hand with uniformity since no such wire meshes could be obtained commercially. The second difficulty lay in the choice of the two conductive materials whose resistivity ratio had to be as high as 10^4. The problem was eventually solved by using a manufactured wire cloth woven with cotton threads in one direction and steel wires in the perpendicular direction.

The resistivity ratio of such a sheet of cloth would be infinity since the cotton threads were perfect insulators. The resistivities of various coating materials and paints were investigated in the hope of finding a suitable coating to apply on the wire cloth, and a suitable lead paint was selected.

To have a reasonably even layer of paint on the wire cloth, it was necessary to put a number of coatings of diluted paint on both sides of the sheet. Care was taken not to bend the painted sheet to prevent any cracking of the coating. The actual resistivity ratio of the painted wire cloth could be varied to some extent by the thickness of the paint applied. The specimen on test was found to have a resistivity ratio of $1{\cdot}7 \times 10^4$, which was sufficiently near the required value.

(3.2.2) **Technique and Results.**

For the purpose of comparison of *IR* drops, the differential network was made with the same dimensions as the aluminium specimen in the previous test. Also, the flux density was kept constant at the same value as that in the last test. Care was taken not to damage the paintwork of the specimen by the two pins of the probe as a result of excessive pressure. As might be expected, only the *IR* drops along the direction of the cotton threads were measurable, since the *IR* drops in the direction of the steel wires were of negligible magnitude owing to the low resistivity in this direction. The eddy-current densities are given graphically in Fig. 8. The *IR* drops of a single turn with the dimensions of the periphery of the section were calculated for comparison. It is of interest to note that the magnitude of the *IR* drop along the outer edge in the direction of high resistance was approximately twice that of the *IR* drops in the turn. This can readily be deduced from the theoretical consideration of the stray eddy current given earlier. Apart from

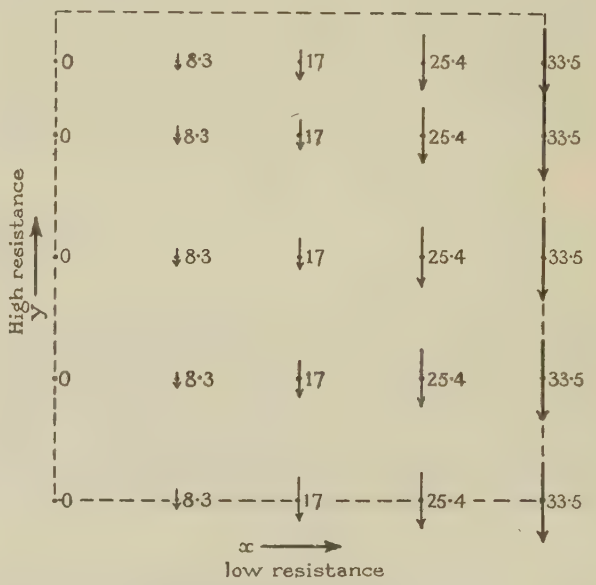

Fig. 8.—Anisotropic section.
Distribution of average eddy-current density in first quadrant (A/m²).

the dropping-off of the *IR* drops towards the two edges of the network (to be explained later), the variation of *IR* drops along any particular line in the direction of high resistance is up to 4%. Considering that the surface of the woven wire cloth was not perfectly smooth and flat, the accuracy obtained in the test was quite satisfactory.

(3.3) **Short-Circuited Differential Network**

Many electrical-machine cores are subjected to one of the following manufacturing processes: welding, riveting, bolting, grinding, machining, etc. It may be considered that each of these operations forms an interlaminar short-circuiting path in the core section. In the theoretical considerations it is

deduced that the distribution of *IR* drops will be modified according to the position of this short-circuiting path. The same apparatus was again used to investigate experimentally the eddy-current distribution in a differential network with one short-circuit present. The short-circuit in the wire cloth was effected by carefully pulling out one of the cotton threads and replacing it with a tinned copper wire of the same diameter. To ensure good electrical contact, the inserted wire was woven in position with its ends spot-soldered to the two end steel wires before the paint was applied. Three short-circuited differential networks were made such that the short-circuits in the networks were respectively (*a*) at the centre, (*b*) at one edge, and (*c*) half-way between the centre and the edge. The eddy-current distribution of the network short-circuited at the centre was found to be practically the same as that of an unshort-circuited network; the measured *IR* drops of the other two networks are given in Fig. 9, (*a*) and (*b*). The above results

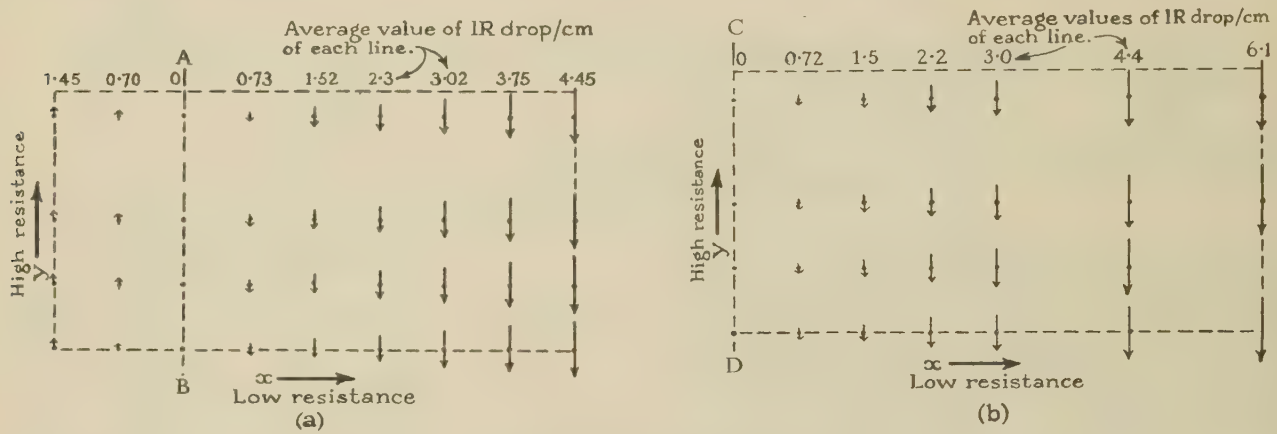

Fig. 9.—Short-circuited section.

Distribution of *IR* drop/cm in half-section (mV).
(*a*) Short-circuit at A–B.
(*b*) Short-circuit at C–D.

generally agree with the theoretical deductions [Fig. 5(*b*)], thus confirming the belief that any short-circuit at the centre of a core section will have the minimum effect on the stray core loss. Further investigations on current distributions in differential networks which had more than one short-circuit were also made. The results were found to be quite arbitrary according to the relative magnitudes of resistances between the steel wires and the short-circuiting wires and therefore of no value.

(4) CONCLUSIONS

(*a*) The network analogy for the laminated core section enables us to obtain a clear picture of the distribution of stray eddy currents in a core.

(*b*) The validity of the theoretical considerations is based on the assumptions that there is a constant resistivity in the interlaminar direction and that this resistivity is much greater than that of the core material. The first assumption has been justified by the results of a number of preliminary tests on interlaminar resistance.[10] The second assumption is justified by the fact that there is always an inherent natural oxide film on steel surfaces and thus a contact resistance always exists between any two adjacent laminations.

(*c*) The ratio of stray eddy-current loss to legitimate eddy-current loss is seen to be a function of the resistivity ratio. For large values of this ratio, the eddy-current loss ratio is inversely proportional to the resistivity ratio.

(*d*) For a machine with an appreciable amount of stray eddy-current loss, the distribution of stray eddy current should b taken into account for any assessment of temperature rise o the core, as there is a concentration of current in the oute laminations.

(*e*) The effect of a short-circuit across a laminated core i seen to alter the distribution of eddy-current densities and thu to increase the stray eddy-current loss. The most favourabl position for such a short-circuit is at the centre of the cor section, where its effect on stray eddy-current loss is minimum The formulae given for stray eddy-current loss in a short circuited core are valid only for core sections with one inter laminar short-circuited path. With more than one short-circui the interlaminar resistance plays little part in the resultant loss

(*f*) The experimental technique of measuring the *IR* drops a various positions of a conductive section serves as an excelle check for the theoretical results of eddy-current distributions i both isotropic and anisotropic sections. The technique will b particularly useful for irregular core sections whose stray eddy current density and loss are difficult to assess theoretically.

(*g*) The use of painted wire cloths as differential network was very satisfactory for this purpose. The uniformity of the thickness of paint was an important factor. The result i Fig. 9(*a*) shows that a decrease of *IR* drop occurred along the top edge of the section. It was subsequently found that thi was due to the thickness of paint being appreciably greate along the edge.

(5) ACKNOWLEDGMENTS

This report formed part of the authors' work under a researc programme of the British Electrical and Allied Industrie Research Association on stray eddy-current losses in f.h.p motors. One of the authors gratefully acknowledges the receip of a maintenance grant from the Association during the perio of compilation.

The authors are indebted to Professor G. W. Carter for hi valuable advice and useful suggestions and for his permission t use the facilities of the Electrical Engineering Laboratory o Leeds University.

(6) REFERENCES

(1) FRANKLIN, R. F.: 'Measurement and Control of Inter laminar Resistance of Laminated Magnetic Cores' *Bulletin of the American Society for Testing Materials* January, 1947, p. 57.

(2) BEILER, A. C., and SCHMIDT, P. L.: 'Interlaminar Eddy-Current Loss in Laminated Cores', *Transactions of the American I.E.E.*, 1947, p. 872.
(3) TAYLOR, E. D.: 'The Measurement of Interlaminar Resistance of Varnish-Insulated Silicon-Steel Sheet for Large Electrical Machines', *Proceedings I.E.E.*, Paper No. 1019, June, 1951 (**98**, II, p. 377).
(4) BEWLEY, L. V., and PORITSKY, H.: 'Intersheet Eddy-Current Loss in Laminated Cores', *Transactions of the American I.E.E.*, 1937, **56**, p. 344.
(5) BARTON, J. P.: 'Interlaminar Resistance', *ibid.*, 1944, **63**, p. 670.
(6) CARTER, G. W.: 'The Electromagnetic Field in its Engineering Aspects' (Longmans, Green, 1954), p. 200.
(7) JONES, D. A.: 'Variation of Interlaminar Losses in Electrical Machines', *Electrical Energy*, 1958, **2**, p. 137.
(8) LEUNG, W. S.: 'Stray Losses in Laminated Cores with Particular Reference to F.H.P. Motors' (E.R.A. Report Ref. Z/T120; 1958).
(9) JONES, D. A., and LEUNG, W. S.: 'Stray Eddy-Current Losses in Induction Motors', *Hawker-Siddeley Technical Journal*, November, 1960, **2**, p. 21.
(10) LEUNG, W. S.: 'An Investigation of Stray Core Losses in Electrical Machines' (University of Leeds Thesis, 1959).

(7) APPENDIX

(7.1) Voltage Measurements in Flux-Enclosing Sections

Consider a conductive section traversed by a sinusoidal magnetic field. An e.m.f. is induced in the section, in which eddy current will flow. When the voltage between any two points in a flux-enclosing network is measured, the voltmeter and its leads inevitably present themselves as an addition to the network. Referring to Fig. 10, let P and Q be any two points in such a section ABCD. In order to obtain the eddy current along PQ, we connect P and Q to the voltmeter V. The loop PVQ is known as the voltage-measurement loop. It is evident that the reading on the voltmeter is the potential difference between the induced e.m.f. in the loop PVQ and the *IR* drop in the loop. Since there is no *IR* drop between P and V and between V and Q in this loop, the voltage reading is thus the potential difference between the induced e.m.f. of the loop and the *IR* drop in PQ as a result of the eddy current in the network.

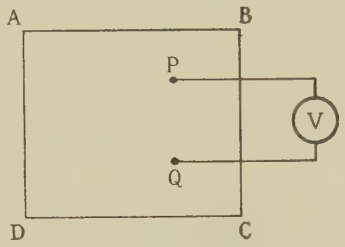

Fig. 10.—Voltage measurement.

In order to measure the *IR* drop directly between any two points in the network, there must be no induced e.m.f. in the voltage-measurement loop for the two points. For instance, if the *IR* drop between PQ is to be measured, the loop PVQ should be situated in such a way that it encloses no magnetic flux. Under these circumstances, the reading of the voltmeter will simply be the *IR* drop in PQ. The above deductions have been confirmed by the measurement of *IR* drops in chosen portions of a number of simple networks (in place of the conductive section) whose *IR* drops can readily be calculated for the purpose of comparison.

621.313.32.018.6

The Institution of Electrical Engineers
Monograph No. 454 S
June 1961

A HUNTING ANALYSIS OF A PERMANENT-MAGNET ALTERNATOR AND A SYNCHRONOUS MOTOR

By M. H. WALSHAW, B.Sc.(Eng.), Graduate, and J. W. LYNN, M.Sc., Ph.D., Associate Member.

(*The paper was first received* 17*th September*, 1960, *and in revised form* 28*th March*, 1961. *It was published as an* INSTITUTION MONOGRAPH *in June* 1961.)

SUMMARY

Little has hitherto been written about the transient analysis of interconnected salient-pole synchronous machines of comparable size, where infinite busbars cannot be assumed to exist.

The paper describes theoretical and practical work carried out on a simple power system of this type, in which a 60 kW permanent-magnet alternator supplies power to a synchronous motor. For analytical purposes the permanent-magnet alternator is shown to be equivalent to a conventional alternator with a constant field voltage. The measurement of the parameters of the machines is described and the steady-state performance of the interconnected system is predicted by Kron's method of analysis.

The hunting equations of the system are examined, and a frequency-response method involving Nyquist's stability criterion is used to predetermine the effects of armature resistance on the hunting stability of the system under various conditions of load and saturation. A digital computer is used to perform the calculations and the predicted results are found to agree well with those obtained experimentally from the actual system.

LIST OF SYMBOLS

v, V = Instantaneous voltages, V.
i = Instantaneous current, A.
R = Resistance, Ω.
X = Reactance, Ω.
L = Self-inductance, H.
$L(p)$ = Operational inductance, a function of p, H.
M = Mutual inductance, H.
τ = Time-constant, sec.
N = Equivalent turns of direct-axis armature winding.
B = Magnetic flux density, Wb/m^2.
H = Magnetizing force, AT/m.
Φ = Magnetic flux, Wb.
ψ = Magnetic flux-linkages, Wb-T.
Λ = Permeance, Wb/AT.
μ_0 = Permeability of free space = $4\pi \times 10^{-7}$ H/m.
μ_r = Recoil permeability.
l = Length of magnetic circuit, m.
a = Cross-sectional area of magnets, m^2.
G = Torque constant of fluxmeter, weber-turns per division.
θ = Angle defining rotor position, electrical radians.
δ = Angle between the rotors of two interconnected synchronous machines, electrical radians.
$p\theta$ = Electrical rotor speed, rad/sec.
P_m = Mechanical power, W.
T = Torque, N-m.
I = Moment of inertia, kg-m^2.
n = Number of pairs of poles.
t = Time, sec.
p = Differential operator, d/dt.
ω = Synchronous angular frequency, rad/sec.
h = Per-unit hunting frequency.
$\boldsymbol{p}$ = Generalized force matrix (voltage and torque).
$\boldsymbol{v}$ = Voltage matrix.
$\boldsymbol{i}$ = Current matrix.
$\boldsymbol{R}$ = Resistance matrix.
$\boldsymbol{L}$ = Inductance matrix.
$\boldsymbol{G}$ = Torque matrix.
$\boldsymbol{Z}$ = Transient-impedance matrix.
$\boldsymbol{\bar{Z}}$ = Transient-motional-impedance matrix.
$\boldsymbol{C}$ = Connection matrix.

Superscripts and Subscripts.

l = Leakage magnetic circuit.
g = Gap or useful magnetic circuit.
ds = Direct-axis stator axis.
de = Direct-axis eddy-current axis.
kd = Permanent-magnet alternator damper axis.
f = Field axis.
dr, d = Direct-axis armature axis.
qr, q = Quadrature-axis armature axis.
qe = Quadrature-axis eddy-current axis.
s = Mechanical reference axis.
1 = Synchronous motor
2 = Permanent-magnet alternator
} when interconnected.

(1) INTRODUCTION

The steady-state and dynamic analyses of salient-pole synchronous machines connected to infinite busbars have been adequately dealt with in the literature.[1, 2, 3] Less has been written, however, about the analysis of such machines when interconnected, and it has been usual to consider steady-state conditions[4] or to represent the machines by a constant voltage behind transient reactance with zero saliency.[5, 6] In some power systems, such as those in aircraft where the resistances and reactances are relatively higher and the inertias lower, a fresh analysis may be required to take account of resistance and of the saliency and inertia of the several machines. The subject of the paper is an analysis of this type.

The paper describes theoretical and practical work carried out on an experimental aircraft power system consisting of a 60 kW 3-phase permanent-magnet alternator supplying a synchronous motor. The descriptive parameters of the two machines are measured, and these enable the steady-state and hunting performances of the system to be predicted from the analysis. Experiments on the actual machines are then made to confirm the predicted results.

The increasingly exact analysis required of electrical machinery nowadays generally leads to the use of fictitious quantities to simplify the equations. Direct and quadrature components are used in this paper, but there still remains the problem of interconnecting the machines. To do this use is made of the methods of tensor analysis developed by Kron.[7, 8, 9] Tensor analysis deals with transformations between the sets of variables that

Correspondence on Monographs is invited for consideration with a view to publication.
Mr. Walshaw is at the Royal Aircraft Establishment, Farnborough, and was attached to the University of Liverpool. Dr. Lynn is in the Electrical Engineering Department, University of Liverpool.

may be used to describe a system,[10] and gives rules for transforming functions of the variables such as voltages and impedances. Transformations may either change the reference axes of a system from one set to another or alter the configuration of the system by interconnections.

Kron has devised a generalized 'primitive electrical machine', in which the armature quantities are expressed along direct and quadrature axes, and whose voltage and torque equations are known.[2, 8, 9] The equations of two interconnected salient-pole synchronous machines have then been obtained by Kron[7] from those of the primitive machine by means of a suitable transformation. His equations are used here to predict the steady-state load characteristics of the experimental system, and the armature resistance necessary to cause hunting.

Frequency-response methods have recently come into prominence for synchronous-machine problems.[11, 12, 24] These prove to be a valuable means of expressing the operational inductances of machines with solid field systems and of predetermining system stability by means of Nyquist's criterion.

The permanent-magnet (p.m.) alternator used in the experimental work was designed and built at the Royal Aircraft Establishment to investigate the use of such machines for power generation in aircraft. P.M. alternators may offer advantages over conventional wound-field machines, but their design, operation and control present many difficulties. Most of the information published so far on p.m. alternators has been concerned with these problems,[13, 14, 15] and a general transient analysis is therefore first derived to relate the machine to the conventional wound-field alternator, and thence to Kron's primitive machine.

(2) DESCRIPTION OF THE TWO SYNCHRONOUS MACHINES

The p.m. alternator was designed to generate a 3-phase output of 60 kW at 208 V, 160 A/phase, 400 c/s and 24 000 r.p.m., but for mechanical reasons tests were carried out only at speeds up to 9 000 r.p.m. The rotor has two poles and contains two permanent magnets made of Columax[16] arranged side by side along the axis. Its cross-section is shown in Fig. 1. Solid-steel pole-

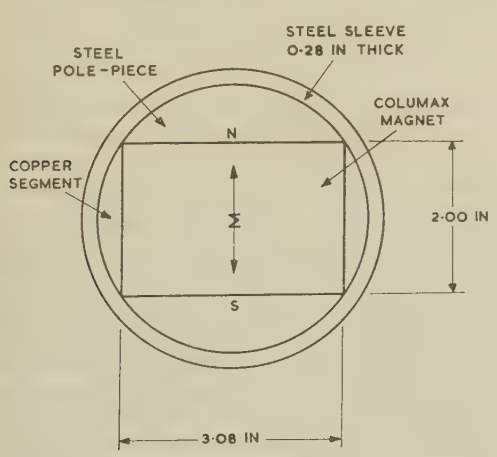

Fig. 1.—Cross-section through the rotor of the permanent-magnet alternator.

pieces are fitted, and the structure is held together by shrinking round it a steel sleeve. It is desirable to protect the magnets from the severely demagnetizing effects of transient armature currents, such as occur on sudden short-circuit. For this purpose a damper winding, in the form of a copper slug, is fitted round each magnet. The copper segments shown in Fig. 1 form part of this damper, and it is completed by copper discs fitted at the outer ends of the magnets and between them. The stator carries a conventional 3-phase star-connected winding.

The synchronous motor used in the interconnection tests was an aircraft alternator having a rated output of 12 kVA at 208 V, 400 c/s and 8 000 r.p.m. It had a conventional laminated rotating field-system, with six salient poles and three small damper bars set in each pole-face.

(3) ANALYSIS OF THE PERMANENT-MAGNET ALTERNATOR

(3.1) Permanent-Magnet Operation

The magnets of the p.m. alternator operate on the section of the B/H curve known as the demagnetization characteristic,[19] shown in Fig. 2. On removal from the magnetizer, the magnets

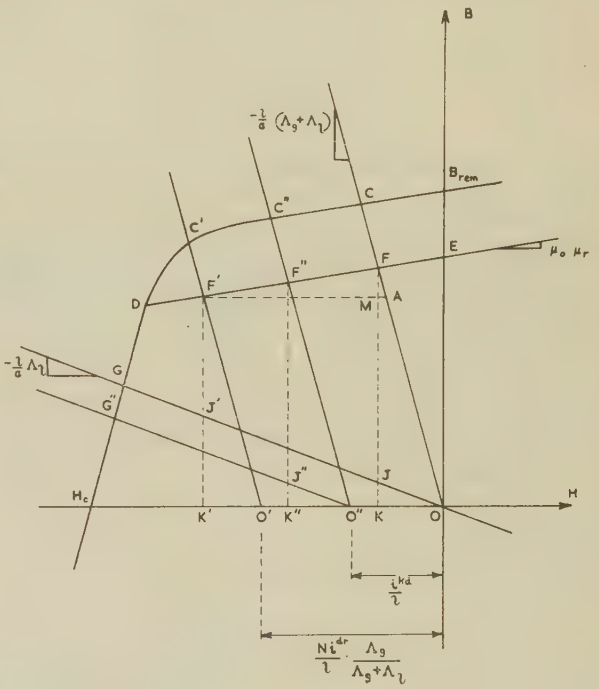

Fig. 2.—Permanent-magnet operating diagram.

operate at point C, and after stabilization to ensure consistent performance they work on a recoil loop such as DE, assumed to be a straight line. The working point on DE then depends upon the direct-axis currents, i^{dr} and i^{kd}, both of which are taken as positive when opposing the magnet.

Fig. 3 shows how the magnet flux, Φ, divides into leakage

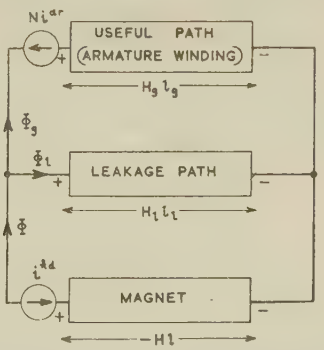

Fig. 3.—Magnetic circuit of the permanent-magnet alternator, showing m.m.f.s, magnetic potential drops and fluxes.

flux, Φ_l, and gap flux, Φ_g, which links the direct-axis armature winding, all leakage fluxes having been referred to the magnet terminals. Ni^{dr} and i^{kd} are the demagnetizing m.m.f.s set up in the useful and magnet paths respectively when currents flow.

(3.1.1) **Operating Condition on No-Load.**

Summing the magnetic potential drops in Fig. 3 when the currents are zero

$$Hl + H_g l_g = 0$$

$$Hl + H_l l_l = 0$$

Also

$$\Phi = Ba = \Phi_g + \Phi_l$$

$$= H_g l_g \Lambda_g + H_l l_l \Lambda_l$$

Therefore

$$B = -\frac{l}{a}(\Lambda_g + \Lambda_l)H \quad . \quad . \quad . \quad . \quad (1)$$

and

$$\frac{\Phi_l}{a} = H_l \frac{l_l}{a} \Lambda_l = -\frac{l}{a}\Lambda_l H \quad . \quad . \quad . \quad (2)$$

Eqn. (1) gives the straight line OC (Fig. 2), called the total unit permeance line. The magnet must operate on this line and also on the recoil loop, DE, so that F must be the no-load working point. Eqn. (2) gives the component of magnet flux density which contributes the leakage flux, and is the equation of the straight line OG, called the leakage unit permeance line. Hence the portion JK of the total magnet flux density, FK, contributes the leakage flux, while FJ contributes the useful flux.

(3.1.2) **Operating Condition with Direct-Axis Armature Current.**

From Fig. 3, equating magnetic potential drops to m.m.f.s,

$$Hl + H_g l_g = -Ni^{dr}$$

$$Hl + H_l l_l = 0$$

whence

$$\Phi = -(Ni^{dr} + Hl)\Lambda_g - Hl\Lambda_l$$

or

$$B = -\frac{l}{a}(\Lambda_g + \Lambda_l)\left[H + \frac{Ni^{dr}}{l}\frac{\Lambda_g}{(\Lambda_g + \Lambda_l)}\right] \quad (3)$$

and

$$\frac{\Phi_l}{a} = -\frac{l}{a}\Lambda_l H \quad . \quad . \quad . \quad . \quad . \quad . \quad . \quad (4)$$

The current, i^{dr}, has caused the total unit permeance line to shift to the left by an amount $Ni^{dr}\Lambda_g/l(\Lambda_g + \Lambda_l)$ to a new position O′C′. The leakage unit permeance line remains unchanged, so that the leakage flux density in the magnet is J′K′ and the useful flux density F′J′.

(3.1.3) **Operating Condition with Damper Current.**

Again from Fig. 3,

$$Hl + H_g l_g = -i^{kd}$$

$$Hl + H_l l_l = -i^{kd}$$

whence

$$B = -\frac{l}{a}(\Lambda_g + \Lambda_l)\left(H + \frac{i^{kd}}{l}\right) \quad . \quad . \quad (5)$$

and

$$\frac{\Phi_l}{a} = -\frac{l}{a}\Lambda_l\left(H + \frac{i^{kd}}{l}\right) \quad . \quad . \quad . \quad . \quad (6)$$

Eqns. (5) and (6) give the lines O″C″ and O″G″, both of which have been shifted to the left by an amount i^{kd}/l. The leakage flux density in the magnet is now J″K″ and the useful flux density F″J″.

(3.2) **Flux-Linkage and Voltage Equations**

On no-load, the useful flux density in the magnet is B_0, equal to FJ, but it is reduced by an amount

$$kNi^{dr}\Lambda_g(\mu_0\mu_r + l\Lambda_l/a)/l(\Lambda_g + \Lambda_l)$$

when i^{dr} flows, and by an amount $ki^{kd}\mu_0\mu_r\Lambda_g/l(\Lambda_g + \Lambda_l)$ when i^{kd} flows, where k is the ratio $F'M/F'A$. The resultant useful flux density in the magnet is therefore

$$B_g = B_0 - \frac{kN\Lambda_g}{l(\Lambda_g + \Lambda_l)}\left(\mu_0\mu_r + \frac{l}{a}\Lambda_l\right)i^{dr} - \frac{k\mu_0\mu_r\Lambda_g}{l(\Lambda_g + \Lambda_l)}i^{kd}$$

Hence the flux linkages with the direct-axis armature winding are

$$\psi_{dr} = -B_g aN + (\text{armature leakage flux linkages})$$

or

$$\psi_{dr} = -B_0 aN + \frac{kaN^2\Lambda_g}{l(\Lambda_g + \Lambda_l)}\left(\mu_0\mu_r + \frac{l}{a}\Lambda_l\right)i^{dr} + \frac{kaN\mu_0\mu_r\Lambda_g}{l(\Lambda_g + \Lambda_l)}i^{kd} + L_{dl}i^{dr} \quad (7)$$

Similarly the flux linkages with the damper circuit are

$$\psi_{kd} = -Ba = -B_1 a + \frac{kaN\mu_0\mu_r\Lambda_g}{l(\Lambda_g + \Lambda_l)}i^{dr} + \frac{ka\mu_0\mu_r}{l}i^{kd} \quad (8)$$

where B_1 is the no-load magnet flux density, FK.

The coefficient of i^{kd} in eqn. (7) is the same as that of i^{dr} in eqn. (8), and is the mutual inductance, M_d, between dr and kd. The sum of the coefficients of i^{dr} in eqn. (7) is the total self inductance L_{dr}, and the coefficient of i^{kd} in eqn. (8) is the self-inductance L_{kd}. If L_{qr} is the self-inductance of the quadrature-axis armature winding, three flux-linkage equations can be written:

$$\left.\begin{aligned}\psi_{kd} &= -B_1 a + L_{kd}i^{kd} + M_d i^{dr}\\ \psi_{dr} &= -B_0 aN + M_d i^{kd} + L_{dr}i^{d}{}_{r}\\ \psi_{qr} &= L_{qr}i^{qr}\end{aligned}\right\} \quad . \quad . \quad (9)$$

If sinusoidal flux distribution is assumed, the following direct- and quadrature-axis voltage equations can be derived[8]:

$$\left.\begin{aligned}v_{kd} &= (R_{kd} + L_{kd}p)i^{kd} + M_d p i^{dr} = 0\\ v_{dr} &= M_d p i^{kd} + (R_r + L_{dr}p)i^{dr} + L_{qr}p\theta i^{qr}\\ v_{qr} &= B_0 aNp\theta - M_d p\theta i^{kd} - L_{dr}p\theta i^{dr} + (R_r + L_{qr}p)i^{qr}\end{aligned}\right\} (10)$$

The term $B_0 aNp\theta$ is the open-circuit generated e.m.f., V. Comparison of eqns. (10) with the field and armature equations of the conventional synchronous machine[1, 2, 8] shows that if i^{kd} is replaced by the field current the equations are of the same form, except that there is now zero applied voltage in the field equation, while an additional generated e.m.f., V, appears in the equation for v_{qr}. The permanent-magnet field system is therefore equivalent to a conventional field winding, of resistance R_{kd} and inductance L_{kd}, to which is connected a constant-voltage battery of zero internal impedance. The battery circulates a constant current i^f, which generates V, given by

$$V = M_d p\theta i^f \quad . \quad . \quad . \quad . \quad . \quad (11)$$

The voltage, V_f, of the battery must therefore be $R_{kd}i^f$. During transients an additional current will be induced in the circuit,

exactly equal to i^{kd}. Let i^{ds} be the instantaneous current in this equivalent, but fictitious, field winding. Then

$$i^{ds} = i^{kd} - i^{f} \text{ and } pi^{ds} = pi^{kd}.$$

Eqns. (10) can then be written in terms of i^{ds}, if $-V_f = -R_{kd}i$ is added to the first equation:

$$\left.\begin{aligned} -V_f &= (R_{kd} + L_{kd}p)i^{ds} + M_d p i^{dr} \\ v_{dr} &= M_d p i^{ds} + (R_r + L_{dr}p)i^{dr} + L_{qr}p\theta i^{qr} \\ v_{qr} &= -M_d p\theta i^{ds} - L_{dr}p\theta i^{dr} + (R_r + L_{qr}p)i^{qr} \end{aligned}\right\} \quad (12)$$

The solid parts of the field system provide abundant paths for eddy currents and can be represented formally by short-circuited windings *de* and *qe*. The voltage equations can then be put into a matrix form similar to that for the conventional machine[2, 7, 8, 9]:

$$\begin{array}{c} \\ de \\ ds \\ dr \\ qr \\ qe \end{array}\!\!\begin{bmatrix} 0 \\ -V_f \\ v_{dr} \\ v_{qr} \\ 0 \end{bmatrix} = \begin{array}{c} \begin{array}{ccccc} de & ds & dr & qr & qe \end{array} \\ \begin{bmatrix} R_{de} + L_{de}p & M_{ke}p & M_{de}p & 0 & 0 \\ M_{ke}p & R_{kd} + L_{kd}p & M_d p & 0 & 0 \\ M_{de}p & M_d p & R_r + L_{dr}p & L_{qr}p\theta & M_q p\theta \\ -M_{de}p\theta & -M_d p\theta & -L_{dr}p\theta & R_r + L_{qr}p & M_q p \\ 0 & 0 & 0 & M_q p & R_{qe} + L_{qe}p \end{bmatrix} \end{array} \begin{bmatrix} i^{de} \\ i^{ds} \\ i^{dr} \\ i^{qr} \\ i^{qe} \end{bmatrix} \quad . \quad . \quad . \quad . \quad (13)$$

(3.3) Elimination of Unwanted Currents

The currents in the equivalent eddy-current windings and in the damper circuit cannot in practice be measured, but can however be eliminated from eqn. (13) by partitioning[8] to give the following result:

$$\begin{array}{c} \\ d \\ q \end{array}\!\!\begin{bmatrix} v_d \\ v_q - V \end{bmatrix} = \begin{array}{c} \begin{array}{cc} d & q \end{array} \\ \begin{bmatrix} R + L_d(p)p & L_q(p)p\theta \\ -L_d(p)p\theta & R + L_q(p)p \end{bmatrix} \end{array} \begin{bmatrix} i^d \\ i^q \end{bmatrix} \quad (14)$$

The rotor (armature) suffix, *r*, has now been discarded as the stator (field) quantities have been eliminated.

The operational inductances $L(p)$ in eqn. (14) can be expressed approximately, for conventional synchronous machines at least, in terms of the time-constants[2] as

$$L_d(p) = L_d \frac{(1 + \tau'_d p)(1 + \tau''_d p)}{(1 + \tau'_{d0} p)(1 + \tau''_{d0} p)} \quad . \quad . \quad . \quad (15)$$

and

$$L_q(p) = L_q \frac{(1 + \tau''_q p)}{(1 + \tau''_{q0} p)} \quad . \quad . \quad . \quad . \quad . \quad . \quad (16)$$

Under balanced steady-state conditions, $p = 0$, and $L_d(p)$ and $L_q(p)$ reduce to the synchronous values L_d and L_q. Under conditions of sinusoidal variation in the direct and quadrature axes, $p = jh\omega$. $L_d(jh\omega)$ and $L_q(jh\omega)$ are then complex and can be plotted as frequency-response loci in the complex plane.[11] As the frequency tends to infinity, the inductances reduce to the real subtransient values L''_d and L''_q. Eqns. (15) and (16) give a semicircular form of frequency-response locus. In practice, however, the loci for the p.m. alternator may be distorted from this form because the distributed eddy-current paths cannot be accurately represented by an equivalent winding in each axis. As a result it is better to express the operational inductances of the p.m. alternator by measured frequency-response curves, rather than by analytical expressions with constant coefficients.

(3.4) Performance Equations

The voltage equations, (13), apply to all conditions and show that the p.m. alternator can be treated as a conventional machine with a constant and fixed field-excitation voltage. With this proviso, therefore, its electrical and mechanical performance equations are similar to those of the conventional machine.

(4) MEASUREMENT OF MACHINE PARAMETERS

(4.1) Parameters of the Permanent-Magnet Alternator

Although most of the parameters of p.m. machines can be calculated with reasonable accuracy,[15] it was decided to make actual measurements of $L_d(p)$, $L_q(p)$, R and I. The most important components of the operational inductances are the synchronous values and their variation with saturation.

(4.1.1) Synchronous Inductances, L_d and L_q.

Most of the tests[20] normally used for the measurement of synchronous inductance were inapplicable to the p.m. alternator because its field could not be switched off or varied, so the following alternative methods were used:

(*a*) *Steady-State 3-Phase Load Tests.*—A balanced 3-phase load of known magnitude was connected to the p.m. alternator, and the load angle was measured by means of a stroboscope triggered by the terminal voltage of the alternator. To ensure that the stroboscope fired at the same point in each cycle, as the magnitude of the terminal voltage varied, it was fed at a constant voltage by a voltage divider. The direct and quadrature components of voltage and current could then be calculated, enabling the synchronous inductances to be derived from the steady-state voltage equations. In order to reduce cross-saturation effects the load phase angle was adjusted so that the major part of the current was in the required axis. Measurements were made at frequencies of 75, 100 and 150c/s, but the results, plotted in Fig. 4, show no significant differences between these frequencies. The direct- and quadrature-axis currents shown in Fig. 4 were calculated from the 3-phase currents by the transformations of Lewis.[18]

(*b*) *Fluxmetric-Bridge Tests.*—The fluxmetric bridge is a method of measuring inductance under d.c. conditions by recording the change in flux linkages in an inductor when a direct current passing through it is changed. It can be used to measure the self-inductance of electrical machines and is carried out with the rotor stationary. The method has previously been described by several authors,[21, 22, 23] but their analyses do not take account of stray inductance in the ratio arms of the bridge, which can be troublesome when measuring low inductances.

The basic circuit is shown in Fig. 5. F is the fluxmeter, L_1 is the inductance to be measured, L_2, L_3, L_4 and L_f are the stray inductances, and I_1 and I_0 are the initial currents. It is shown in Section 10 that when the d.c. supply switch is opened, the deflection $\Delta\theta$ of the fluxmeter is given by

$$L_1 I_1 - L_3 I_0 + \frac{(R_1 + R_3)}{(R_2 + R_4)}(L_4 I_0 - L_2 I_1) = \left[1 + \frac{(R_1 + R_3)}{(R_2 + R_4)}\right] G\Delta\theta \quad (17)$$

The stray error terms can be reduced by making I_0 and

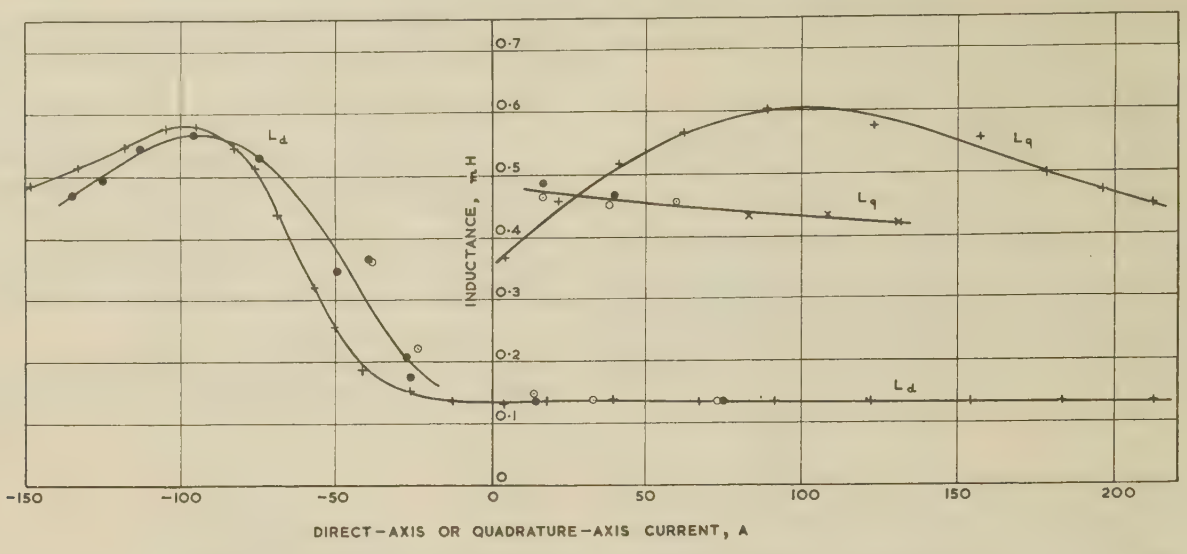

Fig. 4.—Synchronous inductances, L_d and L_q, of the permanent-magnet alternator.

+ Fluxmetric bridge test.
○ Load test at 75 c/s.
× Load test at 100 c/s.
● Load test at 150 c/s.

$(R_1 + R_3)/(R_2 + R_4)$ small. As the bridge is initially balanced like a Wheatstone bridge, this is equivalent to making the ratios R_1/R_3 $(= R_2/R_4)$ and R_1/R_2 $(= R_3/R_4)$ both small.

The resistors R_4 and R_2 in effect shunt the fluxmeter, but if they are designed to reduce the stray errors they will have little shunting effect. Additional shunting is obtained by connecting a resistor across the fluxmeter arm of the bridge, where it will introduce no stray inductance error.

The connections to the armature windings can be made in either of the two ways shown in Fig. 4 of Reference 23, and the rotor is locked so that the armature m.m.f. is in either the direct or the quadrature axis. The experimental circuit was designed to give a maximum stray error of about 0·5%, and the results obtained by it are given in Fig. 4.

(*c*) *Steady-State Short-Circuit Test.*—The steady-state short-circuit test gave a direct-axis synchronous inductance of 0·131 mH. The direct-axis current was very large at 355 A, which is well outside the range plotted on Fig. 4. If the fluxmetric bridge results are extrapolated, however, they agree to within 1 or 2% with this value for L_d.

Comments on the Methods of Measuring Synchronous Inductance.—The values for L_d obtained by the three methods agree well, although the short-circuit test is limited to a single high-current value. When i^d is negative, the inductance is increased considerably for the following reason. The steel sleeve of the rotor is normally saturated, but when i^d becomes negative, Fig. 2 shows that the magnetic potential across the leakage path (proportional to the magnet field, H) becomes zero and then reverses. Hence the leakage path becomes unsaturated and then saturates again in the reverse direction, so that the leakage unit permeance line OG should be drawn with an S-curve at the origin. The increased change of flux linkages per direct-axis unit current in this region accounts for the increased value of L_d. The divergence between the two sets of measured results is attributed to hysteresis in the sleeve.

The fluxmetric and load tests give appreciably different results for L_q although they are basically similar tests. These differences may be due to hysteresis or to eddy currents in the solid parts of the field structure during the load tests. It is not obvious, however, why eddy currents should affect only the quadrature axis.

It will be noted that L_q is about $3 \cdot 5\, L_d$ (when i^d is positive).

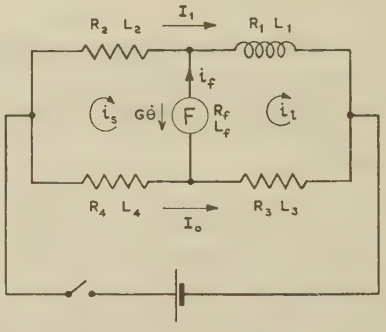

Fig. 5.—Basic circuit of the fluxmetric bridge.

This is because the permeability of the quadrature axis of the magnet is like that of a normal steel, while paths for the quadrature-axis flux are also provided by the pole-pieces and sleeve. In the direct axis, however, the recoil permeability, μ_r, of the magnets is very low (2·5–3·5 for modern materials) and the incremental permeability of the saturated steel sleeve approaches unity.

(4.1.2) **Operational Inductances, $L_d(p)$ and $L_q(p)$.**

(*a*) *Sudden 3-Phase Short-Circuit Test.*—A number of sudden short-circuit tests were carried out on the p.m. alternator using a high-speed pneumatic short-circuiting switch. The oscillograms of phase current were analysed in the usual way,[2] and the following are the average values of the parameters obtained from four tests at 150 c/s:

Synchronous inductance, L_d	0·131 mH.
Transient inductance, L'_d	0·064 mH.
Subtransient inductance, L''_d	0·021 mH.
Transient short-circuit time-constant, τ'_d	13·2 ms.
Subtransient short-circuit time-constant, τ''_d	3·3 ms.
Transient open-circuit time-constant, τ'_{d0}	27 ms.
Subtransient open-circuit time-constant, τ''_{d0}	10 ms.

The expression normally used[2] for the sudden short-circuit current is based on the following assumptions:

(i) The armature resistance is small compared with the reactances.
(ii) The subtransient time-constants are small compared with the transient time-constants.
(iii) All the time-constants are large compared with $1/\omega$.

The first and third assumptions were justified by running the p.m. alternator at the highest possible speed, but the results show that the second assumption was not completely justified. In spite of this the sudden short-circuit test will give L_d'' moderately accurately, and will give some indication of the time-constants.

It seems likely that the eddy-current paths in the solid iron of the field structure will have a shorter time-constant than the copper damper. They are therefore responsible for the sub-transient component of current, and the copper damper provides the transient component.

(*b*) *Static A.C. Impedance Tests.*—A single-phase a.c. supply is connected to two armature phases in series and the rotor is locked with the armature m.m.f. in either the direct or the quadrature axis. The measured line-to-line impedance is then $Z = 2[R + L_{d,q}(p)p]$. If the angular frequency is $h\omega$, the complex operational inductances $L_{d,q}(jh\omega)$ can be determined and should compare with the idealized loci of Reference 11.

Static a.c. impedance measurements were carried out at frequencies of 50, 500 and 1 600 c/s. The results, for a peak direct- or quadrature-axis current of 30 A, are shown in Fig. 6, together

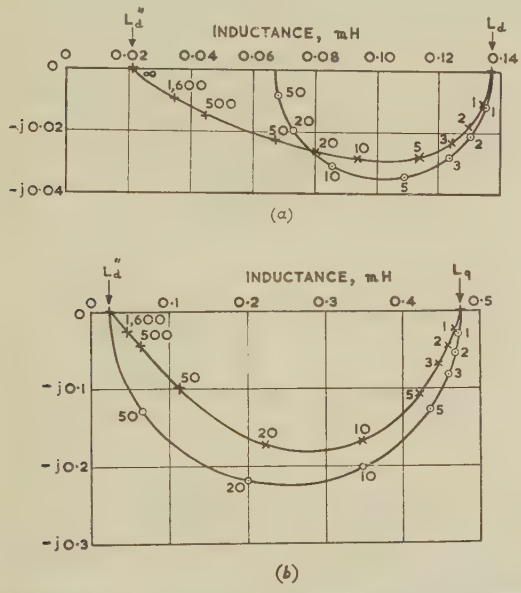

Fig. 6.—Frequency-response loci of the operational inductances of the permanent-magnet alternator.

(*a*) Direct axis, $L_d(jh\omega)$; (*b*) Quadrature axis, $L_q(jh\omega)$.
+ Measured points.
○ Calculated points.
× Estimated points.
Frequencies in cycles per second.

with the synchronous values from Fig. 4. L_d'' from the sudden short-circuit test is also plotted on the real axis as the point $p = j\infty$, and the three measured-frequency points line up well with it on the direct axis, and very nearly on the quadrature. Therefore L_q'' is approximately equal to L_d''; this seems reasonable since, at high frequencies, little alternating flux will penetrate the steel sleeve, and the armature inductance in both axes will tend towards the leakage inductance.

One of the standard methods of measuring subtransient inductance is the static a.c. impedance test carried out at rated frequency.[20] Fig. 6 shows that this frequency (400 c/s) is certainly not high enough for the p.m. alternator and for similar machines with solid rotors and short time-constants.

To predict the hunting characteristics of the interconnected system, the operational inductances at frequencies in the range 1–10 c/s must be known. On account of supply and measurement difficulties, actual tests in this range were not undertaken, and instead the frequency-response loci were derived from the known data. Their shapes were estimated from experimental curves given by Adkins and Sen,[11] while the distribution of the frequency points was estimated from calculated loci, derived as follows.

It was assumed that, at low frequencies, $L_d(jh\omega)$ was controlled by the copper damper, so that it is given by

$$L_d(1 + jh\omega\tau_d')/(1 + jh\omega\tau_{d0}').$$

This is the semicircular locus plotted in Fig. 6(*a*), from which the frequency points on the estimated locus are derived. $L_q(jh\omega)$ is controlled by eddy currents, and the approximation was made that their open-circuit time-constant, τ_{q0}'', was equal to τ_{d0}''. The short-circuit time-constant, τ_q'', is then obtained from the relation $\tau_q''/\tau_{q0}'' = L_q''/L_q$, after which $L_q(jh\omega)$ can be calculated as $L_q(1 + jh\omega\tau_q'')/(1 + jh\omega\tau_{q0}'')$. This is the semicircular locus of Fig. 6(*b*), and from it the frequency points are again fitted to the estimated locus. These estimated loci are probably not very accurate, but should be sufficient for the accuracy of the hunting experiments.

A difficulty with direct measurement is that at low frequencies the operational impedances, $jh\omega L_{d,q}(jh\omega)$, become small compared with the armature resistance, R, from which they must be separated. For example at 3 c/s, $jh\omega L_d(jh\omega)$ would be approximately $(0{\cdot}00045 + j\,0{\cdot}0025)\,\Omega$, and must be separated from R, which measurement showed to be about $0{\cdot}004\,\Omega$.

(4.1.3) Moment of Inertia, *I*.

The total moment of inertia of the rotor and its associated belt-drive pulley was measured to be $0{\cdot}0283$ kg-m^2.

(4.2) Parameters of the Synchronous Motor

(4.2.1) Field Self-Inductance, L_f, and Mutual-Inductance, M_d.

The unsaturated field self-inductance was measured by means of the fluxmetric bridge to be 65 mH, while the mutual inductance, M_d, calculated from the air-gap line of the open-circuit characteristic, had an unsaturated value of 10·7 mH.

(4.2.2) Synchronous Inductances, L_d and L_q.

The unsaturated value of L_d from a steady-state 3-phase short-circuit test was 1·93 mH. The variation of L_d and L_q with field and armature excitation was then measured by means of the fluxmetric bridge, with the field continuously excited during each test. Both the inductances were considerably decreased by field excitation; their values are given in Reference 17 together with all the other motor parameters.

(4.2.3) Field Resistance, R_f.

The field resistance between terminals includes the brush contact resistance; the terminal voltage and current, measured at a speed corresponding to 150 c/s, followed the relation

$$V_f = 1{\cdot}35 + 0{\cdot}95i^f$$

The incremental field resistance between terminals, to be used in calculating the direct-axis operational inductance, is therefore $0{\cdot}95\,\Omega$.

(4.2.4) Estimation of the Operational Inductances.

(*a*) *Direct-Axis Operational Inductance, $L_d(p)$.*—Static a.c. impedance measurements gave the following results. At 50 c/s the inductance was reduced from the synchronous value of 1·93 mH to 1·40 mH with the field winding open-circuited (owing to the action of the damper alone), and to 0·29 mH with the field short-circuited. At 500 c/s the inductance was 0·31 mH when the field winding was open-circuited, and 0·29 mH

when it was short-circuited. At the hunting frequencies of 1–10 c/s the effect of the damper can therefore be ignored in comparison with that of the field winding. The operational inductance is then given by[1, 8]

$$L_d(p) = L_d - \frac{M_d^2 p}{R_f + L_f p} \quad . \quad . \quad . \quad . \quad (18)$$

As p tends to infinity, $L_d(p)$ becomes the transient value (0·29 mH) given by

$$L_d' = L_d - \frac{M_d^2}{L_f} \quad . \quad . \quad . \quad . \quad . \quad (19)$$

from which M_d can be calculated as 10·2 mH (unsaturated). This value is slightly less than that previously obtained, and it will be regarded as the more accurate value for the calculation of the operational inductance.

To allow for saturation, the saturated value of L_d must be substituted into eqn. (18), but the values of M_d and L_f to be used must be incremental values at the particular working condition, rather than total inductances. Since L_d is itself a form of incremental inductance, a suitable incremental saturation factor, s, is the ratio of the saturated value of L_d to the unsaturated value. This factor will take account approximately of the saturating effect of both field and armature excitation. The operational inductance is then given by

$$L_d(p)_{sat} = sL_d - \frac{s^2 M_d^2 p}{R_f + sL_f p} \quad . \quad . \quad . \quad (20)$$

$$\begin{array}{c} \\ ds1 \\ dr1 \\ qr1 \\ ds2 \end{array} \begin{bmatrix} -V_{f1} \\ 0 \\ 0 \\ -V_{f2} \end{bmatrix} = \begin{array}{c} \begin{array}{cc} ds1 & dr1 \end{array} \\ \begin{bmatrix} R_{f1} & 0 \\ 0 & R_1 + R_2 + (X_{q2} - X_{d2}) \sin\delta\cos\delta \\ -X_{md1} & -X_{d1} - X_{d2}\cos^2\delta - X_{q2}\sin^2\delta \\ 0 & 0 \end{bmatrix} \end{array} \begin{array}{c} \begin{array}{cc} qr1 & ds2 \end{array} \\ \begin{bmatrix} 0 & 0 \\ X_{q1} + X_{q2}\cos^2\delta + X_{d2}\sin^2\delta & X_{md2}\sin\delta \\ R_1 + R_2 - (X_{q2} - X_{d2})\sin\delta\cos\delta & X_{md2}\cos\delta \\ 0 & R_{kd} \end{bmatrix} \end{array} \begin{bmatrix} -i^{f1} \\ i^{d1} \\ i^{q1} \\ -i^{f2} \end{bmatrix} \quad . \quad (21)$$

(*b*) *Quadrature-Axis Operational Inductance, $L_q(p)$.*—In the quadrature axis, there will be losses in the high-resistance paths between the damper bars of adjacent poles, and there will also be some eddy-current and hysteresis losses in the field iron. At hunting frequencies these will be small, and the operational inductance will be little different from the synchronous value of 1·09 mH (unsaturated). An estimate of the operational inductance at hunting frequencies had therefore to be made from static a.c. impedance tests at 50 and 500 c/s. By plotting the measured values in the complex plane the unsaturated operational inductance at hunting frequencies can be estimated, as shown in Fig. 7. Under saturated conditions it is assumed that both components are reduced by the same saturation factor, proportional to the reduction in L_q.

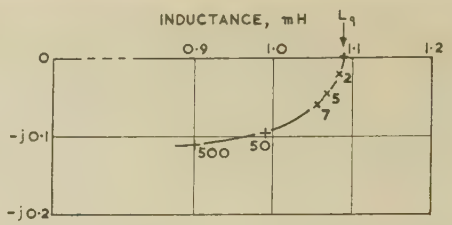

Fig. 7.—Frequency-response locus of the quadrature-axis operational inductance, $L_q(jh\omega)$, of the synchronous motor.
+ Measured points.
× Estimated points.
Frequencies in cycles per second.

(4.2.5) **Moment of Inertia, *I*.**

The total moment of inertia of the rotor and the brake drum fitted for the interconnection tests was 0·0106 kg-m².

(5) STEADY-STATE ANALYSIS OF THE INTERCONNECTED MACHINES

The impedance matrices of the p.m. alternator and the synchronous motor are known and their parameters have been measured. It is now possible to predict their performance when the armature windings are interconnected and a mechanical load is placed on the motor. The analysis of the interconnected system is first undertaken for steady-state conditions, in which the speed and currents of each machine are constant.

(5.1) Performance Equations

Kron[7, 8] has derived the direct- and quadrature-axis connection matrix by which the impedance matrices of the individual machines may be multiplied to interconnect them, and his final voltage equation for the connected system is

It will be noted that the armature reference axes $dr1$ and $qr1$ of the connected system are those of machine 1, the synchronous motor, and that balanced steady-state working has been assumed so that $p = 0$ and $p\theta = \omega$.

Eliminating the constant field currents, i^{f1} and i^{f2}, by partitioning gives the reduced voltage equation

$$\begin{array}{c} \\ d1 \\ q1 \end{array} \begin{bmatrix} V_2\sin\delta \\ V_2\cos\delta - V_1 \end{bmatrix} = \begin{array}{c} \begin{array}{cc} d1 & q1 \end{array} \\ \begin{bmatrix} R + (X_{q2} - X_{d2})\sin\delta\cos\delta & X_{q1} + X_{q2}\cos^2\delta + X_{d2}\sin^2\delta \\ -X_{d1} - X_{d2}\cos^2\delta - X_{q2}\sin^2\delta & R - (X_{q2} - X_{d2})\sin\delta\cos\delta \end{bmatrix} \end{array} \begin{bmatrix} i^{d1} \\ i^{q1} \end{bmatrix} \quad . \quad . \quad . \quad . \quad (22)$$

where R is the total armature resistance ($R_1 + R_2$), and V_1 and V_2 are the open-circuit generated e.m.f.s of the machines.

Eqn. (22) can be solved for the currents by matrix inversion to give

$$i^{d1} = \frac{1}{D}\{V_1[X_{q1} + \tfrac{1}{2}(X_{d2} + X_{q2}) - \tfrac{1}{2}(X_{d2} - X_{q2})\cos 2\delta] + V_2[R\sin\delta - (X_{q1} + X_{q2})\cos\delta]\} \quad (23)$$

and

$$i^{q1} = \frac{1}{D}\{V_1[\tfrac{1}{2}(X_{d2} - X_{q2})\sin 2\delta - R] + V_2[R\cos\delta + (X_{d1} + X_{q2})\sin\delta]\} \quad (24)$$

where D, the determinant of the matrix, is given by

$$D = R^2 + X_{d1}X_{q1} + X_{d2}X_{q2} + \tfrac{1}{2}(X_{d1} + X_{q1})(X_{d2} + X_{q2}) - \tfrac{1}{2}(X_{d1} - X_{q1})(X_{d2} - X_{q2}) \cos 2\delta \quad (25)$$

The steady-state mechanical power developed by the motor, in watts, is then[7, 8]

$$P_{m1} = V_1 i^{q1} - (X_{d1} - X_{q1}) i^{d1} i^{q1} \quad . \quad . \quad . \quad (26)$$

(5.2) Solution of the Equations

It is desired to predict the 3-phase r.m.s. armature current for any given power loading and excitation of the motor. It is not possible to eliminate δ from the equations, and therefore the method of solution is to assume a series of values for δ and calculate for each the currents i^{d1} and i^{q1} from the above equations using the measured parameters, whence the phase current and power may be found. These calculations are laborious and repetitive and they were therefore carried out on a digital computer.

To confirm the predictions, experiments were made on the actual connected system, and for this purpose the synchronous motor was fitted with a small rope brake. Tests were carried out at a frequency of 100 c/s, and the experimental and predicted results are shown in Fig. 8. The agreement between these

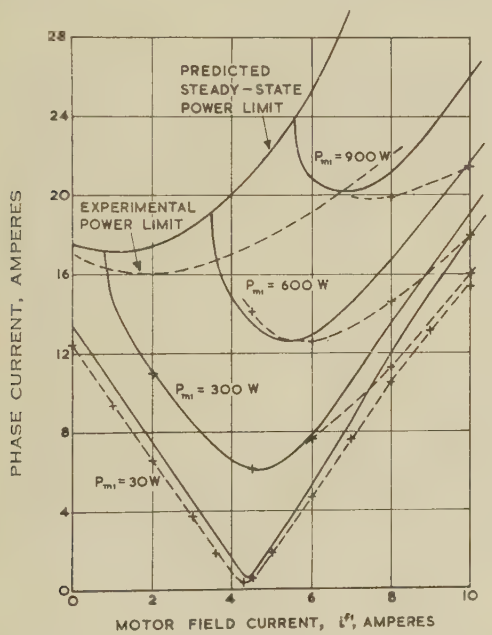

Fig. 8.—V-curves for the interconnected machines running in the steady state at 100 c/s.
——— Predicted curves.
– – – – – Experimental curves.

results is generally very good, although for field currents above 6A the predicted results tend to be high. This may be due to cross-saturation or to inaccuracies in measuring the parameters under saturated conditions, although allowance was made in the predictions for the saturating effect of both field and armature excitation.

(6) HUNTING ANALYSIS OF THE INTERCONNECTED MACHINES

Much has been written about the hunting of salient-pole synchronous machines connected to infinite busbars,[3, 5, 12] but the authors can find no reference, except by Kron, to the hunting of two interconnected salient-pole synchronous machines with armature resistance included.

Kron[7, 8] shows how the hunting equations for a single machine, or a group of unconnected machines, analysed along direct and quadrature axes, may be obtained by taking small increments in the transient voltage and torque matrix equations

$$\boldsymbol{v} = (\boldsymbol{R} + \boldsymbol{L}p + \boldsymbol{G}p\theta)\boldsymbol{i} \text{ and } T = Ip^2\theta/n - \boldsymbol{n}i_t\boldsymbol{G}i.$$

As the reference axes are fixed to the field structure or structures, $\boldsymbol{R}$, $\boldsymbol{L}$ and $\boldsymbol{G}$ are constant, and the following equation of small oscillations is obtained:

$$\Delta \boldsymbol{p} = \boldsymbol{Z}(\Delta \boldsymbol{i} + \Delta\theta)$$

or

$$\begin{bmatrix} \Delta \boldsymbol{v} \\ \Delta T/n \end{bmatrix} = \begin{bmatrix} \boldsymbol{Z} & \boldsymbol{G}ip \\ -\boldsymbol{i}_t(\boldsymbol{G} + \boldsymbol{G}_t) & Ip^2/n^2 \end{bmatrix} \begin{bmatrix} \Delta \boldsymbol{i} \\ \Delta\theta \end{bmatrix} \quad . \quad (27)$$

where $\boldsymbol{Z} = \boldsymbol{R} + \boldsymbol{L}p + \boldsymbol{G}p\theta$.

The transient motional impedance, $\boldsymbol{Z}$, in this equation consists of the transient-impedance matrix, $\boldsymbol{Z}$, together with additional rows and columns for the mechanical quantities.

Kron then shows that the transient motional impedance, $\boldsymbol{Z}'$, of a connected system may be derived from that of the unconnected system, $\boldsymbol{Z}$, by the following transformation equation:

$$\boldsymbol{Z}' = \boldsymbol{C}_t\boldsymbol{Z}\boldsymbol{C} + \boldsymbol{C}_t\boldsymbol{L}(p\boldsymbol{C}) + \boldsymbol{C}_t\boldsymbol{Z}\frac{\partial \boldsymbol{C}}{\partial \theta'}\boldsymbol{i}' + \boldsymbol{C}_t\boldsymbol{L}\left(p\frac{\partial \boldsymbol{C}}{\partial \theta'}\right)\boldsymbol{i}' + \boldsymbol{C}_t\boldsymbol{L}\frac{\partial \boldsymbol{C}}{\partial \theta'}(p\boldsymbol{i}') + \frac{\partial \boldsymbol{C}_t}{\partial \theta'}\boldsymbol{v} - \frac{\partial \boldsymbol{v}'}{\partial \theta'} \quad (28)$$

The small-oscillation equation of the connected system is then

$$\Delta \boldsymbol{p}' = \boldsymbol{C}_t\Delta \boldsymbol{p} = \boldsymbol{Z}'(\Delta \boldsymbol{i}' + \Delta\theta') \quad . \quad . \quad . \quad (29)$$

These equations have been applied by Kron[7] to a system of two interconnected salient-pole synchronous machines running at the same electrical speed. In this system

$$\Delta \boldsymbol{p}' = \begin{matrix} d1 \\ q1 \\ s1 \\ s2 \end{matrix}\begin{bmatrix} 0 \\ 0 \\ \Delta T_1/n_1 \\ \Delta T_2/n_2 \end{bmatrix} \text{ and } (\Delta \boldsymbol{i}' + \Delta\theta') = \begin{matrix} d1 \\ q1 \\ s1 \\ s2 \end{matrix}\begin{bmatrix} \Delta i^{d1} \\ \Delta i^{q1} \\ \Delta\theta_1 \\ \Delta\theta_2 \end{bmatrix} \quad (30)$$

where $s1$ and $s2$ refer to the torque equations, ΔT_1 and ΔT_2 are the applied oscillating torques, Δi^{d1} and Δi^{q1} are the oscillating currents of machine 1, and $\Delta\theta_1$ and $\Delta\theta_2$ are the small increments in rotor angle from the synchronous positions. The transient motional impedance matrix, $\boldsymbol{Z}'$, of the system is given by eqn. (31).

As in Section 5, the armature reference axes of the connected system are those of machine 1. The unwanted oscillating currents in the eddy-current paths and damper and field windings have been eliminated by partitioning to give operational inductances. The currents and voltages appearing in $\boldsymbol{Z}'$ are steady-state quantities existing before the oscillation and, for direct and quadrature axes, are unidirectional.

(6.1) Torque Equations

Eqns. (30) and (31) form the electrical and mechanical small-oscillation equations of the system. To investigate hunting stability the torque equation of each machine must be examined. If the machines oscillate at different frequencies they must be treated separately, but if the oscillations are of the same frequency the torque equations are simultaneous. As an approximation, however, it will be assumed that the p.m. alternator

$$Z' = \begin{array}{c|cccc} & d1 & q1 & s1 & s2 \\ \hline d1 & \begin{array}{c} R + L_{d1}(p)p \\ + [L_{d2}(p)\cos^2\delta + L_{q2}(p)\sin^2\delta]p \\ + [L_{q2}(p) - L_{d2}(p)]\sin\delta\cos\delta\, p\theta \end{array} & \begin{array}{c} [L_{q2}(p) - L_{d2}(p)]\sin\delta\cos\delta\, p \\ + L_{q1}(p)p\theta \\ + [L_{q2}(p)\cos^2\delta + L_{d2}(p)\sin^2\delta]p\theta \end{array} & \begin{array}{c} L_{q1}i^{q1}p \\ + \{L_{d2}(p)\sin\delta\, p\theta - [R_2 + L_{d2}(p)p]\cos\delta\}i^{q2} \\ + \{L_{q2}(p)\cos\delta\, p\theta + [R_2 + L_{q2}(p)p]\sin\delta\}i^{d2} \\ + v_{q1} \end{array} & \begin{array}{c} -[L_{q2}i^{q2}\cos\delta + (M_{d2}i^{f2} - L_{d2}i^{d2})\sin\delta]p \\ - \{L_{d2}(p)\sin\delta\, p\theta - [R_2 + L_{d2}(p)p]\cos\delta\}i^{q2} \\ - \{L_{q2}(p)\cos\delta\, p\theta + [R_2 + L_{q2}(p)p]\sin\delta\}i^{d2} \\ - v_{q1} \end{array} \\ \hline q1 & \begin{array}{c} [L_{q2}(p) - L_{d2}(p)]\sin\delta\cos\delta\, p \\ - L_{d1}(p)p\theta \\ - [L_{d2}(p)\cos^2\delta + L_{q2}(p)\sin^2\delta]p\theta \end{array} & \begin{array}{c} R + L_{q1}(p)p \\ + [L_{q2}(p)\cos^2\delta + L_{d2}(p)\sin^2\delta]p \\ - [L_{q2}(p) - L_{d2}(p)]\sin\delta\cos\delta\, p\theta \end{array} & \begin{array}{c} (M_{d1}i^{f1} - L_{d1}i^{d1})p \\ + \{L_{d2}(p)\cos\delta\, p\theta + [R_2 + L_{d2}(p)p]\sin\delta\}i^{q2} \\ - \{L_{q2}(p)\sin\delta\, p\theta - [R_2 + L_{q2}(p)p]\cos\delta\}i^{d2} \\ - v_{d1} \end{array} & \begin{array}{c} [L_{q2}i^{q2}\sin\delta - (M_{d2}i^{f2} - L_{d2}i^{d2})\cos\delta]p \\ - \{L_{d2}(p)\cos\delta\, p\theta + [R_2 + L_{d2}(p)p]\sin\delta\}i^{q2} \\ + \{L_{q2}(p)\sin\delta\, p\theta - [R_2 + L_{q2}(p)p]\cos\delta\}i^{d2} \\ + v_{d1} \end{array} \\ \hline s1 & [L_{d1}(p) - L_{q1}]i^{q1} & [L_{d1} - L_{q1}(p)]i^{d1} - M_{d1}i^{f1} & \frac{I_1}{n_1^2}p^2 & 0 \\ \hline s2 & \begin{array}{c} -[L_{d2}(p) - L_{q2}]i^{q2}\cos\delta \\ - \{[L_{d2} - L_{q2}(p)]i^{d2} - M_{d2}i^{f2}\}\sin\delta \end{array} & \begin{array}{c} [L_{d2}(p) - L_{q2}]i^{q2}\sin\delta \\ - \{[L_{d2} - L_{q2}(p)]i^{d2} - M_{d2}i^{f2}\}\cos\delta \end{array} & \begin{array}{c} [L_{d2}(p) - L_{q2}]i^{q2}i^{q2} \\ - \{[L_{d2} - L_{q2}(p)]i^{d2} - M_{d2}i^{f2}\}i^{d2} \end{array} & \begin{array}{c} \frac{I_2}{n_2^2}p^2 - [L_{d2}(p) - L_{q2}]i^{q2}i^{q2} \\ + \{[L_{d2} - L_{q2}(p)]i^{d2} - M_{d2}i^{f2}\}i^{d2} \end{array} \end{array} \quad (31)$$

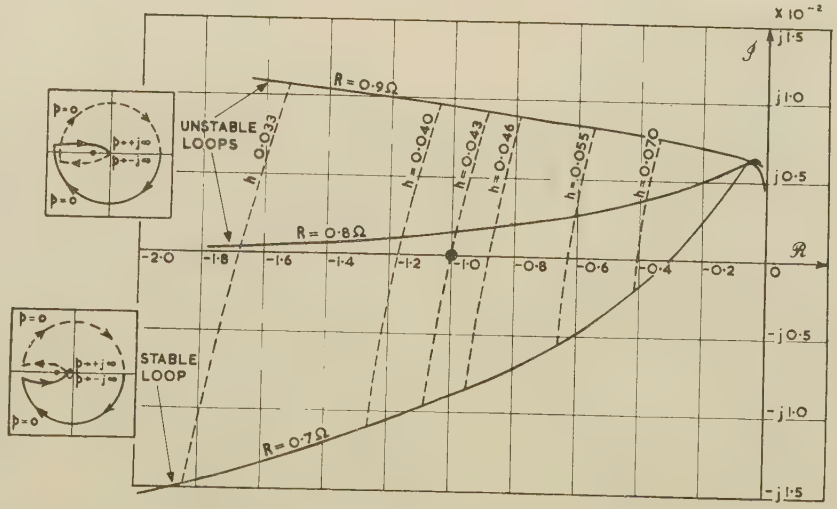

Fig. 9.—Typical frequency-response loci of $A(jh\omega)$ for the motor.

The conditions are: $i^{f1} = 4$A, $P_{m1} = 30$W, $R_f = 10\,\Omega$ for total armature resistances of 0·7, 0·8 and 0·9 Ω. The critical resistance and per-unit hunting frequency can be seen by inspection to be 0·785 Ω and 0·043 respectively.

does not oscillate, because of its relatively high inertia and the stiffness of its drive. Therefore $\Delta\theta_2 = 0$ and the $s2$ row and column can be omitted from the matrix equation, leaving the torque of the motor expressed in terms of $\Delta i'$ and $\Delta\theta_1$. The oscillating currents $\Delta i'$ are not known and are therefore eliminated by partitioning to express the torque as a function of $\Delta\theta_1$ only.

For sinusoidal oscillations $p = jh\omega$, while $p\theta = \omega$. It is then convenient to multiply the torque equation throughout by ω, so that the inductances become reactances and the equation becomes one of power:

$$\frac{\Delta T_1}{n_1}\omega = \left[\frac{C(1-h^2) + jhRF}{D} - K - h^2\omega^3\frac{I_1}{n_1^2}\right]\Delta\theta_1 \quad (32)$$

where

$$C = (i^{q1})^2[X_{d1}(jh\omega) - X_{q1}]^2[X_{q1}(jh\omega) + X_{q2}(jh\omega)\cos^2\delta + X_{d2}(jh\omega)\sin^2\delta] + \{V_1 - i^{d1}[X_{d1} - X_{q1}(jh\omega)]\}^2$$
$$[X_{d1}(jh\omega) + X_{d2}(jh\omega)\cos^2\delta + X_{q2}(jh\omega)\sin^2\delta] + \sin 2\delta\, i^{q1}[X_{d1}(jh\omega) - X_{q1}][X_{q2}(jh\omega) - X_{d2}(jh\omega)]$$
$$\{V_1 - i^{d1}[X_{d1} - X_{q1}(jh\omega)]\}$$

$$F = (i^{q1})^2[X_{d1}(jh\omega) - X_{q1}]^2 + \{V_1 - i^{d1}[X_{d1} - X_{q1}(jh\omega)]\}^2$$

$$K = (i^{q1})^2[X_{d1}(jh\omega) - X_{q1}] + i^{d1}\{V_1 - i^{d1}[X_{d1} - X_{q1}(jh\omega)]\}$$

$$D = R^2 + jhR[X_{d1}(jh\omega) + X_{q1}(jh\omega) + X_{d2}(jh\omega) + X_{q2}(jh\omega)] + (1-h^2)\{X_{d1}(jh\omega)X_{q1}(jh\omega) + X_{d2}(jh\omega)X_{q2}(jh\omega)$$
$$+ [X_{d1}(jh\omega)X_{q2}(jh\omega) + X_{q1}(jh\omega)X_{d2}(jh\omega)]\cos^2\delta + [X_{d1}(jh\omega)X_{d2}(jh\omega) + X_{q1}(jh\omega)X_{q2}(jh\omega)]\sin^2\delta\}$$

(6.2) Stability Criterion

It has been shown by Aldred and Shackshaft[12] that the stability of a synchronous machine may be investigated by a frequency-response method using Nyquist's criterion. In operational form the oscillating torque equation of a machine may be written as

$$\Delta T = [f(p) + Ip^2]\Delta\theta$$

where $f(p)\Delta\theta$ is the electrically developed torque. The equation may be rewritten as

$$\frac{\Delta\theta}{\Delta T} = \frac{1/Ip^2}{1 + f(p)/Ip^2}$$

and can be represented by a simple closed-loop system, the stability of which can be investigated by applying Nyquist's criterion to its open-loop transfer function, $A(p) = f(p)/Ip^2$.

The conventional approach to hunting analysis[3] is to express the electrically developed torque for sinusoidal oscillations as the sum of a real 'synchronizing' component and an imaginary 'damping' component, thus

$$\Delta T = (T_s + jh\omega T_d - h^2\omega^2 I)\Delta\theta \quad . \quad . \quad (33)$$

The condition for self-excited oscillations is $T_d = 0$ and $T_s = h^2\omega^2 I$. This is the same as the condition that the open-loop frequency response, $A(jh\omega)$, which is now equal to $(T_s + jh\omega T_d)/-h^2\omega^2 I$, should pass through the point $(-1, 0)$.

The advantage of plotting the open-loop frequency response is that it enables the degree of stability, in terms of phase and gain margins, to be determined. It also gives a better visual picture of the effects of changes in the parameters,[24] and enables their critical values and the hunting frequency to be obtained more easily.

(6.3) Prediction and Measurement of the Hunting Stability of the System

A means has now been found of predicting the hunting stability of the system under any given conditions. It is known that resistance in the armature circuit can cause instability by cancelling out the positive damping of the field and damper windings. It was therefore decided to predict and measure the critical armature circuit resistance, R, necessary to cause hunting under various conditions of excitation and load. To do this the open-loop frequency response, $A(jh\omega)$, of the motor must be plotted for a range of values of R. The critical value, which would make the locus pass through the point $(-1, 0)$, can then be determined by inspection.

$A(jh\omega)$ is obtained from eqn. (32):

$$A(jh\omega) = \frac{[C(1-h^2) + jhRF]/D - K}{-h^2\omega^3 I_1/n_1^2} \quad . \quad . \quad (34)$$

This expression involves the steady-state currents and angle δ, which must first be predicted as described in Section 5.2 for the conditions being considered. The evaluation of $A(jh\omega)$ for ranges of R and h is very laborious, and a digital computer was used to do this. Computations were carried out for a synchronous frequency of 100 c/s, and two values of field resistance, R_f, were considered: (*a*) 10 Ω, to allow for a fairly high field-control resistance, and (*b*), 1·15 Ω to allow for the field to be connected directly to the supply (with a wiring resistance of 0·2 Ω).

Fig. 9 shows a typical frequency-response plot of $A(jh\omega)$ in the complex plane, from which the critical resistance and hunting frequency can be determined. Figs. 10 and 11 show some of the predicted and experimental results obtained.

Confirmatory experiments on the interconnected system were carried out under the same conditions as those for which the predictions were made. Variable resistances were inserted in each phase and were gradually increased until the motor would just maintain a small oscillation, which was detected by a stroboscope. The hunting frequency, h, was measured by recording the voltage across one of the phase resistors on a Duddell oscillograph to show the hunting-frequency component of current.

In spite of the complexity of the calculation and the possible inaccuracies in some of the parameters, the agreement between the predicted and experimental results is generally good. It was found, however, that the predicted critical resistance was particularly sensitive to changes in certain parameters, notably the quadrature-axis operational inductances. For example, if the eddy-current damping in the quadrature axis of the motor were ignored by equating the imaginary component of $L_{q1}(jh\omega)$ to zero (it is only about 4% of the real component at hunting frequencies), the predicted critical resistance for operation at low saturation would fall by as much as 50%.

The predictions described above were made on the assumption that the p.m. alternator would not hunt, its inertia term, I/n^2, being 24 times that of the motor. The oscillating currents set up by the motor may, however, force the alternator to hunt, even if with only a very small amplitude. This was observed in the experimental system, but the motor oscillations had to be large to enable those of the alternator to be detected.

Kron's hunting equations, which have been used in this

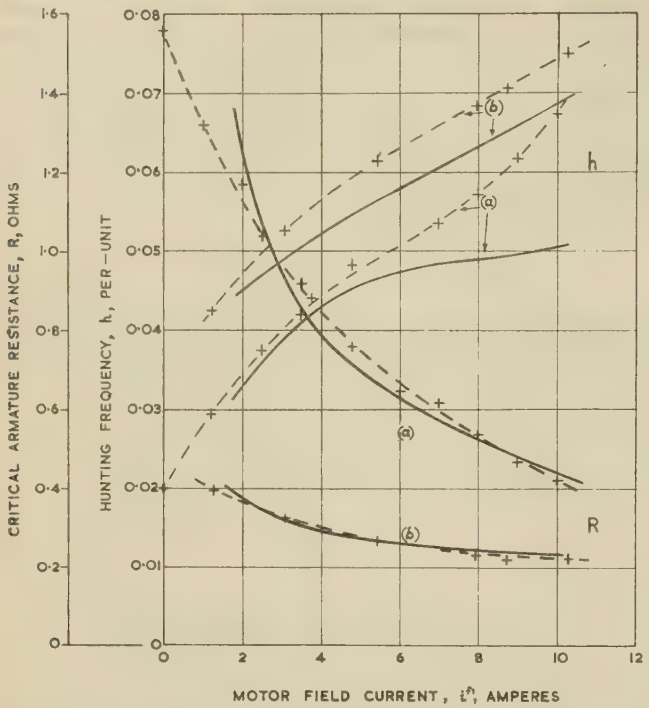

Fig. 10.—Variation of critical resistance, R, and hunting frequency, h, with motor excitation, when running on no-load.

——— Predicted curve.
– – – – – Experimental curve.
(*a*) High field resistance, $R_f = 10\,\Omega$.
(*b*) Direct field supply, $R_f = 1{\cdot}15\,\Omega$.

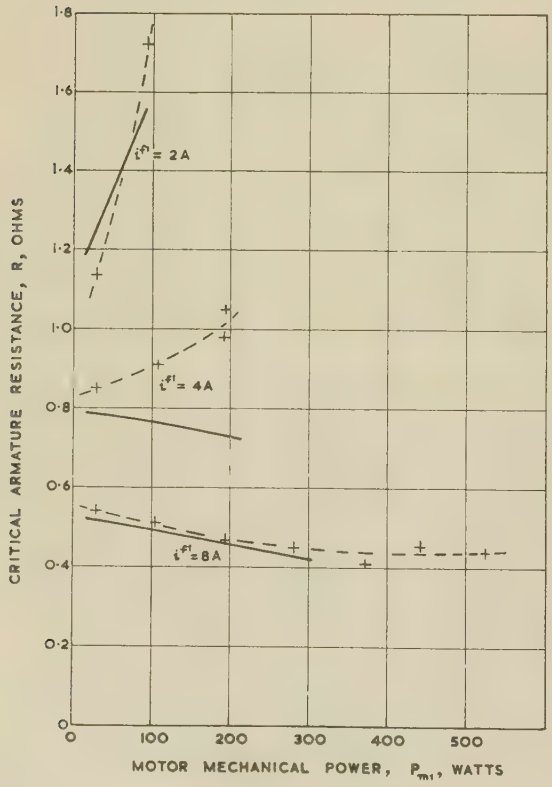

Fig. 11.—Variation of critical resistance with load for high field resistance, $R_f = 10\Omega$.

——— Predicted curve.
– – – – – Experimental curve.

Section, are more exact than those generally used to determine synchronizing and damping torques. It is common to ignore the voltages generated by the rate of change of armature flux-linkage, and frequently resistance can be neglected too. All these terms have been retained in this analysis, but it is recognized that under certain conditions the equations could be simplified a little by making suitable approximations.

(7) CONCLUSION

The p.m. alternator is quite amenable to analysis and is shown to behave in a basically similar way to a conventional wound-field machine with a constant field voltage. The direct-axis armature inductance of the experimental machine was found to be low, only about one-third of the quadrature-axis inductance, and the time-constants were also very low. The operational inductances are best represented by frequency-response loci, as they are controlled by eddy currents in the solid parts of the field and by the damper current, none of which can be measured.

The paper has shown that the steady-state performance and hunting stability of a pair of interconnected salient-pole synchronous machines can be closely predetermined if their parameters are known with sufficient accuracy. No practical conclusions have been drawn concerning the performance of the system, but in any specific case the analysis could be used to find ways of improving the performance by systematically varying the parameters. The labour of substituting numerical data into the equations can be greatly eased by the use of a digital computer, and indeed the availability of computers has now made practical the solution of many difficult problems of interconnected machines.

(8) ACKNOWLEDGMENTS

The authors wish to thank Professor J. M. Meek for his encouragement and interest in the work, and acknowledgment is made to the Controller of H.M. Stationery Office for permission to publish the paper.

(9) REFERENCES

(1) Concordia, C.: 'Synchronous Machines' (Wiley, 1951).
(2) Adkins, B.: 'The General Theory of Electrical Machines' (Chapman and Hall, 1957).
(3) Concordia, C.: 'Synchronous Machine Damping and Synchronising Torques', *Transactions of the American I.E.E.*, 1951, **70**, Part I, p. 731.
(4) Walker, J. H., and Kerruish, N.: 'Parallel Operation of Two Synchronous Machines', *Proceedings I.E.E.*, Paper No. 2423 S, February, 1958 (**105** A, p. 47).
(5) Crary, S. B.: 'Power System Stability' (Wiley, 1957), Vol. 2.
(6) Shankle, D. F., Murphy, C. M., Long, R. W., and Harder, E. L.: 'Transient Stability Studies—1. Synchronous and Induction Machines', *Transactions of the American I.E.E.*, 1954, **73**, Part III B, p. 1563.
(7) Kron, G.: 'The Application of Tensors to the Analysis of Rotating Electrical Machinery' (General Electric Review, 1942).
(8) Kron, G.: 'Tensors for Circuits' (Dover, 1959).
(9) Gibbs, W. J.: 'Tensors in Electrical Machine Theory' (Chapman and Hall, 1952).
(10) McConnell, A. J.: 'Applications of Tensor Analysis' (Dover, 1957).
(11) Sen, S. K., and Adkins, B.: 'The Application of the Frequency-Response Method to Electrical Machines', *Proceedings I.E.E.*, Monograph No. 178 S, May, 1956 (**103** C, p. 378).

(12) ALDRED, A. S., and SHACKSHAFT, G.: 'A Frequency-Response Method for the Predetermination of Synchronous-Machine Stability', *ibid.*, Monograph No. 340S, August, 1959 (**107** C, p. 2).
(13) STRAUSS, F.: 'Synchronous Machines with Rotating Permanent-Magnet Fields', *Transactions of the American I.E.E.*, 1952, **71**, Part III, p. 887.
(14) GOZZOLI, P.: 'Contributo al Calcolo degli Alternatori a Magneti Permanenti', *L'Elettrotecnica*, 1953, **40**, p. 537.
(15) GINSBERG, D., and MISENHEIMER, L. J.: 'Design Calculations for Permanent Magnet Generators', *Transactions of the American I.E.E.*, 1953, **72**, Part III, p. 96.
(16) GOULD, J. E.: 'Progress in Permanent-Magnet Materials', *Proceedings I.E.E.*, Paper No. 3069 M, December, 1959 (**106** A, p. 493).
(17) WALSHAW, M. H., and LYNN, J. W.: 'An Analytical Study of a Permanent Magnet Alternator including its Interaction with another Synchronous Machine', Report No. EL. 1491, Royal Aircraft Establishment, Farnborough.
(18) LEWIS, W. A.: 'A Basic Analysis of Synchronous Machines', *Transactions of the American I.E.E.*, 1958, **78**, Part III, p. 436.
(19) SPREADBURY, F. G.: 'Permanent Magnets' (Pitman, 1949), Chapters 1 and 6.
(20) 'Test Code for Synchronous Machines', American I.E.E. Publication No. 503, June, 1945.
(21) FATTOUH, A. F.: 'Experimental Determination of Synchronous Machine Parameters', Thesis for the Degree of M.Eng., Liverpool University, 1954.
(22) JONES, C. V.: 'An Analysis of Commutation for the Unified-Machine Theory', *Proceedings I.E.E.*, Monograph No. 302 U, April, 1958 (**105** C, p. 476).
(23) PRESCOTT, J. C., and EL-KHARASHI, A. K.: 'A Method of Measuring Self-Inductances Applicable to Large Electrical Machines', *ibid.*, Paper No. 2871 M, April, 1959 (**106** A, p. 169).
(24) ALDRED, A. S., and SHACKSHAFT, G.: 'Frequency Response Analysis of the Stabilizing Effect of a Synchronous Machine Damper', *ibid.*, Monograph No. 393 S, July, 1960 (**108** C, p. 58).

(10) APPENDIX

(10.1) Theory of the Fluxmetric Bridge

The circuit is shown in Fig. 5. Initially the supply switch is closed and the bridge is balanced so that the fluxmeter pointer is stationary. On opening the switch, the magnetic energy stored by the unknown inductor, L_1, is discharged, and at the end of the transient has deflected the fluxmeter by an angle $\Delta\theta$. Let i_s and i_l be the instantaneous currents round the two loops, and i_f be the instantaneous fluxmeter current.

Then

$$i_f = i_l - i_s \quad . \quad . \quad . \quad . \quad . \quad . \quad . \quad (35)$$

Applying Ohm's law to each loop

$$G\dot{\theta} = (R_2 + R_4)i_s + (L_2 + L_4)\frac{di_s}{dt} - R_f i_f - L_f\frac{di_f}{dt} \quad (36)$$

$$-G\dot{\theta} = (R_1 + R_3)i_l + (L_1 + L_3)\frac{di_l}{dt} + R_f i_f + L_f\frac{di_f}{dt} \quad (37)$$

Whence, by eliminating i_l and i_s,

$$-\left[1 + \frac{(R_1 + R_3)}{(R_2 + R_4)}\right]G\dot{\theta} = \left[R_1 + R_3 + R_f + \frac{(R_1 + R_3)}{(R_2 + R_4)}R_f\right]i_f + L_f\left[1 + \frac{(R_1 + R_3)}{(R_2 + R_4)}\right]\frac{di_f}{dt} - (L_2 + L_4)\frac{(R_1 + R_3)}{(R_2 + R_4)}\frac{di_s}{dt} + (L_1 + L_3)\frac{di_l}{dt} \quad (38)$$

Integrating with respect to time over the transient,

$$-\left[1 + \frac{(R_1 + R_3)}{(R_2 + R_4)}\right]G\Delta\theta = \left[R_1 + R_3 + R_f + \frac{(R_1 + R_3)}{(R_2 + R_4)}R_f\right]q_f + L_f\left[1 + \frac{(R_1 + R_3)}{(R_2 + R_4)}\right](i_f^2 - i_f^1) - \frac{(R_1 + R_3)}{(R_2 + R_4)}[L_2(i_{L2}^2 - i_{L2}^1) + L_4(i_{L4}^2 - i_{L4}^1)] + L_1(i_{L1}^2 - i_{L1}^1) + L_3(i_{L3}^2 - i_{L3}^1) \quad . \quad . \quad . \quad . \quad . \quad . \quad . \quad . \quad (39)$$

The superscripts 1 and 2 denote initial and final values respectively. The integrals of the type $\int L di$ have been split up into separate terms for each circuit element. The initial currents are $i_f^1 = 0$, $i_{L1}^1 = i_{L2}^1 = I_1$ and $i_{L3}^1 = i_{L4}^1 = -I_0$. The final currents, i^2, are all zero. The charge q_f passing through the fluxmeter is proportional to the viscous damping of the meter, and if this is small, together with the expression

$$[R_1 + R_3 + R_f + R_f(R_1 + R_3)/(R_2 + R_4)]$$

the term in q_f in eqn. (39) can be neglected. The final equation is then

$$L_1 I_1 - L_3 I_0 + \frac{(R_1 + R_3)}{(R_2 + R_4)}(L_4 I_0 - L_2 I_1) = \left[1 + \frac{(R_1 + R_3)}{(R_2 + R_4)}\right]G\Delta\theta \quad (40)$$

DISCUSSION ON 'ORTHOGONAL CODES'*

Dr. D. A. Bell (*communicated*): The idea of two independent elements per unit of time-bandwidth is fundamental to communication theory,[A] and the possibility of choosing these in the form of sine and cosine functions having an integral number of periods in a standard interval follows naturally,[B] but Dr. Harmuth's paper is probably the first detailed description of a proposed complete system. As the author recognizes, synchronization is the major practical problem. Is it intended that periods of synchronizing signal should be interpolated in the message from time to time? Or is it intended that the synchronizing signal should be transmitted continuously on a separate channel? The bandwidth needed for the transmission of the synchronizing signal would be governed by the steepness of transition between $+1$ and -1, which in the author's diagrams is portrayed as being infinite. If the tolerable error of just under ± 3 millisec is equated to a quarter-cycle of the maximum frequency transmitted, the necessary bandwidth is about 85 c/s, which is $1 \cdot 77$ times the highest of the character fundamental frequencies.

The author refers to the difficulty of assessing the redundancy of a trigonometric code such as that of his Fig. 2, but it is easy to evaluate the related concept of 'packing factor'. A closely packed binary code capable of detecting 3 errors and having characters of length n digits would contain M distinct characters, where[C]

$$M = \frac{2^n}{1 + \binom{n}{1} + \binom{n}{2} + \binom{n}{3}}$$

It is true that there is no such close-packed code for $n = 16$, the first known case being Golay's code[D] for $n = 23$. But as an indication of the quality of packing, one can say that for $n = 16$ the formula gives $M \simeq 94$. This means that in fact one could only include 6 bits of information ($M = 64$) in a 3-error-correcting code of total length 16 digits, and the value of 5 bits obtained in the orthogonal code does not seem too unreasonable.

Another packing consideration is that an e-error-correcting code requires only a minimum distance of $2e + 1$ digits between characters. A 7-element orthogonal code satisfies this requirement for 3 errors but has only 14 characters. It is now apparent that the packing factor of orthogonal codes decreases rapidly as the length is increased. As an example, Golay's 23-digit code contains 12 information digits and therefore 4096 characters; and it can correct 3 errors. A 23-digit orthogonal code would contain only 46 characters and be capable of correcting 5 errors, since the minimum distance between characters would be at least 11 digits. According to the formula given above, a 23-digit code capable of correcting 5 errors should include 190 characters compared with the 46 of a 23-digit orthogonal code.

References

(A) Gabor, D.: 'Communication Theory and Physics', *Philosophical Magazine*, 1950, **41**, p. 1161.

(B) Bell, D. A.: 'Information Theory and its Engineering Applications', 2nd edition (Pitman, 1956).

(C) Hamming, R. W.: 'Error Detection and Error Correction Codes', *Bell System Technical Journal*, 1950, **29**, p. 147.

(D) Golay, M. J. E.: 'Notes on Digital Coding', *Proceedings of the Institute of Radio Engineers*, 1949, **17**, p. 697.

* Harmuth, H. F.: Monograph No. 369 E, March, 1960 (see 107 C, p. 242).

Mr. D. S. Blacklock (*communicated*): Fig. 4 of this monograph shows that for acceptable levels of error probability there would be a 3 dB saving in signal power if a 5-bit 'ortho-trig' code were used instead of normal 5-digit binary. Thus, only 6·7 dB signals would be needed for 99% freedom from error, 8·0 dB for 99·9% and 9·0 dB for 99·99% reliability.

Dr. Harmuth, commenting on this comparison, says that the gain is obtained at the cost of increased bandwidth. In order to meet the U.S. teleprinter standard transmission rate (six characters per second) the bandwidth would need to be widened from 24 c/s to 60 c/s.

Since Gabor and others have shown that signal strength can always be exchanged for extra bandwidth, irrespective of coding, it would be interesting to compare this extra 36 c/s of bandwidth with what would be needed for a 3 dB saving when 5-digit binary is retained. I should then be able to assess the value of an ortho-trig code when all other factors were kept constant.

Dr. Harmuth distinguishes the more practical ortho-trig coding from the simpler ortho-step coding where the steps or bits can be classified as informational and redundant, 5 and 11 respectively for the 32 combinations of normal ABC coding. He asserts that this classification does not hold for the ortho-trig coding, but in commenting on Fig. 4 he does in fact refer to the 5 bits of information in the ortho-trig code. Does this reference not imply that the remaining 11 crests and troughs of $\sqrt{2} \sin 16\pi\theta$ or $\sqrt{2} \cos 16\pi\theta$ are in fact redundant?

With ortho-trig coding there are two square-wave characters that may be transmitted as an alternating series for the correct phasing of the receiver. Am I right in thinking that with normal 5-digit binary coding an extra digital load of 50% has to be transmitted for the correct phasing of the receiver?

I am puzzled by the absence of any claim of superiority for the orthogonal coding, other than the claim of practicality for the trig variant in comparison with the step variant. Are these codes with 5 or more bits of information better than the 5-digit binary code of everyday business?

I can, however, make a comparison within Dr. Harmuth's ortho-trig field, as illustrated in the communication-system block diagram of Fig. 5, between our outmoded ABC coding and a 'Tunish' coding of an English language so modified as to make more intensive use of the 'th', 'sh' and other phonetic characteristics which already distinguish English from other languages. Tunish would provide the 3 dB saving along with a bandwidth saving (using fundamental frequencies of 6 c/s and 12 c/s only) and a terminal-equipment saving of 75% in the count of oscillators, multipliers, integrators and sampling switches; these gains would be accompanied by a 10% gain in transmission rate (counting words, not characters) and by many educational and other benefits. The Simpler Spelling Association of Lake Placid, N.Y., claim a 16·6% saving in writing and printing costs for their 40-symbol alphabet. Tunish makes a 50% claim and enlarges its view by including telegraphy. Thus, the 7000 bits needed to transmit Lincoln's 266 words at Gettysburg would be reduced to 3630 for Tunish language and writing. Every new age requires a revolution in human thinking and the advent of electronics in communication merits a new set of symbols along with greater semantic consistency in the phonetics of our English language.

DISCUSSION ON 'CALCULATION OF THE CURRENT IN NON-LINEAR SURGE-CURRENT-GENERATOR CIRCUITS'*

Messrs. M. Darveniza and **R. Kelly** (*Queensland: communicated*): The study of the non-linear circuit described in this paper has not considered the more general case which includes a linear resistance R. In surge-current-generator circuits it is found that current waveshapes and magnitudes are more easily controlled by introducing the additional resistive (linear) element. This circuit has been studied on an electronic analogue computer at the University of Queensland, Department of Electrical Engineering.

Preliminary work has shown that the values of the circuit elements (R, L and C) required to test the non-linear element of a surge diverter may be accurately determined from the computer study. Fig. A shows the values of charging voltage and of R, L and C required for the surge testing of an 11 kV surge diverter with 8/20 microsec currents between 1 and 5 kA. In this case, the characteristics of the non-linear element were approximately known and the results obtained during actual test conditions agreed to within 3% of the values from the analogue study.

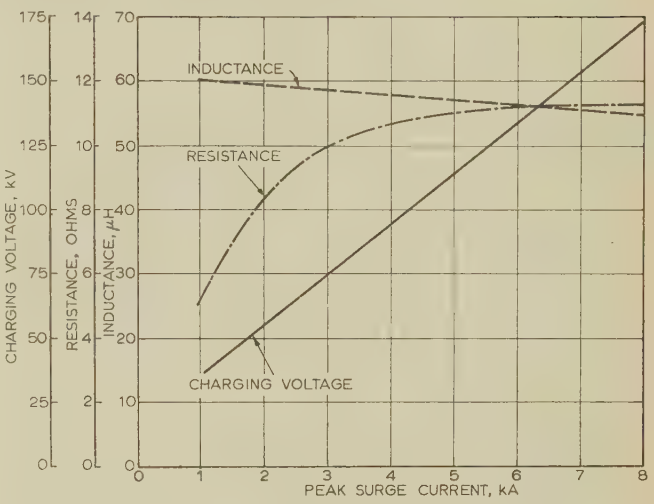

Fig. A.—Tests on surge diverter.
Surge-current generator parameters:
Test waveform, 8/20 microsec
Plant capacitance, 1 μF

It is clear that Mr. Monahan's circuit analysis and study of the more general circuit greatly simplifies the procedure in testing the non-linear elements of surge diverters. This Department is carrying out further work to provide generalized data for the circuit containing a linear resistive element. A function generator representing the non-linear element in the form $V = KI^{\beta}$ is being developed to simplify the use of the analogue computer.

Mr. T. F. Monahan (*in reply*): The inclusion of linear resistance in the non-linear circuit greatly increases the amount of calculation required to produce a general solution covering a range of values of the parameters. As was mentioned in the paper, the solutions ignoring linear resistance have been found to give a useful guide, in many cases, to the performance of a circuit in which linear resistance is present. However, it is better to calculate the effect of the linear resistance, and Messrs. Darveniza and Kelly are fortunate in having an analogue computer on which this can be done. It is to be hoped that they will be able to publish generalized data in due course and also give information on the use of the analogue computer.

*Monahan, T. F., *Proceedings I.E.E.*, Monograph No. 376S, April, 1960 (see 107C, p. 288).

DISCUSSION ON 'EDDY-CURRENT EFFECTS IN RECTANGULAR FERROMAGNETIC RODS'*

Mr. P. Graneau (*communicated*): As a result of the growing belief that eddy currents influence the performance of electromagnetic devices to a larger extent than has hitherto been expected, any advance in our understanding of the mechanism by which they are generated is a very welcome development.

What may delay acceptance of a new theoretical outlook is as much the disappointing experience with older eddy-current theories as the lack of simple and convincing experiments that can be carried out in industrial laboratories. In view of this, it seems essential to demonstrate, beyond reasonable doubt, that a rigorous analysis based on uniform scalar permeability could not account for all the observed losses. Dr. Lee conveys the impression that this has been done. Reading the papers quoted by him left me unconvinced, for three reasons:

All attempts to derive loss formulae start with Maxwell's field equations. Now, almost a century after their formulation, they have still not been solved for the geometrical arrangements of conductors which represent electromagnetic devices. Approximations have been obtained from the three known exact solutions, which all refer to geometrical systems that cannot be realized in practice, but we are unable to estimate how far they may depart from the correct solutions.

Every method of arriving at an approximation terminates in a different loss formula, and hence the loss ratio depends partly on the choice of formula. Moreover, even the losses measured in non-magnetic metals differ widely from those predicted by the various approximations.

With regard to the frequency dependence of the observed loss (Section 2.2.1), it should be stressed that agreement between classical theory and measurement requires constant magnetizing current, with frequency the only variable. Instead, most producers and users of magnetic materials determine the loss/frequency characteristic under constant flux-density conditions.

* Lee, E. W.: Monograph No. 371 M, April, 1960 (see 107 C, p. 257).

This is a useful test of the performance of transformers, but it should not yield losses which agree with classical formulae.

Mr. E. W. Lee (*in reply*): I agree with Mr. Graneau that the classical eddy-current equations can be rigorously derived from Maxwell's equations only for a few simple configurations, which invariably are such that the sample is assumed to be infinite in one or more dimensions so that the number of independent variables in the equations is reduced from three to two or even one. Obviously care must be exercised in applying the formulae derived from such treatments to real physical systems. One would not expect the theory for a thin lamination of infinite extent to apply to a cylinder of square cross-section, for example. However, one would expect it to apply to a strip in which the ratio of breadth to thickness was 100. When this sort of care has been exercised it seems to me that there are at least three instances where the agreement between the calculated effects and those experimentally observed is very good. These are: (*a*) the non-magnetic strip at low frequencies; (*b*) the ferromagnetic strip which is appreciably thicker than the average domain width, also at low frequencies and measured in a field sufficiently small to ensure that the relation between B and H is linear; and (*c*) the skin effect in non-magnetic circular cylinders. It seems too much to expect that the good agreement between theory and experiment is in all cases due to a fortuitous cancellation of errors.

However, in example (*b*) definite discrepancies between theory and experiment become apparent when the thickness of the strip is reduced, in spite of the fact that such a reduction should make the strip a better approximation to an infinite lamina. The discrepancies between theory and experiment become more pronounced as the strip thickness is reduced, although the other magnetic properties are not significantly affected. In addition, by suitable heat treatment one can vary the grain size of a single polycrystalline strip. One then observes a definite correlation between the anomaly factor and the grain size whilst the thickness of the strip remains unaltered.

It is the contention of my paper that the most probable explanation of these phenomena lies in the over-simplification of the eddy-current calculations which results if the domain structure of the material is ignored and the permeability of a ferromagnetic sheet is treated as a uniform scalar quantity. Since the war, theoretical and experimental studies of domains in ferromagnetic media have contributed immensely to our understanding of magnetization processes. On the basis of domain theory one can account, at least in principle, for initial permeability, remanence and coercive force, and the variation of these quantities with internal stresses, temperature and the composition of homogeneous alloys. In view of the undoubted success of domain theory in accounting for almost every aspect of the magnetization curve, it seems rather illogical to ignore it when calculating eddy currents.

With Mr. Graneau's final remark I am in complete agreement. However, Section 2.2.1 is intended to apply only in the low-frequency limit in which the skin depth is very much greater than the thickness d. In these conditions the flux density and the field are both uniform, and if the applied field is sinusoidal so is the flux density.

DISCUSSION ON 'ELECTRIC AND MAGNETIC IMAGES'*

Dr. K. C. Mukherji (*India: communicated*): While I fully agree with the author's conclusion in Section 3.2 regarding the criterion for uniqueness of the image distribution in a magnetostatic field, I find it difficult to follow the latter part of the formal derivation following eqn. (9). It is not clear there if the expressions

$$(\boldsymbol{n} \times \boldsymbol{C}) \iint_S (\nabla \times \boldsymbol{C}) \times \boldsymbol{n} dS \quad \text{and} \quad \boldsymbol{n} \times \boldsymbol{C} \iiint_v (\nabla \times \nabla \times \boldsymbol{C}) dv$$

are meant to represent vectors or scalars, while the expression

$$\iint_S (\boldsymbol{n} \times \boldsymbol{C}) \,.\, (\nabla \times \boldsymbol{C}) dS$$

to which each of these has in turn been equated, definitely represents a scalar; neither do the former two expressions appear to be equal to each other.

The following steps lead to the same conclusion as the author's:

$$\iint_S (\boldsymbol{n} \times \boldsymbol{C}) \,.\, (\nabla \times \boldsymbol{C}) dS = \iint_S \boldsymbol{C} \,.\, (\boldsymbol{n} \times \boldsymbol{C}) \times \nabla dS$$

$$= -\iint_S \boldsymbol{C} \,.\, \nabla \times (\boldsymbol{n} \times \boldsymbol{C}) dS$$

which vanishes if the tangential component of $\boldsymbol{C}$ is constant everywhere on the surface S.

Mr. P. Hammond (*in reply*): I am grateful to Dr. Mukherji for drawing attention to an obscurity in my treatment of the magnetostatic field. All the quantities which he mentions are scalars, but the dot indicating a scalar product was inadvertently omitted.

A clearer way of writing the expressions would be as follows:

$$\iint_S (\boldsymbol{C} \times \nabla \times \boldsymbol{C}) \,.\, \boldsymbol{n} dS = \iint_S (\nabla \times \boldsymbol{C}) \times \boldsymbol{n} \,.\, \boldsymbol{C} dS$$

Hence, if the tangential components of $\nabla \times \boldsymbol{C}$ are zero on S, uniqueness is assured.

Also $\iint_S (\nabla \times \boldsymbol{C}) \times \boldsymbol{n} \,.\, \boldsymbol{C} dS = \boldsymbol{C} \,.\, \iint_S (\nabla \times \boldsymbol{C}) \times \boldsymbol{n} dS$ if the tangential components of $\boldsymbol{C}$ are constant on S.

But $\iint_S (\nabla \times \boldsymbol{C}) \times \boldsymbol{n} dS = -\iiint_v \nabla \times \nabla \times \boldsymbol{C} dv = 0$

Thus constant tangential components of $\boldsymbol{C}$ also assure uniqueness.

Dr. Mukherji's alternative proof relies on a rather free manipulation of the vector operator ∇, and I am not convinced about the validity of the method. However, the important thing is that we both reach the same conclusions.

* HAMMOND, P.: *Proceedings I.E.E.*, Monograph No. 379, May, 1960 (107 C, p. 306).

DISCUSSION ON

'OPTIMUM COMBINATION OF PULSE SHAPE AND FILTER TO PRODUCE A SIGNAL PEAK UPON A NOISE BACKGROUND'*

Dr. D. A. Bell (*communicated*): The author has made an interesting contribution to a somewhat intricate mathematical topic, but his work is likely to be put to practical use more readily if it can be shown to have a non-mathematical interpretation. The author appears to imply that the transmission function $T(\omega)$ of the medium is independent of the noise spectrum $\sigma(\omega)$, but such an assumption is disallowed by the fluctuation-dissipation theorem.[A,B] This theorem is to the effect that in all equilibrium systems a mechanism of dissipation must be a source of noise, and vice versa. Therefore independence of $T(\omega)$ and $\sigma(\omega)$ can apply only if the noise is due to active elements, e.g. if it is interference from other man-made devices, rather than noise inherent in the attenuating part of the communication channel. In what practical situations does one find the effective noise decreasing rapidly with frequency as suggested in eqn. (26)?

In eqn. (19) the factor $1/T(\omega)$ appears to say that the filter should equalize the system, by compensating for the distortion in the medium, before one constructs a matched filter for the transmitted waveform $V_i(t)$. The usual interpretation of the matched filter is that it provides a combination of time delays such that all 'samples' add together at the chosen instant of discrimination. By means of the inverse Fourier transform this time specification may be translated into the required $H(\omega)$, but it is also possible to design the filter in the time domain.†

The statement towards the end of Section 4, that a linear filter cannot recombine two identical signals separated by a time delay, is true of 2-port lumped-parameter networks, but is not true of a distributed system combined with a detector which does not absorb power. For example, the use of a delay line for 'integrating' successive pulse returns in a radar system is a simple method of combining identical signals which are separated by a prescribed time interval. Will the optimum pulse for a system in which delay lines are permitted differ from that specified for a system using only a single channel through a linear filter?

The statement in Section 6, that, for fixed d, λ_0 increases very rapidly as n increases, prompts two questions. First, is not the required minimum bandwidth simply proportional to n, and is it not then unrealistic to regard $T(\omega)$ as a separately and independently specified function? In radio signalling it does not appear reasonable to have transducers, etc., of so great a bandwidth that the transfer characteristic of the system is defined by the propagation characteristics of the medium; and it is not obvious that this would be useful in other applications such as under-water signalling. Secondly, at the end of Section 3 the author states the entirely reasonable result that, if the medium is non-distorting, $\lambda_0 = n$. If, then, in Section 6 we find that $n = 10$ can lead to $\lambda_0 = 250$ for a particular pulse duration and form of $|\sigma(\omega)|^2/|T(\omega)|^2$, does not this mean simply that a substantial part of the signal energy has been put in a part of the spectrum where the noise is negligible?

* Heaps, H. S.: Monograph No. 407 E, October, 1960 (see 108 C, p. 153).

† A review of methods of designing in the time domain has been carried out by A. M. Rosie (publication pending), but the most useful technique appears to be that described by Pucel.[C]

References

(A) Callen, H. B., and Welton, T. A.: 'Irreversibility and Generalized Noise', *Physical Review*, 1951, **83**, p. 34.

(B) Weber, J.: 'Fluctuation Dissipation Theorem', *ibid.*, 1956, **101**, p. 1620.

(C) Pucel, R. A.: 'Network Synthesis for a Prescribed Impulse Response using a Real Part Approximation', *Journal of Applied Physics*, 1957, **28**, p. 124.

Prof. H. S. Heaps (*in reply*): I appreciate Dr. Bell's comments and agree with him as to the desirability of further, and if possible non-mathematical, interpretation of the results.

The method described and the validity of eqns. (15) and (16) do not depend upon the assumption that the transmission function $T(\omega)$ is independent of the noise spectrum $\sigma(\omega)$. It is assumed, however, that both $T(\omega)$ and $\sigma(\omega)$ are independent of the transmitted signal.

With reference to under-water sound propagation, the noise spectrum $\sigma(\omega)$ may include noise caused by wave motion at the surface of the bottom and also noise caused by man-made, or other, disturbances within the water. The propagation function $T(\omega)$ may include the effect of a sound channel and also the frequency response of any transducers that are placed between the signal generator and signal processing equipment. There is no reason why $T(\omega)$ and $\sigma(\omega)$ should not contain common factors. For example, the filtering effect of the transducers affects both $T(\omega)$ and $\sigma(\omega)$ by a common factor.

The statement that a linear filter cannot recombine two identical signals so as to eliminate the time delay between them may be explained by the following example, which is illustrated

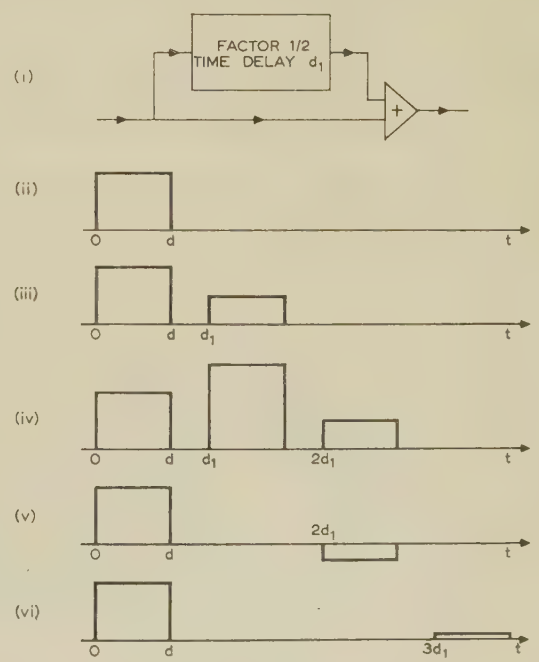

Fig. A

by Fig. A. The linear filter (i) is equivalent to the transmission function

$$T(\omega) = 1 + \tfrac{1}{2}\exp(-j\omega d_1)$$

which transforms the single pulse at (ii) into the two pulses at (iii). A further filter of transfer function $1/T(\omega)$ would transform these two pulses into the single pulse at (ii).

The transfer function

$$1 + \exp(-j\omega d_1) \quad . \quad . \quad . \quad . \quad . \quad . \quad (A)$$

would add together the two pulses at (iii) to form the pulse at (iv) beginning at time d_1, but it would not form a single pulse and some of the output energy would be contained in the subsidiary pulses that begin at times $t = 0$ and $t = 2d_1$. The required transfer function $1/T(\omega)$ may be written in the form

$$1/T(\omega) = [1 + \tfrac{1}{2}\exp(-j\omega d_1)]^{-1}$$
$$= 1 - \tfrac{1}{2}\exp(-j\omega d_1) + \tfrac{1}{4}\exp(-2j\omega d_1) - \ldots \quad (B)$$

The first two terms in the above series for $1/T(\omega)$ correspond to a filter that transforms the pulses at (iii) into those at (v). The first three terms in the series correspond to a filter that transforms the pulses at (iii) into those at (vi). Inclusion of further terms in the series produces further delay in the subsidiary pulse and reduces its amplitude. Although to synthesize $1/T(\omega)$ exactly would require an infinite number of time delays, a synthesis to within any required accuracy may be achieved by the use of a sufficiently large number of time delays. The non-realizability of $1/T(\omega)$ is thus true in the exact mathematical sense but not in the practical sense in which a sufficiently close approximation to $1/T(\omega)$ is sufficient.

The particular form of eqn. (26) was chosen to provide a simple illustration of the theory and to verify that the theory then leads to reasonable conclusions. As noted by Dr. Bell, as n is increased the optimization process places the signal energy in the higher frequencies where the noise is of small amplitude.

In the general case, for sufficiently large values of n, $n - 1$ is the maximum number of sign changes that may occur in the transmitted signal $V_i(t)$. Thus, for a given noise spectrum $\sigma(\omega)$, a given transfer function $T(\omega)$ of the medium, and a given value of n, eqns. (15) determine the envelope of the optimum signal of frequency $2n/d$.

DISCUSSION ON 'AN ANALYTICAL REVIEW OF POWER-SYSTEM FREQUENCY, TIME AND TIE-LINE CONTROL'*

Dr. H. K. Messerle (*New South Wales*: *communicated*): It is interesting to see the integral square error criterion applied to system control studies, and the results indicate that optimum control conditions can be determined quite readily. I wonder, however, whether this criterion leads to a practical optimum.

The integral square error becomes a minimum under conditions for which system response is oscillatory. Consequently we have a system which is not very far from instability when this error is minimized. This feature does not matter in a conventional controller with 'fixed' components which do not vary with time. On a power system which undergoes a considerable change every day the controlling and controlled elements are not fixed and change continuously. Consequently integral square error minimization can lead to difficulties on a practical system.

A solution might be found by searching for system conditions for which the application of the integral square error criterion leads to the smallest controller gain. To do this it would be necessary to know how system components modify the criterion. Have the authors investigated this point, and are there any general trends apparent from their work? It is possible that the integral square error criterion becomes very insensitive for low controller gains, since system transients might contain oscillating components which were independent of controller action. This feature has shown up in a number of similar control problems and might be significant in the work discussed in this paper.

Messrs. D. Broadbent and **K. N. Stanton** (*in reply*): Dr. Messerle stresses the important point that minimization of the integral square error leads to an oscillatory system and, as we pointed out, this feature must be watched carefully; however, when dealing with errors in electrical systems an integral square error of power does seem to be relevant, as its minimization reduces the time over which large errors occur.

Fig. 7 shows that a minimum integral square error for tie power can be obtained for a particular value of tie-line controller gain, K_t, and that this minimum depends to some extent on the type of governor used. The reason for this is that tie-line oscillations, which are affected only to a minor degree by the tie-line controls, depend on conditions prevailing in the individual areas before interconnection. The tie-line controls affect the time required to correct any deviation in the average (over 2–3 sec, say) scheduled tie power. At low values of K_t this correction is slow and the integral square error large; as K_t is increased the integral square errors are reduced until finally the tie-line controller tends to become oscillatory causing the integral square error to increase once more as is shown in Fig. 7. The minor effect which K_t has on tie-line oscillations is not a problem, since increasing K_t actually improves the stability of these oscillations.

For values of K_t below about 0·015 the tie-line controller is quite stable, and it is not expected that the variation in system parameters will be sufficient to disturb seriously this control loop, provided that K_t remains roughly proportional to system capacity. Another fact in our favour is that the optimum value of K_t is not sharply defined. For example, from curve 1(*a*) of Fig. 7, K_t in the range 0·01–0·018 would be suitable for all practical purposes.

A more serious problem is the effect that variation of system parameters will have on tie-line oscillations, and this seems to be a good reason for conservative design of governors. Some results have been obtained to show the effect of tie-line synchromizing-torque coefficient on tie-line oscillations, but it does seem that the most critical parameter is the effective damping, and the way in which it varies with changes of the system is most relevant; for this reason a conservative value of damping has been used in the study, and work is now in progress on the investigation of this parameter in an actual power system.

* Broadbent, D., and Stanton, K. N.: Monograph No. 395 S, September, 1960 (see 108 C, p. 71).

DISCUSSION ON
'NUMERICAL EVALUATION OF INDUCTANCE AND A.C. RESISTANCE'*

Dr. H. McKibbin (*communicated*): It is almost ten years since I first made use of Southwell's relaxation methods to obtain flux plots for current-carrying conductors housed in slots in iron. My object was to determine the 'slot constant' of any slot shape. I was successful, in that I developed special residual equations for nodes on curved boundaries along which only the normal gradient of the sought function is specified, and obtained flux plots and slot constants for rectangular, tapered and circular semi-closed slots. Unfortunately I had not access to a computer and had to obtain all the solutions manually—a very tedious task since the convergence was very slow. I was therefore very impressed by the computer times quoted in the monograph.

Turning now to the finite-difference approximations used in the monograph I wish to raise two points: (*a*) the numbering of the nodes; and (*b*) the order of the neglected terms.

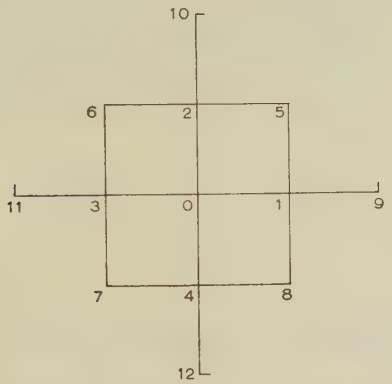

Fig. A

(*a*) Was there any special reason for not using the commonly accepted node numbering system (see Fig. A)?

Writing $A_1 = \varepsilon^{h\frac{\partial}{\partial x}}A_0$, $A_3 = \varepsilon^{-h\frac{\partial}{\partial x}}A_0$; $A_2 = \varepsilon^{h\frac{\partial}{\partial y}}A_0$, and $A_4 = \varepsilon^{-h\frac{\partial}{\partial y}}A_0$ (Fig. B),

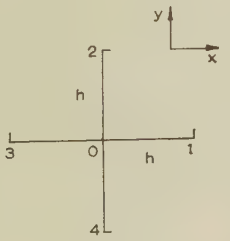

Fig. B

we find that

$$h^2\left[\left(\frac{\partial^2 A}{\partial x^2}\right)_0 + \left(\frac{\partial^2 A}{\partial y^2}\right)_0\right] = A_1 + A_2 + A_3 + A_4 - 4A_0 - \left\{\frac{h^4}{12}\left[\left(\frac{\partial^4 A}{\partial x^4}\right)_0 + \left(\frac{\partial^4 A}{\partial y^4}\right)_0\right] + \ldots\right\}$$

so that the use of

$$h^2\left[\left(\frac{\partial^2 A}{\partial x^2}\right)_0 + \left(\frac{\partial^2 A}{\partial y^2}\right)_0\right] \simeq A_1 + A_2 + A_3 + A_4 - 4A_0$$

as in the monograph, neglects terms in h^4, etc.

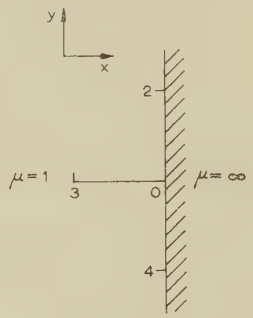

Fig. C

If, however, the line of nodes 4, 0, 2, coincides with an iron boundary (Fig. C) the use of

$$h^2\left[\left(\frac{\partial^2 A}{\partial x^2}\right)_0 + \left(\frac{\partial^2 A}{\partial y^2}\right)_0\right] \simeq A_2 + 2A_3 + A_4 - 4A_0$$

as in the monograph, neglects

$$-\frac{h^4}{12}\left[\left(\frac{\partial^4 A}{\partial x^4}\right)_0 + \left(\frac{\partial^4 A}{\partial y^4}\right)_0\right] + \text{etc.} + \frac{h^3}{3}\left(\frac{\partial^3 A}{\partial x^3}\right)_0 + \text{etc.}$$

Thus at nodes not on the iron boundaries the error is of order h^4 at most, but at those on the boundaries the error is of order h^3.

It is possible, however, to obtain finite-difference approximations for boundary nodes which also have an error of order h^4 at most, as follows.

Writing $A_3 = \varepsilon^{-h\frac{\partial}{\partial x}}A_0$

and $A_{11} = \varepsilon^{-2h\frac{\partial}{\partial x}}A_0$ (Fig. D)

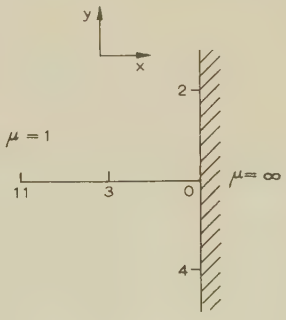

Fig. D

we obtain, since $\left(\frac{\partial A}{\partial n}\right)_0 = \left(\frac{\partial A}{\partial x}\right)_0 = 0$,

* Mamak, R. S., and Laithwaite, E. R.: Monograph No. 418 U, November, 1960 (see 108 C, p. 252).

$$h^2\left(\frac{\partial^2 A}{\partial x^2}\right)_0 = 4A_3 - 0{\cdot}5A_{11} - 3{\cdot}5A_0 + \frac{h^4}{6}\left(\frac{\partial^4 A}{\partial x^4}\right)_0 + \ldots$$

Now $$h^2\left(\frac{\partial^2 A}{\partial y^2}\right)_0 = A_2 + A_4 - 2A_0 - \frac{h^4}{12}\left(\frac{\partial^4 A}{\partial y^4}\right) + \ldots$$

Therefore

$$h^2\left[\left(\frac{\partial^2 A}{\partial x^2}\right)_0 + \left(\frac{\partial^2 A}{\partial y^2}\right)_0\right] - A_2 + 4A_3 + A_4 - 0{\cdot}5A_{11} - 5{\cdot}5A_0 + \frac{h^4}{12}\left[2\left(\frac{\partial^4 A}{\partial x^4}\right)_0 - \left(\frac{\partial^4 A}{\partial y^4}\right)_0\right] + \text{etc.} - \frac{h^5}{10}\left(\frac{\partial^5 A}{\partial x^5}\right)_0 + \ldots$$

So we may write

$$h^2\left[\left(\frac{\partial^2 A}{\partial x^2}\right)_0 + \left(\frac{\partial^2 A}{\partial y^2}\right)_0\right] \simeq A_2 + 4A_3 + A_4 - 0{\cdot}5A_{11} - 5{\cdot}5A_0$$

with an error of order of h^4 at most.

Similarly, we obtain for a corner node (Fig. E)

$$h^2\left[\left(\frac{\partial^2 A}{\partial x^2}\right)_0 + \left(\frac{\partial^2 A}{\partial y^2}\right)_0\right] \simeq 4(A_2 + A_3) - 0{\cdot}5(A_{11} + A_{12}) - 7A_0$$

also with an error of order h^4 at most.

In conclusion I would point out that the above equations result from the coincidence of the domain boundaries with lines of nodes; curved boundaries, with their fractional meshes, do not allow the h^3-terms to be eliminated easily.

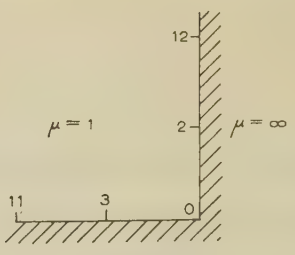

Fig. E

Dr. R. S. Mamak and Dr. E. R. Laithwaite (*in reply*): There was no particular reason for numbering the nodal points as we did, and as Mr. McKibbin points out, most British textbooks use the system which he illustrates.

Regarding his second point, in general the accuracy of the system may be improved by means of a more complex finite-difference equation. Mr. McKibbin obtains greater accuracy at the boundary at the cost of greater complexity inasmuch as it requires a knowledge of a_{11}.

It should also be pointed out that the finite-difference equations for the boundaries between media having different permeabilities, and between current-carrying and non-current regions, are accurate only to the order of h^3, and thus the extra complexity may not be justified.

DISCUSSION ON 'FREQUENCY SPECTRUM DISTORTION OF RANDOM SIGNALS IN NON-LINEAR FEEDBACK SYSTEMS'*

Mr. P. I. Boulton (*Canada: communicated*): In this paper a condition is derived such that the signal and distortion terms in the output of a zero memory non-linearity are non-correlated. The output of the non-linearity is written in the form

$$x_0 = f(x_i) = Kx_i(t) + D(t) \quad . \quad . \quad . \quad . \quad \text{(A)}$$

where K = A constant dependent on the characteristics of the input x_i.

$Kx_i(t)$ = Signal term.

$D(t)$ = Distortion term.

The result obtained is

$$K = \frac{1}{\sigma_i^2}\int_{-\infty}^{\infty} x_i f(x_i) p(x_i) dx_i \quad . \quad . \quad . \quad . \quad \text{(B)}$$

where $p(x_i)$ = First probability density of the input.

σ_i^2 = Power of the input.

It is stated that for this value of K the cross-correlation between the signal and the distortion, $g_{sD}(\tau)$, is zero.

This conclusion is not justified for two reasons. The first is that the method of obtaining eqn. (B), i.e. assuming $g_{sD}(\tau) = 0$ and then determining the value of K from this assumption, leads only to the conclusion that this equation is a *necessary* condition for $g_{sD}(\tau) = 0$. It must be independently shown that this is also a *sufficient* condition. The second is that the derivation given in the paper is carried out for $\tau = 0$ and hence if eqn. (B) is to be taken to be the condition for $g_{sD}(\tau) = 0$ for all τ, it must also be shown that (*a*) $g_{sD}(\tau) \leqslant g_{sD}(0)$, all τ; (*b*) $g_{sD}(\tau) \geqslant 0$, all τ. In general the further proofs mentioned above cannot be carried out; hence eqn. (B) is not a sufficient condition for non-correlation of the signal and distortion.

As mentioned in the paper, eqn. (B) was also obtained by Booton,[A] from a consideration of the non-correlation between input and distortion. However, he obtained this result only after assuming that the input, x_i, was Gaussian, a restriction not given by West *et al.*

A sufficient condition for non-correlation of signal and distortion for an arbitrary input can be obtained as follows: Let the output of the non-linearity be

$$x_0(t) = f[x_i(t)] = Kx_i(t) + D(t)$$

Hence $$D(t) = f[x_i(t)] - Kx_i(t) \quad . \quad . \quad . \quad . \quad . \quad \text{(C)}$$

The cross-correlation between the signal and distortion terms is thus given by

$$g_{sD}(\tau) = \overline{Kx_i(t)D(t+\tau)} = \overline{Kx_i(t)f[x_i(t+\tau)]} - \overline{K^2 x_i(t)x_i(t+\tau)}$$

where the bar denotes time average.

* West, J. C., Douce, J. L., and Leary, B. G.: Monograph No. 419 M, November, 1960 (see 108 C, p. 259).

Writing $x_i(t)$ as x_1 and $x_i(t+\tau)$ as x_2, and expressing the averages in terms of the second probability density of the input, gives[B]

$$g_{sD}(\tau) = K\int_{-\infty}^{\infty}\int_{-\infty}^{\infty} x_1 f(x_2) p_2(x_1, x_2, \tau) dx_1 dx_2$$

$$- K^2 \int_{-\infty}^{\infty}\int_{-\infty}^{\infty} x_1 x_2 p_2(x_1, x_2, \tau)\, dx_1, dx_2$$

The second integral can be recognized as the autocorrelation of the input, $g_{xx}(\tau)$. Making this substitution and equating $g_{sD}(\tau)$ to zero gives

$$\int_{-\infty}^{\infty}\int_{-\infty}^{\infty} x_1 f(x_2) p_2(x_1, x_2, \tau) dx, dx_2 - K g_{xx}(\tau) = 0 \qquad (D)$$

This is a necessary and obviously also a sufficient condition for non-correlation of the signal and distortion, and also defines the value of K. As pointed out earlier, Booton has shown that for x_i Gaussian this can be reduced to eqn. (B).

It should be noted that, since K must be a constant for any given x_i [in order that we may logically speak of the terms in eqn. (C) as signal and distortion], it is often impossible to satisfy eqn. (D) for an arbitrary $p_2(x_1, x_2, \tau)$ and $f(x_i)$. In such cases the output cannot be split into non-correlated signal and distortion terms.

In conclusion it should be mentioned that the comments made here have no effect on the applications and other conclusions presented in the paper as they were all Gaussian cases.

References

(A) Booton, R. C.: 'Analysis of Non-linear Control Systems with Random Inputs', Proceedings of the Symposium on Non-linear Circuit Analysis, Polytechnic Institute of Brooklyn, New York, 1953.

(B) Newton, G. C., Gould, L. A., and Kaiser, J. L.: 'Analytical Design of Linear Feedback Controls' (Wiley, 1957).

Prof. J. C. West, Dr. J. L. Douce and **Mr. B. G. Leary** (*in reply*): We should like to thank Mr. Boulton for his comments on the validity of the derivation of eqn. (B). This equation was first derived by Booton, who showed that the value of K thus defined is that producing minimum mean squared error. This applies for all probability distributions $p(x)$.

The more rigorous method presented by Mr. Boulton leads to his eqn. (D), which is in general insoluble. However, it reduces to Booton's equation for all probability distributions for $\tau = 0$. For instantaneous non-linearities this is the case of importance.

We suggest, on experimental evidence, that there is always a satisfactory solution to eqn. (D) for the simple non-linearities and probability distributions arising in practice. Analytical justification of this statement would form a useful subject for further research.

DISCUSSION ON 'THE STABILITY OF PERMANENT MAGNETS'*

Dr. A. G. Clegg (*communicated*): It is interesting to compare the results given in this paper with those of other workers. The magnetization changes with time, before one day has elapsed, are not given, but we should expect them to be linear with log t as has been published previously.[A,B] The slope of the magnetization log t curve compares well with values found before for Alnico and for Alcomax III with working point above $(BH)_{max}$. Alcomax III working around and below $(BH)_{max}$ is, however, shown to be more stable in this paper than has been observed elsewhere.

A comparison is also possible of the losses of magnetization due to heating with those found by other investigators. The losses obtained for both Alcomax III and Alnico are considerably less than those previously reported.[C,D] It is stated in Section 5(*h*) that there are differences in the conditions of the tests. Are these merely the difference between assemblies and straight bars, or was there a time interval between magnetizing and the start of the heating test, and if so what was this time interval?

References

(A) Kronenberg, K. J., and Bohlmann, M. A.: 'Long Term Magnetic Stability of Alnico V and other Permanent-Magnet Materials', Wright Air Development Center Technical Report 58–535, December, 1958.

(B) Gould, J. E.: 'Permanent Magnet Stability', *Instrument Practice*, 1958, **12**, p. 1083.

(C) Tenzer, R. K.: 'Effects of Temperature Variations on the Remanence of Permanent Magnets', Conference on Magnets and Magnetic Materials (held in Boston, Mass.), p. 203 (New York. American Institute of Electrical Engineers, 1957).

(D) Clegg, A. G., and McCaig, M.: 'The High Temperature Stability of Permanent Magnets of the Iron-Nickel-Aluminium System', *British Journal of Applied Physics*, 1958, **9**, p. 194.

Mr. C. E. Webb (*in reply*): The differences in results to which Dr. Clegg draws attention are of interest though they do not affect the general significance of the observations recorded in the paper. While there is, as far as I know, no direct experimental evidence on the point, it seems probable that the main reason for the differences lies in the different forms of specimen used. My Alnico and Alcomax samples all consisted of short blocks assembled with soft-iron limbs and pole-pieces, so that the magnetization was approximately uniform throughout the permanent-magnet material. In all the other investigations to which Dr. Clegg refers the samples were short bars on open magnetic circuit in which large variations in magnetization between the middle and ends must have occurred. If, as indicated by the results in Table 2 for Alcomax III (Group E) magnets, the stability decreases rapidly below the $(BH)_{max}$ point, it is to be expected that in magnets working around and below $(BH)_{max}$ this non-uniformity will cause greater instability towards the ends of the magnet and hence greater weakening of the magnet. Some support for this explanation is given by the fact that in Alcomax III magnets working above $(BH)_{max}$ and

* Webb, C. E. (see page 317).

in Alnico magnets, where the variation of stability with the working point is much smaller, the results given in the paper agree fairly closely with those previously published.

With reference to the thermal tests, the mention of different conditions of test in Section 5(*h*) related to the difference between assemblies and straight bars, which may be expected to influence the effect of high-temperature treatment as well as the long-term stability. As Dr. Clegg suggests, however, there may be a further cause of discrepancy in the thermal tests, since in my tests the initial readings, as in the long-term tests, were made approximately 24 hours after magnetization and the measured losses in magnetization would be less than those relative to the strength a few minutes after magnetization, as measured in previously published investigations.

DISCUSSION ON 'MATRIX ANALYSIS OF CONSTRAINED NETWORKS'*

Mr. S. Louis (*communicated*): In general, a network that incorporates n_d constraints has its number of degrees of freedom reduced by n_d. When admittance-analysing an n-node network, $n-1$ cut-sets represent the degrees of freedom; hence $n-1$ voltages corresponding to these cut-sets and $n-1$ external currents completely define the state of the network. Now when n_d degrees of freedom are deducted, only $n_f = n - n_d - 1$ external currents that feed the n_f cut-sets generate the whole set of voltages: n_f directly by the n_f currents, and the remaining n_d by the n_d transmittances. The $n_f + n_d$ equations relating the currents $\boldsymbol{i}_f$ to the complete set of voltages are

$$\begin{bmatrix} \boldsymbol{i}_f \\ 0 \end{bmatrix} = \begin{bmatrix} \bar{y}_{ff} & \bar{y}_{fd} \\ \bar{y}_{df} & \bar{y}_{dd} \end{bmatrix} \begin{bmatrix} \boldsymbol{v}_{[f} \\ \boldsymbol{v}_{[d} \end{bmatrix} \quad . \quad . \quad . \quad (A)$$

The upper n_f equation are Kirchhoff's current law applied to the free nodes, and therefore submatrices y_{ff} and y_{fd} are obtained by partitioning the ordinary matrix y. The lower part should contain the parameters of the constraints.†

This matrix y is much simpler to construct and apply than that of eqn. (34) since no manipulations with rows and columns are needed. Moreover, y of eqn. (34) is in fact the $\bar{y}$ of eqn. (A) with $\boldsymbol{v}_{[d}$ eliminated:

$$y = \bar{y}_{ff} - \bar{y}_{fd}\bar{y}_{dd}^{-1}\bar{y}_{df} \quad . \quad . \quad . \quad . \quad . \quad (B)$$

One may assert now that there is no need at all to define the so-called 'separable case' as in Section 3.2.

In Section 3.3 the author eliminates only some of the n_d voltages: the rest he designates $\boldsymbol{v}_{[ne}$—'not eliminated' voltages. By eqn. (A) it is evident that there is no special need for having a n.e. voltage in each transmittance loop, as is stated in Section 3.4(*b*). Obviously any number of voltages from 0 to n_d can be eliminated to form equations of the form (B).

Finally the operations needed to obtain y of eqn. (34) are quite complicated even in the case of one constraint, as in eqn. (44) the bigger n_f is, the more manipulations are needed.

This last argument is clearly enhanced in the case of a dual-control, and much more in a multi-control constraint:

$$v_j = \sum_k t_{kj} v_k \quad . \quad . \quad . \quad . \quad . \quad . \quad (C)$$

This reasoning brings us to the conclusion that if v_d is not eliminated at all, as is in eqn. (A), much labour will be saved in the application to practical problems.

Dr. A. Nathan (*in reply*): Mr. Louis's eqn. (A) is not explicit but I think that only a minor variation in notation is involved as compared with my paper.

In fact, writing

$$t = (I \mid \underline{t}) \quad . \quad . \quad . \quad . \quad . \quad . \quad . \quad (D)$$

and putting in eqn. (A)

$$\left.\begin{aligned} \underline{y}_{[f} &= (\bar{y}_{ff} \mid \bar{y}_{fd}) \\ \bar{y}_{df} &= \underline{t}' \qquad \bar{y}_{dd} = -I \end{aligned}\right\} \quad . \quad . \quad . \quad (E)$$

(which is, I presume, what Mr. Louis has in mind) eqn. (A) becomes identical with eqns. (28) and (31), when $\boldsymbol{v}_{(s)} = 0$.

The paper goes on to eliminate $\boldsymbol{v}_{[d}$ from the equations which lead to eqn. (34). Eqn. (B) states how, in general, elimination is effected. Substitution of eqn. (E) into eqn. (B) yields, for the present case,

$$y = \bar{y}_{ff} + \bar{y}_{fd}\underline{t}' = (\bar{y}_{ff} \mid \bar{y}_{fd}) \begin{pmatrix} I \\ \underline{t}' \end{pmatrix} = \underline{y}_{[f} t' \quad . \quad . \quad . \quad (F)$$

where the last step follows from eqn. (D), and this is identical with eqn. (34). Thus the only pertinent point is the obvious fact that $y = \underline{y}_{[f} t'$ can be produced by the prescription in the second expression of eqn. (F).

In the general case the equations of constraint can be written

$$\bar{y}_{df}\boldsymbol{v}_{[f} + \bar{y}_{dd}\boldsymbol{v}_{[d} = 0 \quad . \quad . \quad . \quad . \quad (G)$$

where $\bar{y}_{dd}$ is of rank $(d-i)$. The non-negative integer i designates the 'feedback index' of the constraining structure. In general only $d-i$ components of $\boldsymbol{v}_{[d}$ can be eliminated, which shows the reason for assigning a special position to the 'separable' case which corresponds to $i = 0$.

I fail to see how simplification of operations is to be achieved. The whole point of the method is the production of a non-singular admittance matrix of least order.

* Nathan, A.: *Proceedings I.E.E.*, Monograph No. 399 E, September, 1960 (see 108 C, p. 98).

† Rigorous proof will be given in a paper to be published.

INDEX TO VOLUME 108, PART C

1961

ABBREVIATIONS

(P)—Paper. (D)—Discussion.

THE BENEVOLENT FUND

The number of applications for assistance from the Fund has shown a marked increase during the last few years, and this year these fresh demands exceed the increase in contributions. The state of the Fund has enabled the Court of Governors to maintain for the present their standard of assistance in the necessitous cases but they are anxious that their ability to help should not be impaired.

The Fund is supported by about a third of the members, and the Governors' best thanks are accorded to those who subscribe. They do, however, specially appeal to those who do not at present contribute to the Fund to do so, preferably under deed of covenant.

Subscriptions and Donations may be sent by post to

THE INCORPORATED BENEVOLENT FUND OF
THE INSTITUTION OF ELECTRICAL ENGINEERS
SAVOY PLACE, LONDON, W.C.2

or may be handed to one of the Local Hon. Treasurers of the Fund.

THE FUND IS SUPPORTED BY SUBSCRIPTIONS, DONATIONS, LEGACIES

LOCAL HON. TREASURERS OF THE FUND:

EAST MIDLAND CENTRE . . . . . *L. Adlington*	SCOTTISH CENTRE . . . . *R. H. Dean, B.Sc.Tech.*
IRISH BRANCH . . . . . *A. Harkin, M.E.*	NORTH SCOTLAND SUB-CENTRE. . . . *P. Philip*
MERSEY AND NORTH WALES CENTRE *D. A. Picken*	SOUTH MIDLAND CENTRE . . . *H. M. Fricke*
TEES-SIDE SUB-CENTRE . . . . *W. K. Harrison*	RUGBY SUB-CENTRE . . . . . *P. G. Ross, B.Sc.*
NORTH-EASTERN CENTRE . . . . *R. G. Scotson*	SOUTHERN CENTRE . . . . . *J. E. Brunnen*
NORTH MIDLAND CENTRE *E. C. Walton, Ph.D., B.Eng.*	WESTERN CENTRE (BRISTOL) . . . *A. H. McQueen*
SHEFFIELD SUB-CENTRE . . . . . *F. Seddon*	WESTERN CENTRE (CARDIFF) . . . *E. W. S. Watt*
NORTH-WESTERN CENTRE . *E. G. Taylor, B.Sc.(Eng.)*	WEST WALES (SWANSEA) SUB-CENTRE *O. J. Mayo*
NORTH LANCASHIRE SUB-CENTRE . . *H. Charnley*	SOUTH WESTERN SUB-CENTRE . . *W. E. Johnson*
NORTHERN IRELAND CENTRE . . *G. H. Moir, J.P.*	

Members are asked to bring to the notice of the Court of Governors any deserving cases of which they may have knowledge.

PAPERS FOR THE PROCEEDINGS

Handbook for Authors

Anyone who is thinking of submitting a Paper to The Institution should apply to the Secretary for a copy of the **Handbook for Authors**. The price is 3s. (post free), but a copy will be supplied free of charge if the application is accompanied by a summary of the Paper. The following are some of the main points considered in the Handbook.

Acceptability

To be acceptable, a Paper should normally contribute to the advancement of electrical science or technology. The Institution does not accept Papers which have been published elsewhere.

Length

No Paper should occupy more than 10 pages in the *Proceedings*. Authors can generally keep well within this limit. For example, the average Paper published in 1960 consisted of 6 000 words (5 pages) and, with its illustrations and mathematics, occupied a total of 8 pages.

Summary

An essential part of a Paper is the **Summary**, which should not exceed 200 words.

Text

The **Text** should begin with sufficient introductory matter to enable the Paper to be understood without undue reference to other publications.

The Text should include no more mathematics than is essential. Extended mathematical treatment and lengthy digressions—if they must be included—should be put in **Appendices.**

Proprietary articles should not be mentioned by name unless this is unavoidable.

The rationalized M.K.S. system of units is preferred.

Acknowledgments

Assistance in the preparation of the Paper, and sources of information, should be acknowledged. References to manufacturers should be made only under **Acknowledgments.**

References

Bibliographical **References** should be numbered and listed in a special section, and indicated in the Text by means of 'indices'.

Numbering

The Text should be appropriately sectionalized, the sections and their subdivisions being numbered according to the 'decimal' system. Acknowledgments, References and Appendices should be numbered as though they were sections of the Text.

Typing

Typing should be on one side of the paper only, with double spacing between lines and a 1½ inch margin on the left. Besides the original typescript, two carbon copies are required by The Institution.

Advice on the typing of mathematics is given in the **Handbook for Authors,** which includes a facsimile of a typewritten page containing mathematics.

Illustrations should not be drawn or pasted on the typewritten pages. They are of no use to the printer, but he does need a complete list of captions, again with double spacing. The list should be attached to the typescript.

Drawings

Three sets of drawings, which may be in the form of dye-line prints, should accompany the typescript. Tracings, which will be required later, should be in indian ink with the lettering in pencil. The reduction in the size of the drawings, and therefore the size of lettering required, is not settled before the Paper has been accepted.

Dispatch

The typescript and illustrations should be packed flat, not rolled, and addressed to *The Secretary, The Institution of Electrical Engineers, Savoy Place, London, W.C.2.*

PROCEEDINGS OF THE INSTITUTION OF ELECTRICAL ENGINEERS

PART C—MONOGRAPHS, SEPTEMBER 1961

CONTENTS

Bibliographical References.—It is requested that bibliographical reference to an Institution paper should always include the serial number of the paper and the month and year of publication, which will be found at the top right-hand corner of the first page of the paper. This information should precede the reference to the Volume and Part.

Example.—Smith, J.: 'Overhead Transmission Systems', *Proceedings I.E.E.*, Paper No. 5001 S, December, 1960 (107 B, p. 1234).

Published by The Institution, Savoy Place, London, W.C.2. *Telephone:* COVent Garden 1871. *Telegrams:* 'Voltampere, Phone, London.'
Printed by Unwin Brothers Limited, Woking and London.